Author:
Resendiz-Lara, Diego

Title:
Catalytic Dehydropolymerisation of Amine– and Phosphine–Boranes as a Route to Structurally Diverse Materials

Catalytic Dehydropolymerisation of Amine– and Phosphine–Boranes as a Route to Structurally Diverse Materials

Diego Alejandro Resendiz–Lara

A dissertation submitted to the University of Bristol in accordance with the requirements for the degree of Doctor of Philosophy in the School of Chemistry, Faculty of Science

October 2018

Word Count: 42,960

Abstract

This thesis describes the synthesis and characterisation of polyamino– and polyphosphinoboranes, targeting the use of catalytic dehydropolymerisation as a route to obtain polymers with varied structures.

Chapter 1 puts into context of the area of metal-catalysed dehydrocoupling chemistry of main group compounds with an emphasis on amine– and phosphine–boranes as precursors to polymeric materials, and the properties and potential applications of the related inorganic polymers.

Chapter 2 describes the synthesis of a family of aryl-substituted phosphine–boranes with electron-donating and electron-withdrawing groups and the polymerisation of these monomers by metal-catalysed dehydropolymerisation using [$CpFe(CO)_2OTf$] as a precatalyst. The discussion focuses on the influences of the electronics of the substituents in the side chains on the properties of the polymers, and the study of their thermal properties, as well as their potential applications.

Chapter 3 describes the expanded use of [$CpFe(CO)_2OTf$] as a versatile precatalyst for the dehydropolymerisation of a range of alkyl-substituted phosphine–boranes with varied structures. Although preliminary investigation was hampered by monomer purity, the discussion focuses on the potential factors that could affected the monomer's reactivity. The thermal properties of poly(alkylphosphinoboranes) are also discussed.

Chapter 4 presents the use of amine–boranes substituted by aryl-containing alkyl groups at nitrogen *via* catalytic dehydropolymerisatiom aided by transition metal precatalysts. The formation of high molar mass homopolymers and copolymers is described along with thermal stability and cross-linking studies. Discussion on the molar mass characterisation of polyaminoboranes by different analytical techniques is also described.

Chapter 5 describes the unprecedented synthesis and characterisation of the BN inorganic analogues of polystyrene, poly(*B*-arylaminoboranes) through metal-catalysed dehydropolymerisation of B-substituted amine–boranes. In addition, the stability studies in the solid state and in solution for these polymers is presented.

Chapter 6 presents ongoing and potential ideas for future work based upon the results presented in Chapter 2–5.

Acknowledgements

Firstly, I would like to thank Prof. Ian Manners for his guidance and for allowing me to be a part of the history of this very dynamic and diverse group. It is inevitable not to be inspired by the passion with which Prof Manners conducts his research and has made this experience invaluable. In the same manner, I would like to thank Dr. George Whittell for his immeasurable help, patience and knowledge when things went south in the laboratory. And to Deborah O'Hanlon Manners for her kindness and assistance even before I arrived to this country.

In addition, I would like to thank my parents, Olga and Braulio, whose decisions in life has led me to this point in mine. None of this would be possible without your love and support. There are not enough words in the English or Spanish language which can express the pride and gratitude I feel for your hard work. Also, I would like to thank Thalia and Braulio, whose lives are complementary of mine. Los amo.

I have been particularly lucky to meet and work with amazing and talented people of whom I praise to be friends with during these four years in Bristol. In particular, I would like to thank to my fellow lab-mates in N418: Vincent Annibale, Marius Arz, Laura Beckett, Theresa Dellermann, Becs Hailes, Ali Knights and Nicola Oldroyd. The past members: Saurabh Chitnis, Titel Jurca, Erin Leitao, Becca Musgrave, André Schäfer, Owen Metters, Naomi Stubbs, Josh Turner and Lipeng Wu.

I also want to thank the "First Years" Paul Choi, Charlie Jarrett-Wilkins, Liam MacFarlane and Alex Oliver for sharing and making this experience extra special.

Also, I would like to extend my gratitude to the people next door, present: Charlotte Ellis, Diego Garcia Horatio He, Sam Pearce, Huda Shaikh, Steve Street; and past: John Finnegan, Charlotte Boott, Jess Gwyther, Emily Kynaston, Ali Nazemi, Mahbouhbeh Hadapour and Matt Robinson.

Finally, I would like to thank to the all the people involved during my “Senior Resident” period, especially to Beth Benker. And I want to thank to my Mexican gang, Alberto Ávila and Dulce Rodriguez, and all the people involved in the Mexican Culture Society; and to CONACyT and all the taxpayers in Mexico for the financial support. Also, I want to thank to Nacho Cervera for his invaluable support.

Declaration

I declare that the work in this dissertation was carried out in accordance with the requirements of the University's *Regulations and Code of Practice for Research Degree Programmes* and that it has not been submitted for any other academic award. Except where indicated by specific reference in the text, the work is the candidate's own work. Work done in collaboration with, or with the assistance of, others, is indicated as such. Any views expressed in the dissertation are those of the author.

Diego Alejandro Resendiz Lara

University of Bristol

19/October/2018

Table of Contents

List of Figures

List of Schemes

List of Tables

List of Abbreviations

°	Degrees
°C	Degrees centigrade
1D	One-dimensional
Å	Angstrom
Ad	Adamantyl
Ar	Aryl
b	Broad
BAr^{F}_{4}	$B(C_6H_3(m\text{-}CF_3)_2)_4)$
Cat.	Catalyst
COD	1,5-Cyclooctadiene
Cp	Cyclopentadienyl
Cp*	Pentamethylcyclopentadiene
Cy	Cyclohexyl
CVD	Chemical vapor deposition
d	Doublet
Da	Daltons
DFT	Density functional theory
Dipp	2,6-diisopropylphenyl
DLS	Dynamic light scattering
DOSY	Diffusion-Ordered Spectroscopy
DP_n	Degree of polymerisation
dppe	1,2-bis(diphenylphosphino)ethane
DSC	Differential scanning calorimetry
E	Main-group element
EA	Elemental Analysis
EDX	Energy dispersive X-ray sprectroscopy
Equiv.	Equivalents
ESI-MS	Electrospray ionisation mass
Et	Ethyl
Et_2O	Diethyl ether
eV	Electron-volt
Fc	Ferrocenyl
FLP	Frustrated Lewis pairs

GPC	Gel permeation chromatography
h	Hour
Hz	Hertz
*i*Bu	*Iso*-butyl
*i*Pr	*Iso*-propyl
IR	Infrared
K	Kelvin
kcal	Kilocalorie
m	Multiplet
M	Molar
m/z	Mass to charge ratio
Me	Methyl
Mes	1,3,5-trimethylbenzene
min	Minute
mg	Milligram
mL	Millilitre
M_n	Number average molecular weight
mol	Mole
M_w	Weight averaged molecular weight
*n*Bu	*n*-butyl
*n*Hex	*n*-hexyl
nm	nanometre
NHC	N-heterocyclic carbene
NMR	Nuclear Magnetic Resonance
Oct	Octyl
PDI	Polydispersity index
PDMS	Polymethylsiloxane
Ph	Phenyl
POCOP	k^3-1,3-$(OPtBu_2)_2C_6H_3$
ppm	Parts per million
R_H	Hydrodynamic radius
RI	Refractive Index
ROP	Ring-opening polymerisation
rpm	Revolutios per minute
s	singlet
SAXS	Small-angle X-ray scattering

SEM	Scanning electron microscopy
t	triplet
tBu	*Tertiary*-butyl
TEM	Transmission electron microscopy
Tf	Triflate
TGA	Thermogravimetric analysis
THF	Tetrahydrofuran
TMS	Trimethylsilane
Tol	Toluene
UV-vis	Ultraviolet-visible
v.	Very
wt.	Weight
XRD	X-ray diffraction
xantphos	4,5-bis(diphenylphosphino)-9,9-dimethylxanthene
δ	Chemical Shift
μL	Microlitre

Chapter 1.

Introduction

1.1 Research Objectives

In recent years, the investigation on the catalytic dehydrocoupling of amine– and phosphine–boranes has primarily focused on the study of the release and potential storage of molecular hydrogen for fuel-cell applications. In addition, the catalytic dehydrocoupling reaction of amine– and phosphine–boranes has been found to provide a viable route for the synthesis of macromolecules containing B–N and P–B bonds in the main chain. These materials possess diverse potential applications as, for example, precursors to ceramic materials or elastomers and thermoplastics. Although there are well-established catalytic routes to access these types of inorganic polymers, the range of monomers that undergoes the dehydropolymerisation reaction is relatively restricted thereby limiting the materials available. In the case of amine–boranes, only monomers with small alkyl groups attached to nitrogen have been successfully polymerised to polyaminoboranes. On the other hand, until now, the polymerization of phosphine–borane monomers has only been efficient with aryl substituents at the phosphorus centre for the synthesis of polyphosphinoboranes,

The aim of the research described in this thesis is to continue the investigation on the dehydropolymerisation of primary amine– and phosphine–boranes using metal-catalysed systems in order to tackle the synthesis of more structurally diverse polyaminoboranes and polyphosphinoboranes, respectively. This introductory chapter describes the general aspects of dehydrocoupling chemistry and places the work on the aforementioned inorganic polymers in context. Moreover, each chapter has detailed background associated with the dehydrocoupling of the array of amine– and phosphine–boranes used in this work.

1.2 Background Introduction

1.2.1 Catalytic Bond Formation for Main Group Elements: Historic Aspects

The ability to form or break C–C bonds by transition-metal-catalysed routes has played a pivotal role in the development of the area of synthetic organic chemistry since the 1950s. This has led to breakthroughs in olefin metathesis,[1] the establishment of different palladium-based cross-coupling systems,[2] and olefin polymerisation.[3] Many efficient catalytic processes have also been developed for the formation of bonds between carbon and other elements.

In contrast, analogous catalytic bond-forming routes to non-carbon main group elements E–E' (E, E' = *p*-block element) are still emerging. In particular, salt metathesis and reductive coupling routes have traditionally provided the main routes to the formation of main group element–element bonds. These involve the generation of unwanted byproducts and often require aggressive reaction conditions. For example, the use of the Wurtz reaction to prepare polysilanes $[SiR_2]_n$ from organochlorosilanes and stoichiometric amounts of alkali metals requires forcing conditions which has hindered the expansion of the field as this methodology was found to be non-catalytic and element-dependant with a limited scope and lack of generality.[4]

Catalytic dehydrocoupling chemistry has emerged as a versatile approach to the formation of *p*-block element–element bonds with concurrent elimination of molecular hydrogen (H_2).[5] Pioneering examples in the mid-1980s of the utilisation of metal-catalysed dehydrocoupling routes were applied to prepare homonuclear bonds between main group elements (E–E). For example, the formation of B–B bonds was achieved by platinum-based catalytic dehydrocoupling of boranes and carboranes to prepare linked borane clusters (Scheme 1.1A)[6] and, around the same time, an analogous process to yield Si–Si bonds from primary silanes using titanocene precatalysts was described (Scheme 1.1B).[7]

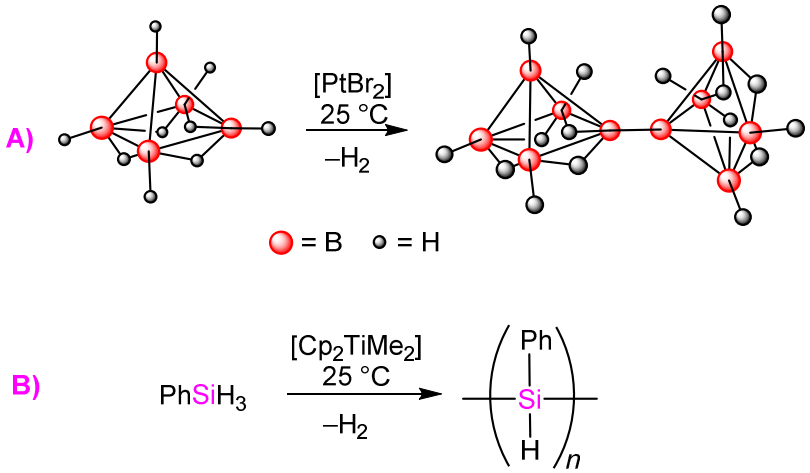

Scheme 1.1. a) Formation of a B–B bond by Pt-based catalytic dehydrocoupling of borane cluster [B_5H_9]. b) Synthesis of polysilanes by Ti-based catalytic dehydrocoupling of silanes.

Metal-catalysed dehydrocoupling reactions to form main group heteronuclear bonds (E–E') were reported shortly thereafter. For example, the formation of Si–N bonds to prepare oligosilazanes (Scheme 1.2A)[8] and the formation of Si–P bonds to prepare silylphosphines (Scheme 1.2B)[9] was achieved by the Ti-catalysed heterodehydrocoupling of silanes with ammonia and phosphines, respectively.

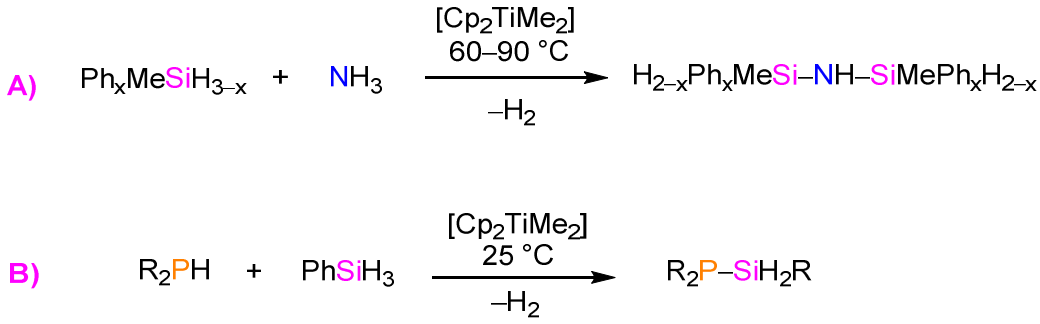

Scheme 1.2. a) Formation of oligosilazanes using Cp_2TiMe_2 by dehydrocoupling of silanes and NH_3. b) Synthesis of P–Si bonds by catalytic dehydrocoupling of phosphines and silanes with Cp_2TiMe_2.

Since then, the area of catalytic dehydrocoupling to form homo- and hetero-nuclear main group bonds (E–E or E–E') has become a promising methodology for the synthesis of a variety of inorganic molecules and materials (e.g. cyclic species, cages, main group multiple bonds, ceramics, etc.).[5a]

1.2.2 Synthesis of Inorganic Polymers: A Synthetic Challenge

Polymeric organic materials are ubiquitous in our everyday modern life. Their technological applications vary from packaging materials, medical implants, and electronics, to their use in the textile, automotive and aerospace industries.[10] This can be attributed to relatively easy access to monomers from petroleum-based sources and to the existence of well-established synthetic organic methodologies (e.g. free radical, anionic and cationic, and addition or condensation polymerisation reactions).[11]

Addition polymerisation (Scheme 1.3A) is a widely used protocol that involves the use of unsaturated organic molecules (e.g. α-olefins such as ethylene and styrene) generally *via* a chain-growth mechanism. However, the application of an analogous technique to synthesise inorganic polymers is usually difficult as the preparation of inorganic molecules with element–element multiple bonds is difficult and, additionally, such species are generally highly reactive and challenging to handle in the absence of sterically bulky substituents which prevent further oligomerisation events.[12] Despite these issues, significant progress in this area has been achieved over the past two decades.[13]

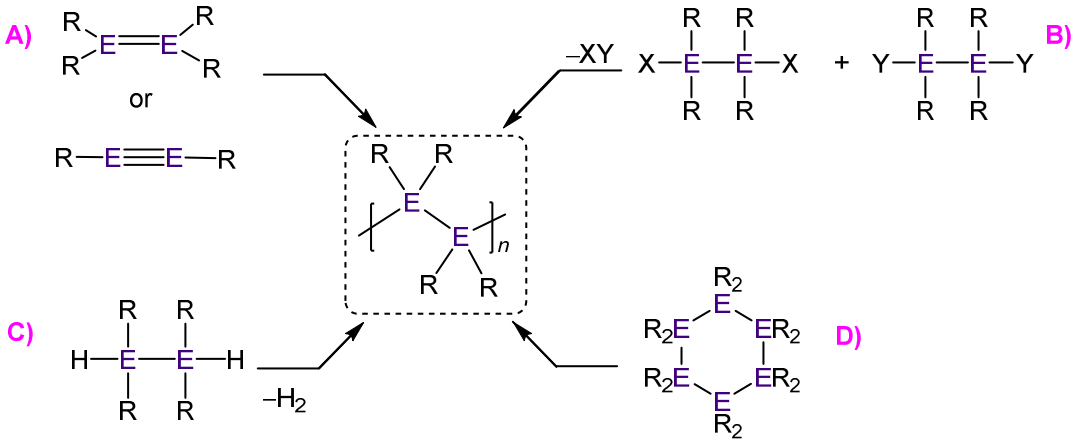

Scheme 1.3. Common routes to prepare inorganic polymers.

The alternative polycondensation protocol (Scheme 1.3B) for all-carbon systems involves a step growth mechanism and requires the use of highly pure difunctional substrates

which are generally easy to access. Moreover, the underlying step-growth mechanism entails the use of strict conditions of stoichiometric balance together with high conversion of monomers to access high molar mass polymers. When this condensation protocol is translated to bifunctionalised inorganic synthons it is found that such species are frequently challenging to synthesise and to purify (e.g. involving preparation of dilithiated monomers) and thus, it leads to low molar mass, oligomeric products.[14]

Despite the challenges in the synthesis of inorganic monomers, the formation of inorganic polymers with main-group elements in their backbones have been circumvented by two alternative synthetic routes: catalytic dehydrocoupling polymerisation (which can be perceived as a catalysed self-condensation reaction) (Scheme 1.3C); and ring-opening polymerisation (ROP) of cyclic monomers (Scheme 1.3D).[15] Both protocols usually follow a chain-growth mechanism with an efficient propagation step which allows for the facile formation of high molar mass polymers. As a consequence, the inorganic polymer field has expanded beyond the classical inorganic polymeric systems (e.g. polysilanes, polysiloxanes and polyphosphazenes) which have been used in a number of different applications such as electroluminescent materials for devices, high-performance elastomers, and flame-retardant materials.[16] Since then, new polymers based on main group elements have been developed: polycarbosilanes, polystannanes, polycarbophosphazenes, metallocene-based polymers, etc. Nevertheless, the exciting prospects of inorganic materials are the remarkable potential related to their unique physical properties, which differ from purely organic carbon-based polymers, as a consequence of the inherent chemistry of main group elements.[17]

Recently, there has been widespread interest in catalytic heterodehydrocoupling strategies for compounds of group 13/15 elements to access novel molecules and materials.[18] Typically, these have involved species such as amine–boranes $RNH_2{\cdot}BH_3$ and phosphine–boranes $RPH_2{\cdot}BH_3$ (R = alkyl, aryl, H). Group 13/15 polymers are relatively

unexplored, yet are important as analogues of polymeric all-carbon systems (e.g. polyolefins). For example, polyaminoboranes $[RNH–BH_2]_n$ and polyphosphinoboranes $[RPH–BH_2]_n$ could potentially have novel thermophysical, preceramic and other useful materials properties of technological relevance.

1.2.3 Catalytic Formation of Nitrogen–Boron Bonds

1.2.3.1 Synthesis of Amine–Borane Adducts

Amine–boranes are a classical representation of a Lewis acid-base adduct formed between a borane Lewis acid (e.g. BH_3) and amine Lewis base (e.g. NH_3) connected by a dative bond. After the discovery of $NH_3{\cdot}BF_3$ in 1809 by Gay-Lussac,[19] different synthetic methodologies to prepare amine–boranes have been developed. The more frequently employed routes to synthesise amine–boranes involve either the direct reaction of amines and borane adducts with labile donors $BH_3{\cdot}L$ (e.g. L = THF or SMe_2) (Scheme 1.4A),[20] or a salt metathesis reaction between ammonium salts and borohydrides (Scheme 1.4B).[21] By the latter route, *B*-substituted amine–boranes can be produced from reduction of boronic acids to form borohydrides that react with commonly available amine hydrochloride salts.[22]

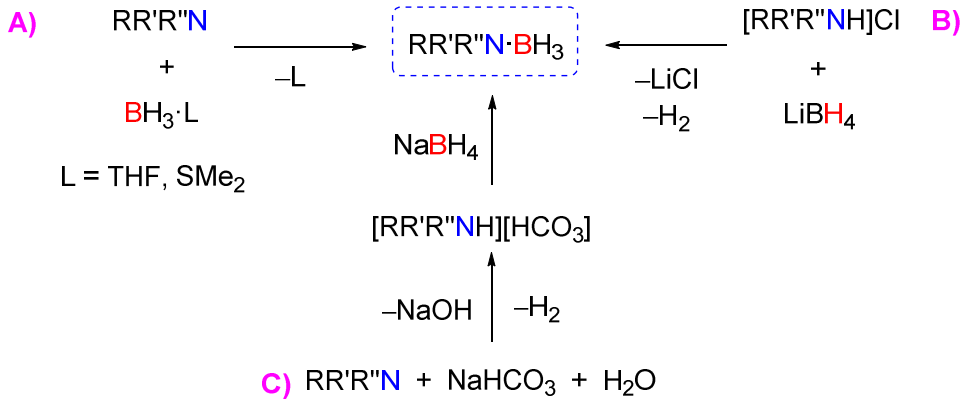

Scheme 1.4. Synthetic routes to amine–boranes.

This metathesis protocol enables the access of a range of amine–boranes with substituents at either boron or nitrogen atoms. Recently, an open-flask synthesis of amine–boranes with high functional group tolerance was described. The reaction involves the formation of alkylammonium carbonate (prepared *in situ* from $NaHCO_3$ and H_2O in the presence of an amine) which subsequently undergoes metathesis with $NaBH_4$ to form the amine–borane (Scheme 1.4C).[23]

1.2.3.2 Reactivity and Applications of Amine–Boranes

Amine–boranes feature a B–N bond with electronegativity difference of 1.0 ($\chi_B = 2$ and $\chi_N = 3$)[24] which induces overall polarisation in these adducts (Figure 1.1).[25] As a consequence, ammonia–borane and related amine–boranes featuring hydrogen substituents at B and N present two fundamental reactions that are dictated by their polar nature; the former is the attack at protic hydrogens at nitrogen by basic reagents, leading to deprotonation; and the latter is the attack at the hydridic hydrogens at boron by acids to lead to loss of a hydride. Furthermore, amine–boranes have been traditionally utilised as reducing and hydroboration reagents,[18a, 26] and in hydrogen storage[27] and transfer.[28] In recent years, amine–boranes have been tested as part of hypergolic rocket fuel components.[29]

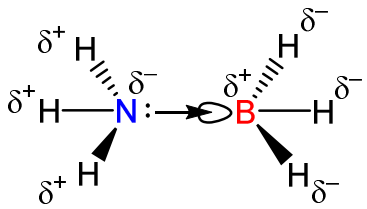

Figure 1.1. Schematic representation of bond polarisation in the Lewis acid/base adduct $NH_3{\cdot}BH_3$.

Moreover, extensive research on the dehydrogenation reaction of ammonia–borane $NH_3{\cdot}BH_3$ has been described,[27b, 30] and this species has been considered to be a potential candidate as a hydrogen storage material due to its high gravimetric hydrogen content (19.6 wt%), low molar mass (30.7 g mol^{-1}) and its thermal stability under ambient

conditions. Although the dehydrogenation of $NH_3{\cdot}BH_3$ by thermal[31] and catalytic routes[32] produces a relatively high yield of H_2, the BN products of such reactions have been found to be difficult to rehydrogenate. The regeneration of the "spent fuel" is one of the critical steps to be addressed if $NH_3{\cdot}BH_3$ is to be used as a realistic hydrogen storage compound for most applications.[21a, 33]

Alternative applications of amine–boranes have been developed in different areas. In materials science, they are ceramic precursors of boron nitride (BN) which exits commonly in two polymorphs, the cubic boron nitride (*c*-BN) and the hexagonal boron nitride (*h*-BN).[34] The former allotropic form has found applications as an abrasive due to its inherent hardness which is similar to diamond.[35] Atomic layers of *h*-BN have been prepared from $NH_3{\cdot}BH_3$ by means chemical vapor deposition (CVD)[36] and have potential applications in graphene-based electronics as a 2D dielectric substrate.[37]

In polymer science, the catalytic dehydrocoupling of amine–boranes has led to the formation of polyaminoboranes which are boron–nitrogen analogues of polyolefins. Although the development of synthetic routes to form high molar mass polyaminoboranes is still nascent, potential applications of these materials have been noted in a few reports. These include precursors to boron nitride[38] or borate nanowires,[39] piezoelectric materials,[40] and for boron neutron capture therapy.[41]

1.2.3.3 General Aspects of Metal-Catalysed Dehydrocoupling of Amine–Boranes

Dehydrocoupling is pivotal to many of the proposed applications of amine–boranes and involves the formation of new B–N bonds with concomitant release of H_2. Amine–boranes can undergo this process either thermally, usually at temperatures above 100 °C,[42] or catalytically at reduced and/or ambient temperatures, usually through the use of a metal catalyst.[18b, 32]

The study of dehydrocoupling reactions has focused to a great extent on secondary amine–boranes $R_2NH{\cdot}BH_3$ for mechanistic investigations on the metal-catalysed reaction.[18b] This is owing to the formation of relatively well-defined intermediates and products. For example, linear diborazanes $R_2NH{\cdot}BH_2NR_2{\cdot}BH_3$ or cyclodiborazanes $[R_2N–BH_2]_2$ can be detected (e.g. R = Me). The exception is when R is a bulky group (e.g. *i*Pr, Cy) and only monomeric aminoboranes, $R_2N{=}BH_2$ are formed.

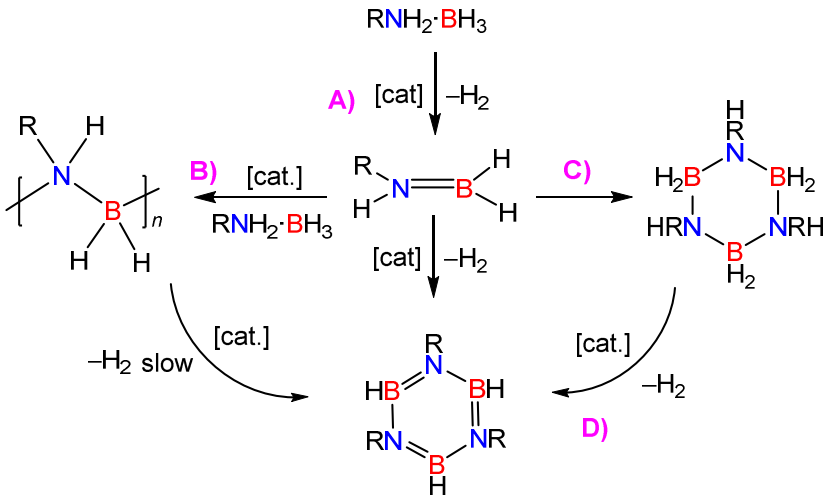

Scheme 1.5. General scheme for the catalytic dehydrocoupling of primary amine–boranes.

In the case for $NH_3{\cdot}BH_3$ and primary amine–boranes $RNH_2{\cdot}BH_3$, the initial loss of H_2 can lead to the formation of an aminoborane $RNH{=}BH_2$ (R = H, Me) (Scheme 1.5A) which has been proposed to be an intermediate in the formation of either cyclic oligomers or linear polymeric material (Scheme 1.5B).[18b] However, the subsequent reactivity of the aminoborane $RNH{=}BH_2$ (R = H, Me) once formed, is poorly understood. One possibility is the initial trimerisation to form borazane $[RNH–BH_2]_3$ (Scheme 1.5C), after which subsequent dehydrogenation processes lead to the formation of the thermodynamic product, borazine $[RN–BH]_3$ (Scheme 1.5D). Nevertheless, an understanding of the fundamental chemistry of free $RNH{=}BH_2$ (R = H, Me) can be approached through their observation as transient intermediates in reactions by *in situ* nuclear magnetic resonance (NMR) spectroscopy,[43] or indirect observation by trapping of stable products (using

hydroboration of cyclohexene),[28a, 44] studies of polymer growth kinetics[45] and catalytic redistribution reactions,[28a] or via their coordination to metal centres.[46]

1.2.3.4 Dehydrocoupling of Amine–Boranes by Transition Metal Catalysts

The number of metal catalysts that mediate dehydrocoupling/dehydrogenation transformations of amine–boranes has increased dramatically in the last decade and are mainly focused on $NH_3{\cdot}BH_3$ and $Me_2NH{\cdot}BH_3$. Among the catalytic systems described, we can find catalysts based on early,[47] mid[28c, 47j, 48] and late transition metals[18b, 32] from the *d* block, and recently, some examples from the *f* block.[49] Moreover, the use of main-group catalysts from the *s*-[50] and *p*-[51] blocks are attracting more attention, and systems based on frustrated Lewis pairs (FLPs)[52] are also emerging as dehydrocoupling agents.

The *Manners* group have contributed significantly to the amine–borane dehydrocoupling area and the main work in this thesis is based on some metal-catalysed systems developed by our group. For example, *Manners* and co-workers reported the first example of the metal-catalysed dehydrocoupling of $Me_2NH{\cdot}BH_3$ using Rh-based precatalysts at room temperature to form the cyclic dimer $[Me_2N–BH_2]_2$. When the same catalytic system was applied to primary amine–boranes $RNH_2{\cdot}BH_3$ (R = H, Me, Ph) the successive formation of borazane $[RBH–NH_2]_3$ to borazine $[RB–NH]_3$ was observed. In the case of $NH_3{\cdot}BH_3$, the formation of B–N oligomers and/or polymers was also detected.[20a]

The catalytic dehydrocoupling reaction has been extended to other amine–borane substrates using $[Rh(\mu\text{-}Cl)(1,5\text{-}COD)]_2$ (COD = cyclooctadiene) as a precatalyst under mild conditions (Scheme 1.6).[20a] For example, this precatalyst has yielded the formation of four-membered B–N rings $[RR'N–BH_2]_2$ from dehydrocoupling of asymmetric $((PhCH_2)(Me)NH{\cdot}BH_3)$ or cyclic $(1,4\text{-}(C_4H_8)NH{\cdot}BH_3)$ amine–borane substrates. The monomeric aminoborane $i Pr_2N{=}BH_2$ was isolated from dehydrogenation of $i Pr_2NH{\cdot}BH_3$.

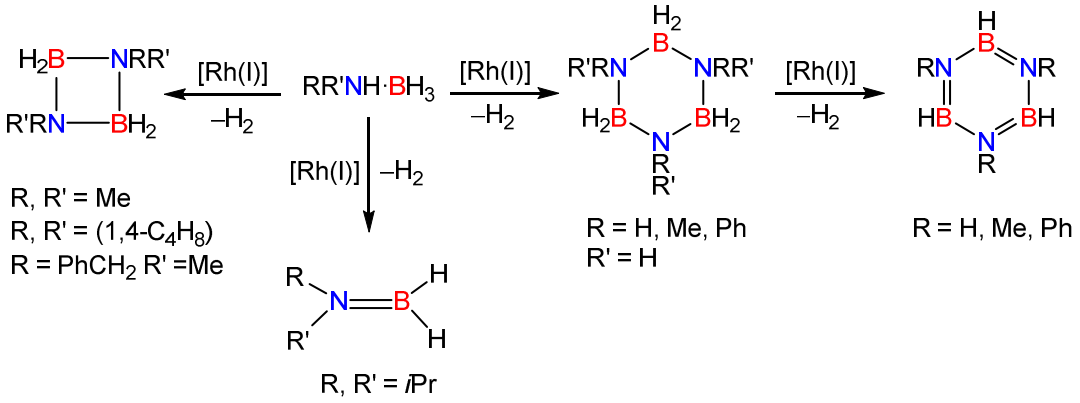

Scheme 1.6. Catalytic dehydrocoupling of amine–boranes by [Rh(μ–Cl)(1,5-COD)]$_2$.

Manners and co-workers suggested through subsequent investigations that the dehydrocoupling by the Rh-based precatalysts was mediated by Rh(0) colloids which were formed *in situ*.[20a, 28h, 53] These investigations were based on multiple factors: observation of a sigmoidal-shaped kinetic curve, an initial induction period and by a change of colour from yellow/orange to black in the solution. Additionally, reaction inhibition was observed: 1) after addition of Hg(0) which suppressed catalysis by amalgam formation, 2) after fractional addition of coordinating ligands and 3) after microfiltration of the reaction mixture through pore membrane filters. After completion of the reaction, the Rh(0) colloids were characterised by transmission electron microscopy (TEM) showing particles of 2 nm in size.

In addition to the Rh-based precatalyst, a heterogenous skeletal nickel system was proved to be active in the dehydrocoupling reaction of amine–boranes by *Manners* and co-workers (Scheme 1.7).[54] The catalytic dehydrocoupling reaction (5 mol% skeletal Ni) of different secondary amine–boranes $R_2NH{\cdot}BH_3$ (R = Me, Et) was demonstrated at room temperature (20 °C) in toluene and produced $[R_2N–BH_2]_2$. The heterogeneous nature of the catalytic system was confirmed by the effects of filtration and addition of mercury to the reaction mixture. Both tests completely ceased the activity of skeletal Ni. This Ni-based catalyst is

an effective alternative for the dehydrogenation of amine–boranes substrates due to its low cost, facile accessibility and simple removal from reaction mixtures by filtration.

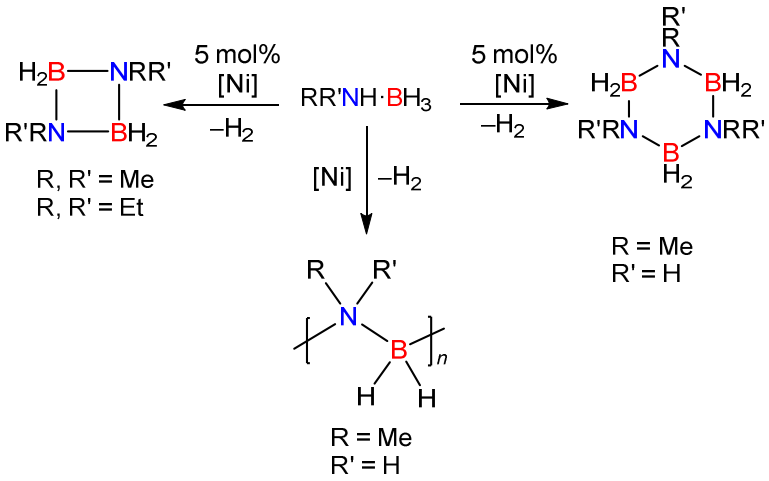

Scheme 1.7. Catalytic dehydrocoupling of amine–boranes by skeletal nickel.

The catalytic dehydrocoupling of $MeNH_2{\cdot}BH_3$ with skeletal Ni (5 mol%) in THF yielded borazane $[MeNH–BH_2]_3$, contrary to dehydrocoupling of $MeNH_2{\cdot}BH_3$ with $[Rh(\mu\text{-}Cl)(1,5\text{-}COD)]_2$ that produced borazine $[MeN–BH]_3$. The formation of high molar mass poly(methylaminoborane) $[MeNH–BH_2]_n$ (M_w = 78,000 g mol^{-1}, PDI = 1.52) was observed when skeletal Ni was used in stoichiometric quantities. The observation that different products are formed upon changing the catalyst loading is significant in the Ni-based system as it reinforces the idea of the participation of the aminoborane intermediate $MeNH{=}BH_2$ in the metal-catalysed polymerisation. It is proposed when catalytic amounts of skeletal Ni are used the aminoborane is found in low quantities, and undergoes subsequent formation of cyclic or linear oligomers. On the contrary, when equimolar amounts of the skeletal Ni are used, the dehydrogenation process is expected to increase, and therefore the aminoborane is likely to be in higher quantities, which allows the formation of polymeric material.

Moreover, *Goldberg*, *Heinekey*, and co-workers have shown that the homogenous precatalyst $[IrH_2(POCOP)]$ (POCOP = κ^3-1,3-$(OP{t}Bu_2)_2C_6H_3$) was very active for the

dehydrogenation of $NH_3{\cdot}BH_3$ which resulted in the rapid elimination of one equivalent of H_2 to produce insoluble $[NH_2–BH_2]_5$, designated as a cyclic pentamer.[55]

When the $[IrH_2(POCOP)]$ catalyst was applied to $MeNH_2{\cdot}BH_3$ in THF in low concentration (0.5 M), the formation of cyclic oligomers $[MeNH–BH_2]_x$ (x = 2–20) and oligomeric linear species $MeNH_2BH_2[MeNH–BH_2]_xNH_2Me$ (x = 4–48) was observed by electrospray ionisation mass spectrometry (ESI-MS).[56] However, when *Manners* and co-workers utilised the same catalytic system with $MeNH_2{\cdot}BH_3$ in THF at higher initial concentrations (10 M) high molar mass poly(methylaminoborane) was isolated and characterised.[57] Further discussion on the synthesis of polyaminoboranes using the $[IrH_2(POCOP)]$ catalyst will be given in further detail in section 1.4.5.

1.2.4 Polymers Containing Boron–Nitrogen Moieties

Over the past decades, the synthesis of macromolecules containing B–N moieties has found applications in the field of inorganic polymers as new materials with interesting properties. For example, B–N cyclolinear polymers containing rings in the main chain have been used as precursors of preceramic materials.[33c, 58] In this case, polyborazylene, a B–N cyclic polymer is structurally formed through fused borazine rings and polycyclic fragments (Figure 1.2A).[33c] The first synthesis of polyborazylene was described by *Sneddon* from thermolysis (70 °C) of $NH_3{\cdot}BH_3$ under vacuum for 48 h.[58a] Later on, *Babonneau*, *Massiot* and co-workers structurally characterised polyborazylene by multinuclear solid-state NMR spectroscopy; and found that this material is formed by tricoordinated boron and nitrogen atoms. The ^{11}B NMR spectrum showed two types of B environments (BHN_2, BN_3) and the ^{15}N NMR showed two types for N sites (NHB_3, NB_3).[38a] Thereafter, the synthesis of polyborazylene from the catalytic dehydrocoupling of $NH_3{\cdot}BH_3$ has been reported from other groups, however, limited characterisation was provided.[59]

In the area of metallopolymers, *Wagner* and co-workers synthesised coordination polymers based on the ready formation of B–N bonds in the backbone from reaction of diborylated ferrocenyl and bifunctional aromatic nitrogen heterocycles (e.g. 4,4'-bypyridine and pyrazine) (Figure 1.2B).[60] These polymeric materials have promising electrical and optical characteristics.

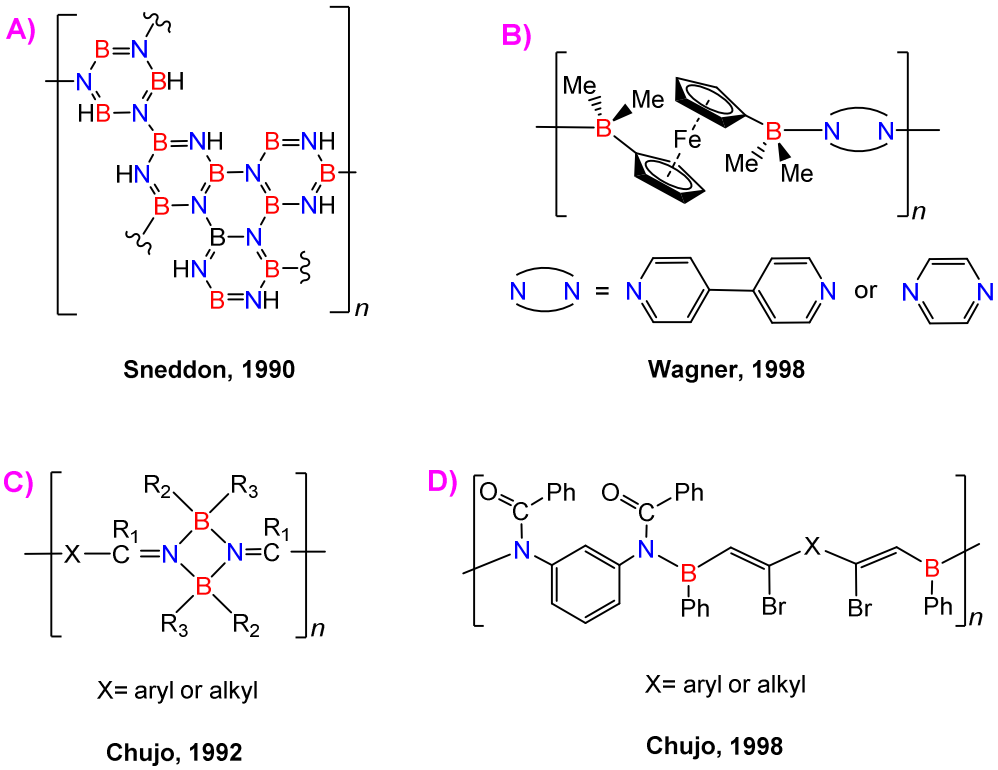

Figure 1.2. Polymers containing BN moieties.

Polymers comprising a cyclic [B_2–N_2] unit have shown to possess nonlinear optical properties. These polymers were described by *Chujo* and co-workers, and were synthesised by hydroboration polymerisation between triallylboranes and dicyano compounds;[61] and also by polyaddition of dicyano compounds with amine–boranes (Figure 1.2C).[62] The N–B–N polymers synthesised by these methodologies are stable under air and moisture.

Additionally, the synthesis of polymers comprising π systems along the backbone has been explored. *Chujo* and co-workers prepared copolymers containing B=N units in the backbone with acyl groups substituted at nitrogen, using an alternating haloboration-

phenylboration polymerisation technique (Figure 1.2D).[63] These copolymers presented low π-conjugation and no bathochromic effect was detected by ultraviolet-visible (UV-Vis) absorption spectroscopy. The results are attributed to the presence of cross-linked points which break the polymer conjugation

Recently, the substitution of C=C units by isoelectronic B=N bonds into polycyclic aromatic hydrocarbon molecules[64] or in polymeric materials,[65] has emerged as an alternative strategy to produce a new catalogue of hybrid organic-inorganic materials with structural similarities to classical all-carbon frameworks.

In this context, the functionalisation of polystyrene by replacement of the phenyl ring by borazinyl groups have been achieved *via* radical polymerization by *Allen*[66] and *Sneddon*[67] in the 1990s. The interest in these new types of borazine-containing polymeric materials arose from the potential applications as flame-retardant materials, materials with high thermal stability, and boron-nitride precursors.

Recently, the synthesis of B–N analogues of polystyrene containing 1,2-azaborininines groups were the subject of recent interest by *Jäckle and Liu*,[68] *Staubitz*[69] and *Klausen*,[70] as these materials can present interesting electronic properties (Figure 1.3A). Also, further post-polymerisation functionalisation reactions have allowed for a variety of different polymeric architectures to be achieved.[70b-d]

Helten and coworkers synthesised BN analogues of *para*-phenylene[71] and poly(p-phenylene vinylene) (PPV)[72] by the use of Si/B exchange of silazanes with boron-containing precursors as an alternative B–N coupling method (Figure 1.3B). These two polymers displayed π-conjugation extended over the B=N bonds and aryl groups. *Lacôte*, *Raynaud* and coworkers reported a new pathway to prepare polymers with $–BH_2–NH_2–$ units alternating with organic spacers from the reductive one-step polycondensation of bisboronic acids with diammonium salts (Figure 1.3C).[73] These polymers acted as H_2

reservoirs which were applied in the transfer hydrogenation to reduce imines and carbonyl molecules.

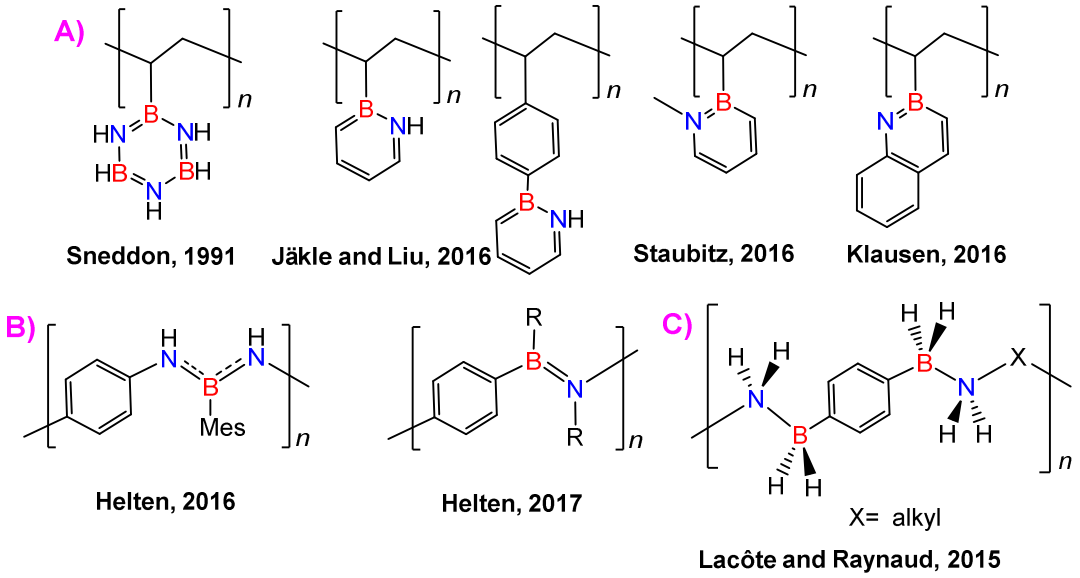

Figure 1.3. Hybrid BN containing polymers.

Among the examples of hybrid BN polymers which have interesting potential properties, the synthesis of inorganic polymers containing exclusively main chain B–N bonds has not been extensively studied (Figure 1.4). In 1984, the isolation of polyiminoboranes, $[RN{=}BR]_n$, which are isoelectronic to polyacetylene, was reported by *Paetzold* and coworkers from the thermolysis reaction of azidoboranes to generate monomeric iminoboranes in the gas phase which were trapped at −196 °C.[74] These materials were described as air- and moisture stable waxy solids which were insoluble in common organic solvents. Nevertheless, the limited characterisation reported was based on elemental analysis and mass spectrometry. Recently, the preparation and convincingly structural characterised oligoiminoborane was achieved by *Helten* and coworkers by the Si/B exchange of 1,3-TMS-1,3,2-diazaborolidine with $OctBCl_2$.[75] By GPC, the oligomeric nature of the material was determine (M_n = 1800 g mol^{-1}) and by SAXS it was suggested that the oligomers adopt a helical conformation in solution. Another example of a class of B–N main chain polymers is the inorganic analogues of polyolefins, the so-called polyaminoboranes.

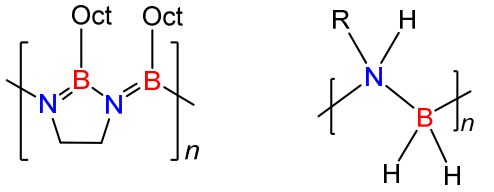

Figure 1.4. Polymers containing exclusively B–N bonds in the main chain.

1.2.5 Synthesis of High Molar Mass Polyaminoboranes

Polyaminoboranes are characterised by the presence of alternating sigma-bonded boron and nitrogen atoms in the backbone. Historically, attempts to prepare polyaminoborane $[NH_2–BH_2]_n$ by noncatalytic methods, have involved the thermal decomposition of $NH_3{\cdot}BH_3$[76] or borazane[77] or subjecting borazine to a radio frequency discharge.[78] However, the products from this reaction were insoluble materials and poorly characterised.

As mentioned before, the first demonstration of metal-catalysed methods to prepare oligoaminoboranes was achieved by *Goldberg*, *Heinekey* and co-workers by dehydrogenation of amine–boranes in low concentrations.[56] $[IrH_2(POCOP)]$ was found to be highly active in the dehydrogenation of $NH_3{\cdot}BH_3$ and $MeNH_2{\cdot}BH_3$, and the isolated materials were tentatively assigned as the cyclic pentamer $[NH_2–BH_2]_5$[55] in the former case (in 2006), and as a product formulated as oligo(methylaminoborane) $[MeNH–BH_2]_x$ (x = 2–48) assigned as a mixture of cyclic and linear species based on mass spectrometric evidence (in 2008), in the latter.

The formation of high molar mass polyaminoborane $[MeNH–BH_2]_n$ by catalytic dehydrocoupling of $MeNH_2{\cdot}BH_3$ using $[IrH_2(POCOP)]$ was accomplished in 2008 around the same time by *Manners* and coworkers using both low and high concentrations (Scheme 1.8).[45, 57] The products were characterised by GPC and also by dynamic light scattering which confirmed the high molar mass nature of the materials. Thereafter, a variety of

other metal-based precatalysts have found use in the dehydropolymerisation reaction to synthesise high molar mass polyaminoboranes.[47e, 79]

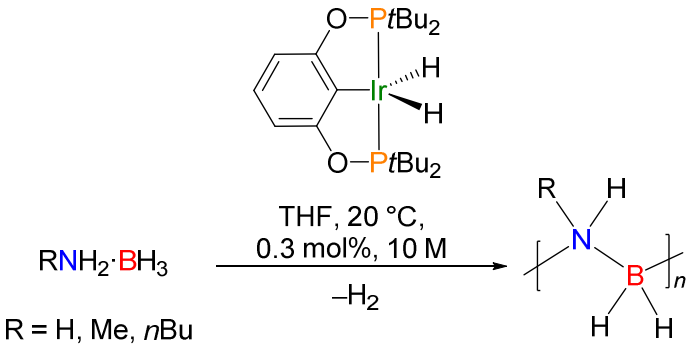

Scheme 1.8. Synthesis of polyaminoboranes by catalytic dehydrocoupling of amine–boranes by [IrH_2POCOP].

The polyaminoborane $[MeNH–BH_2]_n$ formed from the dehydropolymerisation of $MeNH_2{\cdot}BH_3$ *via* [IrH_2(POCOP)] at low catalyst loading (0.3 mol%) was found to be high molar mass (M_n = 160,000 g mol^{-1}, PDI = 2.9) by gel permeation chromatography (GPC) versus polystyrene standards and by dynamic light scattering (DLS), the value of the hydrodynamic radius (R_H = 3 nm) supports the polymeric nature of the material.[45, 80] Analysis of the resulting polyaminoboranes by multinuclear (^{13}C, ^{11}B and ^{1}H) NMR spectroscopy both in solution and in solid state, suggested that the polymers are essentially linear based on the simplicity of the NMR data. The same catalytic system was applied to nBuNH$_2{\cdot}$BH$_3$ to produce polymer $[n$BuNH–BH$_2]_n$ as a very soluble material with high molar mass (M_n = 400,000 g mol^{-1}, PDI = 1.6). The dehydropolymerisation of the parent $NH_3{\cdot}BH_3$ yielded the insoluble polymer $[NH_2–BH_2]_n$, which was characterised by solid state ^{11}B NMR spectroscopy. It was determined that this material is also linear and possessed a degree of polymerisation of around 20 units as suggested by end group analysis.[45]

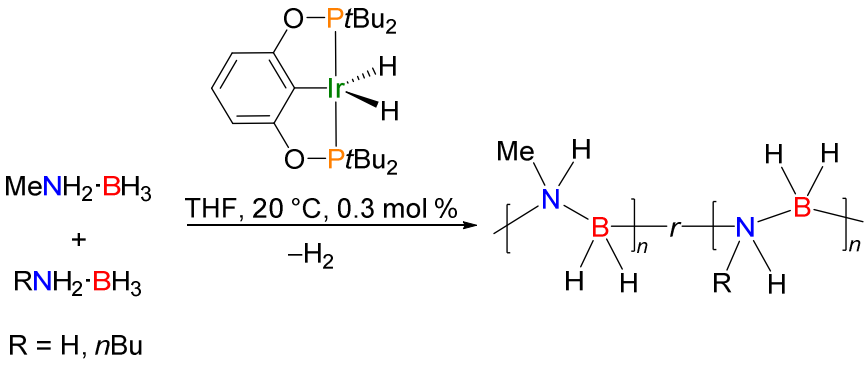

Scheme 1.9. Synthesis of random copolymers *via* catalytic dehydrocoupling of amine–boranes by [IrH$_2$POCOP].

The Ir-based precatalyst was also found to be efficient for the formation of random copolymers (Scheme 1.9) by dehydrocoupling of different amine–borane monomers. For example, when MeNH$_2$·BH$_3$ and *n*BuNH$_2$·BH$_3$ were mixed in different ratios (3:1 and 1:1), the resulting copolymers in each case were very soluble with high molar masses, as determined by GPC. In contrast, for copolymers made from mixtures of MeNH$_2$·BH$_3$ and NH$_3$·BH$_3$ both the molar mass and solubility of the resulting materials decreased when the incorporation of NH$_3$·BH$_3$ was increased from 25% to 50% (Table 1.1). Copolymerisation is an alternative strategy to efficiently incorporate [NH$_2$–BH$_2$]$_n$ units into the backbone of polyaminoboranes. Nevertheless, the incorporation of more than 50% of [NH$_2$–BH$_2$]$_n$ units into copolymers produced insoluble materials.[45]

Table 1.1. Polyaminoboranes synthesised *via* catalytic dehydrocoupling of amine–boranes by [IrH$_2$POCOP].

Polyaminoboranes	Monomer Precursors (Ratio)	Mw (PDI) / Da (GPC)	R_H / nm (DLS)
[MeNH–BH$_2$]$_n$	MeNH$_2$·BH$_3$	160,000 (2.9)	3
[MeNH–BH$_2$]$_n$–*r*–[NH$_2$–BH$_2$]$_m$	MeNH$_2$·BH$_3$/NH$_3$·BH$_3$ (3:1)	156,000 (11.0)	3
[MeNH–BH$_2$]$_n$–*r*–[NH$_2$–BH$_2$]$_m$	MeNH$_2$·BH$_3$/NH$_3$·BH$_3$ (1:1)	47,000 (3.9)	4
[*n*BuNH–BH$_2$]$_n$	*n*BuNH$_2$·BH$_3$	405,000 (1.6)	5
[*n*BuNH–BH$_2$]$_n$–*r*–[MeNH–BH$_2$]$_m$	*n*BuNH$_2$·BH$_3$/ MeNH$_2$·BH$_3$ (3:1)	183,000 (1.9)	4
[*n*BuNH–BH$_2$]$_n$–*r*–[MeNH–BH$_2$]$_m$	*n*BuNH$_2$·BH$_3$/ MeNH$_2$·BH$_3$ (1:1)	244,000 (2.2)	4

1.2.6 Mechanistic Aspects on the Dehydropolymerisation Reaction of Primary Amine–Boranes.

Mechanistic studies of the B–N coupling step in the dehydropolymerisation reaction of amine–boranes are fundamental to understanding the formation of polyaminoboranes. *Manners* and coworkers studied the polymer growth kinetics (molecular weight versus conversion) for the $[IrH_2(POCOP)]/MeNH_2{\cdot}BH_3$ system and concluded that the polymerisation followed a modified chain-growth mechanism.[45] They suggested that this process involves both slow metal-mediated initial dehydrogenation of the adduct with subsequent fast insertion of the resulting aminoborane $MeNH{=}BH_2$. Additionally, the mechanism of polymerisation of $[IrH_2(POCOP)]/NH_3{\cdot}BH_3$ system was studied by means of DFT calculations by *Paul* and coworkers (Scheme 1.10),[81] and a chain growth mechanism was proposed. They suggested the initial formation of complex $[Ir(\eta^2\text{-}H_2B{=}NH_2)]$ is crucial for subsequent chain propagation. This process occurs by interaction of the lone pair from the NH_2 terminus of a sigma complex with the BH_2 end of a second arriving NH_2BH_2 unit.

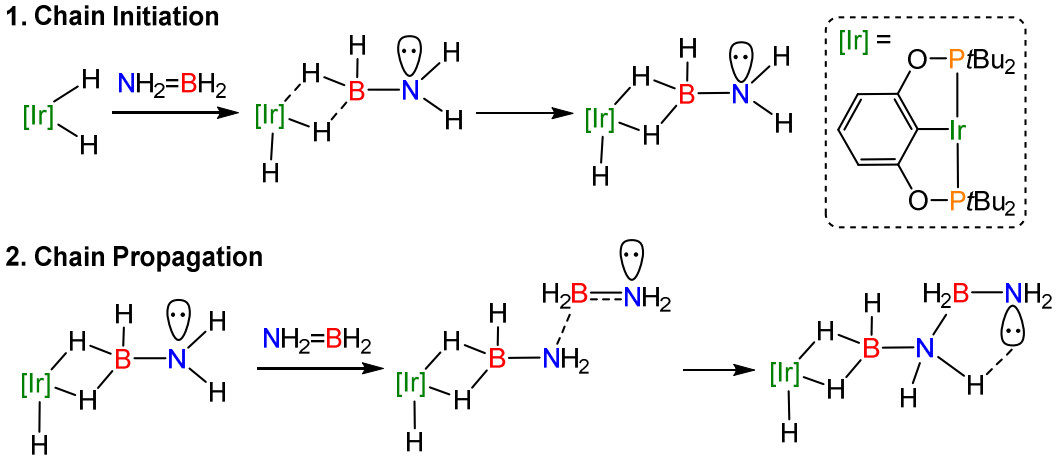

Scheme 1.10. Mechanistic proposal of dehydropolymerisation reaction of $NH_3{\cdot}BH_3$ and $[IrH_2(POCOP)]$ by DFT calculations.

Another approach to study the $[IrH_2(POCOP)]$ system was the use of linear diborazane based on kinetic modelling and redistribution reactions by *Manners*, *Weller* and *Lloyd-*

Jones.[28a, 82] An initial step was the study of dimer $Me_3N{\cdot}BH_2NMe_2{\cdot}BH_3$ as a model adduct, which showed a redistribution process to form $Me_3N{\cdot}BH_3$ and $[Me_2N–BH_2]_2$, respectively.

This redistribution process proceeds both under thermolysis (THF, 70 °C) or at ambient temperature by metal catalysis (THF, 1 mol% [Ir]) to form identical products. When the linear dimer $MeNH_2{\cdot}BH_2MeNH{\cdot}BH_3$ was studied, a similar redistribution of products $MeNH_2{\cdot}BH_3$/$MeNH{=}BH_2$ was observed. In this particular case, formation of $MeNH{=}BH_2$ led to formation of borazane under thermolysis, and to polymeric material under catalytic conditions (Scheme 1.11). Under thermolysis, the $MeNH{=}BH_2$ fragment could be trapped *via* the hydroboration reaction with cyclohexene which evidenced the presence of free monomeric aminoborane in solution. By contrast, no evidence of trapping of aminoborane could be detected in the Ir-catalysed reaction which suggests two viable options: either the polymerisation only proceeds "on metal" or the rate of the trapping reaction is much slower relative to the polymerisation of free aminoborane that could be produced in solution.

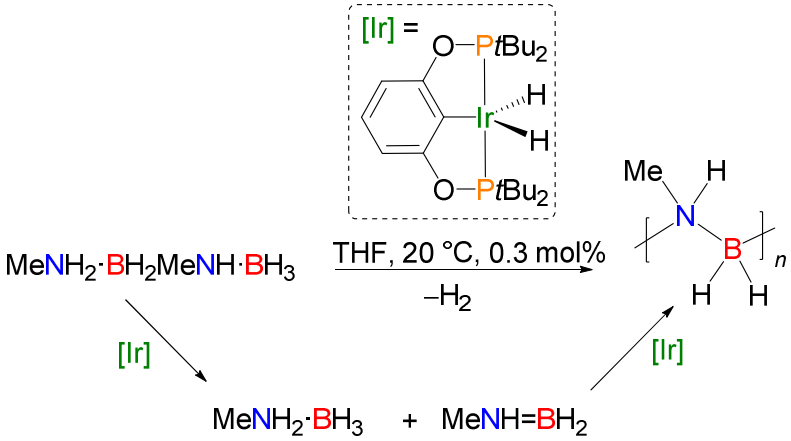

Scheme 1.11. Proposed redistribution process of linear amine–borane dimer by $[IrH_2POCOP]$.

Likewise, the mechanism of polymerisation with the $[IrH_2(POCOP)]$ system can be approached by the use of $[Ir(PCy_3)_2(H)_2(\eta^2\text{-}H_2)][BAr^F{}_4]$ ($Ar^F = 3,5\text{-}C_6H_3(CF_3)_2$) as a model compound, which reacts with one equivalent of $MeNH_2{\cdot}BH_3$ to produce the complex $[[Ir(PCy_3)_2(H)_2(\eta^2\text{-}H_3B{\cdot}NMeH_2)][BAr^F{}_4]$. In this respect, *Manners*, *Weller* and coworkers reacted $[[Ir(PCy_3)_2(H)_2(\eta^2\text{-}H_3B{\cdot}NMeH_2)][BAr^F{}_4]$ with a second equivalent of $MeNH_2{\cdot}BH_3$

that led to the single oligomerisation product $[Ir(PCy_3)_2(H)_2(\eta^2\text{-}H_3B{\cdot}MeNH\text{–}BH_2{\cdot}NMeH_2)][BAr^F{}_4]$ which suggests that the oligomerisation process can occur "on metal" (Scheme 1.12).[83] The latter complex was found to be active in the catalytic dehydrogenation of $MeNH_2{\cdot}BH_3$ to form the linear dimer $MeNH_2{\cdot}BH_2MeNH{\cdot}BH_3$. When the same precursor $[Ir(PCy_3)_2(H)_2(\eta^2\text{-}H_2)][BAr^F{}_4]$ was studied with the parent $NH_3{\cdot}BH_3$, the oligomeric intermediates $[Ir(PCy_3)_2(H)_2(\eta^2\text{-}H_3B{\cdot}(NH_2\text{–}BH_2)_n{\cdot}NH_3)][BAr^F{}_4]$ could be detected by ESI (n = 1–4) and structurally characterised by X-ray crystallography (n = 0–2).[84] A computational study of such species revealed the following mechanistic steps: 1) an initial dehydrogenation of $NH_3{\cdot}BH_3$, 2) dehydrogenation of a second adduct $NH_3{\cdot}BH_3$ and 3) final B–N coupling. The initial dehydrogenation step was found to possess a higher barrier than subsequent B–N coupling processes which promotes the oligomerisation reaction. Significantly, when $MeNH_2{\cdot}BH_3$ was studied, the barrier of the B–N coupling step was higher and is similar to the two consecutive dehydrogenation processes in this adduct. This is in accordance with the experimental observation of only one B–N coupling process.

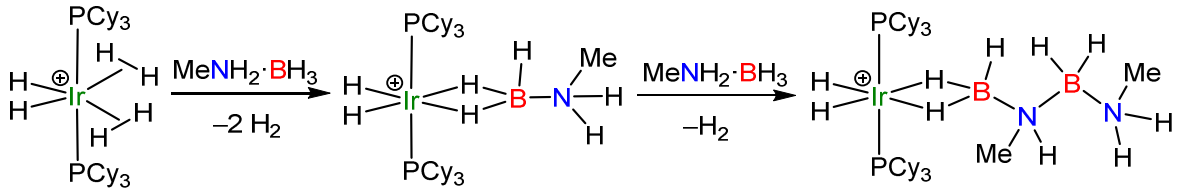

Scheme 1.12. Synthesis of a η^2-amine-borane complex from the reaction of $[Ir(PCy_3)_2(H)_2(\eta^2\text{-}H_3B{\cdot}NMeH_2)]^+$ and $MeNH_2{\cdot}BH_3$. Counterion $[BAr^F{}_4]$ is not shown.

1.2.7 Metal-free Dehydropolymerisation of Amine–Boranes

The synthesis of amine–boronium cations from the parent amine-borane has been reported by *Manners* and coworkers.[43] These amine–boronium species undergo deprotonation with sterically hindered bases to yield free aminoborane monomers $RR'N{=}BH_2$ (R, R' = alkyl, H), which are detected by low temperature ^{11}B NMR spectroscopy. When a primary

amine–borane precursor is used, poly(methylaminoborane) with notably lower molar mass compared to the transition metal-catalysed dehydropolymerization is obtained (Scheme 1.13A).

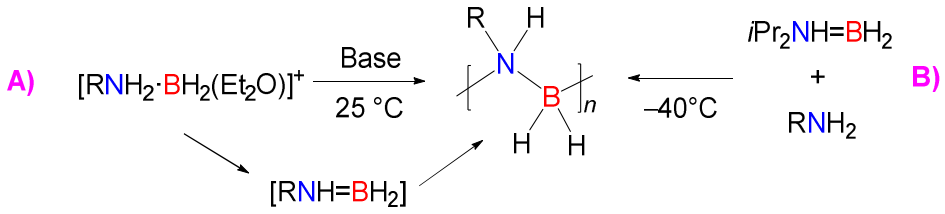

Scheme 1.13. Synthesis of polyaminoboranes by metal-free routes.

Very recently, *Alcaraz* and coworkers developed an innovative synthetic strategy to produce ultra-high molar mass polyaminoboranes $[RNH–BH_2]_n$ by reaction of *i*PrNH=BH_2 with a variety of primary amines in solventless conditions (Scheme 1.13B).[85] A significant contribution is the synthesis of a functional polyaminoboranes such as $[(allyl)NH–BH_2]_n$, which are otherwise difficult to prepare through transition metal catalysed routes. However, further work on establishing the mechanism is needed and the resulting polymers are of low solubility, possibly due to their high molar mass.

1.2.8 Catalytic Formation of Phosphorus–Boron Bonds

1.2.8.1 Synthesis of Phosphine–Borane Adducts

Phosphine–boranes are adducts consisting of a phosphine Lewis base (e.g. PH_3) and a borane Lewis acid (e.g. BH_3) connected by a dative bond. The first phosphine–borane adduct $PH_3·BCl_3$ was reported by *Besson* in 1890,[86] and since then further methodologies have been established similar to the synthesis of amine–boranes. The most common route is the direct addition of primary, secondary, or tertiary phosphines to $BH_3·L$ (L = THF or SMe_2) where replacement of the labile donor by the phosphine occurs (Scheme 1.14A).[87]

Another route is the preparation of phosphine–boranes by reduction of chlorophosphines with $NaBH_4$ (Scheme 1.15B).[88]

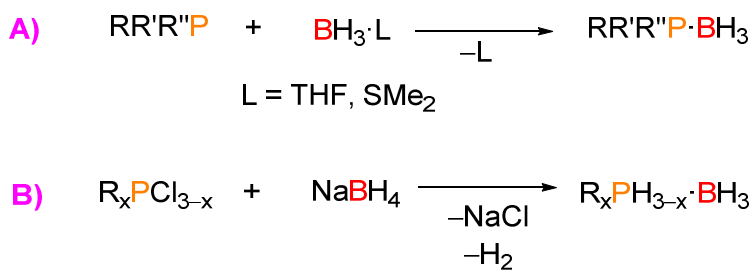

Scheme 1.14. Synthetic routes to obtain phosphine–boranes.

1.2.8.2 Reactivity and Applications of Phosphine–Boranes

The fundamental reactivity of amine–boranes shows similarity to that of phosphine–boranes. However, in the context of dehydrogenation, the P–H bond is significantly non-polar (χ_P =2.19 and χ_H = 2.20)[24] which makes that hydrogen less acidic and, for similar reasons, the hydride at boron is also less basic. This makes hydrogen release less favourable kinetically.

By analogy to amine–boranes, a single dehydrogenation process with phosphine–boranes would yield the intermediate phosphinoborane PH_2=BH_2. In the 1990s, computational studies suggested that the π-component of PH_2=BH_2, where the phosphorus atom is in a planar disposition, possesses similar bond strengths to NH_2=BH_2.[89] However, it was determined that PB molecules do not present the same facility to form planar structures as BN compounds, as the phosphorus atom on the P=B fragment presents a strong tendency to have a pyramidal geometry. Other computational calculations proposed that the high inversion barrier of the PH_3 group is related to the lack of planarity of the PH_2BH_2 moiety.[90]

In the pyramidalization process in phosphines a hybridisation change of the P atom from sp^3 to sp^2 takes place. The latter process is involved in the pyramidal inversion in

phosphines and amines,[91] and the stereoisomerisation process in phosphines has higher energy barriers 30 kcal mol^{-1} (or noticeably greater in the case of trihalophosphines)[92] than the corresponding energy in amines (5−10 kcal mol^{-1}).[92a, 92b, 93] The reduction of the inversion barrier from 31.8 kcal mol^{-1} in phosphine, PH_3, to 5.9 kcal mol^{-1}, in $PH_2{=}BH_2$, strengthens the π component contribution to the B–P bond.[89b]

As a consequence, from a hybridisation perspective, the formation of the planar conformation of phosphinoborane monomers from the dehydrogenation of phosphine–boranes would be more hindered than the formation of the aminoborane analogues.

Nevertheless, applications of phosphine–boranes are diverse and include uses as hydrophosphination reagents,[94] hydrogen storage materials,[95] and also as reducing agents under biological conditions.[96] Additionally, the formation of phosphine–boranes adducts can be used as a methodology to protect phosphines susceptible to oxidation by oxidising agents.[18a, 97]

1.2.8.3 Catalytic Dehydrocoupling of Phosphine–Boranes

Generally, dehydrocoupling of phosphine–boranes can proceed under thermal conditions above 150–200 °C in the absence of a catalyst or at 60–120 °C with the assistance of catalysts (Scheme 1.15).

In the case of the parent phosphine–borane $PH_3{\cdot}BH_3$ and primary phosphine–boranes $RPH_2{\cdot}BH_3$ (R = aryl), the catalytic dehydrocoupling reaction affords oligomeric or polymeric materials, respectively. Monomeric phosphinoboranes $PH_2{=}BH_2$ or $RPH{=}BH_2$ have not been observed experimentally due to their propensity to polymerise, but more substituted phosphinoboranes $PR_2{=}BR_2$ compounds have been comprehensively studied.[12a, 98]

In pioneer studies on the thermal dehydrogenation (150 °C) of secondary phosphine–boranes, the formation of cyclic trimers $[R_2P–BH_2]_3$ or cyclic tetramers $[R_2P–BH_2]_4$ was observed. The cyclic trimers have been reported to possess considerable stability as minimal decomposition was reported under thermolysis (300 °C) in the presence of HCl.[99] *Manners* and coworkers reinvestigated the thermal dehydrocoupling (170 °C) reaction of neat secondary phosphine–borane $Ph_2PH{\cdot}BH_3$ which afforded the cyclic trimer $[Ph_2P–BH_2]_3$ and the cyclic tetramer $[Ph_2P–BH_2]_4$ in a 8:1 ratio respectively.[95a] However, when the thermal dehydrocoupling was attempted at a lower temperature (120 °C), negligible conversion of the phosphine–borane adduct was observed .

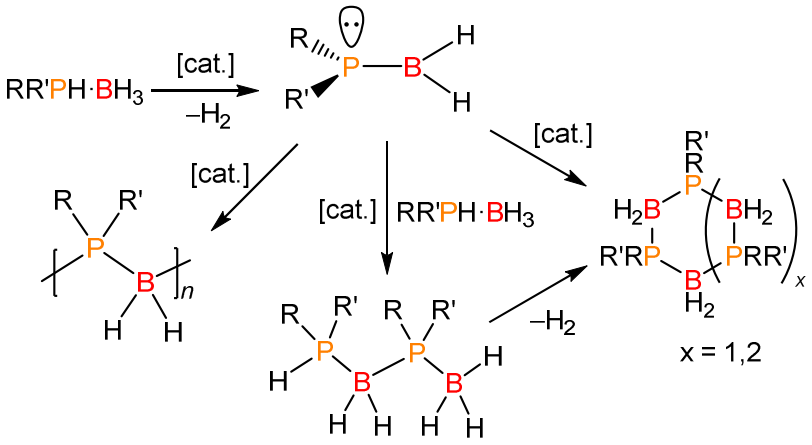

Scheme 1.15. General scheme for the catalytic dehydrocoupling of phosphine–boranes.

When $Ph_2PH{\cdot}BH_3$ was treated with a catalytic amount of $[Rh(\mu\text{-}Cl)(1,5\text{-}COD)]_2$ or [Rh(1,5-COD)][OTf] (OTf = $^-SO_3CF_3$) (1 mol%) at 120 °C, the formation of $[Ph_2P–BH_2]_3$ and $[Ph_2P–BH_2]_4$ in a 2:1 ratio was reported. At 90 °C, exclusive formation of the linear diphosphinoborane $Ph_2PH{\cdot}BH_2PPh_2{\cdot}BH_3$ was observed under otherwise identical reaction conditions. It was proposed that this linear dimer is an intermediate in the formation of the cyclic products. Discussion on the catalytic dehydrocoupling of primary phosphine–boranes will be given with further details in Section 1.5.5.

1.2.9 Polymers Containing Phosphorus–Boron in the Backbone

A limited number of polymers containing P–B moieties in the backbone have been studied in the last two decades. For example, polymers containing PB units arise either from post functionalisation of macromolecules with tricoordinated phosphorus or from oligo/polymerisation of chiral trialkylphosphine–boranes.

Gates and coworkers developed the synthesis of poly(methylenephosphine) *n*Bu[MesP–CPh_2]$_n$H by anionic polymerisation of phosphaalkene MesP=CPh_2.[100] This polymer containing trivalent phosphorus was treated with BH_3·SMe_2, to afford the phosphine–borane polymer (Figure 1.5A). Protection of this polymer by the borane moiety was used to increase polymer stability.

A phosphine–borane metallopolymer was synthesized by Manners and coworkers from ROP of *P*-phenylphosphan[1]ferrocenophane monomer where the BH_3 was coordinated either before or after polymerisation (Figure 1.5B). However, the polymeric materials obtained were poorly soluble.[101]

Additionally, *Chujo* and coworkers developed the synthesis of optically active phosphine–borane oligomers from a stepwise oxidative coupling process from the enantiomerically pure (S,S)-1,2-bis(boranato-(*t*-butyl)methylphosphino)ethane (Figure 1.5C).[102] This substrate could be further functionalised to prepare a range of bifunctional monomers which were converted into polymeric materials.[103]

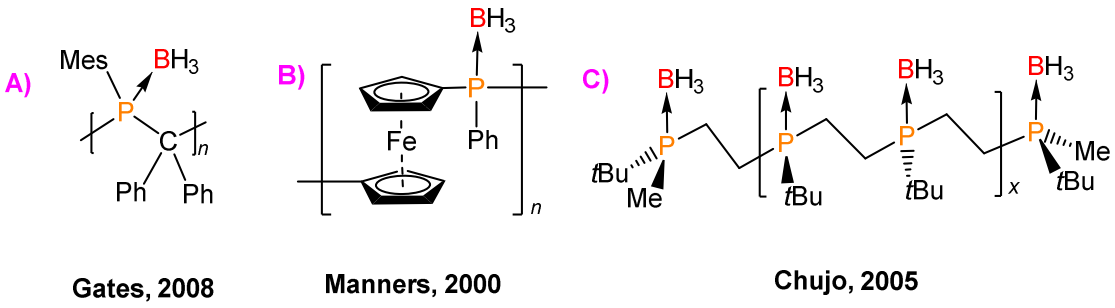

Figure 1.5. Phosphine–borane polymers.

Since the early discovery of methodologies towards the synthesis of PB main chain macromolecules, only a few examples of phosphinoborane polymers were described in patents[104] and in rare occasions in some scientific journals that reported low yield and low molar mass materials with limited characterisation. For example, from the thermal treatment (175–200 °C) of $Me_2P–PMe_2{\cdot}BH_3$[105] or $RMePH{\cdot}BH_3$ (R = Me or Et)[106] with amines the synthesis of $[RMeP–BH_2]_n$ with low molar masses was claimed.

Polyphosphinoboranes, $(RR'P{\cdot}BH_2)_n$ (R, R' = H, alkyl, aryl), received significant attention in the 1950's and 1960's as these polymeric materials were anticipated to possess valuable properties such as high-temperature stability.[107] The pioneering synthesis involves the thermolysis (150–250 °C) of $PhPH_2{\cdot}BH_3$ for 13 h resulting in the formation of a benzene-soluble solid which was claimed to be polymeric $[PhPH–BH_2]_n$ with low molar mass (M_n = 2,200–2,700 g mol^{-1}).[108]

Nevertheless, the synthesis and convincing characterisation of high molar mass polyphosphinoboranes comprising only P–B bonds in the main chain was achieved by *Manners* and coworkers in 1999 leading to renewed interest in these materials.

1.2.10 Synthesis of High Molar Mass Polyphosphinoboranes

The reinvestigation of the uncatalysed thermolytic reaction of $PhPH_2{\cdot}BH_3$ by the *Manners* group showed that the product $[PhPH–BH_2]_x$ is oligomeric in nature with undefined structure.[95a, 109] In contrast, when $PhPH_2{\cdot}BH_3$ was heated in toluene at 110 °C in the presence of Rh precatalysts $[Rh(\mu\text{-}Cl)(1,5\text{-}COD)]_2$ or [Rh(1,5-COD)][OTf], well-defined polyphosphinoborane $[PhPH–BH_2]_n$ of low molar mass (M_w = 5,600 g mol^{-1}) was found. The formation of high molar mass $[PhPH–BH_2]_n$ (M_w = 33,000 g mol^{-1}) was achieved at higher temperatures (130 °C) in the presence of a Rh catalyst under solventless conditions (Scheme 1.16). The resulting polymers were soluble, air- and moisture-stable solids and

were structurally characterised by multinuclear NMR spectroscopy. When the high temperature catalytic reaction is prolonged, insoluble solids are formed which become swellable gels in the presence of solvents. This observation is consistent with the formation of cross-linked materials *via* intermolecular dehydrogenation between P–H and B–H bonds. The formation of other polyphosphinoboranes $[RPH–BH_2]_n$ (R = *i*Bu, *p*-*n*BuC_6H_4, *p*-dodecylC_6H_4) was achieved under similar reaction conditions.[110] These polymers had high polydispersity index (PDI) values which can be correlated with a certain degree of branching and also yielded gels after extended thermolysis.

Hey-Hawkins and coworkers took inspiration from the [Rh(μ-Cl)(1,5-COD)]$_2$ system to extend the synthesis to metal-containing polyphosphinoboranes from the adducts $FcPH_2{\cdot}BH_3$ and $FcCH_2PH_2{\cdot}BH_3$ (Fc = ferrocenyl) to afford polymers with low molar mass when prepared in toluene solution (M_w = 4,000–7000 g mol^{-1}) and moderate molar mass in the absence of solvent (M_w = 10,000–16,000 g mol^{-1}) with relatively low PDI values (1.5–2.1). This methodology was extended to prepare polycationic phosphinoboranes with planar chirality from a quaternised ammonium phosphine–borane derivative.[111]

Manners and coworkers observed that the temperature of the dehydropolymerisation reaction *via* [Rh(μ-Cl)(1,5-COD)]$_2$ can be reduced to 60 °C when aryl phosphine–boranes $RPH_2{\cdot}BH_3$ are substituted with electron withdrawing groups (i.e. R = *p*-$CF_3C_6H_5$) to produce $[RPH–BH_2]_n$ with high molar mass (M_n = 56,200 g mol^{-1}, PDI = 1.67).[112]

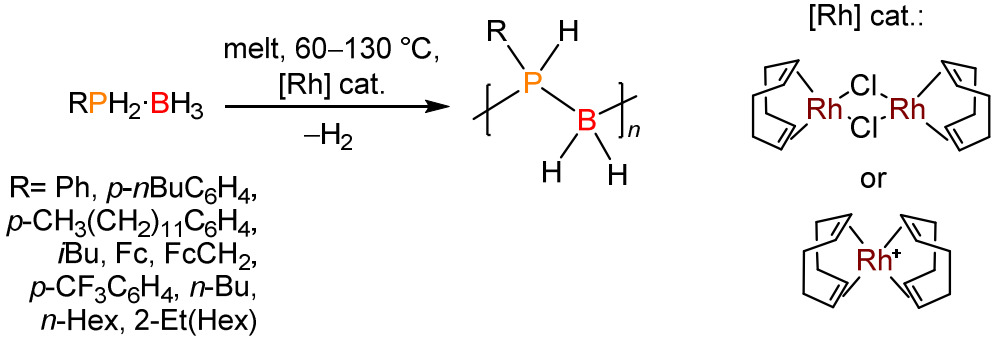

Scheme 1.16. Synthesis of polyphosphinoboranes by Rh-based precatalysts.

The metal-catalysed dehydropolymerisation works effectively with a limited substrate scope, with focus on aryl-containing adducts. Very recently, the reinvestigation of a series of alkyl phosphine–boranes were polymerised successfully with the $[Rh(\mu\text{-}Cl)(1,5\text{-}COD)]_2$ system yielding polyphosphinoboranes $[RPH–BH_2]_n$ (R= *n*Bu, *n*Hex, 2-Et(Hex)) with low molar masses (M_n = 1,700–8,800 g mol^{-1}).[113] These polymers presented low glass transition temperatures T_g (−68 to −58 °C).

Recently, the synthesis of polyphosphinoboranes in solution has been reported by Manners and coworkers using a precatalyst based on the earth-abundant metal Fe.[114] The dehydropolymerisation of $PhPH_2{\cdot}BH_3$ catalysed by $[CpFe(CO)_2OTf]$ (1 mol%) in toluene solution at 100 °C, produced polymer $[PhPH–BH_2]_n$ with high molar mass (M_n = 59,000 g mol^{-1}, PDI = 1.6) in 24 h (Scheme 1.17). Significantly, control over the molar mass of the resulting polymer was achieved with this system. For example, when the catalyst loading was increased, the molar mass decreased, which suggested a type of chain-growth mechanism for the polymerisation.

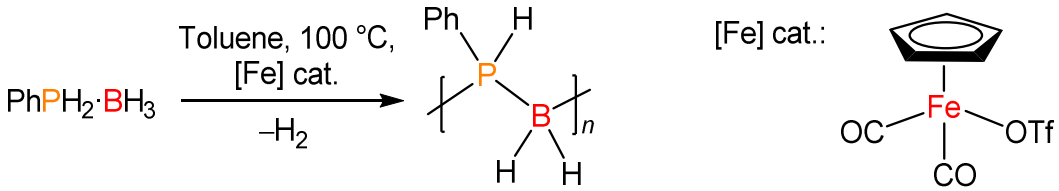

Scheme 1.17. Thermal catalytic dehydrocoupling of $PhPH_2{\cdot}BH_3$ mediated by $[CpFe(CO)_2OTf]$.

Webster and coworkers explored a different Fe-based system for dehydropolymerisation of phosphine–boranes.[115] The catalytic dehydrocoupling of $RPH_2{\cdot}BH_3$ (R = Ph, Cy) *via* Fe(II) *β*-diketiminate precatalyst $LFe(CH_2SiMe_3)$], (L = $[(DippNC(Me))_2CH]^-$, Dipp = 2,6-diisopropylphenyl) (10 mol%) afforded the formation of polyphosphinoboranes in solution of toluene (100 °C) in 72 h. Although the polymer $[PhPH–BH_2]_n$ possessed high molar mass (M_n = 55,000 g mol^{-1}, PDI = 1.85); the alkyl phosphine–borane substrate was fully

converted to form mainly oligomeric material $[CyPH–BH_2]_x$ (M_n < 2,000 g mol^{-1}) with a minor component (< 10%) of high molar mass (M_n = 55,600 g mol^{-1}, PDI = 1.26).

Since the breakthrough by *Manners* and coworkers in the dehydropolymerisation of phosphine–boranes, other metal-based catalysts have been found to be effective. For example, *Weller* and coworkers synthesised $[PhPH–BH_2]_n$ (M_n = 15,000 g mol^{-1}, PDI = 2.2) from the dehydrocoupling of $PhPH_2{\cdot}BH_3$ using $[Cp^*RhMe(PMe_3)(CH_2Cl_2)][BAr^F{}_4]$ (Cp^* = η^5-C_5Me_5) (1 mol%) in solution of toluene at 100 °C for 72h.[116]

Recently, the use of the catalytic system $[IrH_2(POCOP)]$ was applied in the dehydropolymerisation reaction of aryl phosphine–boranes by *Braunschweig*, *Radius* and coworkers.[117] They produced poly(arylphosphinoboranes) $[RPH–BH_2]_n$ (R = Ph, *p*-Tol, Mes) at high temperatures in benzene (80 °C) or toluene (100 °C) with varied molar masses (M_n = 5,000–33,000 g mol^{-1}) and PDI values (1.8–30).

1.2.11 Mechanistic Aspects of the Dehydropolymerisation Reaction of Primary Phosphine–Boranes.

As noted previously, the dehydrocoupling of amine–boranes with Rh-based precatalyst was determined to be a heterogeneous reaction based on different experiments and observations. In the catalytic dehydrocoupling of phosphine–boranes with $[Rh(\mu\text{-}Cl)(1,5\text{-}COD)]_2$, a change of colour from yellow/orange to red was observed with no evidence of black material in the solution which could imply the formation of Rh nanoparticles. Besides these observations, no initial induction period was reported and also no reaction suppression was observed from filtration or from the addition of Hg(0). All these factors lead to the conclusion that the dehydrocoupling of phosphine–boranes is homogeneous in nature.[53]

Additionally, it has been suggested that the dehydropolymerisation of phosphine–boranes using $[Rh(\mu\text{-}Cl)(1,5\text{-}COD)]_2$ precatalyst proceeds *via* a homogeneous step-growth mechanism.[110] A common problem arising in this system is that high monomer conversion (> 99%) is required to produce high molar mass polymers. Since the reaction requires melt conditions as the polymerisation proceeds the viscosity of the reaction mixture increases, this leads to inefficient stirring and generally to the production of materials with uncontrolled molar mass (M_n) ranging from 3,000 to 10,000 g mol^{-1}. Moreover, the use of melt conditions hinders the effective mechanistic study of intermediates. For example, *Weller* and coworkers studied the mechanism of the dehydrocoupling of secondary–phosphine boranes with $[Rh(1,5\text{-}COD)_2][BAr^F{}_4]$ under melt conditions. The observation of the intermediates, $[Rh(PR_2H)_2(\eta^2\text{-}H_3BR_2PBH_2PR_2H)][BAr^F{}_4]$ and the designated active catalytic fragment $\{Rh(PR_2H)_2\}^+$ that arose from the decomposition of the phosphine–borane adduct, could be observed by *in situ* sampling ESI-MS.[118]

Afterwards, a model of the catalytically active fragment $\{Rh(PR_2H)_2\}^+$ was generated by replacement of the monodentate phosphine ligands by a bidentate phosphine, $[Rh(dppp)(\eta^6\text{-}C_6H_5F)][BAr^F{}_4]$ (dppp = $Ph_2P(CH_2)_3PPh_2$), which permitted a better observation of intermediates.[119] In this manner, it was observed that $[Rh(dppp)(\eta^6\text{-}C_6H_5F)]^+$ promotes P–H activation of $Ph_2PH{\cdot}BH_3$ to form a Rh(III)-hydride complex $[Rh(dppp)H(\sigma,\eta\text{-}PPh_2BH_3)(\eta^1\text{-}H_3B{\cdot}Ph_2PH)]^+$ (Scheme 1.18A). This complex underwent dehydrogenation to form a P–B bond in the complex $[Rh(dppp)H(\sigma,\eta^2\text{-}PPh_2{\cdot}BH_2PPh_2{\cdot}BH_3)]^+$. Although these initial processes occur in solution of 1,2-difluorobenzene at ambient temperature within 16 h, melt conditions are required for complete conversion of the substrate. It was also determined that phosphine–boranes substituted with electron withdrawing groups tended to increase the rate of the reaction, meanwhile the opposite is true for adducts substituted with electron donating groups.[120]

Similar intermediates were observed when the complex [Rh(dppp)(η⁶-C₆H₅F)]⁺ was applied to primary phosphine–boranes, where the P–H activation process can lead to the formation of diastereoisomers.[120] For example, when $CyPH_2{\cdot}BH_3$ was reacted with the Rh(I) complex, the reaction proceeded faster (1 h) and hydride Rh(III)-hydride complexes were found to be in an equimolar mixture of two diastereoisomers as a consequence of the activation of the P–H bond at the prochiral phosphorus centre. Furthermore, after the dehydrocoupling process, formation of a P–B bond is also observed, but the subsequent complexes are found in a 6:1 ratio mixture which suggests that a stereocontrol process in the formation of the P–B bond is occurring (Scheme 1.18B).

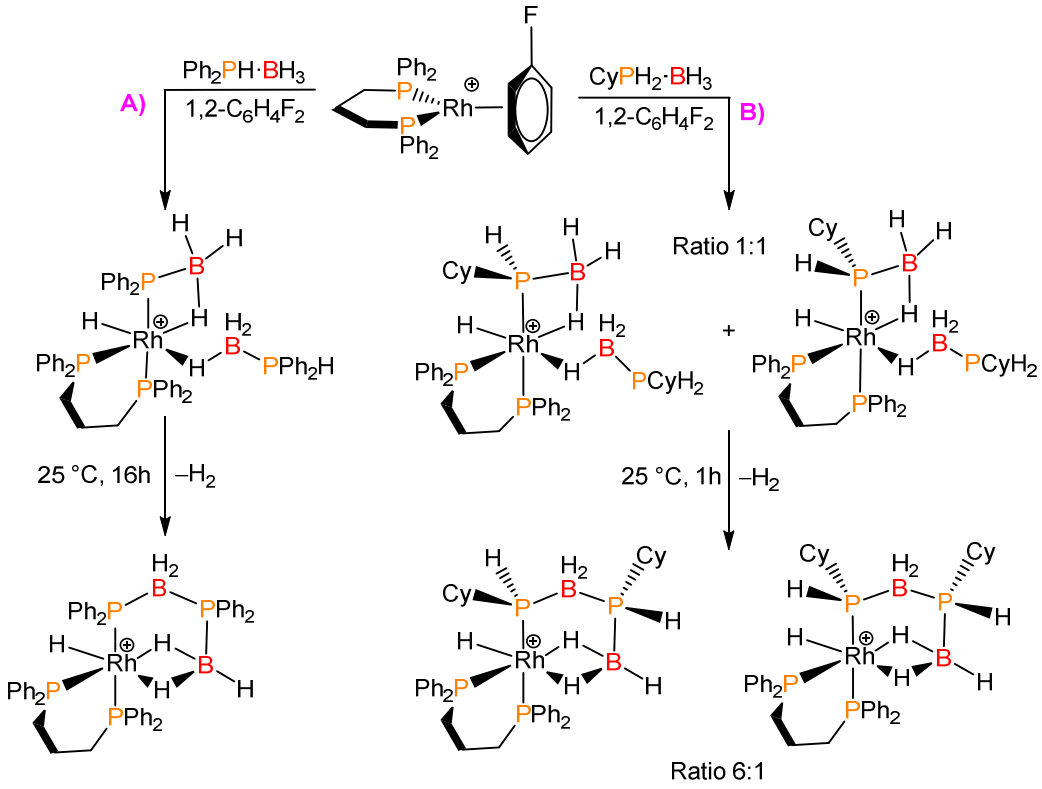

Scheme 1.18. Stoichiometric reaction of [Rh(dppp)(η⁶-C₆H₅F)][BAr$^F_4$] with primary and secondary phosphine–boranes.

The reaction of $CyPH_2{\cdot}BH_3$ with an 'Rh(dppp)' analogue containing a chiral bidentate ligand [Rh(*S*,*S*-bdpp)(η⁶-C₆H₅F)][BAr$^F_4$] (S,S-bdpp = (2*S*,4*S*)-2,4-bis(diphenylphosphino)pentane), resulted in the bias towards the formation of one of the diastereoisomers of the Rh(III)-hydride complex [Rh(S,S-bdpp)H(σ,η-PCyHBH₃)(η¹-

$H_3B{\cdot}PCyH_2)]^+$ in a 1:3 ratio, as opposed to the 1:1 ratio observed with the Rh(dppp) system. This result suggests that selection of appropriate chiral ligands can lead to some diastereoselective control.

Manners and coworkers reported an Fe-based catalytic system that proceeds in solution to produce high molar mass material by a homogeneous chain growth mechanism, in which some aspects were explored by multinuclear NMR, model reaction compounds, DFT computational studies and ESI-MS.[114] It was suggested that the initial protonolysis of the triflate ligand from the complex $[CpFe(CO)_2OTf]$ is followed by the formation of a phosphidoborane complex (Scheme 1.19A). Subsequently, CO dissociation from the former complex is proposed to open a vacant site which is filled by agostic coordination of a σ-bound BH_3 end (Scheme 1.19B).

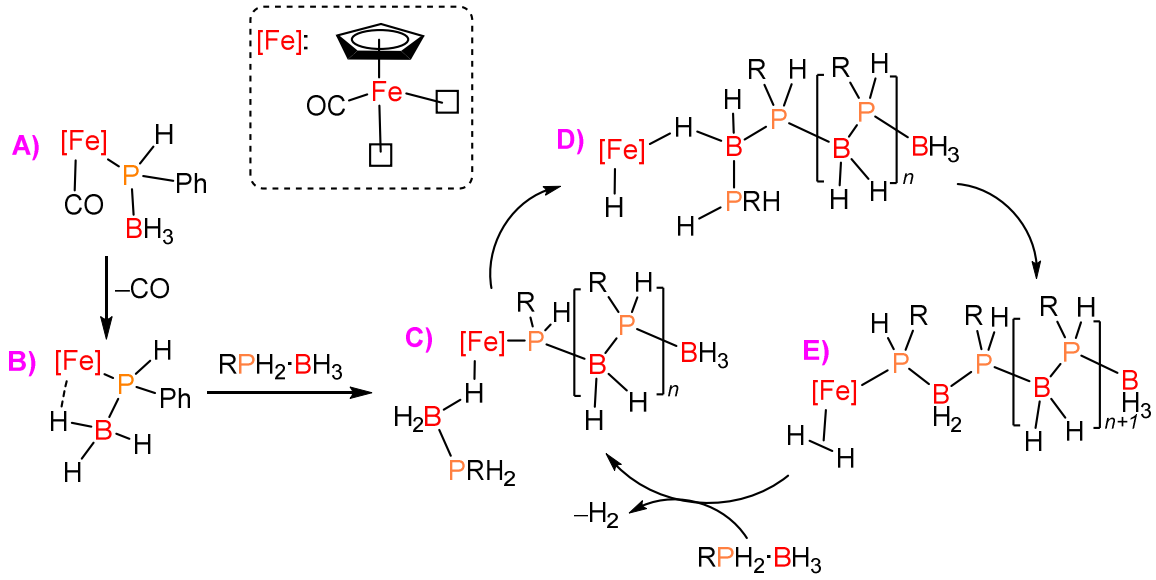

Scheme 1.19. Proposed coordination growth mechanism of the dehydropolymerisation of primary phosphine–boranes *via* $[CpFe(CO)_2OTf]$.

After ligand reorganisation, a second $PhPH_2{\cdot}BH_3$ unit is σ-bound to the Fe centre (Scheme 1.19C) with subsequent B–H activation and P–B coupling to produce Fe-hydride species (by insertion into the [Fe]–P bond) (Scheme 1.19D), in which the phosphine–borane chain is bound by the BH_2 end group to the iron centre. This intermediate undergoes a second

P–H activation to produce phosphidoborane chain species with bound η^2-H_2 (Scheme 1.19E). The final step is the release of molecular hydrogen which allows the formation of a new vacant site for subsequent catalysis (Scheme 1.19).

Weller and coworkers explored the mechanism of dehydrocoupling of phosphine–boranes *via* [RhCp*(PMe_3)Me($ClCH_2Cl$)][BAr^F_4], which proceeded in solution, using both model compounds and computational studies.[116] Initial B–H activation of a $PhPH_2{\cdot}BH_3$ adduct is followed by P–H activation to produce an intermediate hydrido phosphinoborane Rh complex which after ligand reorganisation forms a σ^1-phosphidoborane species. From the formation of this complex, two different polymerisation mechanisms can arise: the first is proposed to be a coordination chain growth mechanism, analogous to the [$CpFe(CO)_2OTf$] system. Interestingly, the second mechanism is proposed to be a reversible chain transfer process, which is based on early detection of significant quantities of the dimer $PhPH_2{\cdot}BH_2PhPH{\cdot}BH_3$ and rapid consumption of monomer $PhPH_2{\cdot}BH_3$, similar to a step growth process (Scheme 1.20).

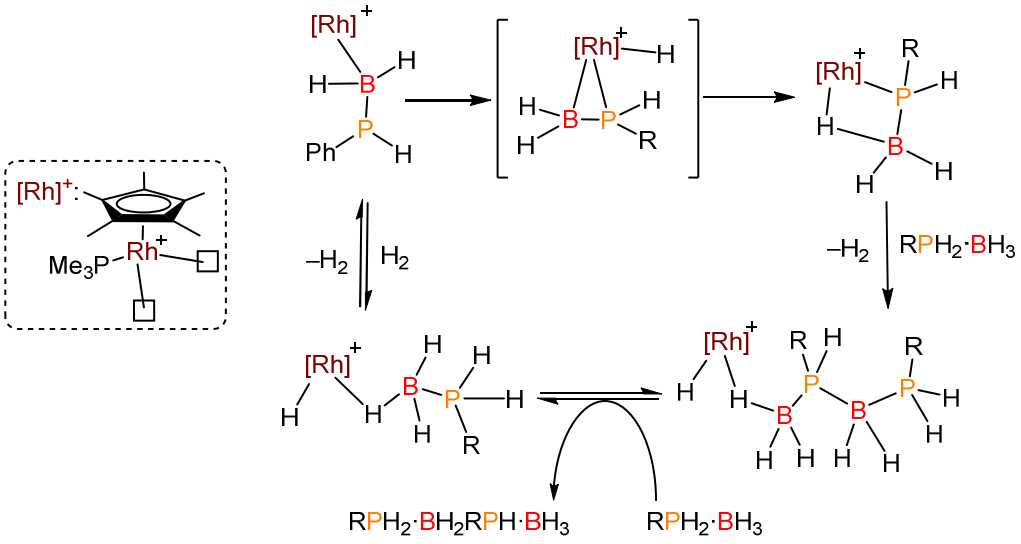

Scheme 1.20. Proposed reversible chain transfer of the dehydropolymerisation of primary phosphine–boranes *via* [RhCp*(PMe_3)Me($ClCH_2Cl$)][BAr^F_4].

Braunschweig, *Radius* and coworkers proposed simultaneous mechanisms for the homogeneous dehydropolymerisation of arylphosphine–boranes using [IrH_2POCOP] in

solution.[117] By initial screening of the catalyst loading, they suggested a step-growth mechanism as higher catalyst loadings led to higher molar mass polymers. Moreover, isolation of high molar mass polymer at low conversion of the monomer, indicated a chain growth mechanism. They concluded that the mechanism can proceed in two different stages. The former, is the initial formation of a phosphinoborane monomer $RPH{=}BH_2$ assisted by the metal centre (similar to the proposed dehydropolymerisation mechanism of amine–boranes) which is followed by rapid chain growth, presumably also metal mediated. No intermediate sigma phosphine–borane complexes or phosphidoborane species were detected in this system.

1.2.12 Metal-Free Dehydropolymerisation of Phosphine–Boranes

Metal-free polymerisation methodologies of phosphine–boranes have been described using catalytic reactions or by stoichiometric reactions of phosphanylboranes in thermal conditions.

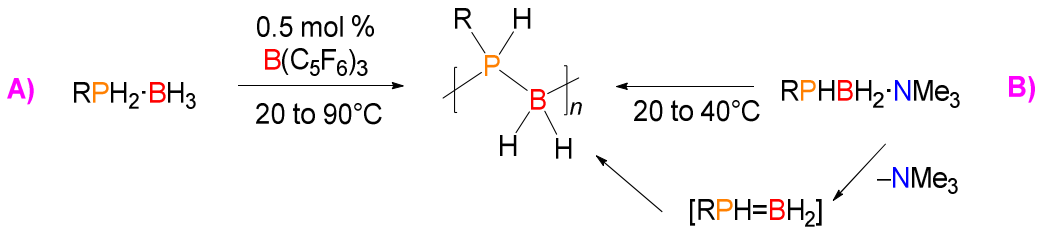

Scheme 1.21. Synthesis of polyphosphinoboranes by metal-free routes.

Gaumont and coworkers reported the dehydropolymerisation reaction of $PhPH_2{\cdot}BH_3$ catalysed by $B(C_6F_5)_3$ (0.5 mol%) in toluene to produce polymers with low molar mass (M_w = 830–3,900 g mol^{-1}) at ambient temperatures (20 °C), however, the full consumption of monomer required 3 days. When the dehydropolymerisation of the parent $PH_3{\cdot}BH_3$ was used at higher temperatures (70–90 °C), formation of an oligomeric material sensitive to air- and moisture was described (Scheme 1.21A).[121]

In a different approach to synthesise polyphosphinoboranes, *Scheer, Manners* and coworkers developed a head-to-tail polymerisation methodology by mild thermolysis (20–40 °C) of phosphanylboranes RR'PBH_2·NMe_3.[122] This methodology produced the parent oligophosphinoborane $[PH_2–BH_2]_n$ as a waxy solid with poor solubility and alkyl-susbtituted polyphosphinoboranes with high molar mass (M_n = 27,800–35,000 g mol^{-1}, PDI = 1.6–1.9) in the case for $[t$BuPH–$BH_2]_n$ and some oligomeric materials ($[MePH–BH_2]_n$ and $[Ph_2P–BH_2]_n$) (Scheme 1.21B).

Very recently, a computational study related to the metal-free head-to-tail polymerisation described that oligomeric chains arising from $PH_2–BH_2$ units possessed marked electronic differences between the cyclic and linear chains for isomers $[PH_2–BH_2]_{15}$.[123] For example, the band gap for the cyclic species (>5 eV) is significantly higher than the linear structure (<0.2 eV). And the molecular orbitals in the oligomeric rings are highly delocalised, whereas for the oligomeric chain, the HOMO and LUMO are localised at the chain ends of the oligomer.

Although the synthesis of polyphosphinoborane materials that could not be accessed to date by catalytic dehydrocoupling can be achieved through this innovative metal-free polymerisation technique, no generalisation on the substrate scope has been accomplished yet.

1.3 Thesis Summary and Collaborators Acknowledgments

The work described in this PhD thesis compiles several research projects on the synthesis, characterisation and properties of polyaminoboranes and polyphosphinoboranes. This thesis is composed of four additional chapters along with a conclusion and future work chapter which are ordered as follows:

- **Chapter 2** explores the iron-catalysed dehydropolymerisation of a range of different aryl-substituted phosphine–boranes. Also, the study of the properties of the polymeric materials obtained is described.
- **Chapter 3** discusses the reinvestigation on the homogeneous Fe-catalyzed dehydropolymerisation of alkyl *P*-monosubstituted phosphine–boranes.
- **Chapter 4** details the synthesis and characterisation of polyaminoboranes with aryl-substituted alkyl groups at nitrogen *via* catalytic dehydrocoupling.
- **Chapter 5** describes the synthesis and characterisation of boron–nitrogen main chain analogues of polystyrene, referred as poly(*B*-aryl)aminoboranes, *via* catalytic dehydrocoupling.
- **Chapter 6**: Conclusions and Future Work

In accordance with the research system implemented by Prof. Ian Manners, each chapter of this thesis can be read as a self-contained manuscript which is targeted for potential publication in peer-reviewed scientific journals. The most part of the body of the work was performed by the author. Additionally, and in favour of the spirit of collaboration as is common practice in strong international groups, this work has been benefited of contributions of other members that are either current or former members within the Manners' research group. These contributions are outlined below:

Chapter 2 has been reproduced from *Macromol. Chem. Phys.* **2017**, *218*, 1700120, in which initial work was performed by Dr. James R. Vance, Dr. Titel Jurca and Dr. Andre Schäfer. The author and Dr. Joshua Turner synthesised and characterised the monomers and polymers. X-ray crystallography was performed by Dr. Rebecca A. Musgrave and Dr. Hazel A. Sparkes. The contact angles measurements were determined by Laura Beckett. Dr. Sean Davis assisted with the TEM and EDX experiments. Dr. George R. Whittell performed powder X-ray diffraction experiments. All of the authors have read and commented on the manuscript.

Chapter 3 contains as yet unpublished results. Dr. Saurabh S. Chitnis conducted the synthesis and characterisation of $[n\text{HexPH–BH}_2]_n$. The author and Dr. Vincent T. Annibale contributed equally in the synthesis and characterisation of the various monomers and polymers used. In addition, the analysis of the results and the manuscript was co-wrote by the author and Dr. Vince T. Annibale.

Chapter 4 contains as yet unpublished results. Initial work was performed by Dr. Erin M. Leitao. The author performed the synthesis and characterisation of the various monomers and polymers. The author analysed the results and wrote the manuscript. Scientific insight was added by Dr. George R. Whittell.

Chapter 5 has been reproduced from *Chem. Commun.,* **2017***, 53,* 11701-11704, in which initial work was performed by Dr. Naomi E. Stubbs. The author performed the synthesis and characterisation of monomers and polymers. The author and Dr. Marius Arz analysed the results and co-wrote the manuscript. Scientific insight and input were added by Dr. George R. Whittell. X-ray crystallography was performed by Dr. Hazel A. Sparkes and Natalie E. Pridmore.

1.4 References

1. (a) Chauvin, Y., *Angew. Chem. Int. Ed.* **2006,** *45*, 3740-3747; (b) Schrock, R. R., *Angew. Chem. Int. Ed.* **2006,** *45*, 3748-3759; (c) Grubbs, R. H., *Angew. Chem. Int. Ed.* **2006,** *45*, 3760-3765.

2. (a) Beletskaya, I. P.; Cheprakov, A. V., *Chem. Rev.* **2000,** *100*, 3009-3066; (b) Stille, J. K., *Angew Chem Int Edit* **1986,** *25*, 508-523; (c) Miyaura, N.; Suzuki, A., *Chem. Rev.* **1995,** *95*, 2457-2483.

3. (a) Natta, G.; Pino, P.; Mazzanti, G.; Giannini, U., *J. Am. Chem. Soc.* **1957,** *79*, 2975-2976; (b) Boor, J., Preface. In *Ziegler–Natta Catalysts Polymerizations*, Boor, J., Ed. Academic Press: 1979; pp xv-xvi.

4. Jones, R. G.; Holder, S. J., *Polym. Int.* **2006,** *55*, 711-718.

5. (a) Leitao, E. M.; Jurca, T.; Manners, I., *Nat. Chem.* **2013,** *5*, 817-829; (b) Waterman, R., *Chem. Soc. Rev.* **2013,** *42*, 5629-5641; (c) Less, R. J.; Melen, R. L.; Wright, D. S., *RSC Adv.* **2012,** *2*, 2191-2199; (d) Melen, R. L., *Chem. Soc. Rev.* **2016,** *45*, 775-788; (e) Hill, M. S.; Liptrot, D. J.; Weetman, C., *Chem. Soc. Rev.* **2016,** *45*, 972-988.

6. (a) Corcoran, E. W.; Sneddon, L. G., *J. Am. Chem. Soc.* **1984,** *106*, 7793-7800; (b) Corcoran, E. W.; Sneddon, L. G., *J. Am. Chem. Soc.* **1985,** *107*, 7446-7450.

7. Aitken, C.; Harrod, J. F.; Samuel, E., *J. Organomet. Chem.* **1985,** *279*, C11-C13.

8. (a) He, J. L.; Liu, H. Q.; Harrod, J. F.; Hynes, R., *Organometallics* **1994,** *13*, 336-343; (b) Biran, C.; Blum, Y. D.; Glaser, R.; Tse, D. S.; Youngdahl, K. A.; Laine, R. M., *J. Mol. Catal.* **1988,** *48*, 183-197; (c) Blum, Y.; Laine, R. M., *Organometallics* **1986,** *5*, 2081-2086.

9. Shu, R. H.; Hao, L. J.; Harrod, J. F.; Woo, H. G.; Samuel, E., *J. Am. Chem. Soc.* **1998,** *120*, 12988-12989.

10. Matyjaszewski, K.; Gnanou, Y.; Leibler, L., *Macromolecular Engineering: Precise Synthesis, Materials Properties, Applications*. John Wiley & Sons: 2007.

11. Mark, H. F.; Kroschwitz, J. I., *Encyclopedia of polymer science and engineering*. Wiley: 1988.

12. (a) Power, P. P., *Chem. Rev.* **1999,** *99*, 3463-3503; (b) Rivard, E.; Power, P. P., *Inorg. Chem.* **2007,** *46*, 10047-10064.

13. Priegert, A. M.; Rawe, B. W.; Serin, S. C.; Gates, D. P., *Chem. Soc. Rev.* **2016,** *45*, 922-953.

14. *Organo-di-Metallic Compounds (or Reagents): Synergistic Effects and Synthetic Applications*. Springer International Publishing: 2014.

15. (a) Chivers, T.; Manners, I.; Chemistry, R. S. o., *Inorganic Rings and Polymers of the P-block Elements: From Fundamentals to Applications*. RSC Pub.: 2009; (b) Rabanzo-Castillo, K. M., Leitao, E. M., Main-Group Rings, Chains, and Polymer Compounds. In *Encyclopedia of Inorganic and Bioinorganic Chemistry*, (Ed.)., R. A. S., Ed. 2017; (c) Manners, I., *Angew. Chem. Int. Ed.* **1996,** *35*, 1602-1621.

16. Mark, J. E.; Allcock, H. R.; West, R., *Inorganic polymers*. Prentice Hall: 1992.

17. Clark, T. J.; Lee, K.; Manners, I., *Chem. Eur. J.* **2006,** *12*, 8634-8648.

18. (a) Staubitz, A.; Robertson, A. P. M.; Sloan, M. E.; Manners, I., *Chem. Rev.* **2010,** *110*, 4023-4078; (b) Johnson, H. C.; Hooper, T. N.; Weller, A. S., *Top. Organometal. Chem.* **2015,** *49*, 153-220.

19. Gay-Lussac, J. L., *Mem. Phys. Chim. Soc. D'Arcueil* **1809,** *2*, 211.

20. (a) Jaska, C. A.; Temple, K.; Lough, A. J.; Manners, I., *J. Am. Chem. Soc.* **2003,** *125*, 9424-9434; (b) Helten, H.; Robertson, A. P. M.; Staubitz, A.; Vance, J. R.; Haddow, M. F.; Manners, I., *Chem. Eur. J.* **2012,** *18*, 4665-4680.

21. (a) Ramachandran, P. V.; Gagare, P. D., *Inorg. Chem.* **2007,** *46*, 7810-7817; (b) Ramachandran, P. V.; Kulkarni, A. S., *Inorg. Chem.* **2015,** *54*, 5618-5620.

22. (a) Beachley, O. T.; Washburn, B., *Inorg. Chem.* **1975,** *14*, 120-123; (b) Paul, V.; Roberts, B. P., *J. Chem. Soc., Perkin Trans. 2* **1988**, 1183-1193; (c) Robertson, A. P. M.; Whittell, G. R.; Staubitz, A.; Lee, K.; Lough, A. J.; Manners, I., *Eur. J. Inorg. Chem.* **2011**, 5279-5287; (d) Campbell, P. G.; Ishibashi, J. S. A.; Zakharov, L. N.; Liu, S. Y., *Aust. J. Chem.* **2014,** *67*, 521-524; (e) Stubbs, N. E.; Schäfer, A.; Robertson, A. P. M.; Leitao, E. M.; Jurca, T.; Sparkes, H. A.; Woodall, C. H.; Haddow, M. F.; Manners, I., *Inorg. Chem.* **2015,** *54*, 10878-10889.

23. Ramachandran, P. V.; Kulkarni, A. S.; Zhao, Y.; Mei, J. G., *Chem. Commun.* **2016,** *52*, 11885-11888.

24. Haynes, W. M., *CRC Handbook of Chemistry and Physics, 95th Edition*. CRC Press: 2014.

25. Liu, Z. Q.; Marder, T. B., *Angew. Chem. Int. Ed.* **2008,** *47*, 242-244.

26. (a) Hutchins, R. O.; Learn, K.; Nazer, B.; Pytlewski, D.; Pelter, A., *Org. Prep. Proced. Int.* **1984,** *16*, 337-372; (b) Sanyal, U.; Jagirdar, B. R., *Inorg. Chem.* **2012,** *51*, 13023-13033.

27. (a) Jacoby, M., *Chemical & Engineering News* **2005,** *83*, 8-8; (b) Stephens, F. H.; Pons, V.; Baker, R. T., *Dalton Trans.* **2007**, 2613-2626; (c) Bluhm, M. E.; Bradley, M. G.; Butterick, R.; Kusari, U.; Sneddon, L. G., *J. Am. Chem. Soc.* **2006,** *128*, 7748-7749.

28. (a) Robertson, A. P. M.; Leitao, E. M.; Manners, I., *J. Am. Chem. Soc.* **2011,** *133*, 19322-19325; (b) Sloan, M. E.; Staubitz, A.; Lee, K.; Manners, I., *Eur. J. Org. Chem.* **2011**, 672-675; (c) Jiang, Y. F.; Blacque, O.; Fox, T.; Frech, C. M.; Berke, H., *Organometallics* **2009,** *28*, 5493-5504; (d) Yang, X. H.; Zhao, L. L.; Fox, T.; Wang, Z. X.; Berke, H., *Angew. Chem. Int. Ed.* **2010,** *49*, 2058-2062; (e) Yang, X. H.; Fox, T.; Berke, H., *Chem. Commun.* **2011,** *47*, 2053-2055; (f) Yang, X. H.; Fox, T.; Berke, H., *Tetrahedron* **2011,** *67*, 7121-7127; (g) Yang, X. H.; Fox, T.; Berke, H., *Org. Biomol. Chem.* **2012,** *10*, 852-860; (h) Jaska, C. A.; Manners, I., *J. Am. Chem. Soc.* **2004,** *126*, 2698-9.

29. (a) Ramachandran, P. V.; Kulkarni, A. S.; Pfeil, M. A.; Dennis, J. D.; Willits, J. D.; Heister, S. D.; Son, S. F.; Pourpoint, T. L., *Chem. Eur. J.* **2014,** *20*, 16869-16872; (b) Pfeil, M. A.; Dennis, J. D.; Son, S. F.; Heister, S. D.; Pourpoint, T. L.; Ramachandran, P. V., *J. Propul. Power* **2015,** *31*, 365-372; (c) Pfeil, M. A.; Kulkarni, A. S.; Ramachandran, P. V.; Son, S. F.; Heister, S. D., *J. Propul. Power* **2016,** *32*, 23-31.

30. (a) Marder, T. B., *Angew. Chem. Int. Ed.* **2007,** *46*, 8116-8118; (b) Hamilton, C. W.; Baker, R. T.; Staubitz, A.; Manners, I., *Chem. Soc. Rev.* **2009,** *38*, 279-293; (c) Staubitz, A.; Robertson, A. P. M.; Manners, I., *Chem. Rev.* **2010,** *110*, 4079-4124; (d) Smythe, N. C.; Gordon, J. C., *Eur. J. Inorg. Chem.* **2010**, 509-521; (e) Bhunya, S.; Malakar, T.; Ganguly, G.; Paul, A., *ACS Catal.* **2016,** *6*, 7907-7934.

31. (a) Rassat, S. D.; Aardahl, C. L.; Autrey, T.; Smith, R. S., *Energ Fuel* **2010,** *24*, 2596-2606; (b) Wang, P., *Dalton Trans.* **2012,** *41*, 4296-4302.

32. Rossin, A.; Peruzzini, M., *Chem. Rev.* **2016,** *116*, 8848-8872.

33. (a) Hausdorf, S.; Baitalow, F.; Wolf, G.; Mertens, F. O. R. L., *Int. J. Hydrogen Energy* **2008,** *33*, 608-614; (b) Davis, B. L.; Dixon, D. A.; Garner, E. B.; Gordon, J. C.; Matus, M. H.; Scott, B.; Stephens, F. H., *Angew. Chem. Int. Ed.* **2009,** *48*, 6812-6816; (c) Sutton, A. D.; Burrell, A. K.; Dixon, D. A.; Garner, E. B.; Gordon, J. C.; Nakagawa, T.; Ott, K. C.; Robinson, P.; Vasiliu, M., *Science* **2011,** *331*, 1426-1429.

34. Bernard, S.; Salameh, C.; Miele, P., *Dalton Trans.* **2016,** *45*, 861-873.

35. Pan, Z. C.; Sun, H.; Zhang, Y.; Chen, C. F., *Phys. Rev. Lett.* **2009,** *102*.

36. Whittell, G. R.; Manners, I., *Angew. Chem. Int. Ed.* **2011,** *50*, 10288-10289.

37. (a) Golberg, D.; Bando, Y.; Huang, Y.; Terao, T.; Mitome, M.; Tang, C. C.; Zhi, C. Y., *Acs Nano* **2010,** *4*, 2979-2993; (b) Kubota, Y.; Watanabe, K.; Tsuda, O.; Taniguchi, T., *Science* **2007,** *317*, 932-934.

38. (a) Kim, D. P.; Moon, K. T.; Kho, J. G.; Economy, J.; Gervais, C.; Babonneau, F., *Polym. Adv. Technol.* **1999,** *10*, 702-712; (b) Wang, X. C.; Hooper, T. N.; Kumar, A.; Priest, I. K.; Sheng, Y. W.; Samuels, T. O. M.; Wang, S. S.; Robertson, A. W.; Pacios, M.; Bhaskaran, H.; Weller, A. S.; Warner, J. H., *CrystEngComm.* **2017,** *19*, 285-294.

39. Du, V. A.; Jurca, T.; Whittell, G. R.; Manners, I., *Dalton Trans.* **2016,** *45*, 1055-1062.

40. Nakhmanson, S. M.; Nardelli, M. B.; Bernholc, J., *Phys. Rev. Lett.* **2004,** *92*.

41. (a) Barth, R. F.; Coderre, J. A.; Vicente, M. G. H.; Blue, T. E., *Clin Cancer Res* **2005,** *11*, 3987-4002; (b) Colebatch, A. L.; Gilder, B. W. H.; Whittell, G. R.; Oldroyd, N. L.; Manners, I.; Weller, A. S., *Chem. Eur. J.* **2018,** *24*, 5450-5455.

42. (a) Burg, A. B.; Randolph, C. L., *J. Am. Chem. Soc.* **1949,** *71*, 3451-3455; (b) Chopard, P. A.; Hudson, R. F., *J. Inorg. Nucl. Chem.* **1963,** *25*, 801-805; (c) Beachley, O. T., *Inorg. Chem.* **1967,** *6*, 870-874; (d) Ryschkew.Ge; Wiggins, J. W., *Inorg. Chem.* **1970,** *9*, 314-&; (e) Carpenter, J. D.; Ault, B. S., *Chem. Phys. Lett.* **1992,** *197*, 171-174.

43. Metters, O. J.; Chapman, A. M.; Robertson, A. P. M.; Woodall, C. H.; Gates, P. J.; Wass, D. F.; Manners, I., *Chem. Commun.* **2014,** *50*, 12146-12149.

44. Pons, V.; Baker, R. T.; Szymczak, N. K.; Heldebrant, D. J.; Linehan, J. C.; Matus, M. H.; Grant, D. J.; Dixon, D. A., *Chem. Commun.* **2008**, 6597-6599.

45. Staubitz, A.; Sloan, M. E.; Robertson, A. P. M.; Friedrich, A.; Schneider, S.; Gates, P. J.; Günne, J. S. A. D.; Manners, I., *J. Am. Chem. Soc.* **2010,** *132*, 13332-13345.

46. (a) Alcaraz, G.; Vendier, L.; Clot, E.; Sabo-Etienne, S., *Angew. Chem. Int. Ed.* **2010,** *49*, 918-920; (b) Johnson, H. C.; Weller, A. S., *J. Organomet. Chem.* **2012,** *721*, 17-22.

47. (a) Clark, T. J.; Russell, C. A.; Manners, I., *J. Am. Chem. Soc.* **2006,** *128*, 9582-9583; (b) Sloan, M. E.; Staubitz, A.; Clark, T. J.; Russell, C. A.; Lloyd-Jones, G. C.; Manners, I., *J. Am. Chem. Soc.* **2010,** *132*, 3831-3841; (c) Beweries, T.; Thomas, J.; Klahn, M.; Schulz, A.; Heller, D.; Rosenthal, U., *ChemCatChem* **2011,** *3*, 1865-1868; (d) Beweries, T.; Hansen, S.; Kessler, M.; Klahn, M.; Rosenthal, U., *Dalton Trans.* **2011,** *40*, 7689-7692; (e) Trose, M.; Reiß, M.; Reiß, F.; Anke, F.; Spannenberg, A.; Boye, S.; Lederer, A.; Arndt, P.; Beweries, T., *Dalton Trans.* **2018**; (f) Pun, D.; Lobkovsky, E.; Chirik, P. J., *Chem. Commun.* **2007**, 3297-3299; (g) Erickson, K. A.; Stelmach, J. P. W.; Mucha, N. T.; Waterman, R., *Organometallics* **2015,** *34*, 4693-4699; (h) Lummis, P. A.; McDonald, R.; Ferguson, M. J.; Rivard, E., *Dalton Trans.* **2015,** *44*, 7009-7020; (i) Miyazaki, T.; Tanabe, Y.; Yuki, M.; Miyake, Y.; Nishibayashi, Y., *Organometallics* **2011,** *30*, 2394-2404; (j) Kakizawa, T.; Kawano, Y.; Naganeyama, K.; Shimoi, M., *Chem. Lett.* **2011,** *40*, 171-173.

48. (a) Garcia-Vivo, D.; Huergo, E.; Ruiz, M. A.; Travieso-Puente, R., *Eur. J. Inorg. Chem.* **2013,** *2013*, 4998-5008; (b) Kawano, Y.; Uruichi, M.; Shimoi, M.; Taki, S.; Kawaguchi, T.; Kakizawa, T.; Ogino, H., *J. Am. Chem. Soc.* **2009,** *131*, 14946-14957; (c) Buss, J. A.; Edouard, G. A.; Cheng, C.; Shi, J. D.; Agapie, T., *J. Am. Chem. Soc.* **2014,** *136*, 11272-11275; (d) Jiang, Y.; Berke, H., *Chem. Commun.* **2007**, 3571-3573.

49. Erickson, K. A.; Kiplinger, J. L., *ACS Catal.* **2017,** *7*, 4276-4280.

50. (a) Bellham, P.; Hill, M. S.; Kociok-Kohn, G.; Liptrot, D. J., *Chem. Commun.* **2013,** *49*, 1960-1962; (b) Liptrot, D. J.; Hill, M. S.; Mahon, M. F.; MacDougall, D. J., *Chem. Eur. J.* **2010,** *16*, 8508-8515; (c) Spielmann, J.; Bolte, M.; Harder, S., *Chem. Commun.* **2009**, 6934-6936; (d) Nolla-Saltiel, R.; Geer, A. M.; Lewis, W.; Blake, A. J.; Kays, D. L., *Chem. Commun.* **2018,** *54*, 1825-1828; (e) Sharpe, H. R.; Geer, A. M.; Blundell, T. J.; Hastings, F. R.; Fay, M. W.; Rance, G. A.; Lewis, W.; Blake, A. J.; Kays, D. L., *Catal. Sci. Technol.* **2018,** *8*, 229-235.

51. (a) Cowley, H. J.; Holt, M. S.; Melen, R. L.; Rawson, J. M.; Wright, D. S., *Chem. Commun.* **2011,** *47*, 2682-2684; (b) Erickson, K. A.; Wright, D. S.; Waterman, R., *J. Organomet. Chem.* **2014,** *751*, 541-545; (c) Hansmann, M. M.; Melen, R. L.; Wright, D. S., *Chem. Sci.* **2011,** *2*, 1554-1559; (d) Less, R. J.; Simmonds, H. R.; Wright, D. S., *Dalton Trans.* **2014,** *43*, 5785-5792.

52. (a) Appelt, C.; Slootweg, J. C.; Lammertsma, K.; Uhl, W., *Angew. Chem. Int. Ed.* **2013,** *52*, 4256-4259; (b) Miller, A. J. M.; Bercaw, J. E., *Chem. Commun.* **2010,** *46*, 1709-1711; (c) Mo, Z. B.; Pit, A.; Campos, J.; Kolychev, E. L.; Aldridge, S., *J. Am. Chem. Soc.* **2016,** *138*, 3306-3309; (d) Metters, O. J.; Flynn, S. R.; Dowds, C. K.; Sparkes, H. A.; Manners, I.; Wass, D. F., *ACS Catal.* **2016,** *6*, 6601-6611.

53. (a) Jaska, C. A.; Manners, I., *J. Am. Chem. Soc.* **2004,** *126*, 9776-85; (b) Jaska, C. A.; Manners, I., *J. Am. Chem. Soc.* **2004,** *126*, 1334-5.

54. Robertson, A. P. M.; Suter, R.; Chabanne, L.; Whittell, G. R.; Manners, I., *Inorg. Chem.* **2011,** *50*, 12680-12691.

55. Denney, M. C.; Pons, V.; Hebden, T. J.; Heinekey, D. M.; Goldberg, K. I., *J. Am. Chem. Soc.* **2006,** *128*, 12048-9.

56. Dietrich, B. L.; Goldberg, K. I.; Heinekey, D. M.; Autrey, T.; Linehan, J. C., *Inorg. Chem.* **2008,** *47*, 8583-5.

57. Staubitz, A.; Soto, A. P.; Manners, I., *Angew. Chem. Int. Ed.* **2008,** *47*, 6212-6215.

58. (a) Fazen, P. J.; Beck, J. S.; Lynch, A. T.; Remsen, E. E.; Sneddon, L. G., *Chem. Mater.* **1990,** *2*, 96-97; (b) Fazen, P. J.; Remsen, E. E.; Beck, J. S.; Carroll, P. J.; Mcghie, A. R.; Sneddon, L. G., *Chem. Mater.* **1995,** *7*, 1942-1956; (c) Li, J.; Bernard, S.; Salles, V.; Gervais, C.; Miele, P., *Chem. Mater.* **2010,** *22*, 2010-2019; (d) Yuan, S.; Toury, B.; Benayoun, S., *Surf. Coat. Tech.* **2015,** *272*, 366-372.

59. (a) Keaton, R. J.; Blacquiere, J. M.; Baker, R. T., *J. Am. Chem. Soc.* **2007,** *129*, 1844-1845; (b) Bhattacharya, P.; Krause, J. A.; Guan, H. R., *J. Am. Chem. Soc.* **2014,** *136*, 11153-11161; (c) Conley, B. L.; Guess, D.; Williams, T. J., *J. Am. Chem. Soc.* **2011,** *133*, 14212-14215; (d) Davis, B. L.; Rekken, B. D.; Michalczyk, R.; Garner, E. B.; Dixon, D. A.; Kalviri, H.; Baker, R. T.; Thorn, D. L., *Chem. Commun.* **2013,** *49*, 9095-9097.

60. (a) Fontani, M.; Peters, F.; Scherer, W.; Wachter, W.; Wagner, M.; Zanello, P., *Eur. J. Inorg. Chem.* **1998**, 2087-2087; (b) Fontani, M.; Peters, F.; Scherer, W.; Wachter, W.; Wagner, M.; Zanello, P., *Eur. J. Inorg. Chem.* **1998**, 1453-1465; (c) Grosche, M.; Herdtweck, E.; Peters, F.; Wagner, M., *Organometallics* **1999,** *18*, 4669-4672.

61. Chujo, Y.; Tomita, I.; Saegusa, T., *Macromolecules* **1992,** *25*, 3005-3006.

62. Chujo, Y.; Tomita, I.; Murata, N.; Mauermann, H.; Saegusa, T., *Macromolecules* **1992,** *25*, 27-32.

63. (a) Matsumi, N.; Kotera, K.; Naka, K.; Chujo, Y., *Macromolecules* **1998,** *31*, 3155-3157; (b) Matsumi, N.; Kotera, K.; Chujo, Y., *Macromolecules* **2000,** *33*, 2801-2806.

64. Morgan, M. M.; Piers, W. E., *Dalton Trans.* **2016,** *45*, 5920-5924.

65. Helten, H., *Chem. Eur. J.* **2016,** *22*, 12972-12982.

66. Jackson, L. A.; Allen, C. W., *J. Polym. Sci., Part A: Polym. Chem.* **1992,** *30*, 577-581.

67. Su, K.; Remsen, E. E.; Thompson, H. M.; Sneddon, L. G., *Macromolecules* **1991,** *24*, 3760-3766.

68. Wan, W. M.; Baggett, A. W.; Cheng, F.; Lin, H.; Liu, S. Y.; Jäkle, F., *Chem. Commun.* **2016,** *52*, 13616-13619.

69. Thiedemann, B.; Gliese, P. J.; Hoffmann, J.; Lawrence, P. G.; Sönnichsen, F. D.; Staubitz, A., *Chem. Commun.* **2017,** *53*, 7258-7261.

70. (a) van de Wouw, H. L.; Lee, J. Y.; Klausen, R. S., *Chem. Commun.* **2017,** *53*, 7262-7265; (b) van de Wouw, H. L.; Lee, J. Y.; Awuyah, E. C.; Klausen, R. S., *Angew. Chem. Int. Ed.* **2018,** *57*, 1673-1677; (c) Mendis, S. N.; Zhou, T.; Klausen, R. S., *Macromolecules* **2018**; (d) van de Wouw, H. L.; Awuyah, E. C.; Baris, J. I.; Klausen, R. S., *Macromolecules* **2018,** *51*, 6359-6368.

71. Lorenz, T.; Lik, A.; Plamper, F. A.; Helten, H., *Angew. Chem. Int. Ed.* **2016,** *55*, 7236-7241.

72. Lorenz, T.; Crumbach, M.; Eckert, T.; Lik, A.; Helten, H., *Angew. Chem. Int. Ed.* **2017,** *56*, 2780-2784.

73. Ledoux, A.; Larini, P.; Boisson, C.; Monteil, V.; Raynaud, J.; Lacote, E., *Angew. Chem. Int. Ed.* **2015,** *54*, 15744-15749.

74. (a) Meier, H. U.; Paetzold, P.; Schroder, E., *Chem. Ber.* **1984,** *117*, 1954-1964; (b) Paetzold, P., *Adv. Inorg. Chem.* **1987,** *31*, 123-170.

75. Ayhan, O.; Eckert, T.; Plamper, F. A.; Helten, H., *Angew. Chem. Int. Ed.* **2016,** *55*, 13321-13325.

76. (a) Komm, R.; Geanangel, R. A.; Liepins, R., *Inorg. Chem.* **1983,** *22*, 1684-1686; (b) Geanangel, R. A.; Rabalais, J. W., *Inorg. Chim. Acta* **1985,** *97*, 59-64.

77. Baumann, J.; Baitalow, E.; Wolf, G., *Thermochim. Acta* **2005,** *430*, 9-14.

78. Kwon, C. T.; Mcgee, H. A., *Inorg. Chem.* **1970,** *9*, 2458-&.

79. (a) Vance, J. R.; Robertson, A. P. M.; Lee, K.; Manners, I., *Chem. Eur. J.* **2011,** *17*, 4099-4103; (b) Johnson, H. C.; Leitao, E. M.; Whitten, G. R.; Manners, I.; Lloyd-Jones, G. C.; Weller, A. S., *J. Am. Chem. Soc.* **2014,** *136*, 9078-9093; (c) Dallanegra, R.; Robertson, A. P. M.; Chaplin, A. B.; Manners, I.; Weller, A. S., *Chem. Commun.* **2011,** *47*, 3763-3765; (d) Johnson, H. C.; Weller, A. S., *Angew. Chem. Int. Ed.* **2015,** *54*, 10173-10177; (e) Anke, F.; Han, D.; Klahn, M.; Spannenberg, A.; Beweries, T., *Dalton Trans.* **2017,** *46*, 6843-6847; (f) Jurca, T.; Dellermann, T.; Stubbs, N. E.; Resendiz-Lara, D. A.; Whittell, G. R.; Manners, I., *Chem. Sci.* **2018,** *9*, 3360-3366; (g) Adams, G. M.; Colebatch, A. L.; Skornia, J. T.; McKay, A. I.; Johnson, H. C.; Lloyd-Jones, G. C.; Macgregor, S. A.; Beattie, N. A.; Weller, A. S., *J. Am. Chem. Soc.* **2018,** *140*, 1481-1495.

80. Staubitz, A.; Besora, M.; Harvey, J. N.; Manners, I., *Inorg. Chem.* **2008,** *47*, 5910-5918.

81. Bhunya, S.; Malakar, T.; Paul, A., *Chem. Commun.* **2014,** *50*, 5919-5922.

82. Robertson, A. P. M.; Leitao, E. M.; Jurca, T.; Haddow, M. F.; Helten, H.; Lloyd-Jones, G. C.; Manners, I., *J. Am. Chem. Soc.* **2013,** *135*, 12670-12683.

83. Johnson, H. C.; Robertson, A. P. M.; Chaplin, A. B.; Sewell, L. J.; Thompson, A. L.; Haddow, M. F.; Manners, I.; Weller, A. S., *J. Am. Chem. Soc.* **2012,** *134*, 3932-3932.

84. Kumar, A.; Johnson, H. C.; Hooper, T. N.; Weller, A. S.; Algarra, A. G.; Macgregor, S. A., *Chem. Sci.* **2014,** *5*, 2546-2553.

85. (a) Singaram, B.; Cole, T. E.; Brown, H. C., *Organometallics* **1984,** *3*, 774-777; (b) Pinheiro, C. A. D.; Roiland, C.; Jehan, P.; Alcaraz, G., *Angew. Chem. Int. Ed.* **2018,** *57*, 1519-1522.

86. Besson, A., *Comptes Rendus* **1890,** *110*, 516.

87. (a) Hurtado, M.; Yanez, M.; Herrero, R.; Guerrero, A.; Davalos, J. Z.; Abboud, J. L. M.; Khater, B.; Guillemin, J. C., *Chem. Eur. J.* **2009,** *15*, 4622-4629; (b) Chan, V. S.; Chiu, M.; Bergman, R. G.; Toste, F. D., *J. Am. Chem. Soc.* **2009,** *131*, 6021-6032; (c) Carreira, M.; Charernsuk, M.; Eberhard, M.; Fey, N.; van Ginkel, R.; Hamilton, A.; Mul, W. P.; Orpen, A. G.; Phetmung, H.; Pringle, P. G., *J. Am. Chem. Soc.* **2009,** *131*, 3078-3092; (d) Seitz, T.; Muth, A.; Huttner, G., *Chem. Ber.* **1994,** *127*, 1837-1842.

88. McNulty, J.; Zhou, Y. H., *Tetrahedron Lett.* **2004,** *45*, 407-409.

89. (a) Power, P. P., *Angew Chem Int Edit* **1990,** *29*, 449-460; (b) Allen, T. L.; Fink, W. H., *Inorg. Chem.* **1992,** *31*, 1703-1705.

90. Gropen, O., *J. Mol. Struct.* **1977,** *36*, 111-120.

91. Montgomery, C. D., *J. Chem. Educ.* **2013,** *90*, 661-664.

92. (a) Rauk, A.; Allen, L. C.; Mislow, K., *Angew. Chem. Int. Ed.* **1970,** *9*, 400-414; (b) Kolmel, C.; Ochsenfeld, C.; Ahlrichs, R., *Theor. Chim. Acta* **1992,** *82*, 271-284; (c) Lehn, J. M.; Munsch, B., *J. Chem. Soc. D.* **1969**, 1327-1329; (d) Fryzuk, M. D.; Giesbrecht, G. R.; Rettig, S. J., *Inorg. Chem.* **1998,** *37*, 6928-6934; (e) Baechler, R. D.; Farnham, W. B.; Mislow, K., *J. Am. Chem. Soc.* **1969,** *91*, 5686-5686; (f) Baechler, R. D.; Mislow, K., *J. Am. Chem. Soc.* **1970,** *92*, 3090-3093; (g) Lambert, J. B.; Jackson, G. F.; Mueller, D. C., *J. Am. Chem. Soc.* **1970,** *92*, 3093-3097.

93. (a) Lambert, J. B.; Oliver, W. L., *J. Am. Chem. Soc.* **1969,** *91*, 7774-7775; (b) Anet, F. A. L.; Trepka, R. D.; Cram, D. J., *J. Am. Chem. Soc.* **1967,** *89*, 357-362; (c) Swalen, J. D.; Ibers, J. A., *J. Chem. Phys.* **1962,** *36*, 1914.

94. (a) Bourumeau, K.; Gaumont, A. C.; Denis, J. M., *J. Organomet. Chem.* **1997,** *529*, 205-213; (b) Busacca, C. A.; Farber, E.; DeYoung, J.; Campbell, S.; Gonnella, N. C.; Grinberg, N.; Haddad, N.; Lee, H.; Ma, S. L.; Reeves, D.; Shen, S.; Senanayake, C. H., *Org. Lett.* **2009,** *11*, 5594-5597.

95. (a) Dorn, H.; Singh, R. A.; Massey, J. A.; Nelson, J. M.; Jaska, C. A.; Lough, A. J.; Manners, I., *J. Am. Chem. Soc.* **2000,** *122*, 6669-6678; (b) Grant, D. J.; Dixon, D. A., *J. Phys. Chem. A* **2005,** *109*, 10138-10147.

96. (a) Schlieve, C. R.; Tam, A.; Nilsson, B. L.; Lieven, C. J.; Raines, R. T.; Levin, L. A., *Exp. Eye Res.* **2006,** *83*, 1252-1259; (b) Seidler, E. A.; Lieven, C. J.; Thompson, A. F.; Levin, L. A., *ACS Chem. Neurosci.* **2010,** *1*, 95-103; (c) Almasieh, M.; Lieven, C. J.; Levin, L. A.; Di Polo, A., *J. Neurochem.* **2011,** *118*, 1075-1086.

97. Carboni, B.; Monnier, L., *Tetrahedron* **1999,** *55*, 1197-1248.

98. (a) Paine, R. T.; Noth, H., *Chem. Rev.* **1995,** *95*, 343-379; (b) Fischer, R. C.; Power, P. P., *Chem. Rev.* **2010,** *110*, 3877-3923; (c) Bailey, J. A.; Pringle, P. G., *Coord. Chem. Rev.* **2015,** *297*, 77-90.

99. Burg, A. B.; Wagner, R. I., *J. Am. Chem. Soc.* **1953,** *75*, 3872-3877.

100. Noonan, K. J. T.; Feldscher, B.; Bates, J. I.; Kingsley, J. J.; Yam, M.; Gates, D. P., *Dalton Trans.* **2008**, 4451-4457.

101. Evans, C. E. B.; Lough, A. J.; Grondey, H.; Manners, I., *New J. Chem.* **2000,** *24*, 447-453.

102. (a) Morisaki, Y.; Ouchi, Y.; Fukui, T.; Naka, K.; Chujo, Y., *Tetrahedron Lett.* **2005,** *46*, 7011-7014; (b) Morisaki, Y.; Ouchi, Y.; Naka, K.; Chujo, Y., *Tetrahedron Lett.* **2007,** *48*, 1451-1455.

103. (a) Ouchi, Y.; Morisaki, Y.; Chujo, Y., *Polym. Bull.* **2007,** *59*, 339-349; (b) Ouchi, Y.; Morisaki, Y.; Ogoshi, T.; Chujo, Y., *Chem. Asian J.* **2007,** *2*, 397-402; (c) Morisaki, Y.; Imoto, H.; Tsurui, K.; Chujo, Y., *Org. Lett.* **2009,** *11*, 2241-2244; (d) Morisaki, Y.; Suzuki, K.; Imoto, H.; Chujo, Y., *Macromol. Rapid Commun.* **2010,** *31*, 1719-1724; (e) Imoto, H.; Morisaki, Y.; Chujo, Y., *Chem. Commun.* **2010,** *46*, 7542-7544.

104. Burg, A. B. W., R. I., *U.S. Patent* **1963,** *3, 071, 553*.

105. Burg, A. B., *J. Inorg. Nucl. Chem.* **1959,** *11*, 258-258.

106. Wagner, R. I.; Caserio, F. F., *J. Inorg. Nucl. Chem.* **1959,** *11*, 259-259.

107. Muetterties, L., *The chemistry of boron and its compounds*. Wiley: 1967.

108. Korshak, V. V. Z., V. A.; Solomatina, A. I, *IzV. Akad. Nauk SSSR, Ser. Khim.* **1964,** *8*, 1541.

109. Dorn, H.; Singh, R. A.; Massey, J. A.; Lough, A. J.; Manners, I., *Angew. Chem. Int. Ed.* **1999,** *38*, 3321-3323.

110. Dorn, H.; Rodezno, J. M.; Brunnhöfer, B.; Rivard, E.; Massey, J. A.; Manners, I., *Macromolecules* **2003,** *36*, 291-297.

111. Pandey, S.; Lonnecke, P.; Hey-Hawkins, E., *Eur. J. Inorg. Chem.* **2014,** *2014*, 2456-2465.

112. Clark, T. L.; Rodezno, J. M.; Clendenning, S. B.; Aouba, S.; Brodersen, P. M.; Lough, A. J.; Ruda, H. E.; Manners, I., *Chem. Eur. J.* **2005,** *11*, 4526-4534.

113. Cayaye, H.; Clegg, F.; Gould, P. J.; Ladyman, M. K.; Temple, T.; Dossi, E., *Macromolecules* **2017,** *50*, 9239-9248.

114. Schäfer, A.; Jurca, T.; Turner, J.; Vance, J. R.; Lee, K.; Du, V. A.; Haddow, M. F.; Whittell, G. R.; Manners, I., *Angew. Chem. Int. Ed.* **2015,** *54*, 4836-4841.

115. Coles, N. T.; Mahon, M. F.; Webster, R. L., *Organometallics* **2017,** *36*, 2262-2268.

116. Hooper, T. N.; Weller, A. S.; Beattie, N. A.; Macgregor, S. A., *Chem. Sci.* **2016,** *7*, 2414-2426.

117. Paul, U. S. D.; Braunschweig, H.; Radius, U., *Chem. Commun.* **2016,** *52*, 8573-8576.

118. Huertos, M. A.; Weller, A. S., *Chem. Commun.* **2012,** *48*, 7185-7187.

119. Huertos, M. A.; Weller, A. S., *Chem. Sci.* **2013,** *4*, 1881-1888.

120. Hooper, T. N.; Huertos, M. A.; Jurca, T.; Pike, S. D.; Weller, A. S.; Manners, I., *Inorg. Chem.* **2014,** *53*, 3716-3729.

121. Denis, J. M.; Forintos, H.; Szelke, H.; Toupet, L.; Pham, T. N.; Madec, P. J.; Gaumont, A. C., *Chem. Commun.* **2003**, 54-55.

122. (a) Marquardt, C.; Jurca, T.; Schwan, K. C.; Stauber, A.; Virovets, A. V.; Whittell, G. R.; Manners, I.; Scheer, M., *Angew. Chem. Int. Ed.* **2015,** *54*, 13782-13786; (b) Stauber, A.; Jurca, T.; Marquardt, C.; Fleischmann, M.; Seidl, M.; Whittell, G. R.; Manners, I.; Scheer, M., *Eur. J. Inorg. Chem.* **2016**, 2684-2687.

123. Pomogaeva, A. V.; Scheer, M.; Timoshkin, A. Y., **2018,** *24*, 17046-17054.

Chapter 2

Synthesis, characterisation and properties of poly(aryl)phosphinoboranes formed *via* iron-catalysed dehydropolymerisation.

Reproduced from:

J. R. Turner, D. A. Resendiz-Lara, T. Jurca, A. Schäfer, J. R. Vance, L. Beckett, G. R. Whittell, R. A. Musgrave, H. A. Sparkes, I. Manners. *Macromol. Chem. Phys.* **2017**, *218*, 1700120.

2.1 Abstract

The dehydropolymerisation of the primary phosphine-boranes, $RPH_2{\cdot}BH_3$ (**2.1a-f**) (R = 3,4-$(OCH_2O)C_6H_3$ (**a**), Ph (**b**), *p*-$(OCF_3)C_6H_4$ (**c**), 3,5-$(CF_3)_2C_6H_3$ (**d**), 2,4,6-$(CH_3)_3C_6H_2$ (**e**), 2,4,6-$(t\text{Bu})_3C_6H_2$ (**f**)) is explored using the precatalyst $[CpFe(CO)_2OTf]$ (**I**) (OTf = $OS(O)_2CF_3$), based on the earth abundant element Fe. Formation of polyphosphinoboranes $[RPH–BH_2]_n$ (**2.2a-e**) was confirmed by multinuclear nuclear magnetic resonance (NMR) spectroscopy, but no conversion of **2.1f** to **2.2f** was detected. Analysis by electrospray ionisation mass spectrometry (ESI-MS) confirmes the presence of the anticipated polymer repeat units for **2.2a-e**. Gel permeation chromatography (GPC) confirmed the polymeric nature of **2.2a-e** and indicated number-average molecular weights (M_n) of 12,000 – 209,000 Da and polydispersity indices (PDI) between 1.14 – 2.17. By contrast, thermal dehydropolymerisation of **2.1a-e** in the absence of added precatalyst led to formation of oligomeric material. Interestingly, polyphosphinoboranes **2.2c** and **2.2d** displayed gel permeation chromatography (GPC) behaviour typical of polyelectrolytes, with a hydrodynamic radius dependant on concentration. The thermal transition behaviour, thermal stability, and surface properties of thin films were also studied.

2.2 Introduction

Macromolecules based on main group elements other than carbon, have been the subject of growing interest over the past two decades.[1,2,3] Current routes to such species are typically based on polycondensation, ring-opening polymerisation and metal-catalysed pathways,[4] which have been successfully exploited to access a broad range of main group polymers; selected examples include polyphosphazenes $[R_2PN]_n$ and related materials,[5] polysiloxanes $[R_2SiO]_n$,[6] polysilanes $[SiR_2]_n$,[7] polystannanes $[SnR_2]_n$ (R = alkyl),[8] boron-nitrogen polymers such as polyaminoboranes $[RNH–BH_2]_n$ (R = alkyl, or H),[9] and their congeneric polyphosphinoboranes $[RPH–BH_2]_n$ (R = aryl).[10] The desirable properties of these materials has facilitated a broad range of applications such as elastomers, biomaterials, polyelectrolytes, ceramic precursors, lithographic resists and in optoelectronics.[1–11] Through the use of metal-catalysed dehydrocoupling routes, an increasing number of main group polymers have been synthesised.[2, 4b]

As polyphosphinoboranes and polyaminoboranes possess main-chains formed of alternating group 13 and 15 elements, they are formally isoelectronic to those based on C–C main chains. This facet has historically aroused fundamental curiosity in such materials.[12] Moreover, polyphosphinoboranes attracted initial interest in the 1950s, when it was postulated that these materials would have high thermal stability and potential flame retardant properties.[13,14] Primary and secondary phosphine-borane adducts ($Me_2PH{\cdot}BH_3$, $MePH_2{\cdot}BH_3$) were thermally dehydrocoupled at ≈200 °C and above. Despite several instances of reports alluding to formation of polymeric materials in low yield, these products were not convincingly structurally characterised by present day standards, and their macromolecular nature was not established.[14,15,16]

Over a decade ago, our group reported the first example of metal-catalysed dehydropolymerisation of primary phosphine–boranes.[10a] This process was promoted by an apparently homogenous mechanism, using Rh-based precatalysts, $[Rh(1,5\text{-}COD)Cl]_2$

(COD = cyclooctadiene) and $[Rh(1,5\text{-}COD)_2][OTf]$ ($OTf = OS(O)_2CF_3$), operating under melt conditions at temperatures of ≈130 °C (Scheme 2.1A).[10a, 10b, 10d, 10g] Soluble polymeric material of high molecular weight (M_n > 10,000 Da) was synthesised, but this method also produced crosslinked, swellable, and insoluble material.[10a] Similar catalyst systems have been used to synthesise other polyphosphinoboranes, and demonstrate selective cross-dehydrocoupling with no evidence for P–P or B–B homocoupling.[10h,17] Furthermore, work has been performed to elucidate a mechanism through experimental work with Rh catalysts.[18,19] Recently, the precatalyst $[IrH_2(POCOP)]$ (POCOP = κ^3-1,3-$(OPtBu_2)_2C_6H_3$) has also been shown to dehydropolymerise primary phosphine-boranes ($RPH_2{\cdot}BH_3$) (R = Ph, *p*Tol, Mes) in solution at 100 °C.[10k] Furthermore, a metal-free thermolysis based route has been developed for the polymerisation of Lewis based-stabilised phosphinoboranes leading to poly(alkylphosphinoboranes) with appreciable molecular weight (28,000 – 35,000 Da, PDI < 2) (Scheme 2.1B).[10j, 20] This metal-free thermolysis route represents an advancement in the field, as the synthesis of high molecular weight poly(alkylphosphinoboranes) by metal catalysed routes has not been reported.[10d]

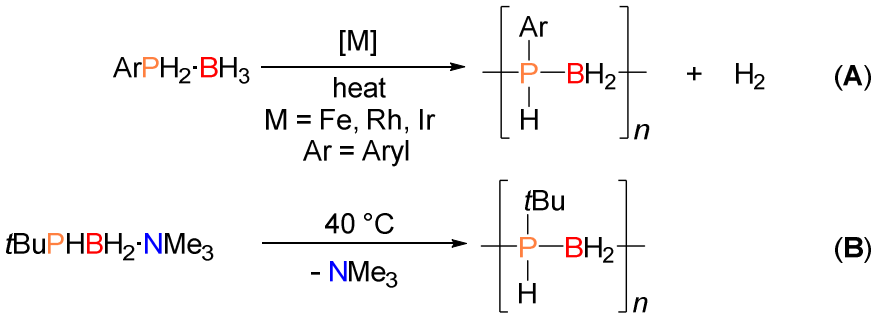

Scheme 2.1. Typical methods of synthesising primary polyphosphinoboranes by A) transition metal catalysed dehydrocoupling or B) via transient formation of phosphinoboranes.

In 2015, our group reported the use of the iron precatalyst $[CpFe(CO)_2OTf]$ (**I**) as a dehydropolymerisation precatalyst to synthesise polyphosphinoboranes with high molar mass, thereby circumventing the use of rare/expensive transition metals.[10i] Unlike previous systems, the homogenous Fe-based catalytic process yielded high molecular

weight poly(phenylphosphinoborane), with polydispersities that were lower than previous reports in the field. This was also achieved with the added advantage of operating under relatively mild conditions (100 °C), and in solution rather than a solvent-free melt. Some degree of control over the molecular weight of the polymer was enabled by changing catalyst loading, such that a lower catalyst loading resulted in higher molecular weights. Furthermore, at low conversion high molecular weight polymer was detected which was indicative of a chain growth polymerisation process. In this chapter we describe an extension of our initial work on the dehydropolymerisation of a range of primary phosphine–borane substrates, catalysed by precatalyst [$CpFe(CO)_2OTf$] (**I**) (OTf = $OS(O)_2CF_3$). The goal was to expand the potential scope of this Fe catalyst to demonstrate its utility in preparing high molecular weight polyphosphinoborane polymers with different properties resulting from the variation of pendant organic groups at phosphorus.

2. 3 Results and Discussion

2.3.1 Synthesis and characterisation of primary phosphine–borane adducts

We targeted the synthesis of a range of sterically and electronically varied phosphine–borane monomers, $RPH_2{\cdot}BH_3$ (**2.1a-f**) (Figure 2.1), of which **2.1a** and **2.1c** and **2.1d** are reported for the first time herein.[10i]

Monomers **2.1a-f** were isolated in good yield 60–70 % by two established literature methods. Adducts, **2.1a**, **2.1c**, **2.1d** and **2.1f** were synthesised by a procedure previously reported by our group,[10g] involving three steps starting from the reaction between a protected phospine $PCl(NEt_2)_2$ and an *in situ* generated organo-lithium reagent LiR (R = **a**, **c**, **d**, **f**) to form $RP(NEt_2)_2$.

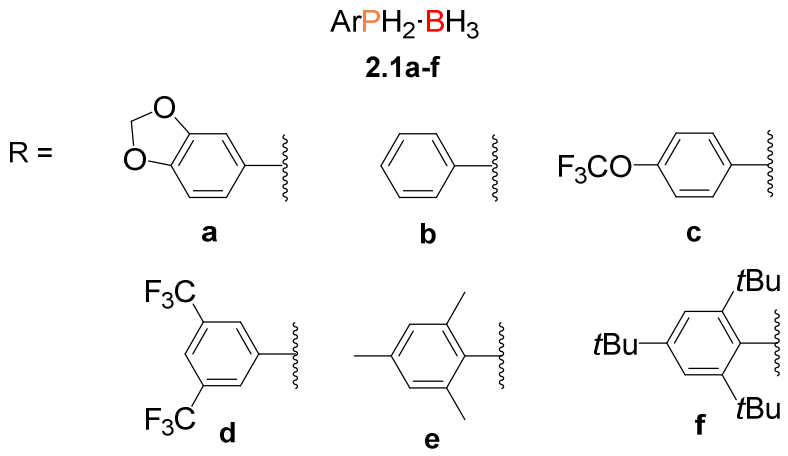

Figure 2.1. Phosphine–borane monomers **2.1a-f**.

The product was subsequently deprotected and reacted with Li[BH_4] to give phosphine–borane adducts **2.1a**, **2.1c**, **2.1d** and **2.1f**. The remaining adducts **2.1b** and **2.1e** were isolated from the reaction between commercially available primary phosphines RPH_2 and BH_3·THF (THF = tetrahydrofuran) (Scheme 2.2). The resulting monomers were characterised by NMR spectroscopy, which afforded spectra consistent with the assigned structures (Table S2.1). For example, the ^{31}P NMR spectrum of **2.1a** consists of a broad triplet at −46.3 ppm, and a doublet of quartets at −43.5 ppm was observed by ^{11}B NMR spectroscopy. In the case of **2.1e** and **2.1f**, where substitution on the aromatic ring was present in the *ortho*-position, the ^{31}P and ^{11}B NMR signals were shifted to higher and lower fields, respectively. By ^{1}H NMR spectroscopy, the chemical shifts for the P–H protons for **2.1a-d** revealed a trend whereby the more electron-withdrawing the aromatic ring, according to its corresponding Hammett parameter, the lower the field of the P–H resonance (Table S2.1).[21]

Single, colourless crystals suitable for X-ray analysis were obtained for **2.1a** and **2.1c-e** by layering a THF solution with either hexanes or pentane at −40 °C. As expected, the structures of **2.1a**, and **2.1c-e** contained tetrahedral phosphorus and boron centres, with

similar P–B bond lengths (**2.1a** 1.922(4) Å, **2.1c** 1.914(8) Å, **2.1d** 1.920(5) Å and **2.1e** 1.925(3) Å) within the range typical for P–B single bonds (1.90 – 2.00 Å) (Figure 2.2).[22]

Method 1: 2.1a, 2.1c, 2.1d, 2.1f

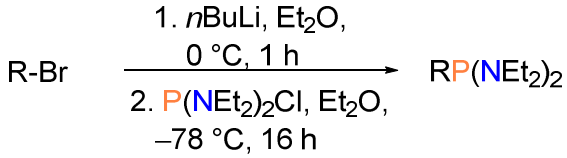

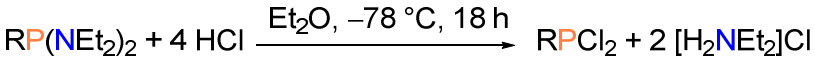

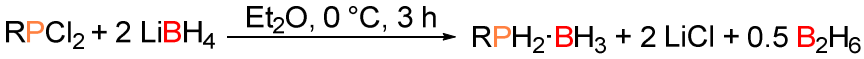

Method 2: 2.1b, 2.1e

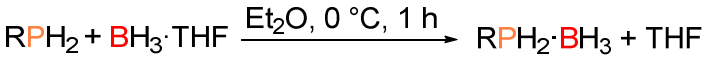

Scheme 2.2. Synthesis of phosphine–borane monomers **2.1a-f**. Method 1 was used to synthesise **2.1a**, **2.1c**, **2.1d** and **2.1f**. Method 2 was used to synthesise **2.1b** and **2.1e**.

Interestingly, close intermolecular contacts were found in the structures of **2.1a**, **2.1c** and **2.1d**. The structure of **2.1a** contained π-π interactions between pairs of molecules, and in addition a short contact (P(1)–H(1B)···O(1) 2.82(3) Å) was identified (Figure S2.1).

The monomer, **2.1c** crystallised with two molecules in the asymmetric unit (z' = 2) and π-π stacking interactions were identified between the aryl rings creating staggered stacks approximately along the *a*-axis direction (Table S2.4). Short intermolecular P–H···H–B contacts were found in **2.1c**, with distances less than the sum of van der Waals radii of two hydrogen atoms (2.4 Å) (Figure 2.3).

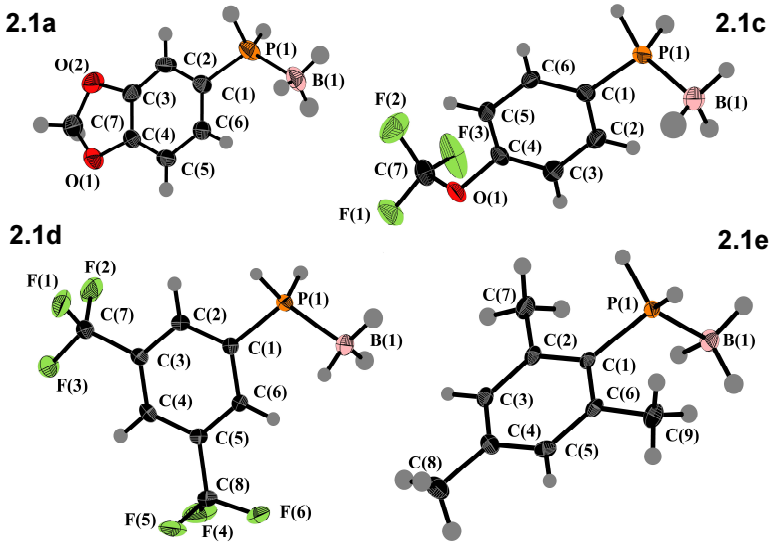

Figure 2.2. Molecular structures for **2.1a**, **2.1c**, **2.1d** and **2.1e** (thermal ellipsoids set at the 50% probability level). Selected bond distances (Å): **2.1a**: B(1)–P(1) 1.922(4); **2.1c**: B(1)–P(1) 1.914(8); **2.1d**: B(1)–P(1) 1.920(5); **2.1e**: B(1)–P(1) 1.925(3).

Furthermore, one P–H bond was found to be in short contact with an oxygen atom (P(2)–H(2B)···O(2), H(2B)···O(2) 2.58(6) Å), which is within the range of a weak electrostatic hydrogen bond interaction (2.2 – 3.2 Å) (Figure S2.2).[23] These close O···H contacts found in **2.1a** and **2.1c** reflect the protic nature of P–H hydrogen. The solid state structure of **2.1d** was also found to contain intermolecular P–H···H–B contacts of 2.42(6) and 2.52(8) Å, close to the sum of the Van der Waals radii of two H atoms (Figure S2.3). In all the instances of short P–H···H–B intermolecular contacts in **2.1c** and **2.1d**, the B–H···H angle (100 – 148°, average: 117°) is smaller relative to the P–H···H angle (118 – 167°, average: 139°), which is consistent to previous reports involving phosphine–boranes and the more thoroughly studied amine–boranes.[24] In the related $NH_3{\cdot}BH_3$, the non-linear N–H···H–B interaction was attributed to charge distribution, such that unfavourable dipole interactions are minimised.[25]

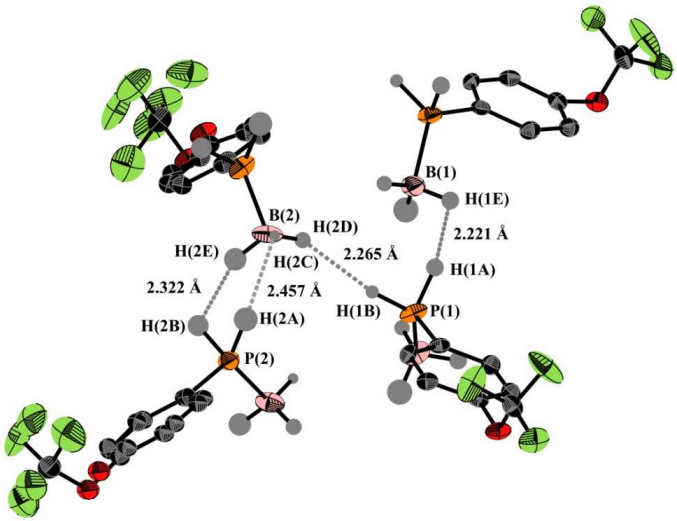

Figure 2.3. Intermolecular P–H···H–B solid state contacts between units of **2.1c**. H atoms on Ph rings have been omitted for clarity and thermal ellipsoids set at the 50% probability level. Selected intermolecular interaction bond lengths (Å) and angles (°): H(1E)···H(1A) 2.22(9), H(1B)···H(2D) 2.27(7), H(2C)···H(2A) 2.46(7), H(2E)···H(2B) 2.3(1), P(1)–H(1B)···H(2D) 167(4), P(1)–H(1A)···H(1E) 144(4), P(2)–H(2B)···H(2E) 118(4), P(2)–H(2A)···H(2C) 129(3), B(2)–H(2E)···H2B 126(5), B(2)–H(2C)···H(2A) 112(3), B(2)–H(2D)···H(1B) 148(5), B(1)–H(1E)···H(1A) 109(4).

In contrast to **2.1a**, **2.1c** and **2.1d**, no analogous intermolecular contacts could be found in the structure of **2.1e**, which we attribute to the increased steric congestion imposed by the mesityl group. This is supported by the report that the primary alkyl phosphine–borane menthylPH$_2$·BH$_3$, does contain short P–B contacts, with the corresponding H···H distances between two monomer units between 2.6 and 2.7 Å.[26] This suggests that intermolecular interactions are still present even for phosphine–boranes with a P–H bond of lower acidity. No intermolecular B–H···H–P contacts could be found for crystallographically characterised secondary phosphine–boranes, such as Mes$_2$PH·BH$_3$ and *p*-CF$_3$(C$_6$H$_4$)$_2$PH·BH$_3$.[10g,27] These examples suggest that the steric demands of the R group induces the molecules to adopt a solid state structure such that no P–H···H–B contacts can form. This would explain that whilst **2.1e** contains a P–H bond of higher polarity than menthylPH$_2$·BH$_3$, the steric demands of the mesityl groups dictate the conformation and packing.

2.3.2 Iron-catalysed dehydrocoupling of the primary phosphine–borane adducts, $RPH_2{\cdot}BH_3$: Polymer synthesis and characterisation

The newly prepared polymers, **2.2a** and **2.2c-e** were synthesised under identical conditions to the previously reported Fe-catalysed formation of **2.2b**.[10i] This involved heating toluene solutions of $RPH_2{\cdot}BH_3$ (R = **2.1a-f**), and 5 mol% **I** at 100 °C for 24 h under N_2 (Scheme 2.3). Consistent with previous work, a colour change from red to yellow was observed within 5 min of heating, consistent with the formation of the intermediate $[CpFe(CO)_2(RPH{\cdot}BH_3)]$ (R = **a-f**).[10i] After 24 h, complete consumption of monomer and subsequent formation of polyphosphinoborane, $[RPH–BH_2]_n$ (**2.2a-e**) was confirmed by *in situ* ^{11}B and ^{31}P NMR spectroscopy. Furthermore, in the reaction mixtures small amounts of the free phosphine RPH_2 were detected by ^{31}P NMR spectroscopy. Monomer **2.1f** did not undergo dehydrocoupling to form **2.2f**.

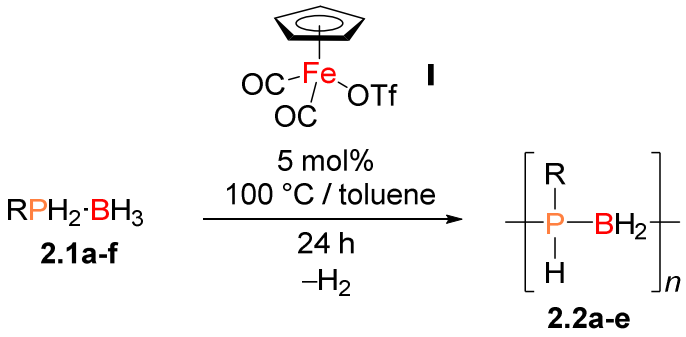

Scheme 2.3. Typical dehydrocoupling reaction for the dehydropolymerisation of monomers **2.1a-f** to form the polyphosphinoboranes **2.2a-e** (**2.2d** was formed using 2 mol% **I**).

Polymers **2.2c** and **22.d**, featuring fluorinated substituents, were purified by precipitation from Et_2O into cold (−78 °C) pentane, whilst **2.2a** and **2.2e** were purified by dissolution in minimal THF and precipitation into pentane at −78 °C.[10i] The polymers obtained were pale yellow/off white solids, where the pale yellow colour likely originates from residual Fe species (Figure S2.8, S2.16, S2.24, S2.29). The presence of catalyst-derived Fe following polymer workup was confirmed by atomic absorption spectroscopy (AAS). A sample of **2.2b**

was added to a solution of nitric acid before being analysed after 24 h. The results revealed an average of 4.5 atoms of Fe per polymeric chain (0.4 wt%). Samples of **2.2a**, **2.2b** and **2.2e** (2 mg mL^{-1}) were also drop cast onto carbon coated Cu grids and analysed by EDX (EDX = energy dispersive X-ray spectroscopy). Areas of sample also contained detectable trace Fe (**Figure S2.50-S2.53**). Polymers **2.2a-e**, could be handled in air, consistent with previous reports on **2.2b** and **2.2e** prepared using precious metal precatalysts.[10i, 10k] Further precipitation steps led to a decrease in the intensity of the yellow colour, however these extra steps reduced the isolated yield of the polymer. Complete removal of encapsulated solvent from the polymers was found to be a challenge, typically requiring heating of the sample (40 °C) *in vacuo* for several days. To aid in the removal of residual solvent, which was typically THF or toluene, the polymers could be dissolved in a minimal amount of dichloromethane, and reprecipitated into cold pentane (−78 °C). In the case of **2.2d**, heating the sample to 60 °C *in vacuo* for several days was required to completely remove encapsulated solvent, otherwise ≈10 wt% toluene remained, as detected by thermogravimetric analysis (TGA). Upon drying, the polymers displayed a slower dissolution rate, typically requiring vigorous stirring for redissolution in either dichloromethane or THF.

At a catalyst loading of 5 mol% of **I**, the dehydropolymerisation of **2.1d** after 24 h of heating at 100 °C in toluene led to formation of a precipitate. This gummy insoluble solid swelled upon solvent addition, consistent with a non-negligible degree of crosslinking (Scheme 2.4). The supernatant was separated from the gel, concentrated and added to cold pentane (−78 °C) which caused a yellow solid to precipitate in 10% yield. A sample of the solid was analysed by GPC and was found contain polymeric material (M_n = 77,000 g mol^{-1}, PDI = 1.35) (Figure S2.35). By reducing the catalyst loading to 2 mol%, isolation of a yellow solid, which did not give a gel in chloroform, was possible and in higher yield (31%). The higher yielding material synthesised at 2 mol% catalyst loading was used for all subsequent analysis. The formation of gels was also found for polymers synthesised by Rh methods at

high degrees of conversion, where a significant degree of cross-linking was suggested to have taken place.[10b] Polymer **2.2d** contains the most electron withdrawing substituent at phosphorus and therefore the most activated P–H bond, which increases the likelihood of cross-linking *via* further H_2 loss leading to formation of gels. By contrast, polymers **2.2a-c** and **2.2e** synthesised through the use of precatalyst **I** did not form solvent swellable cross-linked gels in solvents such as chloroform, THF and dichloromethane. These observations suggest an increased linearity for the polymers synthesised using the Fe-precatalyst **I**, compared to those prepared with Rh catalysts under melt conditions, which is consistent with their lower PDI values.[10d]

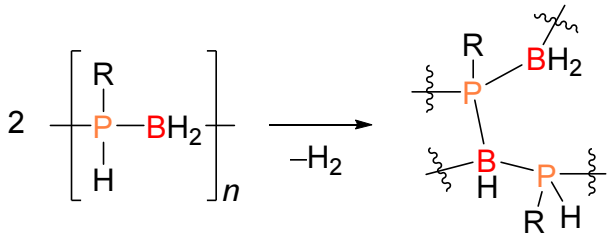

Scheme 2.4. Possible route to crosslinking polyphosphinoborane chains between B and P, enabled by interchain loss of H_2.

Tolerance of catalyst **I** to sterically demanding substituents on the phosphine–borane monomers was explored by comparing the dehydrocoupling reactions of **2.1b**, **2.1e** and **2.1f**, where increasing steric pressure was introduced at the positions *ortho*- and *para*- to the phosphorus on the aromatic ring. While monomers **2.1b** and **2.1e** were successfully converted to polymers **2.2b** and **2.2e**, respectively, no dehydrocoupling was observed for **1f**. Addition of **2.1f** to 5 mol% of **I** in toluene and heating to 100 °C led to a colour change from red to yellow after 1 h. Over the course of 22 h, monitoring the reaction by ^{31}P NMR spectroscopy, only an increase in the amount of free phosphine 2,4,6-(tBu)$_3$C$_6$H$_2$PH$_2$ was detected (Figure S2.32). The ^{11}B and ^{31}P NMR chemical shifts for the isolated samples of polymers **2.2a-e** are summarised in Table 2.1. Consistent with previous reports on polymers **2.2b** and **2.2e**, the ^{11}B NMR chemical shift, found at −35 ppm, was broad mainly

due to the quadrupolar nature of the ^{11}B nucleus **2.2a-e**.[10i, 10k] The ^{31}P NMR chemical shift was found between −46 and −49 ppm for **2.2a-d**, and at −74 ppm for **2e**. The different aromatic groups in **2.2a-d** did not have an obvious impact on the ^{11}B and ^{31}P NMR chemical shifts, except when the polymer contained a substituent in the *ortho*- position (**2.2e**). The expected P–H coupling by ^{31}P NMR spectroscopy could only be resolved for **2.2b** ($^{1}J_{PH}$ = 349 Hz) and **2.2e** ($^{1}J_{PH}$ = 350 Hz).

Furthermore, the ^{31}P NMR spectra of **2.2c** and **2.2d** contained a peak that resembled a virtual 1:2:1 triplet at 46–49 ppm (Figure S2.13 and S2.21). This pattern is consistent with the formation of an atactic polymer, with resolution of the triad structure, which was also reported for primary polyphosphinoboranes, $[p\text{-}(CF_3)C_6H_4PH–BH_2]_n$ and $[t\text{BuPH–}BH_2]_n$.[10g,10j] The triad configurations involves four distinct environments composed of two successive dyads, *mm*, *mr*, *rm* and *rr*, where *m* are the meso (adjacent units of the same configuration) and *r* the racemic (adjacent units of opposite configuration) forms. Since *mr* and *rm* configurations are mirror images, they are indistinguishable by NMR and this leads to the expected distribution 1:2:1 in the ^{31}P NMR spectrum.[28] This fine structure could not be resolved spectroscopically for **2.2a**, **2.2b** or **2.2e**. Compared with the NMR spectra of the monomers **2.1a-e**, the ^{11}B NMR spectra of **2.2a-e** revealed downfield shifted resonances. The P–H chemical shift in the ^{1}H NMR spectrum provided further contrast, where a doublet was found at a higher field than in the monomer. For example, the chemical shift for the PH_2 protons of **2.1a** was found at 5.47 ppm, whilst a value of 4.39 ppm was found for **2.2a**.

2.3.3 Molar mass characterisation

Electrospray ionisation mass spectrometry (ESI-MS) was performed on solutions of **2.2a**, **2.2c**, **2.2d** and **2.2e** in CH_2Cl_2. A repeating pattern corresponding with successive loss of [RPH–BH_2] units, however was only detected up to 2,500–4,000 g mol^{-1} (Figure S2.41-

S2.44). The molecular weight of these polymers was also investigated by GPC, which indicated that the materials were of high molecular weight polymers (Table 2.1). Previous work involving polyphosphinoboranes, analysed by GPC in THF, revealed problems concerning molecular weight characterisation due to facile aggregation and/or adsorption of the polymer chains onto the GPC column solid-phase material.[10d] The problems were resolved through increasing the ionic strength of the eluent through use of $[Bu_4N]Br$, which we have previously found effective in reducing column adsorption effects. By studying variations in the concentration of samples it was evident that poly(phenylphosphinoborane) showed no column adsorption.[10d] Thus, for **2.2a** and **2.2e** the concentration of the GPC sample also had no effect on the elution volume, and therefore the calculated PDI or molecular weight (Figure S2.9 and S2.31). However, for the polymers containing fluorinated groups, **2.2c** and **2.2d**, a reversible, inverse dependency of elution volume on concentration was observed (Figure S2.17 and S2.25).

This GPC behaviour is reminiscent to that of polyelectrolytes, where the lower concentration causes larger intrachain repulsion, thereby increasing the observed hydrodynamic radius.[29,30] Although, there is no clear explanation at this time, we postulate that the presence of electron-withdrawing substituent on phosphorus enhances the existing polarisation of the P–B backbone and results in a partial negative charge at the polymer periphery (Scheme 2.5).[31]

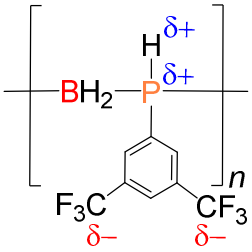

Scheme 2.5. Schematic representation of electron density for polymers **2c** and **2d**.

Formation of polymer **2.2e** has been previously been catalysed by [IrH_2(POCOP)].[10k] Under the optimally reported conditions, which involved a 2.5 mol% catalyst loading and heating of the reaction mixture to 100 °C in toluene for 24 h, polymeric material (M_n = 33,000 g mol^{-1}) with a PDI of 1.8 was isolated. In the case of **I**, a slightly higher molecular weight (M_n = 95,000 g mol^{-1}) polymer with a PDI of 1.14 was formed.

Table 2.1. Summary of ^{11}B NMR and ^{31}P NMR spectroscopy and GPC results for polyphosphinoboranes **2.2a-e**.

Polymer	^{11}B shift[a] (ppm)	^{31}P shift[a] (ppm) ($^1J_{PH}$ (Hz))	M_w (g mol^{-1})[b]	M_n (g mol^{-1})[b]	PDI	DP_n
2.2a	−35	−47 (350)	26,000	12,000	2.17	72
2.2b[c]	−35	−49 (349)	72,000	45,000	1.60	369
2.2c[d]	−35	−49 (350)	107,000	79,000	1.35	383
2.2d[d]	−35	−46 (360)	262,000	209,000	1.25	810
2.2e	−35	−74 (335)	108,000	95,000	1.14	579

[a]NMR spectroscopy was carried out in $CDCl_3$. $^1J_{PH}$ values were calculated by ^1H NMR spectroscopy; [b]2 mg mL^{-1}; [c]Ref. 10i; [d]A concentration based-effect was observed for GPC results, see main text.

Catalyst free, thermal dehydropolymerisation occurred for **2.1a-e** in solution. Thus, heating samples of **2.1a-e** in toluene to 100 °C for 24 h under N_2 resulted in incomplete conversion (70 – 90%) and formation of only low molecular weight (M_n = < 2,300 – 4,500 g mol^{-1}) (Figure S2.36-S2.40) and polydisperse (PDI = 2.0–8.0) material. The metal-catalysed route led to complete consumption of monomer after 24 h leading to formation of a polyphosphinoborane product that had a higher molecular weight and a lower polydispersity. These results suggest that non-metal catalysed reactions can also occur under the conditions used for the metal-catalysed dehydropolymerisation and these may explain the detection of the detected low-molecular weight material for **2.2a-e**.[9b]

2.3.4 Thermal Transitional Behaviour and Stability of Polymers 2.2a-e

The thermal transition behaviour of the polyphosphinoboranes **2.1a**, **2.1c**, **2.1d** and **2.1e** was investigated by differential scanning calorimetry (DSC) and thermogravimetric analysis (TGA) (Table 2.2). Glass transitions temperatures for **2.2a**, **2.2c** and **2.2d** could be determined by DSC, at a scan rate of 10 °C min^{-1} (Figure S2.45-S2.47). The observed glass transition temperature of 82 °C for **2.2a**, is higher than that previously reported for **2.2b** (38 °C). This could be due to increased rigidity of the polymer chain, which is induced by the presence of the –OCH_2O– substituent. Polymer **2.2c** was found to have a lower glass transition temperature of 29 °C relative to that of **2.2b**. The lower glass transition temperature for the former material might be explained by the smaller barrier of rotation for the protruding (trifluoromethoxy)ether group which has the effect of introducing chain flexibility and additional free volume.[32] The T_g of **2.2d** (52 °C), higher than **2.2b** (38 °C), is consistent with the trend detected when comparing the organic polymers polystyrene (105 °C) and poly(2,5-bis(trifluoromethyl)styrene) (116 °C).[33,34] For **2.2e**, no glass transition was observed below ≈135 °C, above which decomposition of the polymer occurred. Compared with polystyrene, the glass transition temperature of **2b** is considerably lower. This difference has previously been attributed to the higher degree of torsional flexibility in the polymer main chain as a result of the longer main chain P–B bonds.[10d]

Table 2.2. Summary of the thermal properties, T_g, $T_{5\%}$, and ceramic yield of **2.2a-e**.

Polymer	R Substituent	T_g (°C)	$T_{5\%}$[a] (°C)	Ceramic Yield[b] (%)
2.2a	3,4-$(OCH_2O)C_6H_3$	82	210	46
2.2b[c]	Ph	38	180 (200[d])	55 (76[d])
2.2c	*p*-$(CF_3O)C_6H_4$	29	170	24
2.2d[e]	3,5-$(CF_3)_2C_6H_3$	52	150 (200[d])	20 (47[d])
2.2e	2,4,6-$(CH_3)_3C_6H_2$	>133	160	21

[a]Temperature at 5% weight loss; [b]Ceramic yields were measured at 700 °C; [c]Ref. 10i; [d]Recorded under a blended air mix (N_2/O_2, 79:21%); [e]Samples contained toluene (<10 wt%).

The thermal stability of **2.2a-e** was further investigated by TGA under an N_2 atmosphere, at a heating rate of 10 °C min^{-1} (Figure 2.4).

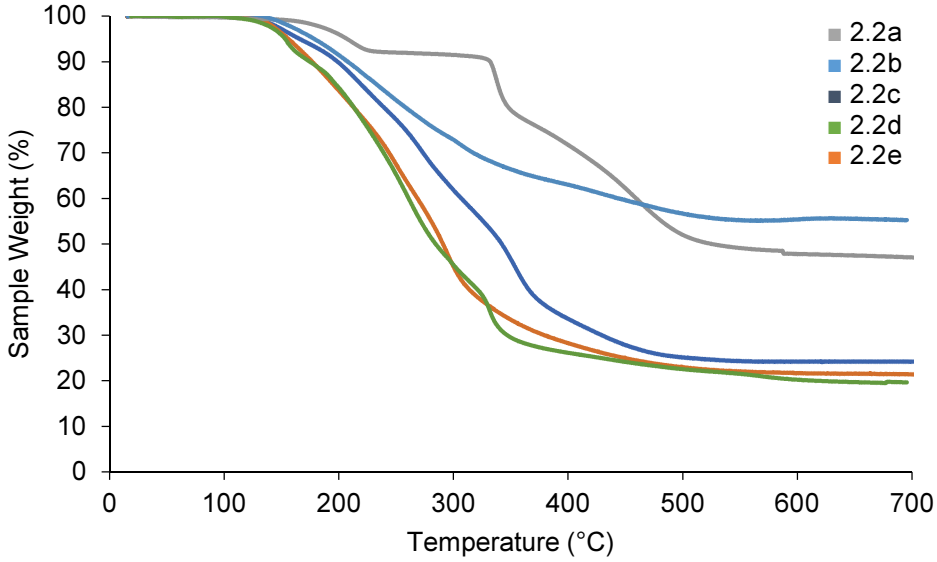

Figure 2.4. TGA thermograms of **2.2a** (■), **2.2b** (■), **2.2c** (■), **2.2d** (■) and **2.2e** (■) (heating rate: 10 °C min^{-1}).

The onset of weight loss for **2.2a** occurred at around 160 °C, and material showed a $T_{5\%}$ (temperature at which the polymer has lost 5% of its original weight) at 210 °C. Minimal weight loss occurred between 230 and 320 °C (< 2 wt%) for **2.2a**, after which a further 30% of mass was lost until 500 °C. For polymers **2.2b**, **2.2c** and **2.2e** the onset of weight loss occurred around 130 °C, after which the majority of mass was lost up until 500 °C. It has previously been suggested that the low thermal stability of these polymers can be explained by the release of a second equivalent of H_2 leading to further decomposition pathways.[10d] Initial weight loss for **2d** was found to occur ca.140 °C, with the majority of loss occurring up to 500 °C. Samples of polymer **2b** prepared with the Fe precatalyst showed a lower temperature for weight loss ($T_{5\%}$ = 180 °C) compared to those synthesised with Rh(I) mediation ($T_{5\%}$ = 240 °C).[10d] This is a likely consequence of a more branched structure in the latter case which would hinder loss of volatile material.

The ceramic yields after heating to 700 °C were also found to be lower than for previous Rh-based dehydropolymerisation products. Ceramic yields for polymers prepared using a Rh precatalyst were typically in the range of 75 – 80% for aryl polymers and 35 – 45% for polymers containing alkyl substituents at phosphorus.[10d] These are noticeably higher ceramic yields than those found for polymers prepared using Fe-precatalyst **I** (Table 2.2). This is especially noticeable when comparing the ceramic yield of **2.2b** between the Rh (75 – 80%) and Fe (55%) catalytic methods.[10d] The lower ceramic yields in this report are consistent with the presence of mainly linear polymeric material since, as noted above, branched polymeric chains hinder the loss of volatile products. In addition to thermal analysis under N_2, polymers **2.2b**, **2.2d** and **2.2e** were analysed under a blended air mix (O_2/N_2, 79:21%) (Figure S2.48-S2.49). This had the effect of increasing the ceramic yields of the polymeric materials, but also slightly increasing the $T_{5\%}$ temperature at which weight loss was observed (Table 2.2).

2.3.5 Soft lithography of polyphosphinoboranes and contact angle measurements

The ability to fabricate polymers into patterns is of key importance for many potential applications.[35] Soft lithography is an attractive approach to achieve this objective and has received widespread attention as a result of the relative simplicity of the method. To further elaborate on our earlier findings that poly(phenylphosphinoborane) could be patterned on silicon wafers using soft lithography techniques, a similar procedure was used for **2.2e**; chosen for the large difference in T_g (> 135 °C) compared to **2.2b** (38 °C).[10i]

The procedure involved drop casting a 2 mg mL^{-1} THF solution of **2.2e** on a clean Si wafer, before patterning using a polydimethylsiloxane stamp at 150 °C for 5 min. Imaging by scanning electron microscopy revealed excellent retention of shape and crisp detail along edges (Figure 2.5). However, as anticipated for **2.2e** on the basis of the higher T_g compared

to **2.2b**, the resulting material contained noticeably more crack features which are present throughout the sample. Since **2.2c** and **2.2d** contain fluorinated groups, we anticipated that thin films of these polymers would display hydrophobic behaviour. Thin films of **2.2a-e** were formed by spin coating a 5 mg mL^{-1} THF solution onto a glass slide, and the advancing water droplet contact angles were subsequently obtained (Figure 2.6).

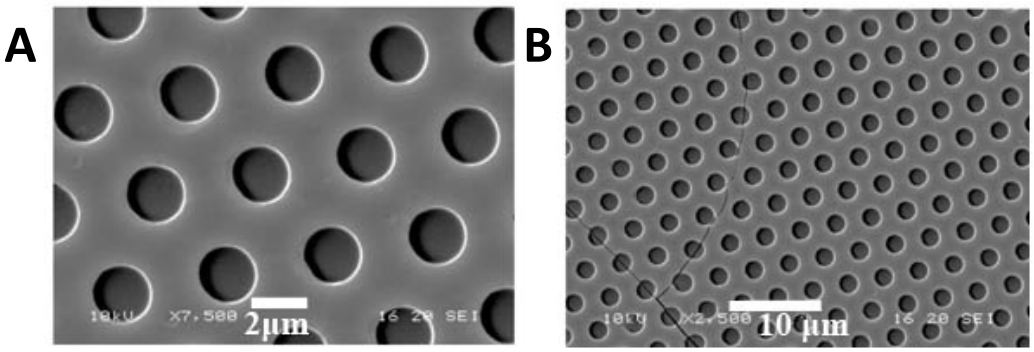

Figure 2.5. Scanning electron microscopy of patterned polymer **2.2e**, scanning electron micrograms obtained with 2 µm (A) and 10 µm (B) scale bars shown.

As expected, the contact angles of 101° and 97° (±2°) obtained for **2.2c** and **2.2d** suggested a hydrophobic surface. These advancing angles are similar to those found for poly(chlorotrifluoroethylene) (99°), but smaller than for the widely used fluorinated polymer, poly(tetrafluoroethylene) (109°).[36] Thin films of **2.2a**, **2.2b** and **2.2e** were found to contain hydrophilic surfaces as supported by their advancing contact angles of 64°, 70° and 78° (±2°), respectively.

The surfaces of polyphosphinoboranes in general, appear to be more hydrophilic in nature than their organic counterparts, highlighted by comparison between **2.2b** (70°) and the organic analogue polystyrene (87°).[37] This is likely to be due to the difference in polarity of the P–H and B–H bonds in the polymer backbone compared with C–H bonds.

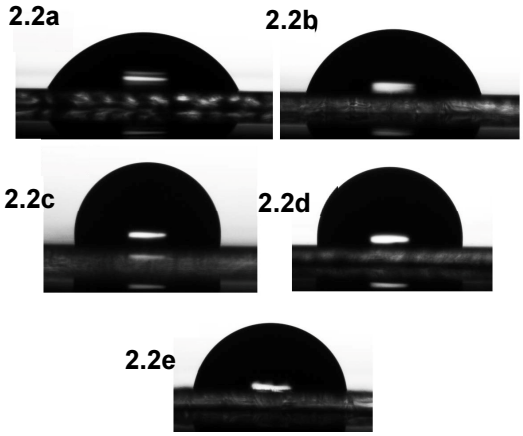

Figure 2.6. Still frames of 2 μL droplets of deionised water deposited on thin films of **2.2a-e**.

2.4 Conclusions

The scope of the Fe complex **I** as a precatalyst for the dehydropolymerisation of phosphine–boranes **2.1a-e** has been explored. Formation of polymers **2.2a-e**, was achieved in solution at 100 °C in under 24 h in the presence of 5 mol% **I**, however, the bulky monomer **2.1f** was resistant to polymerisation under these conditions. GPC analysis of polymers **2.2a-e** revealed the formation of high molecular weight polymeric material, and the presence of the expected repeat unit was confirmed by ESI-MS. A concentration dependence in the cases of polymers **2.2c** and **2.2d** was detected by GPC analysis. This behaviour is reminiscent of polyelectrolytes and was tentatively attributed to the build up of residual charge on the protruding electronegative organic substituent at phosphorus. Analysis of the thermal properties of polymers **2.2a-e** revealed glass transition temperatures that were lower than their organic analogues. Furthermore, these materials possessed lower thermal stability compared with polyphosphinoboranes synthesised by previous Rh based methods. Thin film patterning and contact angle measurements indicate that polymer properties are tuneable by altering the substituents at phosphorus. Addition of fluorine containing functional groups, as with the case of organic polymers, had the expected effect of increasing the hydrophobicity of the surface. Ongoing work involves a mechanistic investigation of the dehydropolymerisation process, optimisation of the reaction with a view to scale up, and further characterisation of the properties of these polymers. We are also exploring routes to polyphosphinoboranes with non-hydrogen substituents at phosphorus, which should show enhanced thermal stability, and potential behaviour as flame retardant materials will be investigated.

2.5 Supporting Information

2.5.1 General procedures, reagents, and equipment.

All manipulations were carried out under an atmosphere of nitrogen gas using standard vacuum line and Schlenk techniques, or under an atmosphere of argon within an M. Braun glovebox. $[CpFe(CO)_2OTf]$[38] (**I**), and $MesPH_2{\cdot}BH_3$[10k] (**2.1e**) were synthesised by literature procedures. The following reagents, $LiBH_4$, $RPCl_2$ (R = **a**, **c**, **d**), RPH_2 (R = **b**, **e**, **f**), and $BH_3{\cdot}THF$ were purchased from Sigma Aldrich. Where stated, anhydrous solvents were dried *via* a Grubbs design solvent purification system.[39] Anhydrous $CDCl_3$ was purchased from Sigma Aldrich and stored over activated molecular sieves (4 Å). NMR spectra were recorded using Oxford Jeol Eclipse 300, 400, Bruker cryo 500 MHz spectrometers. ^1H NMR spectra were calibrated using residual protio signals of the solvent: (δ $^1H(CHCl_3)$ = 7.24). ^{13}C NMR spectra were calibrated using the solvent signals (δ $^{13}C(CDCl_3)$ = 77.0; δ $^{13}C(C_6D_6)$ = 128.0). ^{11}B and ^{31}P NMR spectra were calibrated against external standards (^{31}P: 85% H_3PO_4 (aq) (δ ^{31}P = 0.0); ^{11}B: $BF_3{\cdot}OEt_2$ (δ ^{11}B = 0.0)). GPC was performed on a Malvern RI max Gel Permeation Chromatograph, equipped with an automatic sampler, a pump, an injector, and inline degasser. The columns (T5000) were contained within an oven (35 °C) and consisted of styrene/divinyl benzene gels. Sample elution was detected by means of a differential refractometer. THF (Fisher), containing 0.1 wt% [nBu$_4$N][Br], was used as the eluent at a flow rate of 1 mL min^{-1}. Samples were dissolved in the eluent (2 mg mL^{-1}) and filtered with a Ministart SRP15 filter [poly(tetrafluoroethylene) membrane of 0.45 µm pore size] before analysis. The calibration was conducted using monodisperse polystyrene standards obtained from Aldrich. The lowest (highest) molecular weight standard used was 2,300 (994,000) g mol^{-1}. Single crystal X-ray diffraction experiments on were carried out at 100(2) K, except **2.1a** which was collected at 200(2) K, structures **2.1a** and **2.1c** were collected on a Bruker Apex II diffractometer using Mo Kα radiation (λ = 0.71073 Å) while **2.1d** and **2.1e** were collected on a Bruker Microstar diffractometer using Cu Kα radiation

(λ = 1.54178 Å). Data collection was performed using a CCD area detector. Structures **2.1a** and **2.1d** were solved using SHELXS,[40] **2.1c** was solved using Superflip,[41] and **2.1e** was solved using olex2.solve.[42] All of the structures were refined against F^2 in ShelXL in Olex2.[43] Structures **2.1c** and **2.1e** were refined at two component twins. Crystallographic data collection and refinement details are listed in Table S2.3. All cif-files are available online from the Cambridge Crystallographic Data Centre (see CCDC numbers 1500875–1500878). Contact angles were measured on a Krüss drop shape analyser (DSA100) at 25 °C. DSC was measured on a Thermal Advantage DSCQ100 at 10 °C min^{-1} and TGA was measured on a Thermal Advantage TGAQ500 at 10 °C min^{-1} under N_2, and where stated under a blended air mix (N_2/O_2, 79:21%). DSC and TGA results were analysed using WinUA V4.5A by Thermal Advantage. Powder diffraction experiments were performed on a Bruker D8 Advance diffractometer with Cu-Kα radiation (λ = 1.5406 Å) and measurements were taken at room temperature. The material was placed on a low background silica holder and measurements were run between 5 and 50° 2θ with a step size of 0.01° and 10 seconds per step, with the sample spinning at a rate of 15 rpm. The ESI-MS spectra were obtained using a Waters Synapt G2S instrument equipped with a nanospray ionisation module (Advion TriVersa Nanomate). Solutions (40 μL) of approximately 1 mg mL^{-1} were loaded under ambient conditions into the sample tray, and aliquots of 5 μL were introduced into the spectrometer using a spray voltage of 1.5 kV. Positive (+70 V) and negative (−125 V) ion spectra were recorded at a rate of 1 scan $second^{-1}$ and summed to obtain the final spectra.

2.5.2 Synthesis of phosphine–boranes (2.1a-f)

2.5.2.1 Synthesis of 3,4-$(H_2CO_2)C_6H_3PH_2{\cdot}BH_3$ (2.1a)

To a suspension of $LiBH_4$ (0.234 g, 10.7 mmol) in diethyl ether (100 mL) a solution of 3,4-$(H_2CO_2)C_6H_3PCl_2$ (1.200 g, 5.38 mmol) in diethyl ether (20 mL) was added dropwise at 5 °C. The reaction mixture was stirred for 3 h at 5 °C, and the volatiles were subsequently removed under reduced pressure. Hexanes (150 mL) was added, the white suspension was filtered through celite, and then taken to dryness, yielding **2.1a** as a colorless solid. Colourless crystals of **2.1a** were obtained by dissolving in minimal hexanes and cooling to −40 °C.

Yield = 0.620 g (69%).

^{1}H NMR (400 MHz, $CDCl_3$): δ (ppm) 0.83 (m, 3H, $^{1}J_{BH}$ = 100 Hz, B*H*), 5.47 (dq, 2H, $^{1}J_{PH}$ = 372 Hz, $^{3}J_{HH}$ = 8 Hz, P*H*), 6.02 (s, 2H, OCH_2O), 6.8 – 7.2 (m, 3H, Ar*H*).

^{11}B NMR (128 MHz, $CDCl_3$): δ (ppm) −43.5 (dq, $^{1}J_{BH}$ = 100 Hz, $^{1}J_{BP}$ = 38 Hz).

^{31}P NMR (161 MHz, $CDCl_3$): δ (ppm) −46.3 (br. t, $^{1}J_{PH}$ = 372 Hz).

^{13}C NMR (101 MHz, $CDCl_3$): δ (ppm) 101.9 (s, O*C*H$_2$O), 109.5(d, J_{PC} = 14 Hz, Ar), 111.6 (d, $^{1}J_{PC}$ = 61 Hz, *C*P), 113.0 (d, J_{PC} = 12 Hz, Ar), 129.0 (d, J_{PC} = 11 Hz, Ar), 148.6 (d, J_{PC} = 16 Hz, Ar), 151.2 (d, J_{PC} = 2 Hz, Ar).

ESI-MS (m/z): Calc. 191.0405 [M + Na], found 191.0407 [M + Na].

2.5.2.2 Synthesis of $PhPH_2{\cdot}BH_3$ (2.1b)

$PhPH_2{\cdot}BH_3$ (**2.1b**) was synthesised according to a modified literature procedure.[44] To a round bottom Schlenk flask containing $PhPH_2$ (8.500 g, 77 mmol) and THF (50 mL), cooled to 0 °C, was added $BH_3{\cdot}$THF (77 mL, 77 mmol) dropwise. After 15 min the reaction mixture was allowed to warm to room temperature and was stirred for a further 6 h. The product was obtained by drying the evaporation of the solvent and volatiles *in vacuo* to yield the colourless liquid **2.1b**. Yield = 5.481 g (57%). Spectroscopic data were consistent with reported literature values.[43]

2.5.2.3 Synthesis of *p*-$(CF_3O)C_6H_4PH_2{\cdot}BH_3$ (2.1c)

A solution of *p*-$(CF_3O)C_6H_3PCl_2$ (1.500 g, 5.70 mmol) in Et_2O (20 mL) was added to a suspension of $LiBH_4$ (0.248 g, 11.4 mmol) in diethyl ether (100 mL) at 5 °C. The reaction mixture was then stirred for 3 h at 5 °C, and the volatiles were subsequently removed under reduced pressure. To dissolve the product, hexanes (150 mL) was added, and insoluble salt was removed by filtration. Evaporation of the volatiles *in vacuo* yielded **2.1c** as a colorless solid. Colourless crystals of **2.1c** were obtained by dissolving in minimal hexanes and cooling to −40 °C.

Yield = 0.800 g (67%).

^{1}H NMR (400 MHz, $CDCl_3$): δ (ppm) 0.84 (m, 3H, $^1J_{BH}$ = 102 Hz, B*H*), 5.67 (dq, 2H, $^1J_{PH}$ = 371 Hz, $^3J_{HH}$ = 8 Hz, P*H*), 6.8 – 7.3 (m, 4H, Ar*H*).

^{11}B NMR (128 MHz, $CDCl_3$): δ (ppm) −43.3 (qd, $^1J_{BH}$ = 102 Hz, 31.4 Hz).

^{31}P NMR (161 MHz, $CDCl_3$): δ (ppm) −51.7 (m).

^{19}F NMR (376 MHz, $CDCl_3$): δ (ppm) −58.5.

^{13}C NMR ($CDCl_3$): 118.7 (d, $^1J_{CP}$ = 58 Hz, *C*P), 121.6 (d, J_{CP} = 10 Hz, Ar), 121.8 (s, Ar), 135.9 (d, J_{CP} = 10 Hz, Ar), 152.3 (br, *C*F_3).

2.5.2.4 Synthesis of (*m*-$CF_3)_2C_6H_3PH_2{\cdot}BH_3$ (2.1d)

To a round bottom Schlenk flask containing $LiBH_4$ (0.204 g, 9.37 mmol) in Et_2O (100 mL) was added (*m*-$CF_3)_2C_6H_3PCl_2$ (1.500 g, 4.76 mmol) dissolved in Et_2O (10 mL) dropwise at 5 °C, and stirred for 90 mins. The reaction mixture was dried *in vacuo*, and the product was extracted into hexanes and insoluble salts were removed by filtration through celite. The colourless product **2.1d** was obtained by recrystallisation from hexanes.

Yield = 0.815 g (66%).

^{1}H NMR (400 MHz, $CDCl_3$): δ (ppm) 0.94 (m, 3H, $^1J_{BH}$ = 100 Hz, B*H*), 5.67 (dq, 2H, $^1J_{PH}$ = 377 Hz, $^3J_{HH}$ = 8 Hz, P*H*), 8.05 (s, 1H, *p*-Ar*H*), 8.15 – 8.18 (m, 2H, *o*-Ar*H*).

^{11}B NMR (128 MHz, $CDCl_3$): δ (ppm) −43.4 (dq, $^1J_{BH}$ = 100 Hz, $^1J_{BP}$ = 28 Hz).

^{31}P NMR (161 MHz, $CDCl_3$): δ (ppm) −45.5 (br. t, $^1J_{PH}$ = 377 Hz).

^{19}F NMR (376 MHz, $CDCl_3$): δ (ppm) −63.0.

^{13}C NMR (101 MHz, $CDCl_3$): δ (ppm) 121.7 (s, Ar), 123.9 (s, Ar), 126.2 (br, Ar), 133.0 (d qt, $^1J_{CF}$ = 34 Hz, $^5J_{CF}$ = 10 Hz, *C*F_3) 134.0 (br, Ar).

2.5.2.5 Synthesis of (*t*Bu$_3$)C$_6$H$_2$PH$_2$·BH$_3$ (2.1f)

To a solution of (*t*Bu$_3$C$_6$H$_2$)PH$_2$ (0.500 g, 3.28 mmol) in 20 mL of THF at −78 °C was slowly added 3.3 mL of 1.0 M BH$_3$·THF solution (3.3 mmol). The solution was allowed to stir at −78 °C for 1 h, then warmed to room temperature. The solvent was removed *in vacuo*, and the solid washed with cold hexanes (3 x 2 mL), then dried *in vacuo* to afford **2.1f** as a fine white powder.

Yield = 0.417 g (76%).

^{1}H NMR (400 MHz, $CDCl_3$): δ (ppm) 1.0 – 2.1 (br m, B*H*), 1.17 (s, *t*Bu*H*), 1.42 (s, *t*Bu*H*), 5.44 (br doublet of quartets, P*H*, $^1J_{PH}$ = 390 Hz), 7.44 (br d, Ar*H*).

^{11}B{^{1}H} NMR (128 MHz, $CDCl_3$): δ (ppm) −24 (br s).

^{31}P{^{1}H} NMR (161 MHz, $CDCl_3$): δ (ppm) −61.2 (br s).

Table S2.1. ^{11}B, ^{31}P and ^{1}H NMR chemical shifts for **2.1a-f**, recorded in $CDCl_3$.

Monomer	^{11}B NMR (ppm)	^{31}P NMR (ppm)	^{1}H NMR[c] (ppm)
2.1a	−43.5	−46.3	5.47
2.1b[a]	−42.2	−47.0	5.51
2.1c	−43.3	−51.7	5.67
2.1d	−43.4	−45.5	5.67
2.1e[b]	−39.7	−69.5	4.74
2.1f	−24.0	−61.2	5.44

[a)]Ref. 43. [b)]Spectra recorded in C_6D_6. Ref 2. [c)]Peak corresponding to P*H*$_2$.

Table S2.2. Hammett parameters for the aryl substituent in monomers **2.1a-d**.[21]

Aryl Substituent	Hammett Parameter
a	−0.16
b	0
c	0.35
d	0.43

2.5.3 Crystallography data

Table S2.3. Crystal data and structure refinement for **2.1a**, **2.1c**, **2.1d** and **2.1e**.

Identification code	2.1a	2.1c	2.1d	2.1e
Empirical formula	$C_7H_{10}BO_2P$	$C_7H_9BF_3OP$	$C_8H_8BF_6P$	$C_9H_{16}BP$
Formula weight	167.93	207.92	259.92	166.00
Temperature/K	200(2)	100(2)	100(2)	100(2)
Crystal system	triclinic	orthorhombic	monoclinic	orthorhombic
Space group	*P*-1	$Pca2_1$	$P2_1/c$	$P2_12_12_1$
a/Å	6.6392(9)	7.8523(3)	14.2593(16)	4.6117(8)
b/Å	7.7244(11)	8.7790(4)	8.2563(9)	14.566(3)
c/Å	8.8398(11)	27.7720(12)	9.4680(11)	15.010(3)
α/°	89.111(10)	90	90	90
β/°	89.167(10)	90	108.105(5)	90
γ/°	69.077(9)	90	90	90
Volume/Å^3	423.38(10)	1914.47(14)	1059.5(2)	1008.3(3)
Z	2	8	4	4
ρ_{calc}g/cm^3	1.317	1.443	1.630	1.094
μ/mm^{-1}	0.268	0.288	2.882	1.881
F(000)	176.0	848.0	520.0	360.0
Crystal size/mm^3	0.561 × 0.25 × 0.13	0.4 × 0.23 × 0.11	0.6 × 0.3 × 0.2	0.6 × 0.25 × 0.2
Radiation	MoKα (λ = 0.71073)	MoKα (λ = 0.71073)	CuKα (λ = 1.54178)	CuKα (λ = 1.54178)
2θ range for data collection/°	4.608 to 55.782	2.932 to 54.198	6.522 to 127.372	8.458 to 134.156
Index ranges	−8 ≤ h ≤ 7, −10 ≤ k ≤ 10, −11 ≤ l ≤ 11	−9 ≤ h ≤ 10, −11 ≤ k ≤ 11, −35 ≤ l ≤ 35	−10 ≤ h ≤ 16, −9 ≤ k ≤ 9, −10 ≤ l ≤ 11	−5 ≤ h ≤ 4, −16 ≤ k ≤ 17, −17 ≤ l ≤ 17
Reflections collected	7339	14558	13483	9714
R_{int}	0.0685	0.0667	0.0687	0.0515
Data/restraints/parameters	2023/0/120	4167/256/336	1725/0/165	1771/0/124
Goodness-of-fit on F^2	1.041	1.030	1.139	1.090
Final R indexes [I>=2σ (I)]	R_1 = 0.0471, wR_2 = 0.1155	R_1 = 0.0548, wR_2 = 0.1257	R_1 = 0.0597, wR_2 = 0.1595	R_1 = 0.0360, wR_2 = 0.0926
Final R indexes [all data]	R_1 = 0.0704, wR_2 = 0.1273	R_1 = 0.0896, wR_2 = 0.1425	R_1 = 0.0654, wR_2 = 0.1632	R_1 = 0.0360, wR_2 = 0.0926
Largest diff. peak/hole / e Å^{-3}	0.27/−0.31	0.55/−0.42	0.61/−0.31	0.36/−0.36

Table S2.4. π-π stacking interactions.

Structure	Ring	Ring	Centroid-centroid distance (Å)	Shift Distance (Å)
2.1a	C1−C6	C1−C6[a]	3.706	
2.1c	C1−C6	C1−C6[b]	3.939	1.793
	C1−C6	C1−C6[c]	3.939	1.757
	C8−C13	C8−C13[d]	3.943	1.768
	C8−C13	C8−C13[e]	3.943	1.774

[a)]2-x, -y, -z; [b)]-½+x, 1-y, +z; [c)]½+x, 1-y, +z; [d)]–½+x, 2-y, +z, [e)]½+x, 2-y, +z

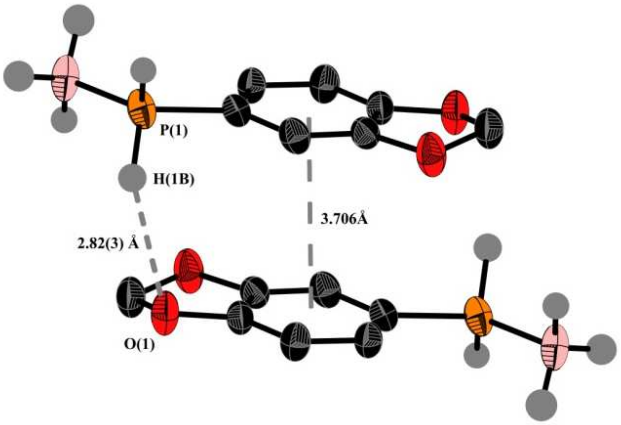

Figure S2.1. Intermolecular solid state contacts between units of **2.1a** including O···H and π-stacking. H atoms on Ph ring have been omitted for clarity and thermal ellipsoids set at the 50% probability level. Selected intermolecular interaction bond lengths (Å): H(1B)–O(1) 2.83(3).

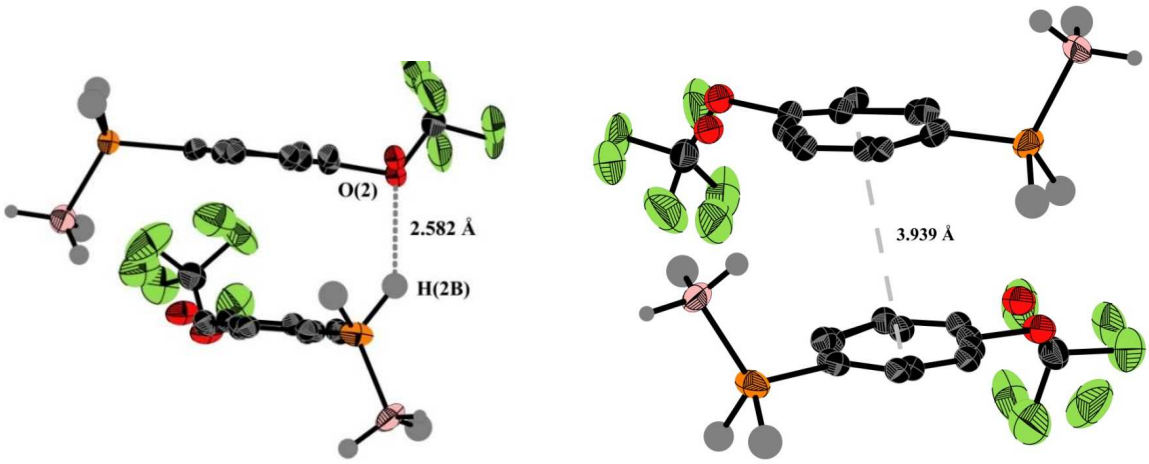

Figure S2.2. Intermolecular solid state contacts between symmetry related monomers of **2.1c**. H atoms on phenyl ring have been omitted for clarity and thermal ellipsoids set at the 50% probability level. Selected intermolecular interaction bond lengths (Å): H(2B)–O(2) 2.58(6).

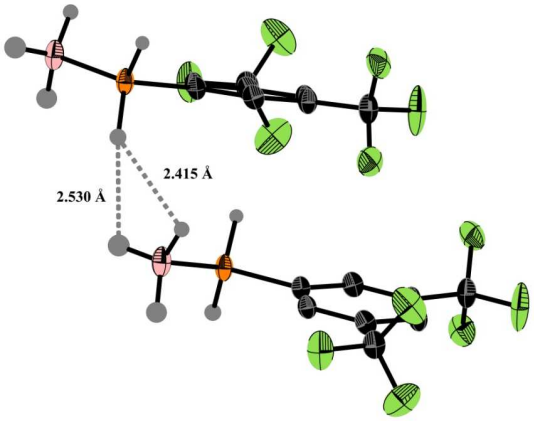

Figure S2.3. Intermolecular solid state contacts between symmetry related monomers of **2.1d**. H atoms on Ph ring have been omitted for clarity and thermal ellipsoids set at the 50% probability level. Selected intermolecular interaction bond lengths (Å) and angles (°): P(1)–H(1B)–H(1D) 136(3), P(1)–H(1B)–H(1C) 137(3), H(1D)–H(1B) 2.52(8), H(1C)–H(1B) 2.42(6), B(1)–H(1D)–H(1B) 100(4), B(1)–H(1C)–H(1B) 105(3).

2.5.4 Polymer Synthesis, NMR and GPC data

2.5.4.1 Catalytic dehydrocoupling of 3,4-$(H_2CO_2)C_6H_3PH_2{\cdot}BH_3$ (2.1a) by precatalyst I (5 mol %)

To a solution of substrate **2.1a** (0.100 g, 0.595 mmol), in 10 mL of anhydrous toluene was added 5 mol% of **I** (0.010 g, 0.031 mmol). The solution was then charged into a J. Young's Schlenk tube, and allowed to react at 100 °C for 24 h, open under N_2, after which time the solvent was evaporated *in vacuo*. The resulting gummy yellow solid was dissolved in minimal Et_2O and transferred into a beaker of cold pentane (−78 °C), which resulted in the precipitation of **2.2a**. The supernatant was then removed, and **2.2a** was dried *in vacuo*, in a vacuum oven at 40 °C for 7 days, yielding an off-white solid.

Yield = 0.045 g (46%).

^{1}H NMR (400 MHz, $CDCl_3$): δ (ppm) 1.0 – 2.0 (br m, 2H, B*H*), 4.39 (d, 2H, $^1J_{PH}$ = 350 Hz, P*H*), 5.88 (br, 2H, CH_2), 6.60 (br, 3H, Ar*H*) (Figure S2.4).

^{11}B NMR (128 MHz, $CDCl_3$): δ (ppm) −35.1 (Figure S2.5).

^{31}P NMR (161 MHz, $CDCl_3$): δ (ppm) −47.3 (Figure S2.6-S2.7).

GPC (2 mg mL^{-1}): M_n = 12,000 g mol^{-1}; PDI = 2.17 (Figure S2.10).

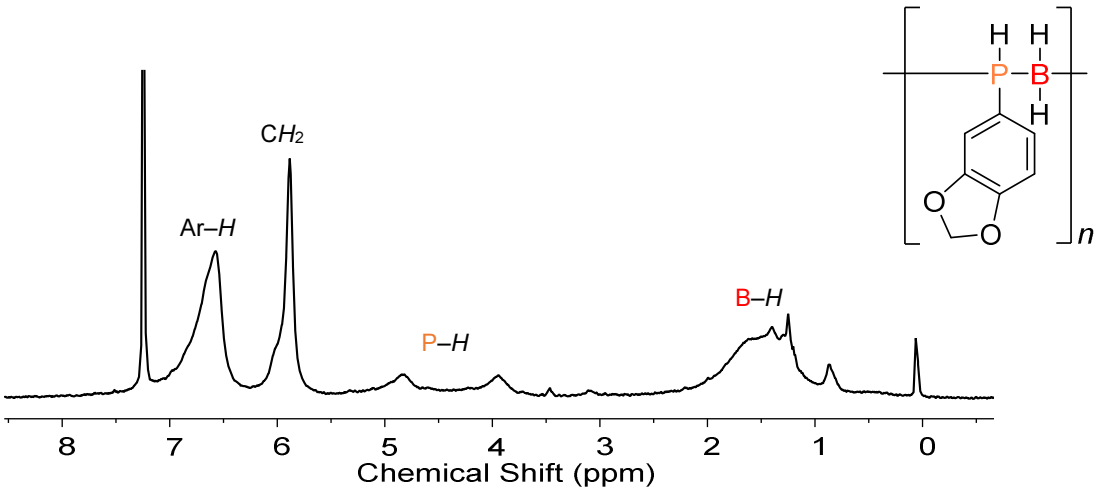

Figure S2.4. ^{1}H NMR spectrum of isolated [3,4-$(H_2CO_2)C_6H_3PH{-}BH_2]_n$ (**2.2a**) in $CDCl_3$ at 20 °C.

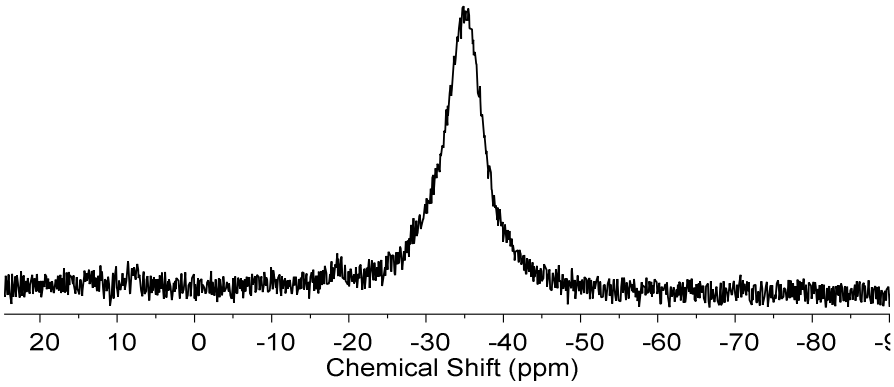

Figure S2.5. $^{11}B\{^{1}H\}$ NMR spectrum of isolated $[3,4\text{-}(H_2CO_2)C_6H_3PH{-}BH_2]_n$ (**2.2a**) in $CDCl_3$ at 20 °C.

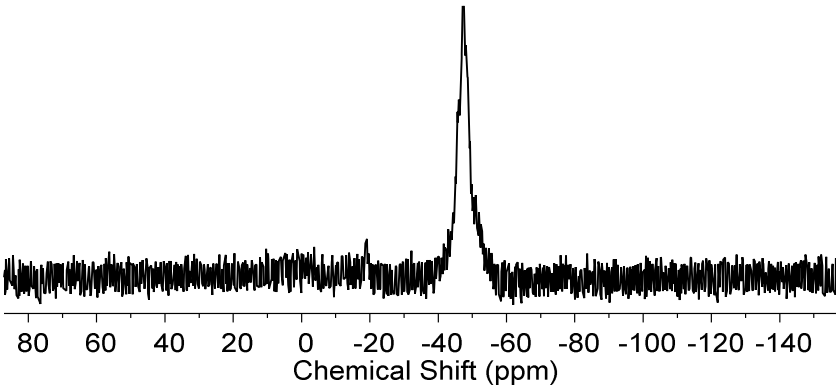

Figure S2.6. $^{31}P\{^{1}H\}$ NMR spectrum of isolated $[3,4\text{-}(H_2CO_2)C_6H_3PH{-}BH_2]_n$ (**2.2a**) in $CDCl_3$ at 20 °C.

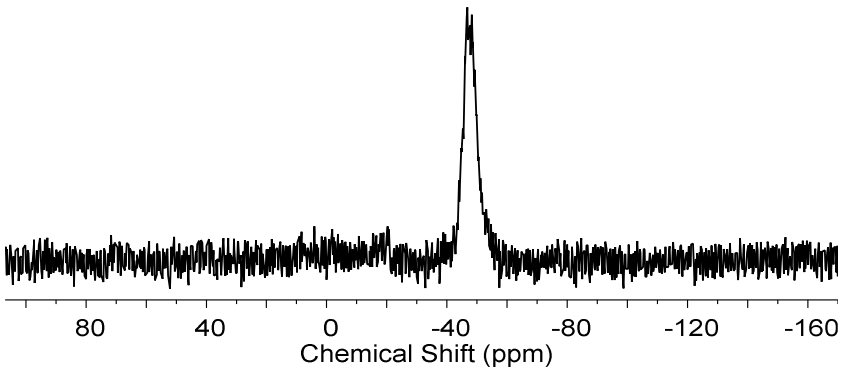

Figure S2.7. ^{31}P NMR spectrum of isolated $[3,4\text{-}(H_2CO_2)C_6H_3PH{-}BH_2]_n$ (**2.2a**) in $CDCl_3$ at 20 °C.

Figure S2.8. Photograph of isolated **2.2a**.

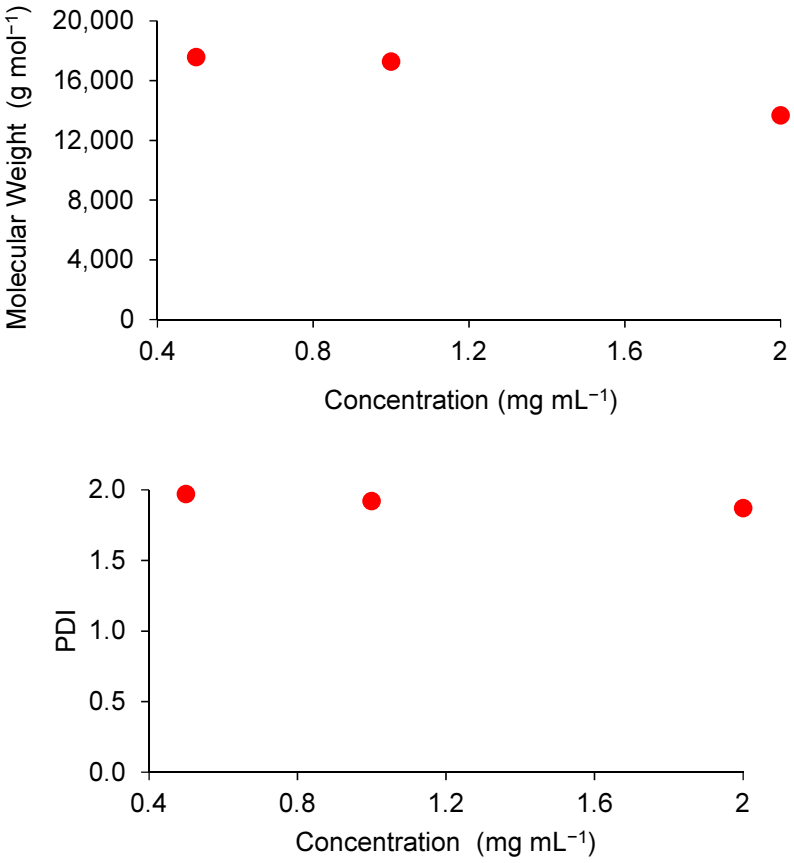

Figure S2.9. Number average molecular weight (M_n) and PDI of **2.2a** as recorded by GPC as a function of concentration of the GPC sample.

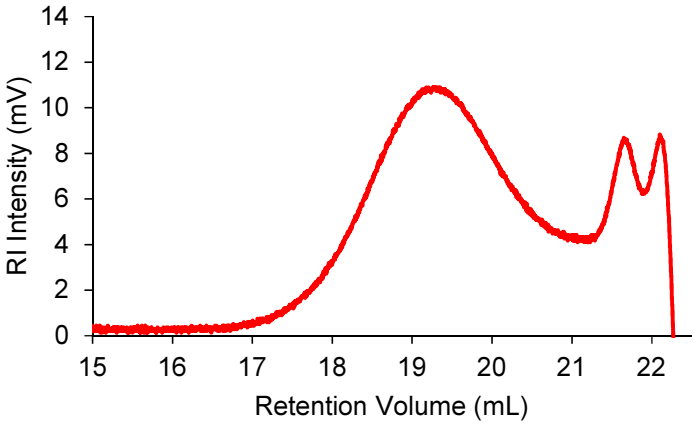

Figure S2.10. GPC chromatogram of polymer **2.2a** at 2 mg mL^{-1} in THF.

2.5.4.2 Catalytic dehydrocoupling of *p*-(OCF$_3$)C$_6$H$_4$PH$_2$·BH$_3$ (2.1c) by precatalyst I (5 mol %)

To a solution of substrate **2.1c** (0.500 g, 2.40 mmol), in 10 mL of anhydrous toluene was added 5 mol % of precatalyst **I** (0.039 g, 0.12 mmol). The solution was then charged into a J. Young's Schlenk tube and allowed to react at 100 °C for 24 h, open under N_2, after which time the solvent was evaporated in *vacuo*. The resulting gummy yellow solid was dissolved in minimal Et_2O and transferred into a beaker of cold pentane (−78 °C), which resulted in the precipitation of **2.2c**. The solution was then removed, and **2.2c** was dried *in vacuo*, in a vacuum oven at 40 °C for 7 days, yielding a pale yellow solid.

Yield = 0.152 g (31%).

^{1}H NMR (400 MHz, $CDCl_3$): δ (ppm) 1.37 (v. br., B*H*), 4.66 (br. d, $^1J_{PH}$ = 360 Hz, P*H*), 6.50 – 8.00 (v. br. m, Ar*H*) (Figure S2.11).

^{11}B NMR (128 MHz, $CDCl_3$): δ (ppm) −34.7 (Figure S2.12).

^{31}P NMR (161 MHz, $CDCl_3$): δ (ppm) −49.1 (Figure S2.13-S2.14).

^{19}F NMR ($CDCl_3$): δ (376 MHz, ppm) −64.5 (br s, C*F*$_3$), −78.5 (s) (Figure S2.15).

GPC (2 mg mL^{-1}): M_n = 79,000 g mol^{-1}; PDI = 1.35 (Figure S2.18).

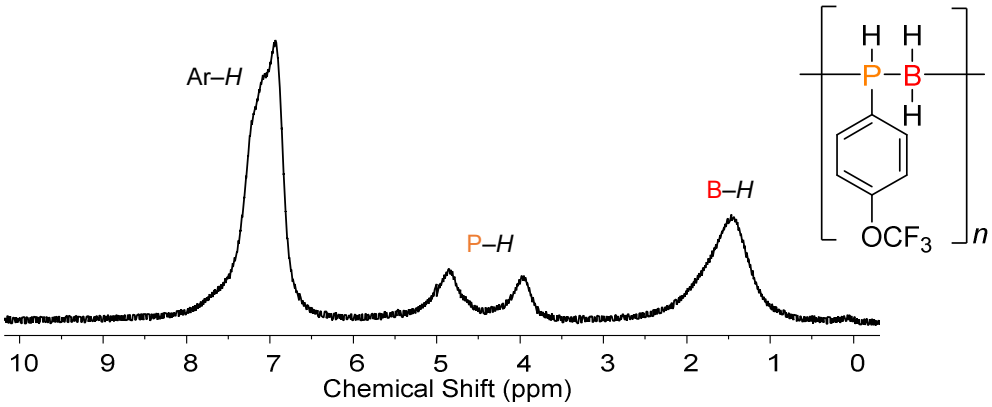

Figure S2.11. ^{1}H NMR spectrum of isolated [*p*-(OCF$_3$)C$_6$H$_4$PH–BH$_2$]$_n$ (**2.2c**) in CDCl$_3$ at 20 °C.

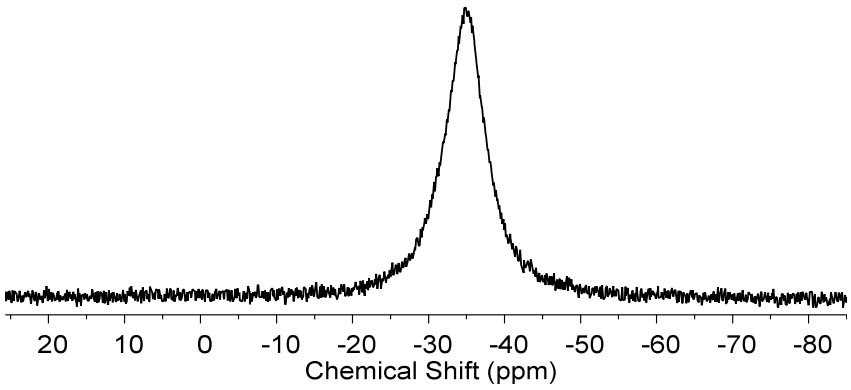

Figure S2.12. ^{11}B{^{1}H} NMR spectrum of isolated [*p*-(OCF$_3$)C$_6$H$_4$PH–BH$_2$]$_n$ (**2.2c**) in CDCl$_3$ at 20 °C.

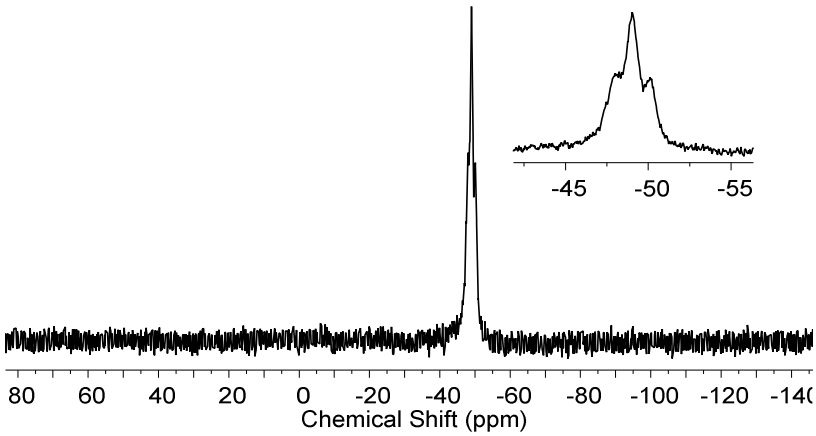

Figure S2.13. ^{31}P{^{1}H} NMR spectrum of isolated [*p*-(OCF$_3$)C$_6$H$_4$PH–BH$_2$]$_n$ (**2.2c**) in CDCl$_3$ at 20 °C.

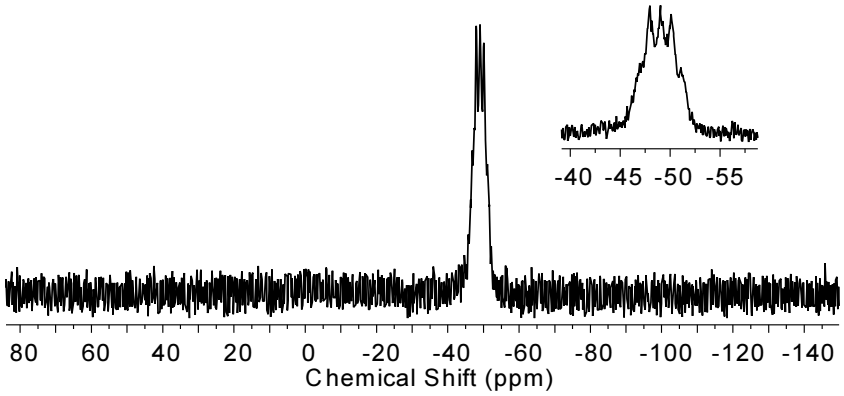

Figure S2.14 ^{31}P NMR spectrum of isolated [*p*-(OCF$_3$)C$_6$H$_4$PH–BH$_2$]$_n$ (**2.2c**) in CDCl$_3$ at 20 °C.

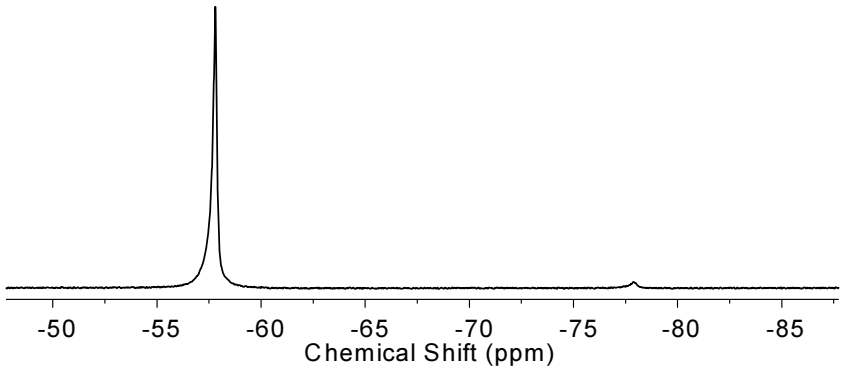

Figure S2.15. ^{19}F NMR spectrum of isolated [*p*-(OCF$_3$)C$_6$H$_4$PH–BH$_2$]$_n$ (**2.2c**) in CDCl$_3$ at 20 °C.

Figure S2.16. Photograph of isolated **2.2c**.

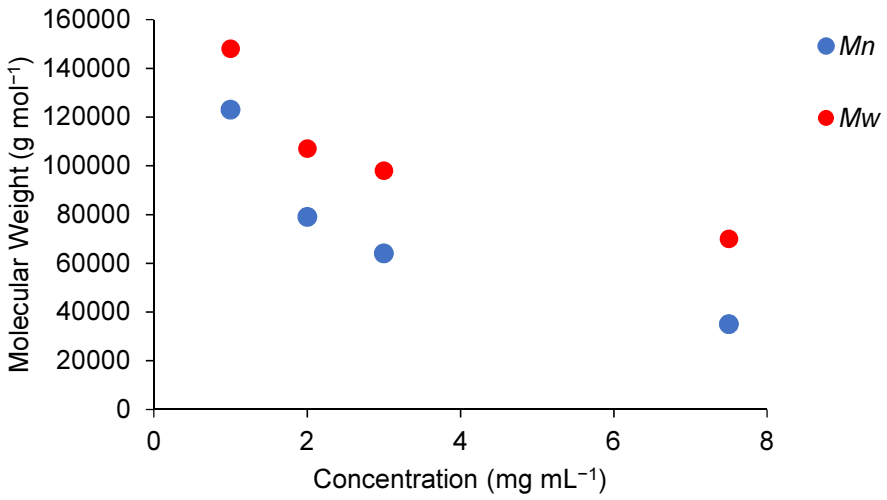

Figure S2.17. Number average molecular weight (M_n) and weight average molecular weight (M_w) of **2.2c** as recorded by GPC as a function of concentration of the GPC sample.

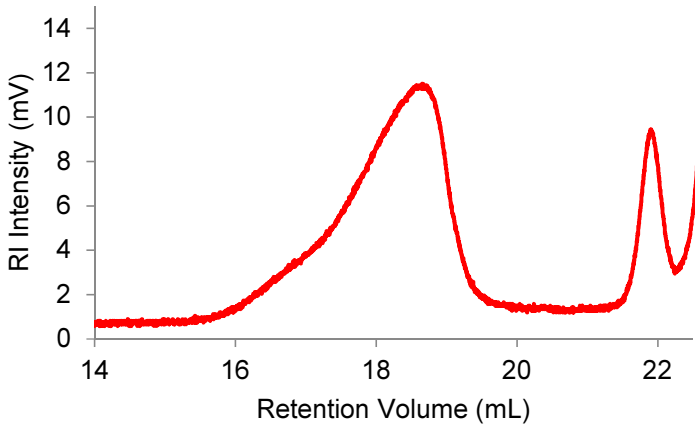

Figure S2.18. GPC chromatogram of **2.2c** at a concentration of 2 mg mL^{-1} in THF.

2.5.4.3 Catalytic dehydrocoupling of (*m*-CF_3)$_2$$C_6H_3PH_2$·$BH_3$ (2.1d) by precatalyst I (2 mol %)

To a solution of substrate **2.1d** (0.400 g, 1.54 mmol), in 10 mL of anhydrous toluene was added 2 mol% of precatalyst **I** (0.010 g, 0.031 mmol). The solution was then charged into a J. Young's Schlenk tube and allowed to react at 100 °C for 24 h under N_2, after which time the solvent was removed *in vacuo*. The resulting gummy yellow solid was dissolved in minimal Et_2O and transferred into a beaker of cold pentane (−78 °C), which resulted in

the precipitation of **2.2d**. The solution was then removed, and **2.2a** was dried *in vacuo*, in a vacuum oven at 40 °C for 7 days, yielding a pale yellow solid.

Yield = 0.123 g (31%).

^{1}H NMR (400 MHz, $CDCl_3$): δ (ppm) 0.80 – 2.20 (v br, B*H*$_2$), 4.62 (br d, $^{1}J_{HP}$ = 364 Hz, P*H*), 7.32 – 7.88 (br m, Ar*H*); (Figure S2.19).

^{11}B NMR (128 MHz, $CDCl_3$): δ (ppm) −35.2 (Figure S2.20).

^{31}P NMR (161 MHz, $CDCl_3$): δ (ppm) −46.3 (d, $^{1}J_{PH}$ = 335 Hz) (Figure S2.21-S2.22).

^{19}F NMR (376 MHz, $CDCl_3$): δ (ppm) −64.5 (br s, CF_3), −78.5 (s) (Figure S2.23).

GPC (2 mg mL^{-1}): M_n = 209,000 g mol^{-1}; PDI = 1.25. (Figure S2.26).

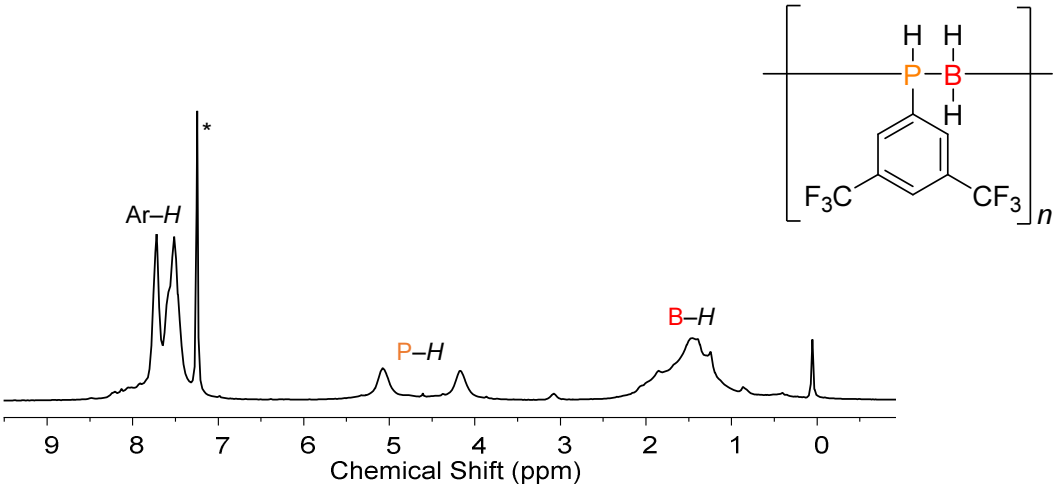

Figure S2.19. ^{1}H NMR spectrum of isolated [(*m*-CF_3)$_2$$C_6H_3$PH–$BH_2$]$_n$ (**2.2d**) in $CDCl_3$ at 20 °C. * $CDCl_3$.

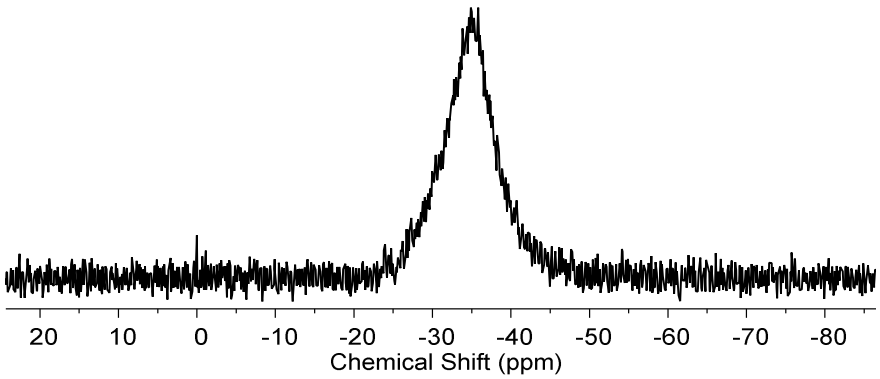

Figure S2.20. ^{11}B{^{1}H} NMR spectrum of isolated [(*m*-CF_3)$_2$$C_6H_3$PH–$BH_2$]$_n$ (**2.2d**) in $CDCl_3$ at 20 °C.

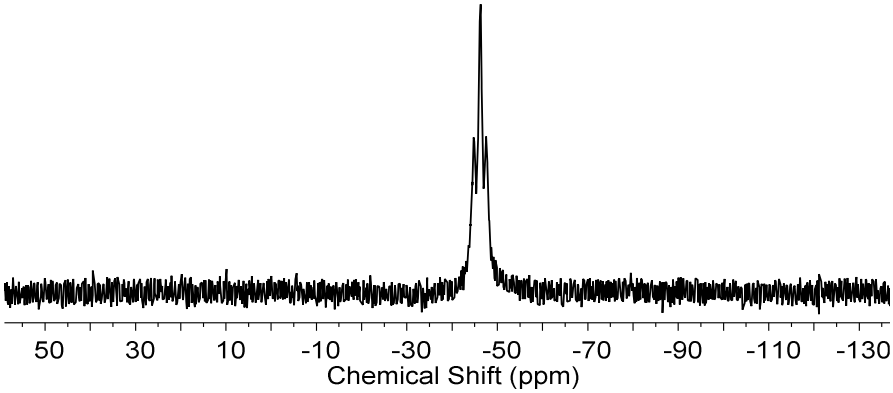

Figure S2.21. $^{31}P\{^{1}H\}$ NMR spectrum of isolated $[(m\text{-}CF_3)_2C_6H_3PH–BH_2]_n$ (**2.2d**) in $CDCl_3$ at 20 °C.

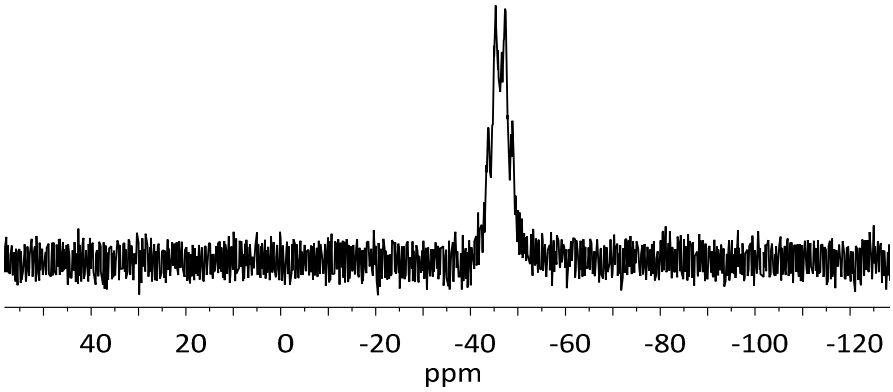

Figure S2.22. ^{31}P NMR spectrum of isolated $[(m\text{-}CF_3)_2C_6H_3PH–BH_2]_n$ (**2.2d**) in $CDCl_3$ at 20 °C.

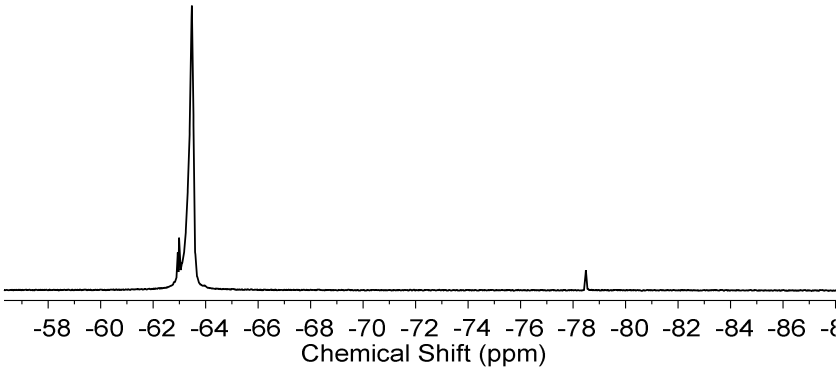

Figure S2.23. ^{19}F NMR spectrum of isolated $[(m\text{-}CF_3)_2C_6H_3PH–BH_2]_n$ (**2.2d**) in $CDCl_3$ at 20 °C.

Figure S2.24. Photograph of isolated **2.2d**.

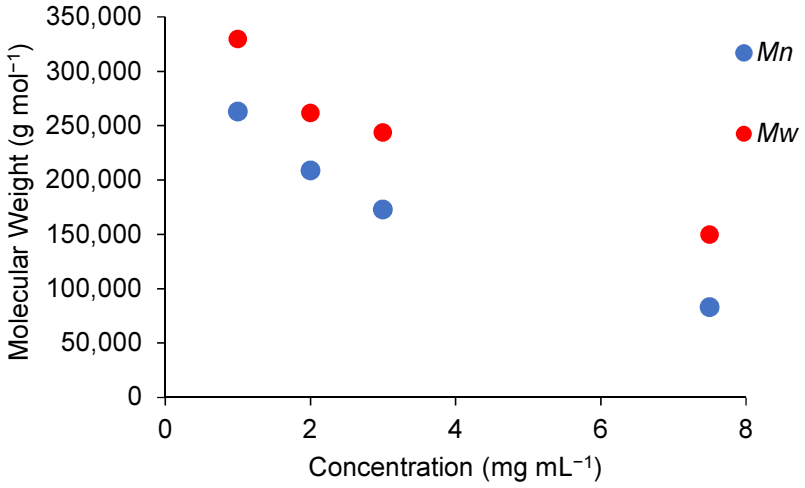

Figure S2.25. Number average molecular weight (M_n) and weight average molecular weight (M_w) of **2.2d** as recorded by GPC as a function of concentration of the GPC sample.

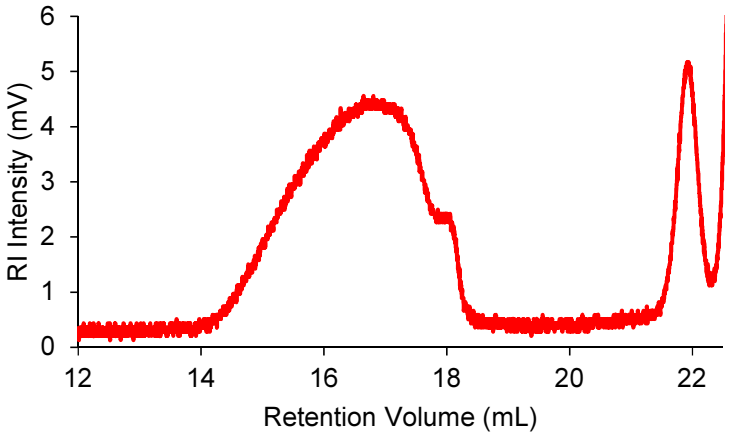

Figure S2.26. GPC chromatogram of **2.2d** at a concentration of 2 mg mL^{-1} in THF.

2.5.4.4 Catalytic dehydrocoupling of $MesPH_2{\cdot}BH_3$ (2.1e) by precatalyst I (5 mol%)

To a solution of substrate **2.1e** (0.664 g, 4.00 mmol), in 10 mL of anhydrous toluene was added 5 mol% of **I** (0.065 g, 0.199 mmol). The solution was then charged into a J. Young's Schlenk flask and allowed to react at 100 °C, open under N_2. The solution turned from dark red to bright yellow within the first hour and remained so throughout the reaction. After 24 h the reaction solution was transferred into a beaker of cold pentane (−78 °C), which resulted in the precipitation of **2.2e**. The product was isolated by filtration and washed several times (3 x 2 mL) with cold pentane and dried *in vacuo* to afford **2.2e** as a pale yellow powder.

Yield = 0.317 g (48%).

^{1}H NMR (400 MHz, $CDCl_3$): δ (ppm) 0.7 – 2.7 (v br., B*H*$_2$ and C*H*$_3$), 4.36 (br. d, $^1J_{PH}$ = 350 Hz, P*H*), 6.25 – 8.0 (br m. Ar*H*) (Figure S2.27).

^{11}B NMR (128 MHz, $CDCl_3$): δ (ppm) −35.3 (br) (Figure S2.28 left).

^{31}P NMR (161 MHz, $CDCl_3$): δ (ppm) −73.2 (d, $^1J_{PH}$ = 335 Hz) (Figure S2.28 middle/right).

GPC (2 mg mL^{-1}): M_n = 79,000 g mol^{-1}; PDI = 1.35. (Figure S2.30).

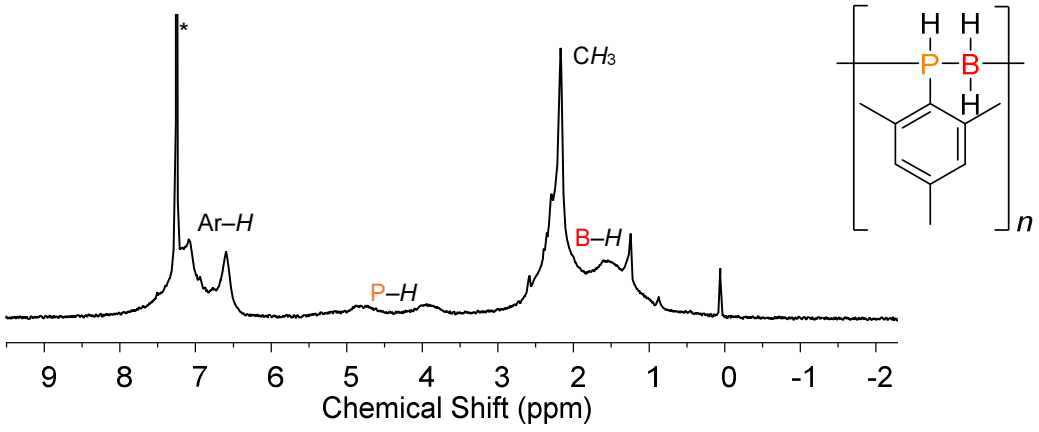

Figure S2.27. ^{1}H NMR spectrum of isolated [MesPH–BH_2]$_n$ (**2.2e**) in $CDCl_3$ at 20 °C. * $CDCl_3$.

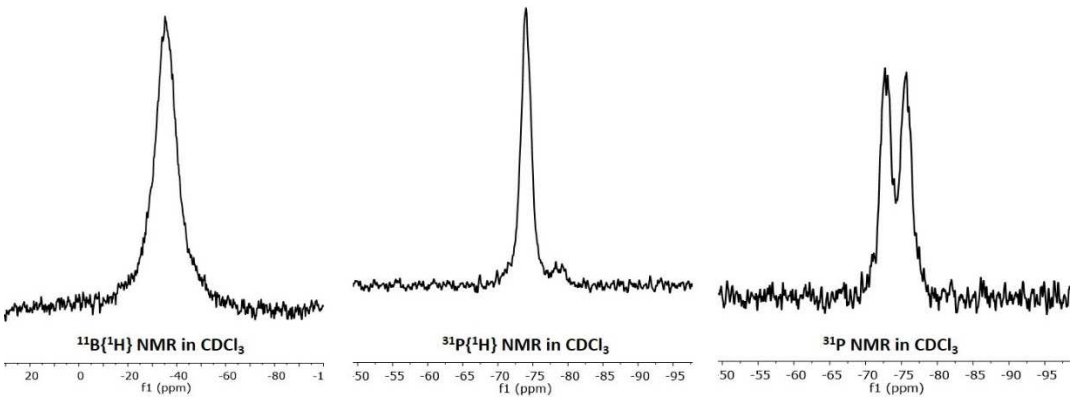

Figure S2.28. NMR spectra of polymer $[MesPH–BH_2]_n$ (**2.2e**) in $CDCl_3$: *(left)* $^{11}B\{^1H\}$ NMR, *(middle)* $^{31}P\{^1H\}$ NMR and *(right)* ^{31}P NMR spectra.

Figure S2.29. Photograph of isolated **2.2e**.

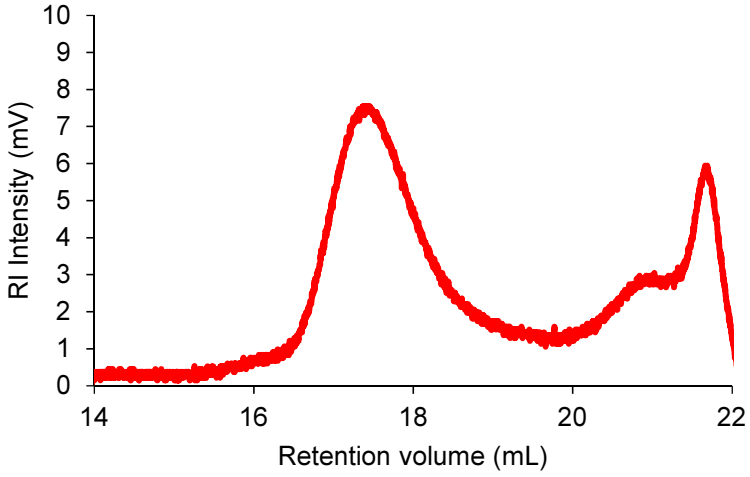

Figure S2.30. GPC chromatogram of **2.2e** at 2 mg mL^{-1} in THF.

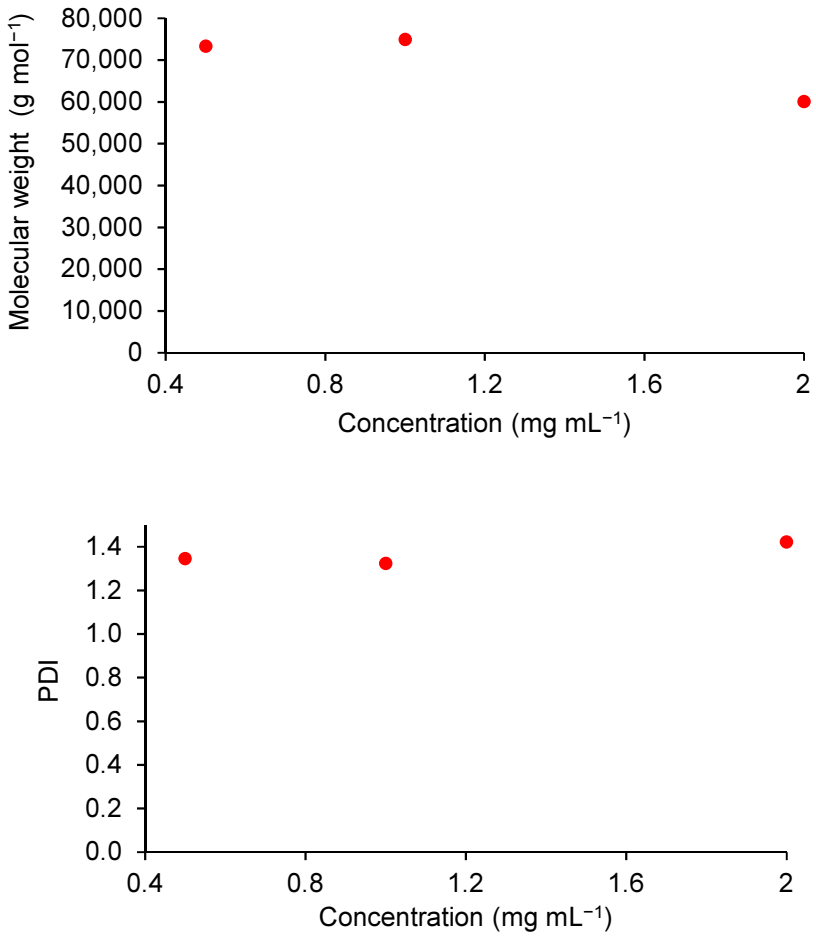

Figure S2.31. Number average molecular weight (M_n) and PDI of **2.2e** as recorded by GPC as a function of concentration of the GPC sample.

2.5.4.5 Attempted catalytic dehydrocoupling of (^{t}Bu$_3$C$_6$H$_2$)PH$_2$·BH$_3$ (2.1f) by I (5 mol%)

To a solution of **1f** (0.073 g, 0.25 mmol), in 0.5 mL of anhydrous toluene was added 5 mol% of precatalyst **I** (0.004 g, 0.012 mmol). The solution was then charged into a quartz J. Young's NMR tube then sealed, and heated to 100 °C. The solution turned from dark red to bright yellow within the first hour,and remained so throughout the reaction. No dehydrocoupling products were observed by multinuclear NMR spectroscopy (Figure S2.32-S2.34).

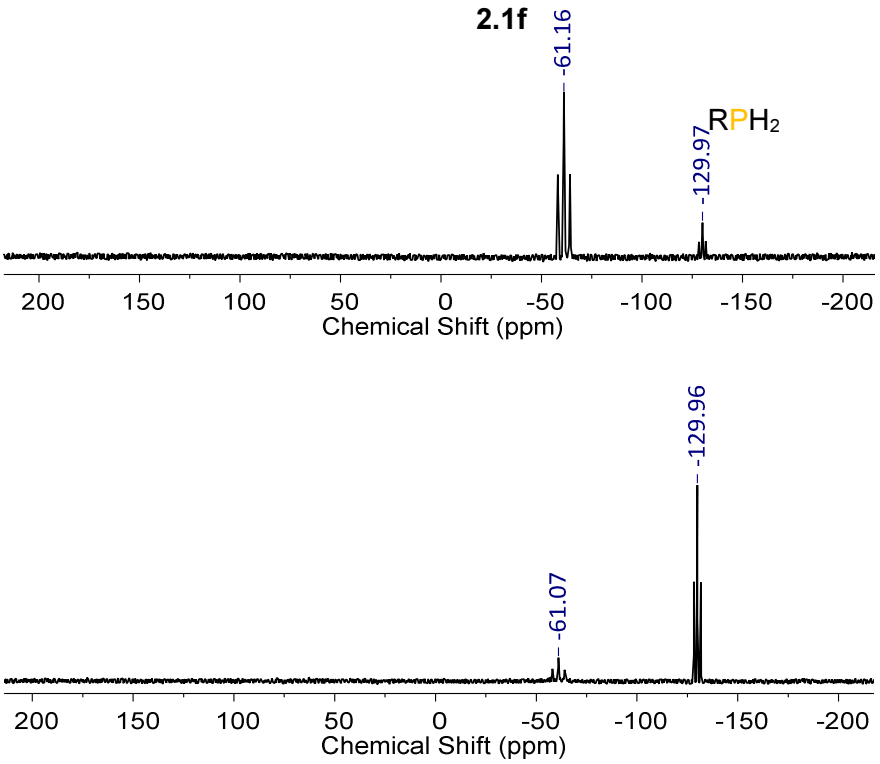

Figure S2.32. ^{31}P NMR spectra of **2.1f** and 5 mol% **I** in toluene-d_8 at 100 °C after 0 h (top) and 22 h (bottom). R= $^{t}Bu_3C_6H_2$

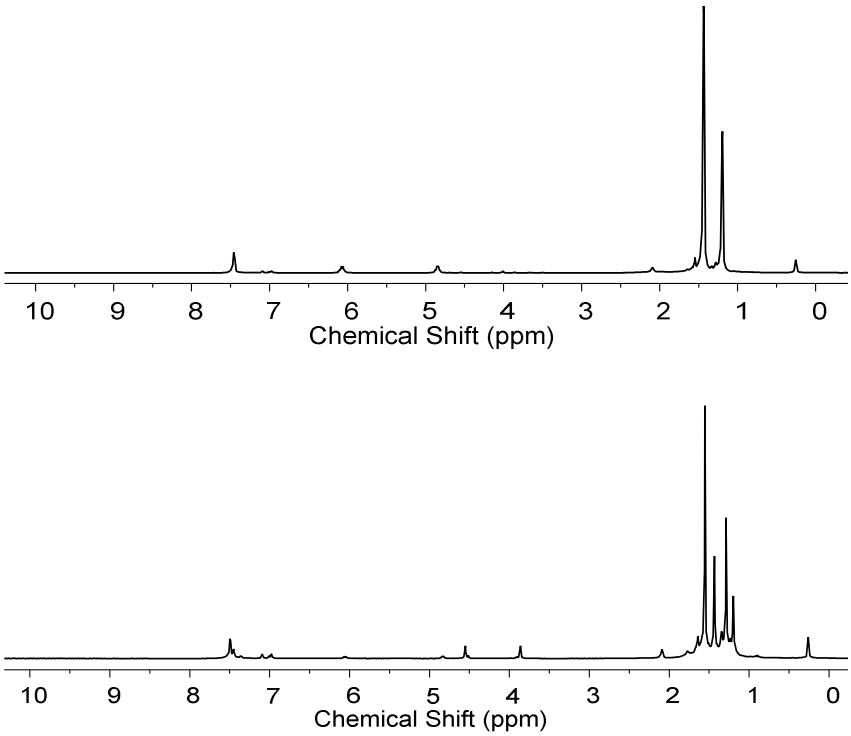

Figure S2.33. ^{1}H NMR specrtra of **2.1f** and 5 mol% **I** in toluene-d_8 at 100 °C after 0 h (top) and 22 h (bottom).

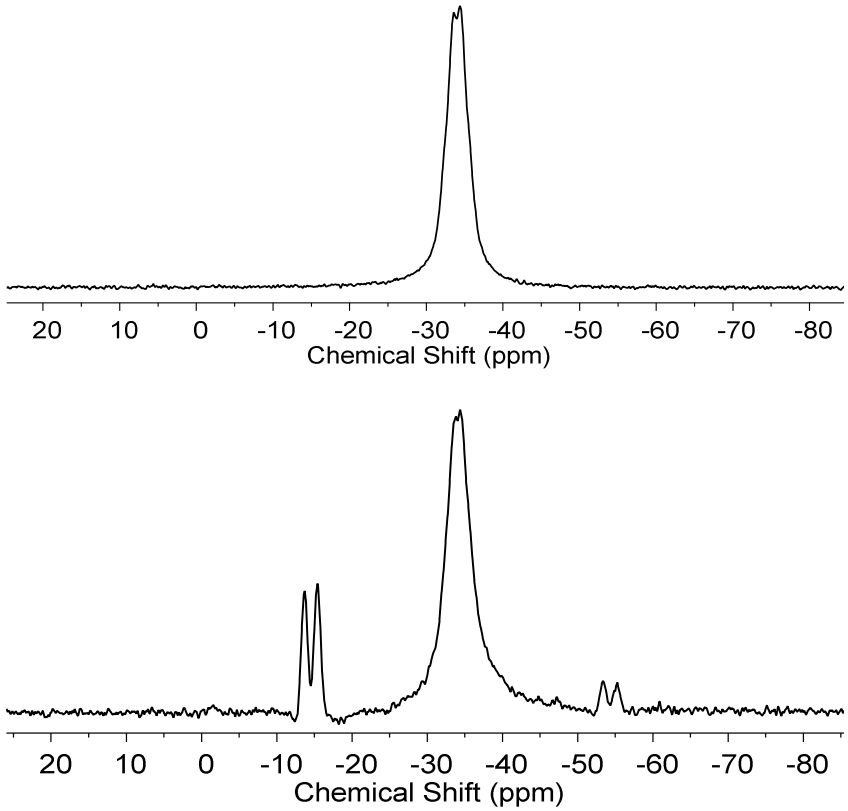

Figure S2.34. ^{11}B NMR spectra of **2.1f** and 5 mol% **I** in toluene-d_8 at 100 °C after 0 h (top) and 22 h (bottom).

2.5.4.6 Catalytic dehydrocoupling of (*m*-CF_3)$_2$$C_6H_3PH_2$·$BH_3$ (2.1d) using precatalyst I (5 mol%)

To a solution of substrate **2.1d** (0.100 g, 0.385 mmol), in 10 mL of anhydrous toluene was added 5 mol% of precatalyst **I** (0.006 g, 0.018 mmol). The solution was then charged into a J. Young's Schlenk tube and allowed to react at 100 °C for 24 h under N_2, after which time the solvent was removed *in vacuo*. Minimal Et_2O was added to the yellow gummy solid, causing some of the solid to swell. The supernatant was transferred into round bottom, concentrated and placed into a beaker of cold pentane (−78 °C), which resulted in the precipitation of **2.2d**. The solution was then removed, and **2.2d** was dried *in vacuo*, yielding a pale yellow solid.

Yield = 0.010 g (10%).

GPC (2 mg mL^{-1}): M_n = 77,000 g mol^{-1}; PDI = 1.35 (Figure S2.35).

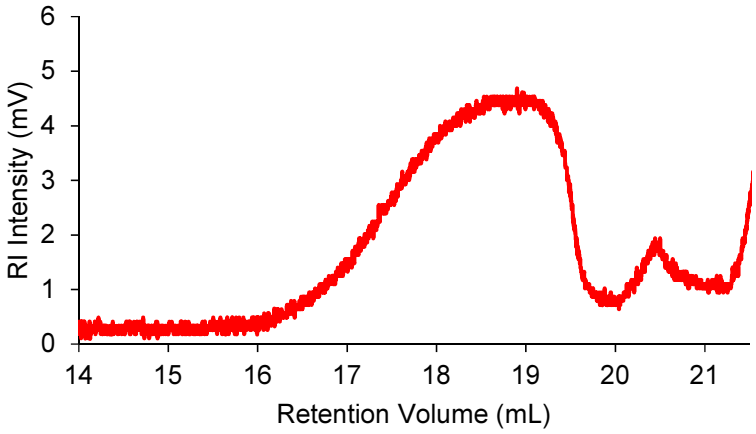

Figure S2.35. GPC chromatogram of **2.2d** at 2mg mL^{-1} in THF.

2.5.5 Thermal dehydropolymerisation of 2.1a-e

A solution of substrate **2.1a-e** (2.3 mmol), in 0.7 mL of toluene was charged into a J. Young's Schlenk tube and allowed to react at 100 °C for 24 h. The resulting reaction mixture after 24 h was analysed by GPC.

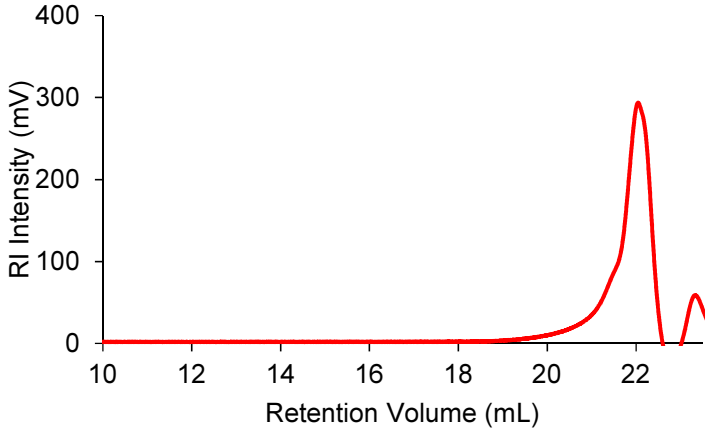

Figure S2.36. GPC chromatogram of the reaction mixture from the thermal dehydrocoupling reaction involving **2.1a**.

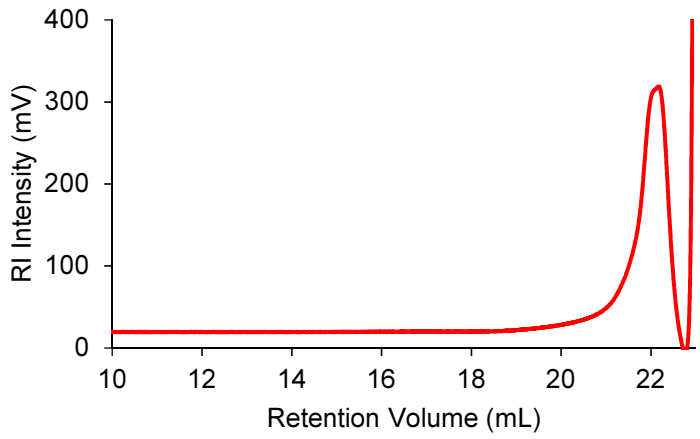

Figure S2.37. GPC chromatogram of the reaction mixture from the thermal dehydrocoupling reaction involving **2.1b**.

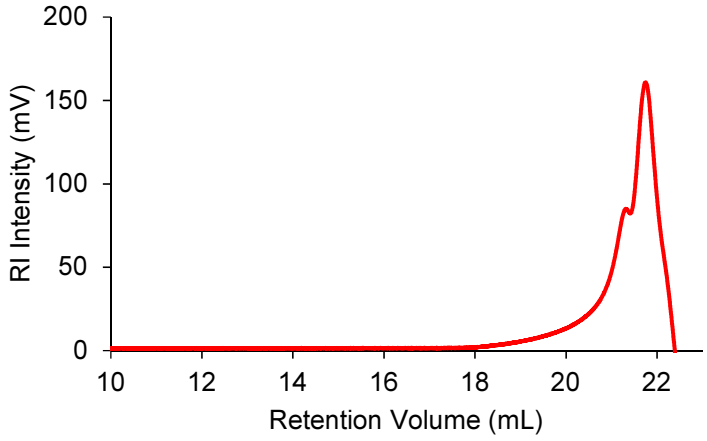

Figure S2.38. GPC chromatogram of the reaction mixture from the thermal dehydrocoupling reaction involving **2.1c**.

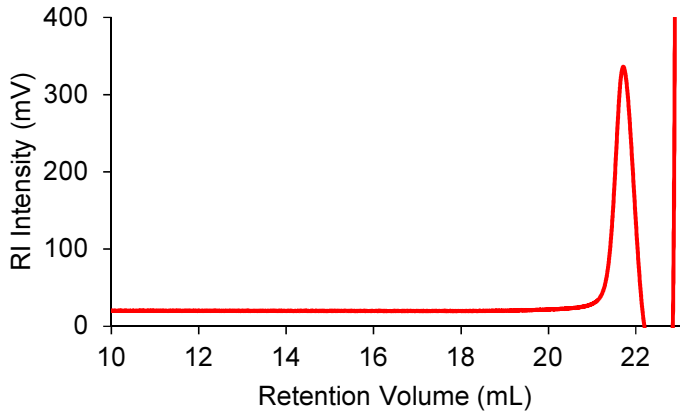

Figure S2.39. GPC chromatogram of the reaction mixture from the thermal dehydrocoupling reaction involving **2.1d**.

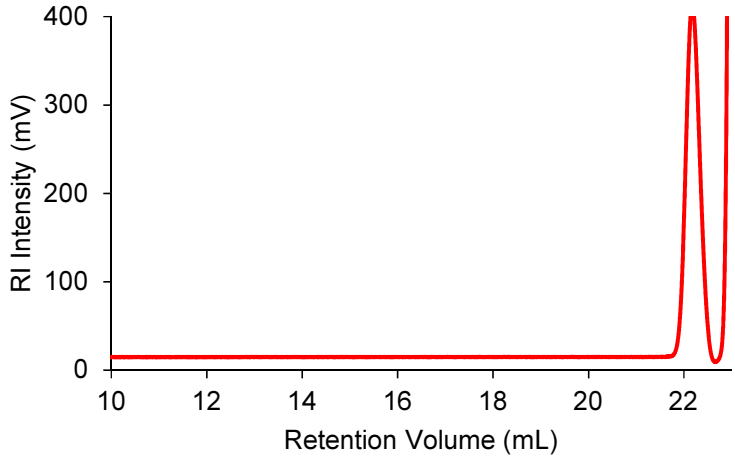

Figure 2.40. GPC chromatogram of the reaction mixture from the thermal dehydrocoupling reaction involving **2.1e**.

2.5.6 Electrospray ionisation mass spectrometry (ESI-MS)

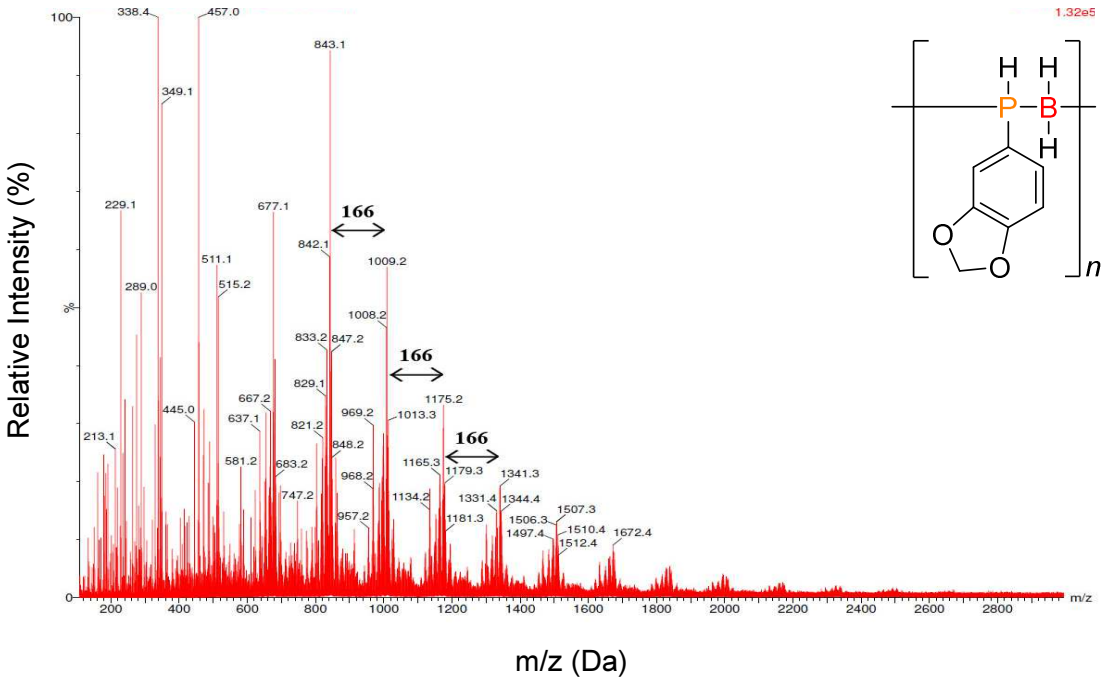

Figure S2.41. ESI-MS (2mg mL^{-1} in CH_2Cl_2) of isolated $[3,4\text{-}(H_2CO_2)C_6H_3PH{-}BH_2]_n$ (**2.2a**).

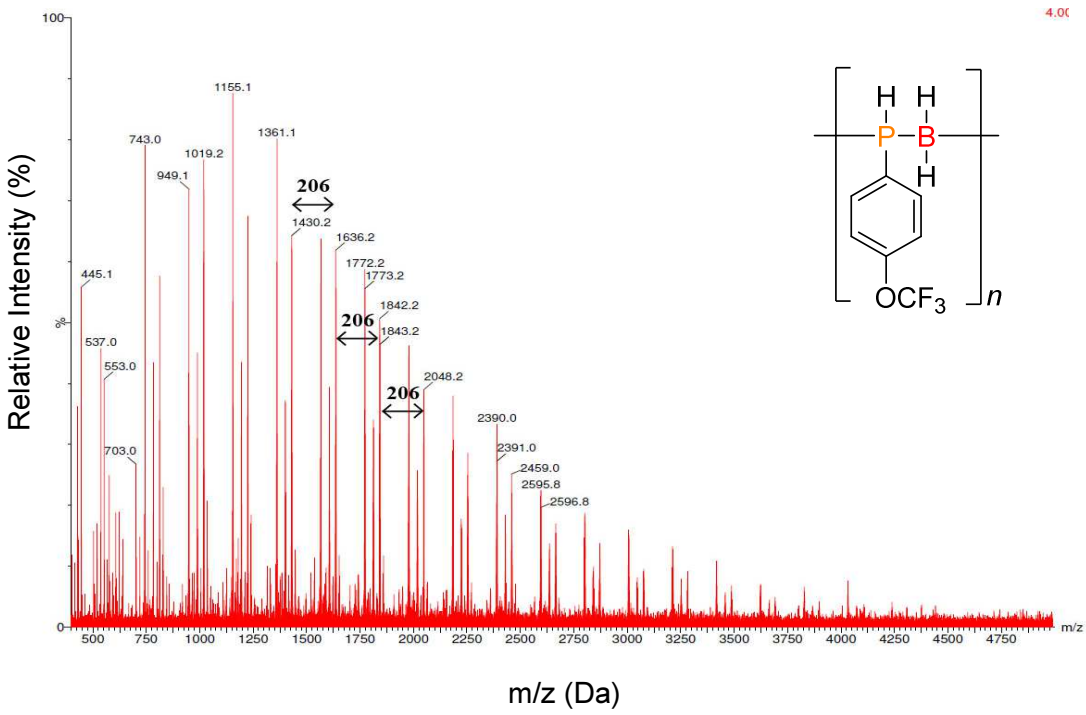

Figure S2.42. ESI-MS (2mg mL^{-1} in CH_2Cl_2) of isolated [*p*-$(OCF_3)C_6H_4PH–BH_2]_n$ (**2.2c**).

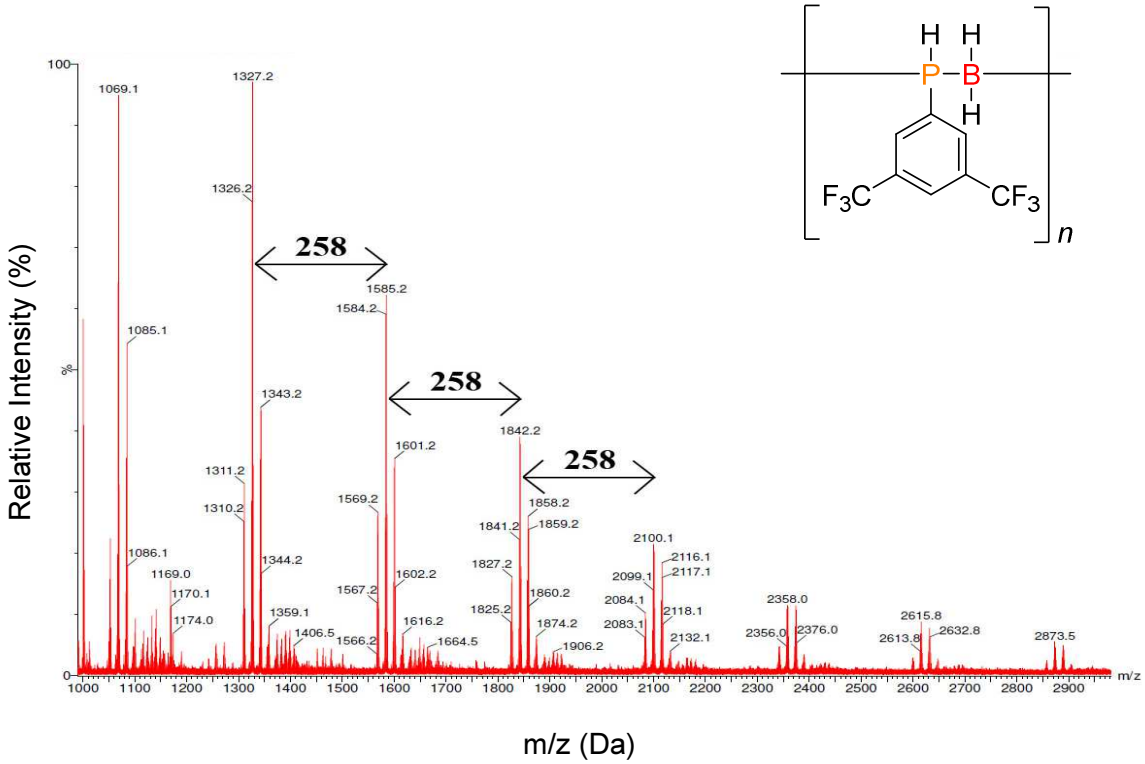

Figure S2.43. ESI-MS (2mg mL^{-1} in CH_2Cl_2) of isolated [(*m*-$CF_3)_2C_6H_3PH–BH_2]_n$ (**2.2d**).

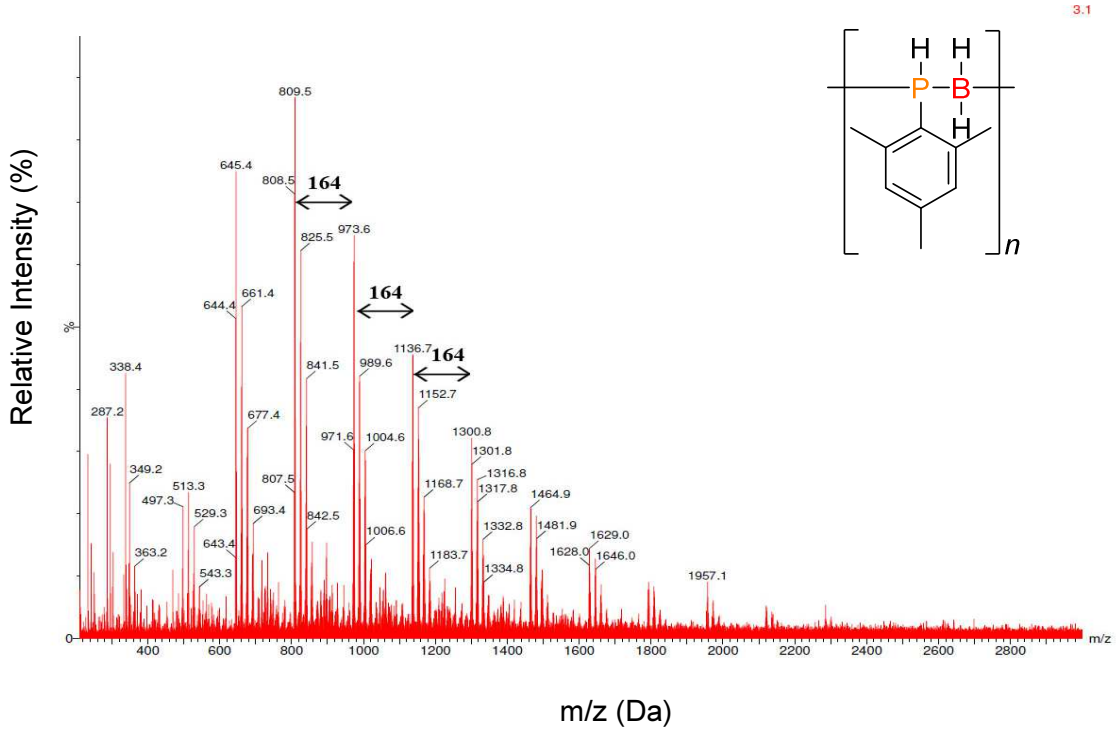

Figure S2.44. ESI-MS (2mg mL^{-1} in CH_2Cl_2) of isolated $[MesPH–BH_2]_n$ (**2.2e**).

2.5.7 DSC Thermograms

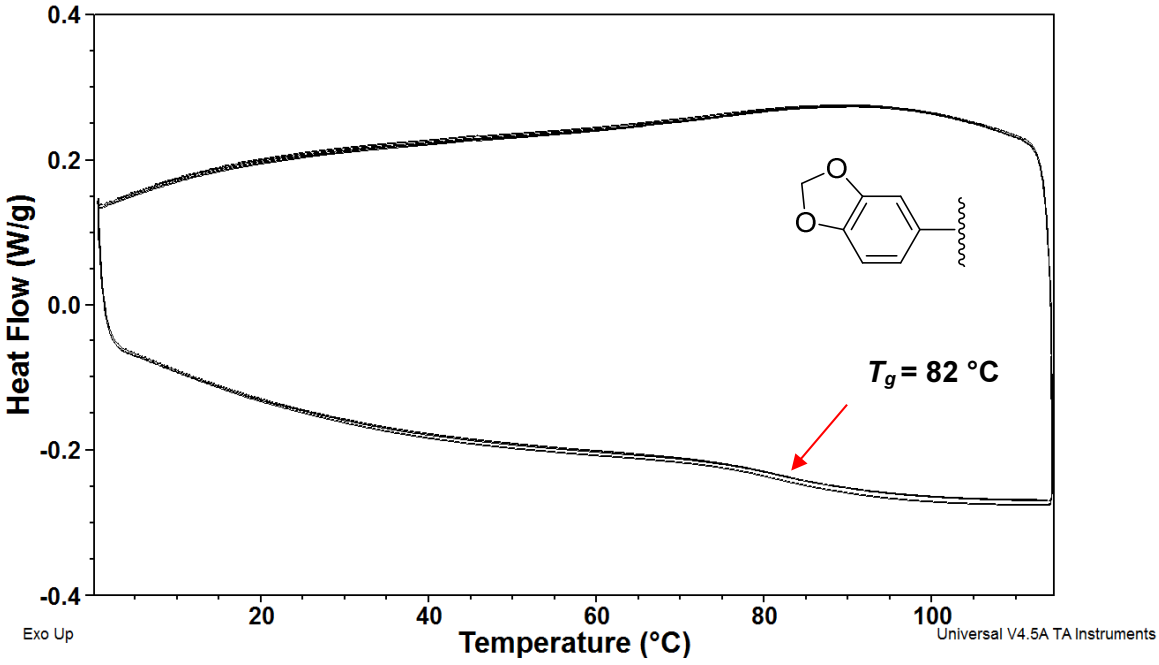

Figure S2.45. DSC thermogram of **2.2a**, first cycle excluded.

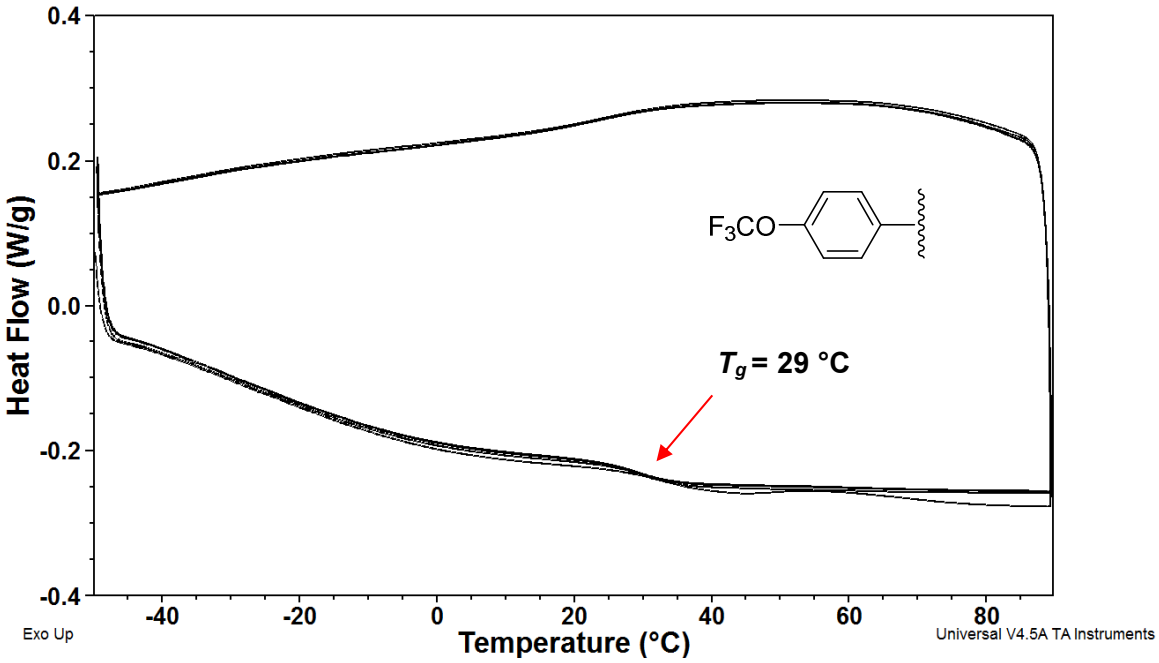

Figure S2.46. DSC thermogram of **2.2c**, first cycle excluded.

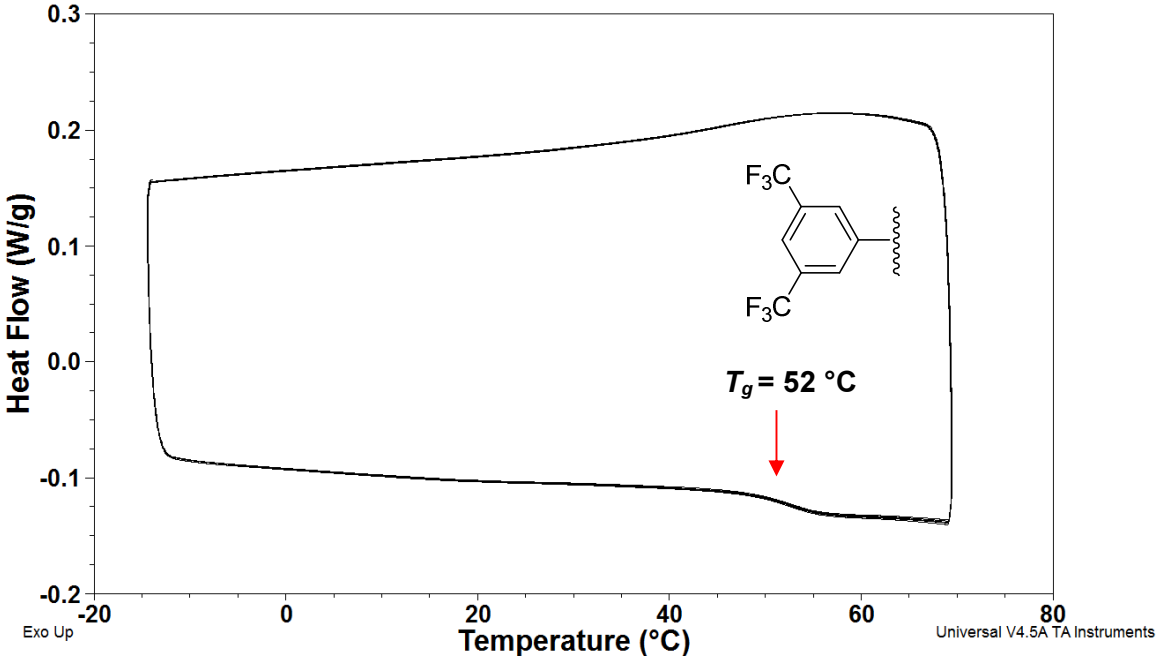

Figure S2.47. DSC thermogram of **2.2d**, first cycle excluded.

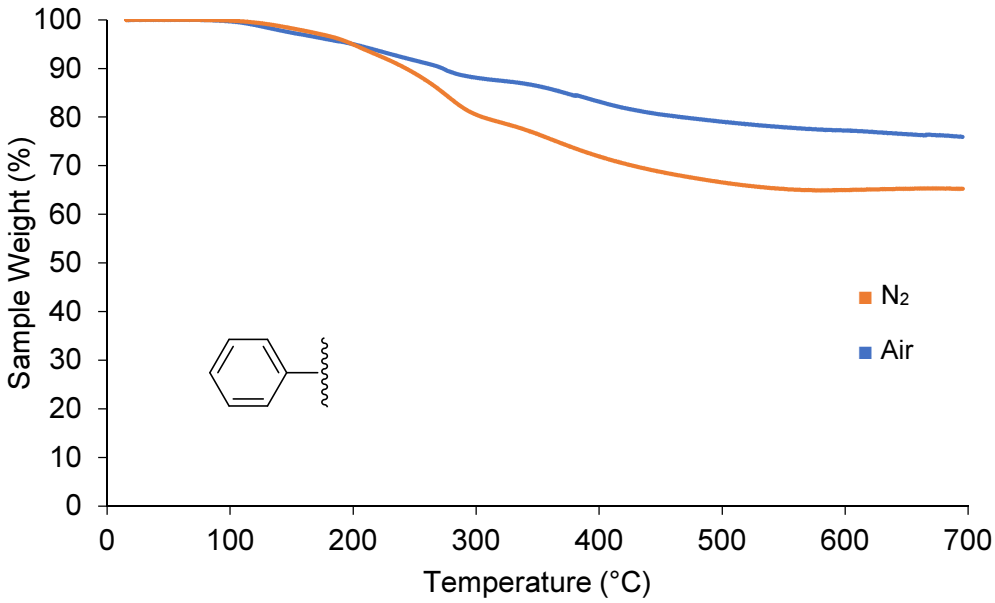

Figure S2.48. TGA thermograms of polymer **2.2b** heated under N_2 (■) and an air blend (O_2/N_2) (■) (heating rate: 10 °C min^{-1}).

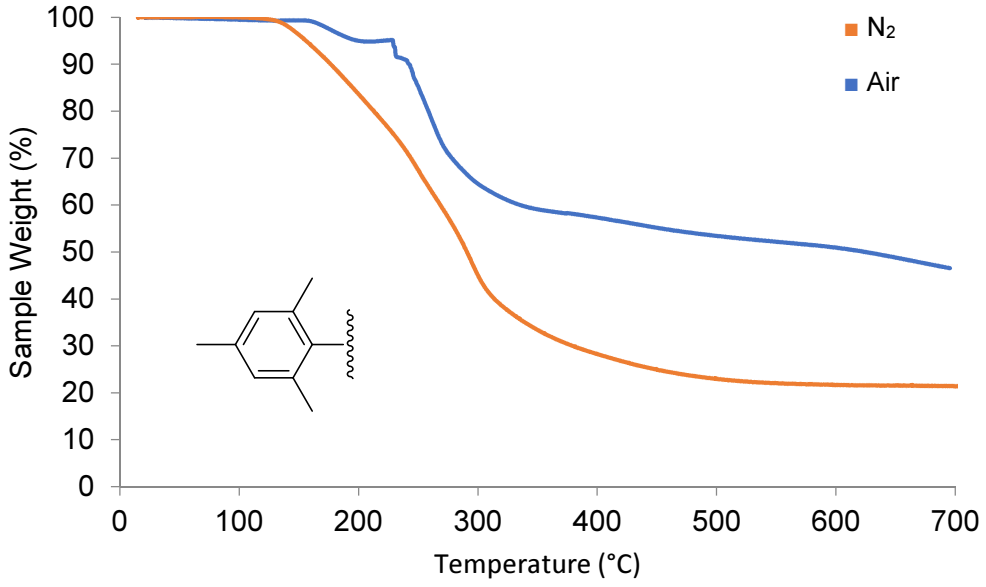

Figure S2.49. TGA thermograms of polymer **2.2e** heated under N_2 (■) and an air blend (O_2/N_2) (■) (heating rate: 10 °C min^{-1}).

2.5.8 Atomic Adsorption Spectroscopy

Sample preparation was carried out by weighing two samples of **2.2b** on a Micro Balance which were subsequently transferred to a 10 mL volumetric flask. 2M nitric acid (trace quality) was added and the samples were agitated over a 24 h period to maximise Fe extraction. Standards of 0.5,1.2, 4.6, 8.0 and 10 ppm were then made up from a 1000 ppm certified Fe standard.

The samples were then run on a GBC sigma Graphite furnace AAS calibrated using the reference standards and the acid as a blank. The conditions used were: DRY 100 °C, ASH 800 °C and Atomize 2300 °C. The experiments were measured at a wavelength of 248.3 nm, a slit of 0.2 nm and lamp current of 7 mA with background correction. Average measured Fe content: 0.40 wt% (0.88 mol%).

2.5.9 Energy Dispersive X-Ray Spectroscopy (EDX)

Samples of **2.2a**, **2.2b** and **2.2e** were dissolved in CH_2Cl_2 (2 mg mL^{-1}) and drop cast onto carbon coated Cu grids, suitable for analysis by EDX.

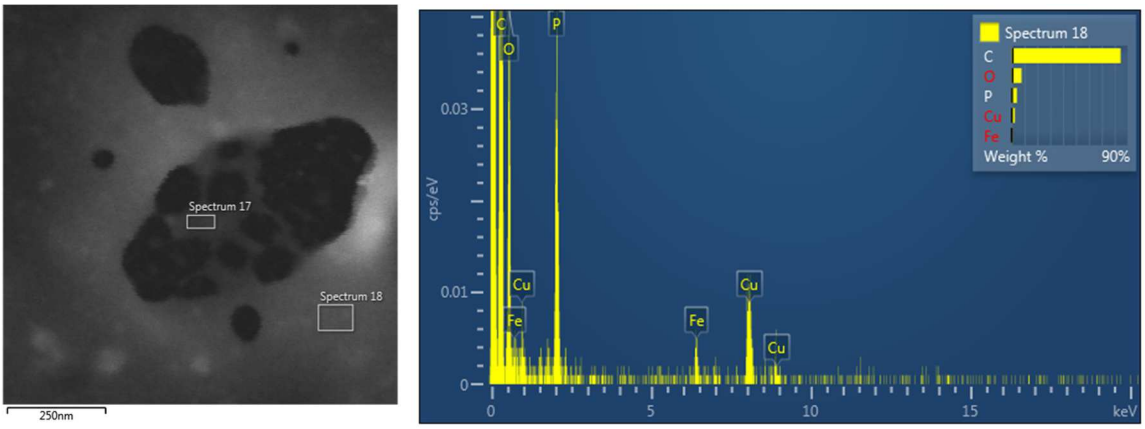

Figure S2.50. TEM Image of **2.2a** (Top) highlighting area analysed by EDX (Spectrum 18, bottom).

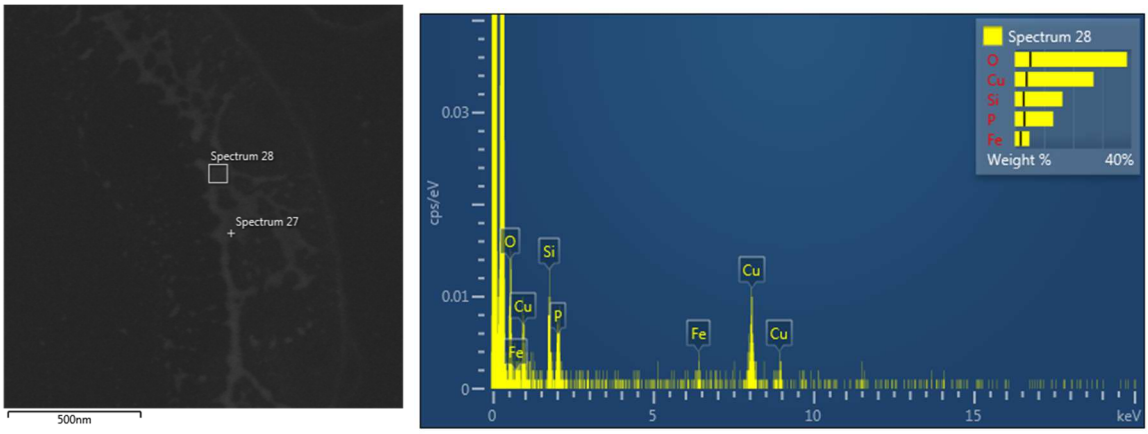

Figure S2.51. TEM Image of **2.2b** (Top) highlighting area analysed by EDX (Spectrum 28, bottom).

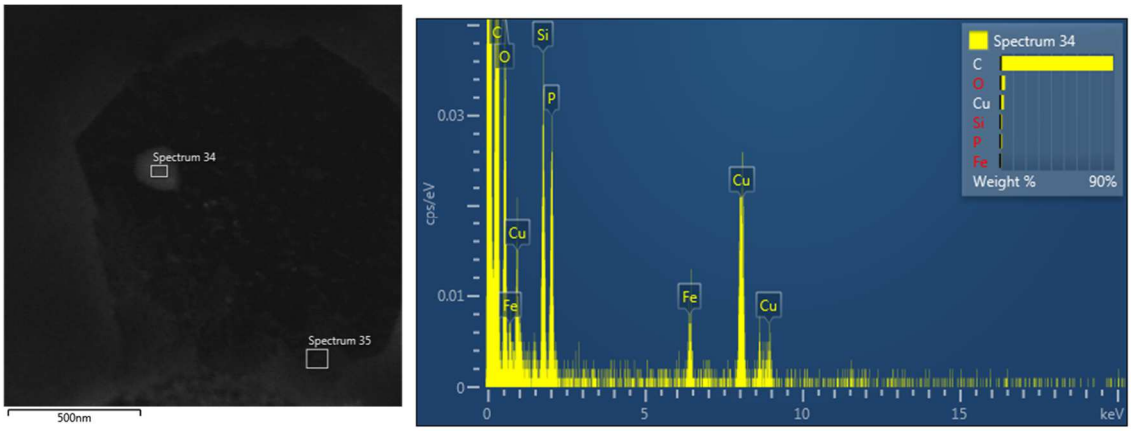

Figure S2.52. TEM Image of **2.2e** (Top) highlighting area analysed by EDX (Spectrum 34, bottom).

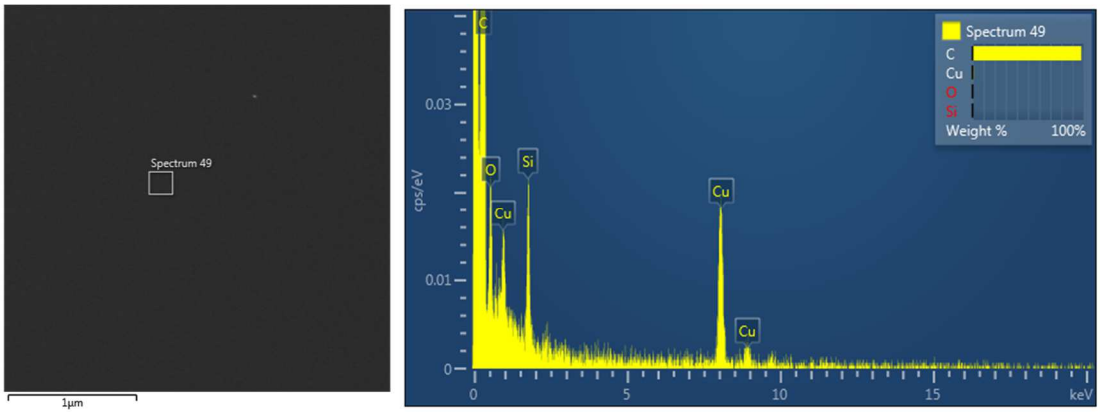

Figure S2.53. TEM Image of a blank Cu grid (Top) highlighting area analysed by EDX (Spectrum 49, bottom).

2.5.10 Thermal analysis of 2.2.b

A sample of **2.2b** was heated to 900 °C at 10 °C min^{-1} (250 mL min^{-1} N_2) in a tube furnace before being held at that temperature for 1h. The sample was allowed to cool and was subsequently analysed by powder XRD.

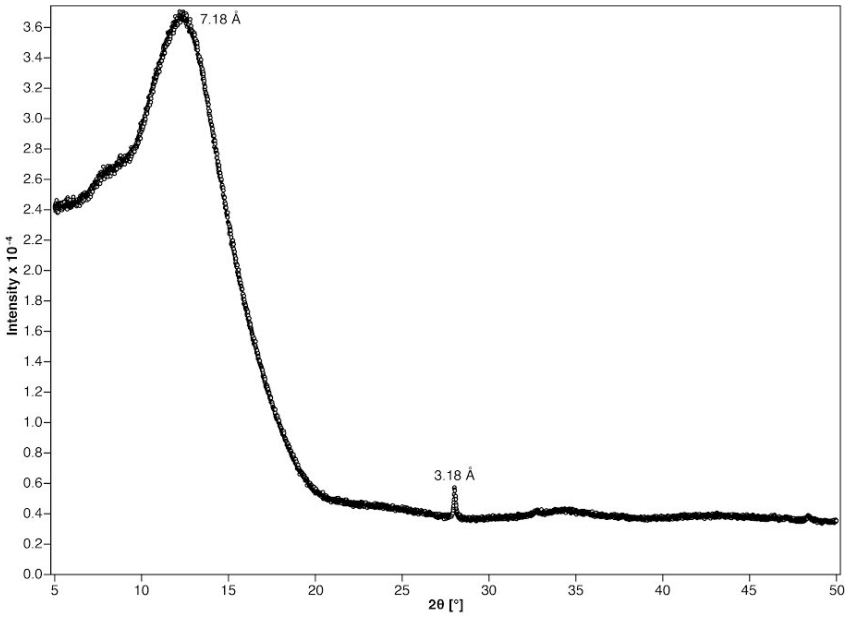

Figure S2.54. Powder X-ray diffraction data at 298 K.

2.5.11 Soft lithography

Samples were prepared by dissolving 2 mg of polymer **2.2e** in 1 mL of THF and drop-casting on a clean silicon wafer (slowly until the entire sample was loaded onto the wafer). A pre-prepared patterned polydimethylsiloxane (PDMS) stamp was then placed on top of the wafer and the sample was heated to the appropriate temperature for 5 min (150 °C) while maintaining pressure on the stamp with a small weight. While still hot, the PDMS stamp was carefully removed to reveal the silicon wafer patterned with polyphosphinoborane **2.2c**. Patterned samples were then imaged by Scanning Electron Microscopy.

2.5.12 Contact angle measurements

Measurements were performed by a Kruss Drop Shape Analyzer - DSA100. Thin films of **2.2a-e** were formed by spin coating, at 3000 rpm, a 5 mg mL^{-1} THF solution of **2.2a-e**. 24 h was allowed to pass to allow for the films to dry, after which time a 2 µL drop was deposited on the surface. The advancing contact angle was recorded immediately and multiple drops were averaged. The error was estimated to be ±2°.

Table S2.5. Measured contact angles of thin films of **2.2a-e** with 2 µL deionised water droplets.

Polymer	Advancing Contact Angle (°)
2.2a	64
2.2b	70
2.2c	101
2.2d	97
2.2e	78

2.6 References

1. Manners, I., *Angew. Chem. Int. Ed.* **1996,** *35*, 1602-1621.

2. Priegert, A. M.; Rawe, B. W.; Serin, S. C.; Gates, D. P., *Chem. Soc. Rev.* **2016,** *45*, 922-953.

3. Jäkle, F., *Chem. Rev.* **2010,** *110*, 3985-4022.

4. (a) Heeney, M.; Zhang, W.; Crouch, D. J.; Chabinyc, M. L.; Gordeyev, S.; Hamilton, R.; Higgins, S. J.; McCulloch, I.; Skabara, P. J.; Sparrowe, D.; Tierney, S., *Chem. Commun.* **2007**, 5061-5063; (b) Leitao, E. M.; Jurca, T.; Manners, I., *Nature Chemistry* **2013,** *5*, 817-829; (c) He, G.; Kang, L.; Torres Delgado, W.; Shynkaruk, O.; Ferguson, M. J.; McDonald, R.; Rivard, E., *J. Am. Chem. Soc.* **2013,** *135*, 5360-5363; (d) Rawe, B. W.; Gates, D. P., *Angew. Chem. Int. Ed.* **2015,** *54*, 11438-11442.

5. (a) Allcock, H. R.; Kugel, R. L., *Inorg. Chem.* **1966,** *5*, 1716-1718; (b) Neilson, R. H.; Wisian-Neilson, P., *Chem. Rev.* **1988,** *88*, 541-562; (c) Liang, M.; Manners, I., *J. Am. Chem. Soc.* **1991,** *113*, 4044-4045; (d) Allcock, H. R., *Chem. Mater.* **1994,** *6*, 1476-1491; (e) Honeyman, C. H.; Manners, I.; Morrissey, C. T.; Allcock, H. R., *J. Am. Chem. Soc.* **1995,** *117*, 7035-7036; (f) Allcock, H. R.; Nelson, J. M.; Reeves, S. D.; Honeyman, C. H.; Manners, I., *Macromolecules* **1997,** *30*, 50-56; (g) De Jaeger, R.; Gleria, M., *Prog. Polym. Sci.* **1998,** *23*, 179-276; (h) Allcock, H. R., *Soft Matter* **2012,** *8*, 7521-7532; (i) Wilfert, S.; Henke, H.; Schoefberger, W.; Brüggemann, O.; Teasdale, I., *Macromol. Rapid Commun.* **2014,** *35*, 1135-1141; (j) Allcock, H. R., *Dalton Trans.* **2016,** *45*, 1856-1862; (k) Rothemund, S.; Teasdale, I., *Chem. Soc. Rev.* **2016,** *45*, 5200-5215; (l) Presa-Soto, D.; Carriedo, G. A.; de la Campa, R.; Presa Soto, A., *Angew. Chem. Int. Ed.* **2016,** *55*, 10102-10107.

6. (a) Li, Y.; Kawakami, Y., *Macromolecules* **1998,** *31*, 5592-5597; (b) Mark, J. E., *Acc. Chem. Res.* **2004,** *37*, 946-953.

7. (a) West, R., *J. Organomet. Chem.* **1986,** *300*, 327-346; (b) Miller, R. D.; Michl, J., *Chem. Rev.* **1989,** *89*, 1359-1410.

8. (a) Imori, T.; Lu, V.; Cai, H.; Tilley, T. D., *J. Am. Chem. Soc.* **1995,** *117*, 9931-9940; (b) Trummer, M.; Choffat, F.; Smith, P.; Caseri, W., *Macromol. Rapid Commun.* **2012,** *33*, 448-460; (c) Harrypersad, S.; Foucher, D., *Chem. Commun.* **2015,** *51*, 7120-7123; (d) Caseri, W., *Chem. Soc. Rev.* **2016,** *45*, 5187-5199.

9. (a) Staubitz, A.; Presa Soto, A.; Manners, I., *Angew. Chem. Int. Ed.* **2008,** *47*, 6212-6215; (b) Staubitz, A.; Sloan, M. E.; Robertson, A. P. M.; Friedrich, A.; Schneider, S.; Gates, P. J.; Günne, J. S. a. d.; Manners, I., *J. Am. Chem. Soc.* **2010,** *132*, 13332-13345; (c) Vance, J. R.; Robertson, A. P. M.; Lee, K.; Manners, I., *Chem. Eur. J.* **2011,** *17*, 4099-4103; (d) Dallanegra, R.; Robertson, A. P. M.; Chaplin, A. B.; Manners, I.; Weller, A. S., *Chem. Commun.* **2011,** *47*, 3763-3765; (e) Marziale, A. N.; Friedrich, A.; Klopsch, I.; Drees, M.; Celinski, V. R.; Schmedt auf der Günne, J.; Schneider, S., *J. Am. Chem. Soc.* **2013,** *135*, 13342-13355; (f) Thiedemann, B.; Gliese, P. J.; Hoffmann, J.; Lawrence, P. G.; Sönnichsen, F. D.; Staubitz, A., *Chem. Commun.* **2017,** *53*, 7258-7261; (g) Wan, W.-M.; Baggett, A. W.; Cheng, F.; Lin, H.; Liu, S.-Y.; Jäkle, F., *Chem. Commun.* **2016,** *52*, 13616-13619; (h) Lorenz, T.; Lik, A.; Plamper, F. A.; Helten, H., *Angew. Chem. Int. Ed.* **2016,** *55*, 7236-7241.

10. (a) Dorn, H.; Singh, R. A.; Massey, J. A.; Lough, A. J.; Manners, I., *Angew. Chem. Int. Ed.* **1999,** *38*, 3321-3323; (b) Dorn, H.; Singh, R. A.; Massey, J. A.; Nelson, J. M.; Jaska, C. A.; Lough, A. J.; Manners, I., *J. Am. Chem. Soc.* **2000,** *122*, 6669-6678; (c) Dorn, H.; Vejzovic, E.; Lough, A. J.; Manners, I., *Inorg. Chem.* **2001,** *40*, 4327-4331; (d) Dorn, H.; Rodezno, J. M.; Brunnhöfer, B.; Rivard, E.; Massey, J. A.; Manners, I., *Macromolecules* **2003,** *36*, 291-297; (e) Denis, J.-M.; Forintos, H.; Szelke, H.; Toupet, L.; Pham, T.-N.; Madec, P.-J.; Gaumont, A.-C., *Chem. Commun.* **2003**, 54-55; (f) Jacquemin, D.; Lambert, C.; Perpète, E. A., *Macromolecules* **2004,** *37*, 1009-1015; (g) Clark, T. J.; Rodezno, J. M.; Clendenning, S. B.; Aouba, S.; Brodersen, P. M.; Lough, A. J.; Ruda, H. E.; Manners, I., *Chem. Eur. J.* **2005,** *11*, 4526-4534; (h) Pandey, S.; Lönnecke, P.; Hey-Hawkins, E., *Eur. J. Inorg.*

Chem. **2014,** *2014*, 2456-2465; (i) Schäfer, A.; Jurca, T.; Turner, J.; Vance, J. R.; Lee, K.; Du, V. A.; Haddow, M. F.; Whittell, G. R.; Manners, I., *Angew. Chem. Int. Ed.* **2015,** *54*, 4836-4841; (j) Marquardt, C.; Jurca, T.; Schwan, K.-C.; Stauber, A.; Virovets, A. V.; Whittell, G. R.; Manners, I.; Scheer, M., *Angew. Chem. Int. Ed.* **2015,** *54*, 13782-13786; (k) Paul, U. S. D.; Braunschweig, H.; Radius, U., *Chem. Commun.* **2016,** *52*, 8573-8576.

11. (a) Clarson, S. J.; Semlyen, J. A., *Siloxane Polymers*. Prentice Hall: Englewood Cliffs: 1993; (b) Archer, R. D., *Inorganic and Organometallic Polymers*. Wiley-VCH: New York: 2004; (c) Choffat, F.; Kaeser, S.; Wolfer, P.; Schmid, D.; Mezzenga, R.; Smith, P.; Caseri, W., *Macromolecules* **2007,** *40*, 7878-7889; (d) Rawe, B. W.; Chun, C. P.; Gates, D. P., *Chem. Sci.* **2014,** *5*, 4928-4938; (e) Linshoeft, J.; Baum, E. J.; Hussain, A.; Gates, P. J.; Nather, C.; Staubitz, A., *Angew. Chem. Int. Ed.* **2014,** *53*, 12916-12920; (f) Cao, W.; Gu, Y. W.; Meineck, M.; Li, T. Y.; Xu, H. P., *J. Am. Chem. Soc.* **2014,** *136*, 5132-5137.

12. Staubitz, A.; Robertson, A. P. M.; Sloan, M. E.; Manners, I., *Chem. Rev.* **2010,** *110*, 4023-4078.

13. Parshall, G. W., *In The Chemistry of Boron and its Compounds*. Wiley: New York, 1967.

14. Burg, A. B.; Wagner, R. I., *J. Am. Chem. Soc.* **1953,** *75*, 3872-3877.

15. Burg, A. B., *J. Inorg. Nucl. Chem.* **1959,** *11*, 258.

16. Burg, A. B., *J. Inorg. Nucl. Chem.* **1959,** *11*, 258-258.

17. Pandey, S.; Lönnecke, P.; Hey-Hawkins, E., *Inorg. Chem.* **2014,** *53*, 8242-8249.

18. Grant, D. J.; Dixon, D. A., *The Journal of Physical Chemistry A* **2006,** *110*, 12955-12962.

19. (a) Hooper, T. N.; Weller, A. S.; Beattie, N. A.; Macgregor, S. A., *Chem. Sci.* **2016,** *7*, 2414-2426; (b) Johnson, H. C.; Hooper, T. N.; Weller, A. S., *Top. Organometal. Chem.* **2015,** *49*, 153-220; (c) Huertos, M. A.; Weller, A. S., *Chem. Sci.* **2013,** *4*, 1881-1888.

20. Stauber, A.; Jurca, T.; Marquardt, C.; Fleischmann, M.; Seidl, M.; Whittell, G. R.; Manners, I.; Scheer, M., *Eur. J. Inorg. Chem.* **2016**, 2684-2687.

21. Hansch, C.; Leo, A.; Taft, R. W., *Chem. Rev.* **1991,** *91*, 165-195.

22. Fox, A.; Hartman, J. S.; Humphries, R. E., *J. Chem. Soc., Dalton Trans.* **1982**, 1275-1283.

23. Jeffrey, G. A., *An Introduction to Hydrogen Bonding*. Oxford University Press: **1997**.

24. Klooster, W. T.; Koetzle, T. F.; Siegbahn, P. E. M.; Richardson, T. B.; Crabtree, R. H., *J. Am. Chem. Soc.* **1999,** 1*21,* 6337-6343.

25. Richardson, T.; de Gala, S.; Crabtree, R. H.; Siegbahn, P. E. M., *J. Am. Chem. Soc.* **1995,** 1*17,* 12875-12876.

26. Blank, N. F.; McBroom, K. C.; Glueck, D. S.; Kassel, W. S.; Rheingold, A. L., *Organometallics* **2006,** 2*5,* 1742-1748.

27. Pelczar, E. M.; Nytko, E. A.; Zhuravel, M. A.; Smith, J. M.; Glueck, D. S.; Sommer, R.; Incarvito, C. D.; Rheingold, A. L., *Polyhedron* **2002,** 2*1,* 2409-2419.

28. Heatley, F., Introduction to NMR and its use in the study of polymer stereochemistry. In *NMR Spectroscopy of Polymers,* Ibbett, R. N., Ed. Springer Netherlands: Dordrecht, **1993**; pp 1-49.

29. Böhme, U.; Scheler, U., *Macromol. Symp.* **2002,** 1*84,* 349-356.

30. Aldebert, P.; Gebel, G.; Loppinet, B.; Nakamura, N., *Polymer* **1995,** 3*6,* 431-434.

31. Jacquemin, D.; Perpète, E. A., *J. Phys. Chem . A* **2005,** 1*09,* 6380-6386.

32. Shishkov, I. F.; Geise, H. J.; Van Alsenoy, C.; Khristenko, L. V.; Vilkov, L. V.; Senyavian, V. M.; Van der Veken, B.; Herrebout, W.; Lokshin, B. V.; Garkusha, O. G., *J. Mol. Struct.* **2001,** 5*67–568,* 339-360.

33. Rieger, J., *J. Therm. Anal. Calorim.* **1996,** 4*6,* 965-972.

34. Teng, H.; Lou, L.; Koike, K.; Koike, Y.; Okamoto, Y., P*olymer* **2011,** 5*2,* 949-953.

35. Lipomi, D. J.; Martinez, R. V.; Cademartiri, L.; Whitesides, G. M., 7.11 - Soft Lithographic Approaches to Nanofabrication. In *Polymer Science: A Comprehensive Reference,* Matyjaszewski, K.; Möller, M., Eds. Elsevier: Amsterdam, 2012; pp 211-231.

36. S. Wu, *Polymer Interface and Adhesion*, Marcel Dekker, New York, NY, **1982**, p. 142-146.

37. Strobel, M.; Thomas, P. A.; Lyons, C. S., *J. Polym. Sci., Part A: Polym. Chem.* **1987,** 2*5,* 3343-3348.

38. Liston, D. J.; Lee, Y. J.; Scheidt, W. R.; Reed, C. A., *J. Am. Chem. Soc.* **1989,** 1*11,* 6643-6648.

39. Pangborn, A. B.; Giardello, M. A.; Grubbs, R. H.; Rosen, R. K.; Timmers, F. J., *Organometallics* **1996,** 1*5,* 1518-1520.

40. Sheldrick, G. M., *Acta Crystallogr A* **2008,** 6*4,* 112-122.

41. (a) Palatinus, L.; Chapuis, G., *J. Appl. Crystallogr.* **2007,** 4*0,* 786-790; (b) Palatinus, L.; Prathapa, S. J.; van Smaalen, S., *J. Appl. Crystallogr.* **2012,** 4*5,* 575-580.

42. Bourhis, L. J.; Dolomanov, O. V.; Gildea, R. J.; Howard, J. A. K.; Puschmann, H., *Acta Crystallogr. A* **2015,** 7*1,* 59-75.

43. Dolomanov, O. V.; Bourhis, L. J.; Gildea, R. J.; Howard, J. A. K.; Puschmann, H., *J. Appl. Crystallogr.* **2009,** 4*2,* 339-341.

44. Bourumeau, K.; Gaumont, A.-C.; Denis, J.-M., *J. Organomet. Chem.* **1997,** 5*29,* 205-213.

Chapter 3

Poly(alkylphosphinoboranes) *via* Iron-Catalysed Dehydropolymerisation

3.1 Abstract

High molar mass polyphosphinoboranes substituted with an alkyl group at phosphorus $[RPH–BH_2]_n$ (R = *t*Bu, 1-Ad, *i*Pr, Cy, *n*Hex, Me) have been successfully prepared *via* the dehydropolymerisation of the phosphine–boranes $RPH_2–BH_3$ using an iron precatalyst, $[CpFe(CO)_2OTf]$ (100 °C, toluene, 2 M, 10–100 h). Substrate purity and the reaction conditions were found to be crucial to obtaining high molar mass (M_n = 14,000 – 57,000 g mol^{-1}) material. For example, the addition of primary phosphines, a potential monomer contaminant, was found to lead to lower molar mass oligomeric material $[RPH–BH_2]_x$. The polymers were characterised through multinuclear NMR spectroscopy, gel permeation chromatography (GPC), and electrospray ionisation mass spectroscopy (ESI-MS). The thermal properties were also investigated by thermogravimetric analysis (TGA), which showed the materials to be stable to weight loss up to 100 – 120 °C and differential scanning calorimetry (DSC), which revealed strongly side-group dependent T_g values that ranged from −76 to 87 °C.

3.2 Introduction

Inorganic macromolecules containing *p*-block elements are of interest as functional materials with properties that differ from those of hydrocarbon-based polymers.[1] For example, boron-containing polymers have attracted attention as precursors to high-performance ceramic materials and as optoelectronic and sensory materials.[2,3] Catalytic dehydrocoupling of primary amine–borane adducts $RNH_2{\cdot}BH_3$ has been developed as a route to high molar mass polyaminoboranes $[RNH–BH_2]_n$,[4] which are isoelectronic, inorganic analogues of polyolefins. These materials possess interesting potential applications as piezoelectrics[5] and as precursors to BN ceramics.[6] Analogous high molar mass aryl *P*-substituted polyphosphinoboranes $[RPH–BH_2]_n$ (R = Ph or *para*-substituted aryl) were initially prepared through catalytic P–B bond formation *via* a dehydropolymerisation reaction involving primary phosphine–boranes $RPH_2{\cdot}BH_3$ assisted by Rh-based precatalysts, at 90–130 °C under melt conditions.[7] The temperature of dehydropolymerisation can be lowered to 60 °C when activated adducts substituted with electron-withdrawing perfluorinated aryl groups are used.[8] Poly(arylphosphinoboranes) are air and moisture stable, with prospective applications as ceramic precursors of boron phosphide[7c, 9] and as electron beam resists in lithography.[8, 10] However, the need for melt conditions to obtain high molar mass polymers has hindered the development of new PB materials.

The recent discovery of $[CpFe(CO)_2OTf]$ as an alternative dehydropolymerisation precatalyst led to access to high molar mass poly(arylphosphinoboranes) $[RC_6H_5PH–BH_2]_n$ (R = electron-withdrawing or -donating groups on aryl) in solution at 100 °C over 24 h. Furthermore, control over the molar mass of the polymer was achieved by varying the catalyst loading, and a coordination chain growth mechanism was proposed.[10] Other metal catalysts based on Ir, Rh, and Fe have also been successfully applied to the production of aryl *P*-substituted polyphosphinoboranes.[4j, 11] Previously, it has been demonstrated that

sterically encumbered phosphine–boranes tBuPH$_2$·BH$_3$ and tBu$_2$HP·BH$_3$ could be dehydrocoupled in the presence of catalytic amounts of Ni or Rh complexes respectively, to form linear dimeric species with no indication of higher mass oligomeric or polymeric material.[12]

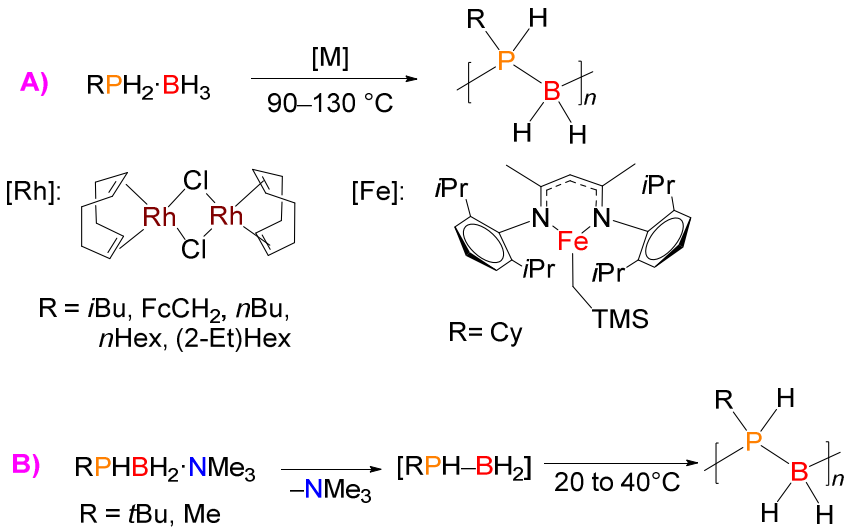

Scheme 3.1. Synthetic routes to poly(alkyl)phosphinoboranes

As a consequence of the development of improved catalytic procedures high molar mass poly(arylphosphinoboranes) are being increasingly studied. In contrast, much less is known about poly(alkylphosphinoboranes). The synthesis of alkyl *P*-substituted polymers would be expected to be significantly more challenging through catalytic dehydrocoupling routes because of the lower acidity of the P–H group in the precursor due to the inductive effect of the alkyl group attached to phosphorus.[7c, 13] Consistent with this, the dehydropolymerisation of iBuPH$_2$·BH$_3$ gave moderate molar mass polymer (M_w = 10,000 – 20,000 g mol^{-1}) [iBuPH-BH$_2$]$_n$ under forcing conditions (melt, 120°C, 13 h) using [Rh(μ-Cl)(1,5-COD)]$_2$ (COD = cyclooctadiene) as a precatalyst (Scheme 3.1A).[7c] More recent studies of the dehydropolymerisation of alkyl phosphine–boranes using the same precatalyst demonstrated that the dehydrocoupling of RPH$_2$·BH$_3$ (R = FcCH$_2$, nBu, nHex, (2-Et)Hex), in general, has given lower molar mass (M_n < 10,000 g mol^{-1}),[9, 13] and relatively branched materials with varied polydispersity index values (PDI = 1.2–5.0) under forcing

thermal conditions (90–130 °C) and in the melt. In collaboration with the *Scheer* group we have demonstrated the viability of an alternative, addition polymerization route to poly(alkylphosphinoboranes) involving metal-free head-to-tail polymerization of transient monomeric phosphinoboranes thermally generated from Lewis base-stabilized precursors. This allowed the isolation of polymeric $[t\text{BuPH–BH}_2]_n$ (M_n = 27,800 – 35,000 g mol^{-1}, PDI = 1.6–1.9) and oligomeric material ($[\text{MePH–BH}_2]_x$ and $[\text{Ph}_2\text{P–BH}_2]_x$; M_n < 2,400 g mol^{-1}) (Scheme 3.1B).[14] Although this method represents an interesting breakthrough the precursors can only be accessed in several synthetic steps.

We have therefore attempted to develop the use of catalysts based on Earth-abundant transition metals that function under more solution and milder conditions in order to promote the exploration of high molar mass poly(alkylphosphinoboranes). In a promising recent report, *Webster* and coworkers studied a low-coordinate Fe(II) β-diketiminate precatalyst [LFe(CH_2SiMe_3)], (L^- = $[(\text{DippNC(Me)})_2\text{CH}]^-$, Dipp = 2,6-diisopropylphenyl) for the dehydrocoupling of $\text{CyPH}_2\cdot\text{BH}_3$ and showed that in solution (110°C, 72 h) formation of low but significant quantities (<10%) of high molar mass $[\text{CyPH–BH}_2]_n$ (M_n = 54,600 g mol^{-1}, PDI = 1.3) was observed, although the main fraction was oligomeric (M_n < 2,000 g mol^{-1}) (Scheme 3.1A).[4j] In a preliminary study, our group attempted the dehydrocoupling of $t\text{BuPH}_2\cdot\text{BH}_3$ with the $[\text{CpFe(CO)}_2\text{OTf}]$ precatalyst and found that at 5 mol% precatalyst loading using 1.0 M concentration of substrate in toluene, and after heating at 100 °C for 176 h only low molecular mass oligomers of $[t\text{BuPH–BH}_2]_x$ (where $x \leq 10$) could be isolated.[14a] Herein, we have reinvestigated the dehydropolymerisation of alkyl substituted phosphine–borane substrates using $[\text{CpFe(CO)}_2\text{OTf}]$ as a precatalyst in detail and found that, under the correct conditions, the process does indeed result in the formation of high molar mass materials. We have used this route to prepare a family of alkyl *P*-monosubstituted polyphosphinoboranes, $[\text{RPH–BH}_2]_n$.

3.3 Results and Discussion

3.3.1 Catalytic Dehydrocoupling of *t*BuPH$_2$·BH$_3$ with the Precatalyst [CpFe(CO)$_2$OTf].

We began our reinvestigation of the Fe-catalysed dehydrocoupling reaction of *t*BuPH$_2$·BH$_3$ (δ = −44.5 ppm and δ = −11.9 ppm) mediated by the precatalyst [CpFe(CO)$_2$OTf] (1.0 mol%) in toluene (2.0 M) with experiments performed on a 1 mmol scale at 100 °C (see Scheme 3.2).

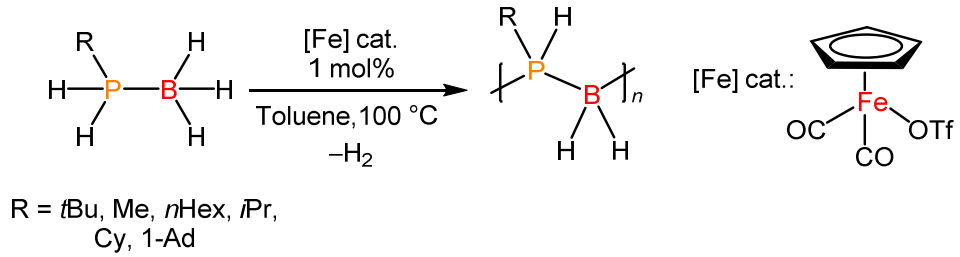

R = *t*Bu, Me, *n*Hex, *i*Pr, Cy, 1-Ad

Scheme 3.2. Catalytic dehydropolymerisation of phosphine–boranes RPH$_2$·BH$_3$ with precatalyst [FeCp(CO)$_2$(OTf)] (1 mol%, toluene, 2.0 M, 100 °C) to give polyphosphinoboranes [RPH–BH$_2$]$_n$.

After 48 h, full conversion to [*t*BuPH–BH$_2$]$_n$ was detected by ^{11}B NMR (δ = −38.6 ppm) and ^{31}P NMR (δ = −19.7 ppm) spectroscopy and the broad signals detected were in accordance to the material prepared previously *via* the thermal-induced polymerisation of *t*BuPHBH$_2$·NMe$_3$.[14a] Surprisingly based on our brief previous study, we found that the majority of the [*t*BuPH–BH$_2$]$_n$ polymer isolated was of high molecular weight (M_n = 31,600 g mol^{-1}, PDI = 1.48) based on gel permeation chromatography (GPC) analysis with THF (0.1 *w*/*w* % *n*Bu$_4$NBr) as an elution solvent (see SI, Fig. S3.10). However, the formation of a much lower mass oligomeric component was also detected. Electrospray ionisation mass spectroscopy (ESI-MS) of the material revealed the expected repeat unit of Δ(m/z) = 102 Da within the oligomeric fraction with a DP$_n$ of 25, and with a residual mass corresponding to a phosphine end group, H–[*t*BuPH–BH$_2$]$_x$–PH$_2$*t*Bu.

In a control experiment a 2.0 M toluene solution of *t*BuPH$_2$·BH$_3$ was heated to 100 °C in a sealed J. Young NMR tube in the absence of catalyst. In contrast to the Fe-catalyzed reaction, after 48 h less than 5% monomer conversion was observed by $^{31}P\{^1H\}$ and $^{11}B\{^1H\}$ NMR spectroscopy. After 30 days, >90% conversion was observed by NMR spectroscopy and the resulting material was isolated. By ^1H NMR spectroscopy, this material showed more sharp signals at δ = 1.4 to 1.1 ppm, corresponding to the CH$_3$ groups, probably arising from mixture of small molecules and oligomeric material which could not be separated (see SI, Fig. S3.7). In addition, the $^{31}P\{^1H\}$ NMR spectrum displayed a set of ill-defined signals at δ = −11, −13, −15, −18, −21, and −23 ppm, which are further broadened in the ^1H-coupled ^{31}P NMR spectrum (see SI, Fig. S3.9). Some of these signals have a similar chemical shift to those reported for the dimer *t*BuPH$_2$BH$_2$P*t*BuHBH$_3$ (δ = −24.5 to −20.0 (m), −14 to −11 (m) ppm) prepared *via* catalytic dehydrocoupling of *t*BuPH$_2$·BH$_3$ with [NiCl$_2$] (10 mol %, 100 °C, 1 h).[12b] In addition, the signals at δ = −18 and −21 ppm, are in a similar chemical shift range as those observed for the oligomeric material [*t*BuPH–BH$_2$]$_x$ prepared *via* dehydrocoupling of *t*BuPH$_2$·BH$_3$ with the [CpFe(CO)$_2$OTf] precatalyst in our previous report (5 mol %, 100 °C, 176 h).[14a] In contrast, the polymer [*t*BuPH–BH$_2$]$_n$ prepared here by the [CpFe(CO)$_2$OTf] catalysed polymerisation of *t*BuPH$_2$·BH$_3$ presented broad signals in both the ^1H NMR and $^{31}P\{^1H\}$ spectra (see Fig. 3.1).

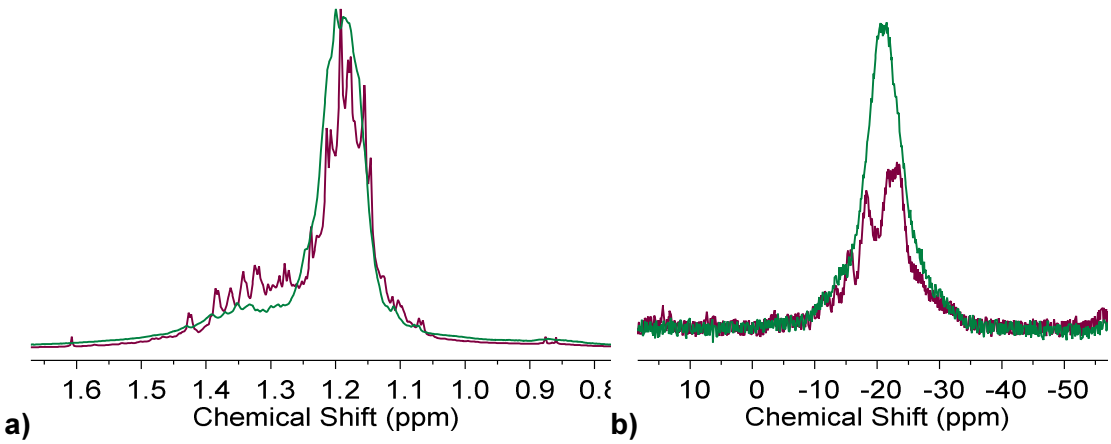

Figure 3.1. a) ^1H and b) $^{31}P\{^1H\}$ NMR spectra for [RPH–BH$_2$]$_x$ prepared in thermal conditions (toluene, 2.0 M, 100 °C, 30 days) (purple) and [RPH–BH$_2$]$_n$ prepared in catalytic conditions with precatalyst [CpFe(CO)$_2$(OTf)] (1 mol%, toluene, 2.0 M, 100 °C, 48 h) (green).

By GPC, the material prepared by the non-catalysed reaction after 30 days at 100 °C in toluene contained a small fraction corresponding to high molar mass [*t*BuPH–BH_2]$_n$ (M_n = 63,400 g mol^{-1}, PDI = 1.50), however, short oligomers (M_n ca. 2,000 g mol^{-1}) and other small molecules which elute with the solvent peak were the main products (see SI, Fig. S3.10). Meanwhile the majority of the material obtained in the dehydropolymerisation reaction using the [$CpFe(CO)_2OTf$] catalyst prepared at 100 °C over 48 h was high molar mass [*t*BuPH–BH_2]$_n$ polymer. Previously, it was shown that the thermal dehydrocoupling of aryl-substituted phosphine–boranes at 100 °C in the absence of catalyst resulted in incomplete conversion of the monomer to produce short chain oligomers (M_n < 4,500 Da) after 24 h.[10b] When the dehydrocoupling of aryl-substituted phosphine–boranes was performed under the same reaction conditions but in the presence of catalytic [$CpFe(CO)_2OTf$] (5 mol%), higher molar mass polymer was observed (M_n = 12,000 – 209,000 g mol^{-1}).[10b] For both aryl and alkyl *P*-substituted phosphine–boranes it appears that under the reaction conditions in toluene at 100 °C both thermally promoted (non-catalysed) and metal-catalysed dehydropolymerisation are likely occurring, but there is a very large (15 fold) rate enhancement and an increase in the high molar mass fraction with added catalyst.

The formation of high molar mass poly(*t*-butylphosphinoborane) under similar conditions of Fe-catalysis to our earlier brief report that yielded oligomers inspired further investigation. In order to obtain further insight into the factors which could have led to oligomeric material in our earlier report,[14a] we performed a series of additional experiments. When the dehydropolymerisation reaction of *t*BuPH$_2$·BH_3 (using 5 mol% of [$CpFe(CO)_2OTf$]) at 100 °C was performed with either ACS lab grade toluene which had not been dried or degassed, or under an atmosphere of air in a sealed J. Young NMR tube, we observed that the dehydrocoupling reaction was complete after 41 h (M_n = 13,800 g mol^{-1}, PDI = 1.86). Although the product was of lower molar mass, the fact that this reaction could be performed using lab grade solvent under air further lends itself to the

user-friendliness of this synthetic methodology given that the reaction is not very sensitive to air or moisture, and rigorous exclusion thereof is not required.

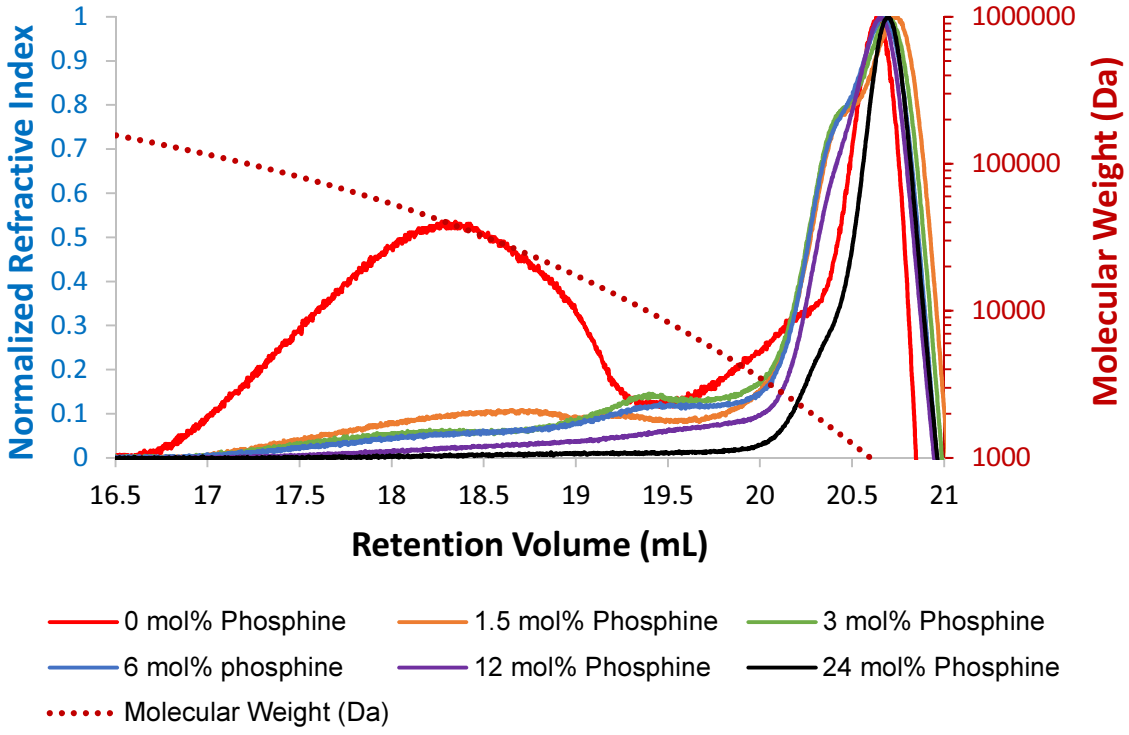

Figure 3.2. Overlay of GPC chromatograms (2 mg mL^{-1}) in THF (0.1 wt% [nBu$_4$N]Br) of [tBuPH–BH$_2$]$_n$ synthesized from the dehydropolymerisation of the phosphine–borane, tBuPH$_2$·BH$_3$, with different amounts of the primary phosphine tBuPH$_2$ added to the initial monomer feed. Reactions were performed with 2.0 M initial concentration of tBuPH$_2$·BH$_3$ in toluene with x mol% tBuPH$_2$ added where x is 0 (red trace), 1.5 (orange trace), 3 (green trace), 6 (blue trace), 12 (purple trace), 24 (black trace), and 1.0 mol% [CpFe(CO)$_2$OTf] catalyst in a sealed J. Young NMR tube at 100 °C for 48 h. Refractive indices were normalized versus the solvent/lower oligomers peak at ~20.7 mL retention volume. Polystyrene-based calibration curve given by dotted dark red trace.

In a series of polymerisation reactions with 1 mol% [CpFe(CO)$_2$OTf] at 100 °C where the amount of the primary phosphine tBuPH$_2$ added into the tBuH$_2$P·BH$_3$ monomer feed was varied in increasing amounts from 0 mol% to 24 mol% relative to the monomer, there was a significant decrease in the molar mass of polymer or oligomers obtained (Figure 3.2). With increasing amounts of added tBuPH$_2$ the majority of the material became increasingly oligomeric (M_n ca. 2,000 g mol^{-1}). Even with 1.5 mol% added tBuPH$_2$ a significant decrease in the fraction of higher weight polymer was detected. This highlights

the potential impact that trace phosphine impurities could have on the dehydropolymerisation process.

The primary phosphine tBuPH$_2$ possesses a sharp ^{31}P{^{1}H} NMR signal at 79.7 ppm in toluene but when tBuPH$_2$ is added in small amounts to solutions containing tBuPH$_2$·BH$_3$ the signal was significantly broadened and, in some cases was invisible in NMR spectra measured at 25 °C. The peak broadening is likely due to dynamic exchange processes occurring due to equilibria associated with dissociation of the P–B coordination bond of the Lewis acid-base adduct. Therefore, it is possible that free tBuPH$_2$ could be present in samples of the phosphine–borane adduct but not detected readily by NMR spectroscopy.

It has been shown that the addition of Lewis bases (LB) to polyphosphinoborane or polyaminoborane polymers under certain conditions can lead to depolymerisation through main-chain scission to afford donor-stabilized LB–BH$_2$–ERH (E = N, P) adducts.[15] Previously we found that [PhPH–BH$_2$]$_n$ was stable towards depolymerisation with diethylamine and tributylphosphine donors in THF solvent at room temperature.[16] When isolated [tBuPH–BH$_2$]$_n$ (sample with M_n = 28,600 g mol^{-1}, and PDI = 1.6) was treated with 1 eq. of tBuPH$_2$ per formula unit of the polymer in C$_6$D$_6$ at 22 °C for 22 h there was no change in the ^{31}P{^{1}H} or ^{11}B{^{1}H} NMR spectra, and upon heating at 100 °C for 48 h, reminiscent of the catalytic reaction conditions, there was also no change. Analysis of the phosphine treated sample by ESI-MS revealed no change in the distribution of peaks, and GPC chromatograms before and after phosphine treatment also revealed no change (see SI, Fig. 3.11). Therefore, it appears likely that additional primary phosphine, or phosphine generated *in situ* from dissociation of the phosphine–borane adduct, plays an intimate role in termination events during the dehydropolymerisation process. Phosphine-based termination processes are further supported by the fact that ESI-MS spectra of isolated materials reveal that the polymer is capped with phosphine end groups. Additional phosphine in the monomer feed led to a shift in [tBuPH–BH$_2$]$_n$ molecular mass distribution

towards low molar mass oligomers, and it appears that the added Lewis basic primary phosphine is not likely to be involved in main-chain scission post-polymerisation.

Previously, it was noted in the synthesis of $[PhPH–BH_2]_n$ with the $[FeCp(CO)_2OTf]$ precatalyst that there was an inverse dependence of the polymer molecular weight *vs.* catalyst loading where decreasing the precatalyst loading led to higher molecular weight polymer.[17] In contrast, in the synthesis of $[t\text{BuPH–BH}_2]_n$ with the $[FeCp(CO)_2OTf]$ precatalyst, there was no significant dependence on polymer molecular weight when the precatalyst loading was varied from 10 mol % (M_n = 23,500 g mol^{-1}, PDI = 1.62), to 0.1 mol % (M_n = 18,400 g mol^{-1}, PDI = 2.16). The initial $t\text{BuPH}_2\cdot\text{BH}_3$ concentration in toluene also had a relatively small effect on the molecular mass of the $[t\text{BuPH–BH}_2]_n$ polymer isolated after reaction at 100 °C with 1.0 mol% $[CpFe(CO)_2OTf]$ catalyst (see SI, Fig. 3.12). The molar mass of the polymer obtained at 10.0 M initial substrate concentration was M_n = 34,800 g mol^{-1}, PDI = 1.53, and at 1.0 M initial substrate concentration the molecular mass was M_n = 29,700 g mol^{-1}, PDI = 1.55. However, the reaction time required to reach over 95% percent conversion did vary drastically from 24 h for the reaction performed at 10.0 M initial substrate concentration, to 13 days for the significantly more dilute reaction at 1.0 M initial concentration (see Figure S3.13).

3.3.2 Synthesis and Characterisation of Other Alkyl Phosphine–Boranes.

Given the successful synthesis of $[t\text{BuPH–BH}_2]_n$ *via* iron-catalysed dehydropolymerisation the previously assumed limitation concerning the efficiency of the catalytic dehydropolymerisation of alkyl substituted phosphine–borane substrates has been tackled.[14a] Since the synthetic methodologies described so far *via* either the metal-catalysed[7c, 13] and metal-free routes[14a, 18] have not been optimised in solution, we attempted the dehydropolymerisation of a range of different phosphine–boranes $RPH_2\cdot BH_3$ that

contain linear, branched or bulky alkyl groups in order to prepare high molecular weight poly(alkylphosphinoboranes).

The $RPH_2{\cdot}BH_3$ monomers (R = 1-Ad, *i*Pr, Cy, *n*Hex, Me) were prepared through either the direct reaction of the primary phosphine with commercially available $BH_3{\cdot}THF$ adduct analogous to Schmidbaur and Müller,[19] or reduction of the phosphine dichloride with $LiBH_4$. The phosphine–boranes $iPrPH_2{\cdot}BH_3$ and $1\text{-}AdPH_2{\cdot}BH_3$ have not been previously reported and were synthesised *via* reduction of the corresponding $RPCl_2$ precursor with 2.2 equivalents of $LiBH_4$ in Et_2O (see Scheme 3.3).

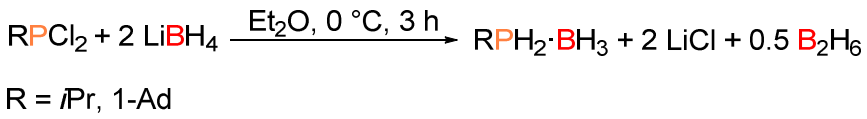

Scheme 3.3. Synthesis of new phosphine–boranes $RPH_2{\cdot}BH_3$ (R = *i*Pr, 1-Ad).

This protocol afforded the phosphine–borane $iPrPH_2{\cdot}BH_3$ in 26% yield as a colourless liquid at 20 °C, and the adduct $1\text{-}AdPH_2{\cdot}BH_3$ in 62% as a colourless solid at room temperature. The NMR data collected for $iPrPH_2{\cdot}BH_3$ and $1\text{-}AdPH_2{\cdot}BH_3$ corroborated the structures, and are comparable to other phosphine–borane adducts that have been previously described.[8, 20] For example, the ^{11}B NMR spectra each displayed a doublet of quartets at −44.6 ppm for $iPrPH_2{\cdot}BH_3$, and −45.0 ppm for $1\text{-}AdPH_2{\cdot}BH_3$, and the ^{31}P NMR spectra each displayed a broad triplet at −26.5 ppm for $iPrPH_2{\cdot}BH_3$, and −14.2 ppm for $1\text{-}AdPH_2{\cdot}BH_3$. The molecular structure of $1\text{-}AdPH_2{\cdot}BH_3$ was determined by single-crystal X-ray diffraction where crystals were obtained from an *n*-pentane solution at −40 °C (Figure 3.3). All of the other primary alkyl phosphine–borane monomers used in this study $RPH_2{\cdot}BH_3$ (R = *t*Bu, Cy, *i*Pr, *n*Hex, Me) are liquids at standard temperature and pressure.

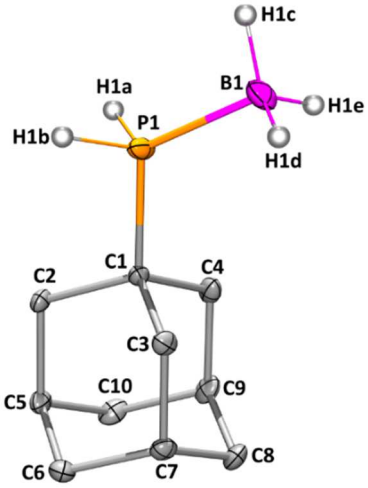

Figure 3.3. X-ray crystal structure of 1-AdPH_2·BH_3 with non-hydrogen atoms shown as 30% probability ellipsoids, and select H-atoms bound to B1 and P1 are shown as spheres of arbitrary radius.

3.3.3 Catalytic Dehydropolymerisation Studies of Other Alkyl Phosphine–Boranes *via* the Precatalyst [CpFe(CO)$_2$OTf].

The synthesis of oligomeric [MePH–BH_2]$_x$ where x is at least 40 repeat units was previously reported in collaboration with the Scheer group through the thermally-induced head-to-tail polymerisation reaction starting from Lewis base stabilized methylphosphinoborane.[14b]

In an initial evaluation of the dehydropolymerisation of adduct MePH_2·BH_3 *via* the [FeCp(CO)$_2$(OTf)] precatalyst (1 mol% precatalyst, toluene, 2.0 M initial MePH_2·BH_3 concentration), different temperatures were screened and the reaction progress was monitored by *in situ* ^{11}B NMR and ^{31}P NMR spectroscopy in a J. Young NMR tube. The reaction was initially heated at 50 °C and we observed a change of colour from red to yellow within 1 h, however, no dehydrocoupling products were observed after 21 h. Subsequently, the reaction temperature was increased to 70 °C in the same system, and moderate conversion (ca. 20%) of MePH_2·BH_3 to form polymer (ca. 17%) [MePH–BH_2]$_n$ was observed after 23 h. Finally, the temperature was further increased to 100 °C, where complete conversion to the polymer was achieved after 13 h (see Table 3.1). It has been mentioned

that the inductive effect of alkyl substituent attached to phosphorus impacts the activation of the P–H bond negatively.[8, 14a]

Based on these results, we continued our dehydropolymerisation studies (1 mol% $[FeCp(CO)_2(OTf)]$, toluene, 2.5 M) at 100 °C with the rest of the adducts $RPH_2{\cdot}BH_3$ (R = 1-Ad, *i*Pr, Cy, *n*Hex) on a 1 mmol scale (see Table 3.1). The consumption of monomer was determined by multinuclear NMR spectroscopy and it was observed that extended periods of time (24–100 h) were needed for complete conversion of the monomers to produce polymeric material.

Recently, the synthesis of soluble polymers $[RPH–BH_2]_n$ (R = *n*Bu, *n*Hex, 2-Et-Hex), was achieved by precatalyst $[Rh(\mu\text{-}Cl)(1,5\text{-}COD)]_2$ (melt, 120 °C), however, the conversion time depended on the precatalyst loading. For example, the synthesis of $[n\text{HexPH–BH}_2]_n$ required 22 h when 0.5 mol% of precatalyst was used; and 4 h when 2.0 mol% of Rh catalyst was added. Additionally, the reaction was monitored visually, and only stopped when the increase in viscosity in the reaction prevented effective mixing.[13] Although the dehydropolymerisation reaction of $n\text{HexPH}_2{\cdot}\text{BH}_3$ took extended periods of time (100 h) to fully convert to $[n\text{HexPH–BH}_2]_n$ using $[FeCp(CO)_2(OTf)]$, it has the advantage that the reaction proceeds in solution and could be tracked by NMR spectroscopy. On the other hand, the synthesis of $[MePH–BH_2]_n$ by thermally-induced (22 °C or 40 °C) reaction of phosphanylboranes $RPHBH_2{\cdot}NMe_3$ was formed in 20 h.[14a, 18] In our case, the formation of the identical polymer was achieved in shorter periods in 13 h, though forcing conditions are required (100 °C).

A trend for a series of aryl phosphine–boranes in which the chemical shift of P–H protons in the ^1H NMR spectrum is related to the electronic effect caused by the *para* substituent group in the phenyl ring was proposed.[10b] In this case, we could not find a specific trend on the chemical shift in the ^1H or ^{31}P NMR spectrum of phosphine–boranes that could be correlated with an electronic effect related to the dehydropolymerisation reaction.

Nevertheless, the alkyl-substituted polymers were obtained after purification either as pale yellow/off white solids or viscous gums in moderate to good yields (50–85%). The pale-yellow colour in some of the polymers presumably arose from trace residual iron-containing species.[10b]

Polyphosphinoboranes $[RPH–BH_2]_n$ (R = 1-Ad, *i*Pr, Cy, *n*Hex, Me) were structurally characterised by multinuclear NMR spectroscopy and molecular weight determinations were achieved by GPC and ESI-MS (see Table 3.1).; the thermal stability and thermal transition behaviour was investigated by thermogravimetric analysis (TGA) and differential scanning calorimetry (DSC), respectively (see Tables 3.2).

Table 3.1. Summary of ^{11}B NMR, ^{31}P NMR, and GPC results for polyalkylphosphinoboranes.

Polymer	Time (h)[a]	^{11}B shift (ppm)[b]	^{31}P shift (ppm)[b]	M_n (g mol^{-1})[c]	M_w (g mol^{-1})[c]	PDI	DP_n[d]
[*t*BuPH–BH$_2$]$_n$	48	−38.8	−24.5	31,600	47,000	1.5	34
[1-AdPH–BH$_2$]$_n$	61	−43.1	−26.1	23,400	35,900	1.5	15
[*i*PrPH–BH$_2$]$_n$	36	−39.9	−39.1	18,200	36,200	1.9	36
[CyPH–BH$_2$]$_n$	76	−40.1	−44.0	31,800	49,100	1.5	27
[*n*HexPH–BH$_2$]$_n$	100	−36.6	−61.8	57,200	86,800	1.5	25
[MePH–BH$_2$]$_n$	13	−34.9	−76.7	14,000[e]	48,100[e]	3.4[e]	24

a) Polymerisation reaction duration (1 mol% $[FeCp(CO)_2(OTf)]$, 100 °C, toluene, 2.0 M) b) NMR spectroscopy was measured in $CDCl_3$. c) GPC in THF (0.1 *w/w* % *n*Bu_4NBr) (2 mg mL^{-1}) of isolated polymers. d) DP_n (degree of polymerisation) obtained by ESI-MS in CH_2Cl_2 (2 mg mL^{-1}). e) Broad, multimodal mass distribution with ca. M_n = 2,000–300,000 g mol^{-1}.

3.3.4 Characterisation by Multinuclear NMR Spectroscopy of Poly(alkylphosphinoboranes)

The ^{11}B and ^{31}P NMR chemical shifts for poly(alkylphosphinoboranes) are summarised in Table 3.1. In the case of the new polyphosphinoboranes synthesised, the ^1H NMR spectra showed a doublet at δ = 3.87 ppm for $[i\text{PrPH–BH}_2]_n$ and at δ = 3.59 ppm for $[1\text{-AdPH–BH}_2]_n$ which corresponds to the resonance of the P–H proton. The ^{11}B NMR spectra for $[i\text{PrPH–BH}_2]_n$ and $[1\text{-AdPH–BH}_2]_n$ showed a single broad resonance at δ = −39.9 ppm and

δ = −43.1 ppm, respectively. The ^{31}P NMR spectra showed a broad main resonance at δ = −39.1 ppm for polyphosphinoborane [*i*PrPH–BH_2]$_n$, and at δ = −26.1 for [1-AdPH–BH_2]$_n$. For the polymer [MePH–BH_2]$_n$, the ^{31}P{^{1}H} NMR spectrum showed a main resonance at δ = −76.7 ppm that splits into a doublet in the coupled ^{31}P NMR spectrum (J_{PH} ≈ 350 MHz). An additional signal at δ = −68.6 ppm displayed a pseudo-triplet in the coupled ^{31}P NMR spectrum which might correspond to a phosphine end group (J_{PH} ≈ 380 MHz) (see SI, Fig. S3.50) as has been suggested for similar signals reported previously.[13]

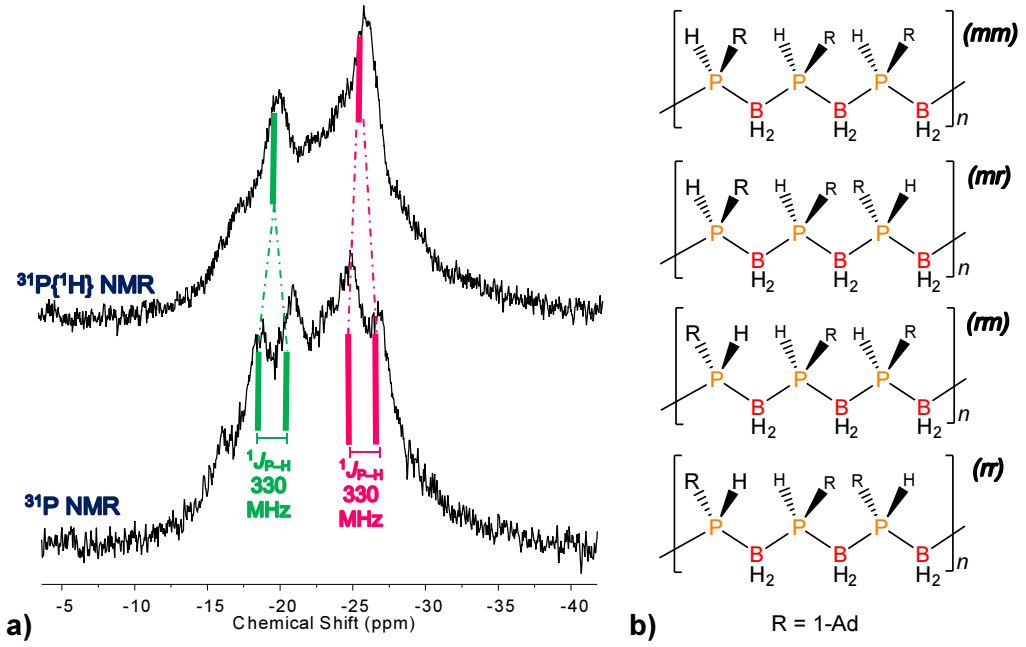

Figure 3.4. a) ^{31}P NMR (bottom) and ^{31}P{^{1}H} NMR (top) spectra for polymer [1-AdPH–BH_2]$_n$. b) Schematic diagram of hypothetical triad sequences for [1-AdPH–BH_2]$_n$.

Moreover, the ^{31}P NMR spectrum of [1-AdPH–BH_2]$_n$ showed overlapped resonances (Figure 3.4), which are not attributed to end groups due to the high molar mass of the polymer. These signals might be related to tactic environments in the polymer, probably imposed by the disposition of the highly bulky adamantyl group. Tacticity in polyphosphinoboranes and poly(methylenephosphine) has been proposed in former reports.[10a, 14a, 21] The ^{31}P{^{1}H} NMR showed an array of resonances, at δ_P = ca. −17, −19, and −26 ppm which are assigned to triads. Some of these signals subsequently split into

doublets ($J_{PH} \approx 330$ MHz) in the coupled ^{31}P NMR spectrum. However, we are reluctant to assign a specific configuration in the ^{31}P NMR spectrum, nevertheless, we suggest that the isotactic triad *mm* has the lowest probability to be formed, attributable to potential steric repulsion of adjacent adamantyl groups.

3.3.5 Molar Mass Characterisation of Poly(alkylphosphinoboranes)

The molar mass characterisation of the polymers was achieved by GPC in THF (0.1 *w*/*w* % *n*Bu$_4$NBr), relative to polystyrene standards, and the analysis showed that polymers are high molar mass in nature (M_n = 36,000–48,000 g mol^{-1}) with polydispersity indices of 1.5–3.4. The polyphosphinoboranes [RPH–BH$_2$]$_n$ where R = 1-Ad, Cy, *n*Hex displayed a bimodal distribution by GPC with a high molecular mass region (see Table 1 for M_n and PDI), and a second overlapped peak assigned to lower molecular weight oligomers below the resolvable exclusion limit area of the GPC, while polymers with R = Me, *i*Pr, *t*Bu displayed a single distribution. The GPC trace for [MePH–BH$_2$]$_n$ possesses the distribution with the highest PDI (3.4), which might suggest some degree of branching arising probably under the dehydropolymerisation reaction conditions.

In several cases, the polymers obtained by Fe-catalysed dehydropolymerisation displayed higher molar mass than analogous poly(alkylphosphinoborane) polymers prepared previously by other means. For example, no evidence of high molar mass was presented for [MePH–BH$_2$]$_n$ prepared by metal-free polymerisation and it was described as an oligomeric material on the basis of ESI-MS and DLS analysis, in which evidence for the formation of aggregates (R_H = 1 nm–5 μm) was reported.[18] Moreover, the molar mass for [*n*HexPH–BH$_2$]$_n$ (M_n = 3,800–8,800 g mol^{-1}) prepared with [Rh(μ-Cl)(1,5-COD)]$_2$ precatalyst possessed a lower value when compared to the identical polymer prepared here with [FeCp(CO)$_2$(OTf)] precatalyst (M_n = 86,800 g mol^{-1}). Also, the polymer [CyPH–BH$_2$]$_n$ prepared here presents high molar mass (M_n = 31,800 g mol^{-1}, PDI = 1.5), contrary to the

identical material previously reported using Fe(II) β-diketiminate based precatalyst which produce mainly oligophosphinoborane (M_n < 2,000 g mol^{-1}).[4j]

ESI-MS spectral analysis of all polyphosphinoboranes synthesised allowed us to confirm the molecular repeat units [RPH–BH_2] of each polymer and the formation of linear oligomeric chains with a phosphine end-group H–[RPH–BH_2]$_x$–PH_2R for each polymer, except for [MePH–BH_2]$_n$ which also gave peaks assigned to linear polymer with H as an end-group H–[RPH–BH_2]$_x$–H. Since only the low molar mass fraction of oligomeric material ([RPH–BH_2]$_x$, where $x \leq 34$) could be detected by ESI-MS, the degree of polymerisation (DP_n) obtained using this method is significantly lower than that obtained by GPC which reveals the entire molar mass distribution. ESI-MS is known to underestimate the molecular weight of polyphosphinoboranes, as well as polyaminoboranes when compared to GPC measurements.[4b, 10b] It is worth noting that matrix-assisted laser desorption/ionization time-of-flight mass spectrometry (MALDI-TOF MS) was unsuccessful for the analysis of polyphosphinoborane samples even after attempts with a range of different matrices.

3.3.6 Thermal Studies of Poly(alkylphosphinoboranes)

The thermal behaviour of polyphosphinoboranes was investigated by DSC and TGA under nitrogen atmosphere (heating rate 10 °C min^{-1}) and the results are shown in Table 3.2. The analysis by DSC showed that the glass transition temperatures (T_g) were below 0 °C temperature for polyphosphinoboranes [RPH–BH_2]$_n$ (R = *i*Pr, Cy, *n*Hex, Me) and above room temperature for [RPH–BH_2]$_n$ (R = *t*Bu, 1-Ad) (see SI, Fig. S3.54–S3.59). As expected, the lowest T_g material in this series corresponded to [*n*HexPH–BH_2]$_n$ which has the most flexible alkyl chain. [*n*HexPH–BH_2]$_n$ (T_g = −76 °C) prepared through the Fe-catalysed reaction presented herein showed a lower glass transition temperature than the identical material prepared via Rh-based precatalyst (T_g = −68 °C).[13] This might be related to the

effect of the degree of branching of polymers on the glass transition temperature.[22] The polymer prepared here has a predominately linear structure (PDI = 1.5)[10] whereas the polymeric materials previously reported with the Rh-based catalyst have been proposed have a branched structure.[7c] It has been suggested that when the degree of branching is low, the influence of molecular rigidity is more pronounced than the contribution of the free volume of chain ends,[23] thus the branching hinders rotation of the polymer which increases the T_g as a consequence. A similar *branching effect* might be affecting the glass transition of the branched poly(n-hexylphosphinoborane) prepared by the Rh-catalyzed route.

Table 3.2. Thermal properties, $T_{5\%}$ and ceramic yield of poly(alkylphosphinoboranes).

Polyalkylphosphinoboranes	$T_{5\%}$[a] (°C)	T_g (°C)	Ceramic Yield[b] (%)
[*t*BuPH–BH_2]$_n$	129	36	25
[1-AdPH–BH_2]$_n$	115	87	21
[*i*PrPH–BH_2]$_n$	135	−22	24
[CyPH–BH_2]$_n$	130	−2	25
[*n*HexPH–BH_2]$_n$	140	−76	29
[MePH–BH_2]$_n$	165	−24	75

a) Temperature at 5% weight loss (heating rate 10 °C min^{-1}). b) Ceramic yields were measured at 700 °C, heating rate 10 °C min^{-1} (under a flow N_2).

The highest glass transition temperature was found for [1-AdPH–BH_2]$_n$ (T_g = 87 °C) in this polymer series. The adamantyl group has been found to generally impart an incremental increase in the glass transition of polymers when it is part of the side chain as a result of impeded chain mobility because of steric factors.[24] For example, for the classic family of inorganic polymers, polyphosphazenes, typical glass transition temperatures are generally around −100 °C when the side groups are small and flexible. However, polyphosphazenes functionalised with adamantyl groups can possess T_g values around

~180 °C.[25] For all poly(alkylphosphinoboranes), the glass transition temperatures are lower when compared to their organic counterparts. For example, polyphosphinoboranes T_g values are: [MePH–BH_2]$_n$ (T_g = −24 °C), [*i*PrPH–BH_2]$_n$ (T_g = −22 °C), [*t*BuPH–BH_2]$_n$ (T_g = 36 °C) and [CyPH–BH_2]$_n$ (T_g = −2 °C). Whereas atactic polypropylene (T_g = −6 °C),[26] atactic poly(iso-propylethylene) (T_g = 50 °C), poly(tert-butylethylene) (T_g = 64 °C) and atactic poly(cyclohexylethylene) (T_g = 120 °C) present higher transition temperatures.[27] The nature of the P–B bonds in the backbone in polyphosphinoboranes confer a high degree of torsional flexibility.[7c]

The analysis of the TGA thermograms (at 700 °C, heating rate: 10 °C min^{-1}) of the polymers showed that the decomposition temperature $T_{5\%}$ (temperature at which each polymer exhibited a 5% loss of mass) ranged from 115 – 165 °C (Figure 3.5). Although a second dehydrogenation process is likely to occur at high temperatures,[10b] it has been suggested that prolonged heating (100 °C) of polyphosphinoboranes produces the scission of the P–B bond on the chain end,[13] which could induce to an "unzipping" process promoting depolymerisation events from the chain ends. Above this temperature ($T_{5\%}$), the polymers [RPH–BH_2]$_n$ (R = 1-Ad, Cy, *n*Hex) decomposed in a single-step process, where degradation was complete at around 400 °C with mass reduction of ca. 60%. On the other hand, polymers [RPH–BH_2]$_n$ (R = Me, *i*Pr, *t*Bu) degraded in a two-step process, and the complete degradation for [*i*PrPH–BH_2]$_n$ and [*t*BuPH–BH_2]$_n$ took place at 350 °C (mass reduction of ca. 50% and 80%, respectively) and for [MePH–BH_2]$_n$ at 500 °C (mass reduction of ca. 15%).

The ceramic yield of some poly(alkylphosphinoboranes) have been previously reported.[7c, 13, 28] It would be anticipated that polymers with greater hydrocarbon content from the side groups lead to lower yields.[13] This is obvious for polymers [RPH–BH_2]$_n$ (R = 1-Ad, *i*Pr, Cy, *n*Hex, *t*Bu) that presented lower ceramic yields (25–47 %) than [MePH–BH_2]$_n$ (75 %). [MePH–BH_2]$_n$ is likely to produce highly volatile products and to produce higher degree of

cross-linking that leads to the highest ceramic yield which makes it a strong candidate as a precursor to boron phosphide.

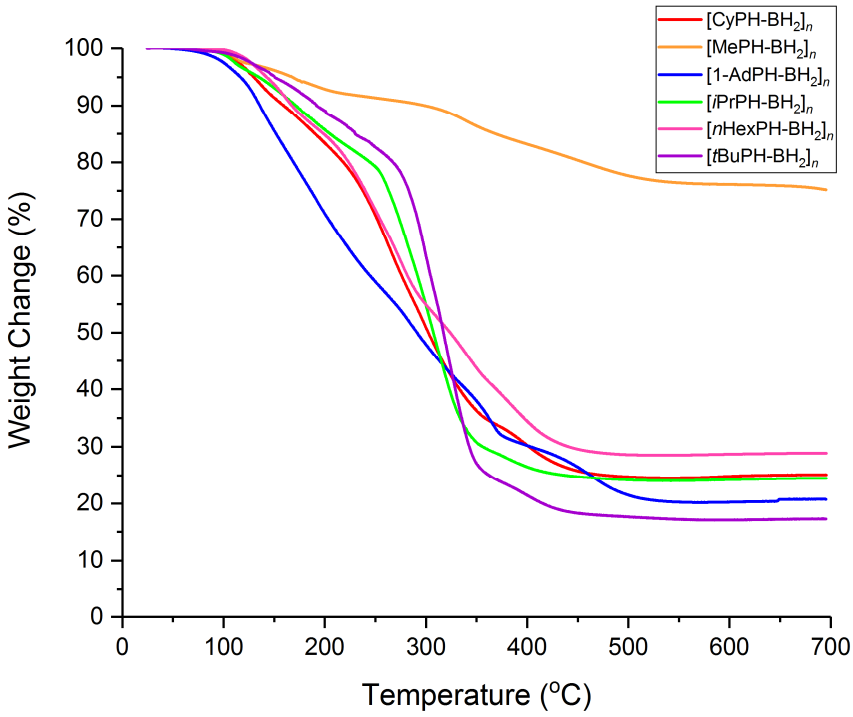

Figure 3.5. TGA thermograms of polyphosphinoboranes at 700 °C (heating rate: 10 °C min $^{-1}$).

We found notable differences in the thermal stability of the polymer [*n*HexPH–BH_2]$_n$ prepared by different catalytic systems, for example, the polymer prepared using the [Rh] system has a higher thermal stability ($T_{5\%}$ = 245 °C) than the polymer prepared by the [Fe] system ($T_{5\%}$ = 140 °C). It has been formerly proposed that dehydropolymerisation by Rh catalysis imparts a certain degree of branching[7c] in the material. On the contrary, polymers synthesised by Fe catalysis are likely to be more structurally linear.[10b] It has been reported that branched polysiloxanes possess higher thermal stability than their linear analogue, as the branched structure promotes cross-linking of the material.[29] We suggest that a similar effect might occur in the case for branched polyphosphinoboranes.

In general, poly(alkylphosphinoboranes) have lower thermal stability temperature ($T_{5\%}$ = 115 – 165 °C) when compared to poly(arylphosphinoboranes) ($T_{5\%}$ = 150–210 °C) prepared by using the same catalytic conditions.[10b] In our previous report, the

dehydropolymerisation of an aryl phosphine–borane *via* the [$FeCp(CO)_2(OTf)$] precatalyst (5 mol%, 100 °C) produced a cross-linked gel. Poly(arylphosphinoboranes) posses P–H bonds which are more susceptible to undergoing cross-linking reaction due to the electron-withdrawing nature of the aryl substituents compared with poly(alkyl)phosphinoboranes. The higher degree of crosslinking in aryl substituted polymers may be one of the factors leading to the increased thermal stability of these materials.

Large substituents that contribute to an increase in steric interactions between side groups, lower overall stability of the polymers.[13] We observed the expected trend for polymers $[RPH–BH_2]_n$; for example, $[t\text{BuPH–BH}_2]_n$ and $[1\text{-AdPH–BH}_2]_n$ possess the lowest $T_{5\%}$ as the bulky side groups destabilize the polymer relative to molecular fragments. In the case for $[n\text{HexPH–BH}_2]_n$,, the increase on thermal stability compared to $[1\text{-AdPH–BH}_2]_n$, can be explained as the *n*-hexyl side chain possessing a smaller steric profile. The low thermal stability and ceramic yields of polymers containing substituents larger than methyl groups suggest that depolymerisation processes are preferred over cross-linking.

3.4 Conclusions

The metal-catalysed dehydropolymerisation of alkyl phosphine–boranes $RPH_2{\cdot}BH_3$ has been achieved using $[CpFe(CO)_2OTf]$ as a precatalyst to produce high molar mass polyphosphinoboranes $[RPH–BH_2]_n$. The thermal non-catalysed dehydropolymerisation is feasible to produce mainly oligomeric material with a small component of high molar mass, whereas the use of the iron-based precatalyst not only favours the formation of high molar mass polymer but also increases the reaction rate dramatically. The purity of the starting materials is fundamental to produce high molar mass polyphosphinoboranes, and it was observed that the iron precatalyst is robust in the absence of anhydrous conditions. Moreover, we have shown that polyphosphinoboranes are stable under high temperatures in solution and no backbone scission from the attack of primary phosphine was observed. Control experiments have unveiled that changing the catalyst loading has no significant. In addition, the rate of the dehydropolymerisation reaction increases with concentration. From the range of polyphosphinoboranes materials synthesised, the analysis of the glass transition temperatures showed a variation from −76 to 87 °C, depending on the side chain group where the P–B backbone of these polymers offers torsional flexibility. On the other hand, it was observed that these polymers possessed low thermal stability and ceramic yield values, except for $[MePH–BH_2]_n$, which has the highest ceramic yield (75%) and makes it a prospective precursor for the formation of boron- based ceramics such as boron phosphide. Further characterisation of the latter ceramic obtained by pyrolysis is under investigation. In addition, detailed mechanistic studies, formation of model compounds and polymer post-functionalisation are in progress in order to obtain a better insight in the polymerisation reaction as well to obtain tailor-made polymers. We have shown that $[CpFe(CO)_2OTf]$ is an excellent precatalyst capable of mediating the dehydropolymerisation of a range of alkyl and aryl substituents to produce a catalogue of polymers with different properties, however, future work entails the synthesis of chiral

catalysts in order to obtain control over the polymer tacticity and the exploration of novel metal-free polymerisation synthetic routes.

3.5 Supporting Information

3.5.1 General Procedures, Equipment and Reagents.

All manipulations were carried out either under an atmosphere of nitrogen gas using standard vacuum line and Schlenk techniques, or under an atmosphere of argon within an M. Braun glovebox MB150G-B maintained at <0.1 ppm of H_2O and <0.1 ppm of O_2. Where stated, anhydrous solvents were dried *via* a Grubbs design solvent purification system.[30] Anhydrous deuterated chloroform or tetrahydrofuran was purchased from Sigma Aldrich and stored over activated molecular sieves (4 Å).

NMR spectra were recorded using Oxford Jeol Eclipse 300, 400, Bruker cryo 500 MHz spectrometers. ^{1}H NMR spectra were calibrated using residual protio signals of the solvent: (δ ^{1}H($CHCl_3$) = 7.24). ^{13}C NMR spectra were calibrated using the solvent signals (δ ^{13}C($CDCl_3$) = 77.0; δ ^{13}C(C_6D_6) = 128.0). ^{11}B NMR spectra were calibrated against external standards (^{11}B: $BF_3 \cdot OEt_2$ (δ ^{11}B = 0.0)). IR spectra were measured using an Agilent Cary FT-IR with ATR sampling module.

Workup of polymeric materials and their characterisation was performed in air using lab grade solvents. The following compounds were synthesized according to literature procedures: [$CpFe(CO)_2(OTf)$],[31] $CyPH_2{\cdot}BH_3$,[32] $MePH_2{\cdot}BH_3$,[33] nHexPH$_2{\cdot}BH_3$,[13] 1-AdPCl$_2$.[34] The substrate tBuPH$_2{\cdot}BH_3$ was synthesized according to a literature procedure but with the following modifications,[14a] the reaction solvent used was Et_2O instead of nBu$_2$O and solvent removal was performed under vacuum while chilling the sample in an ice/water bath, the crude product was trap-to-trap distilled while heating reaction flask at 40 °C and chilling the receiving flask in liquid nitrogen (10^{-3} mbar pressure). The compound tBuPH$_2$ was synthesized according to a literature procedure with the following modification,[35] the reaction solvent used was tetraethylene glycol dimethyl ether instead of butyl diglyme, and the product was purified by trap-to-trap distillation at room temperature while chilling the receiving flask in liquid nitrogen (10^{-3} mbar pressure). The compound

*i*PrPH$_2$·BH$_3$ was previously reported as a byproduct from a reaction,[36] here its intentional synthesis and isolation are reported.

Elemental analyses (C, H, N) were performed externally by Elemental Microanalysis Ltd. in Devon, UK.

GPC was performed on a Malvern RI max Gel Permeation Chromatograph, equipped with an automatic sampler, a pump, an injector, and inline degasser. The columns (T5000) were contained within an oven (35 °C) and consisted of styrene/divinyl benzene gels. Sample elution was detected by means of a differential refractometer. THF (Fisher), containing 0.1 wt% *n*Bu$_4$NBr, was used as the eluent at a flow rate of 1 mL/min. Samples were dissolved in the eluent (2 mg/mL) and filtered with a Ministart SRP15 filter poly(tetrafluoroethylene) membrane of 0.45 µm pore size) before analysis. The calibration was conducted using monodisperse polystyrene standards obtained from Aldrich. The lowest (highest) molecular weight standard used was 2,300 (994,000) g mol^{-1}.

The ESI-MS spectra were obtained using a Waters Synapt G2S instrument equipped with a nanospray ionisation module (Advion TriVersa Nanomate). Solutions (40 µL) of approximately 1 mg/mL were loaded under ambient conditions in air into the sample tray, and aliquots of 3 µL were introduced into the spectrometer using a spray voltage of 1.5 kV. Positive ion spectra were recorded at a rate of 1 scan/second and summed to obtain the final spectra.

DSC was measured on a Thermal Advantage DSCQ100 at 10 °C/min and TGA was measured on a Thermal Advantage TGAQ500 at 10 °C/min under N$_2$. DSC and TGA results were analysed using WinUA V4.5A by Thermal Advantage.

The single crystal X-ray diffraction experiment for 1-AdPH$_2$·BH$_3$ was carried out on a Bruker APEX II diffractometer using Mo Kα radiation (λ = 0.71073 A) and collected at 100 K. The data collection was performed using a CCD area detector from a single crystal

mounted on a glass fibre. Intensities were integrated in SAINT[37] and absorption corrections based on equivalent reflections using SADABS[38] were applied. The structures were solved by the dual-space algorithm SHELXT[39] and refined against all F^2 in ShelXL[40] using Olex2[41]. All the non-hydrogen atoms were refined anisotropically. H atoms bound to P1 and B1 were located directly from the electron density map, while all other hydrogen atoms were calculated geometrically and refined using a riding model.

3.5.2 Catalytic Dehydrocoupling of *t*BuPH$_2$·BH$_3$ with the Precatalyst [CpFe(CO)$_2$OTf].

3.5.2.1 Synthesis and Characterisation of [*t*BuPH–BH$_2$]$_n$

Under dinitrogen atmosphere 1 mmol of *t*BuPH$_2$·BH$_3$ was dissolved in 0.4 mL of toluene, to this solution 0.1 mL of a toluene stock solution of FeCp(CO)$_2$(OTf) (0.1 M) was added. The initially red-orange reaction mixture was transferred to a J. Young NMR tube, sealed, and heated at 100 °C in an oil bath, within the first 5 min a colour change from orange to yellow was observed. The conversion was monitored by ^{31}P{^{1}H} and ^{11}B{^{1}H} NMR spectroscopy. Upon complete consumption of monomer (48 h), the J. Young tube was opened in air carefully to vent H$_2$ generated in the dehydropolymerization reaction, and the solvent was removed by rotary evaporation. The crude yellow-brown residue was dissolved in CH$_2$Cl$_2$ (0.5 mL) and passed through a ~3 cm plug of Florisil® (100-200 mesh) adsorbent, and a short pad of Celite® filtration aid within a glass microfiber plugged pipette, and was eluted with CH$_2$Cl$_2$ (5 mL) afterward the solvent was removed by rotary evaporation and the pale yellow to colorless polymeric product was dried under vacuum overnight followed by in 40 °C vacuum oven for a minimum of 2 days (87 mg, 85 % yield).

^{1}H NMR (CDCl$_3$): δ (ppm) 3.74 (br d, 1H, P*H*); 1.35-1.20 (br s, 11H, B*H*, C*H*$_3$) (Figure S3.1).

^{11}B{^{1}H} NMR (CDCl$_3$): δ (ppm) −38.8 (br) (Figure S3.2).

^{31}P NMR δ (ppm) –24.5 (br) (Figure S3.3).

^{13}C NMR ($CDCl_3$): δ (ppm) 28.8 – 28.0 (br m) (Figure S3.4).

GPC: M_n = 31,600 g mol^{-1}, M_w = 47,000 g mol^{-1}, PDI = 1.5 (Figure S3.5).

ESI-MS: Difference of 102 m/z ([*t*BuHPBH$_2$] subunit) confirms presence of linear oligo(*tert*-butylphosphinoborane) with a phosphine end group H–[*t*BuPH–BH$_2$]$_x$–PH$_2$*t*Bu up to 34 repeat units (Figure S3.6).

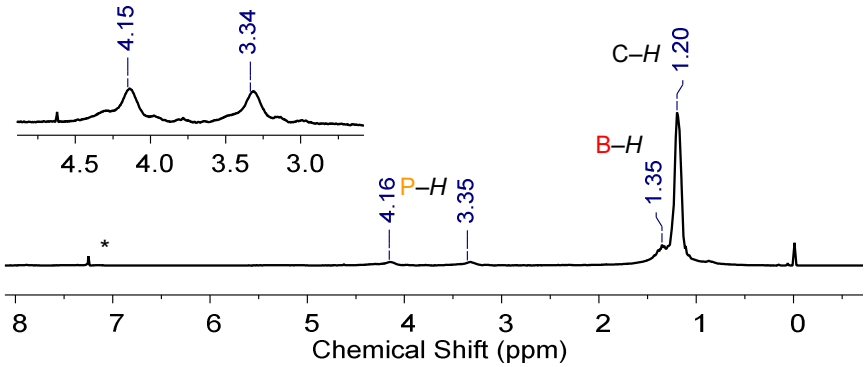

Figure S3.1. ^{1}H NMR spectrum of isolated [*t*BuPH–BH$_2$]$_n$ in $CDCl_3$ at 20 °C. * $CDCl_3$.

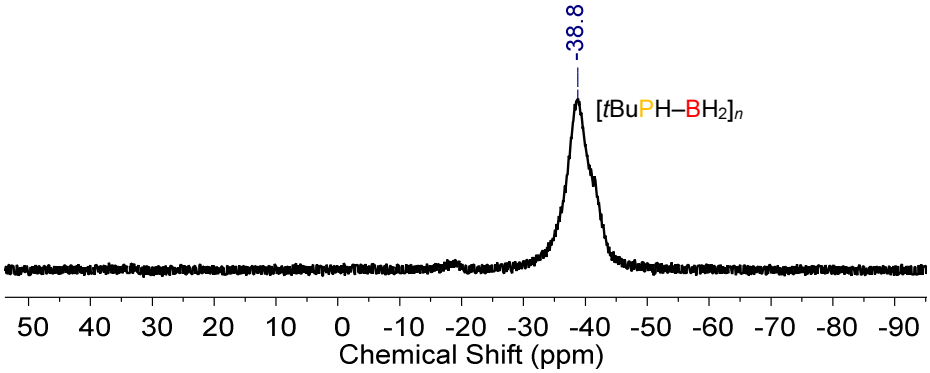

Figure S3.2. ^{11}B{^{1}H} NMR spectrum of isolated [*t*BuPH–BH$_2$]$_n$ in $CDCl_3$ at 20 °C.

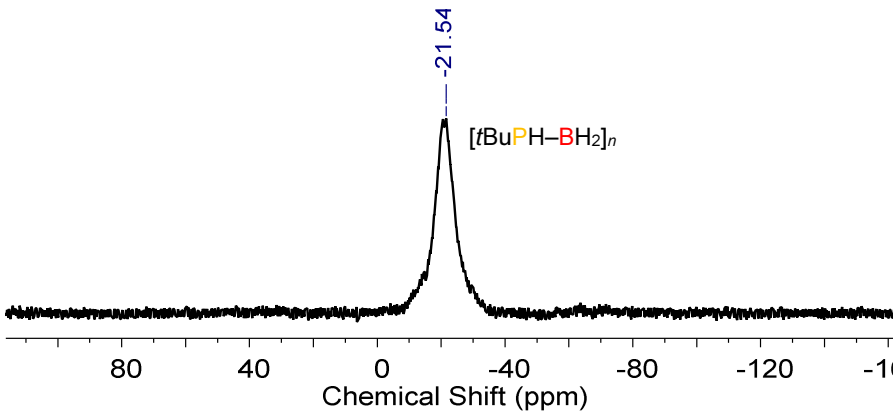

Figure S3.3. ^{31}P{^{1}H} NMR spectrum of isolated [*t*BuPH–BH$_2$]$_n$ in $CDCl_3$ at 20 °C.

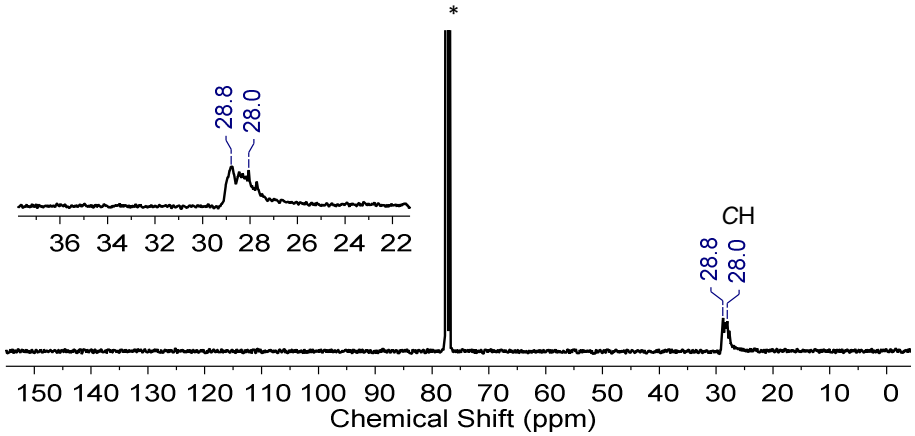

Figure S3.4. ^{13}C NMR spectrum of isolated [*t*BuPH–BH_2]$_n$ in $CDCl_3$ at 20 °C. * $CDCl_3$.

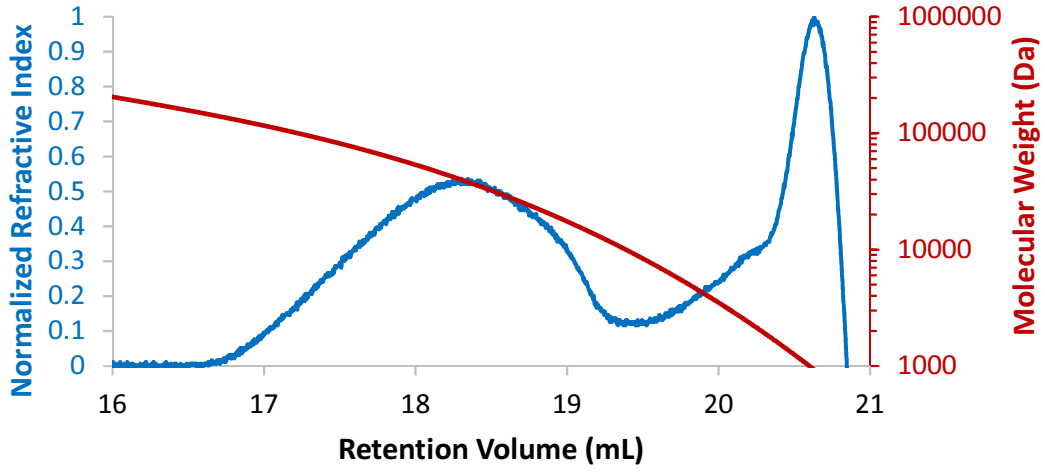

Figure S3.5. GPC chromatogram (2 mg mL^{-1}) of isolated [*t*BuPH–BH_2]$_n$ in THF (0.1 wt% [*n*Bu_4N]Br).

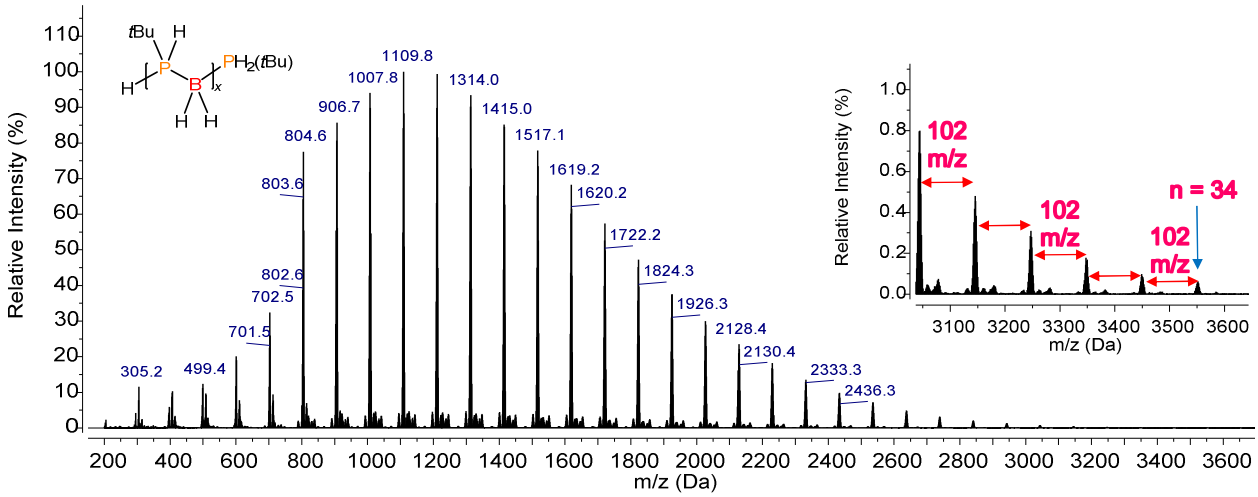

Figure S3.6. ESI-MS (2mg mL^{-1} in CH_2Cl_2) spectrum in positive mode of isolated [*t*BuPH–BH_2]$_x$.

3.5.2.2 Thermal Dehydrocoupling of *t*BuPH$_2$·BH$_3$

*t*BuPH$_2$·BH$_3$ (1.0 mmol) was dissolved in toluene (0.5 mL) at 20 °C. The reaction mixture was transferred to a J. Young NMR tube, sealed, and heated at 100 °C**.** The conversion was monitored by ^{31}P{^{1}H} and ^{11}B{^{1}H} NMR spectroscopy for 30 days. The solvent was removed and dried under vacuum.

Analysis of the Reaction of *t*BuPH$_2$·BH$_3$ after 30 days at 100 °C:

^{1}H NMR {CDCl$_3$}: 3.51 (br d, P*H*); 1.17-0.98 (m, B*H*, C*H*$_3$) (Figure S3.7).

^{11}B{^{1}H} NMR (toluene): [*t*BuPH–BH$_2$]$_n$ [δ −36.4 and −39.5 (br)], *t*BuPH$_2$·BH$_3$ [δ −40.9 and −41.5 (br)] (Figure S3.8).

^{31}P{^{1}H} NMR (toluene): [*t*BuHPBH$_2$]$_n$ [δ −17.8 and −22.4 (br)], *t*BuPH$_2$·BH$_2$–P*t*BuH·BH$_3$ [δ −12.7 and −14.4 (br)] (Figure S3.9).

GPC: Retention time 17.5 mL (M_n = 63,400 g mol^{-1}, PDI = 1.5) and 20.5 mL (M_n ca. 2,000 g mol^{-1}) (Figure S3.10).

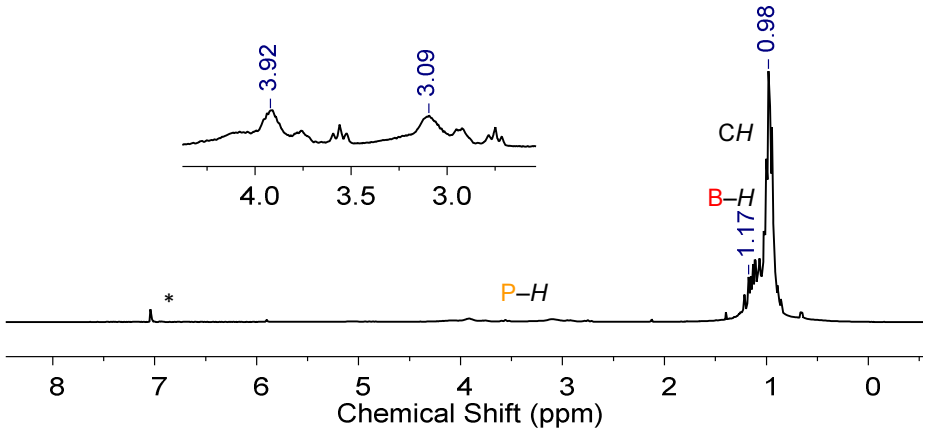

Figure S3.7. ^{1}H NMR spectrum of isolated [*t*BuHP–BH$_2$]$_n$ in CDCl$_3$ at 20 °C. * CDCl$_3$.

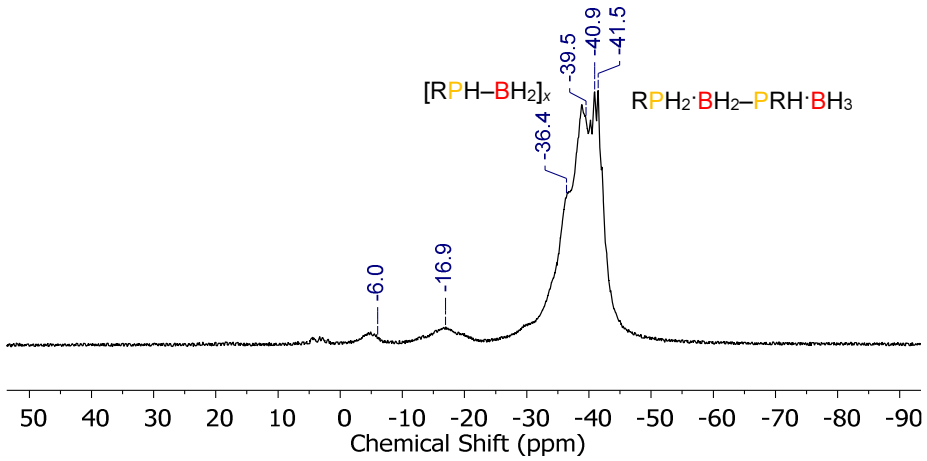

Figure S3.8. $^{11}B\{^1H\}$ NMR spectrum of $[t\text{BuPH–BH}_2]_n$ synthesized thermally at 100 °C for 30 days in toluene at 20 °C. R = *t*Bu

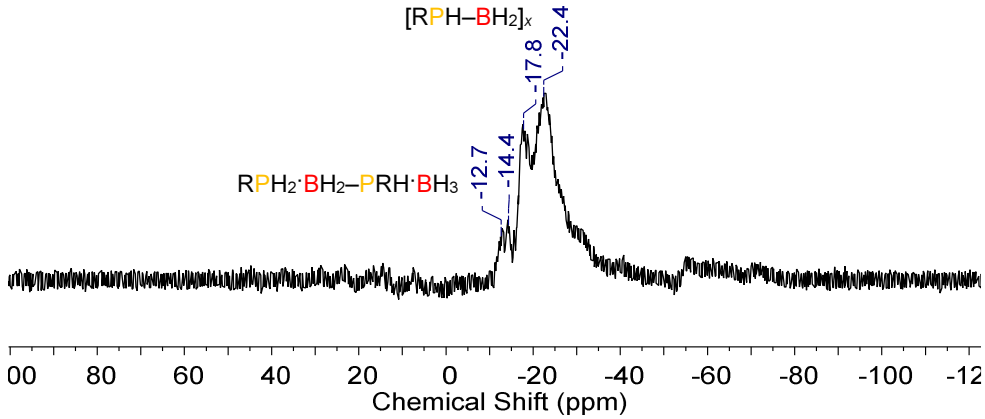

Figure S3.9. $^{31}P\{^1H\}$ NMR spectrum of $[t\text{BuPH–BH}_2]_n$ synthesized thermally at 100 °C for 30 days in toluene at 20 °C.

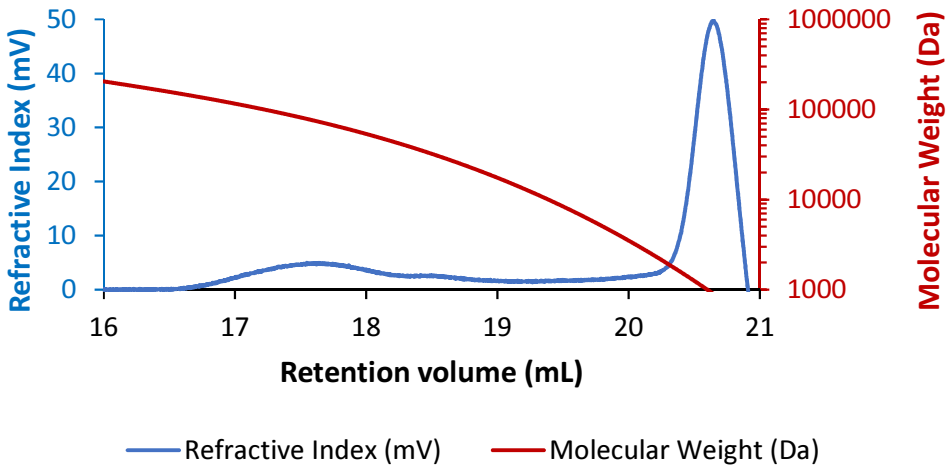

Figure S3.10. GPC chromatogram of isolated $[t\text{BuPH–BH}_2]_n$ (2 mg mL^{-1}) in THF (0.1 wt% $[n\text{Bu}_4\text{N}]\text{Br}$) synthesized thermally in toluene at 100 °C for 30 days.

3.5.2.3 Dehydropolymerisation of *t*BuPH$_2$·BH$_3$ and Stability Studies of [*t*BuPH–BH$_2$]$_n$

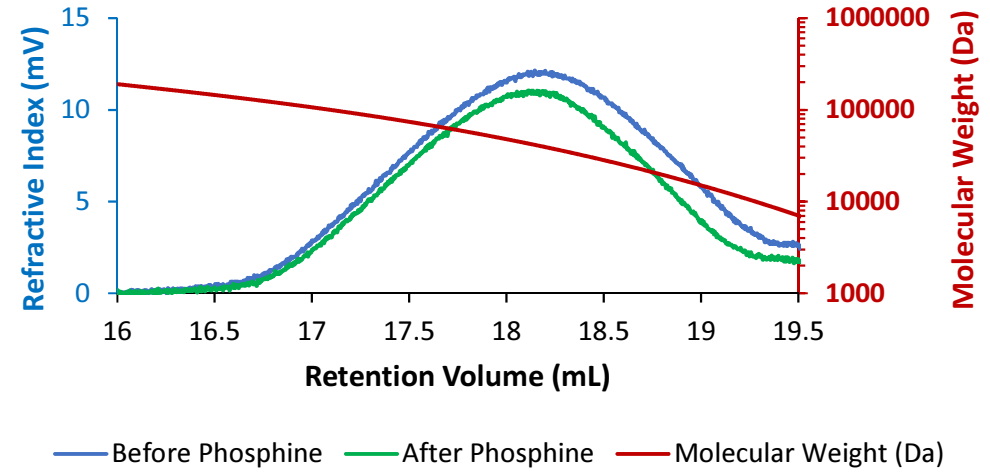

Figure S3.11. Overlay of GPC chromatograms (2 mg mL^{-1}) in THF (0.1 wt% [*n*Bu$_4$N]Br) both before (blue trace) and after (green trace) treatment of [*t*BuPH–BH$_2$]$_n$ (sample with M_n = 28,600 g mol^{-1}, and PDI = 1.6) with 1 eq. of *t*BuPH$_2$ per formula unit of the polymer in C$_6$D$_6$ at 100 °C for 48 h.

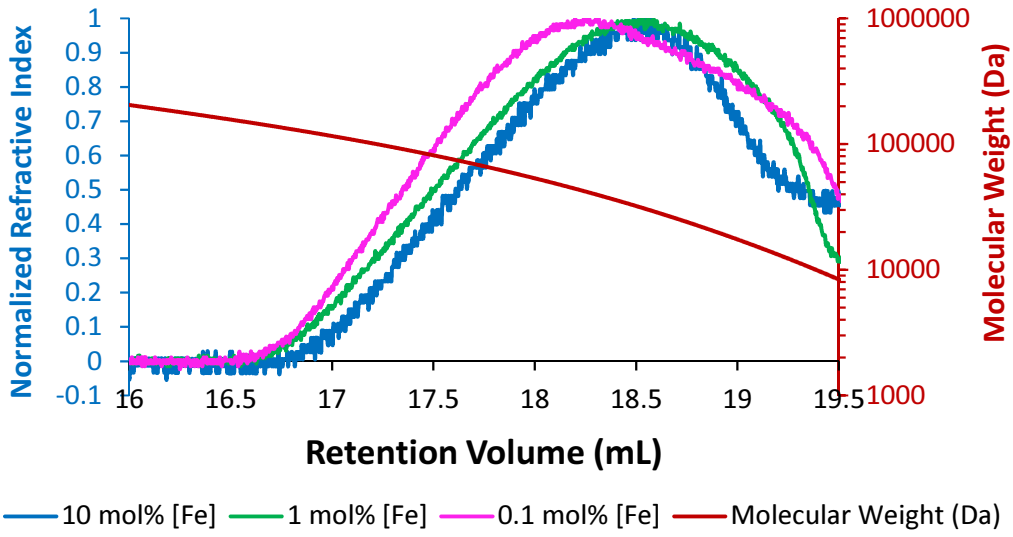

Figure S3.12. Overlay of GPC chromatograms (2 mg mL^{-1}) in THF (0.1 wt% [*n*Bu$_4$N]Br) of [*t*BuPH–BH$_2$]$_n$ synthesized from the dehydropolymerisation of the phosphine borane with different [CpFe(CO)$_2$OTf] catalyst loadings; 10 mol% [Fe] catalyst (blue trace), 1 mol% [Fe] catalyst (green trace), and 0.1 mol% [Fe] catalyst (pink trace). Reactions were performed on 1 mmol scales in terms of *t*BuPH$_2$·BH$_3$ 2.0 M in toluene, in sealed J. Young NMR tubes at 100 °C for 72 h Refractive indices are normalized versus peak maxima.

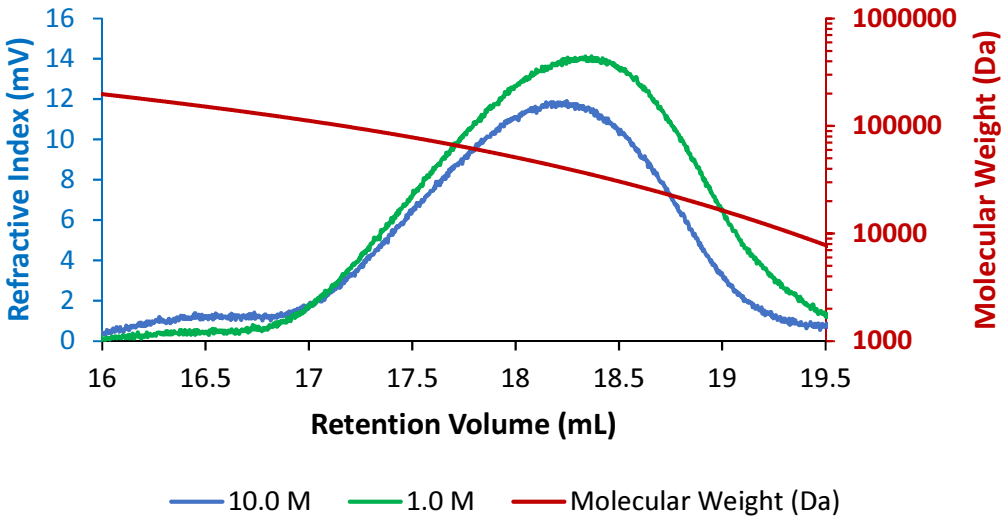

Figure S3.13. Overlay of GPC chromatograms (2 mg mL^{-1}) in THF (0.1 wt% [*n*Bu$_4$N]Br) of [*t*BuPH–BH$_2$]$_n$ synthesized from the dehydropolymerisation of the phosphine borane, *t*BuPH$_2$·BH$_3$, at different initial concentrations in toluene; 10.0 M with 24 h reaction time (blue trace), and 1.0 M with 13 day reaction time (green trace). In both reactions 1.0 mmol of the phosphine-borane and 1.0 mol% [CpFe(CO)$_2$OTf] catalyst loading was used, and reactions were performed in sealed J. Young NMR tubes at 100 °C.

3.5.3 Synthesis and Characterisation of Alkyl Phosphine–Boranes RPH$_2$·BH$_3$ (R = *i*Pr, 1-Ad).

3.5.3.1 Synthesis and Characterisation of *i*PrPH$_2$·BH$_3$:

Under dinitrogen atmosphere 1.65 g (75.9 mmol) of LiBH$_4$ was partially dissolved and suspended in 30 mL of Et$_2$O and chilled in an ice-water bath. Via syringe 5 g (34.5 mmol) of *i*PrPCl$_2$ dissolved in 10 mL of Et$_2$O and added to the cold Et$_2$O slurry of LiBH$_4$. The reaction mixture was stirred at 0 °C for 10 min, afterwards the white suspension was stirred at 25 °C for 1.5 h. The white suspension was filtered through Celite, and the solvent was evaporated from the filtrate under vacuum to give a white cloudy oil. The crude material was purified by short-path vacuum distillation where the heating block was heated at 220 °C, the receiving flask was chilled at -196 °C in a liquid nitrogen bath to yield *i*PrPH$_2$·BH$_3$ as a colorless liquid (0.86 g, 28% yield).

^{1}H NMR (400 MHz, 25 °C, $CDCl_3$) δ 4.85 (m, 1H, *i*PrP$\underline{H}_2$·BH_3), 3.96 (m, 1H, *i*PrP$\underline{H}_2$·BH_3), 2.22 - 2.04 (m, 2H, $(CH_3)_2C\underline{H}PH_2{\cdot}BH_3$), 1.26 (dd, 6H, J = 17.2 Hz, 7.1 Hz, $(C\underline{H}_3)_2CHPH_2{\cdot}BH_3$), 0.90 – 0.16 (m, 3H, *i*PrPH_2·B$\underline{H}_3$). (Figure S3.14)

^{11}B{^{1}H} NMR (128 MHz, $CDCl_3$) δ (ppm) −44.6 (d, J = 39.2 Hz). (Figure S3.15A)

^{11}B NMR (128 MHz, $CDCl_3$) δ −42.6 (ppm) (qd, J = 99.8, 39.2 Hz). (Figure S3.15B)

^{31}P{^{1}H} NMR (162 MHz, $CDCl_3$) δ (ppm) –26.6 (dd, J = 77.8, 37.4 Hz). (Figure S3.16A)

^{31}P NMR (162 MHz, $CDCl_3$) δ (ppm) –26.6 (br t, J = 367 Hz). (Figure S3.16B)

^{13}C{^{1}H} NMR (101 MHz, $CDCl_3$) δ (ppm) 20.1, 20.1 (s, $(\underline{C}H_3)_2CHPH_2{\cdot}BH_3$); 18.9 (d, J = 36.9 Hz, $(CH_3)_2\underline{C}HPH_2{\cdot}BH_3$) (Figure S3.17 and S3.18)

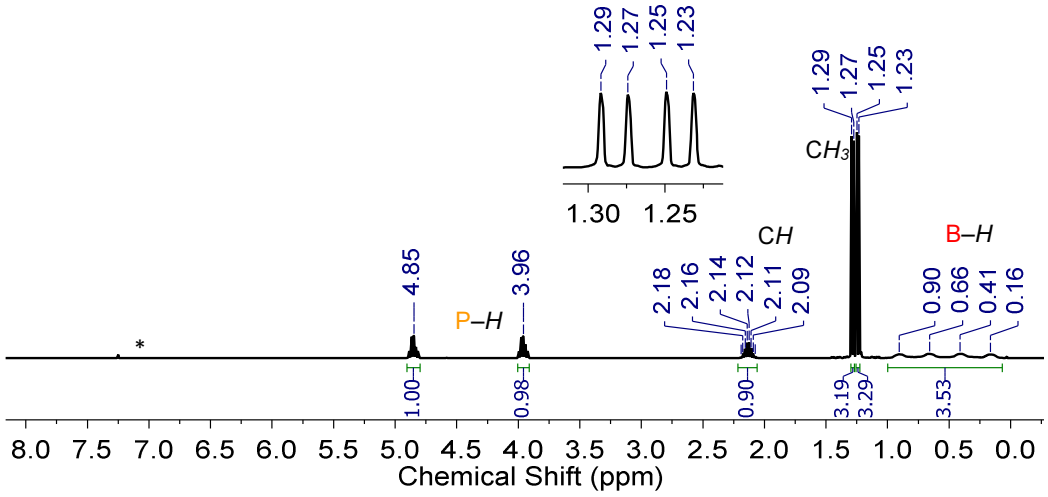

Figure S3.14. ^{1}H NMR spectrum (400 MHz, 25 °C) of *i*$PrPH_2{\cdot}BH_3$ in $CDCl_3$. * $CDCl_3$.

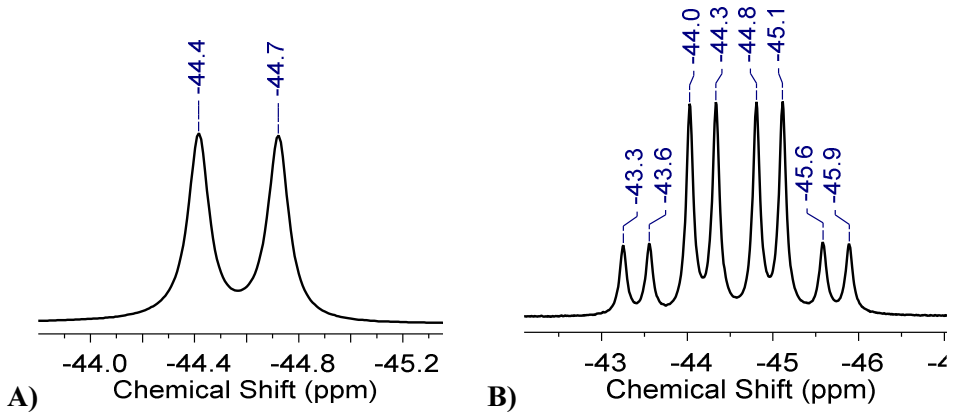

Figure S3.15. a) ^{11}B{^{1}H} NMR spectrum (128 MHz, 25 °C) of *i*$PrPH_2{\cdot}BH_3$ in $CDCl_3$. b) ^{11}B NMR spectrum (128 MHz, 25 °C) of *i*$PrPH_2{\cdot}BH_3$ in $CDCl_3$.

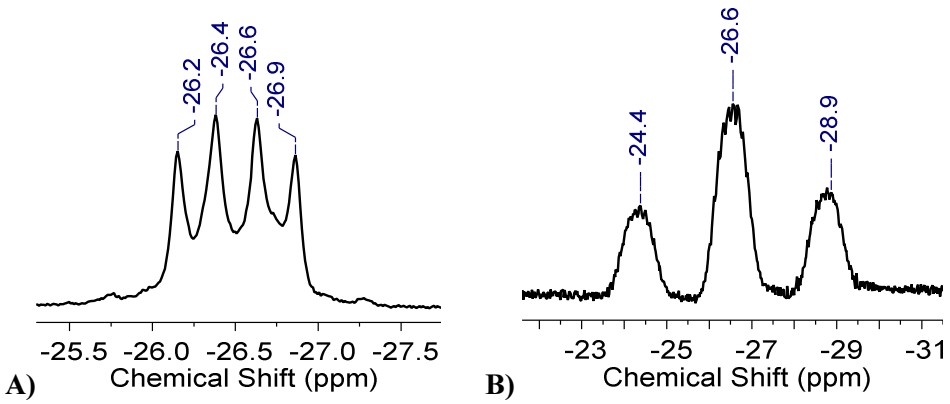

Figure S3.16. a) $^{31}P\{^{1}H\}$ NMR spectrum (162 MHz, 25 °C) of *i*$PrPH_2 \cdot BH_3$ in $CDCl_3$. b) ^{31}P NMR spectrum (162 MHz, 25 °C) of *i*$PrPH_2 \cdot BH_3$ in $CDCl_3$.

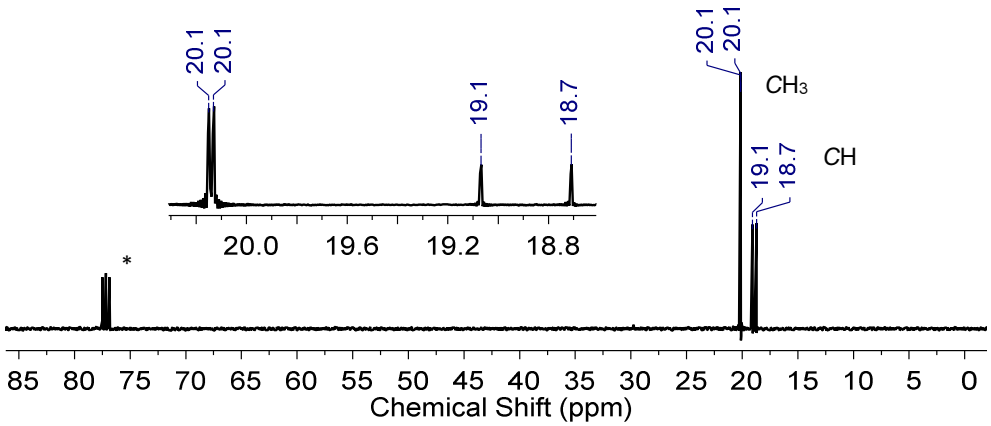

Figures S3.17. $^{13}C\{^{1}H\}$ NMR spectrum (101 MHz, 25 °C) of *i*$PrPH_2 \cdot BH_3$ in $CDCl_3$. * $CDCl_3$.

3.5.3.2 Synthesis and Characterisation of 1-Ad$PH_2 \cdot BH_3$:

Under dinitrogen atmosphere 202 mg (9.27 mmol) of $LiBH_4$ was partially dissolved and suspended in 30 mL of Et_2O and chilled in an ice-water bath. In a separate flask 1.054 g (4.44 mmol) of 1-AdPCl_2 was dissolved in 15 mL of Et_2O and added via cannula to the cold Et_2O slurry of $LiBH_4$. The reaction mixture was stirred at 0 °C for 10 min, afterwards the white suspension was stirred at 25 °C for 2h. The white suspension was filtered through Celite, and the solvent was evaporated from the filtrate under vacuum. The white oily residue was extracted into *n*-pentane, filtered through a glass microfiber filter pad and the filtrate was stored at -40 °C. After 2 days the supernatant was decanted off of colorless X-ray diffraction quality crystals of 1-Ad$PH_2 \cdot BH_3$, the crystals were washed with minimal cold *n*-pentane and dried under vacuum (496 mg, 62% yield).

^{1}H NMR (400 MHz, $CDCl_3$) δ 4.66 (q, J = 7.6 Hz, 1H, 1-AdP$\underline{H}_2$·BH_3), 3.78 (q, J = 7.6 Hz, 1H, AdP$\underline{H}_2$·BH_3), 2.03 (m, 3H, C$\underline{H}$), 1.86 (dd, J = 5.9, 2.8 Hz, 6H, PC(C$\underline{H}_2$)$_3$), 1.79 – 1.70 (m, 6H, C$\underline{H}_2$), 0.86 – 0.14 (m, 3H, AdPH_2·B$\underline{H}_3$). (Figure S3.18)

^{11}B{^{1}H} NMR (128 MHz, $CDCl_3$) δ −45.0 (d, J = 38.7 Hz). (Figure S3.19A)

^{11}B NMR (128 MHz, $CDCl_3$) δ −45.0 (qd, J = 100.0, 38.8 Hz). (Figure S3.19A)

^{31}P{^{1}H} NMR (162 MHz, $CDCl_3$) δ −14.2 (dd, J = 75.0, 32.6 Hz). (Figure S3.20A)

^{31}P NMR (162 MHz, $CDCl_3$) δ −14.2 (t, J = 369.3 Hz). (Figure S3.20B)

^{13}C{^{1}H} NMR (101 MHz, $CDCl_3$) δ 40.0 (d, J = 1.2 Hz, PC($\underline{C}H_2$)$_3$), 36.1 (d, J = 1.7 Hz, $\underline{C}H_2$), 28.7 (d, J = 36.2 Hz, H_3BP$\underline{C}$(CH_2)$_3$), 27.9 (d, J = 9.3 Hz, $\underline{C}$H). (Figure S3.21)

Anal. Calc'd. for $C_{10}H_{20}BP$: C, 65.97; H, 11.07; N, 0.00. Found: C, 65.65; H, 10.63; N, 0.10.

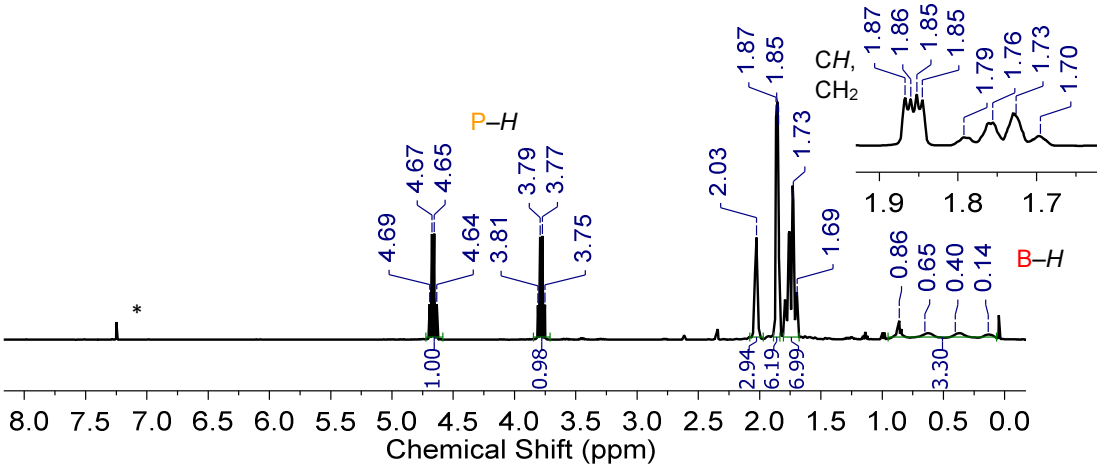

Figure S3.18. ^{1}H NMR spectrum (400 MHz, 25 °C) of 1-AdPH_2·BH_3 in $CDCl_3$. * $CDCl_3$.

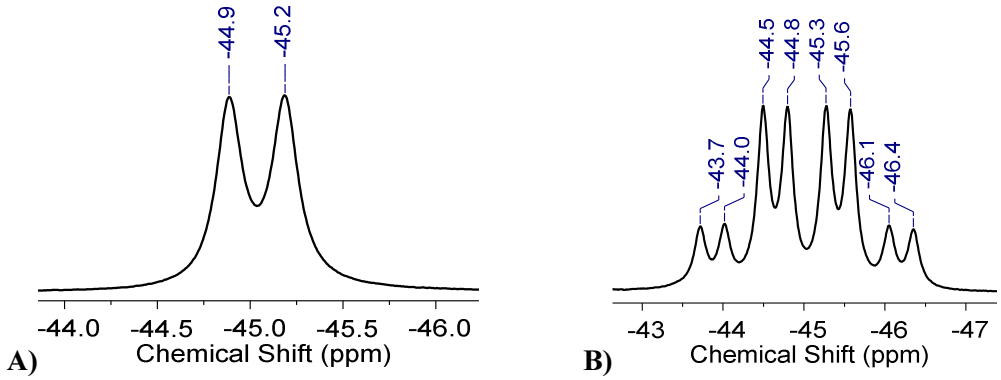

Figure S3.19. a) ^{11}B{^{1}H} NMR spectrum (128 MHz, 25 °C) of 1-AdPH_2·BH_3 in $CDCl_3$. b) ^{11}B NMR spectrum (128 MHz, 25 °C) of 1-AdPH_2·BH_3 in $CDCl_3$.

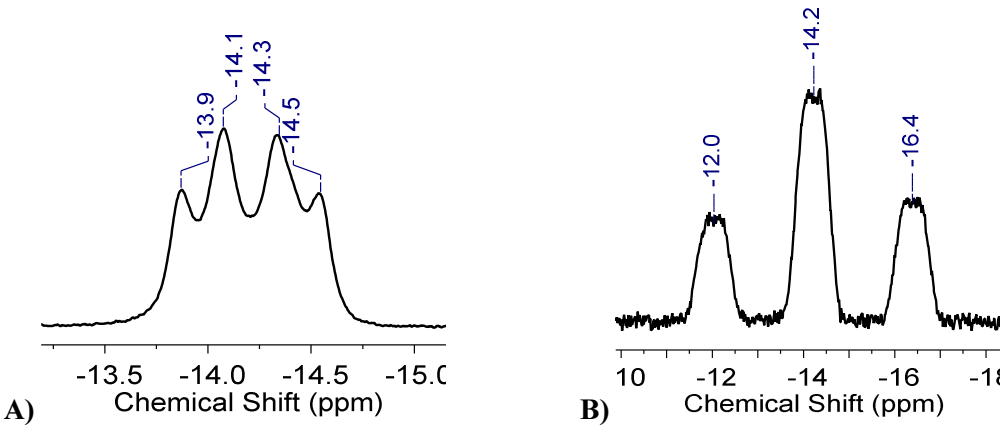

Figure S3.20. a) $^{31}P\{^{1}H\}$ NMR spectrum (162 MHz, 25 °C) of 1-Ad$PH_2{\cdot}BH_3$ in $CDCl_3$. b) ^{31}P NMR spectrum (162 MHz, 25 °C) of 1-Ad$PH_2{\cdot}BH_3$ in $CDCl_3$.

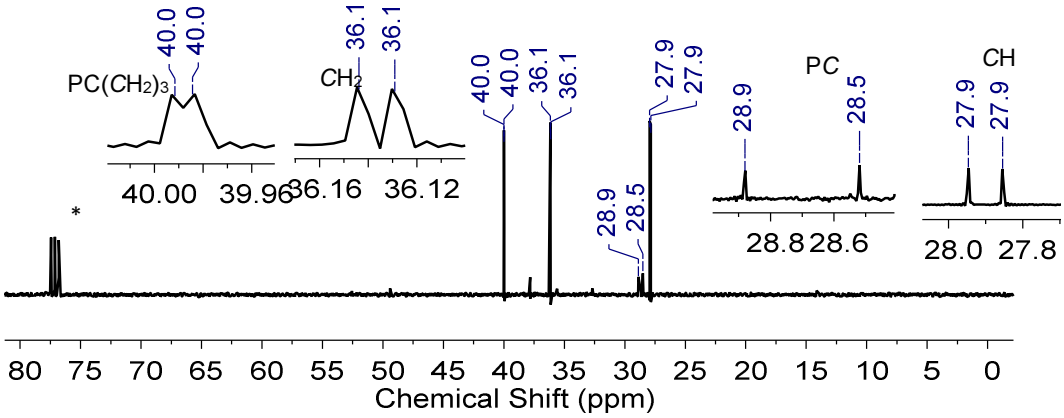

Figures S3.21. $^{13}C\{^{1}H\}$ NMR spectrum (101 MHz, 25 °C) of 1-Ad$PH_2{\cdot}BH_3$ in $CDCl_3$. * $CDCl_3$.

Table S3.1. ^{11}B, ^{31}P and ^{1}H NMR chemical shifts for $RPH_2{\cdot}BH_3$ (R = *i*Pr, 1-Ad), recorded in $CDCl_3$.

Monomer	^{11}B NMR (ppm)	^{31}P NMR (ppm)	^{1}H NMR (ppm)
*i*Pr$PH_2{\cdot}BH_3$	−44.6	−26.5	4.41
1-Ad$PH_2{\cdot}BH_3$	−45.0	−14.2	4.21

Table S3.2. Crystallographic information for 1-AdPH$_2$·BH$_3$.

Identification code	1-AdPH$_2$·BH$_3$
Empirical formula	$C_{10}H_{20}BP$
Formula weight	182.04
Temperature/K	100(2)
Crystal system	orthorhombic
Space group	*Pbca*
a/Å	9.2496(4)
b/Å	10.5381(4)
c/Å	21.9181(8)
α/°	90
β/°	90
γ/°	90
Volume/Å^3	2136.43(15)
Z	8
ρ_{calc}g/cm^3	1.132
μ/mm^{-1}	0.204
F(000)	800.0
Crystal size/mm^3	0.55 × 0.35 × 0.15
Radiation	MoKα (λ = 0.71073)
2θ range for data collection/°	3.716 to 55.066
Index ranges	-11 ≤ h ≤ 12, -13 ≤ k ≤ 13, -28 ≤ l ≤ 28
Reflections collected	18468
Independent reflections	2457 [R_{int} = 0.0439, R_σ = 0.0259]
Data/restraints/parameters	2457/0/129
Goodness-of-fit on F^2	1.043
Final R indexes [I>=2σ (I)]	R_1 = 0.0387, wR_2 = 0.0990
Final R indexes [all data]	R_1 = 0.0520, wR_2 = 0.1063
Largest diff. peak/hole / e Å^{-3}	0.44/-0.29

3.5.4 General Synthesis of Poly(alkylphosphinoboranes)

Under dinitrogen atmosphere 1 mmol of the corresponding phosphine–borane monomer was dissolved in 400 μL of toluene, to this solution 100 μL of a toluene stock solution of FeCp(CO)$_2$(OTf) (0.1 M) was added. The initially red-orange reaction mixture was transferred to a J. Young NMR tube, sealed, and heated at 100 °C, within the first 5 min a colour change from orange to yellow was observed. The J. Young tube was heated at 100 °C for the time specified in Table 1 and the conversion was monitored by ^{31}P{^{1}H} and ^{11}B{^{1}H} NMR spectroscopy. Upon complete consumption of monomer the J. Young tube was opened in air carefully to vent H$_2$ generated in the dehydropolymerisation reaction,

and the solvent was removed by rotary evaporation. The crude yellow-brown residue was dissolved in CH_2Cl_2 (0.5 mL) and passed through a ~3 cm plug of Florisil® (100-200 mesh) adsorbent, and a short pad of Celite® filtration aid within a glass microfiber plugged pipette, and was eluted with CH_2Cl_2 (5 mL). Afterwards the solvent was removed by rotary evaporation and the pale yellow to colorless polymeric product was dried under vacuum overnight followed by in a 40 °C vacuum oven for a minimum of 2 days.

3.5.4.1 Characterisation of $[1\text{-AdPH–BH}_2]_n$ Polymer:

Polymer is an off white powder. Yield: 57 %

^{1}H NMR ($CDCl_3$): δ (ppm) 3.59 (br d, 1H, P*H*); 1.99-1.74 (br m, 17H, B*H*, C*H, CH₂*) (Figure S3.22).

$^{11}B\{^1H\}$ NMR ($CDCl_3$): δ (ppm) −40.5 to −43.1 (br s) (Figure S3.23).

$^{31}P\{^1H\}$ NMR($CDCl_3$): δ (ppm) −19.50 (br); −26.09 (br) (Figure S3.24).

^{31}P NMR($CDCl_3$): δ (ppm) −18.34 to −27.03 (br m) (Figure S3.25).

^{13}C NMR ($CDCl_3$): δ (ppm) (Figure S3.26).

GPC: M_n = 23,400 g mol^{-1}, M_w = 35, 900 g mol^{-1}, PDI = 1.5 (Figure S3.27).

ESI-MS: Difference of 180 m/z ([1-AdPH–BH_2] subunit) confirms presence of linear oligo(adamantylphosphinoborane) with a phosphine end group H–[1-AdPH–BH_2]$_x$–PH_2(1-Ad) up to 15 repeat units (Figure S3.28).

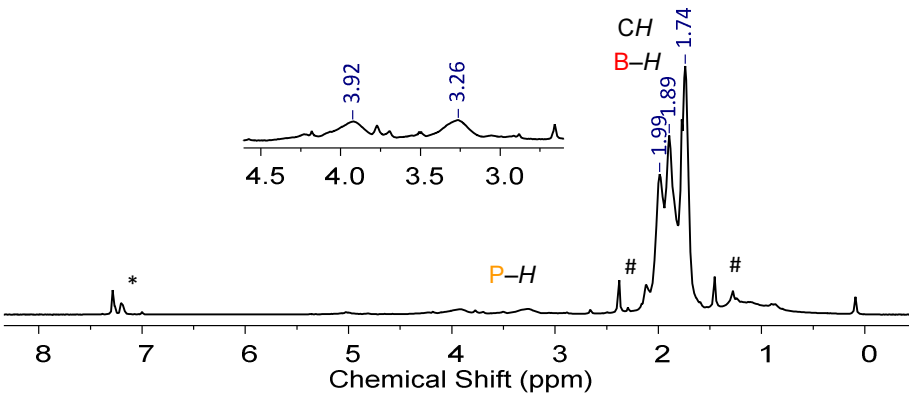

Figure S3.22. ^{1}H NMR spectrum of isolated $[1\text{-AdPH–BH}_2]_n$ in $CDCl_3$ at 20 °C. * $CDCl_3$, # THF.

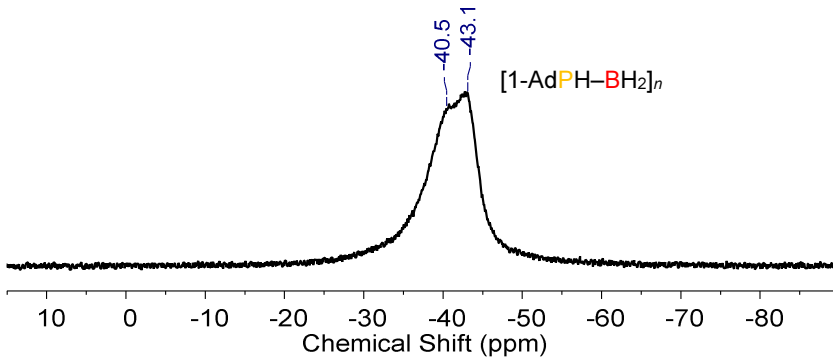

Figure S3.23. $^{11}B\{^{1}H\}$ NMR spectrum of isolated $[1\text{-AdPH–BH}_2]_n$ in $CDCl_3$ at 20 °C.

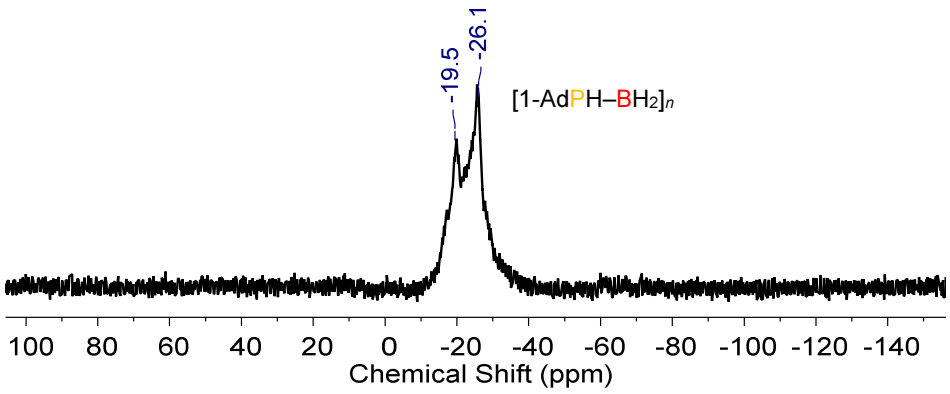

Figure S3.24. $^{31}P\{^{1}H\}$ NMR spectrum of isolated $[1\text{-AdPH–BH}_2]_n$ in $CDCl_3$ at 20 °C.

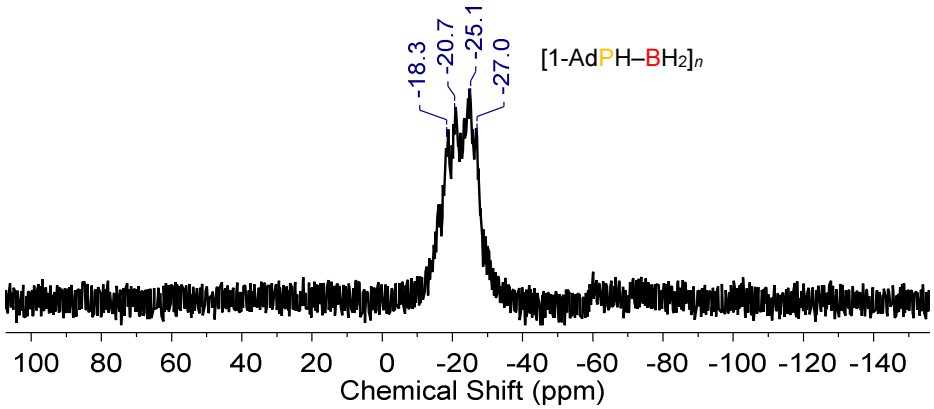

Figure S3.25. ^{31}P NMR spectrum of isolated $[1\text{-AdPH–BH}_2]_n$ in $CDCl_3$ at 20 °C.

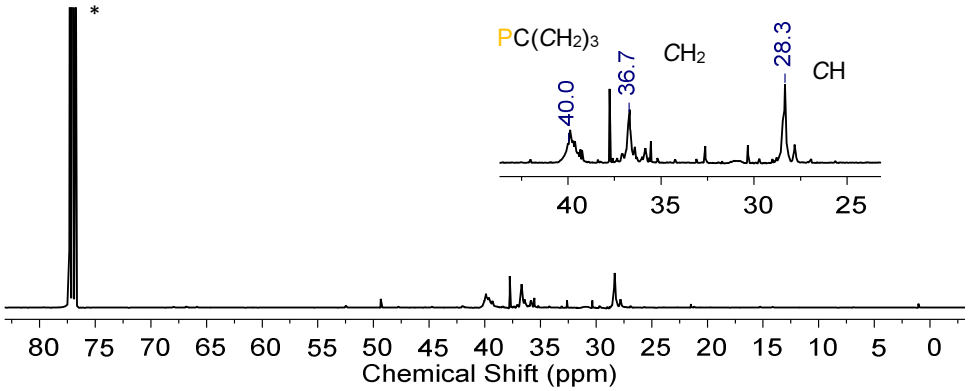

Figure S3.26. ^{13}C NMR spectrum of isolated $[1\text{-AdPH–BH}_2]_n$ in $CDCl_3$ at 20 °C. * $CDCl_3$.

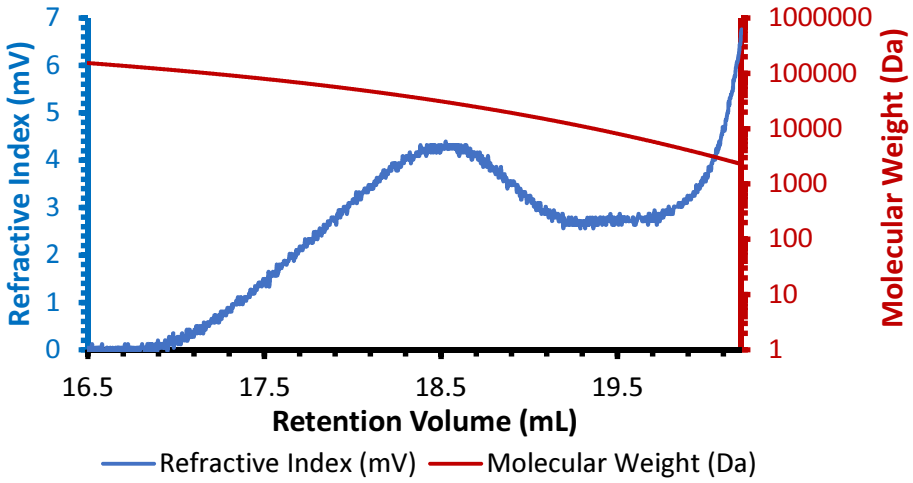

Figure S3.27. GPC chromatogram (2 mg mL^{-1}) of isolated $[1\text{-AdPH–BH}_2]_n$ in THF (0.1 wt% $[n\text{Bu}_4\text{N}]\text{Br}$).

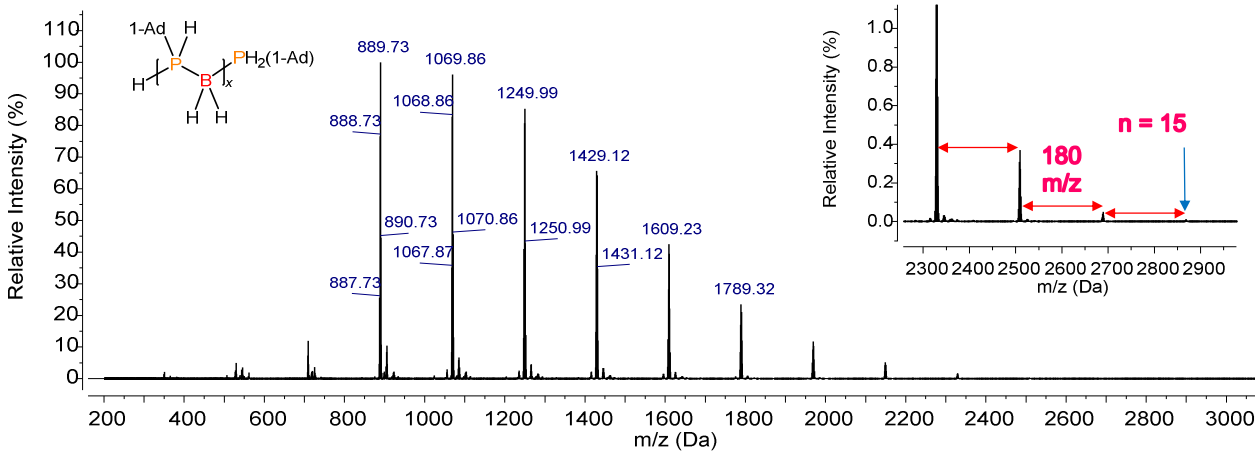

Figure S3.28. ESI-MS (2mg mL^{-1} in CH_2Cl_2) spectrum in positive mode of isolated $[1\text{-AdPH–BH}_2]_x$

3.5.4.2 Characterisation of [*i*PrPH–BH_2]$_n$ Polymer:

Polymer is a pale yellow gum. Yield: 86 %

^{1}H NMR ($CDCl_3$): δ (ppm) 3.87 (br d, 1H, P*H*); 2.20 (br s, C*H*); 1.51-1.34 (br m, B*H*, C*H*$_3$) (Figure S3.29).

^{11}B{^{1}H} NMR ($CDCl_3$): δ (ppm) −39.9 (br) (Figure S3.30).

^{31}P{^{1}H} NMR{^{1}H} NMR ($CDCl_3$): δ (ppm) −30.7 (br); −39.1 (br) (Figure S3.31).

^{13}C NMR ($CDCl_3$): δ (ppm) 20.6–18.7 (br m) (Figure S3.32).

GPC: M_n = 18,200 g mol^{-1}, M_w = 36,200 g mol^{-1}, PDI = 1.99 (Figure S3.33).

ESI-MS: Difference of 88 m/z ([*i*PrPH–BH_2] subunit) confirms presence of linear oligo(isopropylphosphinoborane) with a phosphine end group H–[*i*PrPH–BH_2]$_x$–PH_2*i*Pr up to 36 repeat units (Figure S3.34).

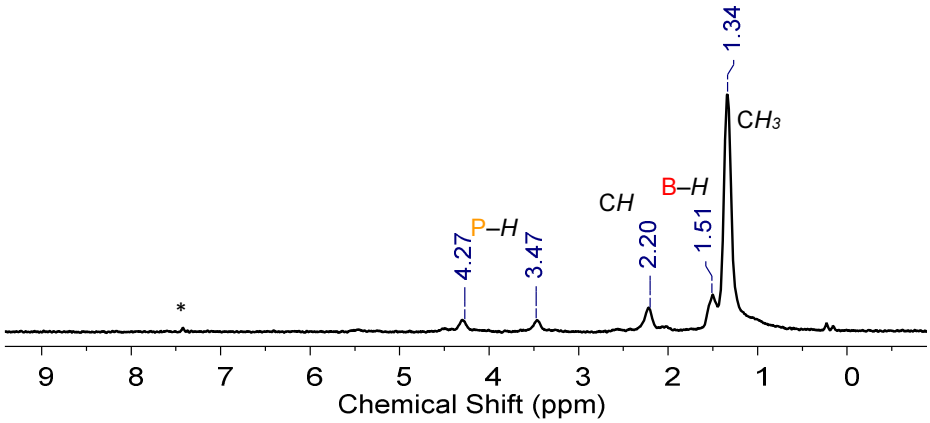

Figure S3.29. ^{1}H NMR spectrum of isolated [*i*PrPH–BH_2]$_n$ in $CDCl_3$ at 20 °C. * $CDCl_3$.

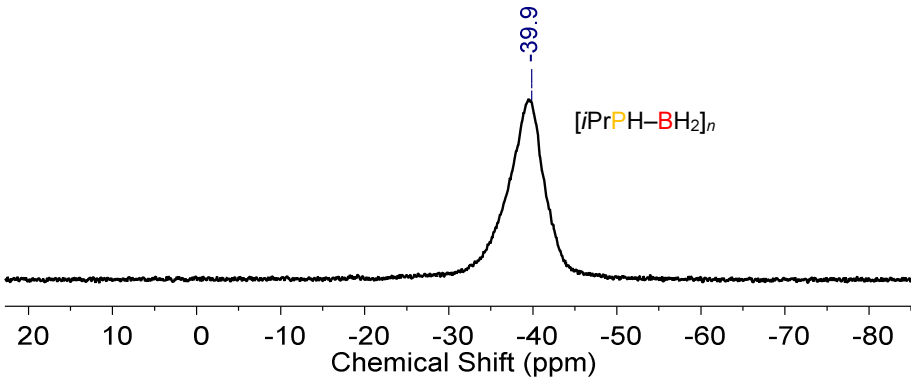

Figure S3.30. ^{11}B{^{1}H} NMR spectrum of isolated [*i*PrPH–BH_2]$_n$ in $CDCl_3$ at 20 °C.

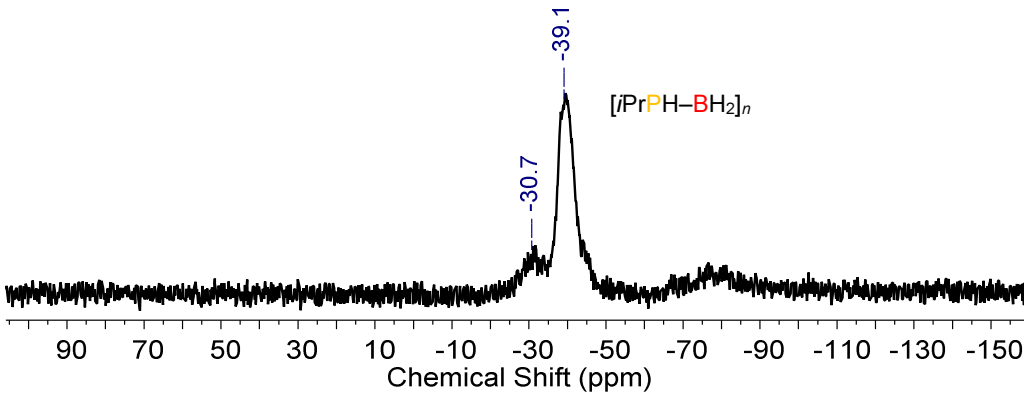

Figure S3.31. $^{31}P\{^{1}H\}$ NMR spectrum of isolated $[i\text{PrPH–BH}_2]_n$ in $CDCl_3$ at 20 °C.

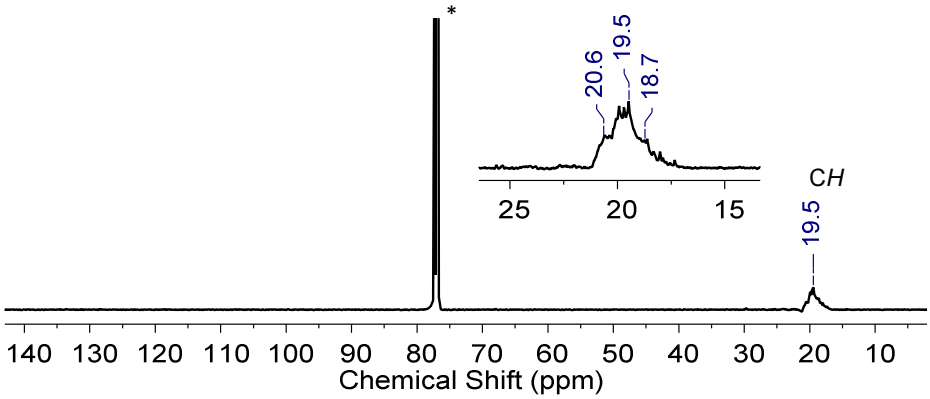

Figure S3.32. $^{31}P\{^{1}H\}$ NMR spectrum of isolated $[i\text{PrPH–BH}_2]_n$ in $CDCl_3$ at 20 °C. * $CDCl_3$.

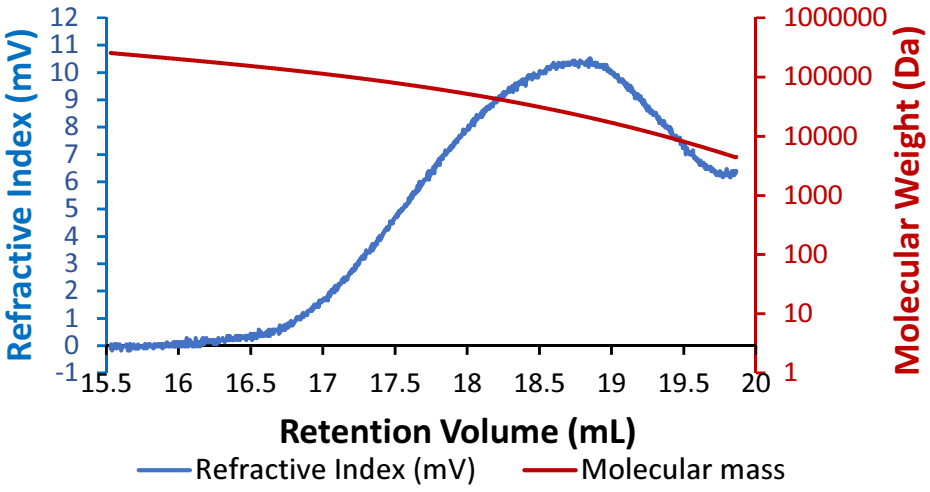

Figure S3.33. GPC chromatogram (2 mg mL^{-1}) of isolated $[i\text{PrPH–BH}_2]_n$ in THF (0.1 wt% $[n\text{Bu}_4\text{N}]\text{Br}$).

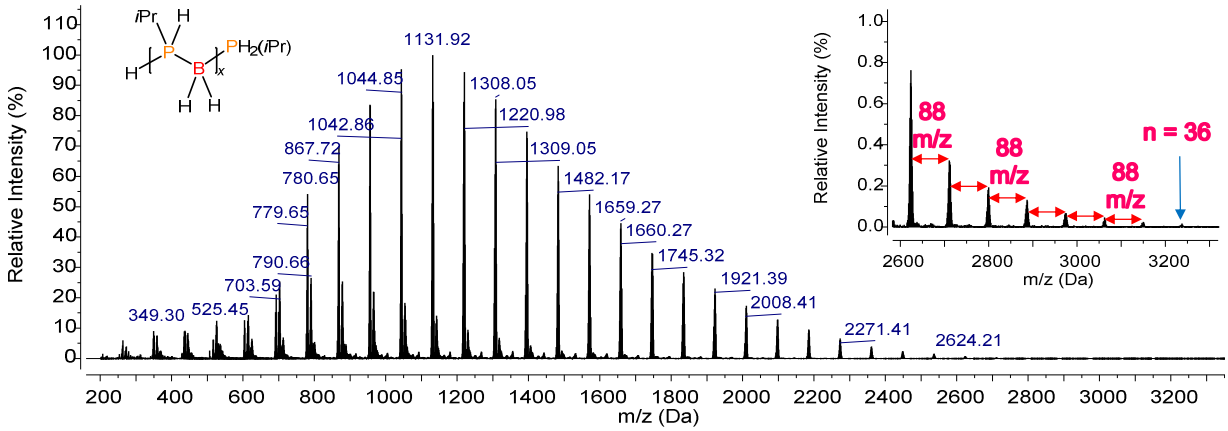

Figure S3.34. ESI-MS (2mg mL^{-1} in CH_2Cl_2) spectrum in positive mode of isolated [*i*PrPH–BH_2]$_x$

3.5.4.3 Characterisation of [CyPH–BH_2]$_n$ Polymer:

Polymer is an off white sticky solid. Yield: 64 %

^{1}H NMR ($CDCl_3$): δ (ppm) 3.65 (br d, P*H*); 1.93-1.65 (br m, C*H*); 1.24 (br s, C*H*, B*H*) (Figure S3.35).

^{11}B{^{1}H} NMR ($CDCl_3$): δ (ppm) −40.1 (br) (Figure S3.36).

^{31}P{^{1}H} NMR ($CDCl_3$): δ (ppm) −34.5 to −48.7 (br m) (Figure S3.37).

^{13}C NMR ($CDCl_3$): δ (ppm) 32.1 (br s); 30.1-29.7 (br m); 26.9 (br s); 25.8 (br s) (Figure S3.38).

GPC: M_n = 31,800 g mol^{-1}, M_w = 49,100 g mol^{-1}, PDI = 1.5 (Figure S3.39).

ESI-MS: ESI-MS: Difference of 128 m/z ([CyHPBH_2] subunit) confirms presence of linear oligo(cyclohexylphosphinoborane) with a phosphine end group H–[CyPH–BH_2]$_x$–PH_2Cy up to 27 repeat units (Figure S3.40).

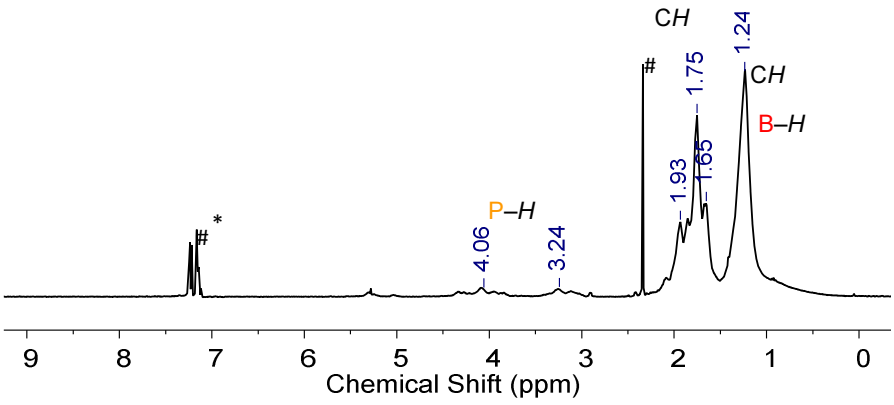

Figure S3.35. ^{1}H NMR spectrum of isolated [CyPH–BH_2]$_n$ in $CDCl_3$ at 20 °C. * $CDCl_3$, # Toluene.

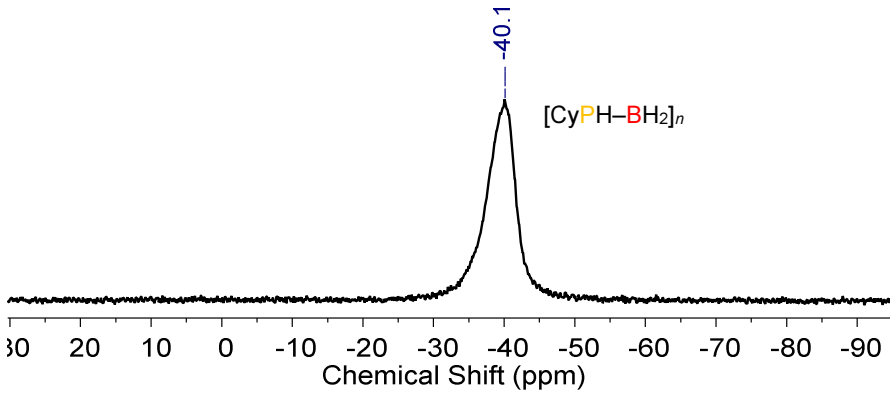

Figure S3.36. $^{11}B\{^{1}H\}$ NMR spectrum of isolated $[CyPH–BH_2]_n$ in $CDCl_3$ at 20 °C.

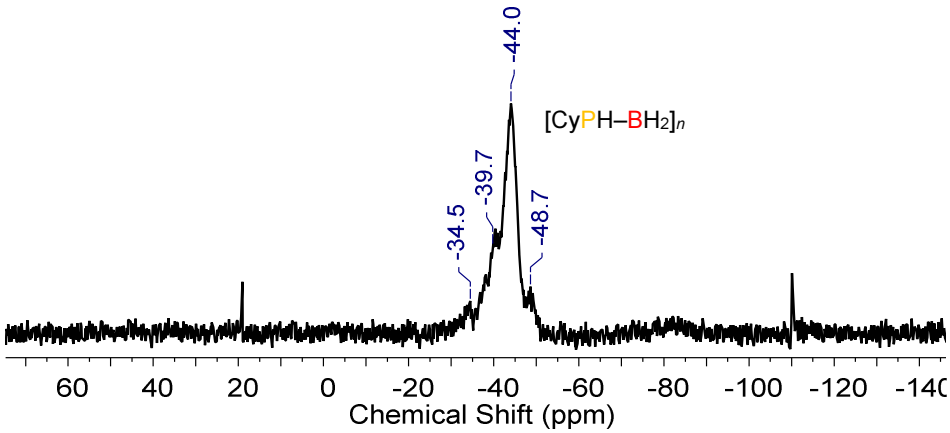

Figure S3.37. $^{31}P\{^{1}H\}$ NMR spectrum of isolated $[CyPH–BH_2]_n$ in $CDCl_3$ at 20 °C.

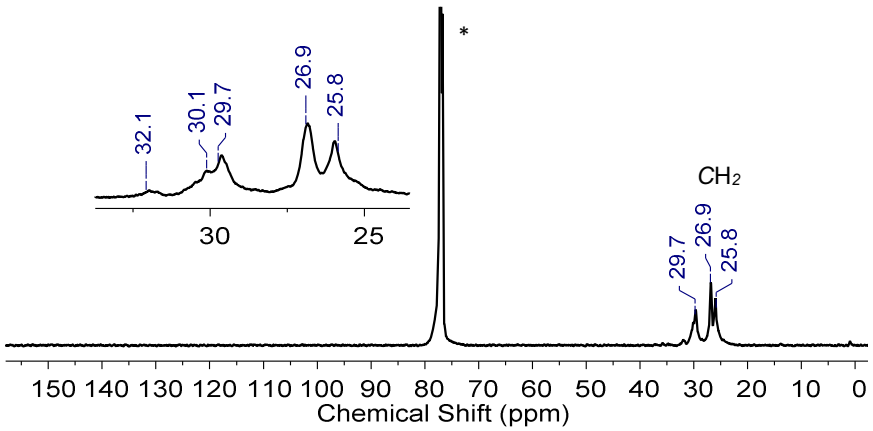

Figure S3.38. ^{13}C NMR spectrum of isolated $[CyPH–BH_2]_n$ in $CDCl_3$ at 20 °C. * $CDCl_3$.

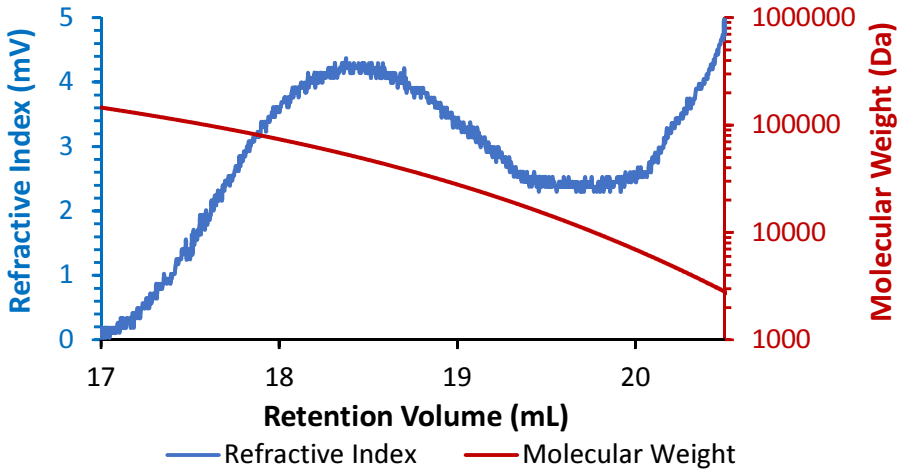

Figure S3.39. GPC chromatogram (2 mg mL^{-1}) of isolated [CyPH–BH_2]$_n$ in THF (0.1 wt% [nBu$_4$N]Br).

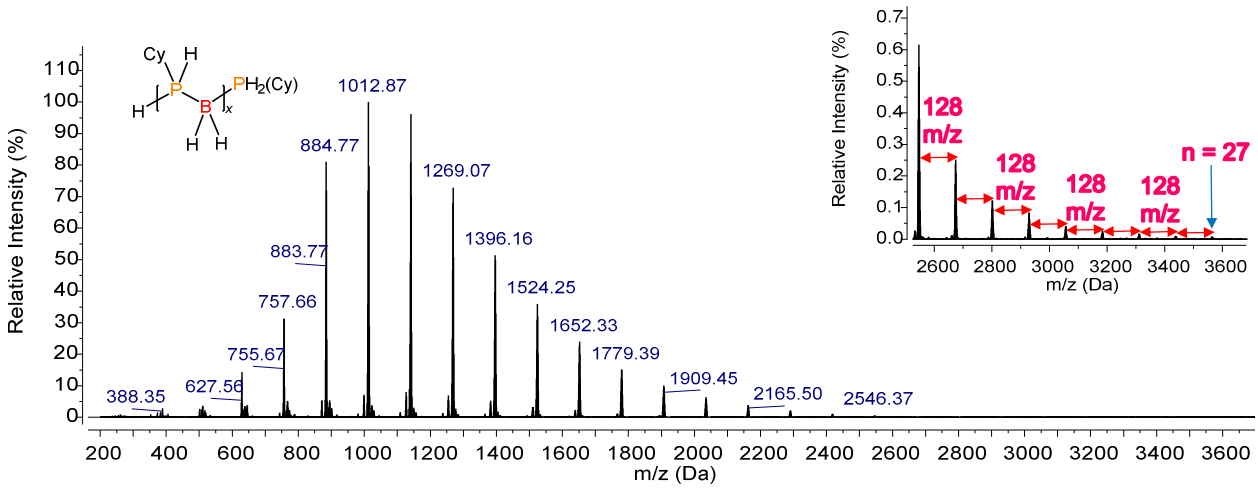

Figure S3.40. ESI-MS (2mg mL^{-1} in CH_2Cl_2) spectrum in positive mode of isolated [CyPH–BH_2]$_x$

3.5.4.4 Characterisation of [*n*HexPH–BH_2]$_n$ Polymer

Polymer is a pale yellow gum. Yield: 61 %

^{1}H NMR ($CDCl_3$): δ (ppm) 3.8 (br d, 1H, P*H*); 1.54- 0.87 (br m, 15H, BH_2, CH_3, CH_2) (Figure S3.41).

^{11}B{^{1}H} NMR ($CDCl_3$): δ (ppm) −36.6 (br) (Figure S3.42).

^{31}P{^{1}H} NMR ($CDCl_3$): δ (ppm) −53.26 (br); −61.81 (br) (Figure S3.43).

^{13}C NMR ($CDCl_3$): δ (ppm) 31.5 (s, $CH_3(\underline{C}H_2)_4CH_2HPBH_2$); 30.7 (s, $CH_3(\underline{C}H_2)_4CH_2HPBH_2$); 26.2 (s, $CH_3(\underline{C}H_2)_4CH_2HPBH_2$); 22.6 (s, $CH_3(\underline{C}H_2)_4CH_2HPBH_2$); 20.6 (br, $CH_3(CH_2)_4\underline{C}H_2HPBH_2$); 14.1 (s, $\underline{C}H_3(CH_2)_4CH_2HPBH_2$) (Figure S3.44).

GPC: M_n = 57,200 g mol^{-1}, M_w = 86,800 g mol^{-1}, PDI = 1.5 (Figure S3.45).

ESI-MS: Difference of 130 m/z ([*n*HexPH–BH_2] subunit) confirms presence of linear oligo(*n*Hexylphosphinoborane) with a phosphine end group H–[*n*HexPH–BH_2]$_x$–PH_2*n*Hex up to 25 repeat units (Figure S3.46).

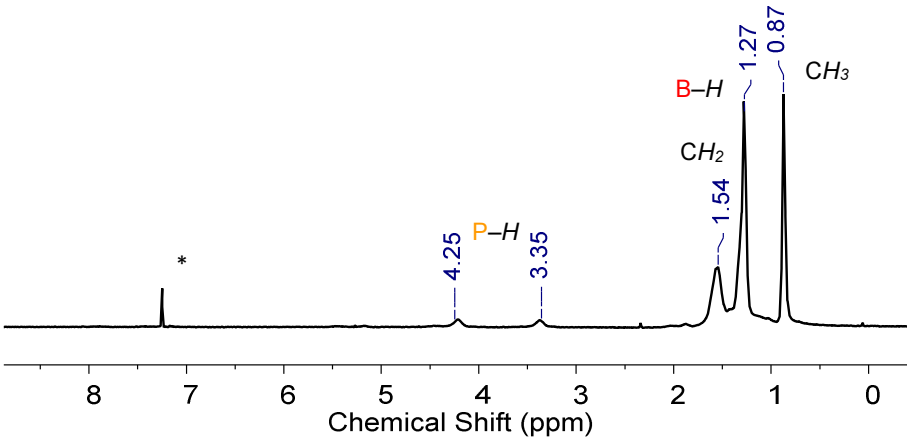

Figure S3.41. ^{1}H NMR spectrum of isolated [*n*HexPH–BH_2]$_n$ in $CDCl_3$ at 20 °C. * $CDCl_3$.

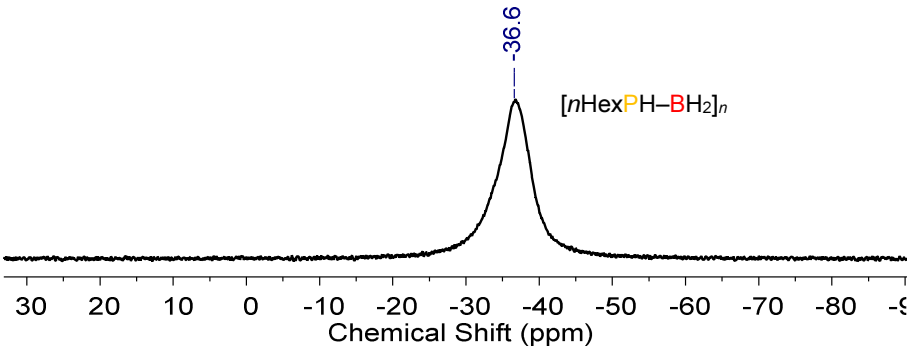

Figure S3.42. ^{11}B{^{1}H} NMR spectrum of isolated [*n*HexPH–BH_2]$_n$ in $CDCl_3$ at 20 °C.

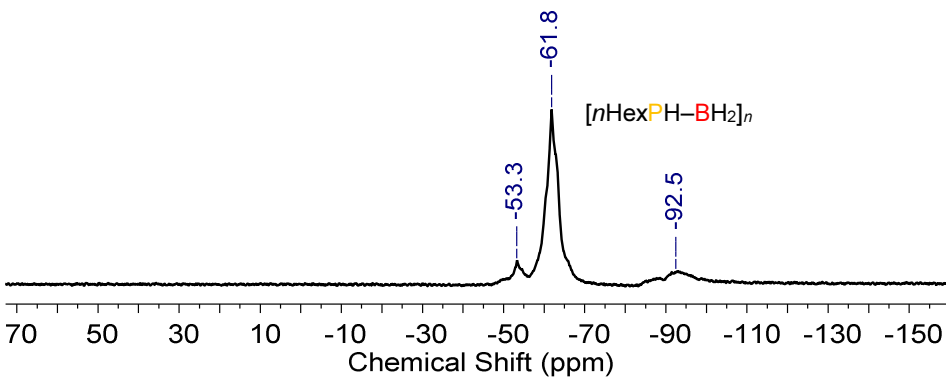

Figure S3.43. ^{31}P{^{1}H} NMR spectrum of isolated [*n*HexPH–BH_2]$_n$ in $CDCl_3$ at 20 °C.

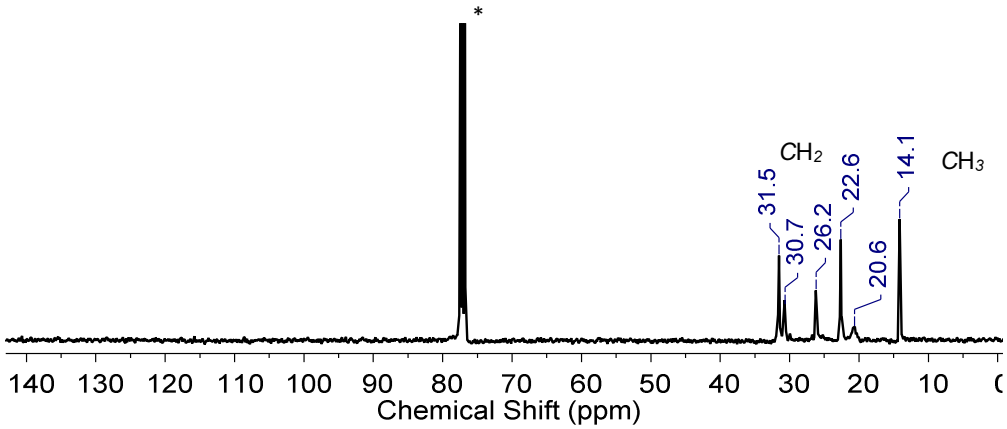

Figure S3.44. ^{13}C NMR spectrum of isolated $[n\text{HexPH–BH}_2]_n$ in $CDCl_3$ at 20 °C. * $CDCl_3$.

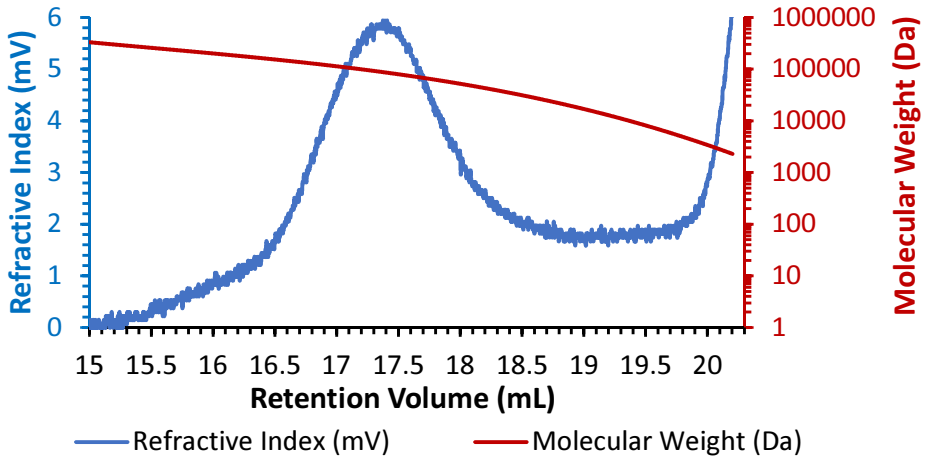

Figure S3.45. GPC chromatogram (2 mg mL^{-1}) of isolated $[n\text{HexPH–BH}_2]_n$ in THF (0.1 wt% $[n\text{Bu}_4\text{N}]\text{Br}$).

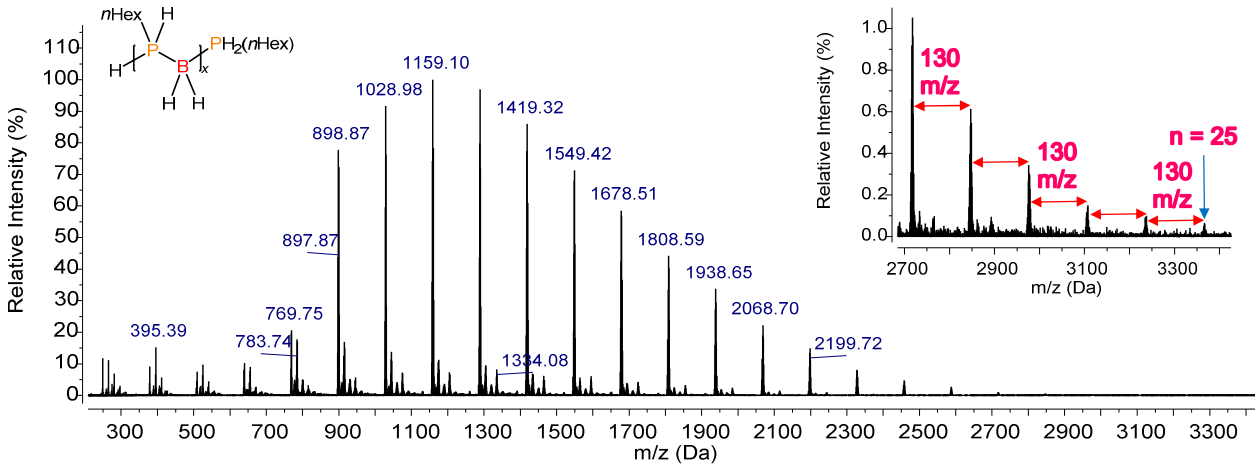

Figure S3.46. ESI-MS (2 mg mL^{-1} in CH_2Cl_2) in positive mode of isolated $[n\text{HexPH–BH}_2]_x$.

3.5.4.5 Characterisation of $[MePH–BH_2]_n$ Polymer:

Polymer is a pale yellow gum. Yield: 80 %

^{1}H NMR ($CDCl_3$): δ (ppm) 3.93 (br d, P*H*); 1.65-0.88 (br m, BH_2, CH_3) (Figure S3.47).

$^{11}B\{^{1}H\}$ NMR ($CDCl_3$): δ (ppm) 4.2 (br); −15.3 (br); −34.9 (br) (Figure S3.48).

$^{31}P\{^{1}H\}$ NMR ($CDCl_3$): δ (ppm) −68.72 (br); −76.70 (br) (Figure S3.49).

^{31}P NMR ($CDCl_3$): δ (ppm) −68.72 (t br) ($J_{PH} \approx 380$ MHz); −76.70 (d br) ($J_{PH} \approx 350$ MHz) (Figure S3.50).

^{13}C NMR ($CDCl_3$): δ (ppm) 5.92–4.91 (br s) (Figure S3.51).

GPC: M_n = 14,000, M_w = 48,000, PDI = 3.4. A broad, multimodal mass distribution with ca. M_n = 2,000–300,000 g mol^{-1} was observed. (Figure S3.52).

ESI-MS: Difference of 60 m/z ([MePH–BH_2] subunit) confirms presence of linear oligo(methylphosphinoborane) H–[MePH–BH_2]$_x$–H up to 9 repeat units and a second distribution with a phosphine end group H–[MePH–BH_2]$_x$–PH_2Me up to 24 repeat units (Figure S3.53).

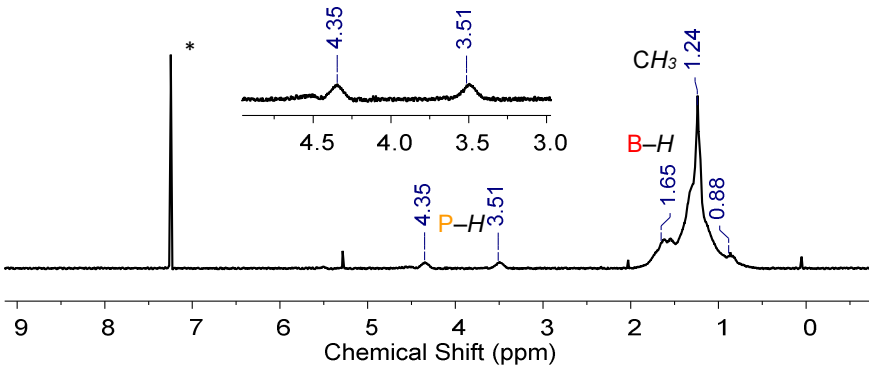

Figure S3.47. ^{1}H NMR spectrum of isolated $[MePH–BH_2]_n$ in $CDCl_3$ at 20 °C. * $CDCl_3$.

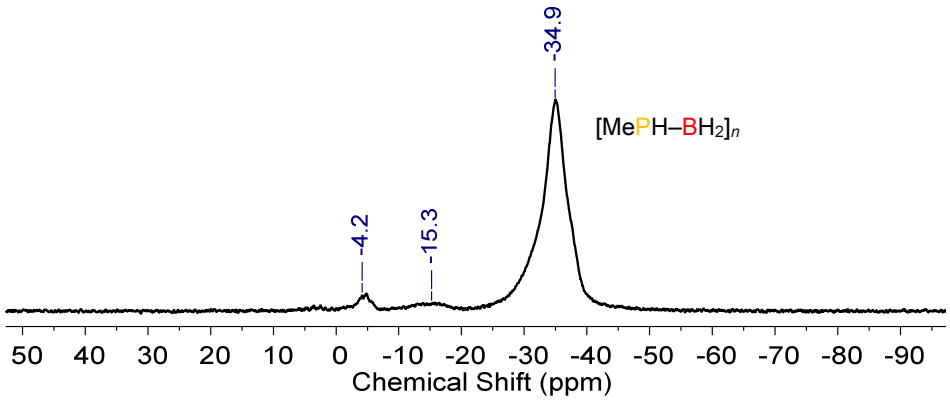

Figure S3.48. $^{11}B\{^{1}H\}$ NMR spectrum of isolated $[MePH–BH_2]_n$ in $CDCl_3$ at 20 °C.

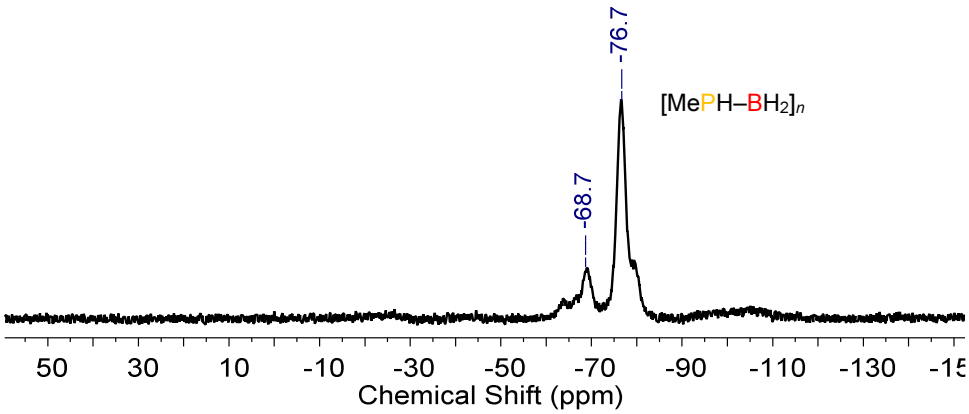

Figure S3.49. $^{31}P\{^{1}H\}$ NMR spectrum of isolated $[MePH–BH_2]_n$ in $CDCl_3$ at 20 °C.

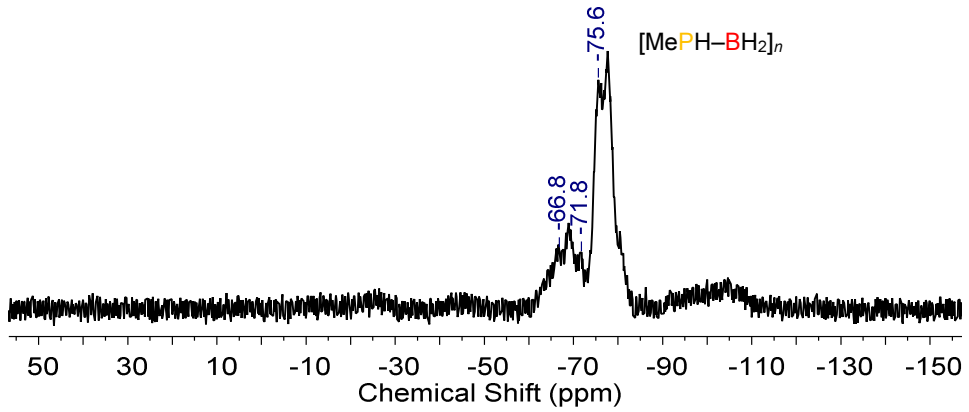

Figure S3.50. $^{31}P\{^{1}H\}$ NMR spectrum of isolated $[MePH–BH_2]_n$ in $CDCl_3$ at 20 °C.

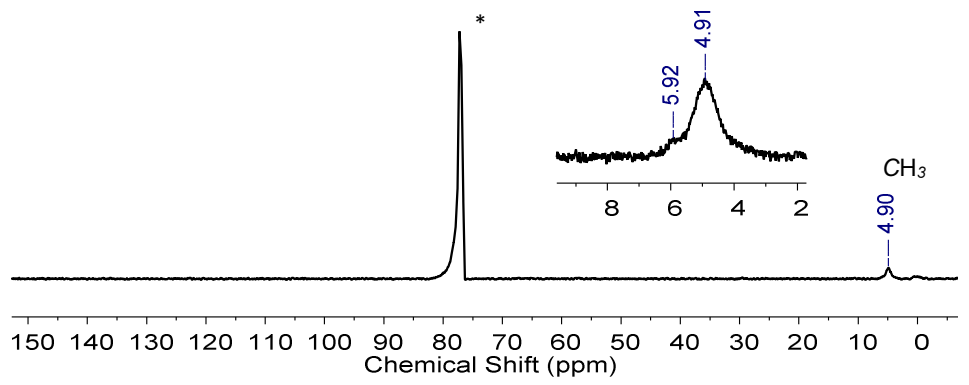

Figure S3.51. ^{13}C NMR spectrum of isolated $[MePH–BH_2]_n$ in $CDCl_3$ at 20 °C. * $CDCl_3$.

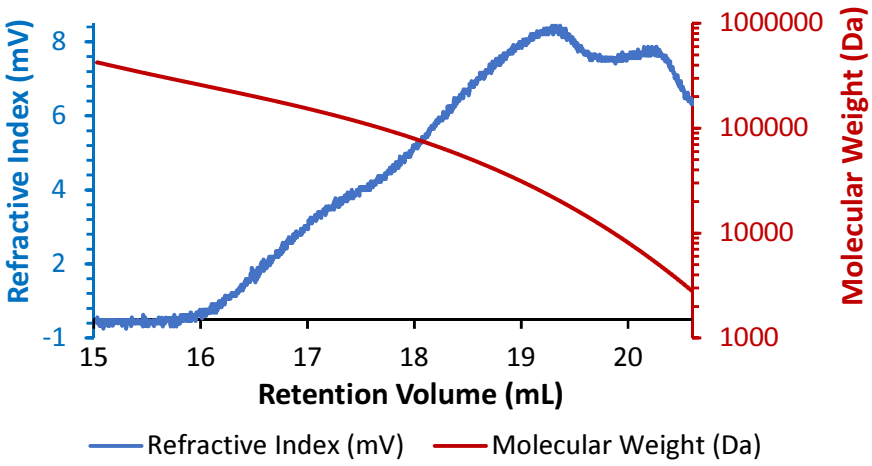

Figure S3.52. GPC chromatogram (2 mg mL^{-1}) of isolated $[MePH–BH_2]_n$ in THF (0.1 wt% $[n Bu_4N]Br$).

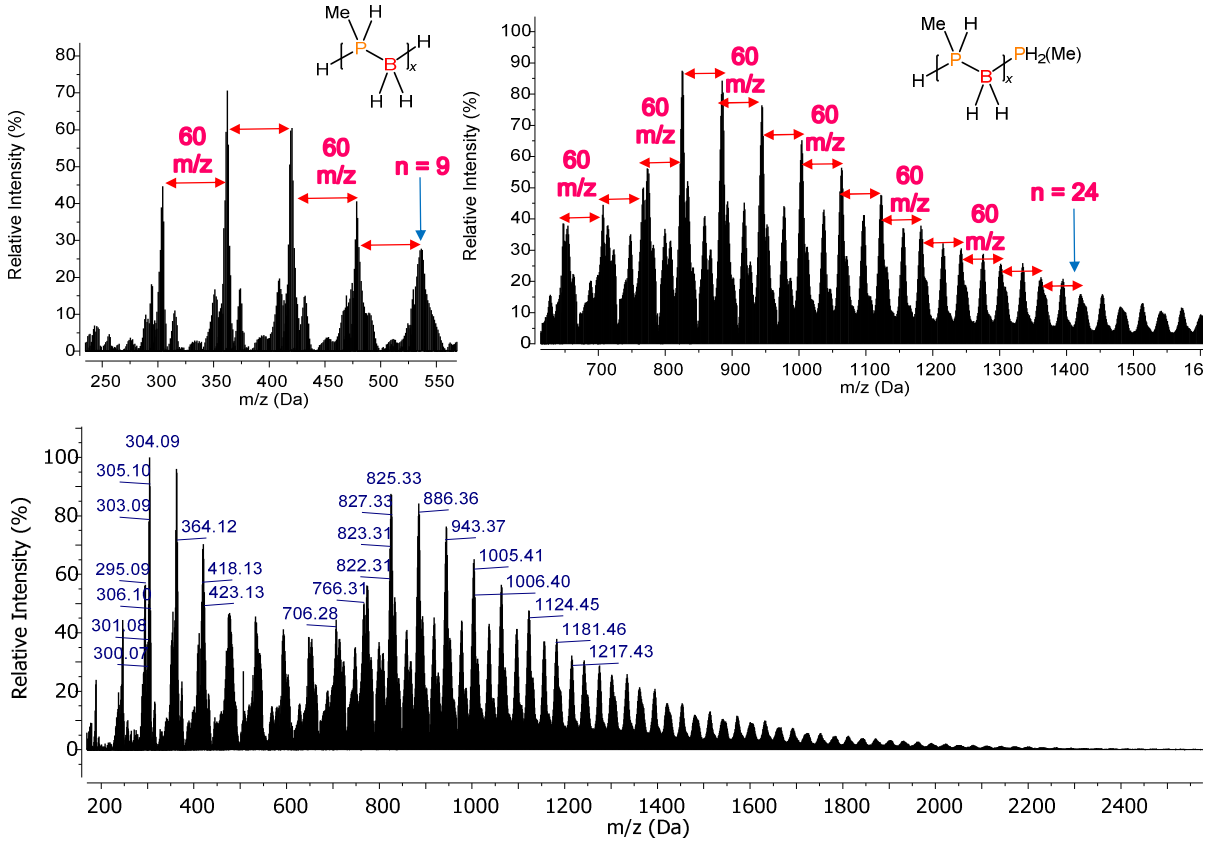

Figure S3.53. ESI-MS (2mg mL^{-1} in CH_2Cl_2) spectrum in positive mode of isolated $[MePH–BH_2]_x$.

3.5.5 DSC Thermograms of Poly(alkylphosphinoboranes)

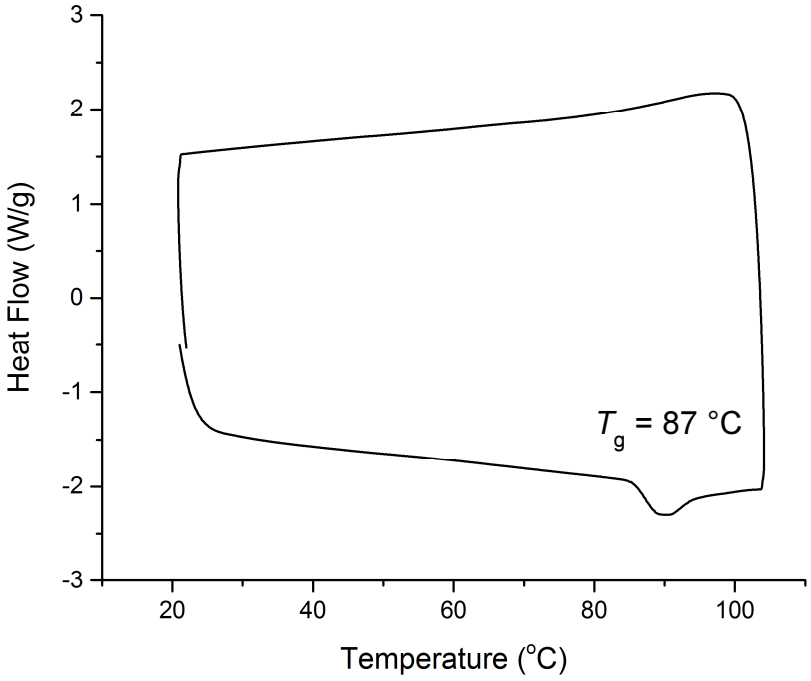

Figure S3.54. DSC thermogram of $[1\text{-AdPH–BH}_2]_n$, 1st cycle excluded.

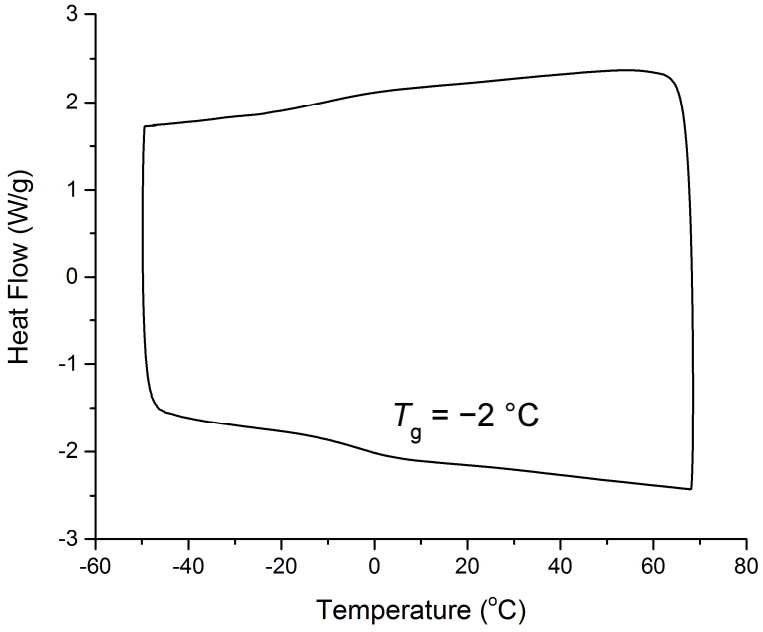

Figure S3.55. DSC thermogram of $[\text{CyPH–BH}_2]_n$, 1st cycle excluded.

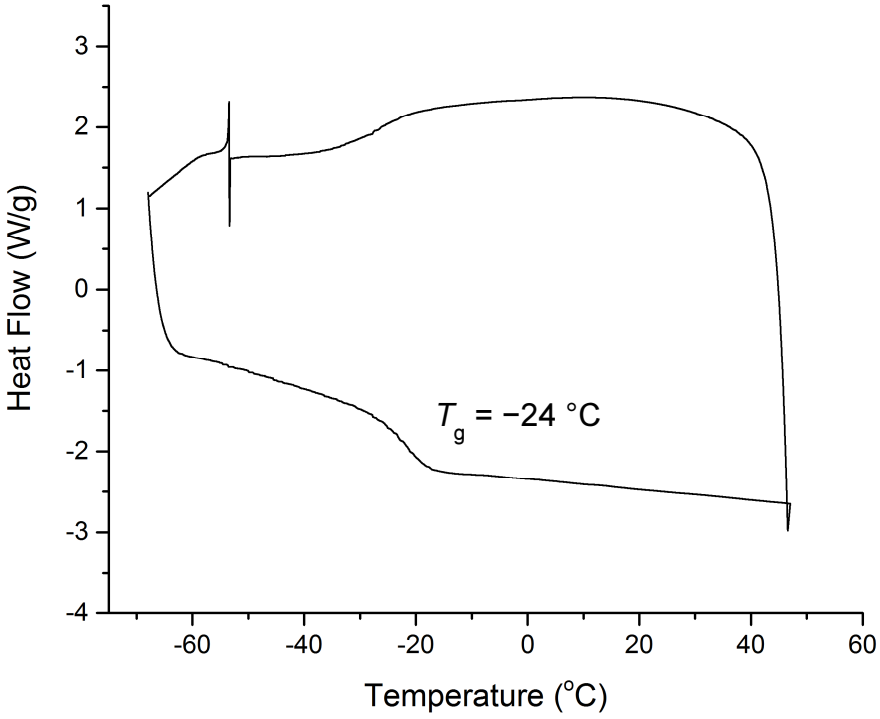

Figure S3.56. DSC thermogram of $[MePH–BH_2]_n$, 1st cycle excluded.

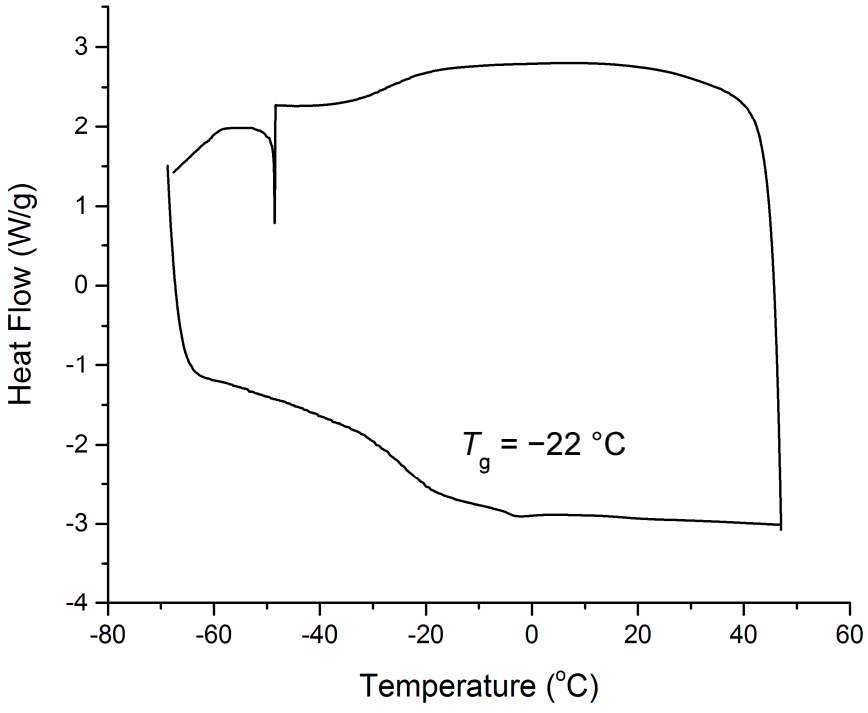

Figure S3.57. DSC thermogram of $[i\text{PrPH–BH}_2]_n$, 1st cycle excluded.

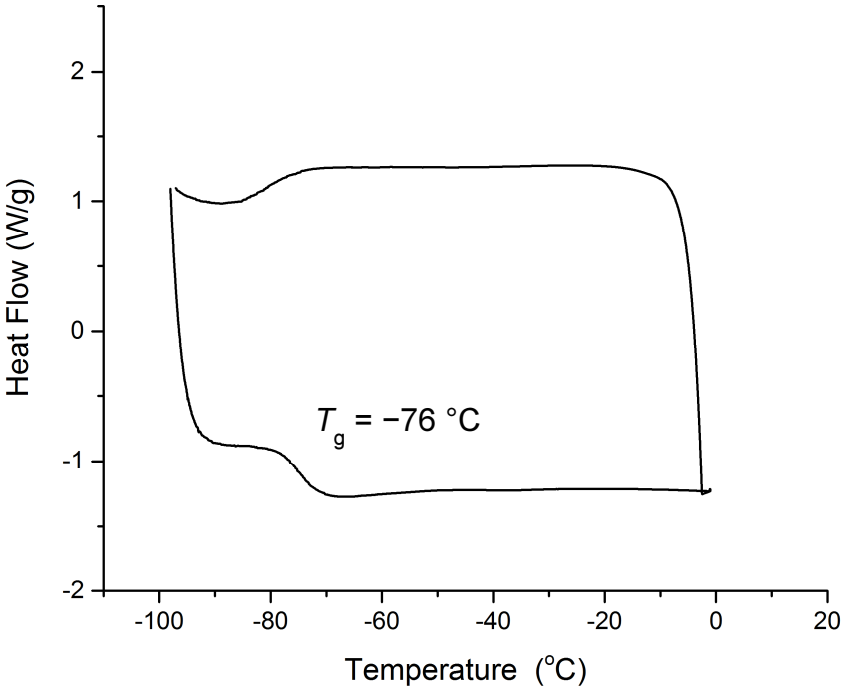

Figure S3.58. DSC thermogram of [*n*HexPH–BH_2]$_n$, 1st cycle excluded.

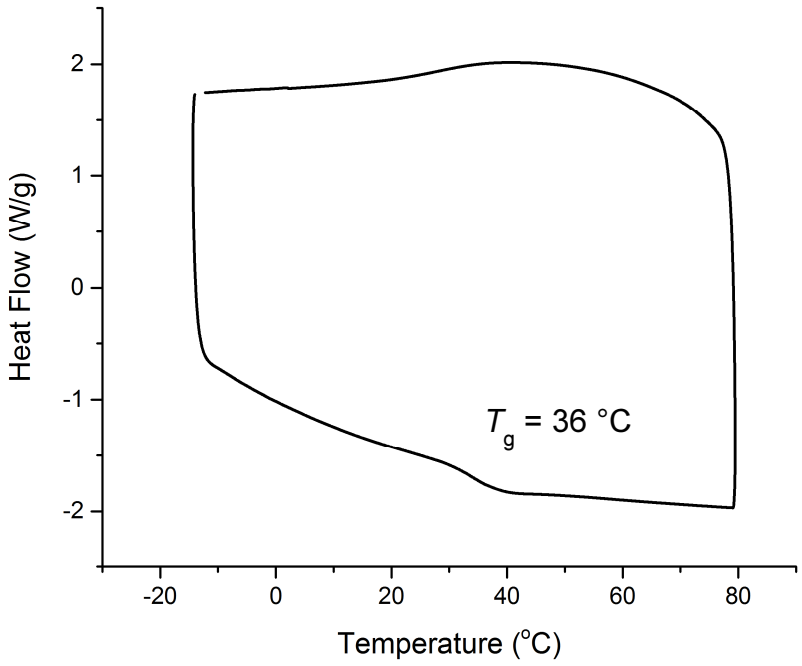

Figure S3.59. DSC thermogram of [*t*BuPH–BH_2]$_n$, 1st cycle excluded.

3.6 References

1. (a) Chivers, T.; Manners, I.; Royal Society of, C., *Inorganic rings and polymers of the p-block elements : from fundamentals to applications*. RSC Pub.: Cambridge, 2009; (b) Manners, I., *Angew. Chem. Int. Ed.* **1996,** *35*, 1602-1621; (c) Priegert, A. M.; Rawe, B. W.; Serin, S. C.; Gates, D. P., *Chem. Soc. Rev.* **2016,** *45*, 922-953.

2. (a) Fazen, P. J.; Remsen, E. E.; Beck, J. S.; Carroll, P. J.; Mcghie, A. R.; Sneddon, L. G., *Chem. Mater.* **1995,** *7*, 1942-1956; (b) Fazen, P. J.; Beck, J. S.; Lynch, A. T.; Remsen, E. E.; Sneddon, L. G., *Chem. Mater.* **1990,** *2*, 96-97; (c) Ren, Y.; Jäkle, F., Incorporation of Group 13 Elements into Polymers. In *Main Group Strategies towards Functional Hybrid Materials*, Baumgartner, T.; Jäkle, F., Eds. 2018; (d) Lorbach, A.; Bolte, M.; Li, H. Y.; Lerner, H. W.; Holthausen, M. C.; Jakle, F.; Wagner, M., *Angew. Chem. Int. Ed.* **2009,** *48*, 4584-4588; (e) Li, H.; Jakle, F., *Angew. Chem. Int. Ed.* **2009,** *48*, 2313-2316.

3. (a) Wan, W. M.; Baggett, A. W.; Cheng, F.; Lin, H.; Liu, S. Y.; Jäkle, F., *Chem. Commun.* **2016,** *52*, 13616-13619; (b) Thiedemann, B.; Gliese, P. J.; Hoffmann, J.; Lawrence, P. G.; Sönnichsen, F. D.; Staubitz, A., *Chem. Commun.* **2017,** *53*, 7258-7261; (c) van de Wouw, H. L.; Lee, J. Y.; Klausen, R. S., *Chem. Commun.* **2017,** *53*, 7262-7265; (d) van de Wouw, H. L.; Lee, J. Y.; Awuyah, E. C.; Klausen, R. S., *Angew. Chem. Int. Ed.* **2018,** *57*, 1673-1677; (e) Mendis, S. N.; Zhou, T.; Klausen, R. S., *Macromolecules* **2018**; (f) van de Wouw, H. L.; Awuyah, E. C.; Baris, J. I.; Klausen, R. S., *Macromolecules* **2018,** *51*, 6359-6368.

4. (a) Staubitz, A.; Soto, A. P.; Manners, I., *Angew. Chem. Int. Ed.* **2008,** *47*, 6212-6215; (b) Staubitz, A.; Sloan, M. E.; Robertson, A. P. M.; Friedrich, A.; Schneider, S.; Gates, P. J.; Günne, J. S. A. D.; Manners, I., *J. Am. Chem. Soc.* **2010,** *132*, 13332-13345; (c) Dallanegra, R.; Robertson, A. P. M.; Chaplin, A. B.; Manners, I.; Weller, A. S., *Chem. Commun.* **2011,** *47*, 3763-3765; (d) Johnson, H. C.; Leitao, E. M.; Whitten, G. R.; Manners, I.; Lloyd-Jones, G. C.; Weller, A. S., *J. Am. Chem. Soc.* **2014,** *136*, 9078-9093; (e) Colebatch, A. L.; Gilder, B. W. H.; Whittell, G. R.; Oldroyd, N. L.; Manners, I.; Weller, A. S., *Chem. Eur. J.* **2018,** *24*, 5450-5455; (f) Adams, G. M.; Colebatch, A. L.; Skornia, J. T.; McKay, A. I.; Johnson, H. C.; Lloyd-Jones, G. C.; Macgregor, S. A.; Beattie, N. A.; Weller, A. S., *J. Am. Chem. Soc.* **2018,** *140*, 1481-1495; (g) Vance, J. R.; Robertson, A. P. M.; Lee, K.; Manners, I., *Chem. Eur. J.* **2011,** *17*, 4099-4103; (h) Anke, F.; Han, D.; Klahn, M.; Spannenberg, A.; Beweries, T., *Dalton Trans.* **2017,** *46*, 6843-6847; (i) Trose, M.; Reiß, M.; Reiß, F.; Anke, F.; Spannenberg, A.; Boye, S.; Lederer, A.; Arndt, P.; Beweries, T., *Dalton Trans.* **2018**; (j) Coles, N. T.; Mahon, M. F.; Webster, R. L., *Organometallics* **2017,** *36*, 2262-2268; (k) Jurca, T.; Dellermann, T.; Stubbs, N. E.; Resendiz-Lara, D. A.; Whittell, G. R.; Manners, I., *Chem. Sci.* **2018,** *9*, 3360-3366.

5. (a) Nakhmanson, S. M.; Nardelli, M. B.; Bernholc, J., *Phys. Rev. Lett.* **2004,** *92*; (b) Bernholc, J.; Nakhmanson, S. M.; Nardelli, M. B.; Meunier, V., *Comput. Sci. Eng.* **2004,** *6*, 12-21.

6. (a) Du, V. A.; Jurca, T.; Whittell, G. R.; Manners, I., *Dalton Trans.* **2016,** *45*, 1055-1062; (b) Wang, X. C.; Hooper, T. N.; Kumar, A.; Priest, I. K.; Sheng, Y. W.; Samuels, T. O. M.; Wang, S. S.; Robertson, A. W.; Pacios, M.; Bhaskaran, H.; Weller, A. S.; Warner, J. H., *CrystEngComm.* **2017,** *19*, 285-294; (c) Staubitz, A.; Robertson, A. P. M.; Sloan, M. E.; Manners, I., *Chem. Rev.* **2010,** *110*, 4023-4078; (d) Leitao, E. M.; Jurca, T.; Manners, I., *Nat. Chem.* **2013,** *5*, 817-829; (e) Kim, D. P.; Moon, K. T.; Kho, J. G.; Economy, J.; Gervais, C.; Babonneau, F., *Polym. Adv. Technol.* **1999,** *10*, 702-712.

7. (a) Dorn, H.; Singh, R. A.; Massey, J. A.; Lough, A. J.; Manners, I., *Angew. Chem. Int. Ed.* **1999,** *38*, 3321-3323; (b) Dorn, H.; Singh, R. A.; Massey, J. A.; Nelson, J. M.; Jaska, C. A.; Lough, A. J.; Manners, I., *J. Am. Chem. Soc.* **2000,** *122*, 6669-6678; (c) Dorn, H.; Rodezno, J. M.; Brunnhöfer, B.; Rivard, E.; Massey, J. A.; Manners, I., *Macromolecules* **2003,** *36*, 291-297.

8. Clark, T. L.; Rodezno, J. M.; Clendenning, S. B.; Aouba, S.; Brodersen, P. M.; Lough, A. J.; Ruda, H. E.; Manners, I., *Chem. Eur. J.* **2005,** *11*, 4526-4534.

9. Pandey, S.; Lonnecke, P.; Hey-Hawkins, E., *Eur. J. Inorg. Chem.* **2014**, 2456-2465.

10. (a) Schäfer, A.; Jurca, T.; Turner, J.; Vance, J. R.; Lee, K.; Du, V. A.; Haddow, M. F.; Whittell, G. R.; Manners, I., *Angew. Chem. Int. Ed.* **2015,** *54*, 4836-4841; (b) Turner, J. R.; Resendiz-Lara, D. A.; Jurca, T.; Schäfer, A.; Vance, J. R.; Beckett, L.; Whittell, G. R.; Musgrave, R. A.; Sparkes, H. A.; Manners, I., *Macromol. Chem. Phys.* **2017,** *218*, 1700120.

11. (a) Paul, U. S. D.; Braunschweig, H.; Radius, U., *Chem. Commun.* **2016,** *52*, 8573-8576; (b) Hooper, T. N.; Weller, A. S.; Beattie, N. A.; Macgregor, S. A., *Chem. Sci.* **2016,** *7*, 2414-2426.

12. (a) Dorn, H.; Vejzovic, E.; Lough, A. J.; Manners, I., *Inorg. Chem.* **2001,** *40*, 4327-4331; (b) Oohara, N.; Imamoto, T., *Bull. Chem. Soc. Jpn.* **2002,** *75*, 1359-1365.

13. Cayaye, H.; Clegg, F.; Gould, P. J.; Ladyman, M. K.; Temple, T.; Dossi, E., *Macromolecules* **2017,** *50*, 9239-9248.

14. (a) Marquardt, C.; Jurca, T.; Schwan, K. C.; Stauber, A.; Virovets, A. V.; Whittell, G. R.; Manners, I.; Scheer, M., *Angew. Chem. Int. Ed.* **2015,** *54*, 13782-13786; (b) Stauber, A.; Jurca, T.; Marquardt, C.; Fleischmann, M.; Seidl, M.; Whittell, G. R.; Manners, I.; Scheer, M., *Eur. J. Inorg. Chem.* **2016,** *2016*, 2684-2687.

15. (a) Marquardt, C.; Hegen, O.; Vogel, A.; Stauber, A.; Bodensteiner, M.; Timoshkin, A. Y.; Scheer, M., *Chem. Eur. J.* **2018,** *24*, 360-363; (b) Stubbs, N. E.; Jurca, T.; Leitao, E. M.; Woodall, C. H.; Manners, I., *Chem. Commun.* **2013,** *49*, 9098-9100.

16. Dorn, H.; Rodezno, J. M.; Brunnhofer, B.; Rivard, E.; Massey, J. A.; Manners, I., *Macromolecules* **2003,** *36*, 291-297.

17. Schäfer, A.; Jurca, T.; Turner, J.; Vance, J. R.; Lee, K.; Du, V. A.; Haddow, M. F.; Whittell, G. R.; Manners, I., *Angew. Chem. Int. Ed.* **2015,** *54*, 4836-4841.

18. Stauber, A.; Jurca, T.; Marquardt, C.; Fleischmann, M.; Seidl, M.; Whittell, G. R.; Manners, I.; Scheer, M., *Eur. J. Inorg. Chem.* **2016**, 2684-2687.

19. Schmidbaur, H.; Weiß, E.; Müller, G., *Synth. React. Inorg. Met.-Org. Chem.* **1985,** *15*, 401-413.

20. Rudolph, R. W.; Parry, R. W.; Farran, C. F., *Inorg. Chem.* **1966,** *5*, 723-&.

21. Tsang, C. W.; Yam, M.; Gates, D. P., *J. Am. Chem. Soc.* **2003,** *125*, 1480-1481.

22. Askadskii, A. A.; Kovriga, O. V., *Polymer Science U.S.S.R.* **1991,** *33*, 1821-1831.

23. Zhu, Q.; Wu, J. L.; Tu, C. L.; Shi, Y. F.; He, L.; Wang, R. B.; Zhu, X. Y.; Yan, D. Y., *J. Phys. Chem. B* **2009,** *113*, 5777-5780.

24. Ishizone, T.; Goseki, R., *Polym. J.* **2018,** *50*, 805-819.

25. Allcock, H. R.; Krause, W. E., *Macromolecules* **1997,** *30*, 5683-5687.

26. Burfield, D. R.; Doi, Y., *Macromolecules* **1983,** *16*, 702-704.

27. Vasile, C., *Handbook of Polyolefins, Second Edition*. CRC Press: 2000.

28. Pandey, S.; Loennecke, P.; Hey-Hawkins, E., *European Journal of Inorganic Chemistry* **2014,** *2014*, 2456-2465.

29. Zhou, W. J.; Yang, H.; Guo, X. Z.; Lu, J. J., *Polym. Degrad. Stab.* **2006,** *91*, 1471-1475.

30. Pangborn, A. B.; Giardello, M. A.; Grubbs, R. H.; Rosen, R. K.; Timmers, F. J., *Organometallics* **1996,** *15*, 1518-1520.

31. Liston, D. J.; Lee, Y. J.; Scheidt, W. R.; Reed, C. A., *J. Am. Chem. Soc.* **1989,** *111*, 6643-6648.

32. Mohr, B.; Lynn, D. M.; Grubbs, R. H., *Organometallics* **1996,** *15*, 4317-4325.

33. Hurtado, M.; Yanez, M.; Herrero, R.; Guerrero, A.; Davalos, J. Z.; Abboud, J. L. M.; Khater, B.; Guillemin, J. C., *Chem. Eur. J.* **2009,** *15*, 4622-4629.

34. Ohashi, A.; Matsukawa, S.; Imamoto, T., *Heterocycles* **2000,** *52*, 905-910.

35. Kou, K. G. M.; Longobardi, L. E.; Dong, V. M., *Adv. Synth. Catal.* **2015,** *357*, 2233-2237.

36. Wrackmeyer, B.; Klimkina, E. V.; Milius, W., *Eur. J. Inorg. Chem.* **2014**, 4865-4876.

37. Bruker-AXS Apex II software, Madison, WI, 2008.

38. G. M. Sheldrick, SADABS V2012/1, University of Göttingen, Germany.

39. Sheldrick, G. M., *Acta Crystallogr., Sect. A: Found. Crystallogr.* **2015,** *71*, 3-8.

40. Sheldrick, G. M., *Acta Cryst. C* **2015,** *71*, 3-8.

41. Dolomanov, O. V.; Bourhis, L. J.; Gildea, R. J.; Howard, J. A. K.; Puschmann, H., *J. Appl. Crystallogr.* **2009,** *42*, 339-341.

Chapter 4

Synthesis and Characterisation of Polyaminoboranes with Aryl-Substituted Alkyl Groups at Nitrogen.

4.1 Abstract

Polyaminoboranes are boron–nitrogen analogues of polyolefins, however, to date, few soluble, well-characterised examples have been described. Herein, we show that metal-catalysed dehydrogenation/dehydrocoupling of amine–boranes $Ph(CH_2)_xNH_2{\cdot}BH_3$ (x = 2–4) yields soluble polyaminoboranes $[Ph(CH_2)_xNH–BH_2]_n$ together with bis(amino)borane $[Ph(CH_2)_4NH]_2BH$ and borazines $[Ph(CH_2)_xN–BH]_3$ as byproducts, using skeletal nickel, $[Rh(\mu\text{-}Cl)(1,5\text{-}COD)]_2$ (COD = cyclooctadiene) and $[IrH_2(POCOP)]$ (POCOP = κ^3-1,3-$(OP{t}Bu_2)_2C_6H_3$) as precatalyst systems at room temperature (20 °C). Application of the most efficient precatalyst system (1 mol %, $[IrH_2(POCOP)]$) at low temperature (−40 °C), enabled the isolation of high molar mass polyaminoborane $[Ph(CH_2)_4NH–BH_2]_n$ in moderate (ca. 40 %) yield after precipitation. Structural characterisation was achieved by multinuclear NMR, IR, and EA; and the molar mass was determined to be high (M_n > 10,000 g mol^{-1}) by GPC, DLS, and ^1H DOSY methods. The optimised dehydropolymerisation conditions (1 mol %, $[IrH_2(POCOP)]$ at −40 °C) were also used to prepare copolymers from mixtures of $Ph(CH_2)_4NH_2{\cdot}BH_3$ with $MeNH_2{\cdot}BH_3$, $Ph(CH_2)_2NH_2{\cdot}BH_3$, or $NH_3{\cdot}BH_3$. Significantly, in contrast to previous copolymers incorporating the $[NH_2–BH_2]$ moiety, the formation of $[Ph(CH_2)_4NH–BH]_n$–*r*–$[NH_2–BH_2]_m$ [n: 1, m: 2] is a soluble processable polyaminoborane containing up to 67 % $[NH_2–BH_2]$ repeat units. The thermal stability of the polyaminoborane homopolymers and copolymers was studied by TGA. The use of a cross-linker ($BH_3{\cdot}NH_2(CH_2)_8NH_2{\cdot}BH_3$) in the

dehydropolymerisation reaction led to an improvement in the resulting ceramic yield after pyrolysis suggesting that these materials are of potential future interest as precursors of ceramic boron nitride.

4.2 Introduction

Macromolecules that incorporate main-group elements in their repeat units are of interest as a result of their interesting properties.[1] Boron-containing polymers have attracted particular attention in a diversity of areas, including their utilisation as precursors of high-performance ceramics, flame retardants, and sensory materials.[1c, 2] Polymers comprising B–P bonds in the backbone have been prepared by the catalytic dehydrocoupling of primary phosphine–boranes $RPH_2{\cdot}BH_3$ to form high molar mass polyphosphinoboranes $[RPH–BH_2]_n$, which are isoelectronic analogues to industrially ubiquitous polyolefins.[3] Polyphosphinoboranes have potential applications as ceramic precursors[3b, 4] and as lithographic resists for patterning due to their electro-beam sensitivity.[3c, 5] On the other hand, recent research has targeted the synthesis of molecules[6] and polymers[7] with boron–nitrogen motifs and has led to the synthesis of BN-based π-conjugated materials.[8] Inorganic polymers whose backbone contains exclusively alternating B–N units are known as polyaminoboranes $[RNH–BHR']_n$ (when R' = H, R = alkyl; when R = H, R' = aryl). These polymers are of potential interest as they are precursors of preceramic and piezoelectric materials.[9,10]

The state-of-the-art in the synthesis of polyaminoboranes involves either metal-catalysed[3g, 11] or metal-free routes.[12] The metal-catalysed dehydropolymerisation routes have produced solution processable polymeric materials with high molecular weight (Scheme 4.1A). The first examples of a homogeneous catalytic dehydropolymerisation of primary amine–boranes $RNH_2{\cdot}BH_3$ (R = H, Me, *n*Bu) was achieved by $[IrH_2(POCOP)]$ to form $[RNH–BH_2]_n$ homopolymers and random copolymers.[11b]

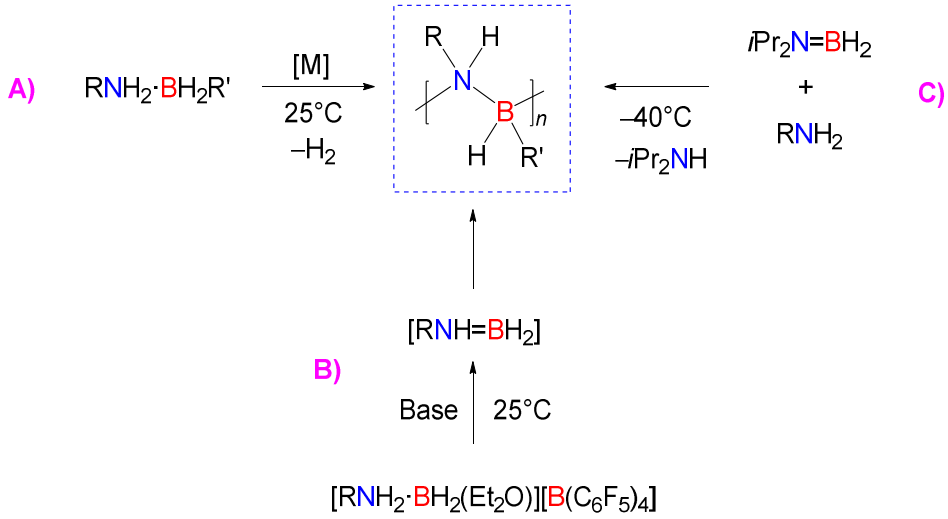

Scheme 4.1. The metal-catalysed and metal-free state-of-the-art routes to form polyaminoboranes.

Thereafter, different catalytic systems have been found to be active in the dehydropolymerisation reaction including [Cp^RTiCl_2] / 2 equiv. *n*BuLi (Cp^R = η^5-C_5Me_5),[13] $[CpFe(CO)_2]_2$,[11c] [(PNHP)Fe(H)(CO)(HBH_3)] (PNHP = HN-($CH_2CH_2PiPr_2$)$_2$),[11f] [Rh($Ph_2P(CH_2)_4PPh_2$)][14] and [Rh(κ^2-P,P-xantphos){η^2-$H_2B(CH_2CH_2tBu)\cdot NMe_3$}]$^+$.[11d, 11g, 15] In some cases the mechanistic aspects of the polymerisation have been systematically studied and been found to be metal-dependent. For example, the Ti-catalysed system proceeds *via* a step-growth mechanism,[13] whereas the Rh(κ^2-P,P-xantphos) system involves a chain-growth process.[11g]

Furthermore, the synthesis of polyaminoboranes by metal-free routes has resulted in the formation of low molecular weight $[MeNH–BH_2]_n$ *via* generation of a transient monomeric aminoborane intermediate generated in a stoichiometric reaction involving amine–boronium cations under dilute conditions (Scheme 4.1B).[12a] Recently, the synthesis of new polyaminoboranes $[RNH–BH_2]_n$ (R = H, Me, Et, *n*Pr, *n*Bu, allyl) by primary-amines/aminoborane exchange in the absence of solvent (Scheme 4.1C) was achieved.[12b, 12c] Although the latter is a fascinating new route that allows the formation of very high molecular weight polymers, these are mainly insoluble and the mechanism by which the polymerisation proceeds is currently unclear.

To date, the polyaminoboranes that have been reported possess sterically unencumbered alkyl substituents at nitrogen. Recently, the synthesis of deuterated polyaminoboranes $[MeNR–BR_2]_n$ (R = H, D) was described.[11h] Despite all these efforts, polyaminoboranes containing aryl substituents are still scarce. For example, the dehydrocoupling of *N*-aryl amine–boranes (p-$RC_6H_4NH_2{\cdot}BH_3$, R = H, OMe, CF_3) by $[IrH_2(POCOP)]$ led to formation of an array of dehydrogenation products other than the polymer.[16] In contrast, *B*-aryl amine–boranes can be dehydropolymerised using the same Ir-based precatalyst, allowing the first synthesis of B–N main chain analogues of polystyrene which will be discussed in Chapter 5.[17]

To date, metal-catalysed routes have been focused on a restricted range of amine–borane substrates with an *N*-alkyl group at nitrogen. We have therefore attempted to extend the scope of the catalytic dehydrocoupling route to prepare aryl-substituted *N*-alkyl polyaminoboranes. The use of aryl-substituted alkyl groups in organic polyolefins has provided interesting properties to the materials. For example, the use of α-olefins such as $Ph(CH_2)_xCH=CH_2$ (x = 1, 2, 4) in olefin copolymerisation has resulted in the change of either the physical properties of polynorbonene[18] (e.g. solubility and glass transition temperature), or in an improvement of the radiation resistance of polypropylene against high-energy radiation exposure[19] as a consequence of the incorporation of the alkylbenzene moieties.

In this chapter, we report the metal-catalysed dehydrogenation reaction for $Ph(CH_2)_xNH_2{\cdot}BH_3$ (x = 1–4) substrates to produce well-defined, high molecular weight polymers and copolymers. The introduction of the alkyl spacer in the present work was intended to increase the solubility of copolymers and the incorporation of the phenyl group into the polymers to improve molar mass characterisation using solution-based methods by increasing the refractive index and light scattering.

4.3 Results and Discussion

4.3.1 Dehydrocoupling Reactions of Aryl-Containing N-Alkyl Amine–Boranes Using Different Catalytic Systems

With the aim of evaluating the metal-catalysed dehydrogenation reaction of aryl-containing alkyl amine–boranes, different transition metal catalysts were explored. Specifically, we investigated the dehydrocoupling reaction using skeletal nickel, [Rh(μ-Cl)(1,5-COD)]$_2$ and [IrH$_2$(POCOP)], which have previously been established as active precatalysts for the dehydropolymerisation of other amine–boranes.[11a, 20] As mentioned previously, the catalytic dehydrocoupling of PhNH$_2$·BH$_3$ does not yield the polymer [PhNH-BH$_2$]$_n$.[16] In order to exclude any negative steric effect that the phenyl group might contribute in the dehydrogenation reaction, we envisage that the incorporation of longer –(CH$_2$)$_x$– linkers that increase the distance of the aryl group from the amine–borane reaction centre could lead to monomers which would undergo the dehydrocoupling reaction.

We initiated our investigation using the amine–borane Ph(CH$_2$)$_4$NH$_2$·BH$_3$ (δ_B = −19.7 ppm) with a catalytic amount of skeletal nickel (5.0 mol %) in THF at 20 °C (Table 4.1, Entry 1-2).[21] After 9 h, the ^{11}B{^{1}H} NMR spectrum showed modest conversion (*ca.* 6 %) to a product with a signal around δ_B = 27.4 ppm, which did not split into a doublet in the ^{1}H-coupled experiment, and was assigned to [Ph(CH$_2$)$_4$NH]$_2$BH based on the similarity in chemical shift compared with similar bis(amino)boranes reported by others.[12b, 22] For example, the ^{11}B NMR spectrum of the related bis(amino)borane, [BuNH]$_2$BH, displays a signal at δ_B = 27.6 ppm (d, $J_{B–H}$ ~ 127 Hz).[12b] Under stoichiometric conditions (Table 4.1, Entry 3-4), it was observed that after 6 h over 70 % conversion was achieved. The ^{11}B{^{1}H} NMR spectrum showed two main signals. The first corresponded to a broad symmetrical signal around (δ_B = −7.1 ppm) (*ca.* 13 %) and was assigned to the polymer [Ph(CH$_2$)$_4$NH–BH$_2$]$_n$. This signal appears in a similar region (δ_B = −6 to −7 ppm) to that of [MeNH–BH$_2$]$_n$ from former

reports.[11b, 11f] The second signal was observed around (δ_B = 27.2 ppm) and assigned to $[Ph(CH_2)_4NH]_2BH$ (*ca.* 60 %).

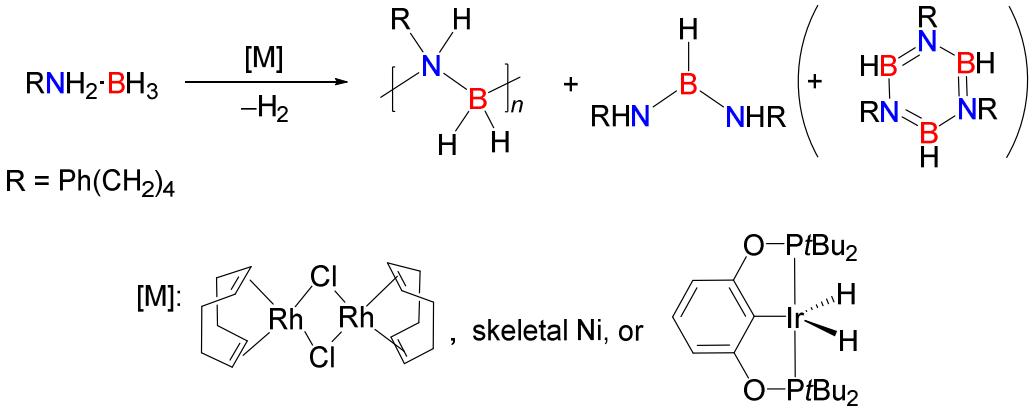

Scheme 4.2. Metal-catalysed dehydrocoupling of $Ph(CH_2)_4NH_2{\cdot}BH_3$ in THF at 20 °C ([M] = 2.5 mol % $[Rh(\mu\text{-Cl})(1,5\text{-COD})]_2$, 1.0 mol % $[IrH_2(POCOP)]$, 5.0 mol % or equimolar amount of skeletal nickel). Borazine $[Ph(CH_2)_4N–BH]_3$ appears only with precatalysts $[Rh(\mu\text{-Cl})(1,5\text{-COD})]_2$ and $[IrH_2(POCOP)]$.

Performing the reaction using $[Rh(\mu\text{-Cl})(1,5\text{-COD})]_2$ (2.5 mol %) as a precatalyst at 20 °C in THF (Table 4.1, Entry 5-7) with $Ph(CH_2)_4NH_2{\cdot}BH_3$, *ca.* 75 % of $Ph(CH_2)_4NH_2{\cdot}BH_3$ conversion was achieved after only 15 min to yield $[Ph(CH_2)_4NH–BH_2]_n$ (*ca.* 30%) and $[Ph(CH_2)_4NH]_2BH$ (ca. 45 %) as observed by $^{11}B\{^1H\}$ NMR spectroscopy.[23] Changing the solvent to toluene (using 2.5 mol % of $[Rh(\mu\text{-Cl})(1,5\text{-COD})]_2$) resulted in a significantly faster reaction (Table 4.1, Entry 8-11). After 15 min, the conversion (*ca.* 85%) of $Ph(CH_2)_4NH_2{\cdot}BH_3$ to form polymer $[Ph(CH_2)_4NH]_2BH$ (*ca.* 55%) and $[Ph(CH_2)_4NH]_2BH$ (ca. 30%) was detected by $^{11}B\{^1H\}$ NMR spectroscopy. After 1.5 h, almost complete consumption of $Ph(CH_2)_4NH_2{\cdot}BH_3$ (ca. 96 %) was achieved,[24] to produce $[Ph(CH_2)_4NH]_2BH$ (ca. 30%) along with the formation of borazine $[Ph(CH_2)_4N–BH]_3$ (See SI, Fig. S4.4).[25]

Table 4.1. Product distribution of the catalytic dehydrocoupling of $Ph(CH_2)_4NH_2{\cdot}BH_3$ in solution at 20 °C ([Rh] = [Rh(μ-Cl)(1,5-COD)]$_2$, [Ir] = [IrH_2(POCOP)], [Ni] = skeletal nickel).

	Conditions[a]	Time (Min)	Conversion [%][b]	Yield [%][c]	
			$Ph(CH_2)_4NH_2{\cdot}BH_3$	$[Ph(CH_2)_4NH{-}BH_2]_n$	$[Ph(CH_2)_4NH]_2BH$
1	5 mol% [Ni]	60	3	0	3
2	5 mol% [Ni]	540	6	0	6
3	100 mol% [Ni]	60	46	3	42
4	100 mol% [Ni]	360	74	13	60
5	2.5 mol% [Rh]	15	76	31	45
6	2.5 mol% [Rh]	45	68	34	35
7	2.5 mol% [Rh]	90	62	34	28
8	2.5 mol% [Rh][d]	15	85	55	30
9	2.5 mol% [Rh][d]	45	88	53	35
10	2.5 mol% [Rh][d]	90	97	52	45[f]
11	2.5 mol% [Rh][d]	180	96	52	44[f]
12	5 mol% Rh/Al_2O_3	60	1	0	1
13	5 mol%, Rh/Al_2O_3	540	9	1	8
14	1 mol% [Ir]	15	63	36	38
15	1 mol% [Ir]	30	92	31	61[f]
16	1 mol% [Ir]	45	90	28	62[f]
17	1 mol% [Ir][e]	30	92	45	42[f]
18	1 mol% [Ir][e]	60	91	43	44[f]

a) Reaction conditions: THF solution, room temperature (20 °C), 2.0 M substrate concentration for [Ni] and [Rh] and 2.5 M for [Ir] reactions. b) Conversion determined by $^{11}B\{^1H\}$ NMR spectroscopy. c) Approximate values determined by integration of the broad signals in the $^{11}B\{^1H\}$ NMR of the reaction mixtures. d) Reaction was performed in toluene. e) Reaction was performed at low temperature (−40 °C). f) Mixture of $[Ph(CH_2)_4NH]_2BH$/$[Ph(CH_2)_4N{-}BH]_3$. The signals observed by $^{11}B\{^1H\}$ NMR spectroscopy are overlapping for these products.

Polymeric material was isolated at different reaction times through precipitation and high molecular weight polymer was observed in all cases (e.g. 15 min: (M_n = 111,500 g mol^{-1}, PDI = 1.18, PDI = polydispersity index); after 3h: (M_n = 188,000 g mol^{-1}, PDI = 1.04) as detected by GPC (See SI, Section 4.2.3). These polymers were isolated as dark-grey solids after precipitation in hexanes, presumably the grey colour is due to the presence of Rh metal. Attempts to remove the catalyst trapped in the polymeric structure *via* filtration of the reaction mixture through celite, alumina, or activated carbon, were all unsuccessful.

These resulted in most of the product being retained in the solid phase and the final solid *post* solvent removal was still dark grey and likely still contaminated with residual metal.

Heterogeneous Rh/Al_2O_3 has previously been reported to produce $[MeNH–BH_2]_n$ with moderate molecular weight (M_n = 26 000 g mol^{-1}, PDI = 8.5) from $MeNH_2·BH_3$.[11b] Therefore, we investigated the reaction of $Ph(CH_2)_4NH_2·BH_3$ with Rh/Al_2O_3 (5 mol % Rh) in THF at 20 °C. After 1 h no significant dehydrocoupling reaction was observed and only after 4 h minor amounts of $[Ph(CH_2)_4NH–BH_2]_n$ (ca. 1 %) and $[Ph(CH_2)_4NH]_2BH$ (ca. 8 %) were detected by $^{11}B\{^1H\}$ NMR spectroscopy. (Table 4.1, Entry 12-13).

We finally investigated the dehydropolymerisation of $Ph(CH_2)_4NH_2·BH_3$ using $[IrH_2(POCOP)]$ (1.0 mol %) as a catalyst in THF at 20 °C. The reaction was monitored at different time points by $^{11}B\{^1H\}$ NMR spectroscopy and after 30 min maximum conversion of monomer $Ph(CH_2)_4NH_2·BH_3$ (ca. 92%) along with the concomitant formation of polymeric material $[Ph(CH_2)_4NH–BH_2]_n$ (ca. 31%) and the mixture of $[Ph(CH_2)_4NH]_2BH$ and $[Ph(CH_2)_4N–BH]_3$ (ca. 61 %) was observed (Table 4.1, Entry 15).

It has been previously suggested that dehydropolymerisation of $MeNH_2·BH_3$ using $[IrH_2(POCOP)]$ as a precatalyst affords $[MeNH–BH_2]_n$ as the kinetic product which will subsequently form borazine $[MeN–BH]_3$ as the thermodynamic product as a consequence of the entropic gain due to the second dehydrogenation event after extended periods of reactivity.[11b] In the case of $Ph(CH_2)_4NH_2·BH_3$ as the substrate, small molecules $[Ph(CH_2)_4NH]_2BH$ and $[Ph(CH_2)_4N–BH]_3$ form preferentially instead of $[Ph(CH_2)_4NH–BH_2]_n$.

With this in mind, and in order to provide kinetic control, we performed the dehydrogenation reaction of $Ph(CH_2)_4NH_2·BH_3$ (using 1.0 mol % of $[IrH_2(POCOP)]$) in THF at low temperature (−40 °C) and allowed the reaction mixture to reach room temperature (20 °C) over a period of 30 min. Under these conditions, almost quantitative conversion of $Ph(CH_2)_4NH_2·BH_3$ (ca. 93%) was observed by $^{11}B\{^1H\}$ NMR spectroscopy, where the

formation of $[Ph(CH_2)_4NH–BH_2]_n$ (ca. 45 %) is preferred over $[Ph(CH_2)_4NH]_2BH$ and $[Ph(CH_2)_4N–BH]_3$ (ca. 42 %) (See SI, Fig. S4.11). An unidentified boron-containing species was also detected [δ_B = −24.2 ppm] (ca. 4 %). The latter is not observed when the reaction is performed at room temperature. The reaction mixture was precipitated into hexanes at 20 °C to give $[Ph(CH_2)_4NH–BH_2]_n$ as a white solid in 42% yield.

Although the best conversion of $Ph(CH_2)_4NH_2{\cdot}BH_3$ to polymer was achieved by the Rh-based catalyst, the materials obtained were difficult to purify. In contrast, using IrH_2(POCOP) as a catalyst enable the facile isolation of polymeric material only by precipitation. Based on these results, we focused the rest of our dehydropolymerisation study on precatalyst IrH_2(POCOP).

4.3.2 Characterisation of Polyaminoborane $[Ph(CH_2)_4NH–BH_2]_n$

Polymer characterisation was performed by multinuclear NMR spectroscopy, including 2D techniques, infrared spectroscopy (IR) and elemental analysis (EA). The molar mass was determined by gel permeation chromatography (GPC), dynamic light scattering (DLS) and ^{1}H DOSY; and thermal stability was investigated by thermogravimetric analysis (TGA) (See SI, Section 4.4).

Structural characterisation *via* NMR spectroscopy of polymer $[Ph(CH_2)_4NH–BH_2]_n$ was consistent with previous reports for the formation of polyaminoboranes. The $^{11}B\{^1H\}$ NMR spectrum in $CDCl_3$ showed a broad symmetrical peak at (δ_B = −8.6 ppm) which did not show splitting in the proton coupled ^{11}B NMR experiment and the signal is found in a similar region to other polyaminoboranes that have been described as essentially linear polymers.[11a, 11b, 12b] [Fig. 4.1 (b)]. The ^{1}H NMR spectrum (in $CDCl_3$) showed broad signals in the aliphatic and aromatic region and the integration was consistent for the proposed repeat units [Fig. 4.1 (a)]. The signal at δ_H = 2.76 ppm was assigned to the protic N–H hydrogen, which is at a lower frequency compared to the equivalent signal in the monomer

$Ph(CH_2)_4NH_2{\cdot}BH_3$ (δ_H = 3.73 ppm). The hydridic hydrogens on boron B–H are in the region (δ_H = 1.62-1.86 ppm). In the ^{13}C NMR spectrum, all the signals for the phenyl ring and methylene groups could be resolved for $[Ph(CH_2)_4NH–BH_2]_n$. It has previously been reported that $[MeNH–BH_2]_n$ was obtained as an atactic material, in which the methyl resonances for the different diads were distinguishable in the ^{13}C NMR.[11b]

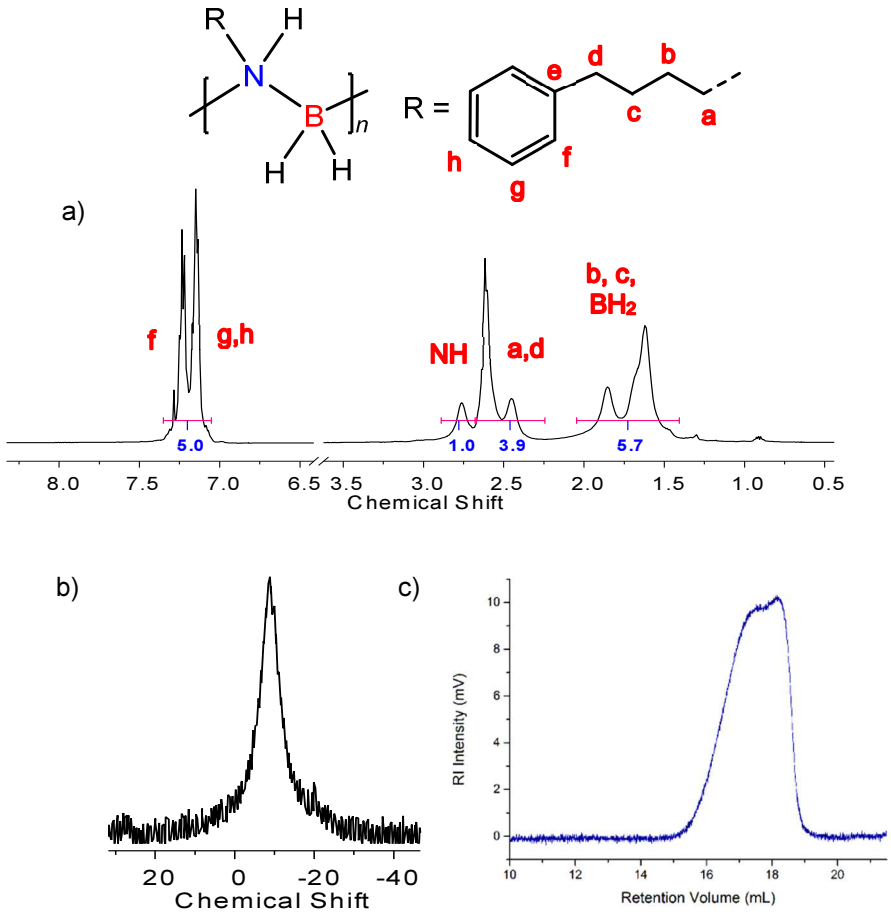

Figure 4.1. (a) ^1H NMR spectrum of $[Ph(CH_2)_4NH–BH_2]_n$ in $CDCl_3$. (b) $^{11}B\{^1H\}$ NMR spectrum of $[Ph(CH_2)_4NH–BH_2]_n$ in $CDCl_3$. (c) GPC chromatogram of $[Ph(CH_2)_4NH–BH_2]_n$ in THF (0.1 *w*/w % *n*Bu_4NBr).

For $[Ph(CH_2)_4NH–BH_2]_n$, we performed ^{13}C NMR experiments with extended data collection times in an attempt to detect any tactic environment, however, only one resonance for the carbon at the α position of the amine–borane moiety was observed (See SI, Fig. S4.14). Further characterisation was accomplished by ATR-IR spectroscopy, which showed a high frequency band at ν = 3252 cm^{-1}, characteristic of N–H stretching

vibrations, and two bands at $\nu = 2384$ cm^{-1} and $\nu = 2295$ cm^{-1} for the B–H stretches, which are in accordance with the vibrational spectra of other reported polyaminoboranes which are claimed to possess a linear structure rather than branched or cyclic.[11a, 11b] The C–H stretching vibrations were assigned on the basis of the vibration spectroscopic study for 4-phenylbutylamine.[26] In this manner, the aromatic C–H vibration was assigned at $\nu = 3025$ cm^{-1} and the C–H asymmetric and symmetric stretching vibrations of the methylene groups, were designated at $\nu = 2928$ cm^{-1} and $\nu = 2857$ cm^{-1}, respectively.

In order to determine the molecular weight of the material, a sample was analysed by GPC in THF (containing 0.1 *w*/*w* % *n*Bu$_4$NBr).[27] The observed chromatogram exhibited a bimodal molecular weight distribution, in which the two components overlapped significantly. When analysed together, this afforded a number-average molecular weight (M_n = 168,300 g mol^{-1}) with a polydispersity index (PDI = 1.16) [Fig. 1 (c)]. Thus, demonstrating the formation of a high molecular weight polymer with a relatively narrow molecular weight distribution. By varying the concentration of [Ph(CH$_2$)$_4$NH–BH$_2$]$_n$ (from 0.5 to 2.0 mg mL^{-1}) we explored the possible variation of the molecular weight by GPC (See SI, Fig. S4.18 and S4.19, Table S4.8). We found that retention times are the same regardless of the concentration which is consistent for macromolecules in solution. In contrast, if aggregates were in solution, shorter retention times by GPC would be expected when the concentration increases.[28] The comparison of the GPC trace of [Ph(CH$_2$)$_4$NH–BH$_2$]$_n$ and [MeNH–BH$_2$]$_n$ was performed at the same concentration (2 mg mL^{-1}) (See SI, Fig. S4.17) and showed a higher refractive index response (RI area [Ph(CH$_2$)$_4$NH–BH$_2$]$_n$ / RI area [MeNH–BH$_2$]$_n$ = 1.32). This can be explained as aromatic rings possess higher refractive indices than methyl groups.[29]

In order to exclude the influence of column interactions during GPC analysis on the molar mass determination the same sample was also characterized by DLS. In THF solution (2 mg mL^{-1}), the size distribution weighted by scattering volume exhibited a single

population at R_H = 4.3 nm. This would correspond to a polystyrene sample of M_n = 25,600 g mol^{-1} in THF.[30] It should be noted, however, that the size distribution weighted by scattered intensity also contained a second population at R_h = ca. 83 nm, which suggests the presence of aggregates, albeit in small quantities. In order to emulate GPC conditions in the DLS experiment, samples of $[Ph(CH_2)_4NH–BH_2]_n$ were prepared with THF containing 0.1 *w*/*w* % *n*Bu$_4$NBr in the same concentration (2 mg mL^{-1}). A similar R_H value (4.2 nm) was obtained by DLS at ambient temperature (20 °C). However, when the DLS experiment was performed at 35 °C, which is the working temperature of the columns in the GPC, it was observed a decrease of the R_H value (3.3 nm). The DLS experiments suggests that the ionic strength at that concentration (0.1 *w*/*w* % *n*Bu$_4$NBr in THF) does not significantly affect the hydrodynamic volume of polyaminoboranes,[31] but that there is a significant effect from temperature.

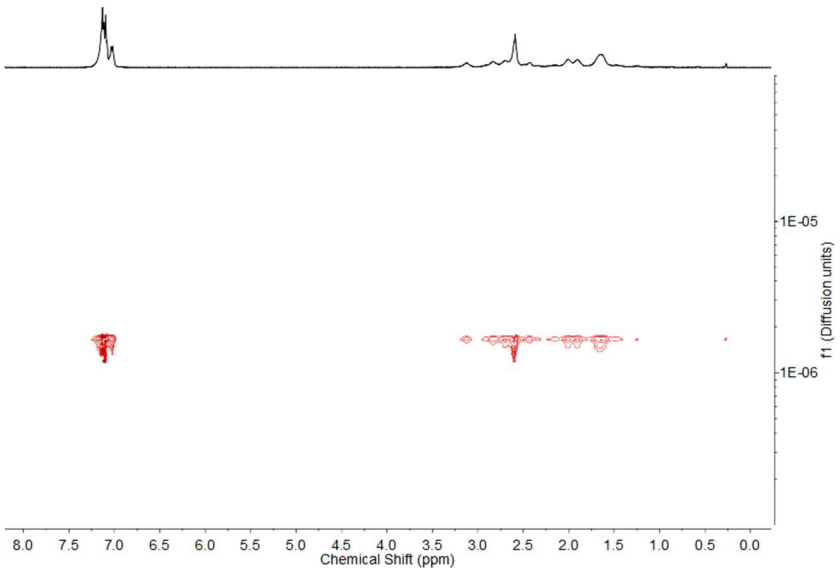

Figure 4.2. ^{1}H DOSY spectrum of isolated $[Ph(CH_2)_4NH–BH_2]_n$ in C_6D_6 at 20 °C.

We also performed diffusion order NMR spectroscopy (DOSY) as a complementary technique to estimate the molecular weight in the same sample of $[Ph(CH_2)_4NH–BH_2]_n$. Applying a method described previously,[32] the diffusion coefficient (D) and the molecular weight of polymers (M_n) can be correlated (See SI, Fig. S4.23). ^{1}H DOSY analysis of a

sample of $[Ph(CH_2)_4NH–BH_2]_n$ (2 mg mL^{-1}, C_6D_6) resulted in a diffusion coefficient of 1.68 x 10^{-10} m^2 s^{-1} (Fig. 4.2) which would correspond to an estimated M_n of ~14,900 g mol^{-1} relative to polystyrene standards. DLS analysis of $[Ph(CH_2)_4NH–BH_2]_n$ in C_6D_6 showed a single population at R_H = 2.9 nm (size distribution by volume) which would correspond to a molecular weight of only ~7,000 g mol^{-1},[30] and indicates that the polymer is found in a significantly more contracted state in benzene than in THF solution due to poorer solvent-segment interactions.

When the molar mass obtained by different analytical techniques of $[Ph(CH_2)_4NH–BH_2]_n$ is compared, we can conclude that the molar mass determination by GPC is overestimated, as it has been previously suggested for polyaminoboranes.[11b] Overestimation of the molecular weight by GPC has been observed for polar polymers such as poly(2-vinylpyridine)[33] due to the poor interactions between the polymer chains and the non-polar styragel columns which leads to faster elution than anticipated.[34] Similar observations have been made for the typical polyelectrolyte sodium poly(styrenesulfonate) in aqueous media.[35] A similar exclusion effect may therefore operate in the GPC analysis of polyaminoboranes, but is weaker due to the polar, rather than ionic, nature of the chain for polyaminoboranes. This might be related to the large dipole moment[36] and/or spontaneous polarisation[37] associated to the B–N backbone which has been suggested by computational studies for polyaminoboranes. For highly polar polyaminoboranes and polyphosphinoboranes, comparable behaviour to polyelectrolytes has been tentatively proposed.[17, 38]

4.3.3 Investigation of the Influence of the Linker Length on $Ph(CH_2)_xNH_2{\cdot}BH_3$ (x = 2–3) in the Dehydropolymerisation Reaction.

We have demonstrated that using $Ph(CH_2)_4NH_2{\cdot}BH_3$ as a substrate in the catalytic dehydropolymerisation reaction is successful. The linkage of a phenyl group to the amine–

borane moiety through methylene chains has not been explored in detail.[39] In order to provide an insight into the catalytic dehydrocoupling reaction, we investigated the use of amine–boranes $Ph(CH_2)_xNH_2 \cdot BH_3$ (x = 1–3), with the intent of assessing the role of the flexible $–(CH_2)_x–$ linker on the dehydrogenation reaction (Scheme 4.3).

An initial evaluation of the dehydrogenation reaction of $PhCH_2NH_2 \cdot BH_3$ (δ_B = −19.6 ppm) *via* the catalytic activity of [IrH_2(POCOP)] (1 mol %) in THF at low temperature (−40 °C) was tested and no conversion was observed after extended periods of time by $^{11}B\{^1H\}$ NMR spectroscopy. Since no dehydrocoupling products were formed, we investigated the dehydrocoupling reaction using the other precatalyst systems (5 mol % skeletal nickel and 2.5 mol % [Rh(μ-Cl)(1,5-COD)]$_2$) in THF at 20 °C, again no reaction was observed by $^{11}B\{^1H\}$ NMR spectroscopy. Moreover, no reaction was observed under stoichiometric conditions of skeletal nickel and the amine–borane. It is proposed that $PhCH_2NH_2 \cdot BH_3$ is behaving similar to other *β*-branched substrates.[40] In this particular case, the steric bulk created by the phenyl ring and the bulkiness of the ligands in the periphery of the catalyst might be impeding either N–H or B–H activation and the subsequent dehydrogenation reaction.

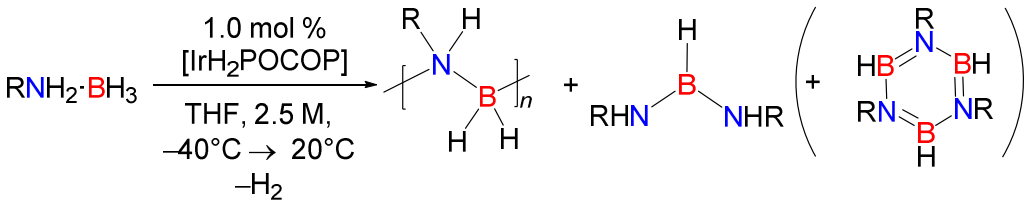

Scheme 4.3. Dehydrocoupling of $Ph(CH_2)_xNH_2 \cdot BH_3$ (x = 2, 3) at low temperature (−40°C) and allowed to reach room temperature (20°C) in THF using 1.0 mol % [IrH_2(POCOP)]. Borazine $[Ph(CH_2)_4N–BH]_3$ appears only with substrate $Ph(CH_2)_2NH_2 \cdot BH_3$.

Through performing the catalytic dehydrogenation reaction (1.0 mol % IrH_2(POCOP) in THF) of amine–boranes $Ph(CH_2)_xNH_2 \cdot BH_3$ (x = 2−3) at low temperature (−40°C), formation of the corresponding polymers $[Ph(CH_2)_2NH–BH_2]_n$ (δ_B = −8.6 ppm) and

$[Ph(CH_2)_3NH–BH_2]_n$ (δ_B = −8.9 ppm), and bis(amino)boranes $[Ph(CH_2)_xNH]_2BH$ (δ_B = 27.1 ppm) and $[Ph(CH_2)_xNH]_2BH$ (δ_B = 26.8 ppm) were achieved after 30 min as detected by $^{11}B\{^1H\}$ NMR spectroscopy (Table 4.2); similar to what was observed in the dehydropolymerisation of $Ph(CH_2)_4NH_2{\cdot}BH_3$. However, the highest conversion from monomer to polymer for $[Ph(CH_2)_2NH–BH_2]_n$ (ca. 57%) was found after 30 min and the formation of $[Ph(CH_2)_3NH–BH_2]_n$ was slower over the same period of time (ca. 32%), under the same reaction conditions.

Table 4.2. Catalytic dehydrocoupling of different amine–boranes $Ph(CH_2)_xNH_2{\cdot}BH_3$ (x = 1–3) in THF at low temperature (−40°C→20°C) using 1.0 mol % [IrH_2POCOP]. Data reported after 30 min.

	Conversion [%][a]	**Yield [%][b]**	
	$Ph(CH_2)_xNH_2{\cdot}BH_3$	**$[Ph(CH_2)_xNH–BH_2]_n$**	**$[Ph(CH_2)_xNH]_2BH$**
x = 1	0	0	0
x = 2	16	57	27[c]
x = 3	59	32	10

a) Conversion determined by $^{11}B\{^1H\}$ NMR spectroscopy. b) Yields determined by integration of the signals in the $^{11}B\{^1H\}$ NMR spectra of the reaction mixtures. c) Mixture of $[Ph(CH_2)_2NH]_2BH$/$[Ph(CH_2)_2N–BH]_3$. The signals observed by ^{11}B NMR$\{^1H\}$ spectroscopy are overlapped for these products.

As $Ph(CH_2)_2NH_2{\cdot}BH_3$ showed the best conversion to polymer, we decided to test the catalytic reaction (1.0 mol % [IrH_2(POCOP)] in THF) on a preparative scale (3.1 mmol) at low temperature (−40°C) which, after 30 min resulted in the isolation of $[Ph(CH_2)_2NH–BH_2]_n$ as a white solid with 56% yield after precipitation (See SI, Section 4.5.1). The $^{11}B\{^1H\}$ NMR spectrum of the polymer $[Ph(CH_2)_2NH–BH_2]_n$ presented a broad peak at (δ_B = −8.7 ppm) in $CDCl_3$. An additional peak was observed at (δ_B = −20.2 ppm) (even after three consecutive precipitations) which could be assigned as an end group (–BH_3) of the polymer. The ^1H NMR spectrum showed broad signals in the aliphatic and aromatic region and the integration matched the monomer unit. GPC analysis in THF showed high molecular weight material (M_n =150,100 g mol^{-1}, PDI = 1.21). By changing the concentration of $[Ph(CH_2)_2NH–BH_2]_n$ in the GPC experiments, it was also determined that discrete

macromolecules are in solution as no influence of concentration on M_n was detected (See SI, Fig. S4.34-S4.35, Table S4.9).

4.3.4 Formation of random copolymers of $Ph(CH_2)_4NH_2{\cdot}BH_3$ using $NH_3{\cdot}BH_3$, $MeNH_2{\cdot}BH_3$ and $Ph(CH_2)_2NH_2{\cdot}BH_3$

As copolymerisation can be used as a tool to change material properties, we also attempted the copolymerisation of $Ph(CH_2)_4NH_2{\cdot}BH_3$ with $NH_3{\cdot}BH_3$, $MeNH_2{\cdot}BH_3$ or with $Ph(CH_2)_2NH_2{\cdot}BH_3$ (Scheme 4.4).

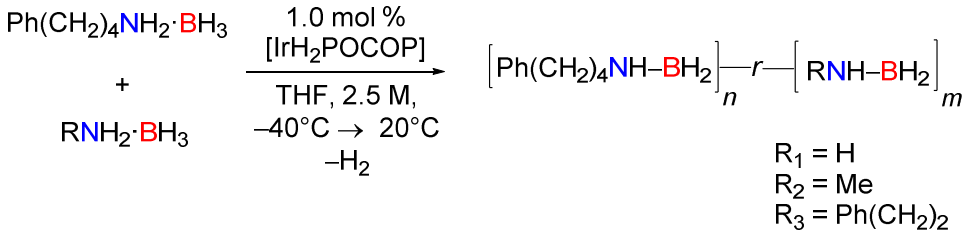

Scheme 4.4. Synthesis of random copolymers of $Ph(CH_2)_4NH_2{\cdot}BH_3$ with different amine–boranes in THF at low temperature (−40°C) and allowed to reach room temperature (20°C) using 1.0 mol % of [IrH_2(POCOP)].

4.3.4.1 Formation of random copolymers with $NH_3{\cdot}BH_3$

Dehydropolymerisation of $NH_3{\cdot}BH_3$ in THF to form $[NH_2–BH_2]_n$ with [IrH_2(POCOP)] (0.3 mol %) yielded material insoluble in common solvents and further characterisation was only possible with solid state Magic Angle Spinning ^{11}B NMR, IR, and EA techniques.[11b] As polymeric $[NH_2–BH_2]_n$ has been proposed as a viable precursor to boron nitride (BN) or as a hydrogen storage material, previous attempts have been made to prepare soluble polymers by copolymerisation of $NH_3{\cdot}BH_3$ with $MeNH_2{\cdot}BH_3$ or nBuNH$_2{\cdot}$BH$_3$.[11a, 11b] It has been described that the *N*-alkyl substituted polyaminoborane $[n$BuNH–BH$_2]_n$ homopolymer is very soluble in most solvents.[11b] This observation, in conjunction with our results, suggests that the introduction of the alkyl chain imparts high solubility to these

polymers and encouraged us to investigate the content limit of [NH_2–BH_2] units that can be introduced to afford soluble copolymers.

We initiated our copolymerisation studies using $Ph(CH_2)_4NH_2 \cdot BH_3$ and $NH_3 \cdot BH_3$ in equimolar quantities. First, $Ph(CH_2)_4NH_2 \cdot BH_3$ and [IrH_2(POCOP)] (1.0 mol %) were mixed at low temperature (−40°C) in THF. Simultaneously, a solution of $NH_3 \cdot BH_3$ in THF was added dropwise to the reaction mixture over a period of 30 min to assure complete monomer consumption. Whenever $NH_3 \cdot BH_3$ was added to the solution vigorous bubbling attributed to H_2 release was observed and the clear yellow reaction mixture increased its viscosity as the reaction was progressing. The polymer could be purified *via* precipitation into hexanes at 20 °C with 80% yield for $[Ph(CH_2)_4NH–BH_2]_n$–*r*–$[NH_2–BH_2]_m$ [n:1, m:1]. GPC analysis of the product in THF indicated that this material is a high molecular weight polymer ($[Ph(CH_2)_4NH–BH_2]_n$–*r*–$[NH_2–BH_2]_m$ [n: 1, m: 1]: M_n =159,700, PDI = 1.33). The $^{11}B\{^1H\}$ NMR spectrum displayed a broad signal at [δ = −9.2 ppm] ($[Ph(CH_2)_4NH–BH_2]_n$–*r*–$[NH_2–BH_2]_m$ [n:1, m:1], in $CDCl_3$).[41]

Next, we attempted to increase the amount of [NH_2–BH_2] units in order to obtain solution-processable copolymers in the dehydropolymerisation reaction. We continued our studies using $Ph(CH_2)_4NH_2 \cdot BH_3$ and $NH_3 \cdot BH_3$ in a molar ratio 1:2, respectively. In this case, the previous reaction conditions were followed, except that the solution of $NH_3 \cdot BH_3$ in THF was added dropwise over a period of 1 h to guarantee the total consumption of $NH_3 \cdot BH_3$. As before, vigorous hydrogen gas evolution was observed, however the solution was opaque. In this case, the polymer yield by precipitation into hexanes at 20 °C was 87 % for $[Ph(CH_2)_4NH–BH_2]_n$–*r*–$[NH_2–BH_2]_m$ [n: 1, m: 2]. The increase in the yield is related to the decreased solubility of the copolymer. GPC analysis of the polymer $[Ph(CH_2)_4NH–BH_2]_n$ – *r*–$[NH_2–BH_2]_m$ [n: 1, m: 2] in solution of THF indicated that it is high molecular weight (M_n =162,100 g mol^{-1}, PDI = 1.28). The $^{11}B\{^1H\}$ NMR spectrum displayed a broad signal at [δ = −12.5 ppm] $[Ph(CH_2)_4NH–BH_2]_n$–*r*–$[NH_2–BH_2]_m$ [n: 1, m: 2] in THF-d_8.[42]

Evidence of the incorporation of the [NH_2–BH_2] units into the copolymers was provided by ^{11}B and ^{1}H NMR spectroscopy. The ^{11}B NMR spectra for [$Ph(CH_2)_4NH$–$BH_2]_n$–*r*–[NH_2–$BH_2]_m$ [n:1, m:1] and [$Ph(CH_2)_4NH$–$BH_2]_n$–*r*–[NH_2–$BH_2]_m$ [n:1, m:2] presented broad resonances for both polymers. When these signals are compared to the homopolymer [$Ph(CH_2)_4NH$–$BH_2]_n$, some subtle differences are observed. The homopolymer [$Ph(CH_2)_4NH$–$BH_2]_n$ presents a very symmetrical broad signal centred at [$\delta = -8.6$ ppm], whereas the copolymer [$Ph(CH_2)_4NH$–$BH_2]_n$–*r*–[NH_2–$BH_2]_m$ [n:1, m:1], presents a broad signal centred at [$\delta = -9.2$ ppm] with a shoulder around [ca. $\delta = -13$ ppm], both in $CDCl_3$. This shoulder is tentatively assigned to the boron environments of [NH_2–BH_2] units in the copolymer. It was reported that polyaminoborane [NH_2–$BH_2]_n$ prepared with [IrH_2(POCOP)] precatalyst, presented an intense signal at [$\delta = -10.7$ ppm] assigned for the –BH_2– groups in the backbone, whereas the signal for [MeNH–$BH_2]_n$, was found in a lower frequency at [$\delta = -5.8$ ppm], as observed by ^{11}B MQMAS NMR spectroscopy.[11b] The ^{11}B NMR spectrum for [$Ph(CH_2)_4NH$–$BH_2]_n$–*r*–[NH_2–$BH_2]_m$ [n:1, m:2] was recorded in THF-d_8, although no direct comparison can be made, it is suggested that the broadness of the signal could represent both boron environments for [$Ph(CH_2)_4NH$–BH_2] and [NH_2–BH_2] units (Figure 4.3).

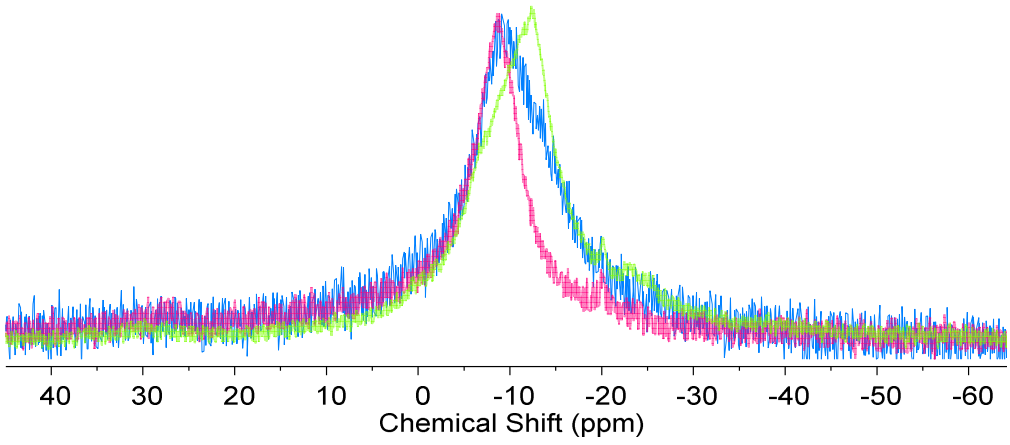

Figure 4.3. (a) Overlapped ^{11}B NMR spectra of [$Ph(CH_2)_4NH$–$BH_2]_n$ (pink, $CDCl_3$), [$Ph(CH_2)_4NH$–$BH_2]_n$–*r*–[NH_2–$BH_2]_m$ (n: 1, m: 1) (blue, $CDCl_3$) and [$Ph(CH_2)_4NH$–$BH_2]_n$–*r*–[NH_2–$BH_2]_m$ (n: 1, m: 2) (green, THF-d_8).

By ^{1}H NMR spectroscopy, both spectra for $[Ph(CH_2)_4NH–BH_2]_n$–*r*–$[NH_2–BH_2]_m$ and $[Ph(CH_2)_4NH–BH_2]_n$–*r*–$[NH_2–BH_2]_{2m}$ where performed in THF-d_8 for direct comparison. The integration of the assigned region for the phenyl substituent [δ = 6.98 to 7.32 ppm] and the region containing the methylene groups, and both N–H and B–H groups [δ = 0.75 to 3.28 ppm] was performed, and it was observed that the integrations approximately matched the expected monomer feed ratio of the copolymers (Fig. 4.4).

Previous attempts only afforded soluble copolymers containing up to 50% $NH_2–BH_2$ repeat units. In this work, we synthesised a copolymer containing up to 67% of $NH_2–BH_2$ repeat units which still could be processed in solution.

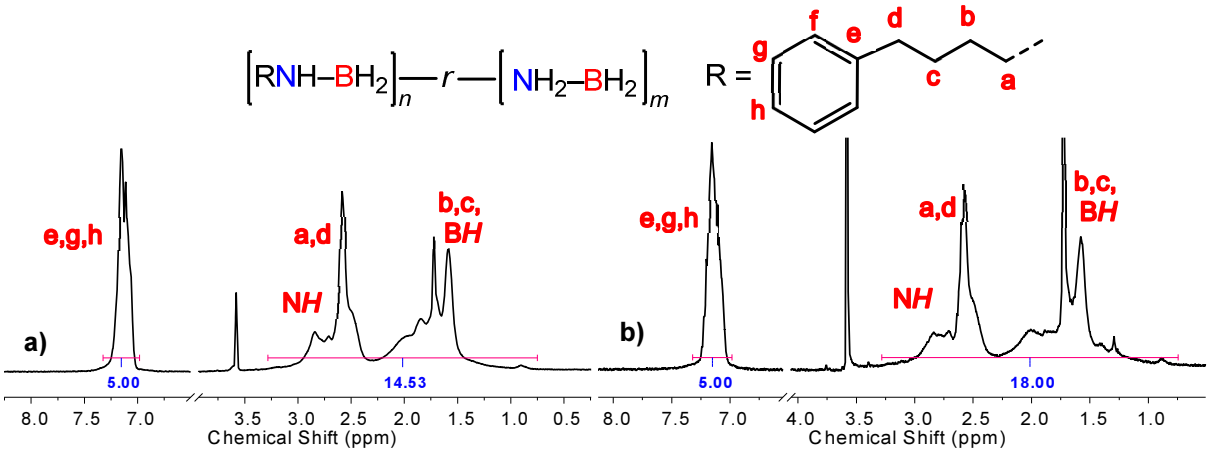

Figure 4.4. (a) ^{1}H NMR spectrum of $[Ph(CH_2)_4NH–BH_2]_n$–*r*–$[NH_2–BH_2]_m$ (n: 1, m: 1) in THF-d_8. (b) ^{1}H NMR spectrum of $[Ph(CH_2)_4NH–BH_2]_n$–*r*–$[NH_2–BH_2]_m$ (n: 1, m: 2) in THF-d_8

4.3.4.2 Formation of random copolymer using $Ph(CH_2)_4NH_2{\cdot}BH_3$ with $MeNH_2{\cdot}BH_3$ and $Ph(CH_2)_2NH_2{\cdot}BH_3$.

To obtain further insight into the ability of $Ph(CH_2)_4NH_2{\cdot}BH_3$ to form copolymers, we investigated the random dehydropolymerisation of $Ph(CH_2)_4NH_2{\cdot}BH_3$ with other amine–boranes. These copolymers were prepared by dehydropolymerisation (1.0 mol % of IrH_2(POCOP) in THF at −40°C) of $Ph(CH_2)_4NH_2{\cdot}BH_3$ and either $MeNH_2{\cdot}BH_3$ or $[Ph(CH_2)_2NH–BH_2]_n$ in a 1:1 mol ratio. The copolymers $[Ph(CH_2)_4NH–BH_2]_n$–*r*–$[MeNH–BH_2]_m$ and $[Ph(CH_2)_2NH–BH_2]_n$–*r*–$[Ph(CH_2)_4NH–BH_2]_m$ were isolated as white solids in

45% and 55% yield, respectively. The GPC chromatograms for both $[Ph(CH_2)_4NH–BH_2]_n$–*r*–$[MeNH–BH_2]_m$ and $[Ph(CH_2)_2NH–BH_2]_n$–*r*–$[Ph(CH_2)_4NH–BH_2]_m$ revealed monomodal molecular weight distributions in the high molecular weight region (M_n =170,100 g mol^{-1}, PDI = 1.18) and (M_n =188,400 g mol^{-1}, PDI = 1.38), respectively. In the $^{11}B\{^1H\}$ NMR spectrum (in $CDCl_3$), the copolymers $[Ph(CH_2)_4NH–BH_2]_n$–*r*–$[MeNH–BH_2]_m$ and $[Ph(CH_2)_2NH–BH_2]_n$–*r*–$[Ph(CH_2)_4NH–BH_2]_m$, showed the characteristic broad peak at (δ_B = −7.7 ppm) and (δ_B = −8.8 ppm), respectively. Nevertheless, the ^1H NMR spectrum for both copolymers showed broad signals in the aromatic and aliphatic regions. Specifically, the signal corresponding to the methyl group can be identified at (δ_H = 2.26 ppm) for the copolymer $[Ph(CH_2)_4NH–BH_2]_n$–*r*–$[MeNH–BH_2]_m$ (Fig. 4.5) and the integration for this polymer matched for a monomer ratio [n: 1, m: 1.56] which is similar to the ratio determined by EA. For copolymer $[Ph(CH_2)_2NH–BH_2]_n$–*r*–$[Ph(CH_2)_4NH–BH_2]_m$, the integration matched the expected ratio [n: 1, m: 1]. In the ^{13}C NMR spectrum, for copolymer $[Ph(CH_2)_4NH–BH_2]_n$–*r*–$[MeNH–BH_2]_m$, the methyl group can be observed at (δ_X = 36.0 ppm). Noteworthy, in the copolymer $[Ph(CH_2)_2NH–BH_2]_n$–*r*–$[Ph(CH_2)_4NH–BH_2]_m$ all signals for both repeat unit components can be assigned.

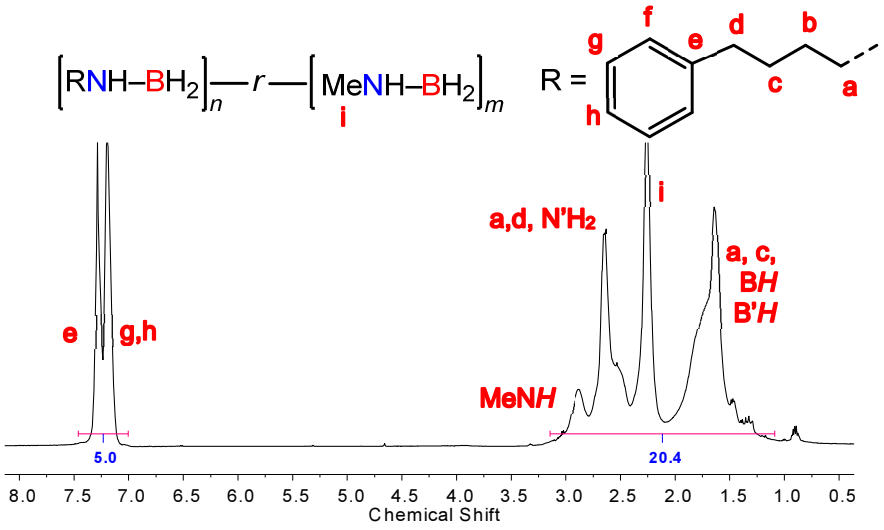

Figure 4.5. ^1H NMR spectrum of isolated $[Ph(CH_2)_4NH–BH_2]_n$–*r*– $[MeNH–BH_2]_m$ (n: 1, m: 2) in $CDCl_3$ at 20 °C.

Table 4.3. Synthesis and characterisation data for polyaminoboranes and copolymers.

Polyaminoborane (Monomer Precursor Ratio) [a]	Isolated Yield (%)	$^{11}B\{^1H\}$ NMR (ppm)[b]	M_n (GPC)	PDI (GPC)
$[Ph(CH_2)_2NH–BH_2]_n$	56	−8.7	158,800	1.25
$[Ph(CH_2)_4NH–BH_2]_n$	42	−8.6	168,300	1.16
$[Ph(CH_2)_2NH–BH_2]_n$–*r*–$[NH_2–BH_2]_m$ (n: 1, m: 1)[c]	80	−9.2	159,700	1.33
$[Ph(CH_2)_2NH–BH_2]_n$–*r*–$[NH_2–BH_2]_{2m}$ (n: 1, m: 2) [c]	87	−12.5[b]	162,100	1.28
$[Ph(CH_2)_2NH–BH_2]_n$–*r*–$[MeNH–BH_2]_m$ (n: 1, m: 1.56) [c]	45	−7.7	170,100	1.18
$[Ph(CH_2)_2NH–BH_2]_n$–*r*–$[Ph(CH_2)_4NH–BH_2]_m$ (n:1, m:1) [c]	55	−8.8	188,400	1.38

a) $^{11}B\{^1H\}$ NMR spectroscopy was measured in $CDCl_3$. b) $^{11}B\{^1H\}$ NMR spectroscopy measured in THF-d_8. c) Monomer ratios obtained by ^1H NMR.

4.3.5 Thermal Decomposition Behaviour and Stability of Polymers

As polyaminoboranes are of potential interest as precursors to BN-based ceramic materials, we investigated the thermal decomposition of the polyaminoboranes synthesised in this study by TGA under N_2 atmosphere (heating rate 10 °C min^{-1} gradient to 900 °C) (Table 4.4). The polymers $[Ph(CH_2)_2NH–BH_2]_n$ and $[Ph(CH_2)_4NH–BH_2]_n$ showed similar $T_{5\%}$ (temperature that represents 5% loss of the original mass of the polymer) at 205 and 210 °C, respectively. Past this temperature, the polymers degraded in a two-step process, where decomposition was complete at around 500 °C. The predicted ceramic yields from boron nitride from $[Ph(CH_2)_2NH–BH_2]_n$ is 18 % and for $[Ph(CH_2)_4NH–BH_2]_n$ is 15 %. We observed a ceramic yield of 32% for $[Ph(CH_2)_2NH–BH_2]_n$ and 19 % for $[Ph(CH_2)_4NH–BH_2]_n$ after heating to 900 °C, which indicates that carbon content in the ceramic product might have been incorporated from the hydrocarbon group.

In the case of copolymers containing $[NH_2–BH_2]$ or $[MeNH–BH_2]$ repeat units, $T_{5\%}$ exhibited values around 145-155 °C, which is lower than the corresponding homopolymers $[Ph(CH_2)_2NH–BH_2]_n$ and $[Ph(CH_2)_4NH–BH_2]_n$. It has been determined that complete decomposition of $[NH_2–BH_2]_n$ and $[MeNH–BH_2]_n$ occurred by 210 °C and 150 °C, respectively,[10b] therefore copolymers containing these repeat units might have similar

decomposition pathways which diminish their overall thermal stability. For $[Ph(CH_2)_2NH–BH_2]_n–r–[Ph(CH_2)_4NH–BH_2]_m$ (n: 1, m: 1), $T_{5\%}$ was slightly higher (160 °C) than the other copolymers.

Table 4.4. Thermal properties, $T_{5\%}$ and ceramic yield of polyaminoboranes.

Polyaminoboranes (Monomer Precursor Ratio)[c]	$T_{5\%}$[a] (°C)	Ceramic Yield[b] (%)
$[Ph(CH_2)_2NH–BH_2]_n$	205	32
$[Ph(CH_2)_4NH–BH_2]_n$	210	19
$[Ph(CH_2)_4NH–BH_2]_n–r–[NH_2–BH_2]_m$ (1:1) [c]	155	16
$[Ph(CH_2)_4NH–BH_2]_n–r–[NH_2–BH_2]_{2m}$ (1:2) [c]	145	24
$[Ph(CH_2)_4NH–BH_2]_n–r–[MeNH–BH_2]_m$ (1:1.56) [c]	145	16
$[Ph(CH_2)_4NH–BH_2]_n–r–[Ph(CH_2)_2NH–BH_2]_m$ (1:1) [c]	160	25

a) Temperature at 5% weight loss (heating rate 10 °C min^{-1}). b) Ceramic yields were measured at 900 °C, heating rate 10 °C min^{-1} (under a flow N_2). c) Monomer ratios obtained by ^1H NMR.

The ceramic yield previously reported for $[NH_2–BH_2]_n$ was 34 % and for $[MeNH–BH_2]_n$ was 16 % (1000 °C under flow of N_2).[10b] For copolymers $[Ph(CH_2)_4NH–BH_2]_n–r–[NH_2–BH_2]_m$ (n: 1, m: 1) and $[Ph(CH_2)_4NH–BH_2]_n–r–[NH_2–BH_2]_m$ (n: 1, m: 2), the TGA experiment showed that the polymer containing more $[NH_2–BH_2]$ repeat units possessed higher ceramic yield (16% vs 24%). The ceramic yield of $[Ph(CH_2)_4NH–BH_2]_n–r–[MeNH–BH_2]_m$ was 16 %, which is similar to the one reported for the homopolymer $[MeNH–BH_2]_n$.

The ceramic yield can be increased when the pyrolysis of polyaminoboranes is performed as compressed pellet. For example, the ceramic yield improved from 36 % to 52 % (at 900 °C), when pyrolysis of $[NH_2–BH_2]_n$ was achieved as a powder and as a pellet, respectively.[11a] We attempted the same experiment with the copolymer $[Ph(CH_2)_4NH–BH_2]_n–r–[NH_2–BH_2]_m$ (n: 1, m: 1), and resulted in the slight improvement on the ceramic

yield (from 16% to 21%) when the pyrolysis at 900 °C was performed with the material as a pellet rather than a powder (See SI, Fig. S4.55).

It has been previously shown that crosslinked polyaminoboranes gave ceramic yields around 75-80% (700 to 1000 °C),[10a, 43] which usually came from insoluble, highly cross-linked precursors. In general, the low thermal stability and ceramic yields of our polymers suggests that further dehydrogenation and depolymerisation processes are favoured over cross-linking.

4.3.6 Synthesis of crosslinked polyaminoboranes

In previous studies, copolymerisation of $NH_3{\cdot}BH_3$ with the cross-linker hydrazine-borane $BH_3{\cdot}NH_2{-}NH_2{\cdot}BH_3$ (ratio 9:1) afforded a insoluble copolymer with a ceramic yield of 52% at 900 °C (10 °C min^{-1} gradient).[11a] In order to determine the effect on the possible increase of the ceramic yield in our materials, we attempted the copolymerization reaction of $Ph(CH_2)_2NH_2{\cdot}BH_3$ (precursor which homopolymer presented the highest ceramic yield by TGA) with the cross-linker octyldiamine–diborane $BH_3{\cdot}NH_2(CH_2)_8NH_2{\cdot}BH_3$ in a ratio 95:5 with [IrH_2(POCOP)] (1.0 mol %) at low temperature (−40 °C) (See SI, Section 4.8). This reaction afforded a white solid soluble in THF with 29% yield, after precipitation in hexanes. The GPC chromatogram of this material showed an asymmetric trace with tailing towards high molecular weight region (M_n = 225,400 g mol^{-1}, M_w = 666,300 g mol^{-1}, PDI = 2.94). The ^{11}B NMR (THF-d_8) spectrum of this material showed a broad signal centred at δ_B = −9.0 ppm. An additional signal around δ_B = −1.6 ppm can be suggestive of the presence of 'BN_3' or 'BN_4' environments,[12a, 44] indicating some crosslinking of the polymer chains in this system. Moreover, the signal around δ_B = −22.0 ppm may correspond to an end group.[13] The ^{1}H NMR spectrum possessed the same pattern as the homopolymer $[Ph(CH_2)_2NH{-}BH_2]_n$ (broad signals in the aliphatic and aromatic region). The thermal stability ($T_{5\%}$ = 210 °C) and the ceramic yield (33 %) are similar when

compared to the corresponding homopolymer. When the copolymerisation reaction was repeated varying the monomer and cross-linker ratio to 90:10, this resulted in an insoluble material where the thermal stability and ceramic yield increased ($T_{5\%}$ = 247 °C; 40%). The copolymerisation of $NH_3 \cdot BH_3$ with $BH_3 \cdot NH_2(CH_2)_8NH_2 \cdot BH_3$ (ratio 90:10) was attempted and the material isolated gave a ceramic yield of 40% at 900 °C (Fig. 4.6).

These results suggest that the effect of controlled crosslinking of the polymer $[Ph(CH_2)_2NH–BH_2]_n$ improved the thermal stability of the material, however, loss of tractability is manifested as insoluble materials are obtained, and only small increases in the ceramic yield are observed.

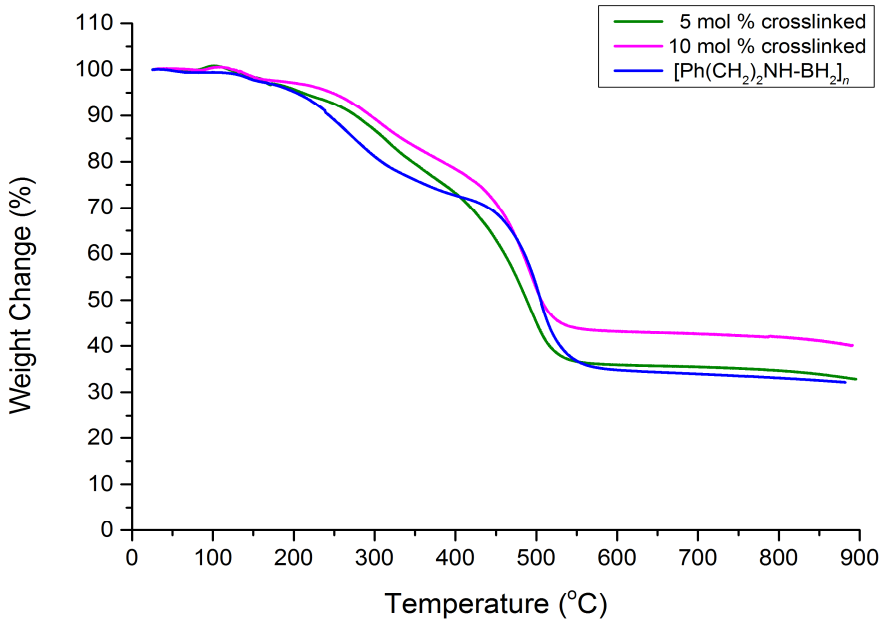

Figure 4.6. TGA thermograms of $[Ph(CH_2)_2NH–BH_2]_n$ crosslinked with $BH_3 \cdot NH_2(CH_2)_8NH_2 \cdot BH_3$ in different ratios at 900 °C(heating rate 10 °C min^{-1}).

4.4 Conclusions

In summary, we present here the metal-catalysed dehydropolymerisation of aryl-containing *N*-alkyl amine-boranes. We found that the *N*-alkyl chain influences the dehydrogenation reaction. By variation of the chain length, we discovered that the *N*-benzyl substrate could not be dehydrogenated whereas substrates with longer methylene chains as spacers between nitrogen of the substrate and the aryl substituent were active in the dehydrocoupling reaction. Based on these results, we synthesised and characterised high molecular weight polyaminoboranes and copolymers using the precatalyst system [IrH_2(POCOP)] that has enabled an expansion of the substrate scope. Formation of random copolymers was possible by mixtures of $Ph(CH_2)_2NH_2 \cdot BH_3$ and different amine-boranes. In particular, the copolymerisation with $NH_3 \cdot BH_3$ produced copolymers containing up to 67 % [NH–BH_2] units to produce soluble materials which has not been previously achieved. The structural analysis of $[Ph(CH_2)_2NH–BH_2]_n$ using solution NMR spectroscopy and IR spectroscopy, which is consistent with previous studies, showed that these materials are essentially linear. Also, evidence of the polymeric nature (M_n > 10,000 g mol^{-1}) of $[Ph(CH_2)_2NH–BH_2]_n$ was achieved by GPC, DLS and ^{1}H DOSY, however, overestimation of the molar mass by GPC is found for these polar polyaminoboranes. Overall, the analysis of the thermal properties of polyaminoboranes and copolymers revealed that these materials possessed low thermal stability and ceramic yield values, which implies that at high temperatures dehydrogenation/dehydropolymerisation events are occurring. We explored the use of a cross-linking agent for the dehydropolymerisation of $Ph(CH_2)_2NH_2 \cdot BH_3$ and found that the resulting copolymeric material improved its thermal stability and ceramic yield, however, low solubility is observed. Detailed systematic studies on the cross-linking of polyaminoboranes and compression of the materials as pellets are in progress as tools to obtain higher ceramic yields for the development of tangible applications. Future work needs to be carried out in order to explore the control on the stereochemistry of the dehydropolymerisation *via* the catalyst

systems (e.g. development of new catalysts or chiral ligands) or the use of chiral substrates in order to control the tacticity of these inorganic polymers.

4.5 Supporting Information

4.5.1 General procedures, equipment and reagents.

All manipulations were carried out under an atmosphere of nitrogen gas using standard vacuum line and Schlenk techniques; except for the use of argon atmosphere within an M. Braun glovebox MB150G-B maintained at <0.1 ppm of H_2O and <0.1 ppm of O_2 where all manipulations with [IrH_2(POCOP)] (POCOP = [κ^3 - 1,3-($tBu_2PO)_2C_6H_3$] were carried out. Where stated, anhydrous solvents were dried *via* a Grubbs design solvent purification system.[45] Anhydrous deuterated chloroform or tetrahydrofuran was purchased from Sigma Aldrich and stored over activated molecular sieves (4 Å). Primary amines $Ph(CH_2)_xNH_2$ (x = 1–3), ammonia-borane, Celite® and chloro(1,5-cyclooctadiene)rhodium(I) dimer [Rh(μ-Cl)(1,5-COD)]$_2$ and Rh/Al_2O_3 (5 wt. % Rh) were purchased from Sigma Aldrich Ltd and used as acquired. BH_3·THF was purchased from Acros Organics and distilled prior use. Ammonia-borane was purified by sublimation (T = 40 °C, p = 10^{-3} bar). [IrH_2(POCOP)][46] and skeletal nickel[20a] were synthesised via literature methods and purified by reprecipitation ([IrH_2(POCOP)]) and washing with *n*-hexane (skeletal nickel). NMR spectra were recorded using Oxford Jeol Eclipse 300, 400 or Bruker 500 MHz cryoprobe spectrometers. ^{1}H NMR spectra were calibrated using residual protio signals of the solvent: (δ ^{1}H ($CHCl_3$) = 7.24). ^{13}C NMR spectra were calibrated using the solvent signals (δ ^{13}C ($CDCl_3$) = 77.0; δ ^{13}C (C_6D_6) = 128.0). ^{11}B NMR spectra were calibrated against external standards (^{11}B: BF_3·OEt_2 (δ ^{11}B = 0.0)). IR spectra were measured using an Agilent Cary FT-IR with ATR sampling module.

Diffusion Ordered Spectroscopy (DOSY) experiments were carried out on a Varian 500 instrument. Samples were analysed at 2 mg/ml concentrations in C_6D_6. To avoid distorted diffusion coefficients, the spectra were collected without sample spinning. Spectra were processed using the MestReNova Bayesian DOSY transform function at a resolution factor of 0.1, 5 repetitions, and 512 points in the diffusion dimension over a range of ($1x10^{-7}$ –

$1x10^{-4}$) cm^2s^{-1}. The estimation of the molecular weight of the polyaminoborane sample was performed using the method described previously by Grubbs *et. al*[32]. using five polystyrene standards of know molecular weight from 820 to 44,000 Da, purchased from Sigma-Aldrich. Plotting log D against log M_n produced a linear calibration curve, to which the polyaminoborane was compared.

GPC was performed on a Malvern RI max Gel Permeation Chromatograph, equipped with an automatic sampler, a pump, an injector, and inline degasser. The columns (T5000) were contained within an oven (35 °C) and consisted of styrene/divinyl benzene gels. Sample elution was detected by means of a differential refractometer. THF (Fisher), containing 0.1 *w*/*w* % *n*Bu_4NBr, was used as the eluent at a flow rate of 1 mL min^{-1}. Samples were dissolved in the eluent (2 mg mL^{-1}) and filtered with a Ministart SRP15 filter poly(tetrafluoroethylene) membrane of 0.45 µm pore size before analysis. The calibration was conducted using monodisperse polystyrene standards obtained from Aldrich. The lowest and highest molecular weight standard used were 2,300 and 994,000 g mol^{-1}, respectively.

Dynamic light scattering experiments were performed using a Malvern Zetasizer Nano S spectrometer at λ = 632 nm in a glass cuvette using dry THF at 20°C, citing the average values for volume and intensity.

TGA was measured on a Thermal Advantage TGAQ500 at 10 °C min^{-1} under N_2. TGA results were analysed using WinUA V4.5A by Thermal Advantage.

Elemental analysis was performed with a Eurovector EA 3000 Elemental Analyzer at the University of Bristol Microanalysis Laboratory.

4.5.2 Synthesis and characterisation of new amine–boranes $Ph(CH_2)_xNH_2{\cdot}BH_3$ (x = 1–4)

General procedure for the formation of $Ph(CH_2)_xNH_2{\cdot}BH_3$ (x = 1–4).

A solution of $BH_3{\cdot}THF$ (20 mL, 20 mmol) at –78 °C was reacted with the corresponding amines $Ph(CH_2)_xNH_2$ (x = 1–4) (20 mmol). The reaction mixture was warmed to 25 °C and stirred for 1 h. Removal of the solvent from the clear, colourless reaction mixture yielded the compound $PhCH_2NH_2{\cdot}BH_3$ as a solid and $Ph(CH_2)_xNH_2{\cdot}BH_3$ (x = 2–4) as colourless oils.

Purification process for $PhCH_2NH_2{\cdot}BH_3$: Recrystallisation from hexanes/DCM at –60 °C, yields the product as a white solid. This amine-borane has been reported in prior literature.[47]

Purification process for $Ph(CH_2)_xNH_2{\cdot}BH_3$ (x = 2–4): These amine–boranes are liquids at room temperature. As a purification step, the amines-boranes were frozen at –78 °C and the resultant solids were washed with hexanes (3 x 10 mL) in order to remove any remaining amine. Then, they were dried under vacuum (10^{-2} mmHg) for 1 h. $Ph(CH_2)_2NH_2{\cdot}BH_3$ has been reported in prior literature.[48]

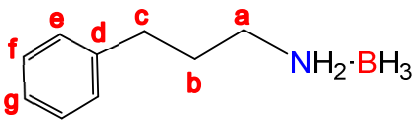

$Ph(CH_2)_3NH_2{\cdot}BH_3$. Colourless liquid. 82% yield.

^{11}B NMR ($CDCl_3$): δ (ppm) −20.4.

^{1}H NMR ($CDCl_3$): δ (ppm) 1.49 (br s, B*H*$_3$); 1.92 (m, 2H, Hb); 2.63 (m, 2H, Hc); 2.78 (m, 2H, Ha); 3,81 ppm (br s, N*H*$_2$); 7.17-7.25 (3H, m, Hg-Hf); 7.28-7,32 (2H, m He).

^{13}C NMR ($CDCl_3$): δ (ppm) 30.53 (Cc); 33.04 (Cb); 48.39 (Ca); 126.43 (Cg); 128.44 (Ce); 128.75 (Cf); 140.69 (Cd).

Elemental analysis calculated for $C_9H_{16}BN$: C, 72.5; H, 10.8; N, 9.4. Found: C, 73.2; H, 10.7; N, 10.2.

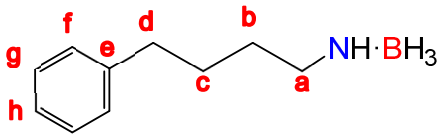

Ph(CH$_2$)$_4$NH$_2$·BH$_3$. Colourless liquid. 98% yield.

^{11}B NMR (CDCl$_3$): δ (ppm) −20.3.

^{1}H NMR (CDCl$_3$): δ (ppm) 1.48 (br s, B*H*$_3$); 1.61-1.69 (m, 4H, Hb-Hc); 2.63 (t, *J*=7.0 Hz, 2H, Hd); 2.73-2.83 (m, 2H, Ha); 3.73 (br s, N*H*$_2$); 7.15-7.22 (m, 3H, Hg-Hh); 7.26-7.32 (m, 2H, Hf).

^{13}C NMR (CDCl$_3$): δ (ppm) 28.40 (Cc); 28.71 (Cb); 35.38 (Cd); 48.75 (Ca); 126.12 (Ch); 128.49 (Cf); 128.56 (Cg); 141.66 (Ce).

Elemental analysis calculated for C$_{10}$H$_{18}$BN: C, 73.7; H, 11.1; N, 8.6. Found: C, 72.6; H, 11.4; N, 9.2.

4.5.3 Dehydropolymerisation Studies of Ph(CH$_2$)$_x$NH$_2$·BH$_3$ Using Different Catalysts (Skeletal Nickel, [Rh(μ-Cl)(1,5-COD)]$_2$ and [IrH$_2$(POCOP)])

4.5.3.1 Dehydropolymerisation of Ph(CH$_2$)$_4$NH$_2$·BH$_3$ with Skeletal Nickel

4.5.3.1.1 Dehydropolymerisation Using 5 mol % Skeletal Nickel After Various Reaction Times

To a solution of Ph(CH$_2$)$_4$NH$_2$·BH$_3$ (163 mg, 1.0 mmol) in THF (0.5 mL) in a vial was added skeletal nickel (5 mol %, 3 mg) at 20 °. At different reactions times at room temperature, the solution was transferred to a Teflon-tapped J. Young quartz NMR tube and monitored by ^{11}B NMR.

Analysis of the reaction of Ph(CH$_2$)$_4$NH$_2$·BH$_3$ with 5 mol % skeletal nickel at 60 min and 540 min: ^{11}B NMR (THF): [Ph(CH$_2$)$_4$NH]$_2$BH [δ$_B$ 27.4 (br)] and Ph(CH$_2$)$_4$NH$_2$·BH$_3$ [δ$_B$ −19.8] (Figure S4.1 and Table S4.1).

Table S4.1*:* Influence of reaction time on the dehydropolymerisation of $Ph(CH_2)_4NH_2{\cdot}BH_3$ in THF at 20 °C with 5 mol % skeletal nickel.

Time	Conversion [%][a]	Yield [%][b]
	$Ph(CH_2)_4NH_2{\cdot}BH_3$	$[Ph(CH_2)_4NH]_2BH$
60 min	3	3
540 min	6	6

a) Conversion determined by ^{11}B NMR spectroscopy. b) Yields determined by integration of the signals in the ^{11}B NMR spectra of the reaction mixtures.

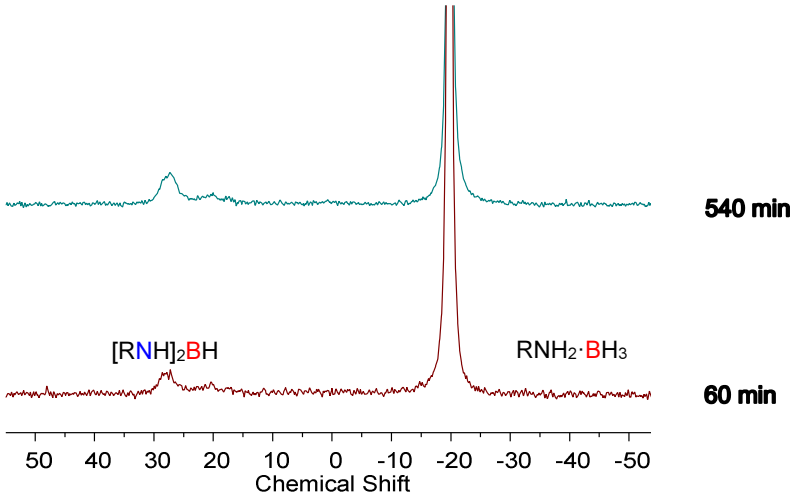

Figure S4.1. $^{11}B\{^1H\}$ NMR spectra of the reaction of $Ph(CH_2)_4NH_2{\cdot}BH_3$ and 5 mol % of skeletal nickel in THF at 20 °C at 1h and 6h. R = $Ph(CH_2)_4$.

4.5.3.1.2 Dehydropolymerisation Using 100 mol % Skeletal Nickel After Various Reaction Times

To a solution of $Ph(CH_2)_4NH_2{\cdot}BH_3$ (163 mg, 1.0 mmol) in THF (0.5 mL) in a vial was added skeletal nickel (100 mol %, 59 mg) at 20 °C. At different reaction times at room temperature (20 °C), the solution was transferred to a Teflon-tapped J. Young quartz NMR tube and monitored by ^{11}B NMR.

Analysis of the reaction of $Ph(CH_2)_4NH_2{\cdot}BH_3$ with 100 mol % skeletal nickel after 60 min and 240 min: ^{11}B NMR (THF): $[Ph(CH_2)_4NH]_2BH$ [δ_B 27.2 (br)], $[Ph(CH_2)_4NH{-}BH_2]_n$ [δ_B −7.1 (br)] and $Ph(CH_2)_4NH_2{\cdot}BH_3$ [δ_B −19.7] (Figure S4.2 and Table 4.2).

Table S4.2*:* Influence of reaction time on the dehydropolymerisation of $Ph(CH_2)_4NH_2{\cdot}BH_3$ in THF at 20 °C with 100 mol % skeletal nickel.

Time	Conversion [%][a]	Yield [%][b]	
	$Ph(CH_2)_4NH_2{\cdot}BH_3$	$[Ph(CH_2)_4NH–BH_2]_n$	$[Ph(CH_2)_4NH]_2BH$
60 min	46	3	42
240 min	74	13	60

a) Conversion determined by ^{11}B NMR spectroscopy. b) Yields determined by integration of the signals in the ^{11}B NMR spectra of the reaction mixtures.

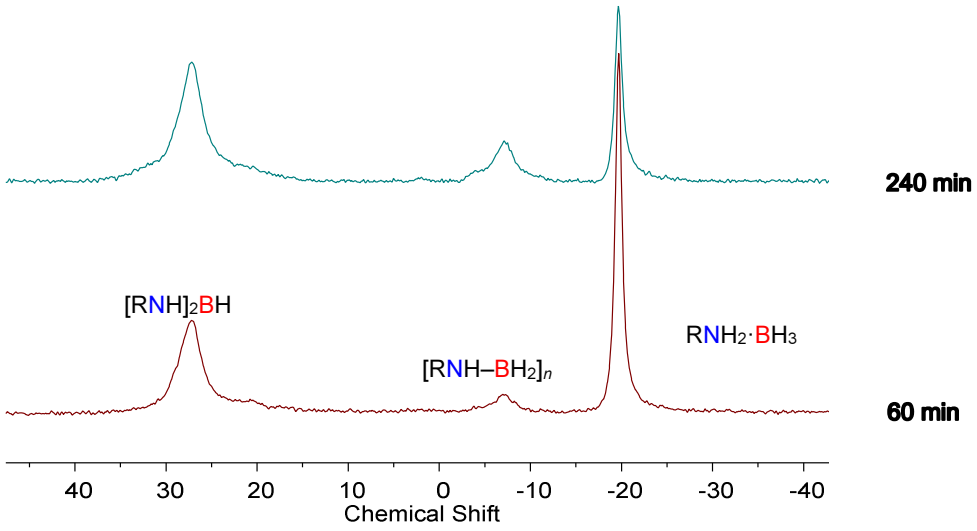

Figure S4.2. $^{11}B\{^1H\}$ NMR spectra of the reaction of $Ph(CH_2)_4NH_2{\cdot}BH_3$ and 100 mol % of skeletal nickel in THF at 20 °C at 60 min and 240 min. R = $Ph(CH_2)_4$.

4.5.3.2 Dehydropolymerisation of $Ph(CH_2)_4NH_2{\cdot}BH_3$ with $[Rh(\mu\text{-}Cl)(1,5\text{-}COD)]_2$.

4.5.3.2.1 Dehydropolymerisation of $Ph(CH_2)_4NH_2{\cdot}BH_3$ with 2.5 mol % $[Rh(\mu\text{-}Cl)(1,5\text{-}COD)]_2$ After Various Reaction Times at Room Temperature in THF.

To a solution of $Ph(CH_2)_4NH_2{\cdot}BH_3$ (163 mg, 1.0 mmol) in THF (0.3 mL) in a vial was added a solution of $[Rh(\mu\text{-}Cl)(1,5\text{-}COD)]_2$ (2.5 mol %, 12 mg) in toluene (0.2 mL) at 20 °C. The solution was transferred to a Teflon-tapped J. Young quartz NMR tube and monitored by ^{11}B NMR at different reaction times at 20 °C.

Analysis of the reaction of $Ph(CH_2)_4NH_2{\cdot}BH_3$ with 2.5 mol % $[Rh(\mu\text{-}Cl)(1,5\text{-}COD)]_2$ at 15 min, 30 min and 90 min: ^{11}B NMR (THF): $[Ph(CH_2)_4NH]_2BH$ [δ_B 27.1 (br)], $[Ph(CH_2)_4NH–BH_2]_n$ [δ_B −8.2 (br)] (*ca.* 20%) and $Ph(CH_2)_4NH_2{\cdot}BH_3$ [δ_B −19.8] (Figure S4.3 and Table S4.3).

Table S4.3*:* Influence of reaction time on the dehydropolymerisation of $Ph(CH_2)_4NH_2{\cdot}BH_3$ in THF at 20 °C with 2.5 mol % $[Rh(\mu\text{-}Cl)(1,5\text{-}COD)]_2$.

Time	Conversion [%][a]	Yield [%][b]	
	$Ph(CH_2)_4NH_2{\cdot}BH_3$	$[Ph(CH_2)_4NH{-}BH_2]_n$	$[Ph(CH_2)_4NH]_2BH$
15 min	76	31	45
45 min	68	34	35
90 min	62	34	28

a) Conversion determined by ^{11}B NMR spectroscopy. b) Yields determined by integration of the signals in the ^{11}B NMR spectra of the reaction mixtures.

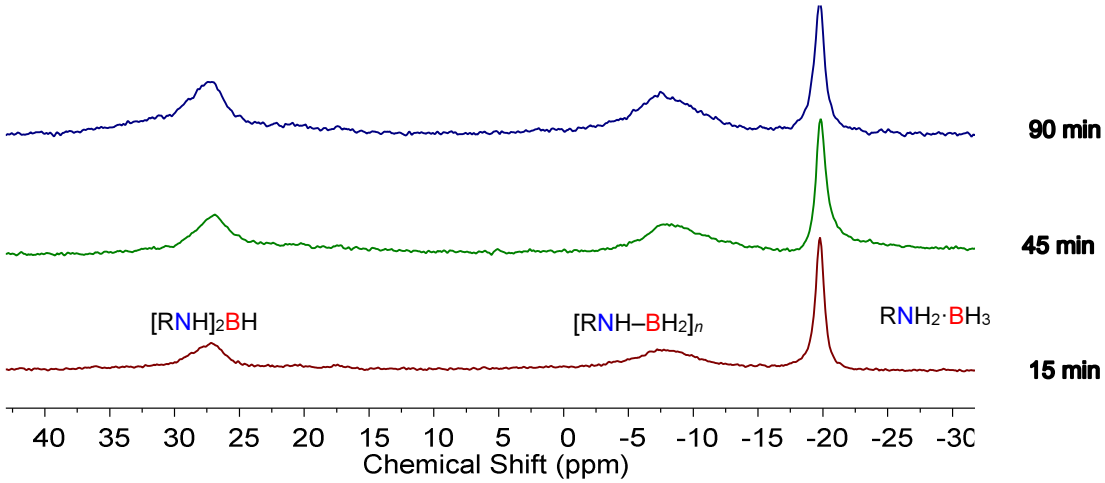

Figure S4.3. $^{11}B\{^1H\}$ NMR spectra of the reaction of $Ph(CH_2)_4NH_2{\cdot}BH_3$ and 2.5 mol % of $[Rh(\mu\text{-}Cl)(1,5\text{-}COD)]_2$ in THF at 20 °C at 15 min, 45 min and 90 min. R = $Ph(CH_2)_4$.

4.5.3.2.2 Dehydropolymerisation of $Ph(CH_2)_4NH_2{\cdot}BH_3$ with 2.5 mol % $[Rh(\mu\text{-}Cl)(1,5\text{-}COD)]_2$ After Various Reaction Times at Room Temperature in Toluene.

To a solution of $Ph(CH_2)_4NH_2{\cdot}BH_3$ (163 mg, 1.0 mmol) in toluene (0.3 mL) in a vial was added a solution of $[Rh(\mu\text{-}Cl)(1,5\text{-}COD)]_2$ (2.5 mol %, 12 mg) in toluene (0.2 mL) at 20 °C. The solution was transferred to a Teflon-tapped J. Young quartz NMR tube and monitored by ^{11}B NMR at different reaction times at 20 °C.

Analysis of the reaction of $Ph(CH_2)_4NH_2{\cdot}BH_3$ with 2.5 mol % $[Rh(\mu\text{-}Cl)(1,5\text{-}COD)]_2$ at 15 min, 45 min, 90 min and 225 min: ^{11}B NMR (THF): $[Ph(CH_2)_4NH]_2BH$ [δ_B 27.2 (br)] and $[Ph(CH_2)_4N{-}BH]_3$ [δ_B ca. 32 (br)], $[Ph(CH_2)_4NH{-}BH_2]_n$ [δ_B −6.9 (br)] (*ca.* 20%) and $Ph(CH_2)_4NH_2{\cdot}BH_3$ [δ_B −19.0] (Figure S4.4 and Table S4.4).

Table S4.4*:* Influence of reaction time on the dehydropolymerisation of $Ph(CH_2)_4NH_2{\cdot}BH_3$ in toluene at 20 °C with 2.5 mol % $[Rh(\mu\text{-}Cl)(1,5\text{-}COD)]_2$.

Time	Conversion [%][a]	Yield [%][b]	
	$Ph(CH_2)_4NH_2{\cdot}BH_3$	$[Ph(CH_2)_4NH{-}BH_2]_n$	$[Ph(CH_2)_4NH]_2BH$
15min	85	55	30
45 min	88	53	35
90 min	97	52	45[c]
180 min	96	52	44[c]

a) Conversion determined by ^{11}B NMR spectroscopy. b) Yields determined by integration of the signals in the ^{11}B NMR spectra of the reaction mixtures. c) Mixture of $[Ph(CH_2)_4NH]_2BH$/$[Ph(CH_2)_4N{-}BH]_3$. The signals observed by $^{11}B\{^1H\}$ NMR spectroscopy are overlapping for these products.

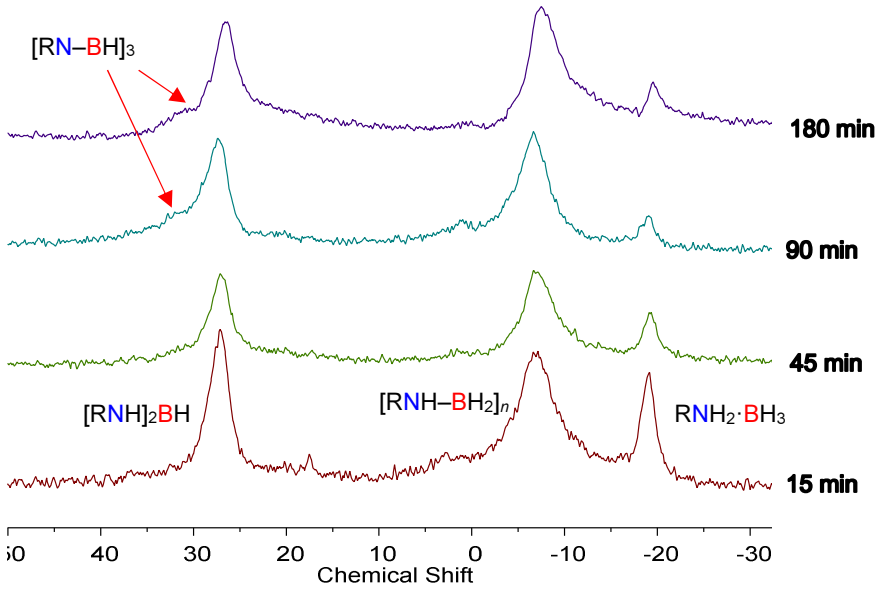

Figure S4.4. $^{11}B\{^1H\}$ NMR spectra of the reaction of $Ph(CH_2)_4NH_2{\cdot}BH_3$ and 2.5 mol % of $[Rh(\mu\text{-}Cl)(1,5\text{-}COD)]_2$ in toluene at 20 °C at 15 min, 45 min, 90 min and 225 min. R = $Ph(CH_2)_4$.

4.5.3.2.3 NMR and GPC Analysis of $Ph(CH_2)_4NH_2{\cdot}BH_3$ with 2.5 mol % $[Rh(\mu\text{-}Cl)(1,5\text{-}COD)]_2$ After 15 min and 180 min of Reaction.

To $Ph(CH_2)_4NH_2{\cdot}BH_3$ (163 mg, 1.0 mmol) was added a solution $[Rh(\mu\text{-}Cl)(1,5\text{-}COD)]_2$ (2.5 mol %, 12 mg) in toluene (0.5 mL) in a vial at 20 °C. After 15 min or 180 min, the solution was transferred into cold (−40 °C) stirred hexanes (20 mL), whereupon a precipitate was observed. Excess solvent was removed via decantation and volatile byproducts were removed *in vacuo*.

Analysis of the reaction of $Ph(CH_2)_4NH_2{\cdot}BH_3$ with 2.5 mol % $Rh(\mu\text{-}Cl)(1,5\text{-}COD)]_2$ after 15 min: ^{11}B NMR (THF): $[Ph(CH_2)_4NH]_2BH$ [δ_B 27.2 (br)] (*ca.* 19%), unassigned product [δ_B 0.8 (s)] (*ca.* 16%), $[Ph(CH_2)_2NH{-}BH_2]_n$ [δ_B −7.4 (br)] (*ca.* 60%) and $Ph(CH_2)_4NH_2{\cdot}BH_3$ [δ_B −19.0] (*ca.* 5%) (Figure S4.5). GPC (M_n = 111,500 g mol^{-1}, M_w = 131,000 g mol^{-1}, PDI = 1.18) (Figure S4.6).

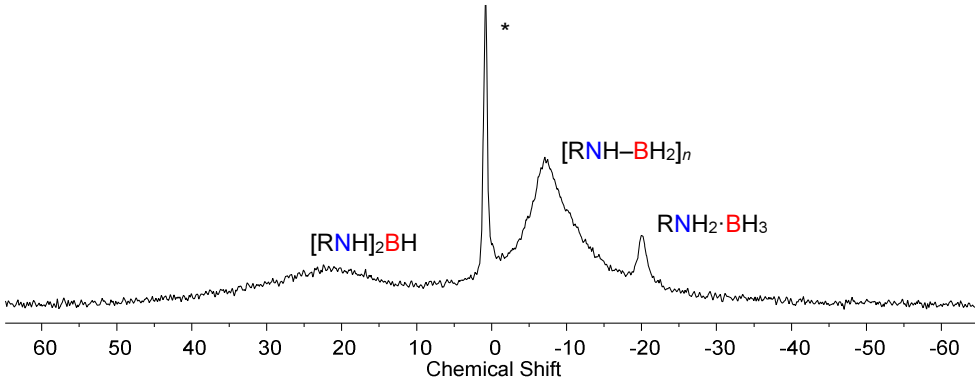

Figure S4.5. $^{11}B\{^1H\}$ NMR spectrum of the product of the reaction of $Ph(CH_2)_4NH_2{\cdot}BH_3$ and 2.5 mol % **[**$Rh(\mu\text{-}Cl)(1,5\text{-}COD)]_2$ in THF at 20 °C after 15min. * Unassigned product. R = $Ph(CH_2)_4$

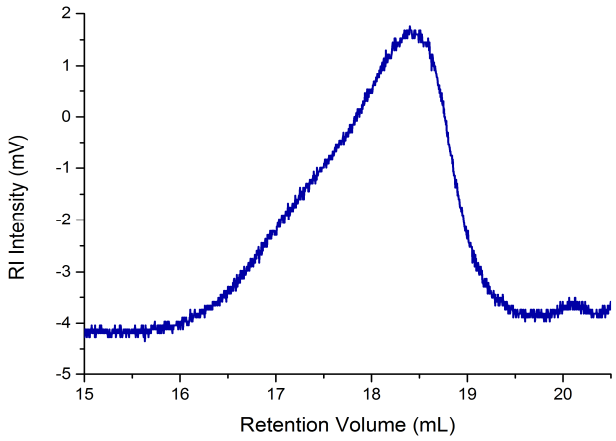

Figure S4.6. GPC chromatogram (2mg mL^{-1}) of the product of the reaction of $Ph(CH_2)_4NH_2{\cdot}BH_3$ and 2.5 mol % **[**$Rh(\mu\text{-}Cl)(1,5\text{-}COD)]_2$ after precipitation in THF (0.1 *w/w* % *n*Bu_4NBr) at 20 °C after 15 min.

Analysis of the reaction of $Ph(CH_2)_4NH{\cdot}BH_3$ with 2.5 mol % $Rh(\mu\text{-}Cl)(1,5\text{-}COD)]_2$ after 180 min: ^{11}B NMR (THF): $[Ph(CH_2)_4NH{-}BH_2]_n$ [δ_B −7.5 (br)] (Figure S4.7). GPC (M_n = 188,000 g mol^{-1}, M_w = 196,300 g mol^{-1}, PDI = 1.04) (Figure S4.8).

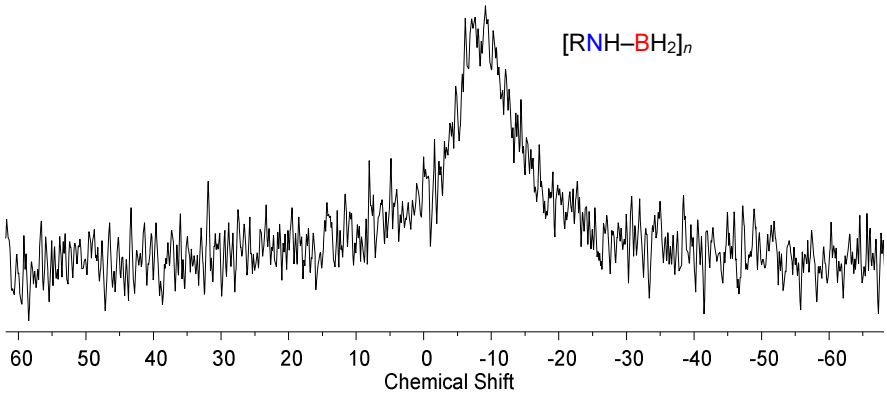

Figure S4.7. $^{11}B\{^{1}H\}$ NMR spectrum of the product of the reaction of $Ph(CH_2)_4NH_2{\cdot}BH_3$ and 2.5 mol % **[**$Rh(\mu\text{-}Cl)(1,5\text{-}COD)]_2$ in THF at 20 °C after 180 min. R = $Ph(CH_2)_4$

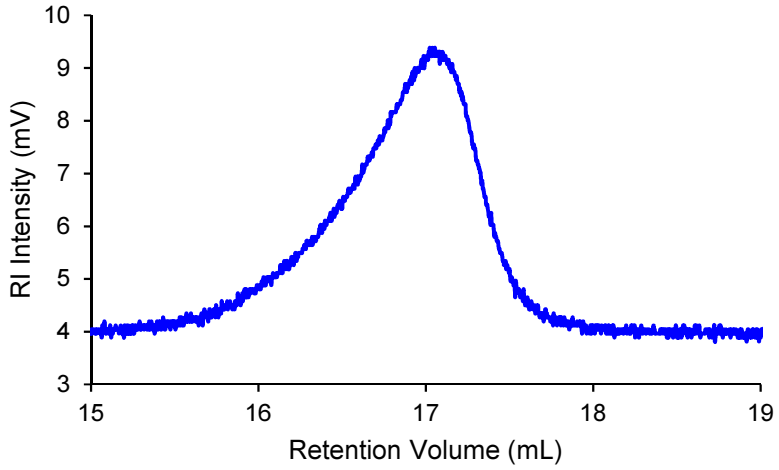

Figure S4.8. GPC chromatogram (2mg mL^{-1}) $[Ph(CH_2)_4NH–BH_2]_n$ in THF (0.1 *w/w* % nBu$_4$NBr) of the product of the reaction of $Ph(CH_2)_4NH_2{\cdot}BH_3$ and 2.5 mol % **[**$Rh(\mu\text{-}Cl)(1,5\text{-}COD)]_2$ after precipitation in THF (0.1 *w/w* % nBu$_4$NBr) at 20 °C after 180 min.

4.5.3.2.4 Dehydropolymerisation of $Ph(CH_2)_4NH_2{\cdot}BH_3$ with Rh/Al_2O_3 at Various Reaction Times.

To a solution of $Ph(CH_2)_4NH_2{\cdot}BH_3$ (163 mg, 1 mmol) in toluene (0.5 mL) in a vial was added Rh/Al_2O_3 (103 mg, ca. 5 w % Rh) at 20 °C. The solution was transferred to a Teflon-tapped J. Young quartz NMR tube and monitored by ^{11}B NMR at different reactions times at room temperature.

Analysis of the reaction of $Ph(CH_2)_4NH{\cdot}BH_3$ with 5 w % $[Rh/Al_2O_3]$ at 60 min and 240 min: ^{11}B NMR (THF): $[Ph(CH_2)_4NH]_2BH$ [δ_B 27.2 (br)], $[Ph(CH_2)_2NH–BH_2]_n$ [δ_B −6.9 (br)] and $Ph(CH_2)_4NH_2{\cdot}BH_3$ [δ_B −19.0 (br)] (Figure S4.9 and Table S4.5).

Table S4.5*:* Influence of reaction time on the dehydropolymerisation of $Ph(CH_2)_4NH_2{\cdot}BH_3$ in THF at 20 °C with 2.5 mol % $[Rh/Al_2O_3]$.

Time	Conversion [%][a]	Yield [%][b]	
	$Ph(CH_2)_4NH_2{\cdot}BH_3$	$[Ph(CH_2)_2NH–BH_2]_n$	$[Ph(CH_2)_4NH]_2BH$
60 min	1	0	1
240 min	9	1	8

a) Conversion determined by ^{11}B NMR spectroscopy. b) Yields determined by integration of the signals in the ^{11}B NMR spectra of the reaction mixtures.

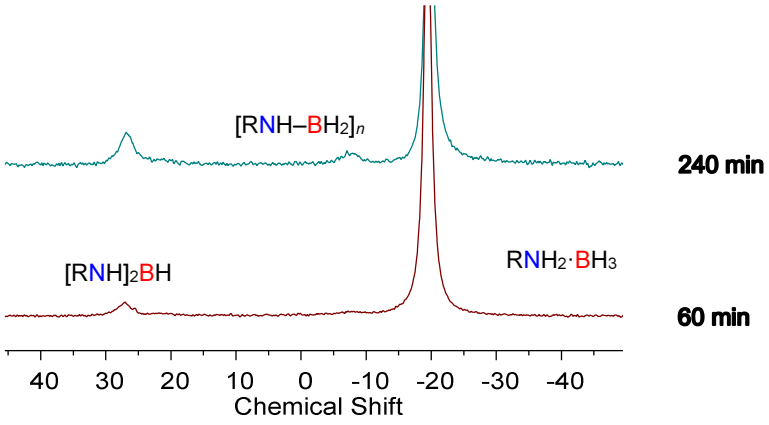

Figure S4.9. $^{11}B\{^1H\}$ NMR spectra of the reaction of $Ph(CH_2)_4NH_2{\cdot}BH_3$ and 2.5 mol % of $[Rh/Al_2O_3]$ in THF at 20 °C at 60 min and 240 min. R = $Ph(CH_2)_4$.

4.5.3.3 Dehydropolymerisation of $Ph(CH_2)_4NH_2{\cdot}BH_3$ with 1.0 mol % $[IrH_2(POCOP)]$ at Various Reaction Times.

4.5.3.3.1 Dehydropolymerisation at Room Temperature.

To a solution of $Ph(CH_2)_4NH_2{\cdot}BH_3$ (82 mg, 0.5 mmol) in THF (0.1 mL) was added a solution of $[IrH_2(POCOP)]$ (1.0 mol %, 3 mg) in THF (0.1 mL) at 20 °C. The solution was transferred to a Teflon-tapped J. Young quartz NMR tube and monitored by ^{11}B NMR at different reactions times at 20 °C.

Analysis of the reaction of $Ph(CH_2)_4NH_2{\cdot}BH_3$ (1a) with 1.0 mol % $[IrH_2(POCOP)]$ at 15 min, 30 min and 45min: ^{11}B NMR (THF): $[Ph(CH_2)_4NH]_2BH$ [δ_B 26.9 (br)] and $[Ph(CH_2)_4N–BH]_3$ [δ_B ca. 32 (br)], $[Ph(CH_2)_4NH–BH_2]_n$ [δ_B −7.5 (br)] (*ca.* 20 %) and $Ph(CH_2)_4NH_2{\cdot}BH_3$ [δ_B −19.8] (Figure S4.10 and Table S4.6).

Table S4.6*:* Influence of different reaction times on the dehydropolymerisation of $Ph(CH_2)_4NH_2{\cdot}BH_3$ in THF at 20 °C with 1.0 mol % $[IrH_2(POCOP)]$.

Time	Conversion [%][a]	Yield [%][b]	
	$Ph(CH_2)_4NH_2{\cdot}BH_3$	$[Ph(CH_2)_2NH–BH_2]_n$	$[Ph(CH_2)_4NH]_2BH$
15 min	63	25	38
30 min	92	31	61[c]
45 min	90	28	62[c]

a) Conversion determined by ^{11}B NMR spectroscopy. b) Yields determined by integration of the signals in the ^{11}B NMR spectra of the reaction mixtures. c) Mixture of $[Ph(CH_2)_4NH]_2BH$/$[Ph(CH_2)_4N–BH]_3$. The signals observed by $^{11}B\{^1H\}$ NMR spectroscopy are overlapping for these products.

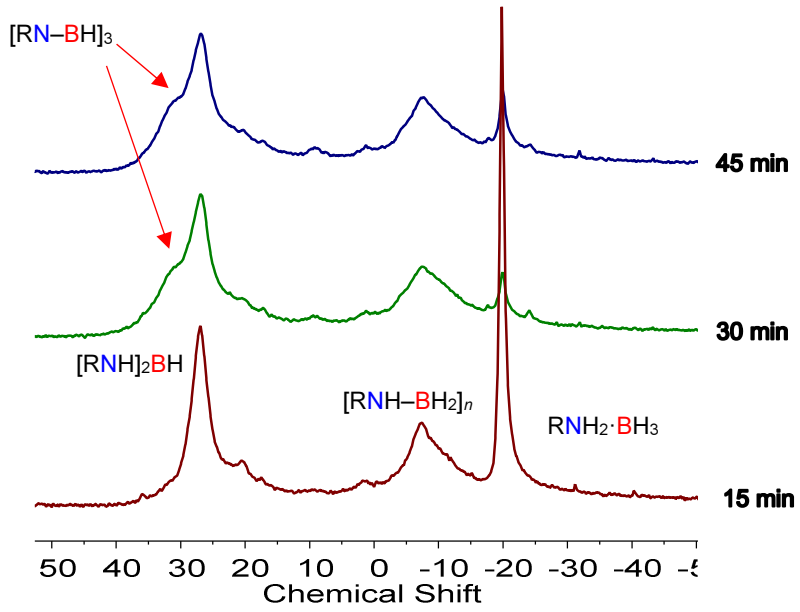

Figure S4.10. $^{11}B\{^1H\}$ NMR spectra of the reaction of $Ph(CH_2)_4NH_2{\cdot}BH_3$ and 1.0 mol % of $[IrH_2(POCOP)]$ in THF at 20 °C at 15 min, 30 min and 45min. R = $Ph(CH_2)_4$.

4.5.3.3.2 Dehydropolymerisation at low temperature.

To a solution of $Ph(CH_2)_4NH_2 \cdot BH_3$ (82 mg, 0.5 mmol) in THF (0.1 mL) at −40 °C, was added a solution of $[IrH_2(POCOP)]$ (1.0 mol %, 3 mg) in THF (0.1 mL) at −40 °C and it was stirred until reaction mixture reached room temperature (20 °C). The solution was transferred to a Teflon-tapped J. Young quartz NMR tube and monitored by ^{11}B NMR at different reaction times at 20 °C.

Analysis of the reaction of $Ph(CH_2)_4NH_2 \cdot BH_3$ (1a) with 1.0 mol % $[IrH_2(POCOP)]$ at 30 min and 60 min: ^{11}B NMR (THF): $[Ph(CH_2)_4NH]_2BH$ [δ_B 26.6 (br)] and $[Ph(CH_2)_4N–BH]_3$ [δ_B ca. 32 (br)], $[Ph(CH_2)_4NH–BH_2]_n$ [δ_B −8.7 (br)] and $Ph(CH_2)_4NH_2 \cdot BH_3$ [δ_B −20.0] and an unassigned product [δ_B −24.2] (Figure S4.11 and Table S4.7).

Table S4.7*:* Influence of reaction time on the dehydropolymerisation of $Ph(CH_2)_4NH_2 \cdot BH_3$ in THF at −40 °C with 1.0 mol % $[IrH_2(POCOP)]$.

Time	Conversion [%][a]	Yield [%][b]	
	$Ph(CH_2)_4NH_2 \cdot BH_3$	$[Ph(CH_2)_2NH–BH_2]_n$	$[Ph(CH_2)_4NH]_2BH$
30min	92	45	42[c]
60 min	91	43	44[c]

a) Conversion determined by ^{11}B NMR spectroscopy. b) Yields determined by integration of the signals in the ^{11}B NMR spectra of the reaction mixtures. c) Mixture of $[Ph(CH_2)_4NH]_2BH$/$[Ph(CH_2)_4N–BH]_3$. The signals observed by $^{11}B\{^1H\}$ NMR spectroscopy are overlapping for these products.

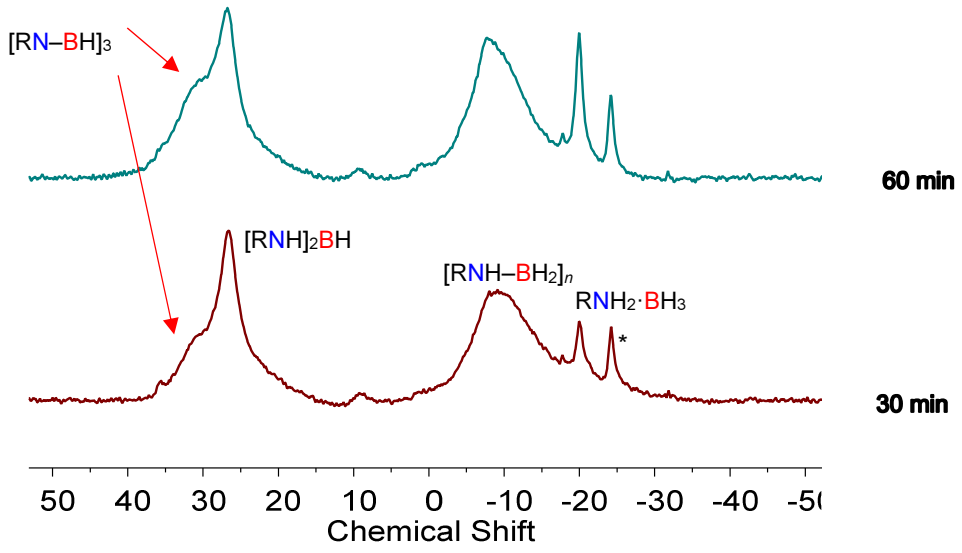

Figure S4.11. $^{11}B\{^1H\}$ NMR spectra from the reaction at low temperature (−40 °C) of $Ph(CH_2)_4NH_2 \cdot BH_3$ and 1.0 mol % of $[IrH_2(POCOP)]$ in THF at 20 °C at 30 min and 60 min. * Unassigned product. R = $Ph(CH_2)_4$.

4.5.3.4 Synthesis and characterisation of $[Ph(CH_2)_4NH–BH_2]_n$.

$Ph(CH_2)_4NH_2 \cdot BH_3$ (500 mg, 3.07 mmol) was dissolved in THF (0.6 mL) in a vial. In a separate vial, the catalyst [IrH_2(POCOP)] (18 mg, 30 μmol, 1 mol %) was dissolved in THF (0.6 mL). Both solutions were cooled to −40 °C. The solution with the catalyst was added slowly at low temperature to the amine-borane solution and immediate bubbling was observed. Then, the solution was allowed to warm up and stirred for 30 min. Then the reaction mixture was precipitated into hexanes (~20 mL) at room temperature and formation of a white solid was observed. The reaction mixture was decanted to remove the solvents and then dried under vaccum for ten minutes giving the polymer as a white powder. The polymer was redissolved in DCM (~1 mL) and the polymer was reprecipitated into hexanes for a second time to produce the polymer as a white solid. To remove any residual solvent that could be retained in the polymeric structure, the polymer was redissolved in DCM and reprecipitated into hexanes (~20 mL). After drying the polymer under vacuum (ca. 10^{-2} mmHg) for 18 h, no residual solvent was detected. (42% yield, 210 mg)

^{11}B NMR ($CDCl_3$): δ (ppm) −8.60 (Figure S4.12).

^{1}H NMR ($CDCl_3$): δ (ppm) 1.62-1.86 (m, 6H, Hc-Hb-B*H*$_2$); 2.45-2.76 (m, 5H, Ha-Hd, N*H*$_2$); 7.13-7.15 (m, 3H, Hg-Hh); 7.23-7.25 (m, 2H, Hf) (Figure S4.13).

^{13}C NMR ($CDCl_3$): δ (ppm) 27.8 (Cc); 29.3 (Cb); 35.7 (Cd); 50.7 (Ca); 125.7 (Ch); 128.3 (Cf-Cg); 142.3 (Ce) (Figure S4.14).

GPC: M_n = 168,300 g mol^{-1}, M_w = 195,200 g mol^{-1}, PDI = 1.16 (Figure S4.16).

FT-IR: ($\tilde{\nu}$ = cm^{-1}) 3252 (N–H); 3025 (C–H); 2928, 2857 (C–H_2); 2384,2295 (B–H) (Figure S4.53).

Elemental analysis calculated for $C_{10}H_{16}BN$: C, 74.6; H, 10.0; N, 8.7. Found: C, 74.5; H, 9.6; N, 8.7.

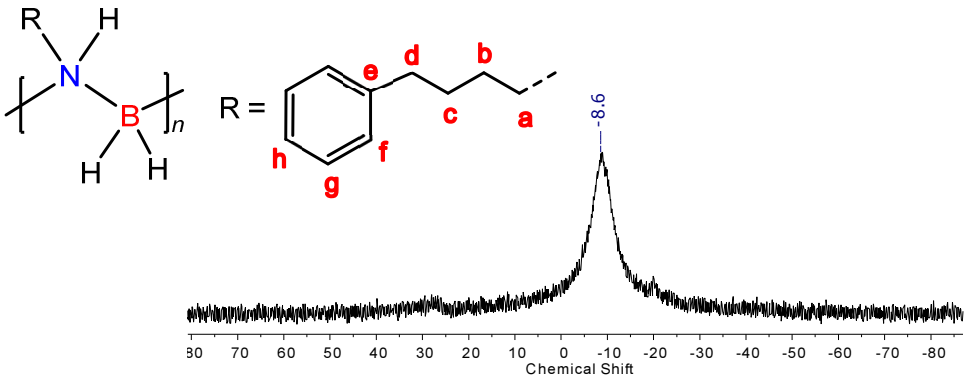

Figure S4.12. $^{11}B\{^{1}H\}$ NMR spectrum of isolated $[Ph(CH_2)_4NH–BH_2]_n$ in $CDCl_3$ at 20 °C.

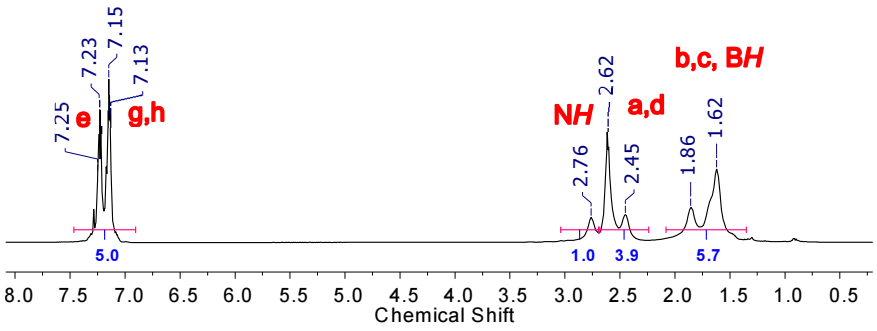

Figure S4.13. ^{1}H NMR spectrum of isolated $[Ph(CH_2)_4NH–BH_2]_n$ in $CDCl_3$ at 20 °C.

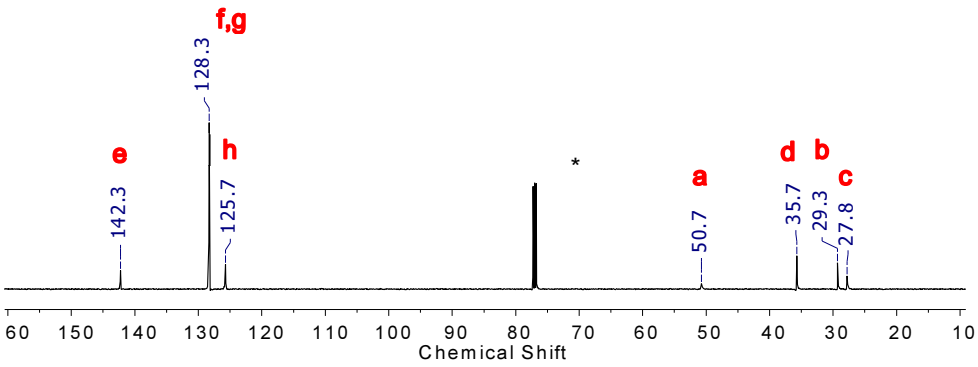

Figure S4.14. ^{13}C NMR spectrum of isolated $[Ph(CH_2)_4NH–BH_2]_n$ in $CDCl_3$ at 20 °C. * $CDCl_3$.

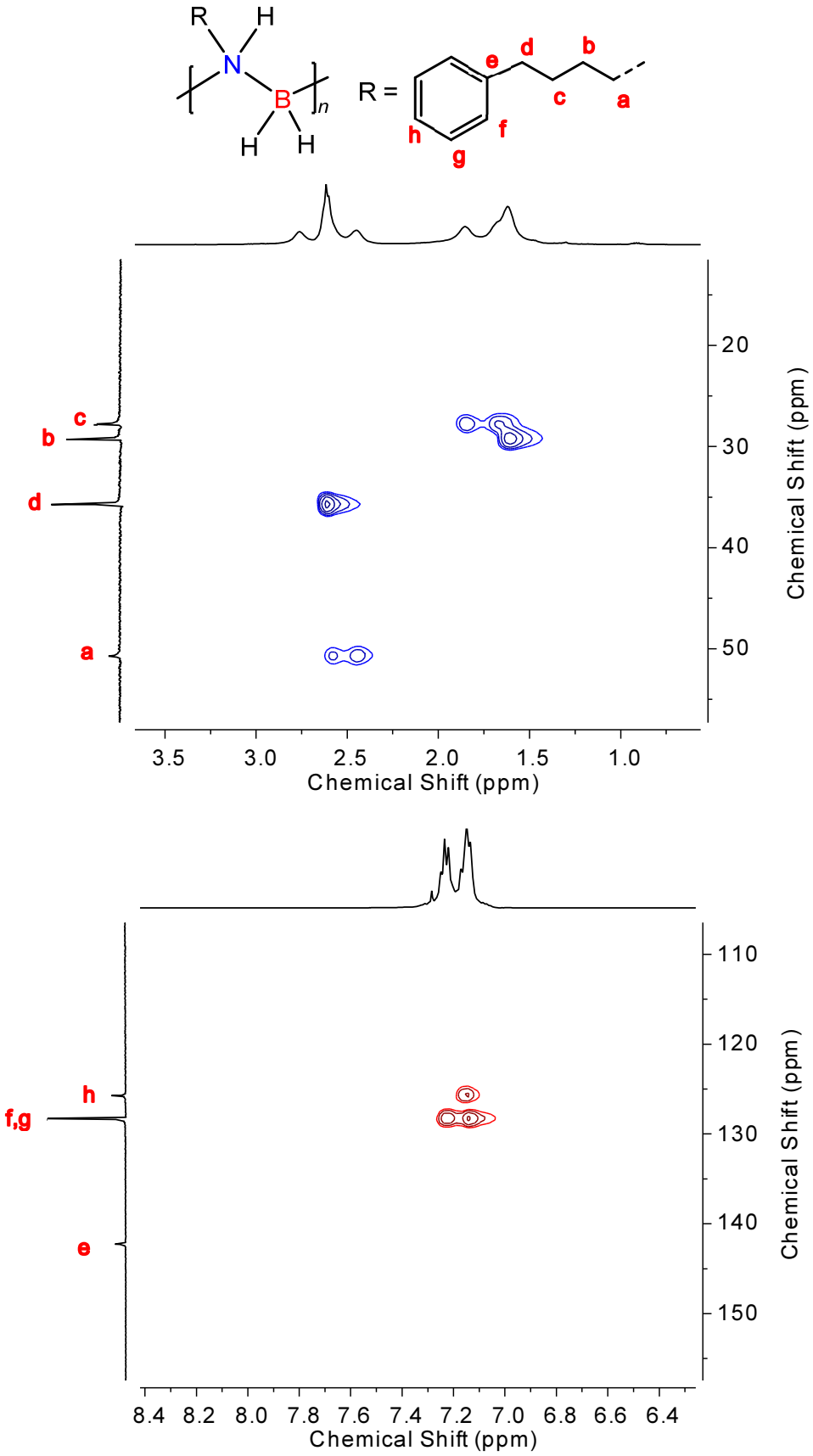

Figure S4.15. HSQC NMR spectrum of isolated $[Ph(CH_2)_4NH–BH_2]_n$ in $CDCl_3$ at 20 °C.

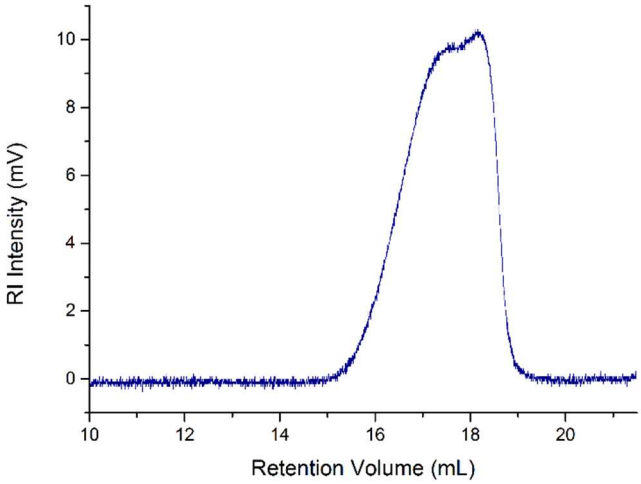

Figure S4.16. GPC chromatogram (2mg mL^{-1}) of isolated $[Ph(CH_2)_4NH–BH_2]_n$ in THF (0.1 *w/w* % nBu_4NBr).

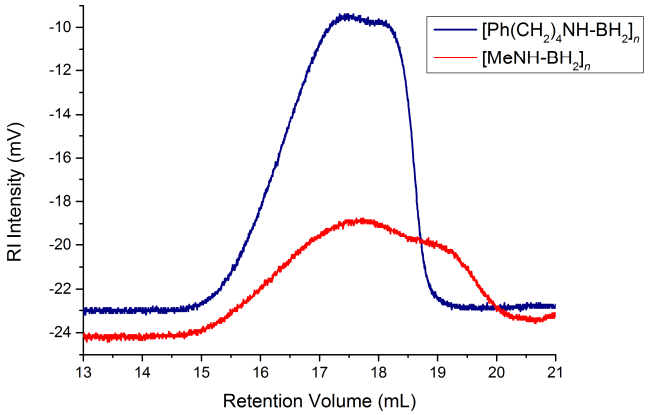

Figure S4.17. GPC chromatogram (2 mg mL^{-1}) of isolated $[Ph(CH_2)_2NH–BH_2]_n$ (Blue trace) [GPC (M_n = 150,000 g mol^{-1}, M_w = 181,600 g mol^{-1}, PDI = 1.21)] and isolated $[MeNH–BH_2]_n$ (Red trace) [GPC (M_n = 82,300 g mol^{-1}, M_w = 151,500 g mol^{-1}, PDI = 1.81)] produced from $MeNH_2{\cdot}BH_3$ and 3 mol % IrH_2POCOP in THF at 20˚C in THF (0.1 *w/w* % nBu_4NBr).

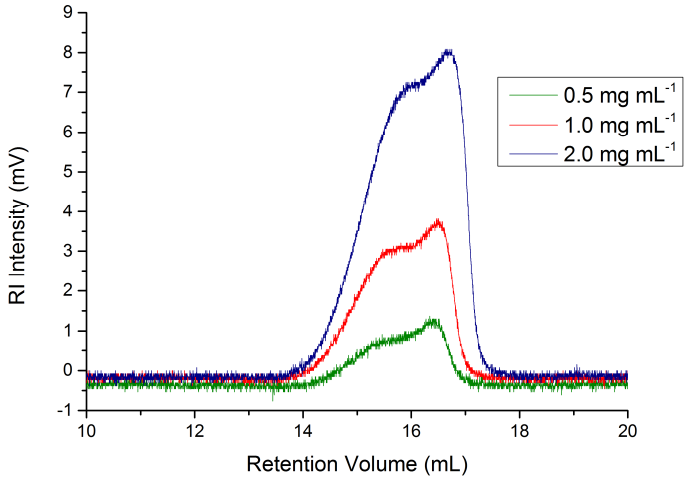

Figure S4.18. GPC chromatograms of $[Ph(CH_2)_4NH–BH_2]_n$ in THF (0.1 *w/w* % nBu_4NBr) at different concentrations.

Table S4.8: Number average molecular weight (M_n), mass average molecular weight (M_w) and polydispersity index (PDI) for $[Ph(CH_2)_4NH–BH_2]_n$ at different concentrations

c **(mg mL^{-1})**	***M*$_n$ (g mol^{-1})**	***M*$_w$ (g mol^{-1})**	**PDI**
0.5	186,600	206,500	1.11
1.0	188,300	213,800	1.14
2.0	168,300	195,200	1.16

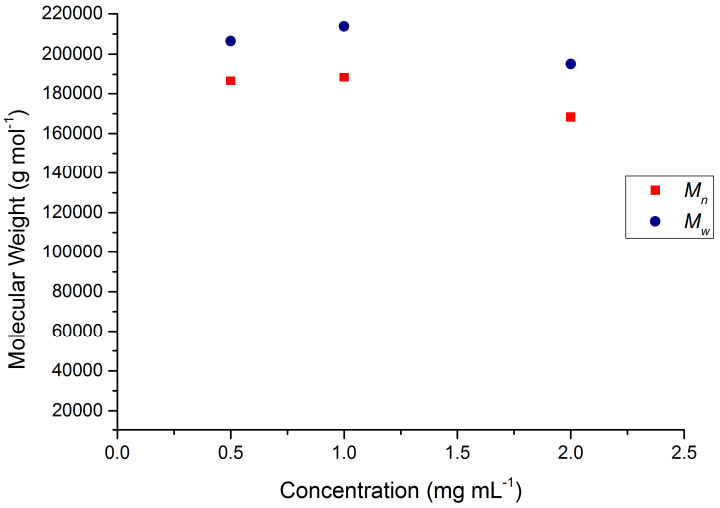

Figure S4.19. Plot of the molecular weight of $[Ph(CH_2)_4NH–BH_2]_n$ versus the concentration in THF.

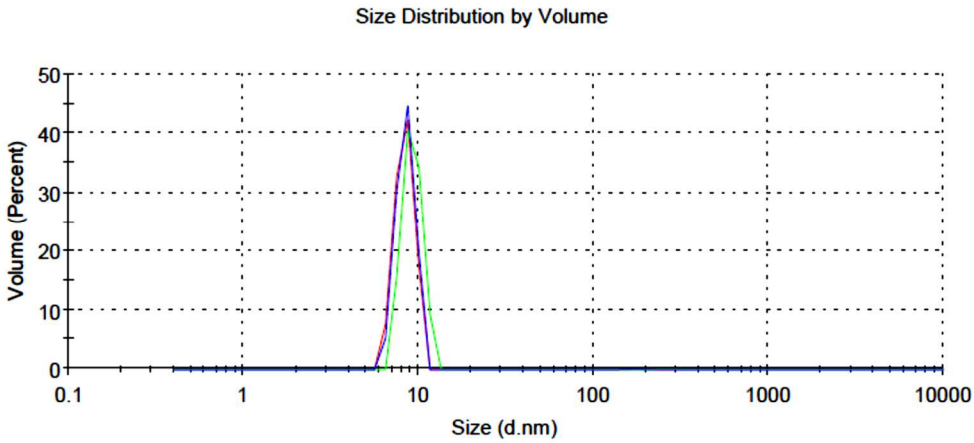

Figure S4.20. DLS (size distribution by volume, repeat scans) of $[Ph(CH_2)_4NH–BH_2]_n$ (2 mg mL^{-1}) in THF [R_H = 4.3 nm (average value)] at 20 °C.

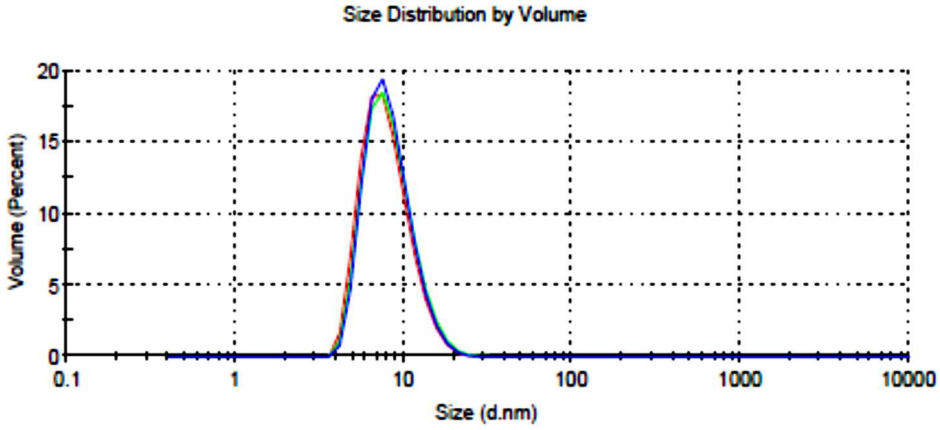

Figure S4.21. DLS (size distribution by volume, repeat scans) of $[Ph(CH_2)_4NH–BH_2]_n$ (2 mg mL^{-1}) in THF (0.1 *w/w* % nBu$_4$NBr). [R_H = 4.1 nm (average value)] at 20 °C.

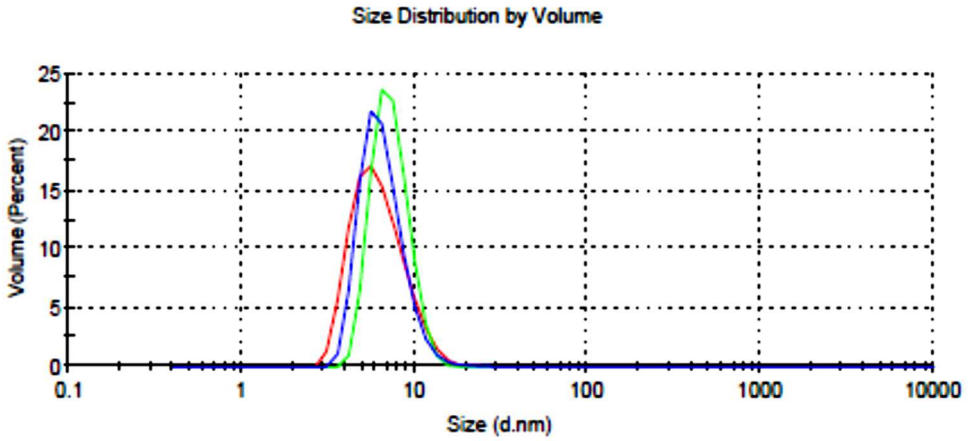

Figure S4.22 DLS (size distribution by volume, repeat scans) of $[Ph(CH_2)_4NH–BH_2]_n$ (2 mg mL^{-1}) in THF (0.1 *w/w* % nBu$_4$NBr). [R_H = 3.3 nm (average value)] at 35 °C.

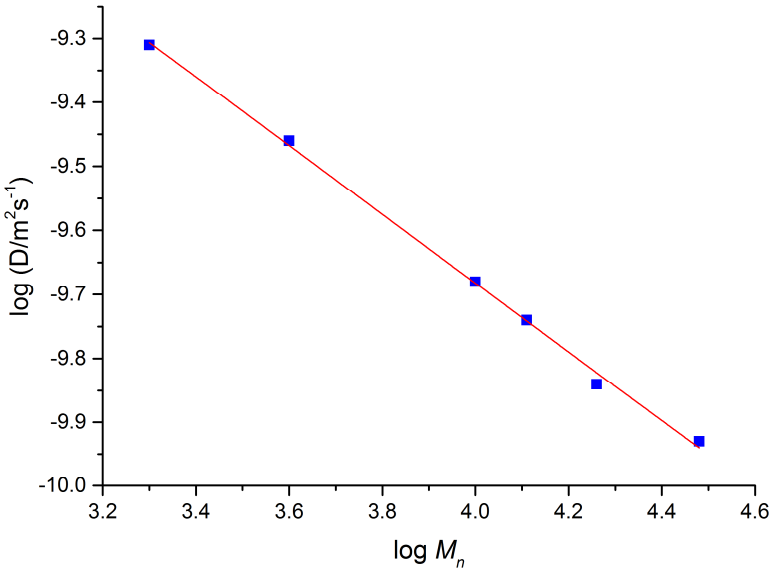

Figure S4.23. Polystyrene standard calibration curve in C_6D_6 for molecular weight prediction. Equation of the polystyrene standard calibration curve is log D = -0.5372 log M_n – 7.5335.

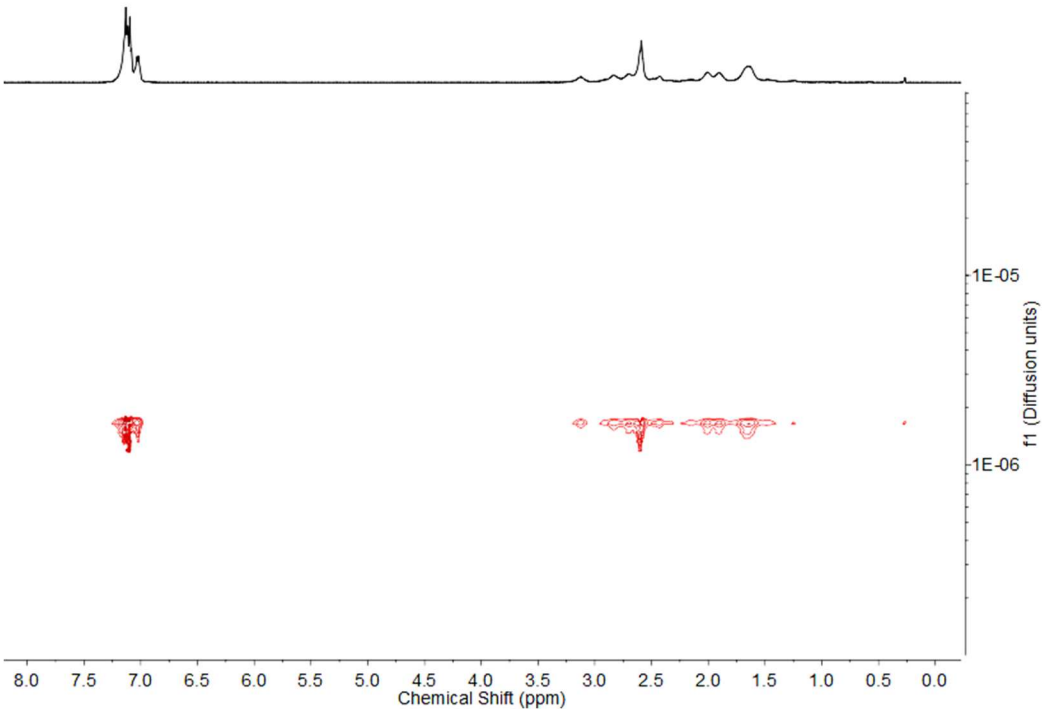

Figure S4.24. ^{1}H DOSY spectrum of isolated $[Ph(CH_2)_4NH–BH_2]_n$ (2b) in C_6D_6 at 20 °C.

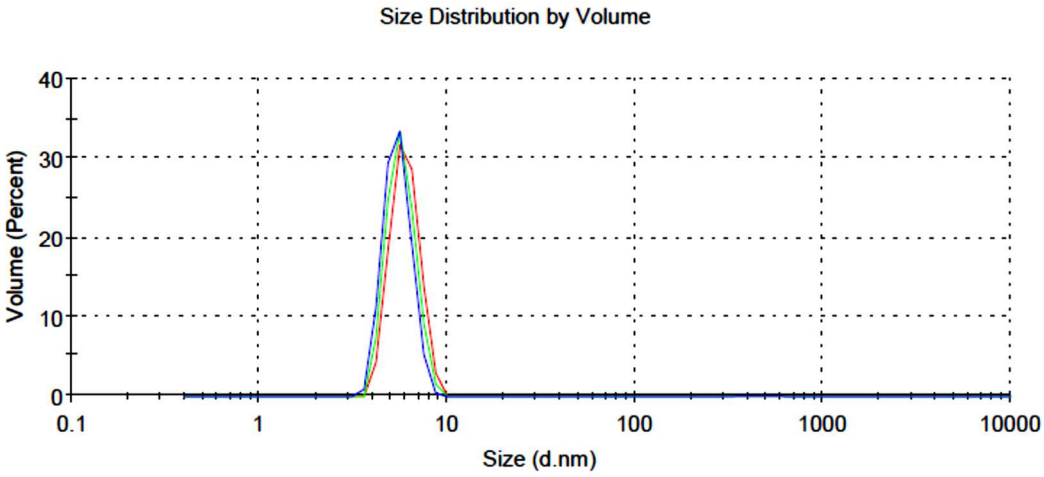

Figure S4.25. DLS (size distribution by volume, repeat scans) of $[Ph(CH_2)_4NH–BH_2]_n$ (2 mg mL^{-1}) in C_6H_6 [R_H = 2.9 nm (average value)] at 20 °C.

4.5.4 Dehydropolymerisation Studies of $PhCH_2NH_2{\cdot}BH_3$ Using Different Catalysts (Skeletal Nickel, $[Rh(\mu\text{-Cl})(1,5\text{-COD})]_2$ and $[IrH_2(POCOP)]$).

To a solution of $PhCH_2NH_2{\cdot}BH_3$ (121 mg, 1.0 mmol) in THF (0.5 mL) was added skeletal nickel (5 mol %, 3 mg) at 20 °C. The solution was transferred to a Teflon-tapped J. Young quartz NMR tube and monitored by ^{11}B NMR, no reaction was observed after 24 h.

To a solution of $PhCH_2NH_2{\cdot}BH_3$ BH_3 (121 mg, 1.0 mmol) in THF (0.5 mL) was added skeletal nickel (100 mol %, 59 mg) at 20 °C. The solution was transferred to a Teflon-tapped J. Young quartz NMR tube and monitored by ^{11}B NMR, no reaction was observed after 24 h.

To a solution of $PhCH_2NH_2{\cdot}BH_3$ (121 mg, 1.0 mmol) in THF (0.3 mL) was added a solution of $[IrH_2(POCOP)]$ (1.0 mol %, 6 mg) in THF (0.2 mL) at 20 °C. The solution was transferred to a Teflon-tapped J. Young quartz NMR tube and monitored by ^{11}B NMR, no reaction was observed after 24 h.

To a solution of $PhCH_2NH_2{\cdot}BH_3$ (121 mg, 1.0 mmol) in THF (0.3 mL) was added a solution of $[Rh(\mu\text{-Cl})(1,5\text{-COD})]_2$ (2.5 mol %, 12 mg) in toluene (0.2 mL) at 20 °C. The solution was

transferred to a Teflon-tapped J. Young quartz NMR tube and monitored by ^{11}B NMR, no reaction was observed after 24 h.

As an example, here is shown the analysis of the reaction of $PhCH_2NH_2{\cdot}BH_3$ with 1.0 mol % [IrH_2(POCOP)]: ^{11}B NMR (THF): $PhCH_2NH_2{\cdot}BH_3$ [δ_B −19.6] (*ca.* 100%) (Figure S4.26).

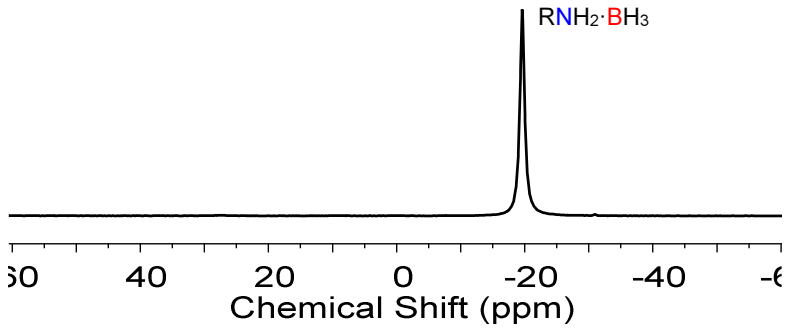

Figure S4.26. ^{11}B{^{1}H} NMR spectrum of the reaction of $PhCH_2NH_2{\cdot}BH_3$ and 1.0 mol % of [IrH_2(POCOP)] in THF at 20 °C at 30 min. R = $PhCH_2$

4.5.5 Dehydropolymerisation Studies of $Ph(CH_2)_xNH_2{\cdot}BH_3$ (x = 2–3) Using [IrH_2(POCOP)].

To a solution of $Ph(CH_2)_2NH_2{\cdot}BH_3$ (68 mg, 0.5 mmol) in THF (0.1 mL) was added a solution of [IrH_2(POCOP)] (3 mg, 1.0 mol %) in THF (0.1 mL) at −40 °C. Then, the solution was allowed to warm up and stirred. The solution was diluted with 0.3 mL of THF and was transferred to a Teflon-tapped J. Young quartz NMR tube and monitored by ^{11}B NMR at room temperature (20 °C).

Analysis of the reaction of $Ph(CH_2)_2NH{\cdot}BH_3$ (1a) with 1.0 mol % [IrH_2(POCOP)] at 30 min: ^{11}B NMR (THF): $[Ph(CH_2)_2NH]_2BH$ [δ_B 27.1 (br)] and $[Ph(CH_2)_2N–BH]_3$ [δ_B ca. 32 (br)] (*ca.* 27%), $[Ph(CH_2)_2NH–BH_2]_n$ [δ_B −8.6 (br)] (*ca.* 57%) and $Ph(CH_2)_2NH_2{\cdot}BH_3$ [δ_B −20.3] (*ca.* 16%) (Figure S4.27).

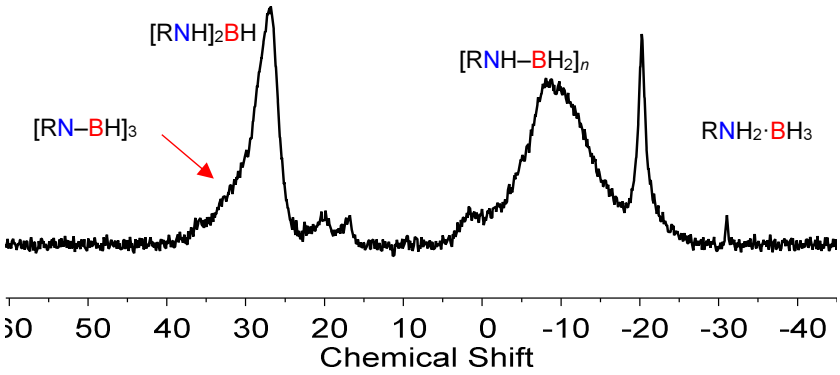

Figure S4.27. $^{11}B\{^1H\}$ NMR spectrum of the reaction of $Ph(CH_2)_2NH_2{\cdot}BH_3$ and 1.0 mol % of $[IrH_2(POCOP)]$ in THF at 20 °C at 30 min. R = $Ph(CH_2)_2$.

To a solution of $Ph(CH_2)_3NH_2{\cdot}BH_3$ (74 mg, 0.5 mmol) in THF (0.1 mL) was added a solution of $[IrH_2(POCOP)]$ (3 mg, 1.0 mol%) in THF (0.1 mL) −40 °C. Then, the solution was allowed to warm up and stirred for 30 min. The solution was diluted with 0.3 mL of THF and was transferred to a Teflon-tapped J. Young quartz NMR tube and monitored by ^{11}B NMR at room temperature (20 °C).

Analysis of the reaction of $Ph(CH_2)_3NH_2{\cdot}BH_3$ (1a) with 1.0 mol % $[IrH_2(POCOP)]$ at 30 min: ^{11}B NMR (THF): $[[Ph(CH_2)_3NH]_2BH$ [δ_B 26.8 (br)] (*ca.* 10%), $[Ph(CH_2)_3NH–BH_2]_n$ [δ_B −8.9 (br)] (*ca.* 32%) and $Ph(CH_2)_3NH_2{\cdot}BH_3$ [δ_B −20.3] (*ca.* 59%) (Figure S4.28).

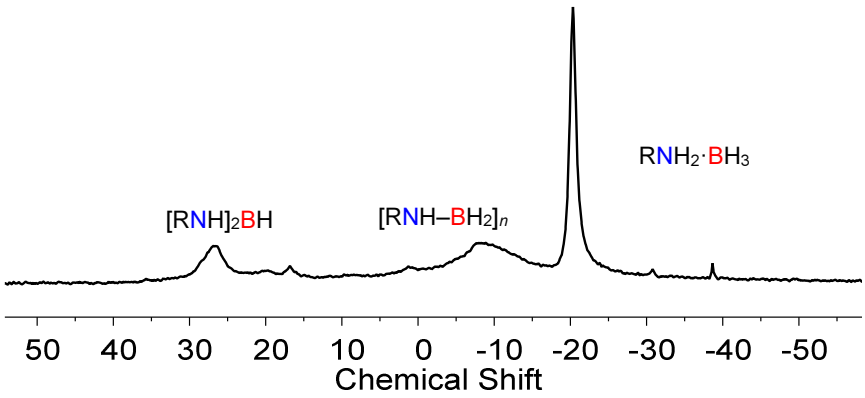

Figure S4.28. $^{11}B\{^1H\}$ NMR spectrum of the reaction of $Ph(CH_2)_3NH_2{\cdot}BH_3$ and 1 mol % of $[IrH_2(POCOP)]$ in THF at 20 °C after 30 min. R = $Ph(CH_2)_3$.

4.5.5.1 Synthesis and Characterisation of $[Ph(CH_2)_2NH–BH_2]_n$.

$Ph(CH_2)_2NH_2 \cdot BH_3$ (405 mg, 3.00 mmol) was dissolved in THF (0.6 mL) in a vial. In a separate vial, the catalyst IrH_2(POCOP) (18 mg, 30 µmol, 1 mol %) was dissolved in THF (0.6 mL). Both solutions were cooled to −40 °C. The solution with the catalyst was added slowly at low temperature (−40 °C) to the amine-borane solution and immediate bubbling was observed. Then, the solution was allowed to warm up to 20 °C and stir for 30 min. Then the reaction mixture was precipitated into hexanes (~20 mL) at room temperature and formation of a white solid was observed. The reaction mixture was decanted to remove the solvents and then dried under vaccum for ten minutes giving the polymer as a white powder. The polymer was redissolved in DCM (~1 mL) and the polymer was reprecipitated into hexanes for a second time to produce the polymer as a white solid, which was dried overnight under vacuum. (42% yield, 210 mg)

^{11}B NMR ($CDCl_3$): δ (ppm) −8.7 (Figure S4.29).

^{1}H NMR ($CDCl_3$): δ (ppm) 1.88-2.19 (m, 2H, B*H*$_2$); 2.71-3.24 (m, 5H, Ha-Hb-N*H*); 7.25 (br s; 5H, Hd-He-Hf) (Figure S4.30).

^{13}C NMR ($CDCl_3$): δ (ppm) 34.6 (Cb); 52.2 (Ca); 126.5 (Cf); 128.7 (Cd); 129.1 (Ce); 139.0 (Cc) (Figure S4.31).

GPC: M_n = 158,800 g mol^{-1}, M_w = 199,000 g mol^{-1}, PDI = 1.25 (Figure S4.33).

FT-IR: ($\tilde{\nu}$ = cm^{-1}) 3247 (N–H); 3026 (C–H); 2950 (C–H_2); 2388,2303 (B–H) (Figure S4.52).

Elemental analysis calculated for $C_8H_{12}BN$: C, 72.3; H, 9.1; N, 10.5. Found: C, 72.1; H, 9.1; N, 10.6.

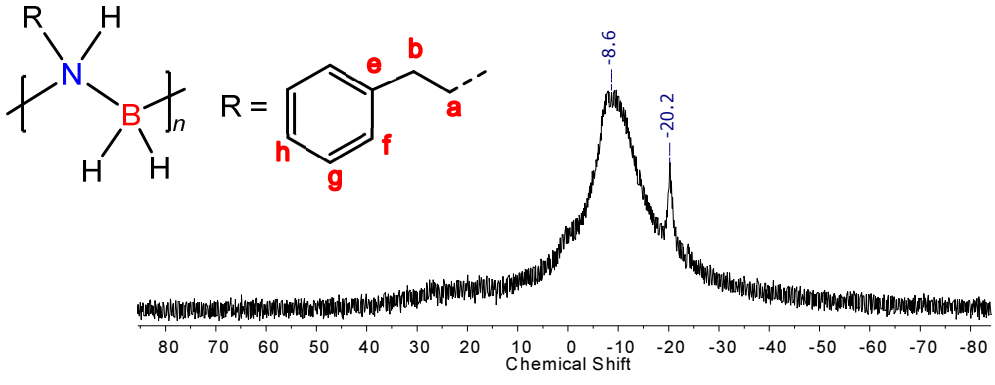

Figure S4.29. ^{11}B{^{1}H} NMR spectrum of isolated $[Ph(CH_2)_2NH–BH_2]_n$ in $CDCl_3$ at 20 °C.

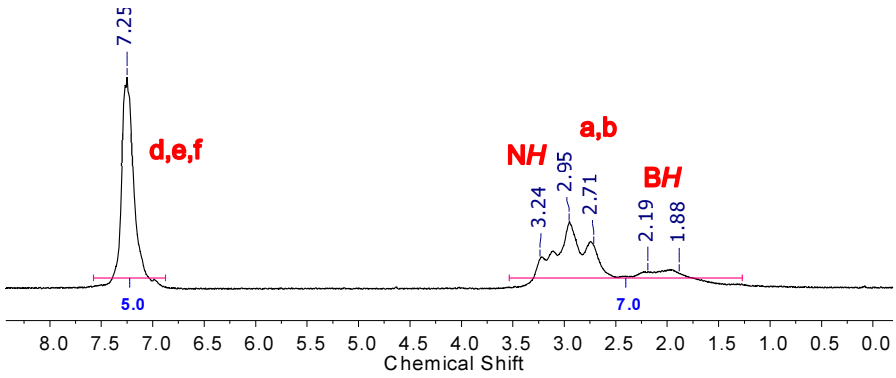

Figure S4.30. ^{1}H NMR spectrum of isolated $[Ph(CH_2)_2NH–BH_2]_n$ in $CDCl_3$ at 20 °C.

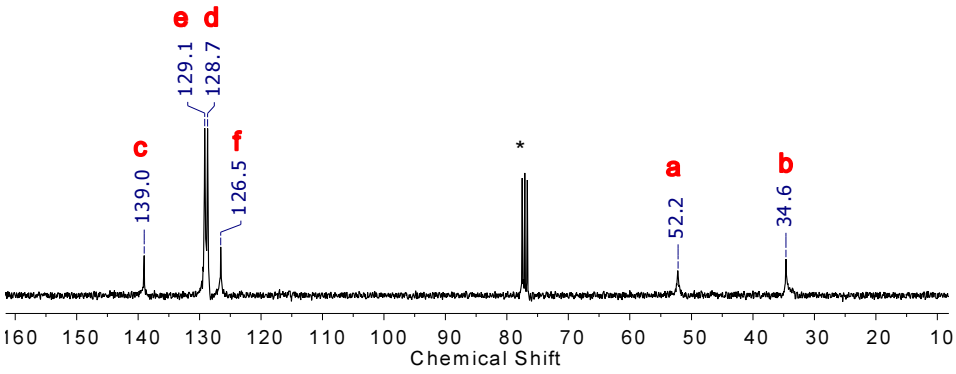

Figure S4.31. ^{13}C NMR spectrum of isolated $[Ph(CH_2)_2NH–BH_2]_n$ in $CDCl_3$ at 20 °C. * $CDCl_3$.

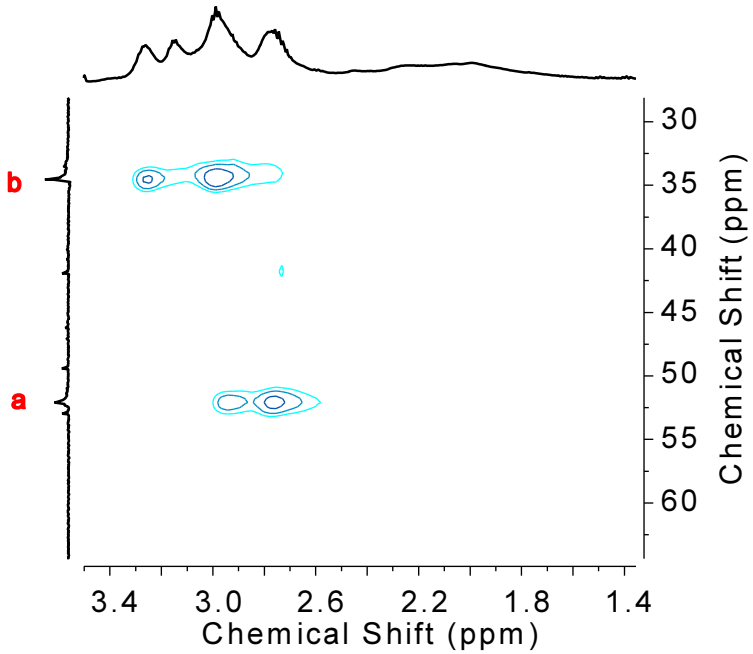

Figure S4.32. HSQC NMR spectrum of isolated $[Ph(CH_2)_2NH–BH_2]_n$ in $CDCl_3$ at 20 °C.

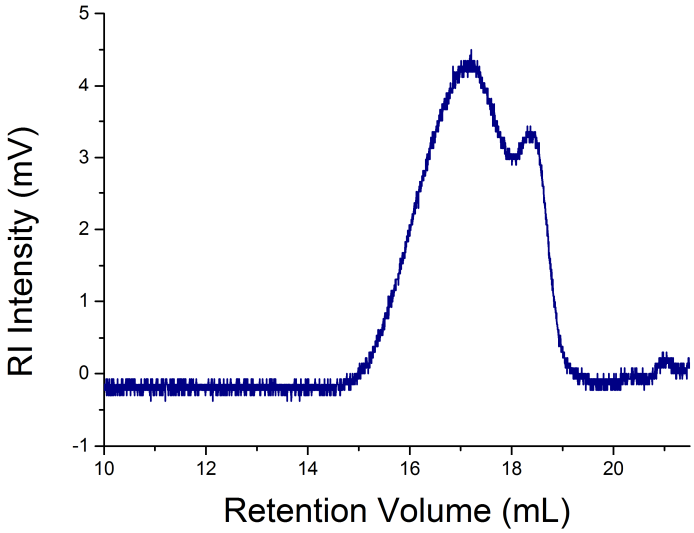

Figure S4.33. GPC chromatogram (2mg mL^{-1}) of isolated $[Ph(CH_2)_2NH–BH_2]_n$ in THF (0.1 *w/w* % nBu_4NBr).

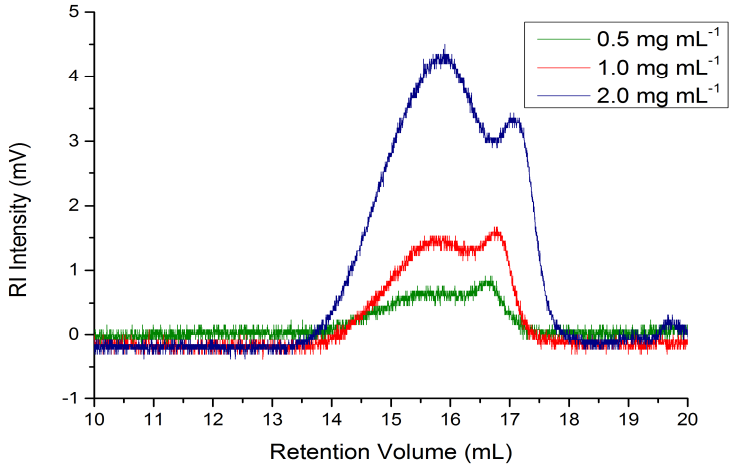

Figure S4.34 GPC chromatograms of $[Ph(CH_2)_2NH–BH_2]_n$ in THF (0.1 *w/w* % nBu_4NBr) at different concentrations.

Table S4.9: Number average molecular weight (M_n), mass average molecular weight (M_w) and polydispersity index (PDI) for $[Ph(CH_2)_2NH–BH_2]_n$ at different concentrations

c **(mg mL^{-1})**	***M_n*** **(g mol^{-1})**	***M_w*** **(g mol^{-1})**	**PDI**
0.5	181,500	209,900	1.16
1.0	172,200	203,300	1.18
2.0	158,800	199,000	1.25

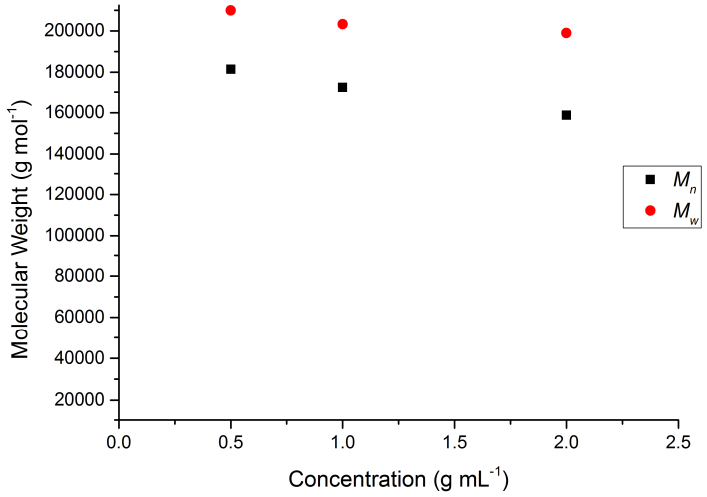

Figure S4.35. Plot of the molecular weight of $[Ph(CH_2)_2NH–BH_2]_n$ versus the concentration in THF.

4.5.6 Synthesis and Characterisation of Copolymers

$[Ph(CH_2)_4NH–BH_2]_n$–*r*– $[NH_2–BH_2]_m$ and $[Ph(CH_2)_2NH–BH_2]_n$–*r*– $[Ph(CH_2)_4NH–BH_2]_m$ were prepared following the procedure described below for $[Ph(CH_2)_4NH–BH_2]_n$–*r*–$[MeNH–BH_2]_m$

$Ph(CH_2)_4NH_2·BH_3$ (224 mg, 1.50 mmol) and $MeNH_2·BH_3$ (67 mg, 1.50 mmol) were dissolved in THF (0.6 mL) in a vial. In a separate vial, the catalyst IrH_2(POCOP) (18 mg, 30 μmol, 1 mol %) was dissolved in THF (0.6 mL). Both solutions were cooled to −40 °C. The solution with the catalyst was added to the amine-boranes solution slowly at −40 °C and immediate bubbling was observed. Then, the solution was allowed to warm up to 20 °C and stir for 30 min. Then the reaction mixture was precipitated into hexanes (~20 mL) at 20 °C and formation of a white solid was observed. The supernatant was decanted and the precipitate dried under vaccum for ten minutes giving the polymer as a white powder. The polymer was redissolved in DCM (~1 mL) and the polymer was reprecipitated into hexanes (~20 mL) for a second time to produce the polymer as a white solid, which was dried overnight under vacuum. (45% yield, 150 mg).

**Copolymers $[Ph(CH_2)_4NH–BH_2]_n$–*r*– $[NH_2–BH_2]_m$ (n: 1, m: 1) and $[Ph(CH_2)_4NH–BH_2]_n$–*r*– $[NH_2–BH_2]_m$ (n: 1, m: 2) were prepared following a slightly modified procedure to above. For the ratio 1:1, the $NH_3 \cdot BH_3$ monomer solution in THF was added dropwise over a period of 30 min and for the ratio 1:2 was added over a period of 60 min in order to assure random formation of the copolymer is occurring.

4.5.6.1 Characterisation of Copolymer $[Ph(CH_2)_4NH–BH_2]_n$–*r*– $[NH_2–BH_2]_m$ (n: 1, m: 1).

^{11}B NMR ($CDCl_3$): δ (ppm) −9.2 (Figure S4.36).

^{1}H NMR ($CDCl_3$): δ (ppm) 1.57-1.81 (m, 6H, Hc-Hb-B*H*$_2$); 2.42-2.72 (m, 5H, Ha-Hd-N*H*); 7.09-7.12 (m, 3H, Hg-Hh); 7.17-7.20 (m, 2H, Hf) (Figure S4.37).

^{13}C NMR ($CDCl_3$): δ (ppm) 27.7 (Cc); 29.3 (Cb); 35.8 (Cd); 50.6 (Ca); 125.8 (Ch); 128.3 (Cf-Cg); 142.3 (Ce) (Figure S4.38).

GPC: M_n = 159,700 g mol^{-1}, M_w = 213,100 g mol^{-1}, PDI = 1.33 (Figure S4.39).

FT-IR: ($\tilde{\nu}$ = cm^{-1}) 3247 (N–H); 3026 (C–H); 2926, 2859 (C–H_2); 2387,2303 (B–H) (Figure S4.53).

Elemental analysis calculated for $C_{10}H_{20}B_2N_2$, corrected for a ratio (1:0.875): C, 64.5; H, 10.5; N, 14.1. Found: C, 64.2; H, 10.1; N, 14.0.

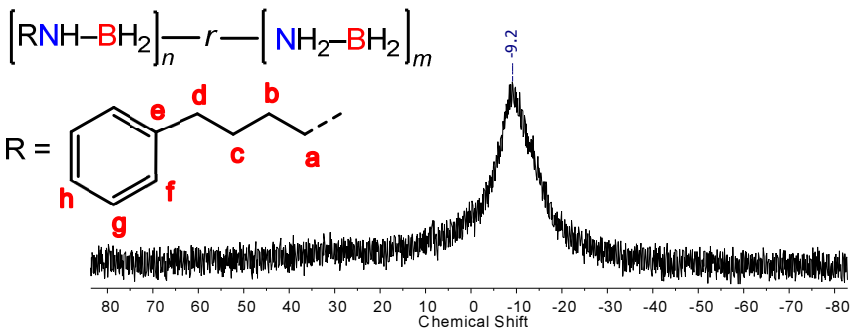

Figure S4.36. $^{11}B\{^{1}H\}$ NMR spectrum of isolated $[Ph(CH_2)_4NH–BH_2]_n$–*r*– $[NH_2–BH_2]_m$ (n: 1, m: 1) in $CDCl_3$ at 20 °C.

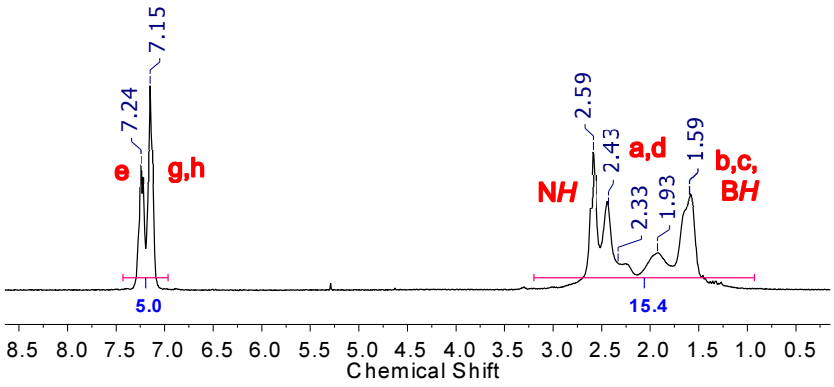

Figure S4.37. ^{1}H NMR spectrum of isolated $[Ph(CH_2)_4NH–BH_2]_n$–*r*– $[NH_2–BH_2]_m$ (n: 1, m: 1) in $CDCl_3$ at 20 °C.

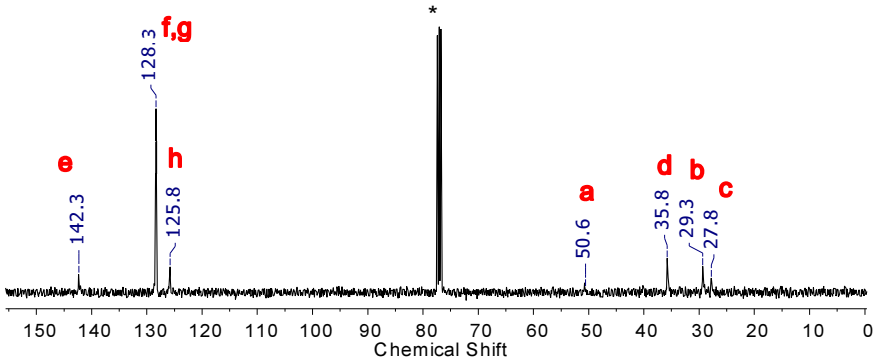

Figure S4.38. ^{13}C NMR spectrum of isolated $[Ph(CH_2)_4NH–BH_2]_n$–*r*– $[NH_2–BH_2]_m$ (n: 1, m: 1) in $CDCl_3$ at 20 °C. * $CDCl_3$.

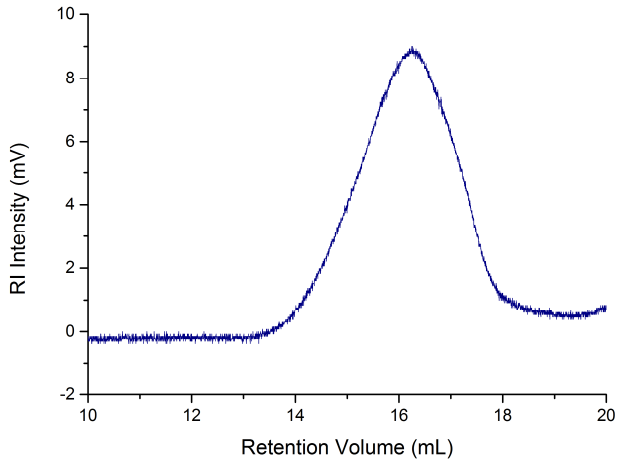

Figure S4.39. GPC chromatogram (2mg mL^{-1}) of isolated $[Ph(CH_2)_4NH–BH_2]_n$–*r*– $[NH_2–BH_2]_m$ (n: 1, m: 1) in THF (0.1 *w/w* % *n*Bu_4NBr).

4.5.6.2 Characterisation of Copolymer $[Ph(CH_2)_4NH–BH_2]_n–r–[NH_2–BH_2]_m$ (n: 1, m: 2).

^{11}B NMR (THF-d_8): δ (ppm) −12.7 (Figure S4.40).

^{1}H NMR (THF-d_8): δ (ppm) 1.59-2.01 (m, H, Hc-Hb-B*H*$_2$-B'*H*$_2$); 2.59-2.85 (m, H, Ha-Hd-N*H*$_2$); 7.16 (br s, 5H, Hf-Hg-Hh) (Figure S4.41).

^{13}C NMR (THF-d_8): δ (ppm) 25.8 (Cc); 27.5 (Cb); 33.9 (Cd); 49.0 (Ca); 123.8 (Ch); 126.3 (Cf-Cg); 140.4 (Ce) (Figure S4.42).

GPC: M_n = 162,100 g mol^{-1}, M_w = 208,400 g mol^{-1}, PDI = 1.28 (Figure S4.43).

FT-IR: $\tilde{\nu}$ = cm^{-1}) 3297, 3247 (N–H); 2929, 2858 (C–H$_2$); 2373,2302 (B–H) (Figure S4.53).

Elemental analysis calculated for $C_{10}H_{24}B_3N_3$: C, 54.9; H, 11.1; N, 19.2. Found: C, 54.9; H, 10.9; N, 18.9.

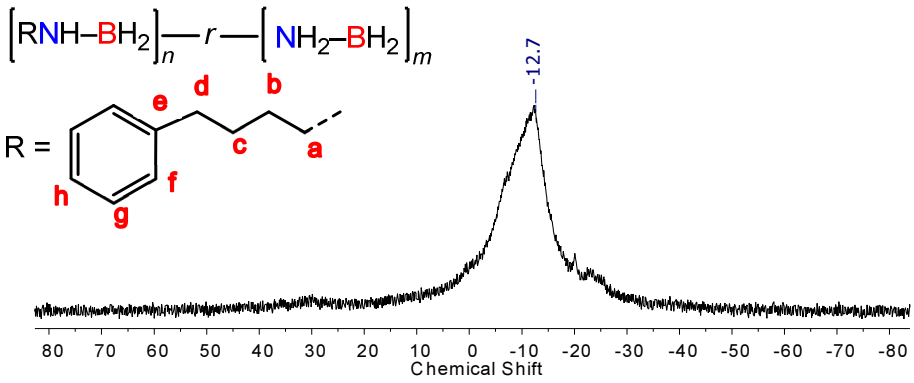

Figure S40. $^{11}B\{^1H\}$ NMR spectrum of isolated $[Ph(CH_2)_4NH–BH_2]_n–r–[NH_2–BH_2]_m$ (n: 1, m: 2) in THF-d_8 at 20 °C.

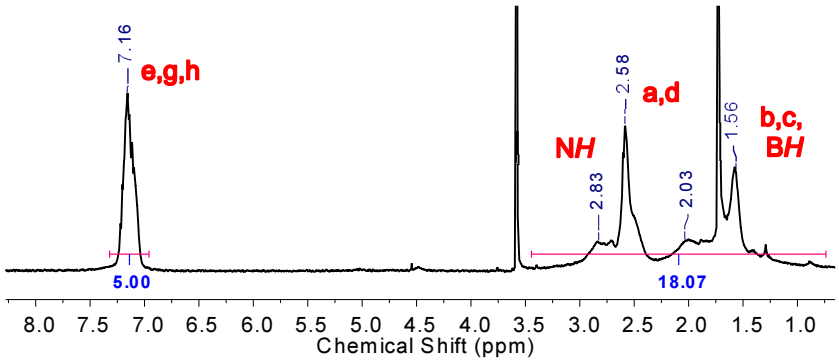

Figure S41. ^{1}H NMR spectrum of isolated $[Ph(CH_2)_4NH–BH_2]_n–r–[NH_2–BH_2]_m$ (n: 1, m: 2) in THF-d_8 at 20 °C.

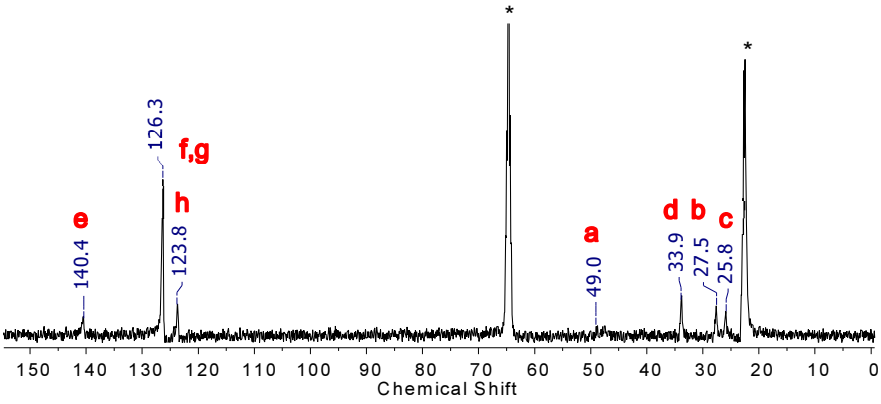

Figure S4.42. ^{13}C NMR spectrum of isolated $[Ph(CH_2)_4NH–BH_2]_n$–*r*– $[NH_2–BH_2]_m$ (n: 1, m: 2) in THF-d_8 at 20 °C. * THF-d_8.

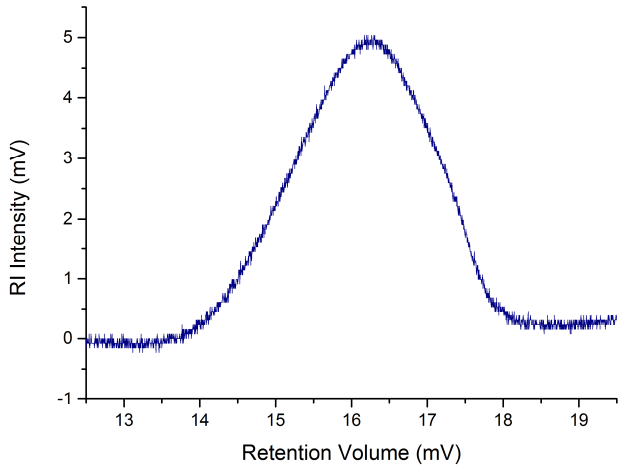

Figure S4.43. GPC (2mg mL^{-1}) chromatogram of isolated $[Ph(CH_2)_4NH–BH_2]_n$–*r*– $[NH_2–BH_2]_m$ (n: 1, m: 2) in THF (0.1 *w/w* % *n*Bu$_4$NBr).

4.5.6.3 Characterisation of Copolymer $[Ph(CH_2)_4NH–BH_2]_n$–*r*–$[MeNH–BH_2]_m$ (n: 1, m: 1.56).

^{11}B NMR ($CDCl_3$): δ (ppm) −7.7 (Figure S4.44).

^{1}H NMR ($CDCl_3$): δ (ppm) 1.63-1.75 (m, 8H, Hb-Hc-B*H*$_2$-B'*H*$_2$); 2.26 (s, 3H, Hi); 2.53-2.65 (m, 6H, H6-N'*H*$_2$); 2.90 (s, 1H, MeN*H*); 7.09-7.12 (m, 3H, Hg-Hh); 7.17-7.20 (m, 2H, Hf) (Figure S4.45).

^{13}C NMR ($CDCl_3$): δ (ppm) 27.5 (Cc); 29.1 (Cb); 35.6 (Cd); 36.0 (Ci); 50.3 (Ca); 125.7 (Ch); 128.4 (Cf-Cg); 142.2 (Ce) (Figure S4.46).

GPC: M_n = 170,100 g mol^{-1}, M_w = 200,700 g mol^{-1}, PDI = 1.18 (Figure S4.47).

FT-IR: ($\tilde{\nu}$ = cm^{-1}) 3260 (N–H); 2928, 2858 (C–H_2); 2373, 2294 (B–H) (Figure S4.53).

Elemental analysis calculated for $C_{11}H_{22}B_2N_2$, corrected for a ratio 1:1.45: C, 61.6; H, 11.1; N, 15.4. Found: C, 61.3; H, 11.2; N, 15.1.

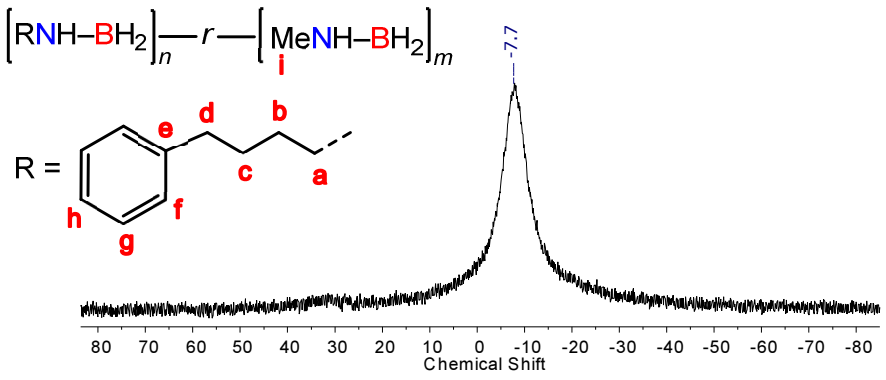

Figure S4.44. $^{11}B\{^1H\}$ NMR spectrum of isolated $[Ph(CH_2)_4NH–BH_2]_n$–*r*– $[MeNH–BH_2]_m$ (n: 1, m: 1.56) in $CDCl_3$ at 20 °C.

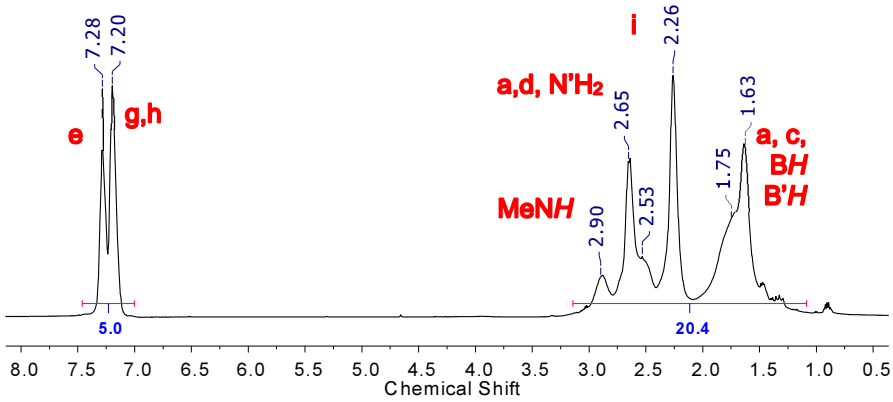

Figure S4.45. ^1H NMR spectrum of isolated $[Ph(CH_2)_4NH–BH_2]_n$–*r*– $[MeNH–BH_2]_m$ (n: 1, m: 1.56) in $CDCl_3$ at 20 °C.

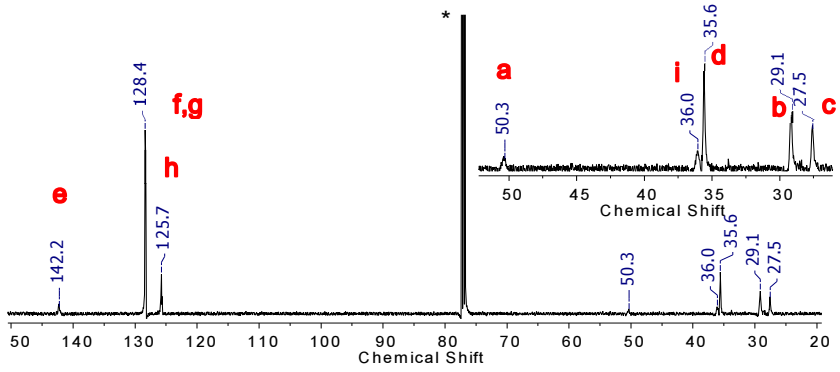

Figure S4.46. ^{13}C NMR spectrum of isolated $[Ph(CH_2)_4NH–BH_2]_n$–*r*– $[MeNH–BH_2]_m$ (n: 1, m: 1.56) in $CDCl_3$ at 20 °C. * $CDCl_3$.

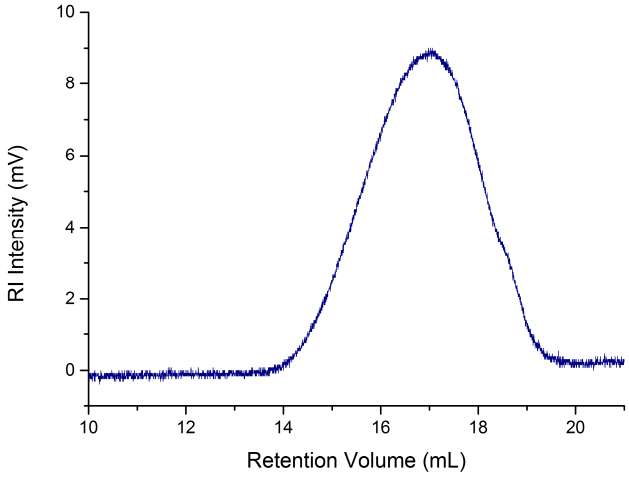

Figure S4.47. GPC chromatogram (2mg mL^{-1}) of isolated [Ph(CH$_2$)$_4$NH–BH$_2$]$_n$–*r*– [MeNH–BH$_2$]$_m$ (n: 1, m: 1.56) in THF (0.1 *w/w* % [*n*Bu$_4$N]Br).

4.5.6.4 Characterisation of Copolymer [Ph(CH$_2$)$_2$NH–BH$_2$]$_n$–*r*–[Ph(CH$_2$)$_4$NH–BH$_2$]$_m$ (n: 1, m: 1).

^{11}B NMR (CDCl$_3$): δ (ppm) −8.8 (Figure S4.48).

^{1}H NMR (CDCl$_3$): δ (ppm) 1.65-1.89 (m, 8H, Hb-Hc- B*H$_2$*-B'*H$_2$*); 2.62-3.14 (m, 10H Ha-Hd-Hi-Hj- N*H$_2$*-N'*H$_2$*); 7.21 (br s, 5H, Hf-Hg-Hh-Hl-Hm-Hn) (Figure S4.49).

^{13}C NMR (CDCl$_3$): δ (ppm) 27.8 (Cc); 29.3 (Cb); 34.4 (Cj); 35.7 (Cd); 50.8 (Ca); 52.1 (Ci); 125.8 (Ch); 126.5 (Cn); 128.4 (Cf-Cg); 128.6 (Cl); 129.1 (Cm); 139.1 (Ck); 142.4 (Ce) (Figure S4.50).

GPC: M_n = 188,400 g mol^{-1}, M_w = 260,500 g mol^{-1}, PDI = 1.38 (Figure S4.51).

FT-IR: $\tilde{\nu}$ = cm^{-1}) 3242 (N–H); 2944, 2857 (C–H$_2$); 2386, 2294 (B–H) (Figure S4.53).

Elemental analysis calculated for C$_{18}$H$_{28}$B$_2$N$_2$: C, 73.5; H, 9.6; N, 9.5. Found: C, 73.3; H, 9.8; N, 9.9.

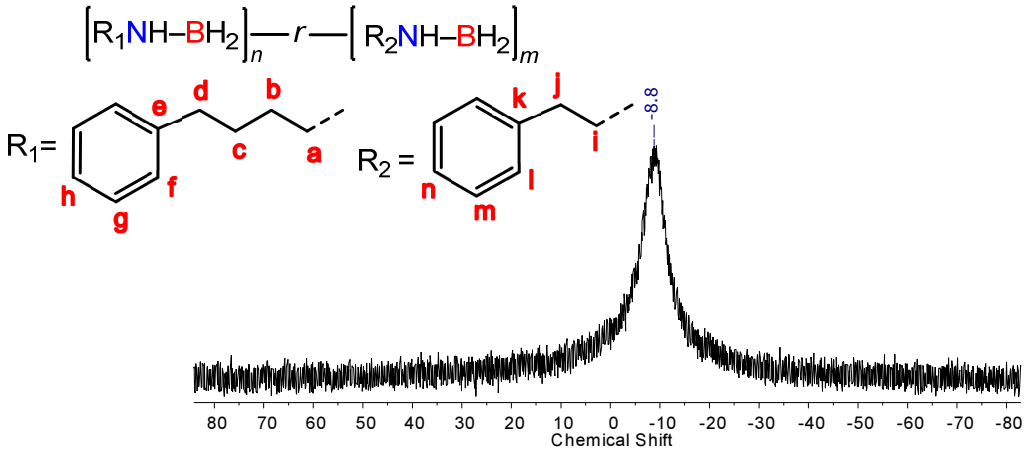

Figure S4.48. $^{11}B\{^{1}H\}$ NMR spectrum of isolated $[Ph(CH_2)_2NH–BH_2]_n$–*r*– $[Ph(CH_2)_4NH–BH_2]_m$ (n: 1, m: 1) in $CDCl_3$ at 20 °C.

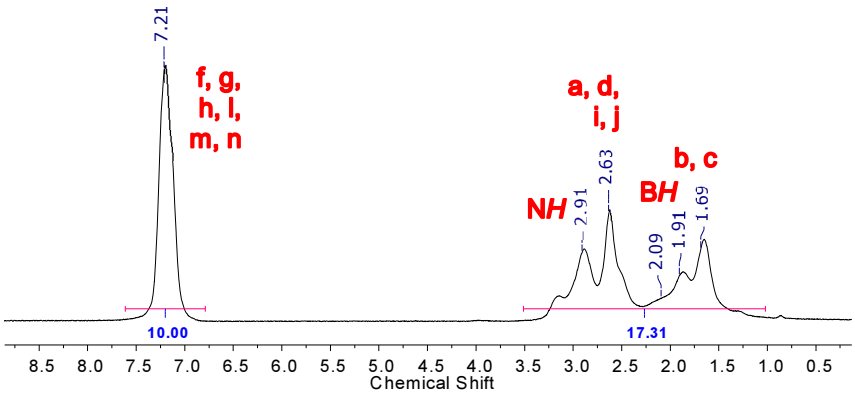

Figure S4.49. ^{1}H NMR spectrum of isolated $[Ph(CH_2)_2NH–BH_2]_n$–*r*– $[Ph(CH_2)_4NH–BH_2]_m$ (n: 1, m: 1) in $CDCl_3$ at 20 °C.

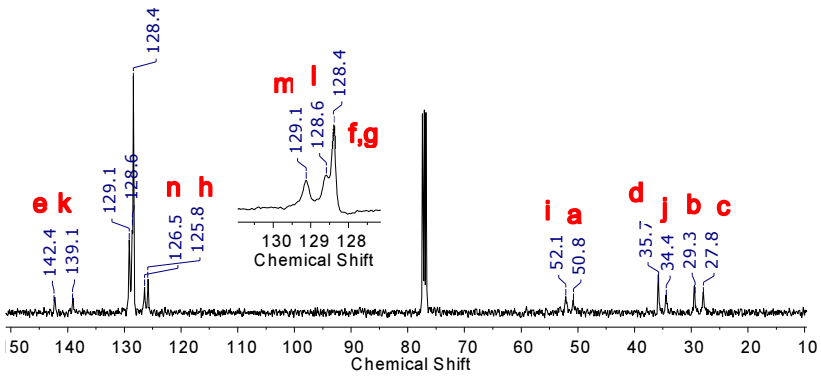

Figure S4.50. ^{13}C NMR spectrum of isolated $[Ph(CH_2)_2NH–BH_2]_n$–*r*– $[Ph(CH_2)_4NH–BH_2]_m$ (n: 1, m: 1) in $CDCl_3$ at 20 °C.

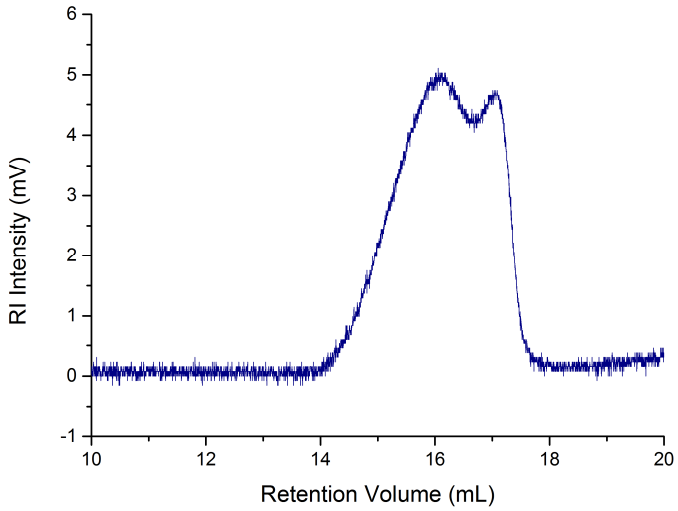

Figure S4.51. GPC chromatogram (2mg mL^{-1}) of isolated $[Ph(CH_2)_2NH–BH_2]_n$–*r*– $[Ph(CH_2)_4NH–BH_2]_m$ (n: 1, m: 1) in THF (0.1 *w*/w % nBu_4NBr).

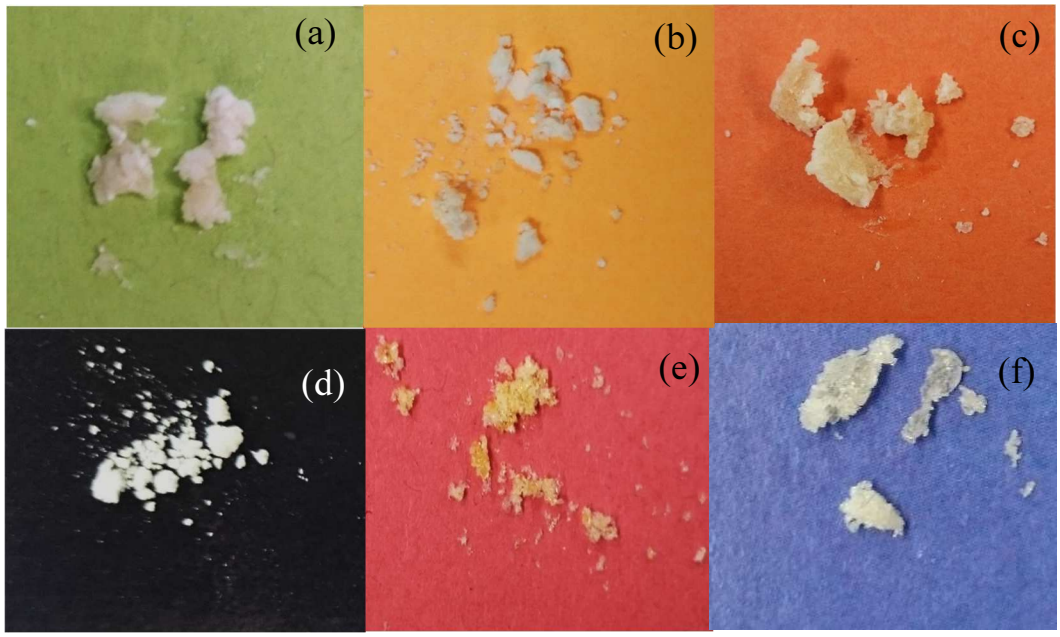

Figure S4.52. Photographs of the physical appearance of polyaminoboranes a) $[Ph(CH_2)_4NH–BH_2]_n$; b) $[Ph(CH_2)_2NH–BH_2]_n$; c) $[Ph(CH_2)_4NH–BH_2]_n$–*r*– $[NH_2–BH_2]_m$ (n: 1, m: 1); d) $[Ph(CH_2)_4NH–BH_2]_n$–*r*– $[NH_2–BH_2]_m$ (n: 1, m: 2); e) $[Ph(CH_2)_4NH–BH_2]_n$–*r*– $[MeNH–BH_2]_m$ (n: 1, m: 1.56) and f) $[Ph(CH_2)_2NH–BH_2]_n$–*r*– $[Ph(CH_2)_4NH–BH_2]_m$ (n: 1, m: 1).

4.5.7 Infrared Spectroscopy of Polyaminoboranes

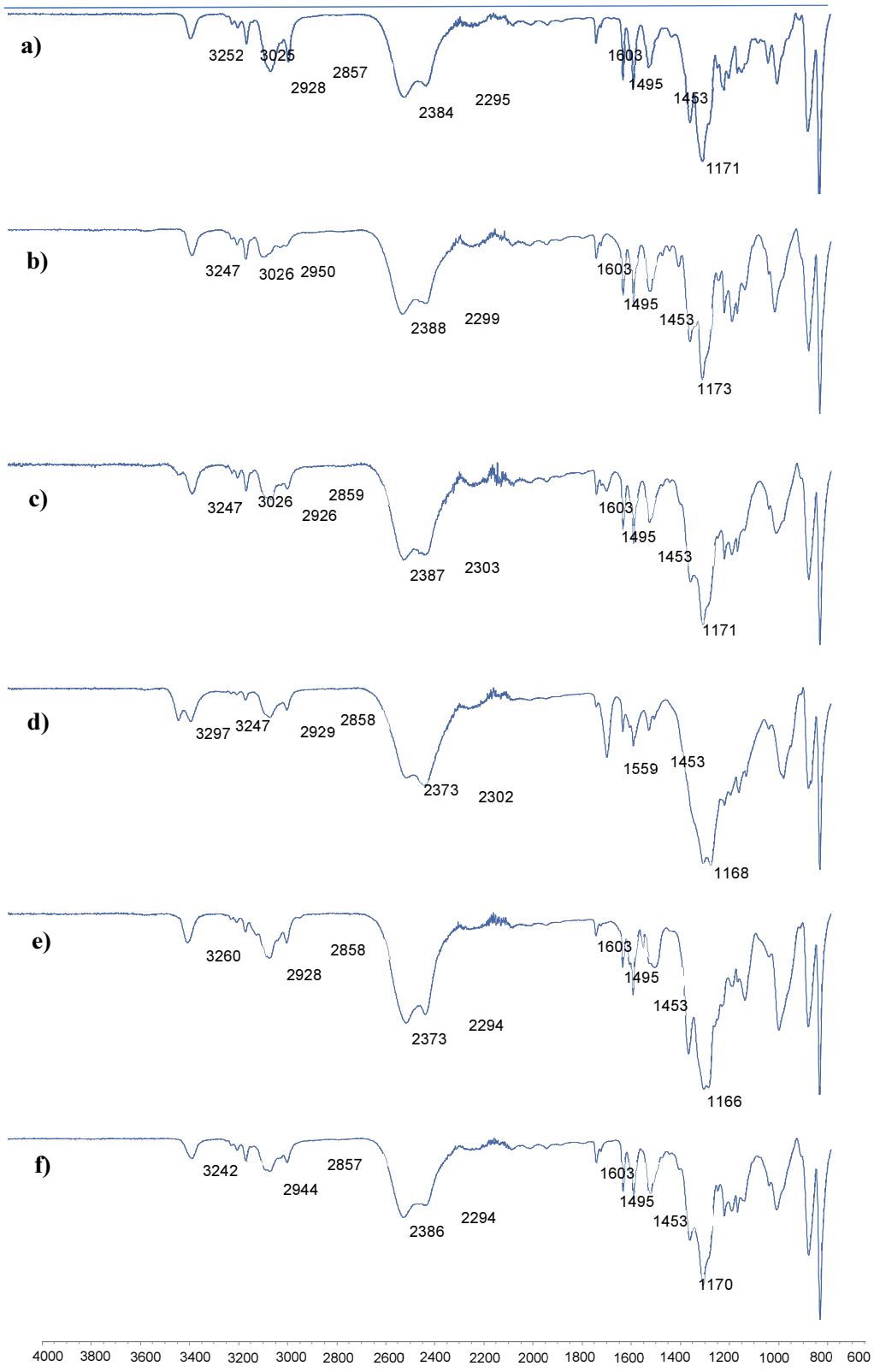

Figure S4.53. FT-IR spectra of a) $[Ph(CH_2)_4NH–BH_2]_n$; b) $[Ph(CH_2)_2NH–BH_2]_n$; c) $[Ph(CH_2)_4NH–BH_2]_n$–*r*– $[NH_2–BH_2]_m$ (n: 1, m: 1); d) $[Ph(CH_2)_4NH–BH_2]_n$–*r*– $[NH_2–BH_2]_m$ (n: 1, m: 2); e) $[Ph(CH_2)_4NH–BH_2]_n$–*r*– $[MeNH–BH_2]_m$ (n: 1, m: 1.56)and f) $[Ph(CH_2)_2NH–BH_2]_n$–*r*– $[Ph(CH_2)_4NH–BH_2]_m$ (n: 1, m: 1).

4.5.8 Thermogravimetric Analysis of Polyamonoboranes.

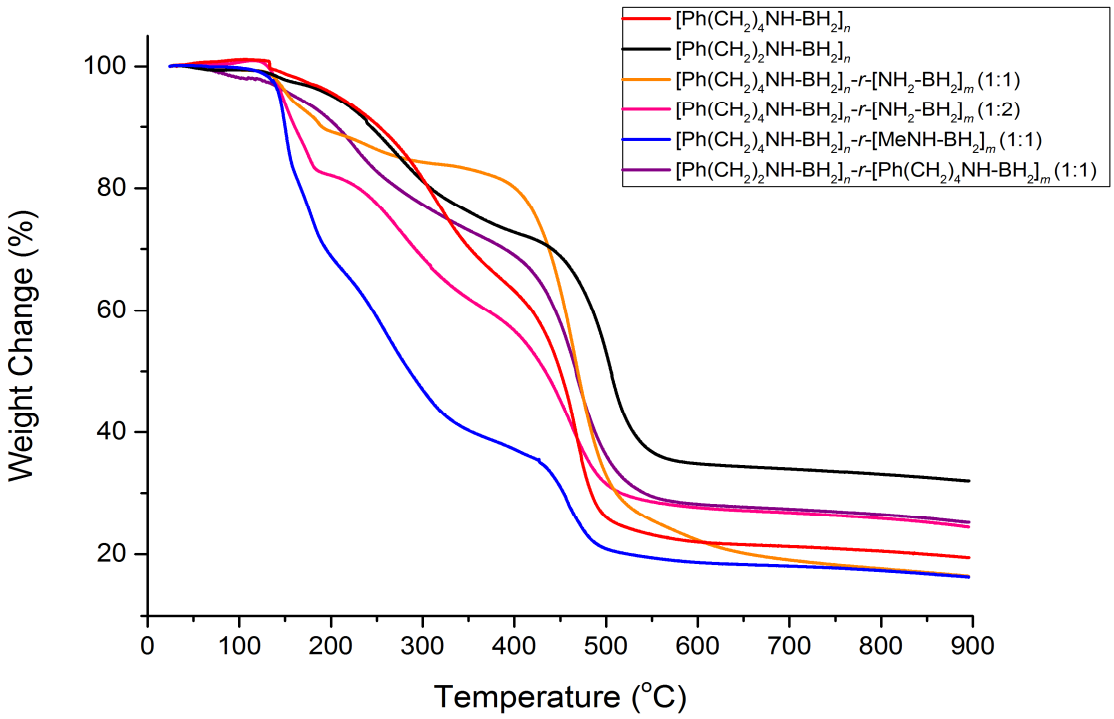

Figure S4.54. TGA thermograms of polyaminoboranes at 900 °C (heating rate: 10 ˚C min $^{-1}$).

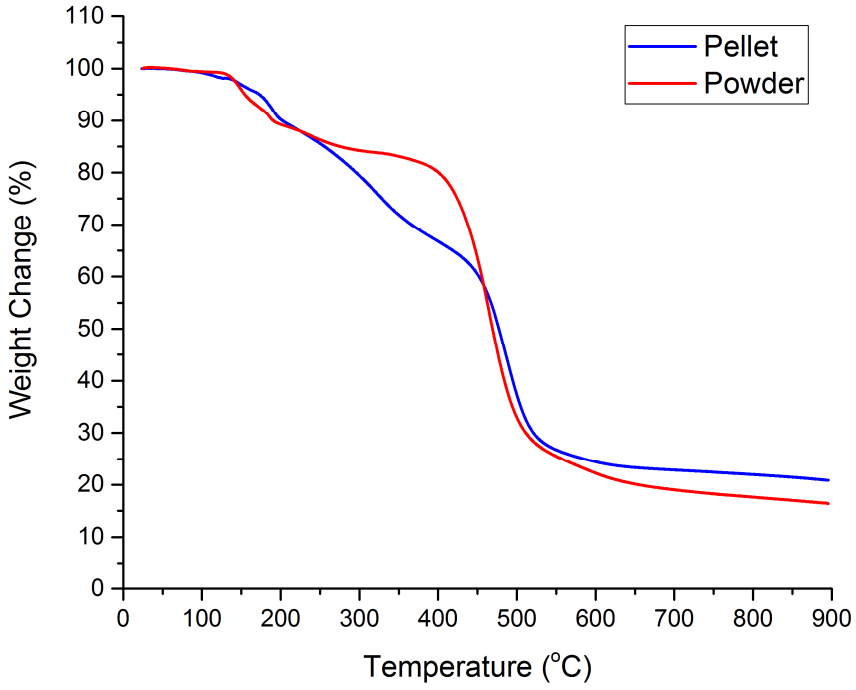

Figure S4.55. TGA thermograms of $[Ph(CH_2)_4NH–BH_2]_n$–*r*– $[NH_2–BH_2]_m$ (n: 1, m: 1) performed as a powder and as a pellet at 900 °C (heating rate: 10 ˚C min $^{-1}$).

4.5.9 Crosslinking Studies.

$Ph(CH_2)_2NH_2{\cdot}BH_3$ (206 mg, 1.5 mmol) was cross-linked with $BH_3{\cdot}NH_2(CH_2)_8NH_2{\cdot}BH_3$ at 5 mol % (13 mg, 0.075 mmol) and at 10 mol % (26 mg, 0.15 mmol) and each reaction was dissolved in THF (0.3 mL) in a vial. In a separate vial, the catalyst IrH_2(POCOP) (1 mol %, 9 mg) was dissolved in THF (0.3 mL). Both solutions were cooled to −40°C and then, the solution with the catalyst was added slowly at low temperature to the amine-borane/cross-linker solution and immediate bubbling was observed. After two minutes, the solutions became sticky solids as it is shown in Fig. S4.56. The reaction mixtures were standing for 16 h to assure monomer reactivity. After this period, it was observed that the reaction mixtures was back into solution. Then they were precipitated into hexanes (~20 mL) at room temperature (20 °C) and formation of white solids was observed. The excess of solvent was decanted and the materials were dried under vaccum overnight. Yield of the material containing 5 mol % crosslinker (29 %, 60 mg). Yield of the material containing 5 mol % crosslinker (39%, 80 mg).

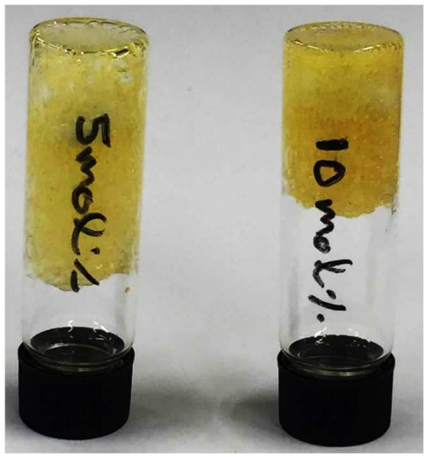

Figure S4.56. Photograph of the reaction mixtures of $Ph(CH_2)_2NH_2{\cdot}BH_3$ with the crosslinker $BH_3{\cdot}NH_2(CH_2)_8NH_2{\cdot}BH_3$ in different ratios (left) 5 mol % cross-linker and (right) 10 mol % crosslinker and 1 mol% of IrH_2(POCOP) in THF.

The resultant material containing 5 mol % crosslinker is soluble in THF.

^{11}B NMR (THF-d_8): δ (ppm) −1.6 ('BN_3'/'BN_4'), −9.0 ppm (polyaminoborane), −22.0 ($Ph(CH_2)_2NH_2 \cdot BH_3$ or end group chain $–BH_3$) (Figure S4.57).

^{1}H NMR (THF-d_8): δ (ppm) 1.32 (BH_2); 2.61-3.13 (m, C*H*-N*H*); 7.25 ($C_{ar}H$) (Figure S4.58).

GPC: M_n = 225,400 g mol^{-1}, M_w = 666,300 g mol^{-1}, PDI = 2.94 (Figure S4.59).

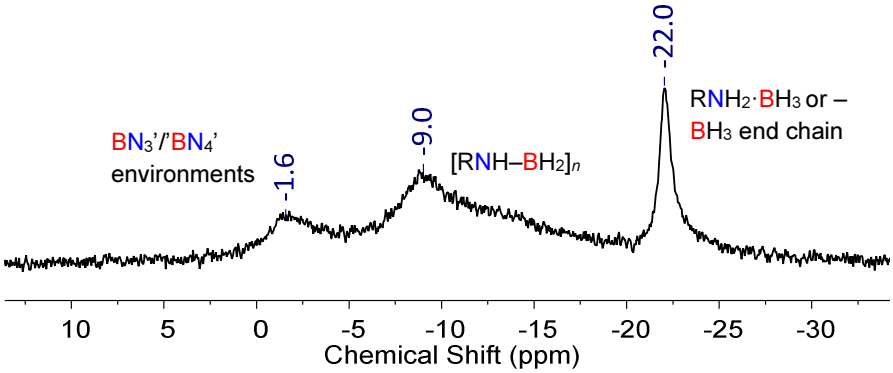

Figure S4.57. $^{11}B\{^1H\}$ NMR spectrum of isolated material of the reaction of $Ph(CH_2)_2NH_2 \cdot BH_3$ /$BH_3 \cdot NH_2(CH_2)_8NH_2 \cdot BH_3$ (Ratio 95:5) and 1 mol% of IrH_2(POCOP) in THF-d_8 at 20 °C.

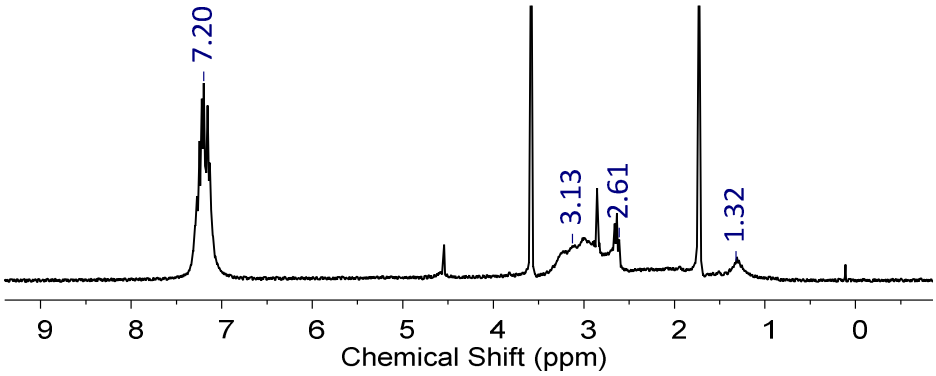

Figure S4.58. ^{1}H NMR spectrum of isolated material of the reaction of $Ph(CH_2)_2NH_2 \cdot BH_3$ /$BH_3 \cdot NH_2(CH_2)_8NH_2 \cdot BH_3$ (Ratio 95:5) and 1 mol% of IrH_2(POCOP) in THF-d_8 at 20 °C.

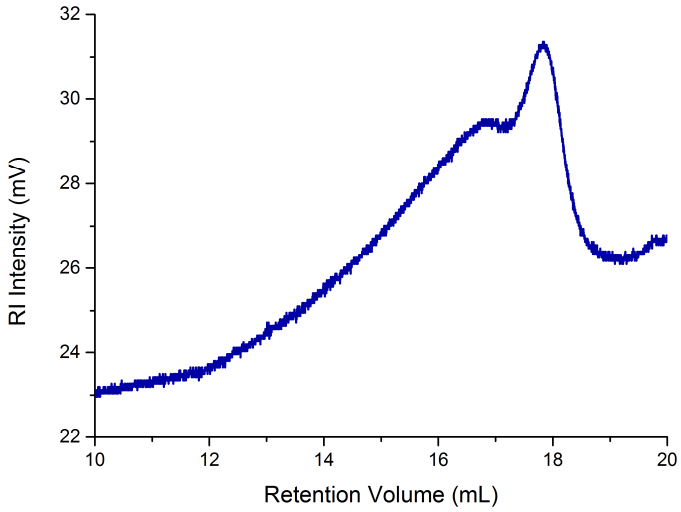

Figure S4.59. GPC chromatogram (2mg mL^{-1}) of isolated material of the reaction of $Ph(CH_2)_2NH_2{\cdot}BH_3$ /$BH_3{\cdot}NH_2(CH_2)_8NH_2{\cdot}BH_3$ (Ratio 95:5) and 1 mol% of IrH_2(POCOP) in THF (0.1 *w/w* % $n$$Bu_4NBr$).

4.6 Notes and References

1. (a) Priegert, A. M.; Rawe, B. W.; Serin, S. C.; Gates, D. P., *Chem. Soc. Rev.* **2016,** *45*, 922-953; (b) Manners, I., *Angew. Chem. Int. Ed.* **1996,** *35*, 1602-1621; (c) Jäkle, F., *Chem. Rev.* **2010,** *110*, 3985-4022.

2. (a) Abd-El-Aziz, A. S.; Carraher, C. E.; Pittman, C. U.; Zeldin, M., *Macromolecules Containing Metal and Metal-Like Elements, Volume 8: Boron-Containing Particles*. Wiley: 2007; (b) Doshi, A.; Jäkle, F., 1.27 - Boron-Containing Polymers. In *Comprehensive Inorganic Chemistry II (Second Edition)*, Reedijk, J.; Poeppelmeier, K., Eds. Elsevier: Amsterdam, 2013; pp 861-891; (c) Qiu, F.; Zhao, W.; Han, S.; Zhuang, X.; Lin, H.; Zhang, F., *Polymers-Basel* **2016,** *8*, 191; (d) Fazen, P. J.; Beck, J. S.; Lynch, A. T.; Remsen, E. E.; Sneddon, L. G., *Chem. Mater.* **1990,** *2*, 96-97; (e) Fazen, P. J.; Remsen, E. E.; Beck, J. S.; Carroll, P. J.; Mcghie, A. R.; Sneddon, L. G., *Chem. Mater.* **1995,** *7*, 1942-1956; (f) Bernard, S.; Miele, P., *Materials* **2014,** *7*, 7436-7459; (g) Bernard, S.; Salameh, C.; Miele, P., *Dalton Trans.* **2016,** *45*, 861-873.

3. (a) Dorn, H.; Singh, R. A.; Massey, J. A.; Nelson, J. M.; Jaska, C. A.; Lough, A. J.; Manners, I., *J. Am. Chem. Soc.* **2000,** *122*, 6669-6678; (b) Pandey, S.; Lonnecke, P.; Hey-Hawkins, E., *Eur. J. Inorg. Chem.* **2014,** *2014*, 2456-2465; (c) Schäfer, A.; Jurca, T.; Turner, J.; Vance, J. R.; Lee, K.; Du, V. A.; Haddow, M. F.; Whittell, G. R.; Manners, I., *Angew. Chem. Int. Ed.* **2015,** *54*, 4836-4841; (d) Marquardt, C.; Jurca, T.; Schwan, K. C.; Stauber, A.; Virovets, A. V.; Whittell, G. R.; Manners, I.; Scheer, M., *Angew. Chem. Int. Ed.* **2015,** *54*, 13782-13786; (e) Hooper, T. N.; Weller, A. S.; Beattie, N. A.; Macgregor, S. A., *Chem. Sci.* **2016,** *7*, 2414-2426; (f) Paul, U. S. D.; Braunschweig, H.; Radius, U., *Chem. Commun.* **2016,** *52*, 8573-8576; (g) Coles, N. T.; Mahon, M. F.; Webster, R. L., *Organometallics* **2017,** *36*, 2262-2268; (h) Cayaye, H.; Clegg, F.; Gould, P. J.; Ladyman, M. K.; Temple, T.; Dossi, E., *Macromolecules* **2017,** *50*, 9239-9248.

4. Dorn, H.; Rodezno, J. M.; Brunnhöfer, B.; Rivard, E.; Massey, J. A.; Manners, I., *Macromolecules* **2003,** *36*, 291-297.

5. Clark, T. L.; Rodezno, J. M.; Clendenning, S. B.; Aouba, S.; Brodersen, P. M.; Lough, A. J.; Ruda, H. E.; Manners, I., *Chem. Eur. J.* **2005,** *11*, 4526-4534.

6. (a) Morgan, M. M.; Piers, W. E., *Dalton Trans.* **2016,** *45*, 5920-5924; (b) Campbell, P. G.; Marwitz, A. J. V.; Liu, S. Y., *Angew. Chem. Int. Ed.* **2012,** *51*, 6074-6092; (c) Belanger-Chabot, G.; Braunschweig, H.; Roy, D. K., *Eur. J. Inorg. Chem.* **2017**, 4353-4368.

7. (a) van de Wouw, H. L.; Lee, J. Y.; Klausen, R. S., *Chem. Commun.* **2017,** *53*, 7262-7265; (b) Thiedemann, B.; Gliese, P. J.; Hoffmann, J.; Lawrence, P. G.; Sonnichsen, F. D.; Staubitz, A., *Chem. Commun.* **2017,** *53*, 7258-7261; (c) Wan, W. M.; Baggett, A. W.; Cheng, F.; Lin, H.; Liu, S. Y.; Jäkle, F., *Chem. Commun.* **2016,** *52*, 13616-13619; (d) Grosche, M.; Herdtweck, E.; Peters, F.; Wagner, M., *Organometallics* **1999,** *18*, 4669-4672; (e) Ledoux, A.; Larini, P.; Boisson, C.; Monteil, V.; Raynaud, J.; Lacote, E., *Angew. Chem. Int. Ed.* **2015,** *54*, 15744-15749.

8. (a) Baggett, A. W.; Guo, F.; Li, B.; Liu, S. Y.; Jäkle, F., *Angew. Chem. Int. Ed.* **2015,** *54*, 11191-11195; (b) Ayhan, O.; Eckert, T.; Plamper, F. A.; Helten, H., *Angew. Chem. Int. Ed.* **2016,** *55*, 13321-13325; (c) Lorenz, T.; Crumbach, M.; Eckert, T.; Lik, A.; Helten, H., *Angew. Chem. Int. Ed.* **2017,** *56*, 2780-2784; (d) Wang, X. Y.; Zhuang, F. D.; Wang, J. Y.; Pei, J., *Chem. Commun.* **2015,** *51*, 17532-17535; (e) Marinelli, D.; Fasano, F.; Najjari, B.; Demitri, N.; Bonifazi, D., *J. Am. Chem. Soc.* **2017,** *139*, 5503-5519; (f) Helten, H., *Chem. Eur. J.* **2016,** *22*, 12972-12982; (g) Huang, J.; Li, Y., *Front. Chem.* **2018,** *6*; (h) Stepien, M.; Gonka, E.; Zyla, M.; Sprutta, N., *Chem. Rev.* **2017,** *117*, 3479-3716.

9. (a) Liu, Z.; Song, L.; Zhao, S. Z.; Huang, J. Q.; Ma, L. L.; Zhang, J. N.; Lou, J.; Ajayan, P. M., *Nano Lett.* **2011,** *11*, 2032-2037; (b) Whittell, G. R.; Manners, I., *Angew. Chem. Int. Ed.* **2011,** *50*, 10288-10289.

10. (a) Kim, D. P.; Moon, K. T.; Kho, J. G.; Economy, J.; Gervais, C.; Babonneau, F., *Polym. Adv. Technol.* **1999,** *10*, 702-712; (b) Du, V. A.; Jurca, T.; Whittell, G. R.; Manners, I., *Dalton Trans.* **2016,** *45*, 1055-1062; (c) Wang, X. C.; Hooper, T. N.; Kumar, A.; Priest, I. K.; Sheng, Y. W.; Samuels, T. O. M.; Wang, S. S.; Robertson, A. W.; Pacios, M.; Bhaskaran, H.; Weller, A. S.; Warner, J. H., *CrystEngComm.* **2017,** *19*, 285-294.

11. (a) Staubitz, A.; Soto, A. P.; Manners, I., *Angew. Chem. Int. Ed.* **2008,** *47*, 6212-6215; (b) Staubitz, A.; Sloan, M. E.; Robertson, A. P. M.; Friedrich, A.; Schneider, S.; Gates, P. J.; Günne, J. S. A. D.; Manners, I., *J. Am. Chem. Soc.* **2010,** *132*, 13332-13345; (c) Vance, J. R.; Robertson, A. P. M.; Lee, K.; Manners, I., *Chem. Eur. J.* **2011,** *17*, 4099-4103; (d) Johnson, H. C.; Leitao, E. M.; Whitten, G. R.; Manners, I.; Lloyd-Jones, G. C.; Weller, A. S., *J. Am. Chem. Soc.* **2014,** *136*, 9078-9093; (e) Lichtenberg, C.; Adelhardt, M.; Gianetti, T. L.; Meyer, K.; de Bruin, B.; Grutzmacher, H., *ACS Catal.* **2015,** *5*, 6230-6240; (f) Anke, F.; Han, D.; Klahn, M.; Spannenberg, A.; Beweries, T., *Dalton Trans.* **2017,** *46*, 6843-6847; (g) Adams, G. M.; Colebatch, A. L.; Skornia, J. T.; McKay, A. I.; Johnson, H. C.; Lloyd-Jones, G. C.; Macgregor, S. A.; Beattie, N. A.; Weller, A. S., *J. Am. Chem. Soc.* **2018,** *140*, 1481-1495; (h) Colebatch, A. L.; Gilder, B. W. H.; Whittell, G. R.; Oldroyd, N. L.; Manners, I.; Weller, A. S., *Chem. Eur. J.* **2018,** *24*, 5450-5455; (i) Trose, M.; Reiß, M.; Reiß, F.; Anke, F.; Spannenberg, A.; Boye, S.; Lederer, A.; Arndt, P.; Beweries, T., *Dalton Trans.* **2018**.

12. (a) Metters, O. J.; Chapman, A. M.; Robertson, A. P. M.; Woodall, C. H.; Gates, P. J.; Wass, D. F.; Manners, I., *Chem. Commun.* **2014,** *50*, 12146-12149; (b) Pinheiro, C. A. D.; Roiland, C.; Jehan, P.; Alcaraz, G., *Angew. Chem. Int. Ed.* **2018,** *57*, 1519-1522; (c) Brown, M. P.; Heseltin.Rw, *J. Inorg. Nucl. Chem.* **1967,** *29*, 1197-1201.

13. Jurca, T.; Dellermann, T.; Stubbs, N. E.; Resendiz-Lara, D. A.; Whittell, G. R.; Manners, I., *Chem. Sci.* **2018,** *9*, 3360-3366.

14. Dallanegra, R.; Robertson, A. P. M.; Chaplin, A. B.; Manners, I.; Weller, A. S., *Chem. Commun.* **2011,** *47*, 3763-3765.

15. Johnson, H. C.; Weller, A. S., *Angew. Chem. Int. Ed.* **2015,** *54*, 10173-10177.

16. Helten, H.; Robertson, A. P. M.; Staubitz, A.; Vance, J. R.; Haddow, M. F.; Manners, I., *Chem. Eur. J.* **2012,** *18*, 4665-4680.

17. Resendiz-Lara, D. A.; Stubbs, N. E.; Arz, M. I.; Pridmore, N. E.; Sparkes, H. A.; Manners, I., *Chem. Commun.* **2017,** *53*, 11701-11704.

18. Tanaka, R.; Goda, M.; Cai, Z. G.; Nakayama, Y.; Shiono, T., *Polymer* **2015,** *70*, 252-256.

19. Ekman, K. B.; Wilen, C. E.; Nasman, J. H.; Starck, P., *Polymer* **1993,** *34*, 3757-3759.

20. (a) Robertson, A. P. M.; Suter, R.; Chabanne, L.; Whittell, G. R.; Manners, I., *Inorg. Chem.* **2011,** *50*, 12680-12691; (b) Jaska, C. A.; Temple, K.; Lough, A. J.; Manners, I., *J. Am. Chem. Soc.* **2003,** *125*, 9424-9434.

21. Our group has previously reported the synthesis of $[MeNH–BH_2]_n$ (M_n = 78 000 g mol^{-1}, PDI = 1.52) *via* the dehydropolymerisation of $MeNH_2{\cdot}BH_3$ at room temperature in 2 h using stoichiometric amounts of skeletal nickel in THF (Ref. 20a).

22. (a) Spielmann, J.; Bolte, M.; Harder, S., *Chem. Commun.* **2009**, 6934-6936; (b) Rosello-Merino, M.; Rama, R. J.; Diez, J.; Conejero, S., *Chem. Commun.* **2016,** *52*, 8389-8392.

23. When $MeNH_2{\cdot}BH_3$ was treated with $[Rh(\mu\text{-}Cl)(1,5\text{-}COD)]_2$ the formation of moderate molecular weight polymer was observed (M_n = 42 000 g mol^{-1}, PDI = 10.5) (Ref. 11b). Similar to the dehydrocoupling of $MeNH_2{\cdot}BH_3$ with $[Rh(\mu\text{-}Cl)(1,5\text{-}COD)]_2$, we observed vigorous bubbling as the solution of THF changed from yellow to a black colour. Previously, reaction of $MeNH_2{\cdot}BH_3$ in

dimethoxyethane (DME) using [Rh(μ-Cl)(1,5-COD)]$_2$ as a precatalyst produced [MeN–BH$_3$]$_n$ at 45 °C, and this process has been associated with Rh(I) being reduced to Rh(0) nanoparticles which are the active species in the dehydrogenation reaction (Ref. 20b).

24. The rate of the dehydropolymerisation of MeNH$_2$·BH$_3$ is significantly different with Ph(CH$_2$)$_4$NH$_2$·BH$_3$; MeNH$_2$·BH$_3$ reaching maximum conversion after 22 h to give polymer (Ref. 11b).

25. The signal assigned to borazine [Ph(CH$_2$)$_4$N–BH]$_3$ appears as broad shoulder of the main peak that corresponds to bis(amino)borane [Ph(CH$_2$)$_4$NH]$_2$BH. The signal assigned to borazine is in agreement to similar products reported previously: E.Framery, M.Vaultier, *Heteroat. Chem.* **2000**, *11*, 218 –225.

26. Ünal, A.; Okur, M., *AIP Conf. Proc.* **2017,** *1815*, 100006.

27. It has been postulated that polyaminoboranes can present significant adsortion effects with the column material surface when analised by GPC in THF. For reducing the interaction between the analyte and the column, the addition of nBu$_4$NBr to THF was used to increase the ionic strength in the mobile phase (Ref. 11b).

28. Solc, K.; Elias, H. G., *J. Polym. Sci. B Polym. Phys.* **1973,** *11*, 137-148.

29. Van Krevelen, D. W.; Te Nijenhuis, K., Chapter 10 - Optical Properties. In *Properties of Polymers (Fourth Edition)*, Elsevier: Amsterdam, 2009; pp 287-318.

30. Fetters, L. J.; Hadjichristidis, N.; Lindner, J. S.; Mays, J. W., *J. Phys. Chem. Ref. Data* **1994,** *23*, 619-640.

31. In the DLS experiment performed in THF (0.1 w/w % nBu$_4$NBr) at 35 ºC has not been considered the change in viscosity, and the slightly change on R_H from the experiment at room temperature indicates that the change in conformation might be negligible.

32. Li, W. B.; Chung, H. Y.; Daeffler, C.; Johnson, J. A.; Grubbs, R. H., *Macromolecules* **2012,** *45*, 9595-9603.

33. Mencer, H. J.; Grubisicgallot, Z., *J. Liq. Chromatogr.* **1979,** *2*, 649-662.

34. Bruessau, R. J., *Makromol. Chem., Macromol. Symp.* **1992,** *61*, 199-218.

35. Mori, S., *Anal. Chem.* **1989,** *61*, 530-534.

36. Jacquemin, D., *J. Phys. Chem. A* **2004,** *108*, 9260-9266.

37. Bernholc, J.; Nakhmanson, S. M.; Nardelli, M. B.; Meunier, V., *Comput. Sci. Eng.* **2004,** *6*, 12-21.

38. Turner, J. R.; Resendiz-Lara, D. A.; Jurca, T.; Schäfer, A.; Vance, J. R.; Beckett, L.; Whittell, G. R.; Musgrave, R. A.; Sparkes, H. A.; Manners, I., *Macromol. Chem. Phys.* **2017,** *218*, 1700120.

39. Very recent, the formation of polyaminoboranes from BzNH$_2$·BH$_3$ (Bz = benzyl) and Ph(CH$_2$)$_4$NH$_2$·BH$_3$ was succesful using the catalyst system Cp$^R_2$TiCl$_2$ and 2*n*BuLi (Ref. 13).

40. Schubert, W. M.; Robins, J., *J. Am. Chem. Soc.* **1958,** *80*, 559-563.

41. This polymer can be recorded both in CDCl$_3$ and THF-d_8.

42. This polymer is poorly soluble in CDCl$_3$ but soluble in THF-d_8.

43. (a) Baumann, J.; Baitalow, E.; Wolf, G., *Thermochim. Acta* **2005,** *430*, 9-14; (b) Pusatcioglu, S. Y.; Mcgee, H. A.; Fricke, A. L.; Hassler, J. C., *J. Appl. Polym. Sci.* **1977,** *21*, 1561-1567.

44. (a) Marziale, A. N.; Friedrich, A.; Klopsch, I.; Drees, M.; Celinski, V. R.; Günne, J. S. A. D.; Schneider, S., *J. Am. Chem. Soc.* **2013,** *135*, 13342-13355; (b) Ewing, W. C.; Marchione, A.; Himmelberger, D. W.; Carroll, P. J.; Sneddon, L. G., *J. Am. Chem. Soc.* **2011,** *133*, 17093-17099.

45. Pangborn, A. B.; Giardello, M. A.; Grubbs, R. H.; Rosen, R. K.; Timmers, F. J., *Organometallics* **1996,** *15*, 1518-1520.

46. Gottker-Schnetmann, I.; White, P. S.; Brookhart, M., *Organometallics* **2004,** *23*, 1766-1776.

47. Ramachandran, P. V.; Kulkarni, A. S.; Zhao, Y.; Mei, J. G., *Chem. Commun.* **2016,** *52*, 11885-11888.

48. Camacho, C.; Paz-Sandoval, M. A.; Contreras, R., *Polyhedron* **1986,** *5*, 1723-1732.

Chapter 5.

Boron–Nitrogen Main Chain Analogues of Polystyrene: Poly(*B*-aryl)aminoboranes *via* Catalytic Dehydrocoupling.

Reproduced from:

D. A. Resendiz-Lara, N. E. Stubbs, M. I. Arz, N. E. Pridmore, H. A. Sparkes, I. Manners, *Chem. Commun.* **2017**, *53*, 11701-11704.

5.1 Abstract

The first high molar mass polyaminoboranes with an organic substituent at boron, namely the *B*-arylated polyaminoboranes $[NH_2–BHPh]_n$ (**5.2a**) and $[NH_2–BH(p\text{-}CF_3C_6H_4)]_n$ (**5.2b**), have been prepared via catalytic dehydropolymerisation. These materials can be considered as inorganic analogues of polystyrene with a B–N main chain. Their synthesis was achieved from *B*-aryl amine–borane precursors in solution using an $[IrH_2(POCOP)]$ precatalyst.

5.2 Introduction

Recent research at the interface of polymer and inorganic chemistry targets the development of hybrid polymers, which combine main group elements with classical organic polymer frameworks leading to novel materials with unique combinations of properties.[1] One well-established strategy to access hybrid polymers involves the formal replacement of C–C units by B–N moieties and has been pursued to create main chain boron–nitrogen analogues of polyolefins[2] and poly(*p*-phenylenes).[3] This approach has very recently been extended to poly(phenylene vinylene),[4] and a range of other interesting BN-based materials have also been prepared.[5] Recently, side chain B–N analogues of polystyrene, namely poly(*B*-vinyl borazines) and poly(*B*-vinyl 1,2-azaborinines) were obtained *via* radical polymerization of the corresponding *B*-substituted monomers.[6] Despite these advances, polystyrene analogues in which the C–C main chain is formally replaced with a B–N skeleton have not been reported to date.

Catalytic dehydrocoupling of amine–boranes, $RR'NH{\cdot}BH_3$ (R = H, alkyl), has attracted considerable attention in recent years due to the potential for applications in hydrogen storage and hydrogen transfer chemistry as well as the potential to access new inorganic polymeric and BN-containing solid state materials.[7,8] However, to date, only a limited number of amine–boranes, $RNH_2{\cdot}BH_3$ (R = H, Me, Et, *n*Bu), have been dehydropolymerised using transition-metal catalysts to yield soluble polyaminoboranes with *N*-alkyl substituents, $[RNH–BH_2]_n$, isolobal congeners of polyolefins, with potential applications as piezoelectric or preceramic materials.[2,9] The attempted dehydropolymerisation of primary *N*-aryl amine–boranes, $RNH_2{\cdot}BH_3$ (R = Ph, *p*-$MeOC_6H_4$, *p*-$CF_3C_6H_4$), to yield polyaminoborane analogues of polystyrene was prevented by their complex dehydrogenation chemistry in the presence or absence of catalysts that leads to a myriad of products within which no high molar mass polymer was detected.[10]

In contrast to the case of (*N*-organo)amine–boranes, the dehydrocoupling behaviour of their *B*-organo analogues is relatively unexplored.[11,12] We recently reported studies of the catalytic dehydrocoupling of sterically unhindered *B*-methylated amine–boranes, $RNH_2{\cdot}BH_2Me$ (R = H, Me), using stoichiometric amounts of skeletal nickel.[11b] Although ^{11}B NMR peaks were tentatively assigned to oligomeric or polymeric *B*-methyl aminoboranes, $[RNH–BHMe]_n$ (R = H or Me), under the reaction conditions these intermediates readily underwent further dehydrogenation to yield mainly the *B*-methylated borazines $[RN–BMe]_3$ (R = H, Me). We attributed the lability of the $[RNH–BHMe]_n$ oligomers/polymers to the inclusion of an electron-donating methyl group at boron,[11b] which lowers the dissociation energy of the B–N dative bond and thermodynamically facilitates hydrogen elimination, which has been predicted theoretically.[13] We therefore envisaged that replacement of the methyl groups at boron by electron-withdrawing aryl groups should increase the strength of the B–N bonds in the main chain and also their overall stability. In this chapter, we present our studies of the catalytic dehydropolymerisation of the *B*-aryl amine–boranes $NH_3{\cdot}BH_2Ph$ (**5.1a**) and $NH_3{\cdot}BH_2(p\text{-}CF_3C_6H_4)$ (**5.2b**) to give poly(*B*-aryl)aminoboranes, $[NH_2–BHR]_n$ (**5.2a**: R = Ph, **5.2b**: R = p-$CF_3C_6H_4$), which are the first examples of inorganic analogues of polystyrene containing a main-chain of alternating B–N groups.

5.3 Results and Discussion

The *B*-aryl amine–boranes **5.2a** and **5.2b** were synthesised *via* the dehydrogenative salt metathesis of $Li[BH_3R]$ and NH_4Cl in an Et_2O/toluene mixture (Scheme 5.1)[11b, 12, 14] The lithium trihydridoborate precursor was generated *in situ via* treatment of commercially available $RB(OH)_2$ with 1.5 equivalents of $LiAlH_4$. This protocol afforded amine–(aryl)borane **5.1a** in 39 % yield as a colourless oil at 25°C, which solidifies upon cooling to −40 °C, and analogue **5.1b** in 69 % yield as a colourless solid at ambient temperature. The

NMR data acquired for **5.1a** (in $CDCl_3$) and **5.1b** (in THF-d_8) was consistent with the expected data for *B*-aryl amine–boranes containing four-coordinate boron centres with two hydrogen atoms. For example, the ^{11}B NMR spectra each displayed a single peak at −13.9 (for **5.1a**) and −16.8 (for **5.1b**) ppm which appeared as triplets in the ^{1}H coupled spectra [$^{1}J_{BH}$ = 95 Hz (**5.1a**), 96 Hz (**5.1b**)].

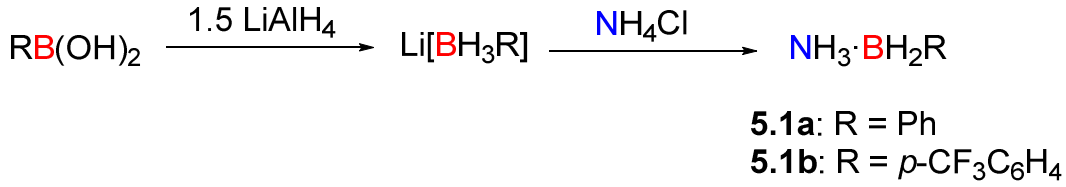

Scheme 5.1. Synthesis of *B*-arylated amine–boranes **5.1a** (R = Ph) and **5.1b** (R = *p*-$CF_3C_6H_4$).

In line with a higher energy required for dissociation of the B–N bond in **5.1b** compared to **5.1a** due to the presence of an electron-withdrawing *p*-CF_3 group, amine–borane **5.1b** is stable in the solid state at 20 °C for 170 h, whereas **5.1a** partially decomposes to give oligomeric $[NH_2–BHPh]_n$ (ca. 20 %) and $NH_3·BH_3$ (ca. 5 %) by ^{11}B NMR spectroscopy. Interestingly, both **5.1a** and **5.1b** are stable in THF solution at 20 °C for 170 h, providing evidence for the importance of intermolecular reactions in the decomposition pathways of **5.1a**. Heating of solid **5.1a** or **5.1b** or their solutions in THF to 70 °C for 170 h led to full conversion to an array of products consisting mainly of the borazine $[HN–BR]_3$, but also small quantities of the aminoborane $H_2N=BPh_2$ as well as the amine–boranes $NH_3·BHPh_2$ and $NH_3·BH_3$ were detected by ^{11}B NMR spectroscopy in case of **5.1a**. These minor products arise from an apparent redistribution of hydrogen and aryl substituents at boron, as found previously for *B*-methyl amine–borane, $NH_3·BH_2Me$, on thermal treatment.[11b] The molecular structures of the borazines $[HN–BR]_3$ (R = Ph, *p*-$CF_3C_6H_4$) were also determined by single crystal X-ray diffraction analysis (Figure 5.1).

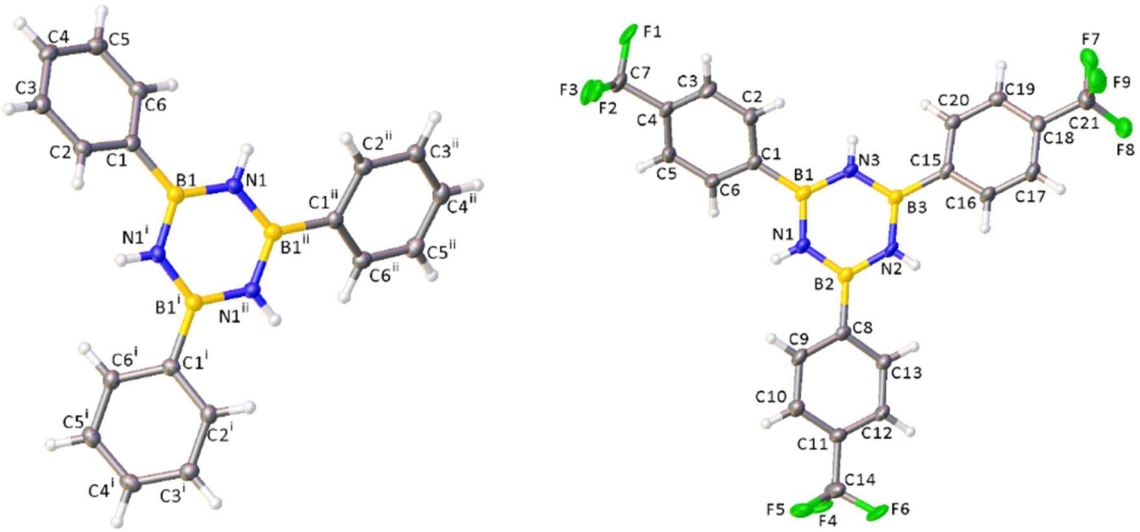

a) b)

Figure 5.1. Molecular structures of the borazines [HN–BPh]$_3$ (a) and [HN–B(*p*-CF$_3$C$_6$H$_4$)]$_3$ in the solid state.

With the aim of preparing high molecular weight poly(*B*-aryl)aminoboranes, we investigated the dehydropolymerisation of **5.1a** using [{Rh(COD)(μ-Cl)}$_2$] (COD = 1,5-cyclooctadiene), skeletal nickel and [IrH$_2$(POCOP)] (POCOP = κ^3-1,3-(*t*Bu$_2$PO)$_2$C$_6$H$_3$), which have previously been reported to be active precatalysts for the dehydrocoupling of amine–boranes (Scheme 5.2 and Table 5.1).[2,9e,9g,15] Reaction of **5.1a** with 2.5 mol % [{Rh(COD)(μ-Cl)}$_2$] (5 % Rh) in THF at 20 °C resulted in the formation of *ca.* 25 % of aminoborane, H$_2$N=BPh$_2$, *ca.* 50 % of borazine, [HN–BPh]$_3$, and *ca.* 25 % of poly(*B*-phenyl)aminoborane, [NH$_2$–BHPh]$_n$ (**5.2a**), as detected by ^{11}B NMR spectroscopy of the reaction mixture after 6 h. A significantly slower reaction was observed for the dehydrocoupling of **5.1a** using 10 mol % skeletal nickel in THF at 20 °C, with only *ca.* 50 % consumption of **5.1a** after 70 h to yield **5.2a** (*ca.* 30 %) and [HN–BPh]$_3$ (*ca.* 20 %). Increasing the amount of skeletal nickel to 100 mol % resulted in quantitative conversion of **5.1a** at 20 °C in THF within 70 h, leading to the formation of mainly borazine [HN–BPh]$_3$ (*ca.* 70 %) and smaller amounts of **5.2a** (*ca.* 20 %) and H$_2$N=BPh$_2$ (*ca.* 10 %). The best results were obtained for the dehydrocoupling of **5.1a** using 5 mol % [IrH$_2$(POCOP)] in THF at 20 °C, which according to ^{11}B NMR spectroscopy resulted in complete

consumption of **5.1a** to yield the highest proportion of polymer **5.2a** (*ca.* 75 %), alongside [HN–BPh]$_3$ (*ca.* 25 %) within 1 h.

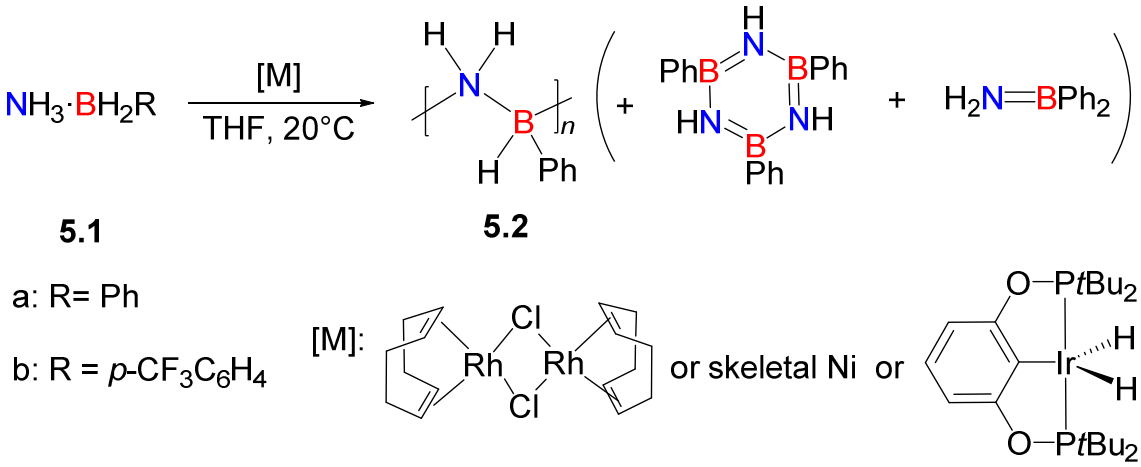

Scheme 5.2. Catalytic dehydrocoupling of **5.1** with different metal catalysts [M]; side products observed in the case of **5.1a** are depicted in brackets.

Table 5.1: Product distribution from the catalytic dehydrocoupling of **5.1a** in THF at 20 °C ([Rh] = [{Rh(COD)(μ-Cl)}$_2$], [Ir] = [IrH$_2$(POCOP)], [Ni] = skeletal nickel).[a]

Conditions	Time [h]	Conversion of 5.1a [%]	Yield of 5.2a [%]	[HN-BPh]$_3$ [%]	H$_2$N=BPh$_2$ [%]
2.5 mol % [Rh]	6	100	25	50	25
10 mol % [Ni]	70	50	30	20	0
100 mol % [Ni]	70	100	20	70	10
5 mol % [Ir]	1	100	75	25	0

[a] Approximate values determined by integration of the broad signals in the ^{11}B NMR spectra of the reaction mixtures.

In order to further optimise the dehydropolymerisation of **5.1a** and isolate polymer **5.2a**, the loading of precatalyst [IrH$_2$(POCOP)] and the reaction time were varied from 0.5 – 5 mol % and 0.5–2 h, respectively (See SI, Section 5.5.2 and 5.5.3). After the specified time, the products were precipitated by transferring the THF solution into precooled (−40 °C), stirred *n*-hexane, which resulted in isolation of a colourless solid. The polymer products were analysed by ^{11}B NMR spectroscopy and gel permeation chromatography (GPC). Full

conversion of **5.1a** was only observed in case of employing 5 mol % [IrH_2(POCOP)] and afforded high molar mass polymer **5.2a** (see below).

Polymer **5.2a** of similar molar mass was prepared on a larger scale by dehydropolymerisation of **5.1a** for 1 h in THF using 5 mol % [IrH_2(POCOP)]. This afforded **5.2a** as an off-white solid in 38 % yield. Using the same protocol, polymer **5.2b** was isolated by dehydropolymerisation of **5.1b** as an off-white solid in 40 % yield. GPC analysis of both solids as solutions in THF (2 mg mL^{-1}, calibration *versus* polystyrene standards) revealed unimodal molecular weight distributions of relatively low dispersity and indicated the presence of high molecular weight polymers in each case (**2a**: M_n = 81,600 g mol^{-1}, PDI = 1.33; **2b**: M_n = 86,800 g mol^{-1}, PDI = 1.37; PDI = polydispersity index) (Figure 5.2a).

Interestingly, analysis of the GPC data for **5.2a** and **5.2b** in the concentration range of 0.5 – 2 mg mL^{-1} revealed a significant dependence of the molar mass data on concentration indicating that the hydrodynamic radius (R_H) of the polymer increased on dilution. This was more pronounced for the fluorinated polymer **5.2b** than **5.2a** (see SI, section 5.5.6.3), and also observed for polymer **5.2b** in DLS in solution of CH_2CL_2, where the hydrodynamic radius increased on dilution (see SI, Figure S5.53). Although no definitive explanation can yet be provided, it is postulated that the presence of electron-withdrawing aryl, and in particular, fluoroaryl substituents enhances the polarity of the polymer structure, which leads to intrachain repulsion.[16] This is suggestive of a non-size-exclusion effects for polyelectrolytes,[17] such as the polyelectrolyte coil expansion or the *polyelectrolyte effect* which are likely to be involved in this case.[18] This effect has also been observed in polyphosphinoboranes bearing fluorinated aryl substituents on phosphorus.[19] This differs from the GPC behaviour observed for poly(*N*-alkyl)aminoboranes where no dependence on the molar mass on concentration was noted[9g] (mentioned in Chapter 4).

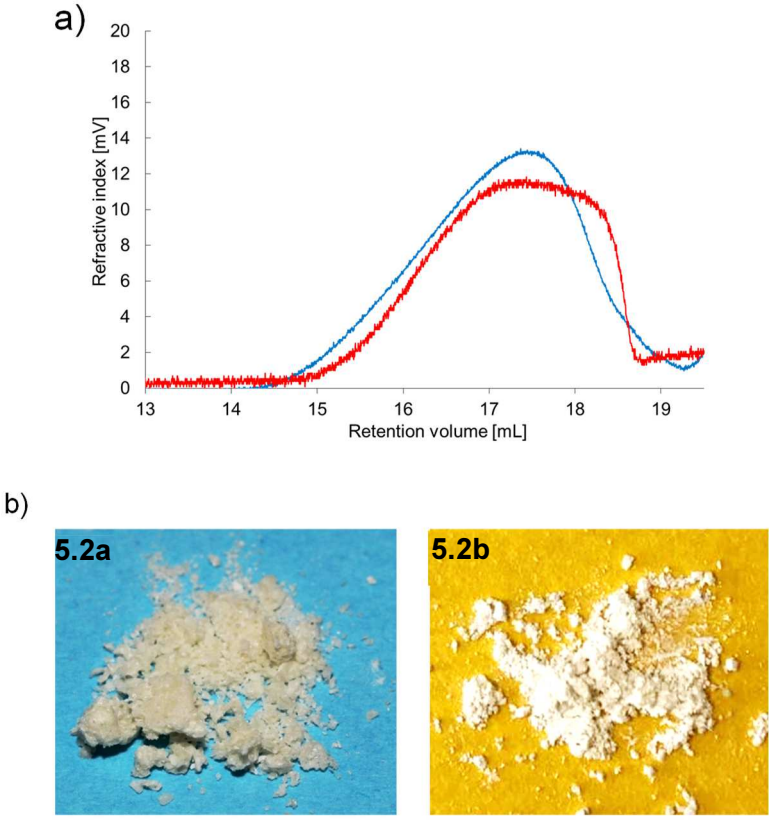

Figure 5.2. a) GPC chromatograms of **5.2a** (blue line) and **5.2b** (red line) in THF (2 mg mL^{-1}) containing 0.1 wt% [*n*Bu$_4$N]Br; b) images of poly(*B*-aryl)aminoboranes **5.2a** and **5.2b**.

The ^{11}B NMR spectra of the polymers displayed broad signals at −7.4 (**5.2a**, THF) and –7.8 ppm (**5.2b**, CD_2Cl_2), which appear in a similar region to that for $[MeNH–BH_2]_n$ (δ_B = −6.7 ppm).[2] The ^{1}H NMR spectra of **5.2a** and **5.2b** both show broad signals, which may result from different stereochemical environments due to tacticity of the polymers, although further conclusions are hampered by the severe quadrupolar broadening. The ESI-MS spectra of **5.2a** (**5.2b**) show multiple peaks with a difference of 105 (173) *m*/*z* up to 14 (8) repeat units, which correspond to [NH_2–BHR] subunits. (see ESI, Figures S5.41 and S5.47).

Polyaminoboranes **5.2a** and **5.2b** are stable to the atmosphere and their thermal stabilities were investigated. This revealed higher stability for the latter material, presumably due to the presence of electron-withdrawing *p*-CF_3 groups in the side chain.

For example, polymer **5.2a** partly decomposes (*ca.* 40 % conversion) after 170 h at 20 °C in the solid state to give mainly monomeric **5.1a** and borazine $[HN–BPh]_3$, whereas polymer **5.2b** is stable under identical conditions. Thermogravimetric analysis is indicative of thermally-induced dehydrogenation and depolymerisation with low ceramic yields as is often found to linear polymers (for example, the char yield of **5.2a** at 275°C is only 5 %). Thermally-induced branching and crosslinking reactions will need to be introduced to exploit potential utility of these materials as ceramic precursors.

5.4 Conclusions

In summary, we report the synthesis and characterisation of the first high molar mass poly(*B*-aryl)aminoboranes **5.2a** and **5.2b**, which can be regarded as B–N analogues of polystyrene. Although similar in appearance to the latter, **5.2a** was found to be of marginal thermal stability. Significant stabilisation was provided by the introduction of an electron withdrawing *para*-CF_3 group on the aryl substituents in **5.2b**. This offers promise for the future formation of thermally stable materials through the introduction of further electron withdrawing groups on boron. We will also explore the accompanying introduction of electron donating groups on nitrogen which would also be anticipated to lead to materials with increased thermodynamic and kinetic stability, therefore laying the foundation for a full exploration of their properties. We are also exploring the addition of crosslinking additives which should increase ceramic yields and allow an exploration of their utility as precursors to BN/graphitic hybrid materials.

5.5 Supporting Information

5.5.1 General procedures and equipment

All manipulations were carried out under an atmosphere of nitrogen using standard vacuum line and Schlenk techniques, or under an atmosphere of argon within an MBraun glovebox. All solvents were dried via a Grubbs design solvent purification system.[20] Phenyl boronic acid ($PhB(OH)_2$), *p*-trifluoromethylphenyl boronic acid [(p-$CF_3C_6H_4$)$B(OH)_2$], lithium aluminium hydride ($LiAlH_4$), ammonium chloride (NH_4Cl) and chloro(1,5-cyclooctadiene)rhodium(I) dimer ([{Rh(COD)(μ-Cl)}$_2$]) were purchased from Sigma Aldrich Ltd. and used as acquired. [IrH_2(POCOP)] (POCOP = [κ^3-1,3-($t$$Bu_2PO$)$_2C_6H_3$][21] and skeletal nickel[9e] were synthesised via literature methods and purified by re-precipitation ([IrH_2(POCOP)]) and washing with *n*-hexane (skeletal nickel). The NMR spectra were recorded at 298 K in J. Young quartz-glass NMR on Jeol ECP(Eclipse) 300 or Jeol ECP(Eclipse) 400 spectrometers. Anhydrous chloroform-*d* and THF-d_8 were purchased from Sigma Aldrich Ltd. and stored over molecular sieves (4 Å) in the glovebox. The ^1H and ^{13}C NMR spectra were calibrated against the residual ^1H and ^{13}C resonances of the respective deuterated solvent [chloroform-*d*: $d(^1H)$ = 7.24 ppm, $d(^{13}C)$ = 77.0 ppm; dichloromethane-d_2: $d(^1H)$ = 5.32 ppm, $d(^{13}C)$ = 54.0 ppm; THF-d_8: $d(^1H)$ = 1.73 ppm, $d(^{13}C)$ = 25.4 ppm] relative to tetramethylsilane [$d(^1H)$ = 0.00 ppm, $d(^{13}C)$ = 0.0 ppm]. The ^{11}B NMR spectra were calibrated against external neat $BF_3{\cdot}Et_2O$ [$d(^{11}B)$ = 0.0 ppm]. Integration of ^{11}B NMR spectra was performed using MestReNova Version 7.1.1 with an estimated accuracy of ± 5%. ESI mass spectra were recorded on a Bruker Daltonics Apex IV Fourier transform Ion Cyclotron resonance mass spectrometer with a cone potential of +150 V using the negative mode in THF or acetonitrile. Elemental analysis was performed with a Eurovector EA 3000 Elemental Analyser at the University of Bristol Microanalysis Laboratory. Gel permeation chromatography (GPC) was performed on a Malvern RI max Gel Permeation Chromatograph, equipped with an automatic sampler, a pump, an

injector, and inline degasser. The columns (T5000) were contained within an oven (35 °C) and consisted of styrene/divinyl benzene gels. Sample elution was detected by means of a differential refractometer. THF (Fisher), containing 0.1 wt% [nBu$_4$N]Br, was used as the eluent at a flow rate of 1 mL min^{-1}. Samples were dissolved in the eluent (2 mg mL^{-1}) and filtered with a Ministart SRP15 filter [poly(tetrafluoroethylene) membrane of 0.45 mm pore size] before analysis. The calibration was conducted using monodisperse polystyrene standards obtained from Sigma Aldrich. The lowest (highest) molecular weight standard used was 2,300 (994,000) g mol^{-1}. Dynamic light scattering (DLS) experiments were carried out using a Malvern Zetasizer Nano S spectrometer using a He-Ne laser (l = 632 nm) in a gas-tight glass cuvette in dry CH_2Cl_2. Thermogravimetric analysis (TGA) was performed on a Thermal Advantage TGAQ500 with a heating rate of 10 °C min^{-1} under nitrogen. The TGA results were analysed using WinUA V4.5A by Thermal Advantage.

4.5.2 Synthesis and characterisation of $NH_3{\cdot}BH_2Ph$ (5.1a) and $NH_3{\cdot}BH_2$(p-$CF_3C_6H_4$) (5.1b)

Synthesis of $NH_3{\cdot}BH_2Ph$ (5.1a): To a suspension of $LiAlH_4$ (2.29 g, 60.3 mmol) in Et_2O (50 mL) was added a solution of $PhB(OH)_2$ (5 g, 40.2 mmol) in Et_2O / toluene (50 mL, 5:2) at 20°C and the suspension was stirred at this temperature for 2 h. The mixture was filtered via cannula to yield a solution of $Li[BH_3Ph]$. This solution was added to a suspension of NH_4Cl (3.23 g, 60.3 mmol) in Et_2O (50 mL) at −78 °C and the mixture was stirred overnight in the cold bath until it reached room temperature. The next day the reaction mixture was filtered through celite. Removal of the solvent from the clear colourless filtrate and drying of the residue under vacuum at room temperature yielded compound **5.1a** a colourless oil, which solidifies at low temperature (−40 °C). Yield: 1.6 g (15.8 mmol, 39 %).

^{11}B NMR (128 MHz, $CDCl_3$): δ = −13.9 (t, $^1J_{BH}$ = 95 Hz) (Figure S5.1).

^{1}H NMR (400 MHz, $CDCl_3$): δ = 2.36 (2 H, q, br, BH_2), 3.12 (3 H, br, NH_3), 7.16 (1 H, t, $^{3}J_{HH}$ = 4 Hz, *para*-Ar*H*), 7.25-7.31 (4 H, m, *meta*-Ar*H* + *ortho*-Ar*H*) (Figure S5.3).

^{13}C{^{1}H} NMR (101 MHz, $CDCl_3$): δ = 125.8(Ar*C*), 127.9 (Ar*C*), 131.9 (Ar*C*), 133.7 (Ar*C*) (Figure S5.4).

Elemental analysis calcd (%) for $C_6H_{10}BN$: C 67.37, H 9.42, N 13.10; found: C 67.66, H 9.67, N 13.13.

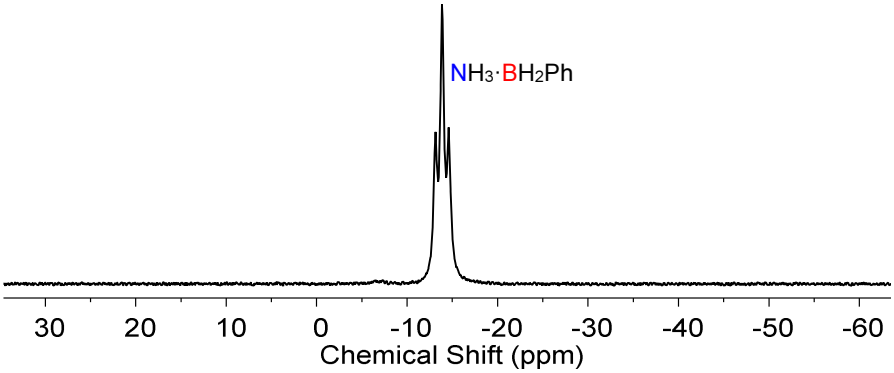

Figure S5.1. ^{11}B NMR spectrum of $NH_3{\cdot}BH_2Ph$ (**5.1a**) in $CDCl_3$

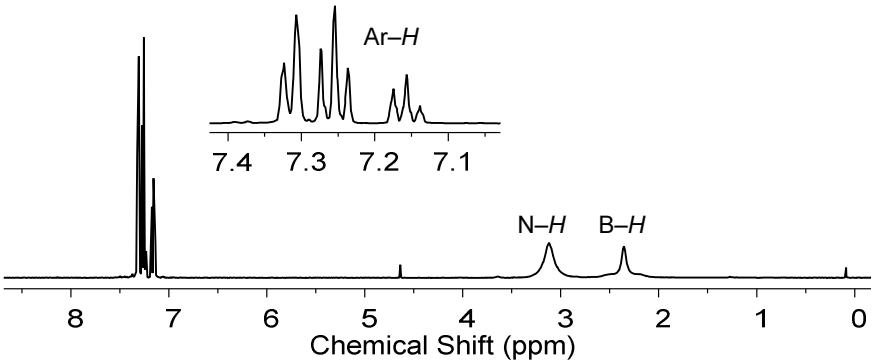

Figure S5.2. ^{1}H{^{11}B} NMR spectrum of $NH_3{\cdot}BH_2Ph$ (**5.1a**) in $CDCl_3$.

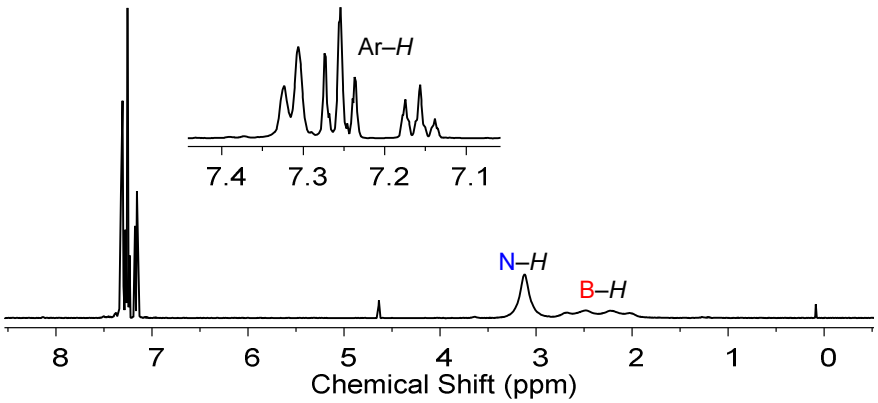

Figure S5.3. ^{1}H NMR spectrum of $NH_3{\cdot}BH_2Ph$ (**5.1a**) in $CDCl_3$.

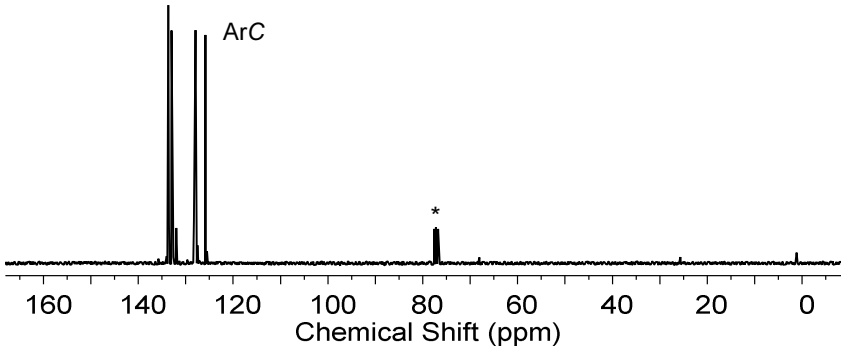

Figure S5.4. $^{13}C\{^{1}H\}$ NMR spectrum of $NH_3{\cdot}BH_2Ph$ (**5.1a**) in $CDCl_3$. * $CDCl_3$.

Synthesis of $NH_3{\cdot}BH_2(p\text{-}CF_3C_6H_4)$ (5.1b): To a suspension of $LiAlH_4$ (1.47 g, 38.7 mmol) in Et_2O (50 mL) was added a solution of $(p\text{-}CF_3C_6H_4)B(OH)_2$ (5 g, 26.3 mmol) in Et_2O / toluene (50 mL, 5:2) at 20°C and the suspension was stirred at this temperature for 2 h. The mixture was filtered via cannula to yield a solution of $Li[BH_3(p\text{-}CF_3C_6H_4)]$. This solution was added to a suspension of NH_4Cl (3.23 g, 60.3 mol) in Et_2O (50 mL) at 20 °C and the suspension was stirred overnight in the cold bath until it reached room temperature. The next day the reaction mixture was filtered through celite. Removal of the solvent from the clear, colourless filtrate and drying of the residue under vacuum afforded compound **5.1b** as a colourless solid. Yield: 3.12 g (17.8 mmol, 69 %).

^{11}B NMR (128 MHz, THF-d_8): δ = −16.8 (t, $^{1}J_{BH}$ = 96 Hz) (Figure S5.5).

^{1}H NMR (400 MHz, THF-d_8): δ = 2.45 (2 H, q, br, BH_2), 4.57 (3 H, br, NH_3), 7.34 (4 H, m, *meta*-Ar*H* + *ortho*-Ar*H*) (Figure S5.6).

$^{13}C\{^{1}H\}$ NMR (101 MHz, THF-d_8): δ = 120.9 (q, $^{3}J_{FC}$ = 4 Hz, *meta*-Ar*C*), 123.3 (q, $^{1}J_{FC}$ = 270 Hz, Ar*C*F_3), 123.8 (q, $^{2}J_{FC}$ = 31 Hz, *para*-Ar*C*), 131.1 (*ortho*-Ar*C*) (the signal for the B-bonded *ipso*-Ar*C* atom was not detected) (Figure S5.7).

$^{19}F\{^{1}H\}$ NMR (376 MHz, THF-d_8): δ = −64.4 (s) (Figure S5.8).

Elemental analysis calcd (%) for $C_7H_9BF_3N$: C 48.05, H 5.19, N 8.01; found: C 48.15, H 5.17, N 7.49.

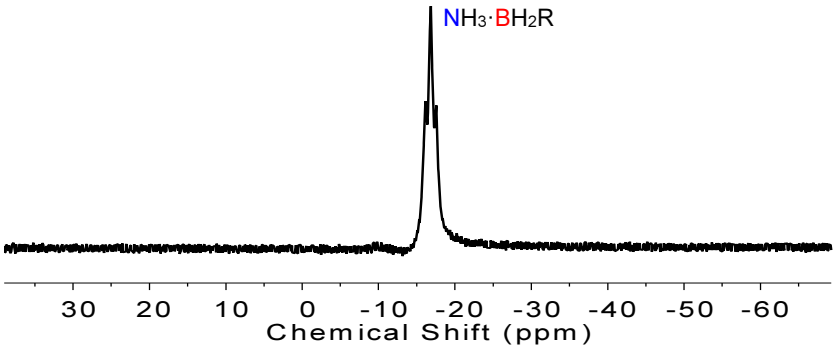

Figure S5.5. ^{11}B NMR spectrum of $NH_3{\cdot}BH_2(p\text{-}CF_3C_6H_4)$ (**5.1b**) in THF-d_8. R = p-$CF_3C_6H_4$

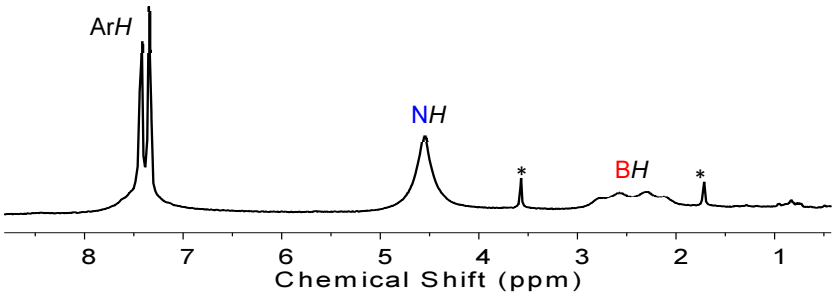

Figure S5.6. ^{1}H NMR spectrum of $NH_3{\cdot}BH_2(p\text{-}CF_3C_6H_4)$ (**5.1b**) in THF-d_8. * THF-d_8.

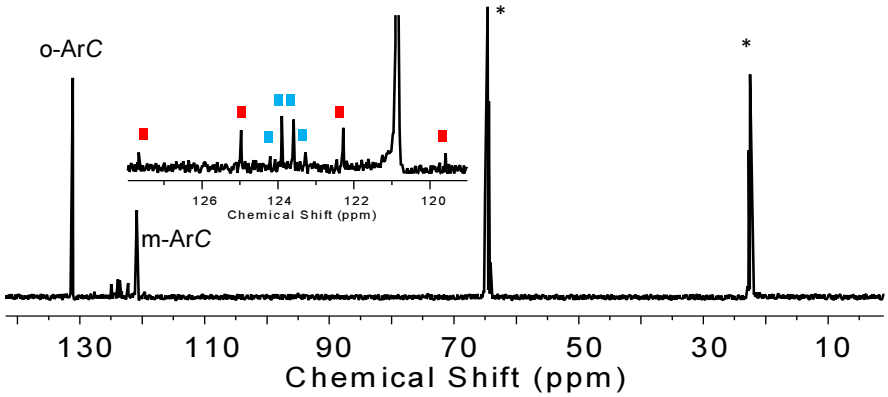

Figure S5.7. ^{13}C{^{1}H} NMR spectrum of $NH_3{\cdot}BH_2(p\text{-}CF_3C_6H_4)$ (**5.1b**) in THF-d_8. Red squares: ArCF_3. Blue squares: p-ArC. * THF-d_8.

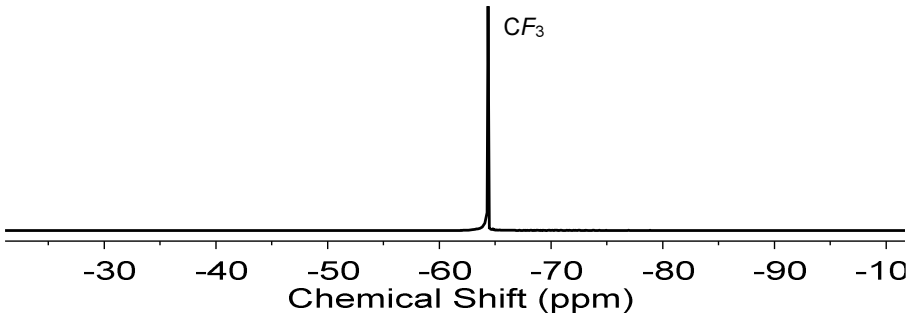

Figure S5.8. $^{19}F\{^{1}H\}$ NMR spectrum of $NH_3 \cdot BH_2(p\text{-}CF_3C_6H_4)$ (**5.1b**) in THF-d_8.

4.5.3 Thermal studies of $NH_3{\cdot}BH_2Ph$ (5.1a) and $NH_3{\cdot}BH_2(p\text{-}CF_3C_6H_4)$ (5.1b)

4.5.3.1 Thermal studies in the solid state:

Thermal stability of solid $NH_3{\cdot}BH_2Ph$ (5.1a) at 20 °C: Solid $NH_3{\cdot}BH_2Ph$ (53 mg, 0.5 mmol) was allowed to stand at 20 °C. After 170 h, the solid was dissolved in THF (0.4 mL) and analysed by ^{11}B NMR spectroscopy to reveal partial consumption of $NH_3{\cdot}BH_2Ph$ [δ_B −14.0 (t, $^1J_{BH}$ = 83 Hz)] (*ca.* 75 %) to yield $[NH_2–BHPh]_n$ [δ_B −7.2 (br)] (*ca.* 20 %) and $NH_3{\cdot}BH_3$ [δ_B −22.9 (q, $^1J_{BH}$ = 107 Hz)] (*ca.* 5 %) (Figures S5.9 and S5.10).

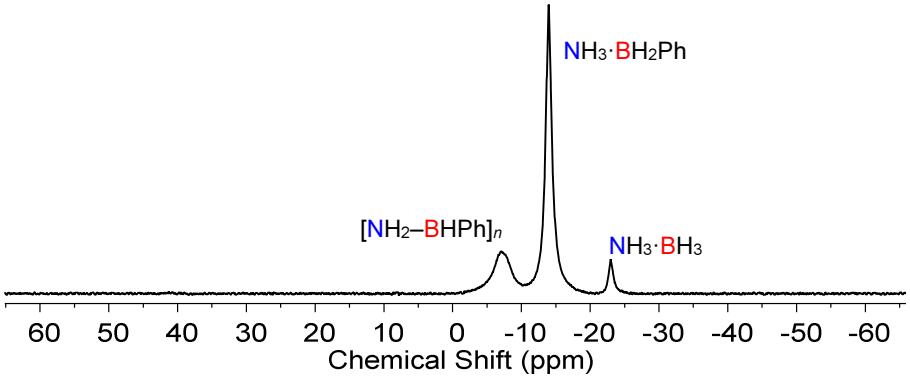

Figure S5.9. $^{11}B\{^1H\}$ NMR spectrum of $NH_3{\cdot}BH_2Ph$ (**5.1a**) in THF after leaving as a solid at 20 °C for 170 h.

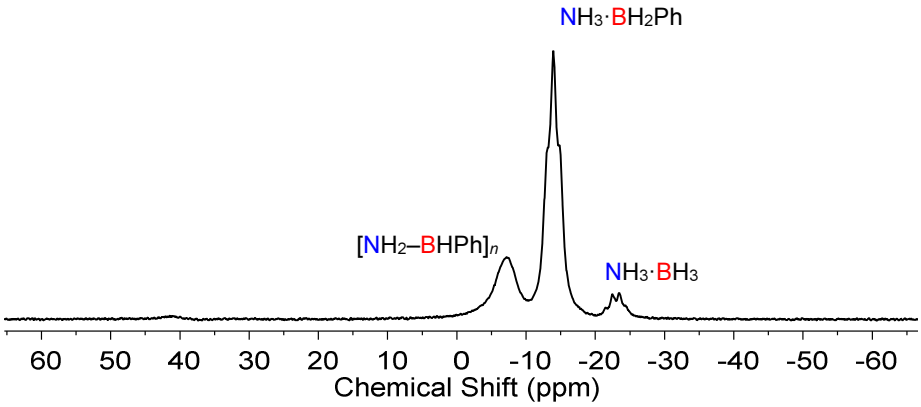

Figure S5.10. ^{11}B NMR spectrum of $NH_3{\cdot}BH_2Ph$ (**5.1a**) in THF after leaving as a solid at 20 °C for 170 h.

Thermal stability of solid $NH_3{\cdot}BH_2Ph$ (5.1a) at 70 °C: Solid $NH_3{\cdot}BH_2Ph$ (53 mg, 0.5 mmol) was transferred to a J. Young quartz-glass NMR tube and heated to 70 °C for 170 h. After cooling to 20 °C, the solid was dissolved in THF (0.4 mL) and analysed by ^{11}B NMR spectroscopy indicating quantitative consumption of $NH_3{\cdot}BH_2Ph$ [δ_B −15.3 (t, $^1J_{BH}$ = 95 Hz)] (trace amounts) to yield $H_2N{=}BPh_2$ [δ_B 40.0 (br)] (*ca.* 10 %), $[HN{-}BPh]_3$ [δ_B 31.4 (s)] (*ca.* 85 %), $NH_3{\cdot}BHPh_2$ [δ_B −9.3 (d, $^1J_{BH}$ = 87 Hz)] (*ca.* 5 %) and $NH_3{\cdot}BH_3$ [δ_B −23.9 (m)] (trace amounts) (Figures S5.11 and S5.12).

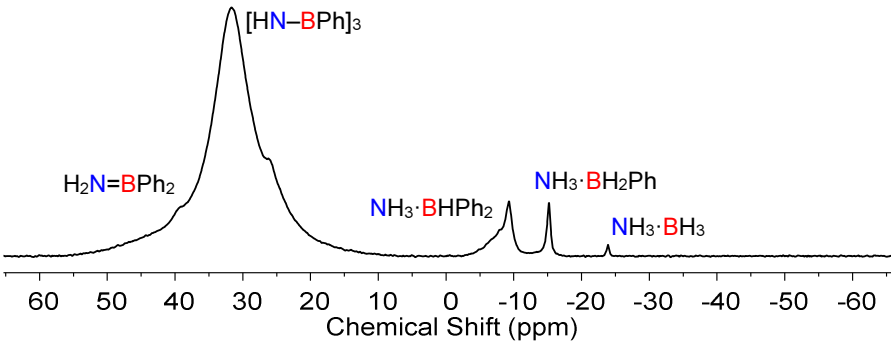

Figure S5.11. $^{11}B\{^1H\}$ NMR spectrum of $NH_3{\cdot}BH_2Ph$ (**5.1a**) as in THF after heating as a solid at 70 °C for 170 h.

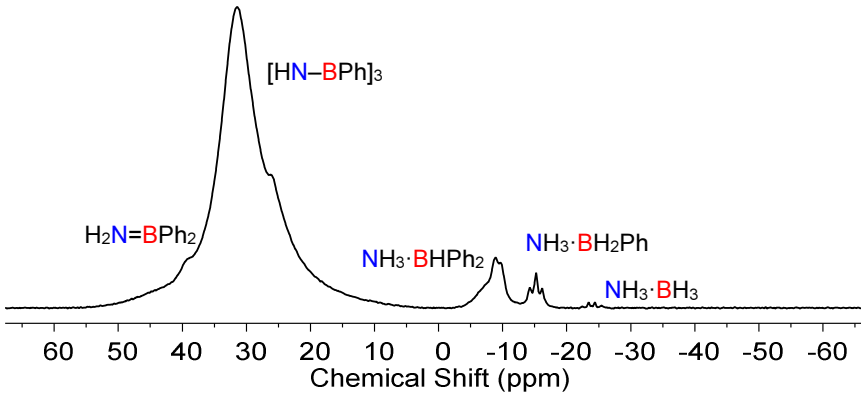

Figure S5.12. ^{11}B NMR spectrum of $NH_3{\cdot}BH_2Ph$ (**5.1a**) in THF after heating as a solid at 70 °C for 170 h.

Thermal stability of solid $NH_3{\cdot}BH_2(p\text{-}CF_3C_6H_4)$ (5.1b) at 20 °C: Solid $NH_3{\cdot}BH_2(p\text{-}CF_3C_6H_4)$ (88 mg, 0.5 mmol) was allowed to stand at 20 °C. After 170 h, the solid was dissolved in THF (0.4 mL) and analysed by ^{11}B NMR spectroscopy to reveal no change [δ_B −11.2 (t, $^1J_{BH}$ = 95 Hz)] (Figure S5.13).

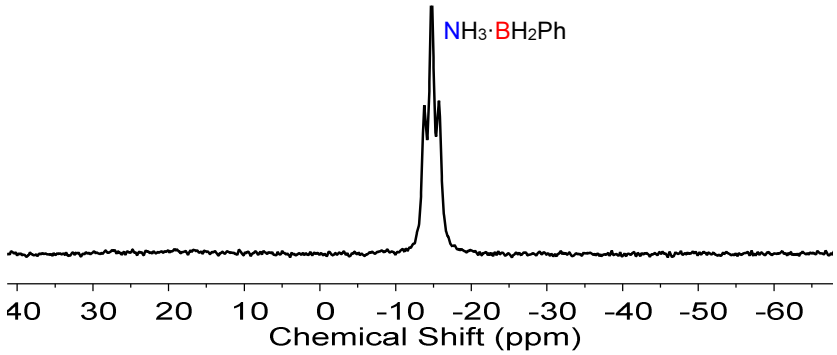

Figure S5.13. ^{11}B NMR spectrum of $NH_3{\cdot}BH_2(p\text{-}CF_3C_6H_4)$ (**1a**) in THF after leaving as a solid at 20 °C for 170 h.

Thermal stability of solid $NH_3{\cdot}BH_2(p\text{-}CF_3C_6H_4)$ (5.1b) at 70 °C: Solid $NH_3{\cdot}BH_2(p\text{-}CF_3C_6H_4)$ (88 mg, 0.5 mmol) was transferred to a J. Young quartz-glass NMR tube and heated to 70 °C for 170 h. After cooling to 20 °C, the solid was dissolved in THF (0.4 mL) and analysed by ^{11}B NMR spectroscopy indicating quantitative consumption of $NH_3{\cdot}BH_2(p\text{-}CF_3C_6H_4)$ to yield $[NH_2{-}BH(p\text{-}CF_3C_6H_4)]_n$ [δ_B −6.0], $[HN{-}B(p\text{-}CF_3C_6H_4)]_3$ [δ_B −32.1] and an array of unknown boron-containing species (Figure S5.14 and S5.15).

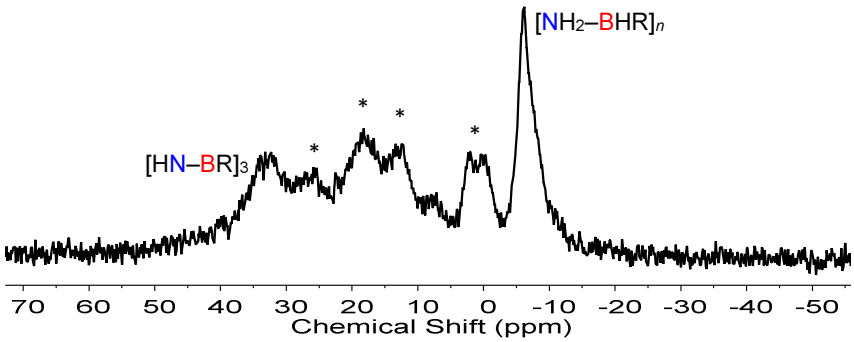

Figure S5.14. $^{11}B\{^1H\}$ NMR spectrum of $NH_3{\cdot}BH_2(p\text{-}CF_3C_6H_4)$ (**1b**) in THF after heating as a solid at 70 °C for 170 h. * Unknown species. R = $p\text{-}CF_3C_6H_4$.

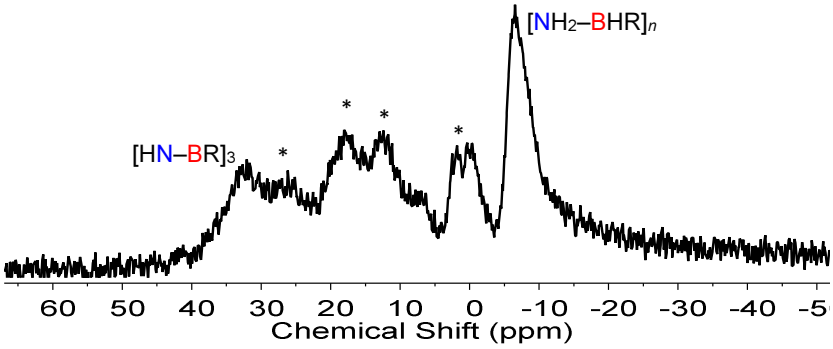

Figure S5.15. ^{11}B NMR spectrum of $NH_3{\cdot}BH_2(p\text{-}CF_3C_6H_4)$ (**5.1b**) in THF after heating as a solid at 70 °C for 170 h. * Unknown species. R = p-$CF_3C_6H_4$.

4.5.3.2 Thermal studies in solution

Thermal stability of $NH_3{\cdot}BH_2Ph$ (5.1a) in THF at 20 °C: An aliquot (0.7 mL) of a solution of $NH_3{\cdot}BH_2Ph$ (53 mg, 0.5 mmol) in THF (2 mL) was stirred for 170 h at 20 °C. The solution was analysed by ^{11}B NMR spectroscopy to reveal no change [δ_B −14.2 (t, $^1J_{BH}$ = 95 Hz)] (Figure S5.16).

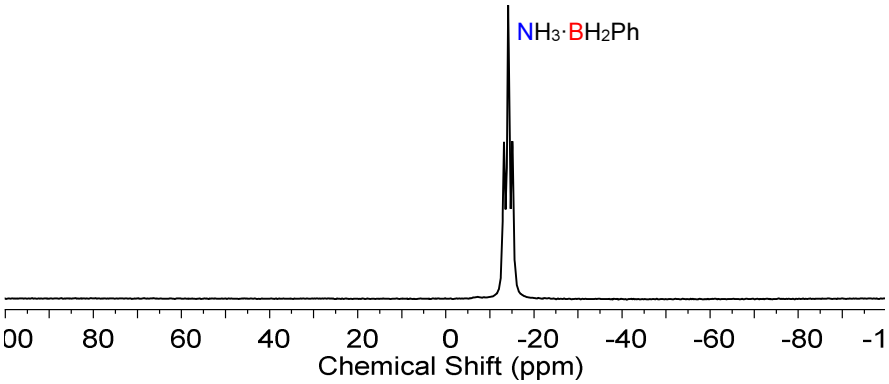

Figure S5.16. ^{11}B NMR spectrum of $NH_3{\cdot}BH_2Ph$ (**1a**) in THF at 20 °C after 170 h.

Thermal stability of $NH_3{\cdot}BH_2Ph$ (1a) in THF at 70 °C: An aliquot (0.7 mL) of a solution of $NH_3{\cdot}BH_2Ph$ (53 mg, 0.5 mmol) in THF (2 mL) was transferred to a J. Young quartz-glass NMR tube and heated to 70 °C for 170 h. After cooling to 20 °C, the mixture was analysed by ^{11}B NMR spectroscopy indicating quantitative consumption of $NH_3{\cdot}BH_2Ph$ [δ_B −14.2 (t, $^1J_{BH}$ = 91 Hz)] (trace amounts) to yield $H_2N{=}BPh_2$ [δ_B 40.2 (s)] (*ca.*

10 %), [HN–BPh]$_3$ [δ_B 31.6 (s)] (*ca.* 70 %), [NH$_2$–BHPh]$_n$ [δ_B −6.2 (br)] (*ca.* 10 %), NH$_3$·BHPh$_2$ [δ_B −8.4 (d, $^1J_{BH}$ = 97 Hz)] (*ca.* 10 %) and an unidentified product [δ_B −11.4 (s)] (trace amounts) (Figures S5.17 and S5.18).

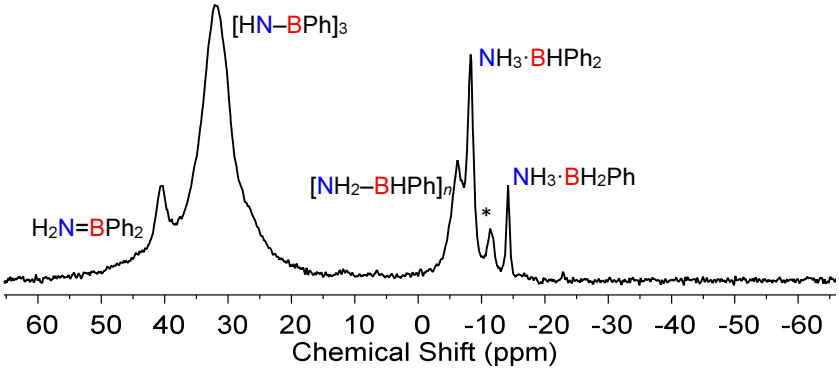

Figure S5.17. $^{11}B\{^1H\}$ NMR spectrum of NH$_3$·BH$_2$Ph (**5.1a**) in THF after heating to 70 °C for 170 h. * Unassigned product.

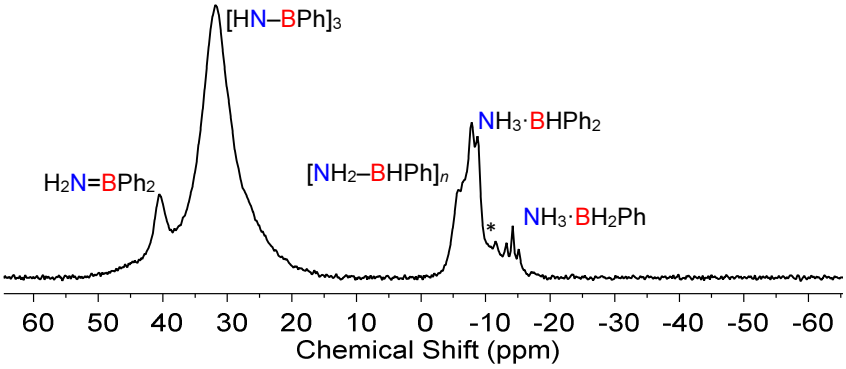

Figure S5.18. ^{11}B NMR spectrum of NH$_3$·BH$_2$Ph (**5.1a**) in THF after heating to 70 °C for 170 h. * Unassigned product.

Thermal stability of NH$_3$·BH$_2$(*p*-CF$_3$C$_6$H$_4$) (5.1b) in THF at 20 °C: An aliquot (0.7 mL) of a solution of NH$_3$·BH$_2$(*p*-CF$_3$C$_6$H$_4$) (88 mg, 0.5 mmol) in THF (2 mL) was stirred for 170 h at 20 °C. The solution was analysed by ^{11}B NMR spectroscopy to reveal no change [δ_B −11.2 (t, $^1J_{BH}$ = 95 Hz)] (Figure S5.19).

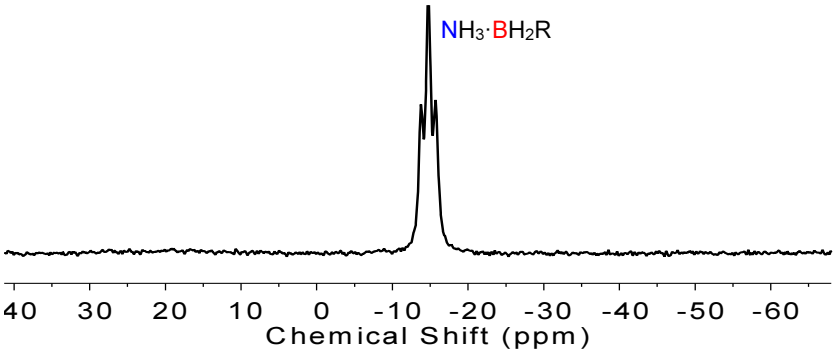

Figure S5.19. ^{11}B NMR spectrum of $NH_3{\cdot}BH_2(p\text{-}CF_3C_6H_4)$ (**5.1b**) in THF at 20 °C after 170 h. R = *p*-$CF_3C_6H_4$.

Thermal stability of $NH_3{\cdot}BH_2(p\text{-}CF_3C_6H_4)$ (5.1b) in THF at 70 °C: An aliquot (0.7 mL) of a solution of $NH_3{\cdot}BH_2(p\text{-}CF_3C_6H_4)$ (88 mg, 0.5 mmol) in THF (2 mL) was transferred to a J. Young quartz-glass NMR tube and heated to 70 °C for 170 h. After cooling to 20 °C, the mixture was analysed by ^{11}B NMR spectroscopy indicating quantitative consumption of $NH_3{\cdot}BH_2(p\text{-}CF_3C_6H_4)$ to yield $[HN{-}B(p\text{-}CF_3C_6H_4)]_3$ [δ_B 31.5 (s)] (*ca.* 80 %), $[NH_2{-}BH(p\text{-}CF_3C_6H_4)]_n$ [δ_B −6.1 (br)] (*ca.* 15 %) and an unidentified product [δ_B 9.3 (s, br)] (*ca.* 5 %) (Figures S5.20 and S5.21).

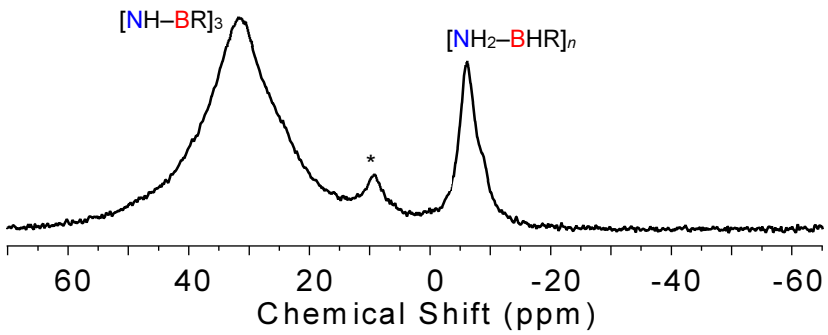

Figure S5.20. ^{11}B{^{1}H} NMR spectrum of $NH_3{\cdot}BH_2(p\text{-}CF_3C_6H_4)$ (**5.1b**) in THF after heating to 70 °C for 170 h. * Unassigned product. R = *p*-$CF_3C_6H_4$.

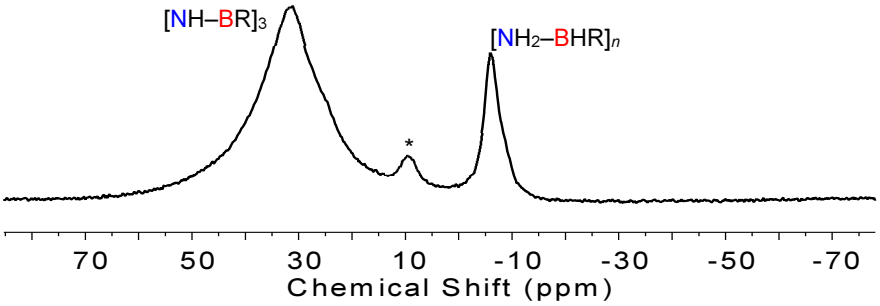

Figure S5.21. ^{11}B NMR spectrum of $NH_3{\cdot}BH_2(p\text{-}CF_3C_6H_4)$ (**5.1b**) in THF after heating to 70 °C for 170 h. * Unassigned product. R = $p\text{-}CF_3C_6H_4$.

5.5.4 Single crystal X-ray diffraction analysis of [HN–BPh]$_3$ and [HN–B(*p*-CF$_3$C$_6$H$_4$)]$_3$

Single crystals of [HN–BPh]$_3$ were isolated upon crystallization from a toluene/diethyl ether mixture at −40 °C and single crystals of [HN–B(*p*-CF$_3$C$_6$H$_4$)]$_3$ were obtained from a *n*-hexane/diethyl ether mixture at room temperature. X-ray diffraction experiments on [HN–BPh]$_3$ and [HN–B(*p*-CF$_3$C$_6$H$_4$)]$_3$ were carried out at 100(2) K on a Bruker APEX II CCD diffractometer using Mo-K$_\alpha$ radiation (λ = 0.71073 Å). Intensities were integrated in SAINT[22] and absorption corrections based on equivalent reflections using SADABS[23] were applied. The structure of [HN-BPh]$_3$ was solved using Superflip[24] and the structure of [HN-B(*p*-CF$_3$C$_6$H$_4$)]$_3$ was solved using olex2.solve;[25] both structures were refined against F^2 in SHELXL[26] using Olex2.[27] All non-hydrogen atoms were refined anisotropically. All hydrogen atoms were located geometrically and refined using a riding model, apart from the N–H protons, which were located in the difference map and refined freely. Squeeze within Platon[28] was used to remove disordered solvent from the lattice of [HN–BPh]$_3$ that could not be sensibly modelled. In the case of [HN–B(*p*-CF$_3$C$_6$H$_4$)]$_3$ the structure was refined as a two component twin against an hklf5 file with the refined occupancies of the two domains 0.44:0.56. In addition, in [HN–B(*p*-CF$_3$C$_6$H$_4$)]$_3$, the CF$_3$ groups were disordered; the occupancies of the fragments were determined by refining them against a free variable with the sum of the two sites set to equal 1, and the occupancies were then fixed at the refined values. Restraints were applied to maintain sensible geometries and thermal parameters. Crystal structure and refinement data are given in Table 5.1. Crystallographic data for compounds [HN–BPh]$_3$ and [HN–B(*p*-CF$_3$C$_6$H$_4$)]$_3$ have been deposited with the Cambridge Crystallographic Data Centre as supplementary publication CCDC 1562257-1562258. Copies of the data can be obtained free of charge on application to CCDC, 12 Union Road, Cambridge CB2 1EZ, UK [fax(+44) 1223 336033, e-mail: deposit@ccdc.cam.ac.uk].

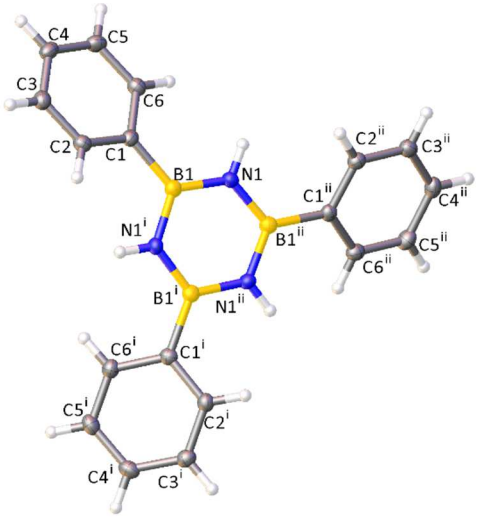

Figure S5.22. Structure of [HN–BPh]$_3$ with the atomic numbering scheme depicted. Ellipsoids are set at the 50% probability level. Symmetry codes ^{i} = 1-*y*, +*x*-*y*, +*z*, ^{ii} = 1+*y*-*x*, 1-*x*, +*z*. Selected bond lengths [Å]: B1–C1 1.573(2), B1–N1 1.424(2), B1–N1^{i} 1.425(2), N1–B1^{ii} 1.425(2). Selected bond angles [°]: N1^{i}–B1–C1 120.92 (12), N1–B1–C1 122.36 (12), N1–B1–N1^{i} 116.65 (14), B1–N1–B1^{ii} 123.30 (14).

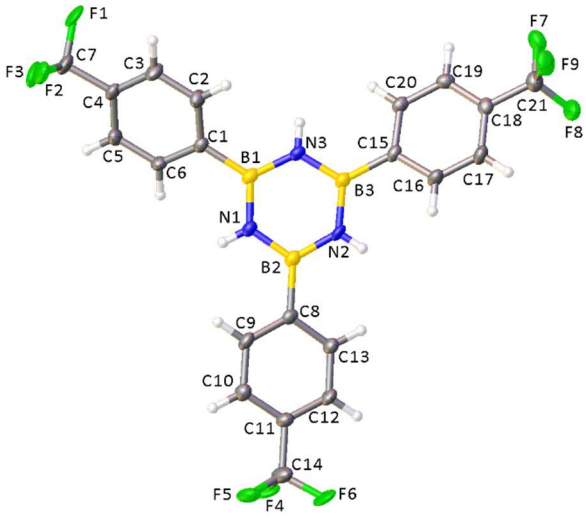

Figure S5.23. Structure of [HN–B(*p*-CF$_3$C$_6$H$_4$)]$_3$ with the atomic numbering scheme depicted. Ellipsoids are set at the 50% probability level. Selected bond lengths [Å]: N1–B1 1.427 (4), N1–B2 1.432 (4), N2–B2 1.425 (4), N2–B3 1.426 (4), N3–B1 1.425 (4), N3–B3 1. 435 (4), B1–C1 1.576 (4), B3–C15 1. 571 (4), B2–C8 1.576 (4). Selected bond angles [°]: B1–N1–B2 124.0 (3), B2–N2–B3 124.3 (2), B1–N3–B3 123.4 (2), N1–B1–C1 121.5 (3), N3–B3–C15 121.6 (2), N2–B2–C8 122.3 (2).

Table S5.1. Crystal data and structure refinement for $[HN–BPh]_3$ and $[HN–B(p\text{-}CF_3C_6H_4)]_3$.

Identification code	**$[HN\text{-}BPh]_3$**	**$[HN\text{-}B(p\text{-}CF_3C_6H_4)]_3$**
Empirical formula	$C_{18}H_{18}B_3N_3$	$C_{21}H_{15}B_3F_9N_3$
Formula weight	308.81	512.79
Temperature/K	100(2)	100(2)
Crystal system	hexagonal	monoclinic
Space group	*P*6*cc*	$P2_1/c$
a/Å	17.1231(6)	11.0171(3)
b/Å	17.1231(6)	23.4105(6)
c/Å	7.1049(3)	8.7127(2)
α/°	90	90
β/°	90	99.1234(15)
γ/°	120	90
Volume/Å^3	1804.07(15)	2218.71(10)
Z	3.9996	4
ρ_{calc}g/cm^3	1.137	1.535
μ/mm^{-1}	0.066	0.143
F(000)	648.0	1032.0
Crystal size/mm^3	0.637 × 0.243 × 0.204	0.59 × 0.41 × 0.25
Radiation	MoK_α (λ = 0.71073)	MoK_α (λ = 0.71073)
2θ range for data collection/°	2.746 to 55.85	3.48 to 55.908
Index ranges	$-22 \le h \le 22$, $-22 \le k \le 22$, $-9 \le l \le 9$	$-14 \le h \le 14$, $0 \le k \le 30$, $0 \le l \le 11$
Reflections collected	38173	5313
R_{int}	0.0477	0.0408
Data/restraints/parameters	1441/1/77	5313/243/413
Goodness-of-fit on F^2	1.073	1.044
Final R indexes [I>=2σ (I)]	R_1 = 0.0285, wR_2 = 0.0760	R_1 = 0.0584, wR_2 = 0.1291
Final R indexes [all data]	R_1 = 0.0309, wR_2 = 0.0773	R_1 = 0.0937, wR_2 = 0.1482
Largest diff. peak/hole / e Å^{-3}	0.21/−0.13	0.70/−0.39

5.5.5 Dehydropolymerisation studies of $NH_3{\cdot}BH_2Ph$ (5.1a)

5.5.5.1 Dehydropolymerisation of 5.1a using different catalysts ([{Rh(COD)(μ-Cl)}$_2$], [IrH_2(POCOP)] and skeletal nickel

Reaction of $NH_3{\cdot}BH_2Ph$ (5.1a) with 2.5 mol % [{Rh(COD)(μ-Cl)}$_2$]: To a solution of $NH_3{\cdot}BH_2Ph$ (53 mg, 0.5 mmol) in THF (1.0 mL) was added a solution of [{Rh(COD)(μ-Cl)}$_2$] (6 mg, 0.01 mmol, 2.5 mol %, 5.0 mol % Rh) in THF (1.0 mL) at 20 °C. After 6 h, an aliquot (0.4 mL) was transferred into a J. Young quartz-glass NMR tube and analysed by ^{11}B NMR spectroscopy revealing quantitative consumption of $NH_3{\cdot}BH_2Ph$ to yield $H_2N{=}BPh_2$ [δ_B 40.9 (s)] (*ca.* 25 %), $[HN{-}BPh]_3$ [δ_B 30.8 (br)] (*ca.* 50 %) and $[NH_2{-}BHPh]_n$ [δ_B −6.5 (br)] (*ca.* 25 %) (Figure S5.24).

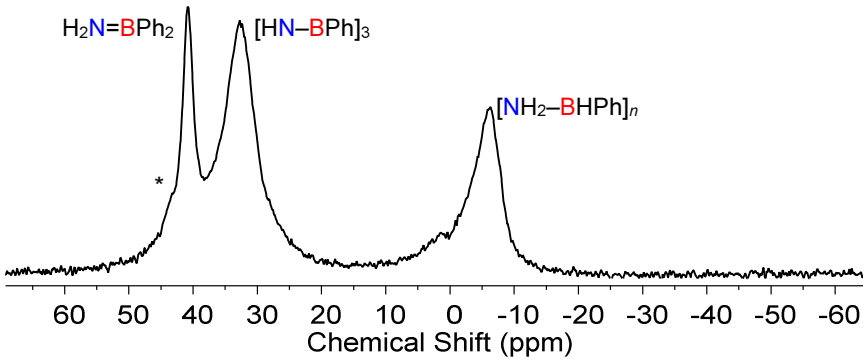

Figure S5.24. $^{11}B\{^1H\}$ NMR spectrum of the reaction of $NH_3{\cdot}BH_2Ph$ (**5.1a**) and 2.5 mol % [{Rh(COD)(μ-Cl)}$_2$] in THF at 20 °C after 6 h. * Unassigned product.

Reaction of $NH_3{\cdot}BH_2Ph$ (5.1a) with 5 mol % [IrH_2(POCOP)]: To a solution of $NH_3{\cdot}BH_2Ph$ (53 mg, 0.5 mmol) in THF (1.0 mL) was added a solution of [IrH_2(POCOP)] (15 mg, 0.025 mmol, 5 mol %) in THF (1.0 mL) at 20 °C. After 1 h, an aliquot (0.4 mL) was transferred into a J. Young quartz-glass NMR tube and analysed by $^{11}B\{^1H\}$ NMR spectroscopy revealing quantitative consumption of $NH_3{\cdot}BH_2Ph$ to yield $[HN{-}BPh]_3$ [δ_B 31.6 (br)] (*ca.* 25 %) and $[NH_2{-}BHPh]_n$ [δ_B −7.2 (br)] (*ca.* 75 %) (Figure S5.25).

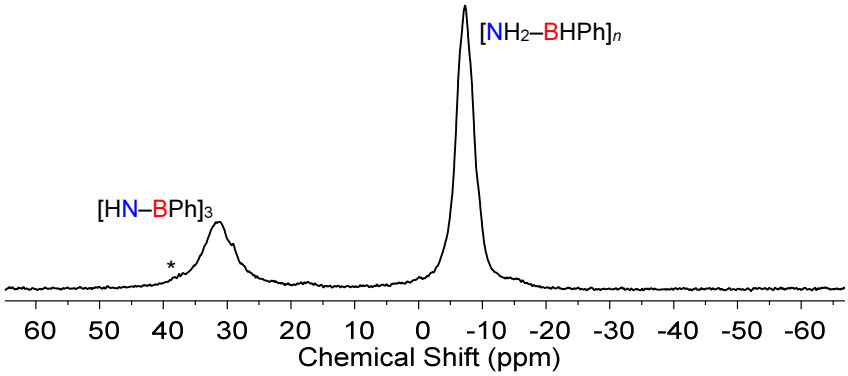

Figure S5.25. $^{11}B\{^{1}H\}$ NMR spectrum of the reaction of $NH_3{\cdot}BH_2Ph$ (**5.1a**) and 5 mol % [IrH_2(POCOP)] in THF at 20 °C after 1 h. * Unassigned product.

Reaction of $NH_3{\cdot}BH_2Ph$ (5.1a) with 10 mol % skeletal nickel: To a suspension of skeletal nickel (3 mg, 0.05 mmol, 10 mol %) in THF (1.0 mL) was added a solution of $NH_3{\cdot}BH_2Ph$ (53 mg, 0.5 mmol) in THF (1.0 mL) at 20 °C. After 70 h, an aliquot (0.4 mL) was transferred to a J. Young quartz-glass NMR tube and analysed by ^{11}B NMR spectroscopy revealing partial consumption of $NH_3{\cdot}BH_2Ph$ [δ_B −14.0 (t, $^{1}J_{BH}$ = 95 Hz)] (*ca.* 50 %) to yield $[HN–BPh]_3$ [δ_B 32.8 (br)] (*ca.* 20 %), and $[NH_2–BHPh]_n$ [δ_B −6.7 (br)] (*ca.* 30 %) (Figure S5.26).

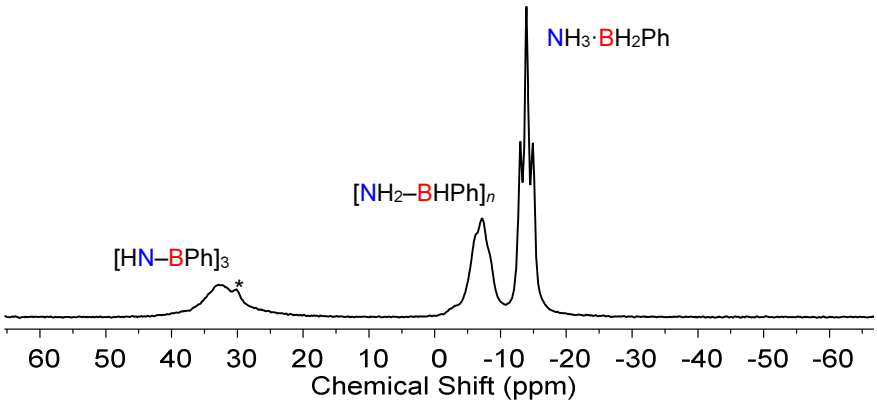

Figure S5.26. ^{11}B NMR spectrum of the reaction of $NH_3{\cdot}BH_2Ph$ (**5.1a**) and 10 mol % skeletal nickel in THF at 20 °C after 70 h. * Unassigned product.

Reaction of $NH_3{\cdot}BH_2Ph$ (5.1a) with 100 mol % of skeletal nickel: To a suspension of skeletal nickel (30 mg, 0.5 mmol) in THF (1.0 mL) was added a solution of $NH_3{\cdot}BH_2Ph$ (53 mg, 0.5 mmol) in THF (1.0 mL) at 20 °C. After 70 h, an aliquot (0.4 mL) was transferred to a J. Young quartz-glass NMR tube and analysed by $^{11}B\{^1H\}$ NMR spectroscopy revealing quantitative consumption of $NH_3{\cdot}BH_2Ph$ to yield $H_2N{=}BPh_2$ [δ_B 41.0 (s)] (*ca.* 10 %), $[HN–BPh]_3$ [δ_B 33.1 (s)] (*ca.* 70 %) and $[NH_2–BHPh]_n$ [δ_B −6.5 (br)] (*ca.* 20 %) (Figure S5.27).

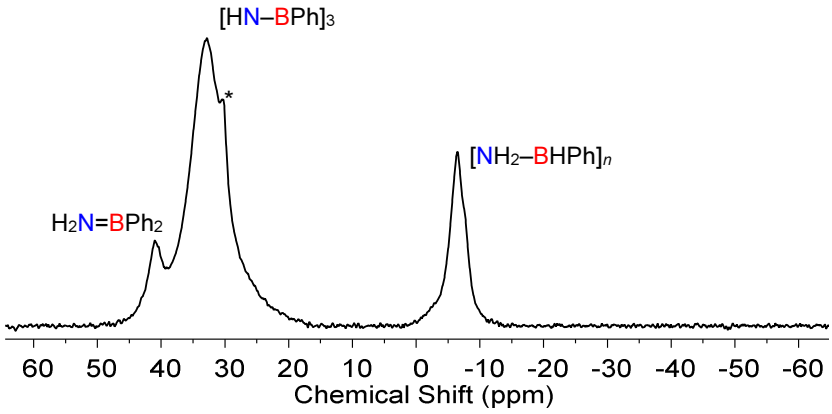

Figure S5.27. $^{11}B\{^1H\}$ NMR spectrum of the reaction of $NH_3{\cdot}BH_2Ph$ (**5.1a**) and 100 mol % of skeletal nickel in THF at 20 °C after 70 h. * Unassigned product.

5.5.5.2 Dehydropolymerisation of $NH_3{\cdot}BH_2Ph$ (5.1a) with various catalyst loadings of $[IrH_2(POCOP)]$

To a solution of $NH_3{\cdot}BH_2Ph$ (200 mg, 1.9 mmol) in THF (0.5 mL) was added a solution of $[IrH_2(POCOP)]$ (0.5, 1 or 5 mol %) in THF (0.5 mL) at 20 °C. After 1 h, the solution was transferred into cold (−40 °C), stirred *n*-hexane, whereupon a colourless precipitate was observed. Excess solvent was removed via decantation and volatile byproducts removed *in vacuo* to yield an off-white solid.

Analysis of the reaction of $NH_3{\cdot}BH_2Ph$ (5.1a) with 0.5 mol % [IrH_2(POCOP)] after 1 h: ^{11}B NMR (THF): $H_2N{=}BPh_2$ [δ_B 39.2 (br)] (trace amounts), $[HN{-}BPh]_3$ [δ_B 30.2 (br)] (trace amounts), $NH_3{\cdot}BH_2Ph$ [δ_B −13.8 (t, br)] (*ca.* 80 %) and $[NH_2{-}BHPh]_n$ [δ_B −6.9 (br)] (*ca.* 20 %) (Figure S5.28); the GPC analysis showed the presence of a trace of high molar mass polymer in the range of 17 to 21 mL in the retention volume (Figure S5.29).

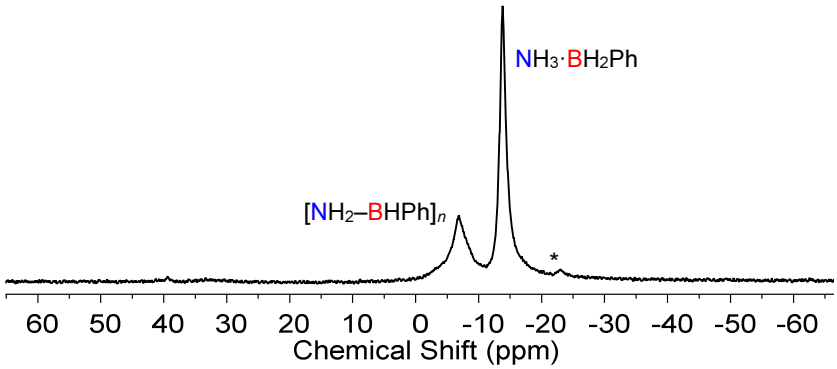

Figure S5.28. $^{11}B\{^1H\}$ NMR spectrum of the product of the reaction of $NH_3{\cdot}BH_2Ph$ (**2.1a**) and 0.5 mol % [IrH_2(POCOP)] in THF at 20 °C after 1 h. * Unassigned product.

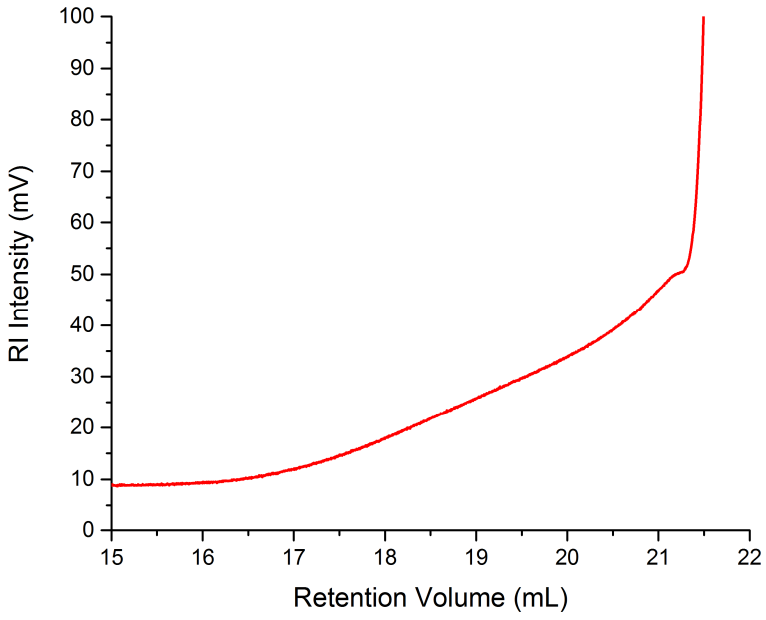

Figure S5.29. GPC chromatogram (2 mg mL^{-1}) of the product of the reaction of $NH_3{\cdot}BH_2Ph$ (**5a**) and 0.5 mol % [IrH_2(POCOP)] in THF (0.1 wt% [nBu$_4$N]Br) at 20 °C after 1 h.

Analysis of the reaction of $NH_3{\cdot}BH_2Ph$ (5.1a) with 1 mol % [IrH_2(POCOP)] after 1 h: ^{11}B NMR (THF): $NH_3{\cdot}BH_2Ph$ [δ_B −12.8 (t, br)] (*ca.* 20 %) and $[NH_2–BHPh]_n$ [δ_B −6.7 (br)] (*ca.* 80 %) (Figure S5.30); GPC (M_n = 96,000 g mol^{-1}, M_w = 121,000 g mol^{-1}, PDI = 1.25) (Figure S5.31).

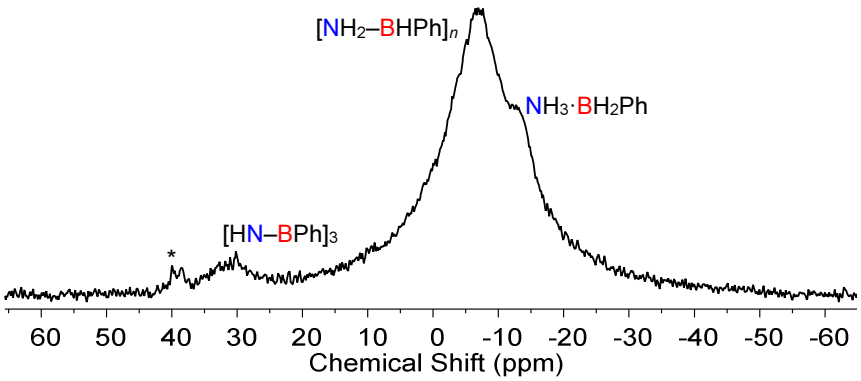

Figure S5.30. $^{11}B\{^1H\}$ NMR spectrum of the product of the reaction of $NH_3{\cdot}BH_2Ph$ (**5.1a**) and 1 mol % [IrH_2(POCOP)] in THF at 20 °C after 1 h. * Unassigned product.

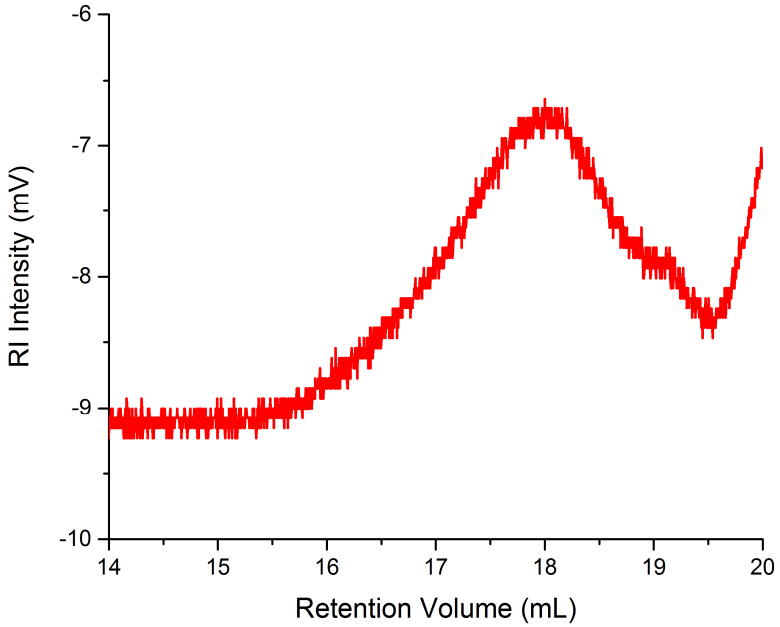

Figure S5.31. GPC chromatogram (2 mg mL^{-1}) of the product of the reaction of $NH_3{\cdot}BH_2Ph$ (**5.1a**) and 1 mol % [IrH_2(POCOP)] in THF (0.1 wt% [nBu$_4$N]Br) at 20 °C after 1 h.

Analysis of the reaction of $NH_3{\cdot}BH_2Ph$ (5.1a) with 5 mol % [IrH_2(POCOP)] after 1 h: $^{11}B\{^1H\}$ NMR (THF): [HN–BPh]$_3$ [δ_B 31.4 (br)] (trace amounts), [NH_2–BHPh]$_n$ [δ_B −6.0 (br)] (Figure S4.32); GPC (M_n = 97,000 g mol^{-1}, M_w = 112,000 g mol^{-1}, PDI = 1.16) (Figure S4.33).

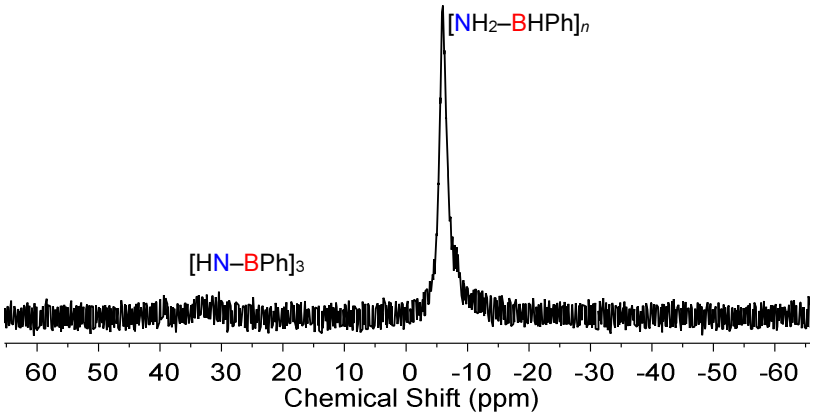

Figure S5.32. $^{11}B\{^1H\}$ NMR spectrum of the product of the reaction of $NH_3{\cdot}BH_2Ph$ (**5.1a**) and 5 mol % [IrH_2(POCOP)] in THF at 20 °C after 1 h.

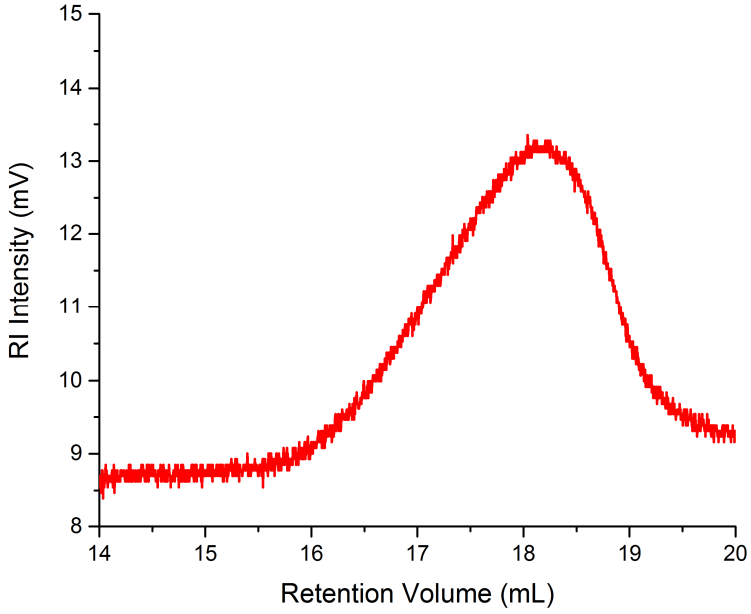

Figure S5.33. GPC chromatogram (2 mg mL^{-1}) of the product of the reaction of $NH_3{\cdot}BH_2Ph$ (**5.1a**) and 5 mol % [IrH_2(POCOP)] in THF (0.1 wt% [nBu$_4$N]Br) at 20 °C after 1 h.

5.5.5.3 Dehydropolymerisation of $NH_3{\cdot}BH_2Ph$ (5.1a) with 1 mol % [IrH_2(POCOP)] after various reaction times

To a solution of $NH_3{\cdot}BH_2Ph$ (200 mg, 1.9 mmol) in THF (0.5 mL) was added a solution of [IrH_2(POCOP)] (1 mol %) in THF (0.5 mL) at 20 °C. After 0.5 or 2 h, the solution was transferred into cold (−40 °C), stirred *n*-hexane, whereupon a colourless precipitate was observed. Excess solvent was removed via decantation and volatile byproducts were removed *in vacuo*.

Analysis of the reaction of $NH_3{\cdot}BH_2Ph$ (5.1a) with 1 mol % [IrH_2(POCOP)] after 0.5 h: ^{11}B NMR (THF): $H_2NH{=}BPh_2$ [δ_B 40.2 (br)] (trace amounts), $[HN{-}BPh]_3$ [δ_B 31.8 (br)] (trace amounts), $NH_3{\cdot}BH_2Ph$ [δ_B −13.4 (t, br)] (*ca.* 20 %) and $[NH_2{-}BHPh]_n$ [δ_B −6.9 (br)] (*ca.* 80 %) (Figure S5.34); GPC (M_n = 30,000 g mol^{-1}, M_w = 63,000 g mol^{-1}, PDI = 2.11) (Figure S5.35).

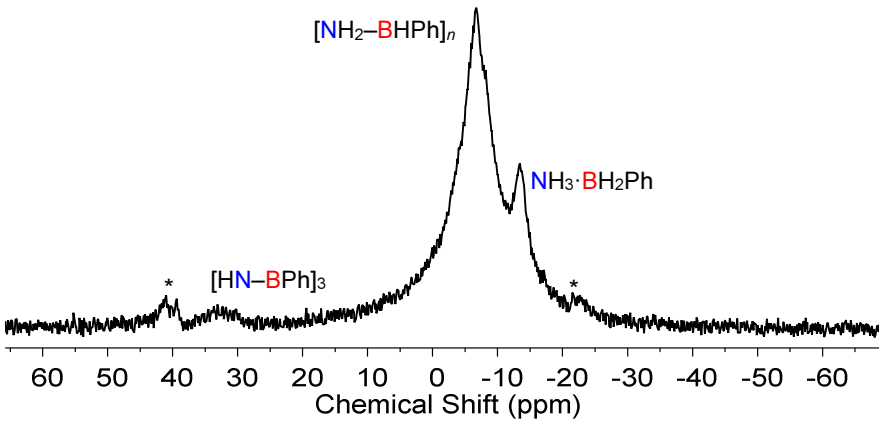

Figure S5.34. $^{11}B\{^1H\}$ NMR spectrum of the product of the reaction of $NH_3{\cdot}BH_2Ph$ (**5.1a**) and 1 mol % [IrH_2(POCOP)] in THF at 20 °C after 0.5 h. * Unassigned product.

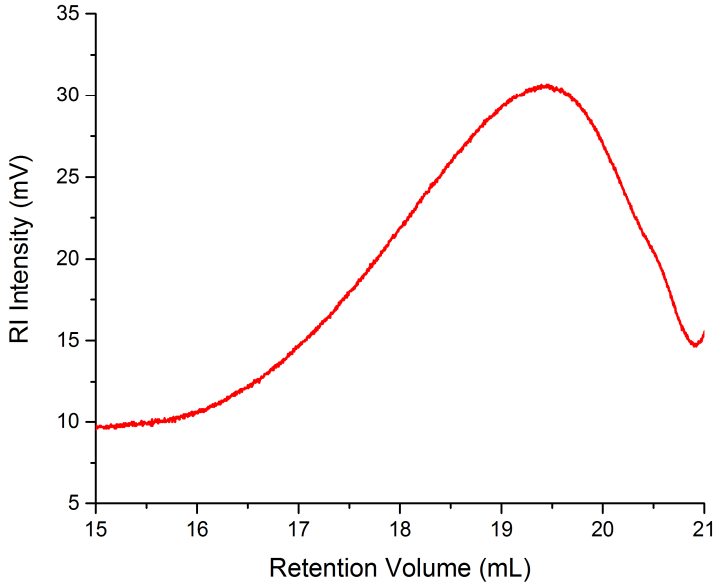

Figure S5.35. GPC chromatogram (2 mg mL^{-1}) of the product of the reaction of $NH_3{\cdot}BH_2Ph$ (**5.1a**) and 1 mol % [IrH_2(POCOP)] in THF (0.1 wt% [*n*Bu_4N]Br) at 20 °C after 0.5 h.

Analysis of the reaction of $NH_3{\cdot}BH_2Ph$ (5.1a) with 1 mol % [IrH_2(POCOP)] after 2 h: ^{11}B NMR ($CDCl_3$): $H_2N{=}BPh_2$ [δ_B 41.2 (br)] (trace amounts), $[HN{-}BPh]_3$ [δ_B 33.3 (br)], $NH_3{\cdot}BH_2Ph$ [δ_B −13.4 (t, br)] (*ca.* 20 %) and $[NH_2{-}BHPh]_n$ [δ_B −4.0 (br)] (*ca.* 80 %) (Figure S5.36); GPC (M_n = 41,000 g mol^{-1}, M_w = 89,000 g mol^{-1}, PDI = 2.15) (Figure S5.37).

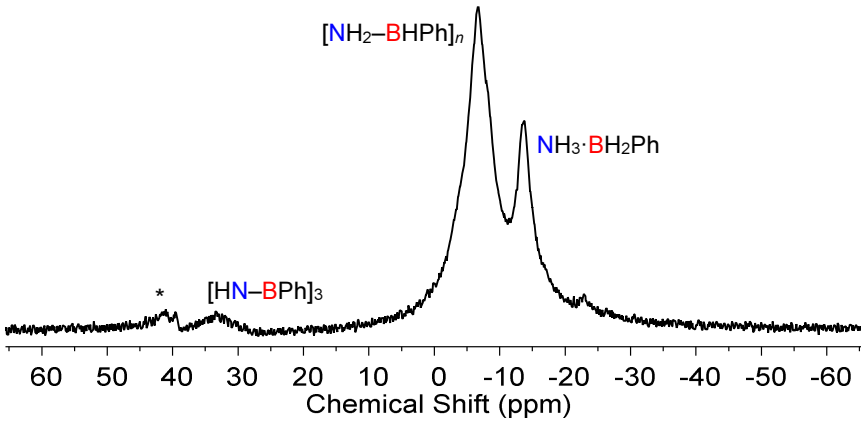

Figure S5.36. $^{11}B\{^1H\}$ NMR spectrum of the product of the reaction of $NH_3{\cdot}BH_2Ph$ (**5.1a**) and 1 mol % [IrH_2(POCOP)] in THF at 20 °C after 2 h. * Unassigned product.

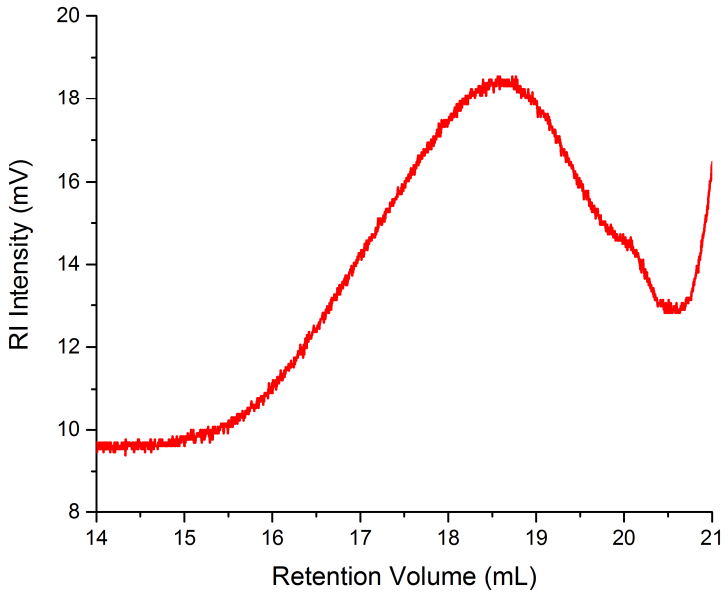

Figure S5.37. GPC chromatogram (2 mg mL^{-1}) of the product of the reaction of $NH_3{\cdot}BH_2Ph$ (**5.1a**) and 1 mol % [IrH_2(POCOP)] in THF (0.1 wt% [*n*Bu_4N]Br) at 20 °C after 2 h.

Table S5.2*:* Influence of different catalyst loadings of [IrH_2(POCOP)] and reaction times on the dehydropolymerisation of **5.1a** in THF at 20 °C.

Catalyst loading [mol %]	Reaction time [h]	Conversion [%][a]	M_n / [g mol^{-1}][b]	PDI[b]
0.5	1	30	–[c]	–[c]
1	1	80	96,000	1.25
5	1	100	97,000	1.16
1	0.5	80	30,000	2.11
1	2	80	41,000	2.15

[a] determined by integration of the signals in the ^{11}B NMR spectra of the reaction mixtures. [b] determined by GPC analysis of the isolated solids in THF containing 0.1 wt% [*n*Bu_4N]Br. [c] the GPC analysis showed that only a trace of high molecular weight material was present.

5.5.6 Synthesis and Characterisation of poly(*B*-aryl aminoboranes)

5.5.6.1 Synthesis and Characterisation of $[NH_2–BHPh]_n$ (5.2a)

To a solution of $NH_3{\cdot}BH_2Ph$ (300 mg, 2.8 mmol) in THF (0.5 mL) was added a solution of $[IrH_2(POCOP)]$ (83 mg, 0.14 mmol, 5 mol %) in THF (0.5 mL) at 20 °C. After 1 h, the solution was transferred into cold (−40 °C) stirred *n*-hexane, whereupon formation of a colourless precipitate was observed. Excess solvent was removed via decantation and the solid was re-precipitated using a minimal amount of CH_2Cl_2 (*ca.* 0.5 mL) and excess *n*-hexane (*ca.* 15 mL). Decantation was then repeated. Residual solvent and volatile byproducts were removed *in vacuo* to yield a colourless solid. Yield: 115 mg (1.1 mmol, 38 %).

$^{11}B\{^1H\}$ NMR (128 MHz, THF-d_8): δ_B −7.4 (br) (Figure S5.38). Trace amounts of unassigned peaks were observed at [δ_B 39.5 (br)] and [δ_B 30.4 (br)].

^1H NMR (400MHz, CD_2Cl_2): δ_H 7.12 (5 H, m, br, Ar*H*), 2.55 (3 H, s, br, B*H*, N*H*) (Figure S5.39).

GPC: M_n = 81,600 g mol^{-1}, M_w = 108,700 g mol^{-1}, PDI = 1.33 (Figure S5.40).

ESI-MS: Difference of 105 *m*/*z* ([NH_2–BHPh] subunit) confirms presence of linear oligo(*B*-phenyl aminoborane) **2a** up to 14 repeat units (Figure S5.41).

TGA: A sample of solid $[NH_2–BHPh]_n$ showed thermal stability up to *ca.* 60 °C, whereupon gradual weight loss occurred until *ca.* 275 °C and *ca.* 5 wt. % remained up to 600 °C (Figure S5.42).

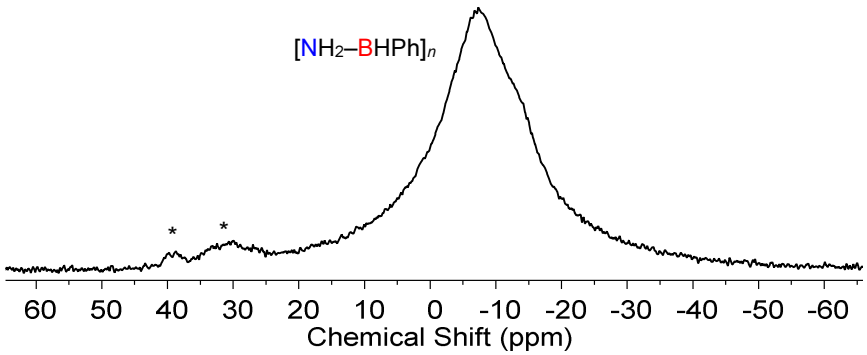

Figure S5.38. $^{11}B\{^{1}H\}$ NMR spectrum of isolated $[NH_2–BHPh]_n$ (**2a**) in THF-d_8 at 20 °C. * Unassigned product.

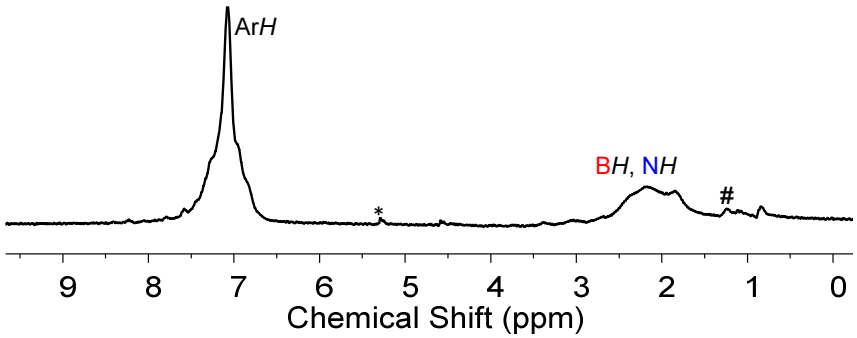

Figure S5.39. ^{1}H NMR spectrum of isolated $[NH_2–BHPh]_n$ (**5.2a**) in CD_2Cl_2. *CD_2Cl_2, # *n*-hexane.

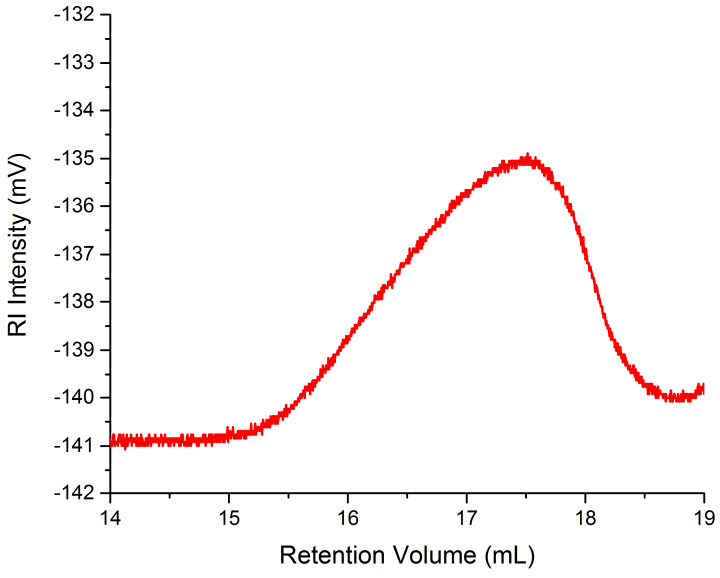

Figure S5.40. GPC chromatogram (2 mg mL^{-1}) of isolated $[NH_2–BHPh]_n$ (**5.2a**) in THF (0.1 wt% [*n*Bu_4N]Br).

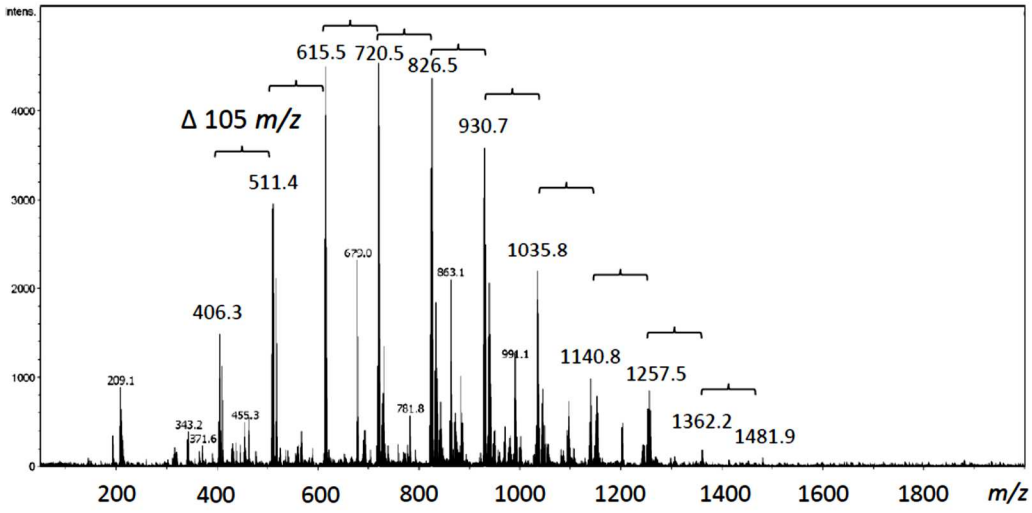

Figure S5.41. ESI mass spectrum of isolated $[NH_2–BHPh]_n$ (**5.2a**) in THF, indicative of oligomeric material of at least 14 subunits.

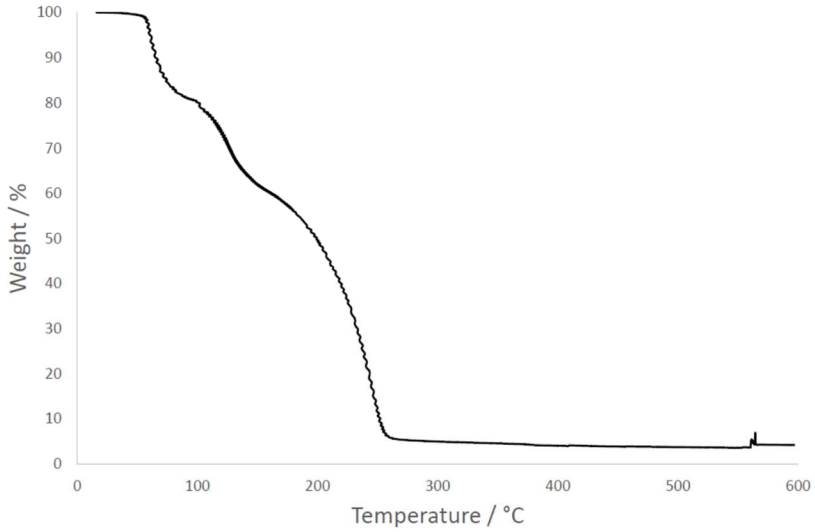

Figure S5.42. TGA plot of isolated $[NH_2–BHPh]_n$ (**5.2a**) (heating rate:10 °C min^{-1}, N_2 gas flow).

5.5.6.2 Synthesis and characterisation of $[NH_2–BH(p\text{-}CF_3C_6H_4)]_n$ (5.2b)

To a solution of $NH_3{\cdot}BH_2(p\text{-}CF_3C_6H_4)$ (300 mg, 1.71 mmol) in a mixture of THF (0.2 mL) and toluene (0.8 mL) was added [IrH_2(POCOP)] (51 mg, 0.086 mmol, 5 mol %) at 20 °C. After 1 h, the solution was transferred into cold (−40 °C), stirred *n*-hexane, whereupon formation of a colourless precipitate was observed. Excess solvent was removed via decantation and the solid was re-precipitated using a minimal amount of CH_2Cl_2 (*ca.* 0.5 mL) and excess *n*-hexane (*ca.* 15 mL). Decantation was then repeated. Residual solvent and volatile byproducts were removed *in vacuo* to yield a colourless solid. Yield: 120 mg (0.69 mmol, 40 %).

$^{11}B\{^1H\}$ NMR (128 MHz, CD_2Cl_2): δ_B −7.8 (br) (Figure S5.43).

^1H NMR (400 MHz, CD_2Cl_2): δ_H 7.25-6.86 (4 H, m, br, *ortho*-Ar*H*, *meta*-Ar*H*), 2.16 (3 H, s, br, B*H*) (Figure S5.44).

$^{19}F\{^1H\}$ NMR (376 MHz, CD_2Cl_2): δ = −62.9 (s) (Figure S5.45).

GPC: M_n = 86,800 g mol^{-1}, M_w = 119,400 g mol^{-1}, PDI = 1.37 (Figure S5.46).

ESI-MS: Difference of 173 *m*/*z* ([NH_2–BH(*p*-$CF_3C_6H_4$)] subunit) confirms presence of linear oligo(*B*-aryl aminoborane) **2b** up to 8 repeat units (Figure S5.47).

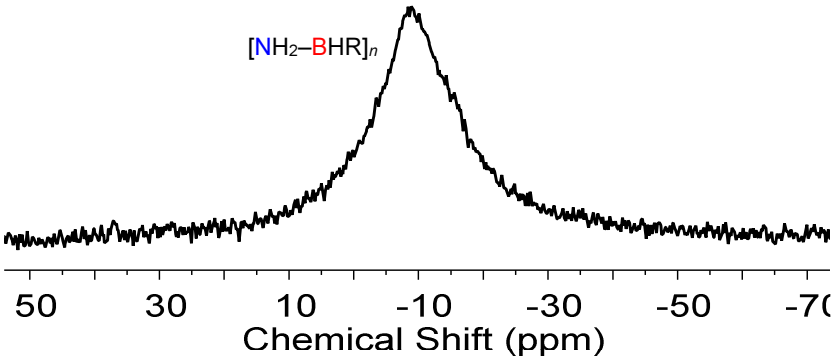

Figure S5.43. $^{11}B\{^1H\}$ NMR spectrum of isolated $[NH_2–BH(p\text{-}CF_3C_6H_4)]_n$ (**5.2b**) in CD_2Cl_2 at 20 °C. R = *p*-$CF_3C_6H_4$

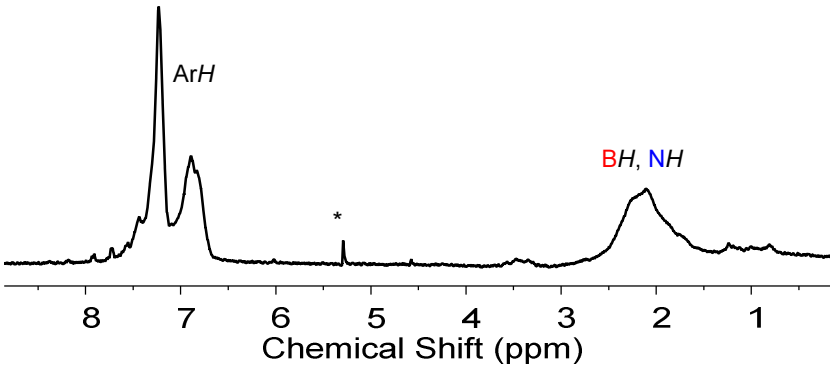

Figure S5.44. ^{1}H NMR spectrum of isolated [NH_2–BH(*p*-$CF_3C_6H_4$)]$_n$ (**5.2b**) in CD_2Cl_2 at 20 °C. * CD_2Cl_2.

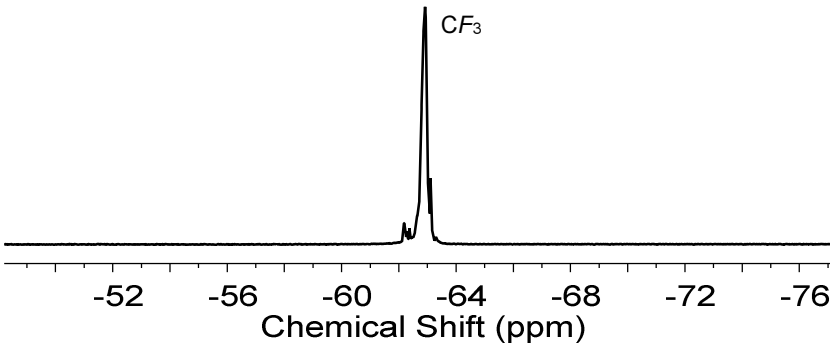

Figure S5.45. ^{19}F{^{1}H} NMR spectrum of isolated [NH_2–BH(*p*-$CF_3C_6H_4$)]$_n$ (**5.2b**) in CD_2Cl_2 at 20 °C.

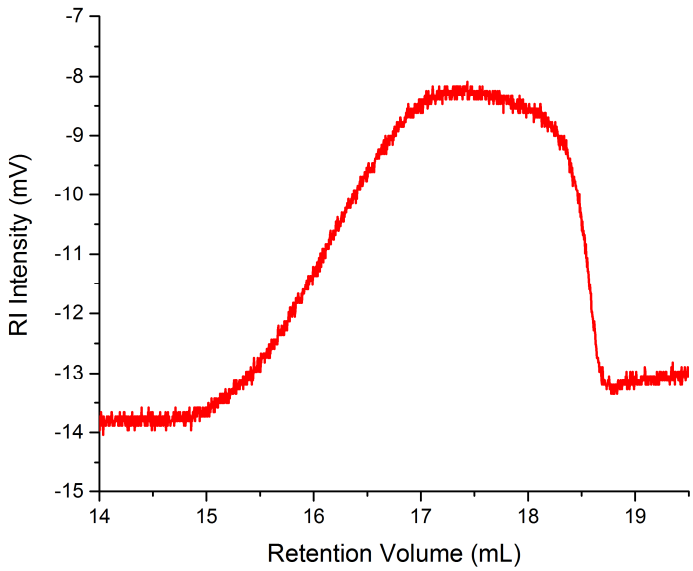

Figure S5.46. GPC chromatogram (2 mg mL^{-1}) of isolated [NH_2–BH(*p*-$CF_3C_6H_4$)]$_n$ (**5.2b**) in THF (0.1 wt% [*n*Bu_4N]Br).

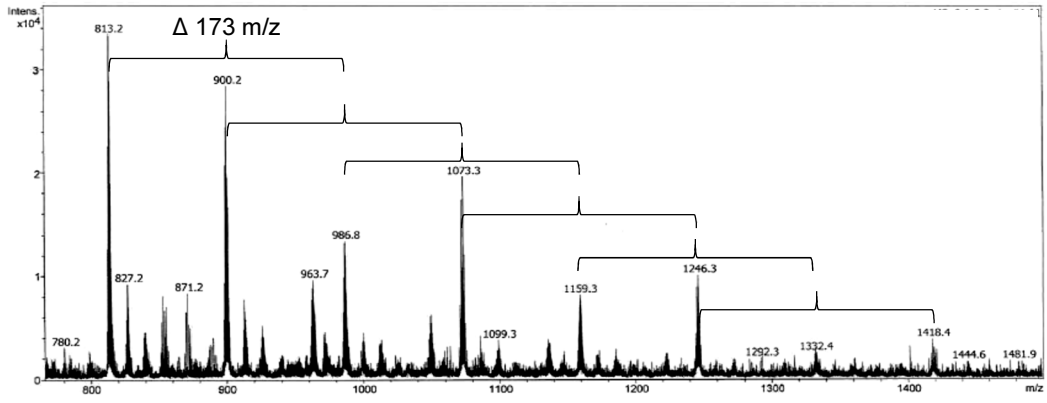

Figure S5.47. ESI mass spectrum of isolated $[NH_2–BH(p\text{-}CF_3C_6H_4)]_n$ (**5.2b**) in CH_3CN, indicative of oligomeric material of at least 8 subunits.

5.5.6.3 GPC analysis of 5.2a and 5.2b at different concentrations

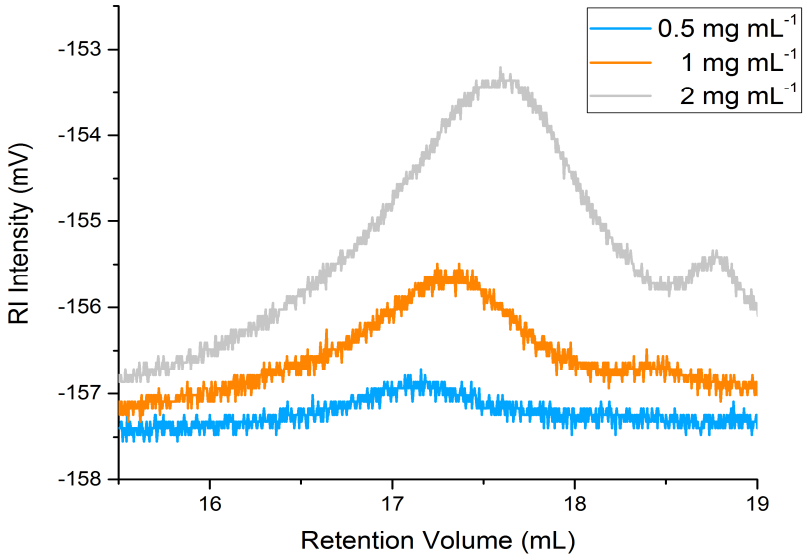

Figure S5.48. GPC chromatograms of $[NH_2–BHPh]_n$ (**5.2a**) in THF (0.1 wt% $[n Bu_4N]Br$) at different concentrations. Note: another batch of polymer was used for the measurement, which was synthesised following exactly the procedure described in section 6.1. Samples were prepared using pure THF.

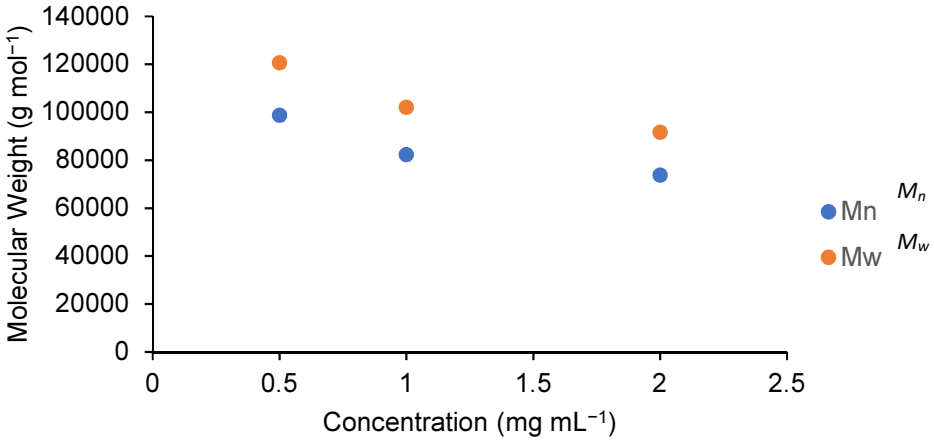

Figure S5.49. Plot of the molecular weight of $[NH_2–BHPh]_n$ (**5.2a**) *versus* the concentration in THF.

Table S5.3. Number average molecular weight (M_n), mass average molecular weight (M_w) and polydispersity index (PDI) for $[NH_2–BHPh]_n$ (**5.2a**) at different concentrations (c).

c (mg mL^{-1})	M_n (g mol^{-1})	M_w (g mol^{-1})	PDI
0.5	98,800	120,700	1.22
1	82,400	102,200	1.24
2	73,900	91,700	1.24

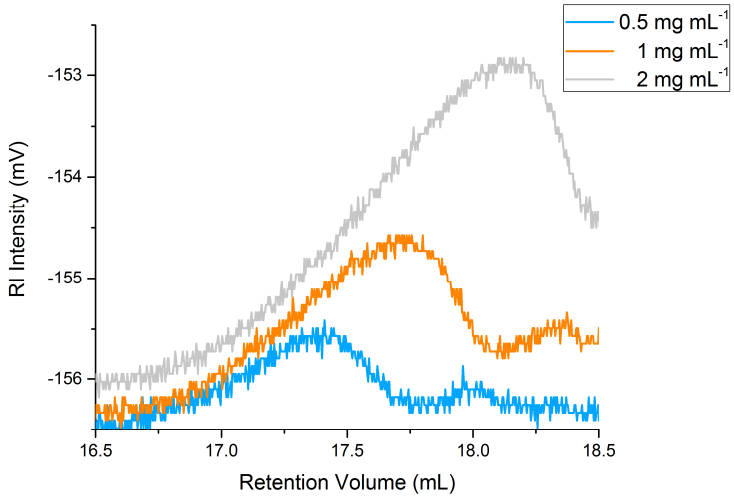

Figure S5.50. GPC chromatograms of [NH_2–BH(*p*-$CF_3C_6H_4$)]$_n$ (**5.2b**) in THF (0.1 wt% [*n*Bu_4N]Br) at different concentrations. Note: another batch of polymer was used for the measurement, which was synthesised following exactly the procedure described in section 6.2. Samples were prepared using pure THF.

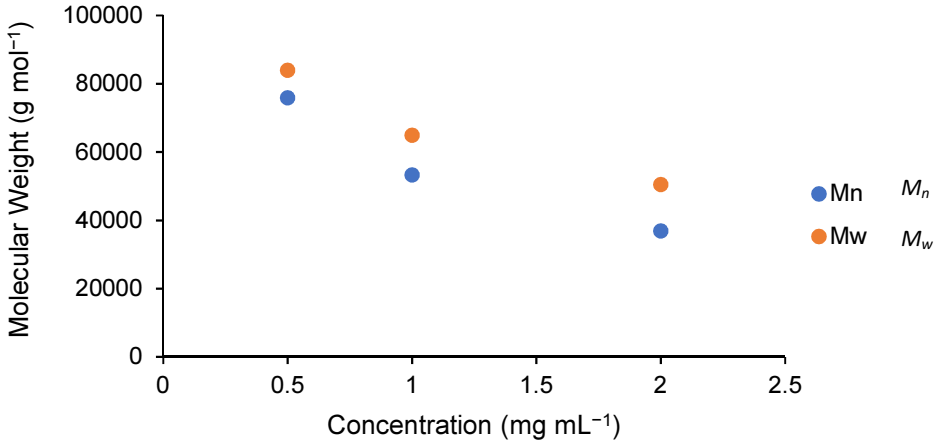

Figure S5.51. Plot of the molecular weight of [NH_2–BH(*p*-$CF_3C_6H_4$)]$_n$ (**5.2b**) *versus* the concentration in THF.

Table S5.4. Number average molecular weight (M_n), mass average molecular weight (M_w) and polydispersity index (PDI) for [NH_2–BH(*p*-$CF_3C_6H_4$)]$_n$ (**5.2b**) at different concentrations (*c*).

c **(mg mL^{-1})**	***M*$_n$ (g mol^{-1})**	***M*$_w$ (g mol^{-1})**	**PDI**
0.5	75,900	84,000	1.11
1	53,300	64,900	1.21
2	36,900	50,500	1.63

5.5.6.4 DLS analysis of 5.2a and 5.2b

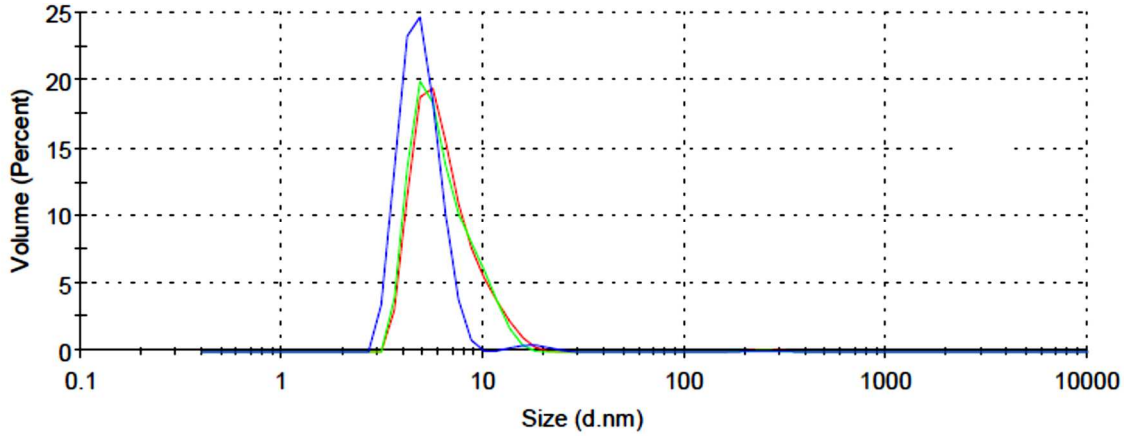

Figure S5.52. DLS (size distribution by volume, repeat scans) of (**5.2a**) in 2 mg mL^{-1} in DCM [R_H = 2.5 nm (average value)].

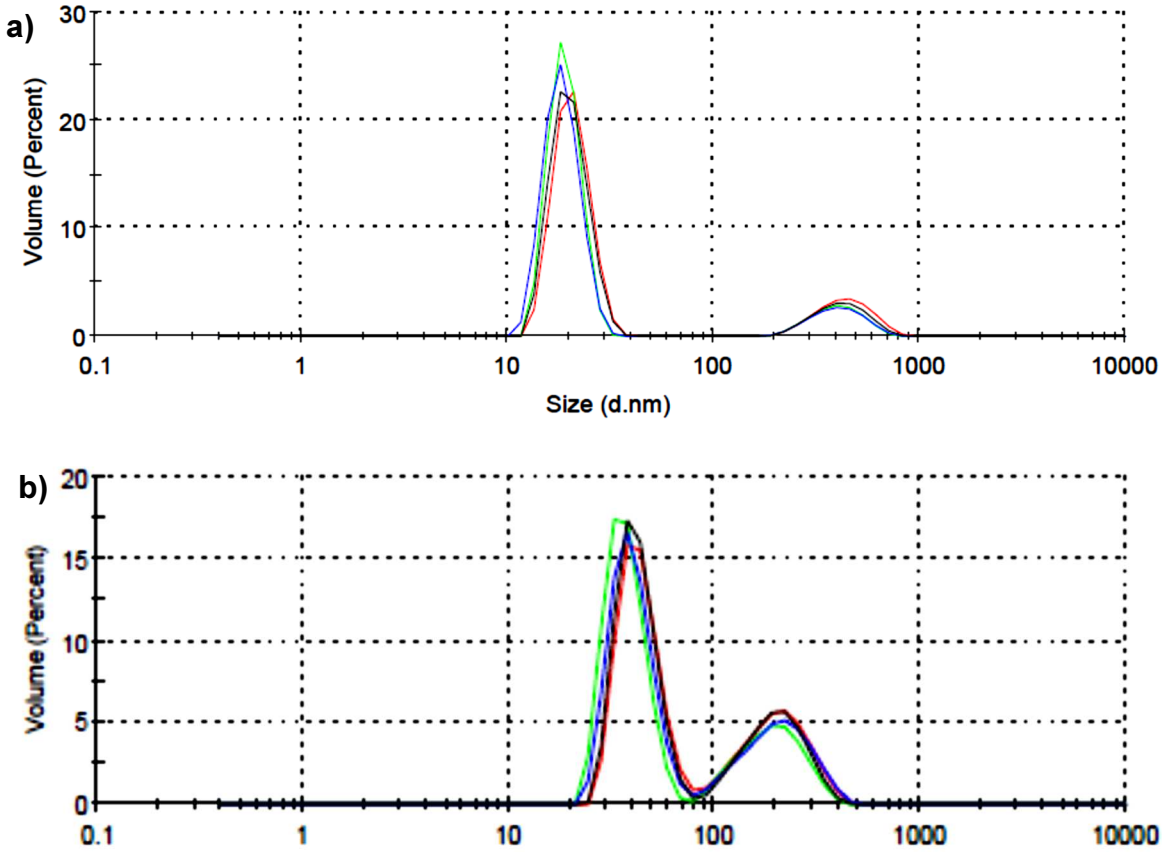

Figure S5.53. DLS (size distribution by volume, repeat scans) of (**5.2b**) in a) 2 mg mL^{-1} in DCM [R_H = 10.1 nm (average value)] and b) 1 mg mL^{-1} in DCM [R_H = 21.2 nm (average value)].

5.5.7 Thermal studies of $[NH_2–BHPh]_n$ (5.2a) and $[NH_2CBH(p\text{-}CF_3C_6H_4)]_n$ (5.2b)

5.5.7.1 Thermal studies in the solid State

Thermal stability of solid $[NH_2–BHPh]_n$ (5.2a) at 20 °C: Solid $[NH_2–BHPh]_n$ (26 mg, 0.25 mmol) was allowed to stand at 20 °C. After 170 h, the solid was dissolved in THF (0.4 mL) and analysed by $^{11}B\{^1H\}$ NMR spectroscopy to reveal partial consumption of $[NH_2–BHPh]_n$ [δ_B −6.8 (br)] (*ca.* 60 %) to yield $H_2N{=}BPh_2$ [δ_B 41.1 (br)] (*ca.* 5 %), $[HN–BPh]_3$ [δ_B 32.7 (br)] (*ca.* 10 %) and $NH_3{\cdot}BH_2Ph$ [δ_B −13.5 (br)] (*ca.* 25 %) (Figure S5.54). Analysis of the solution by GPC confirmed the presence of high molecular weight polymer (M_n = 77,000 g mol^{-1}, M_w = 102,000 g mol^{-1}, PDI = 1.32) (Figure S5.55).

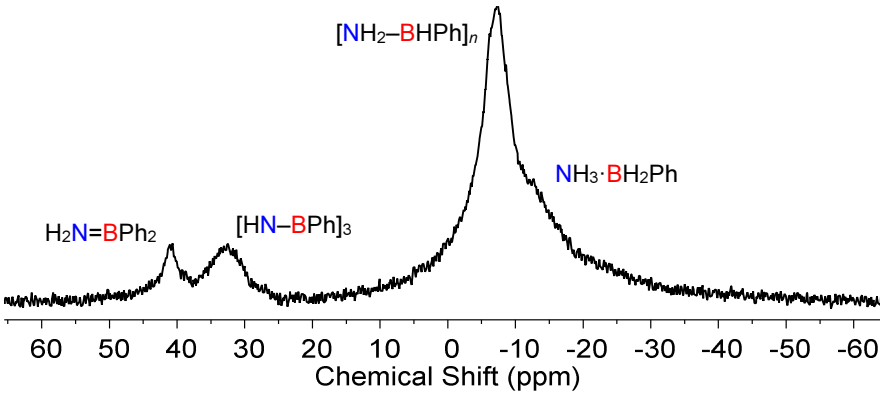

Figure S5.54. $^{11}B\{^1H\}$ NMR spectrum of $[NH_2\text{-}BHPh]_n$ (**2a**) in THF after leaving as a solid at 20 °C for 170 h.

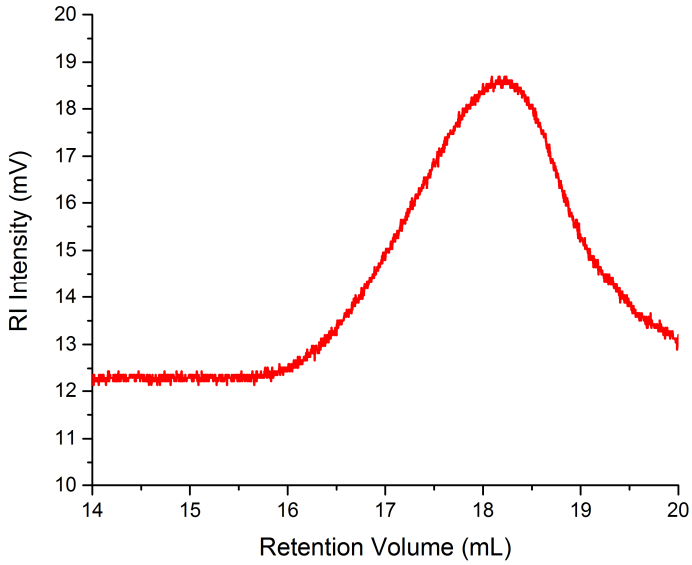

Figure S5.55. GPC chromatogram (2 mg mL^{-1}) of $[NH_2–BHPh]_n$ (**5.2a**) in THF (0.1 wt% $[nBu_4N]Br$) after leaving as a solid at 20 °C for 170 h.

Thermal stability of solid $[NH_2–BHPh]_n$ (5.2a) at 70 °C: Solid $[NH_2–BHPh]_n$ (26 mg, 0.25 mmol) was heated to 70 °C for 24 h. After cooling to 20 °C, the solid was dissolved in THF (0.4 mL). Analysis by ^{11}B NMR spectroscopy revealed quantitative consumption of $[NH_2–BHPh]_n$ [δ_B −6.3 (br)] (trace amounts) to yield $[HN–BPh]_3$ [δ_B 33.5 (br)] as the sole product (Figure S5.56).

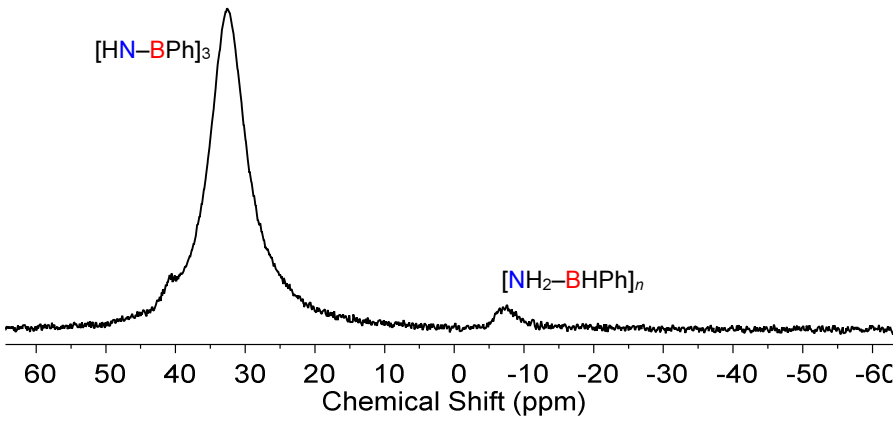

Figure S5.56. $^{11}B\{^1H\}$ NMR spectrum of $[NH_2–BHPh]_n$ (**5.2a**) in THF after heating as a solid at 70 °C for 170 h.

Thermal stability of solid [NH$_2$–BH(*p*-CF$_3$C$_6$H$_4$)]$_n$ (5.2b): Solid [NH$_2$–BH(*p*-CF$_3$C$_6$H$_4$)]$_n$ (43 mg, 0.25 mmol) was allowed to stand at 20 °C. After 170 h, the solid was dissolved in THF (0.4 mL) and analysed by ^{11}B{^{1}H} NMR spectroscopy to reveal no change of [NH$_2$–BHPh]$_n$ [δ_B −6.8 (br)] (Figure S5.57). Analysis of the solution by GPC confirmed the presence of high molecular weight polymer (M_n = 123,900 g mol^{-1}, M_w = 157,500 g mol^{-1}, PDI = 1.27). (Figure S5.58).

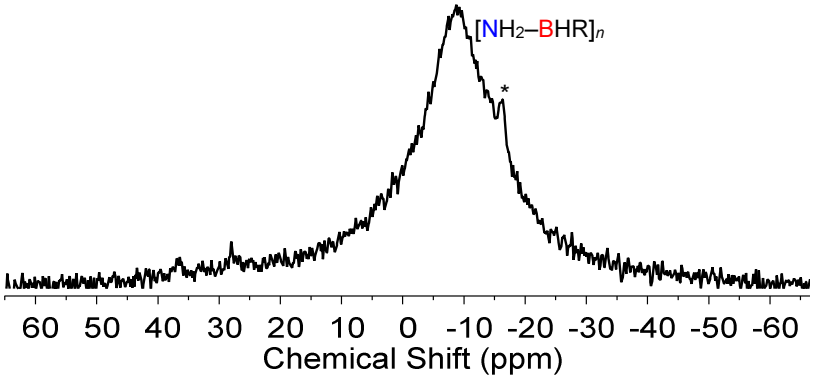

Figure S5.57. ^{11}B{^{1}H} NMR spectrum of [NH$_2$–BH(*p*-CF$_3$C$_6$H$_4$)]$_n$ (**5.2b**) in THF after leaving as a solid at 20 °C for 170 h. R = *p*-CF$_3$C$_6$H$_4$. * Traces of NH$_3$·BH$_2$(*p*-CF$_3$C$_6$H$_4$).

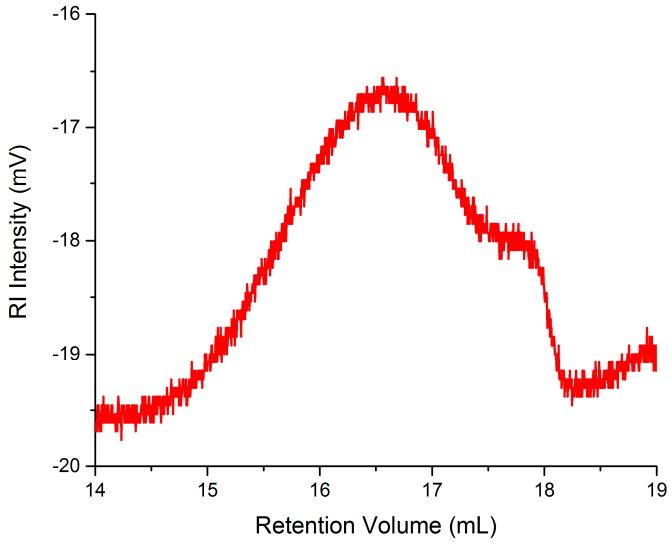

Figure S5.58. GPC chromatogram (2 mg mL^{-1}) of [NH$_2$–BH(*p*-CF$_3$C$_6$H$_4$)]$_n$ (**5.2b**) in THF (0.1 wt% [*n*Bu$_4$N]Br) after leaving as a solid at 20 °C for 170 h.

Thermal stability of solid [NH_2–BH(*p*-$CF_3C_6H_4$)]$_n$ (5.2b) at 70 °C: Solid [NH_2–BH(*p*-$CF_3C_6H_4$)]$_n$ (88 mg, 0.25 mmol) was heated to 70 °C for 170 h. After cooling to 20 °C, the residue was dissolved in THF (0.4 mL). Analysis by ^{11}B NMR spectroscopy revealed partial consumption of [NH_2-BH(*p*-$CF_3C_6H_4$)]$_n$ [δ_B –7.4 (br)] (ca. 60%) to yield an unknown product at [δ_B 12.3 (br)] (ca. 40%) and trace amounts of [HN–B(*p*-$CF_3C_6H_4$)]$_3$ [δ_B 29.3 (br)] (Figure S5.59). Analysis of the solution by GPC confirmed the presence of high molecular weight material (M_n = 77,500 g mol^{-1}, M_w = 81,000 g mol^{-1}, PDI = 1.04) (Figure S5.60).

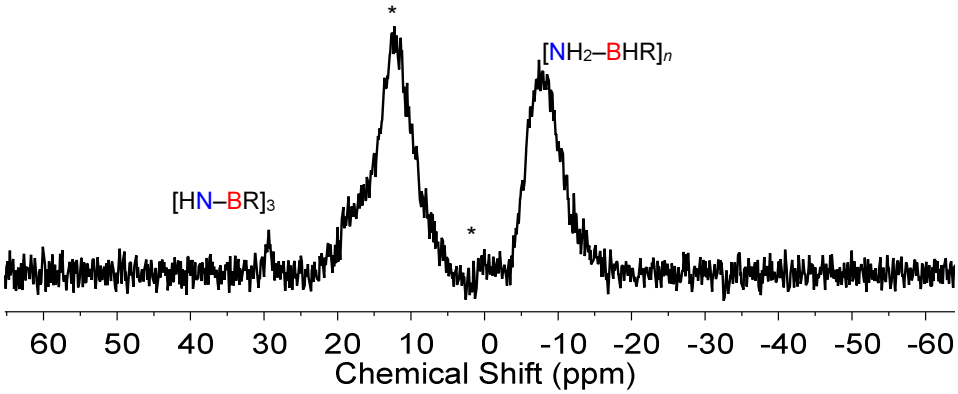

Figure S5.59. ^{11}B{^{1}H} NMR spectrum of [NH_2–BH(*p*-$CF_3C_6H_4$)]$_n$ (**5.2b**) in THF after heating as a solid at 70 °C for 170 h. * Unknown species. R = *p*-$CF_3C_6H_4$.

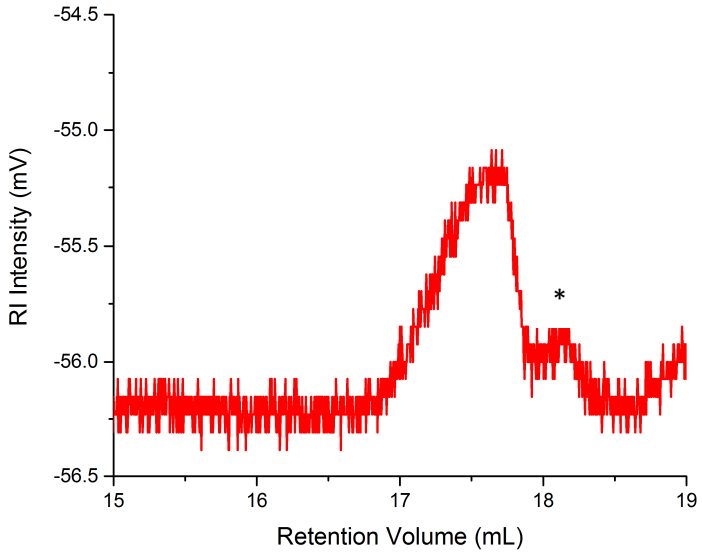

Figure S5.60. GPC chromatogram (2 mg mL^{-1}) of [NH_2–BH(*p*-$CF_3C_6H_4$)]$_n$ (**5.2b**) in THF (0.1 wt% [*n*Bu_4N]Br) after leaving as a solid at 70 °C for 170 h. The asterisk (*) marks an additional trace, which was present in the polymer batch used for the thermal studies.

5.5.7.2 Thermal Studies in Solution

Thermal stability [NH_2–BHPh]$_n$ (5.2a) in THF at 20 °C: A solution of [NH_2–BHPh]$_n$ (26 mg, 0.25 mmol) in THF (0.5 mL) was stirred at 20 °C. After 170 h, the solution was analysed by ^{11}B NMR spectroscopy to reveal partial depolymerisation and redistribution of [NH_2–BHPh]$_n$ to yield H_2N=BPh_2 [δ_B 40.6 (br)] (trace amounts), [HN–BPh]$_3$ [δ_B 32.4 (br)] (*ca.* 20 %), [NH_2–BHPh]$_n$ [δ_B −6.8 (br)] and [δ_B −8.0 (br)] (*ca.* 50 %), NH_3·BH_2Ph [δ_B −14.0 (t, $^1J_{BH}$ = 95 Hz)] (*ca.* 25 %) and NH_3·BH_3 [δ_B −22.8 (q, $^1J_{BH}$ = 96 Hz)] (*ca.* 5 %) (Figures S5.61 and S5.62). Analysis of the solution by GPC confirmed the presence of high molecular weight polymer (M_n = 66,000 g mol^{-1}, M_w = 99,000 g mol^{-1}, PDI = 1.49) (Figure S5.63).

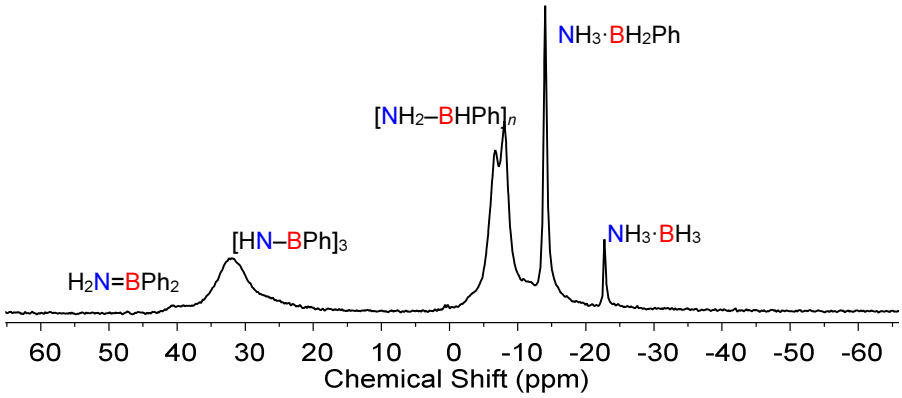

Figure S5.61. ^{11}B{^{1}H} NMR spectrum of [NH_2–BHPh]$_n$ (**5.2a**) in THF at 20 °C after 170 h.

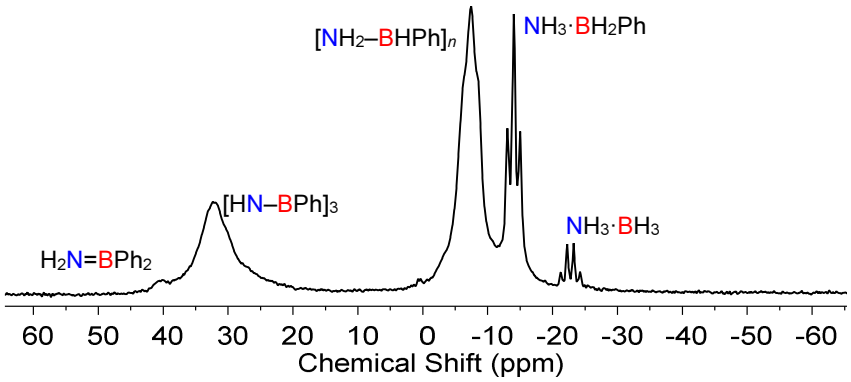

Figure S5.62. ^{11}B NMR spectrum of [NH_2–BHPh]$_n$ (**5.2a**) in THF at 20 °C after 170 h.

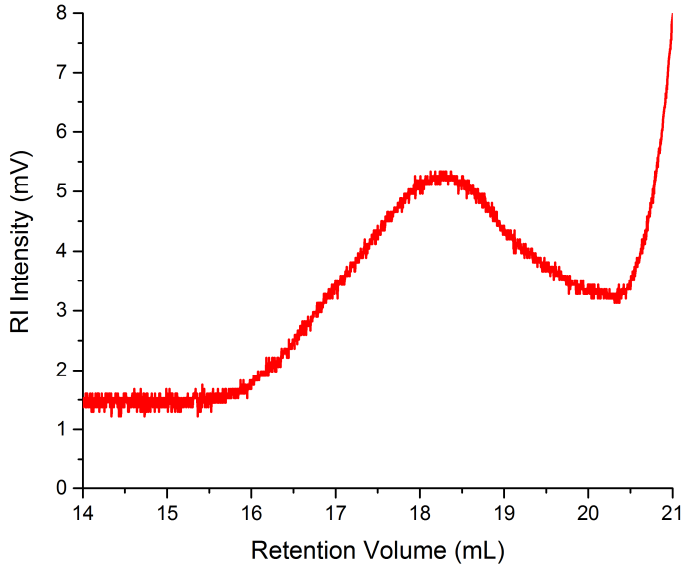

Figure S5.63. GPC chromatogram (2 mg mL^{-1}) of $[NH_2–BHPh]_n$ (**5.2a**) in THF (0.1 wt% [*n*Bu$_4$N]Br) at 20 °C after 170 h.

Thermal stability of $[NH_2–BHPh]_n$ (5.2a) in THF at 70 °C: An aliquot (0.4 mL) of a solution of $[NH_2$-BHPh$]_n$ (26 mg, 0.25 mmol) in THF (0.5 mL) was transferred to J. Young quartz-glass NMR tube and heated to 70 °C for 170 h. After cooling to 20 °C, the mixture was analysed by ^{11}B NMR spectroscopy indicating partial depolymerisation and redistribution of $[NH_2–BHPh]_n$ to yield $H_2N{=}BPh_2$ [δ_B 40.5 (s)] (*ca.* 5 %), $[HN–BPh]_3$ [δ_B 31.9 (br)] (*ca.* 70 %), $[NH_2–BHPh]_n$ [δ_B −6.2 (br)] (*ca.* 5 %), $NH_3{\cdot}BHPh_2$ [δ_B −8.1 (br)] (*ca.* 15 %), $NH_3{\cdot}BH_2Ph$ [δ_B −14.1 (t, $^1J_{BH}$ = 97 Hz)] (*ca.* 5 %), $NH_3{\cdot}BH_3$ [δ_B −22.8, (m)] (trace amounts) and $H_2B(\mu\text{-}H)(\mu\text{-}NH_2)BH_2$ [δ_B −27.6 (br)] (trace amounts) (Figures S5.64 and S5.65). Analysis of the solution by GPC revealed that neither high nor low molecular weight species were present.

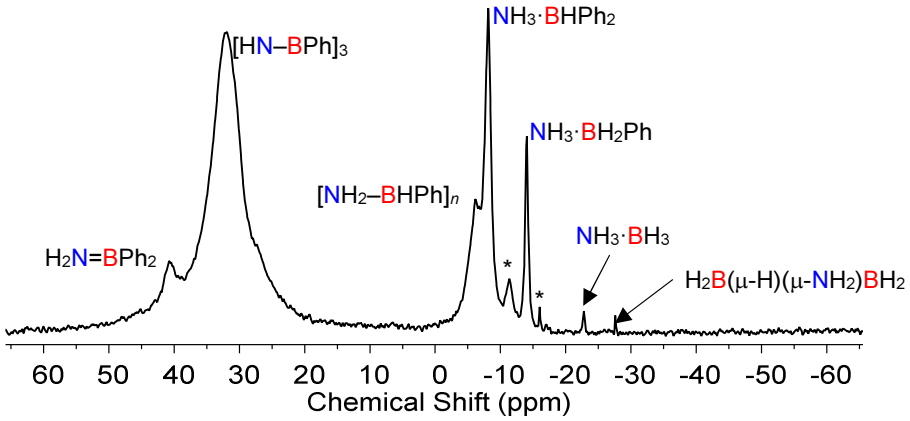

Figure S5.64. $^{11}B\{^{1}H\}$ NMR spectrum of $[NH_2–BHPh]_n$ (**5.2a**) in THF after heating to 70 °C for 170 h. * Unassigned product.

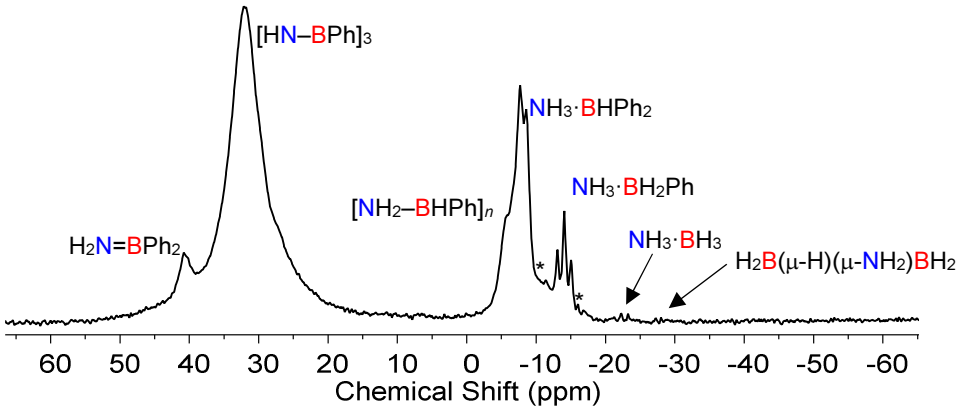

Figure S5.65. ^{11}B NMR spectrum of $[NH_2–BHPh]_n$ (**5.2a**) in THF after heating to 70 °C for 170 h.

Thermal stability of $[NH_2–BH(p\text{-}CF_3C_6H_4)]_n$ (5.2b) in THF at 20 °C: A solution of $[NH_2–BH(p\text{-}CF_3C_6H_4)]_n$ (88 mg, 0.25 mmol) in THF (0.5 mL) was stirred at 20 °C. After 170 h, the solution was analysed by ^{11}B NMR spectroscopy to reveal partial depolymerisation of $[NH_2–BH(p\text{-}CF_3C_6H_4)]_n$ to yield $[HN–B(p\text{-}CF_3C_6H_4)]_3$ [δ_B 32.1 (br)] (*ca.* 35 %), $[NH_2–BH(p\text{-}CF_3C_6H_4)]_n$ [δ_B −7.9 (br)] (*ca.* 45 %), and an unknown species [δ_B 12.1 (br)] (*ca.* 20 %) (Figure S5.66). Analysis of the solution by GPC showed a bimodal distribution containing a high and a low molecular weight fraction (peak at 17.7 mL: M_n = 72,500 g mol^{-1}, M_w = 77,500 g mol^{-1}, PDI = 1.07) (peak 18.5 mL: M_n = 31,500 g mol^{-1} M_w = 33,000 g mol^{-1}, PDI = 1.06) (Figure S5.67).

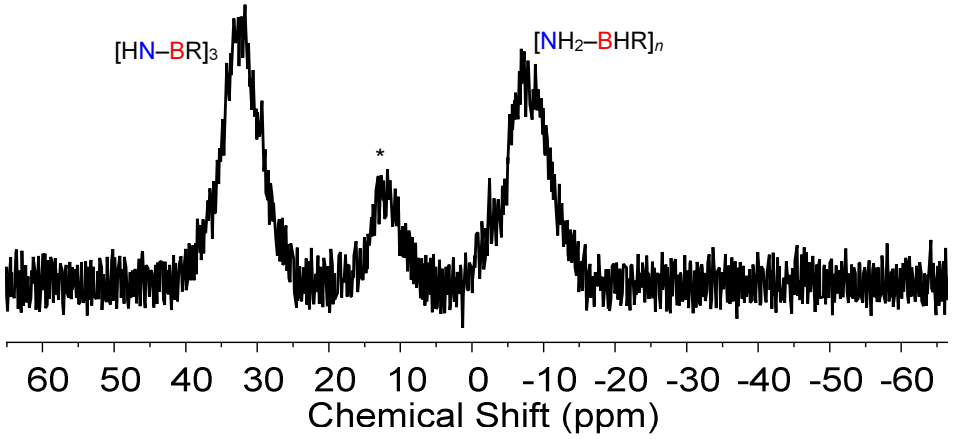

Figure S5.66. $^{11}B\{^{1}H\}$ NMR spectrum of $[NH_2–BH(p\text{-}CF_3C_6H_4)]_n$ (**5.2b**) in THF at 20 °C after 170 h. * Unknown species. R = $p\text{-}CF_3C_6H_4$.

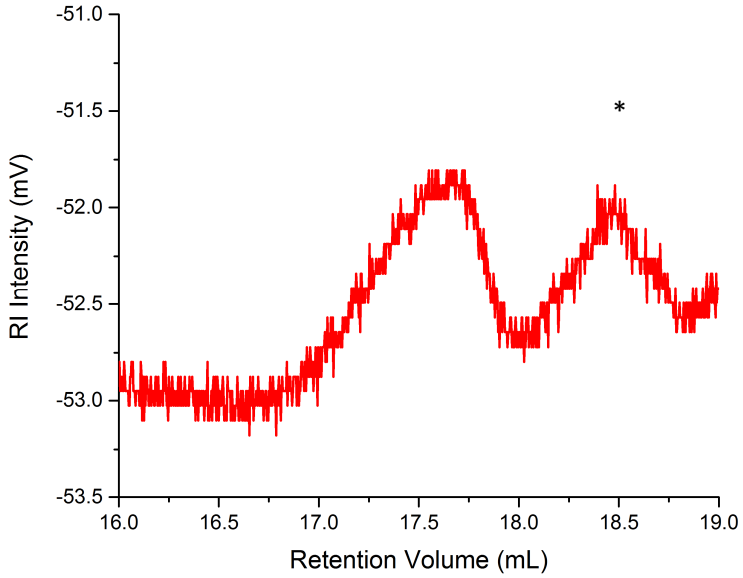

Figure S5.67. GPC chromatogram (2 mg mL^{-1}) of $[NH_2–BH(p\text{-}CF_3C_6H_4)]_n$ (**5.2b**) in THF (0.1 wt% [nBu$_4$N]Br) at 20 °C after 170 h. The asterisk (*) marks an additional trace, which was present in the polymer batch used for the thermal studies.

Thermal stability of [NH$_2$–BH(*p*-CF$_3$C$_6$H$_4$)]$_n$ (5.2b) in THF at 20 °C after three consecutive precipitations: A solution of [NH$_2$–BH(*p*-CF$_3$C$_6$H$_4$)]$_n$ (88 mg, 0.25 mmol) in THF (0.5 mL) was stirred at 20 °C. After 170 h, the solution was analysed by ^{11}B NMR spectroscopy to reveal partial depolymerisation of [NH$_2$–BH(*p*-CF$_3$C$_6$H$_4$)]$_n$ to yield [HN–B(*p*-CF$_3$C$_6$H$_4$)]$_3$ [δ_B 33.1 (br)] (*ca.* 57 %), [NH$_2$–BH(*p*-CF$_3$C$_6$H$_4$)]$_n$ [δ_B −7.9 (br)] (*ca.* 33 %), and NH$_3$·BH$_2$(*p*-CF$_3$C$_6$H$_4$) [δ_B −14.96 (br) (t, $^1J_{BH}$ = 95 Hz)] (*ca.* 10 %) (Figures S5.68 and S5.69). Analysis of the solution by GPC showed a bimodal distribution containing a high and a low molecular weight fraction (peak at 17.3 mL: M_n = 100,000 g mol^{-1}, M_w = 103,800 g mol^{-1}, PDI = 1.03) (peak 19.7 mL: M_n = 7,700 g mol^{-1} M_w = 9,200 g mol^{-1}, PDI = 1.18) (Figure S5.70).

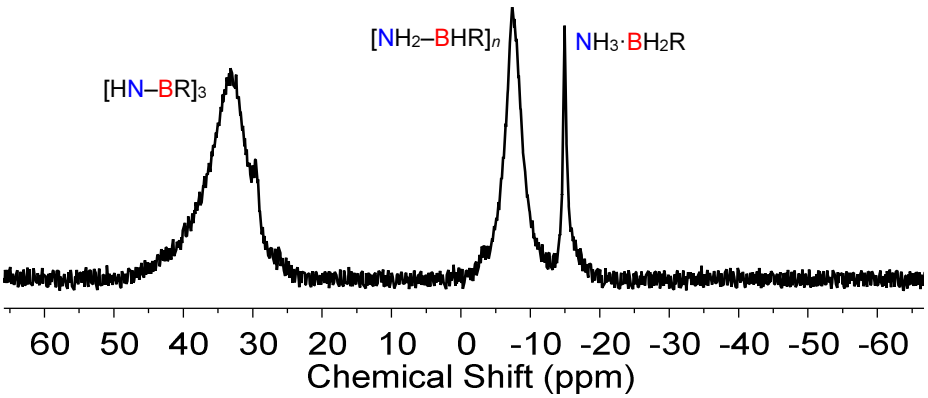

Figure S5.68. ^{11}B{^{1}H} NMR spectrum of [NH$_2$−BH(*p*-CF$_3$C$_6$H$_4$)]$_n$ (**5.2b**) in THF at 20 °C after 170 h.

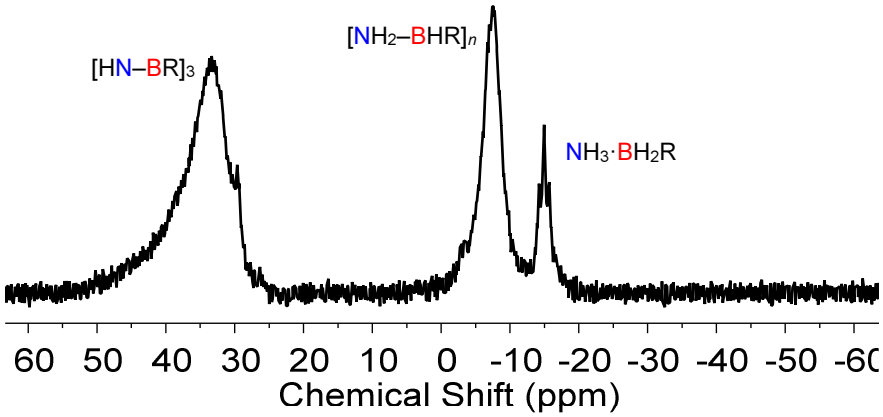

Figure S5.69. ^{11}B NMR spectrum of [NH$_2$−BH(*p*-CF$_3$C$_6$H$_4$)]$_n$ (**5.2b**) in THF at 20 °C after 170 h.

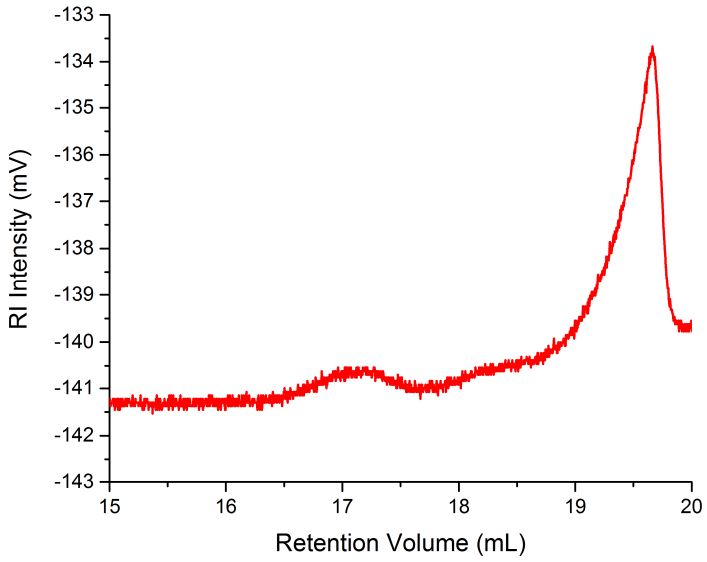

Figure S5.70. GPC chromatogram (2 mg mL^{-1}) of [NH_2–BH(*p*-$CF_3C_6H_4$)]$_n$ (**2b**) in THF (0.1 wt% [*n*Bu_4N]Br) at 20 °C after 170 h.

Thermal stability of [NH_2–BH(*p*-$CF_3C_6H_4$)]$_n$ (5.2b) in THF at 70 °C: An aliquot (0.4 mL) of solution of [NH_2–BH(*p*-$CF_3C_6H_4$)]$_n$ (88 mg, 0.25 mmol) in THF (0.5 mL) was transferred to a J. Young quartz-glass NMR tube and heated to 70 °C for 170 h. After cooling to 20 °C, the mixture was analysed by ^{11}B NMR spectroscopy indicating depolymerisation of [NH_2–BH(*p*-$CF_3C_6H_4$)]$_n$ to yield [HN–B(*p*-$CF_3C_6H_4$)]$_3$ [δ_B 32.7 (br)] (*ca.* 75 %), [NH_2–BH(*p*-$CF_3C_6H_4$)]$_x$ [δ_B −6.2 and −5.21 (br)] (*ca.* 15 %) and an unidentified species [δ_B 12.3 (br)] (*ca.* 10 %) (Figure S5.71 and S5.72). Analysis of the solution by GPC revealed that neither high nor low molecular weight polymer were present.

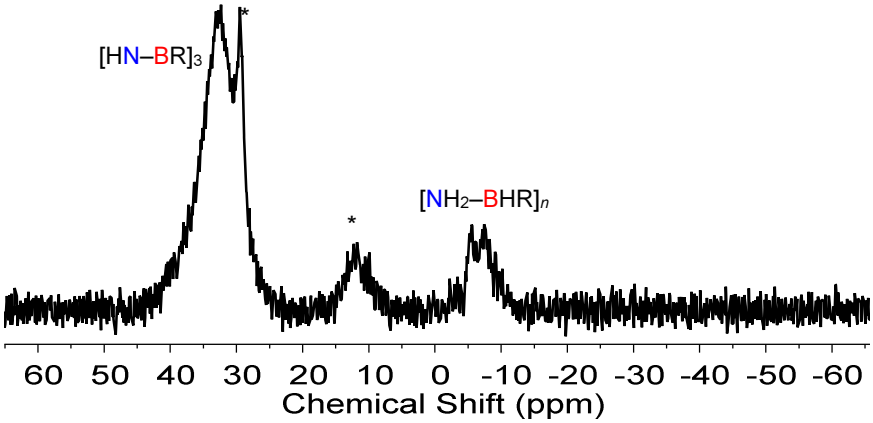

Figure S5.71. $^{11}B\{^{1}H\}$ NMR spectrum of $[NH_2–BH(p\text{-}CF_3C_6H_4)]_n$ (**5.2b**) in THF after heating to 70 °C for170 h. * Unknown species. R = p-$CF_3C_6H_4$.

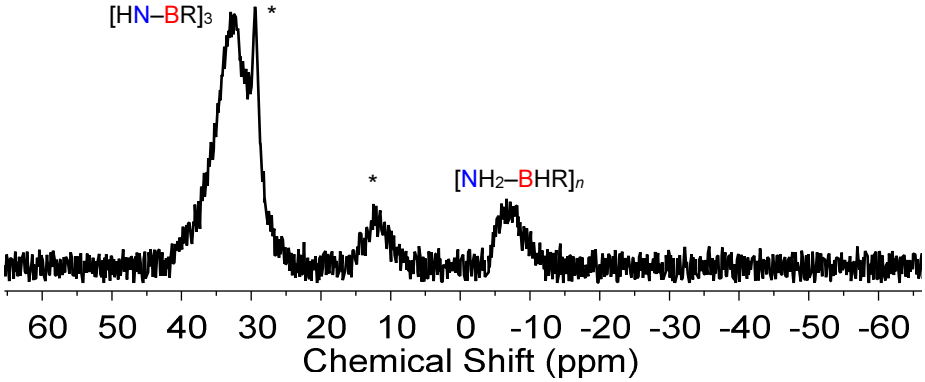

Figure S5.72. ^{11}B NMR spectrum of $[NH_2–BH(p\text{-}CF_3C_6H_4)]_n$ (**5.2b**) in THF after heating to 70 °C for 170 h. * Unknown species. R = p-$CF_3C_6H_4$.

5.6 References

1. (a) Priegert, A. M.; Rawe, B. W.; Serin, S. C.; Gates, D. P., *Chem. Soc. Rev.* **2016,** *45*, 922-953; (b) Jäkle, F., *Chem. Rev.* **2010,** *110*, 3985-4022; (c) Manners, I., *Angew. Chem. Int. Ed.* **1996,** *35*, 1602-1621.

2. Staubitz, A.; Soto, A. P.; Manners, I., *Angew. Chem. Int. Ed.* **2008,** *47*, 6212-6215.

3. Fazen, P. J.; Remsen, E. E.; Beck, J. S.; Carroll, P. J.; Mcghie, A. R.; Sneddon, L. G., *Chem. Mater.* **1995,** *7*, 1942-1956.

4. Lorenz, T.; Crumbach, M.; Eckert, T.; Lik, A.; Helten, H., *Angew. Chem. Int. Ed.* **2017,** *56*, 2780-2784.

5. (a) Marinelli, D.; Fasano, F.; Najjari, B.; Demitri, N.; Bonifazi, D., *J. Am. Chem. Soc.* **2017,** *139*, 5503-5519; (b) Ayhan, O.; Eckert, T.; Plamper, F. A.; Helten, H., *Angew. Chem. Int. Ed.* **2016,** *55*, 13321-13325; (c) Lorenz, T.; Lik, A.; Plamper, F. A.; Helten, H., *Angew. Chem. Int. Ed.* **2016,** *55*, 7236-7241; (d) Ledoux, A.; Larini, P.; Boisson, C.; Monteil, V.; Raynaud, J.; Lacote, E., *Angew. Chem. Int. Ed.* **2015,** *54*, 15744-15749; (e) Grosche, M.; Herdtweck, E.; Peters, F.; Wagner, M., *Organometallics* **1999,** *18*, 4669-4672.

6. (a) van de Wouw, H. L.; Lee, J. Y.; Klausen, R. S., *Chem. Commun.* **2017,** *53*, 7262-7265; (b) Thiedemann, B.; Gliese, P. J.; Hoffmann, J.; Lawrence, P. G.; Sönnichsen, F. D.; Staubitz, A., *Chem. Commun.* **2017,** *53*, 7258-7261; (c) Wan, W. M.; Baggett, A. W.; Cheng, F.; Lin, H.; Liu, S. Y.; Jäkle, F., *Chem. Commun.* **2016,** *52*, 13616-13619; (d) Jackson, L. A.; Allen, C. W., *J. Polym. Sci., Part A: Polym. Chem.* **1992,** *30*, 577-581; (e) Su, K.; Remsen, E. E.; Thompson, H. M.; Sneddon, L. G., *Macromolecules* **1991,** *24*, 3760-3766.

7. (a) Wang, X. C.; Hooper, T. N.; Kumar, A.; Priest, I. K.; Sheng, Y. W.; Samuels, T. O. M.; Wang, S. S.; Robertson, A. W.; Pacios, M.; Bhaskaran, H.; Weller, A. S.; Warner, J. H., *CrystEngComm.* **2017,** *19*, 285-294; (b) Du, V. A.; Jurca, T.; Whittell, G. R.; Manners, I., *Dalton Trans.* **2016,** *45*, 1055-1062.

8. (a) Rossin, A.; Peruzzini, M., *Chem. Rev.* **2016,** *116*, 8848-8872; (b) Hill, M. S.; Liptrot, D. J.; Weetman, C., *Chem. Soc. Rev.* **2016,** *45*, 972-988; (c) Johnson, H. C.; Hooper, T. N.; Weller, A. S., *Top. Organometal. Chem.* **2015,** *49*, 153-220; (d) Leitao, E. M.; Jurca, T.; Manners, I., *Nat. Chem.* **2013,** *5*, 817-829; (e) Less, R. J.; Melen, R. L.; Wright, D. S., *RSC Adv.* **2012,** *2*, 2191-2199; (f) Smythe, N. C.; Gordon, J. C., *Eur. J. Inorg. Chem.* **2010**, 509-521; (g) Stephens, F. H.; Pons, V.; Baker, R. T., *Dalton Trans.* **2007**, 2613-2626.

9. (a) Anke, F.; Han, D.; Klahn, M.; Spannenberg, A.; Beweries, T., *Dalton Trans.* **2017,** *46*, 6843-6847; (b) Johnson, H. C.; Leitao, E. M.; Whitten, G. R.; Manners, I.; Lloyd-Jones, G. C.; Weller, A. S., *J. Am. Chem. Soc.* **2014,** *136*, 9078-9093; (c) Marziale, A. N.; Friedrich, A.; Klopsch, I.; Drees, M.; Celinski, V. R.; Günne, J. S. A. D.; Schneider, S., *J. Am. Chem. Soc.* **2013,** *135*, 13342-13355; (d) Dallanegra, R.; Robertson, A. P. M.; Chaplin, A. B.; Manners, I.; Weller, A. S., *Chem. Commun.* **2011,** *47*, 3763-3765; (e) Robertson, A. P. M.; Suter, R.; Chabanne, L.; Whittell, G. R.; Manners, I., *Inorg. Chem.* **2011,** *50*, 12680-12691; (f) Vance, J. R.; Robertson, A. P. M.; Lee, K.; Manners, I., *Chem. Eur. J.* **2011,** *17*, 4099-4103; (g) Staubitz, A.; Sloan, M. E.; Robertson, A. P. M.; Friedrich, A.; Schneider, S.; Gates, P. J.; Günne, J. S. A. D.; Manners, I., *J. Am. Chem. Soc.* **2010,** *132*, 13332-13345.

10. Helten, H.; Robertson, A. P. M.; Staubitz, A.; Vance, J. R.; Haddow, M. F.; Manners, I., *Chem. Eur. J.* **2012,** *18*, 4665-4680.

11. (a) Kumar, A.; Priest, I. K.; Hooper, T. N.; Weller, A. S., *Dalton Trans.* **2016,** *45*, 6183-6195; (b) Stubbs, N. E.; Schäfer, A.; Robertson, A. P. M.; Leitao, E. M.; Jurca, T.; Sparkes, H. A.; Woodall, C. H.; Haddow, M. F.; Manners, I., *Inorg. Chem.* **2015,** *54*, 10878-10889; (c) Kumar, A.; Ishibashi, J. S. A.; Hooper, T. N.; Mikulas, T. C.; Dixon, D. A.; Liu, S. Y.; Weller, A. S., *Chem. Eur. J.* **2016,** *22*,

310-322; (d) Campbell, P. G.; Ishibashi, J. S. A.; Zakharov, L. N.; Liu, S. Y., *Aust. J. Chem.* **2014,** *67*, 521-524; (e) Campbell, P. G.; Marwitz, A. J. V.; Liu, S. Y., *Angew. Chem. Int. Ed.* **2012,** *51*, 6074-6092; (f) Robertson, A. P. M.; Haddow, M. I. F.; Manners, I., *Inorg. Chem.* **2012,** *51*, 8254-8264; (g) Robertson, A. P. M.; Whittell, G. R.; Staubitz, A.; Lee, K.; Lough, A. J.; Manners, I., *Eur. J. Inorg. Chem.* **2011**, 5279-5287.

12. Kim, S. K.; Han, W. S.; Kim, T. J.; Kim, T. Y.; Nam, S. W.; Mitoraj, M.; Piekos, L.; Michalak, A.; Hwang, S. J.; Kang, S. O., *J. Am. Chem. Soc.* **2010,** *132*, 9954-9955.

13. (a) Anane, H.; Jarid, A.; Boutalib, A.; Nebot-Gil, I.; Tomas, F., *J. Mol. Struc.-Theochem.* **1998,** *455*, 51-57; (b) Grant, D. J.; Matus, M. H.; Anderson, K. D.; Camaioni, D. M.; Neufeldt, S. R.; Lane, C. F.; Dixon, D. A., *J. Phys. Chem. A* **2009,** *113*, 6121-6132; (c) Staubitz, A.; Besora, M.; Harvey, J. N.; Manners, I., *Inorg. Chem.* **2008,** *47*, 5910-5918.

14. Singaram, B.; Cole, T. E.; Brown, H. C., *Organometallics* **1984,** *3*, 774-777.

15. Jaska, C. A.; Temple, K.; Lough, A. J.; Manners, I., *J. Am. Chem. Soc.* **2003,** *125*, 9424-9434.

16. Jacquemin, D.; Perpète, E. A., *J. Phys. Chem. A* **2005,** *109*, 6380-6386.

17. Bruessau, R. J., *Makromol. Chem., Macromol. Symp.* **1992,** *61*, 199-218.

18. (a) Boymirzaev, A. S.; Shomuratov, S.; Turaev, A. S., *Chem. Plant Mater.* **2013,** *2*, 51-55; (b) Young, R. J.; Lovell, P. A., *Introduction to Polymers, Third Edition*. CRC Press: 2011.

19. Turner, J. R.; Resendiz-Lara, D. A.; Jurca, T.; Schäfer, A.; Vance, J. R.; Beckett, L.; Whittell, G. R.; Musgrave, R. A.; Sparkes, H. A.; Manners, I., *Macromol. Chem. Phys.* **2017,** *218*, 1700120.

20. Pangborn, A. B.; Giardello, M. A.; Grubbs, R. H.; Rosen, R. K.; Timmers, F. J., *Organometallics* **1996,** *15*, 1518-1520.

21. Gottker-Schnetmann, I.; White, P. S.; Brookhart, M., *Organometallics* **2004,** *23*, 1766-1776.

22. Bruker, *SAINT+ Integration Engine, Data Reduction Software, Bruker Analytical X-ray Instruments Inc., Madison, WI, USA* **2007**.

23. Bruker, *SADABS, Bruker AXS area detector scaling and absorption correction, Bruker Analytical X-ray Instruments Inc., Madison, Wisconsin, USA* **2001**.

24. (a) Palatinus, L.; Chapuis, G., *J. Appl. Crystallogr.* **2007,** *40*, 786-790; (b) Palatinus, L.; Prathapa, S. J.; van Smaalen, S., *J. Appl. Crystallogr.* **2012,** *45*, 575-580.

25. Bourhis, L. J.; Dolomanov, O. V.; Gildea, R. J.; Howard, J. A. K.; Puschmann, H., *Acta Crystallogr. A* **2015,** *71*, 59-75.

26. (a) Sheldrick, G. M., *Acta Crystallogr., Sect. A: Found. Crystallogr.* **2008,** *64*, 112-122; (b) Sheldrick, G. M., *Acta Crystallogr. C* **2015,** *71*, 3-8.

27. Dolomanov, O. V.; Bourhis, L. J.; Gildea, R. J.; Howard, J. A. K.; Puschmann, H., *J. Appl. Crystallogr.* **2009,** *42*, 339-341.

28. (a) Spek, A., *J. Appl. Crystallogr.* **2003,** *36*, 7-13; (b) Spek, A., *Acta Crystallogr. D* **2009,** *65*, 148-155.

Chapter 6

Outlook and Future Work

The body of work presented in this thesis has focused on the synthesis of polyamino– and polyphosphinoboranes *via* metal-catalysed dehydropolymerisation of amine– and phosphine–boranes to produce materials with varied structures. This chapter will cover some ideas for future investigation, based on results from former chapters.

6.1 Post-functionalisation of Polyphosphinoboranes: Alkene Hydroboration

Chapter 2 and Chapter 3 focused on the synthesis of high molar mass polyphosphinoboranes containing either aryl or alkyl groups with a variety of substituents. This emphasised the versatility of the [$CpFe(CO)_2OTf$] to create a catalogue of new PB materials with different properties..

Post-polymerisation modification has been successfully applied to organic polymers to create materials with a broad range of different functional groups.[1] This technique has also been successfully applied to inorganic polymers, such as polysilanes and polysiloxanes, in which well-stablished Si–H activation routes, as hydrosilation and dehydrocoupling chemistry have been used.[2] In a similar way, the P–H and B–H bonds in polyphosphinoboranes could be activated by subsequent reaction steps, for example, using hydrophosphination or hydroboration routes, respectively, to access polymers that cannot be synthesised by direct polymerisation of the corresponding monomers.

The post-polymerisation route can be potentially applied to polyphosphinoboranes to create tailor-made polymeric materials. For example, B–H activation may be a promising avenue based on work by *Vedejs* and coworkers whom have reported the intramolecular

hydroboration of allylic phosphine–boranes by activation with the Lewis acid $B(C_6F_5)_3$ under catalytic conditions (Scheme 6.1).[3]

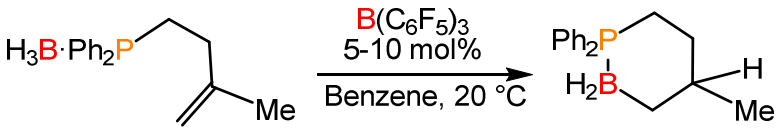

Scheme 6.1. Intermolecular hydroboration of an allylic phosphine–borane by a Lewis acid.

Preliminary experiments exploring the reactivity of polyphosphinoboranes towards hydroboration with alkenes by activation with $B(C_6F_5)_3$ appear promising (Scheme 6.2). These involved the reactivity of $[PhPH–BH_2]_n$ with 3,3-dimethyl-1-butene in equimolar quantities (1,2-$C_6H_4F_2$, 60 °C) with $B(C_6F_5)_3$ (10 mol %).

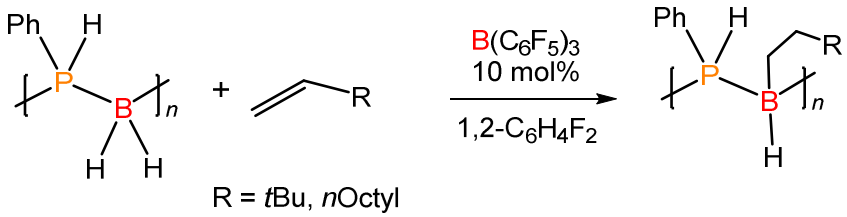

Scheme 6.2. Polyphosphinoborane hydroboration with alkenes assisted by a Lewis acid.

After 46 h, the ^{11}B NMR spectrum showed two signals at ($\delta_B = -34.7$ ppm) and at ($\delta_B = -15$ ppm) which were tentatively assigned to $[PhPH–BH_2]_n$ and to a *B*-substituted polymer $[PhPH–BHR]_n$ respectively. In addition, the signal at ($\delta_B = -25.9$ ppm, $J_{BH} = 94.2$ Hz) corresponded to $[HB(C_6F_5)_3]^-$, which implied the activation of the B–H bond in the polyphosphinoborane by the Lewis acid (Figure 6.1). However, further reactivity was not observed, and future experiments will involve the addition of excess olefin.

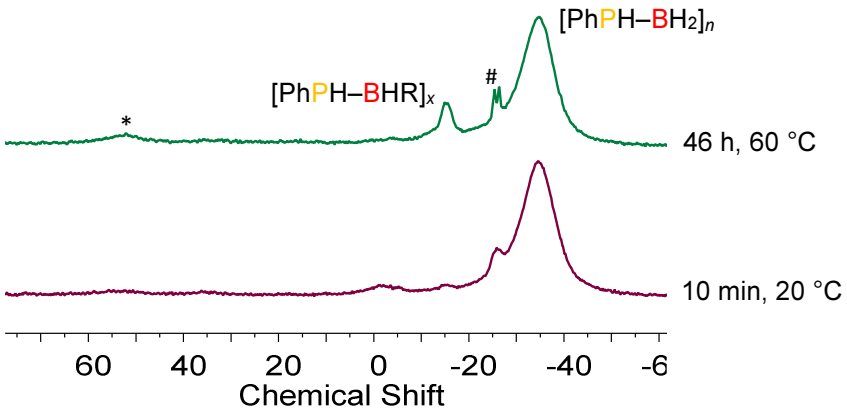

Figure 6.1. ^{11}B NMR spectra of $[PhPH–BH_2]_n$ and 3,3-dimethyl-1-butene using $B(C_6F_5)_3$ (10 mol%) in 1,2-$C_6H_4F_2$. * $B(C_6F_5)_3$ # $[HB(C_6F_5)_3]^-$

Similar experiments with the less sterically encumbered olefin 1-octene showed a signal at ca. (δ_B = −15 ppm) which was assigned to the poly(*B*-octyl)phosphinoborane $[PhPH–BH(CH_2)_8]_n$. These results suggest that functionalisation of polyphosphinoboranes via hydroboration may be a promising future approach to expanding the range of materials available. However, it has to be considered that the increase of the steric repulsion on boron and the decrease of the Lewis acidity by introduction of alkyl groups, could lead to a reduction of the B–P bond stability, possibly promoting scission of the polymer backbone.

6.2 Synthesis and Reactivity of *B*-substituted Phosphine–Boranes

Chapter 5 contained a brief overview of the chemistry of *B*-substituted amine–boranes, $NH_3{\cdot}BH_2R$, and in addition, some examples of these adducts were described which represent a significant contribution to this underveloped field. In phosphine–borane chemistry, the description of analogous *B*-substituted phosphine–boranes, $RPH_2{\cdot}BH_2R$, is almost non-existent.

It has been previously reported that unsaturated phosphinoboranes $PR_2–BR'_2$ exist in their monomeric form when the R groups are sterically demanding substituents. In

contrast, in the absence of steric protection, these species tend to form dimeric or trimeric cyclic compounds or oligomeric species with both B and P atoms in tetracoordinated environments. In the same manner, the elusive RP=BR′ species tend to form four- (RP–BR′)$_2$ or six-membered (RP–BR′)$_3$ rings with B and P atoms display in a tricoordinated geometry.[4] For example, *Power* and coworkers have synthesised examples of four- (PR–BR')$_3$ [R,R′ = 1-Ad,Mes and Mes,Thex] and six-membered (PR–BR')$_3$ [R,R′ = Cy,Mes; Ph.Mes; Mes,Mes; and Mes,Ph] rings from the reaction of the corresponding boranes R'BX$_2$ and the lithium salts of different primary phosphines RPHLi (Figure 6.3). However, no mechanistic studies for the formation of the compounds were provided.[5]

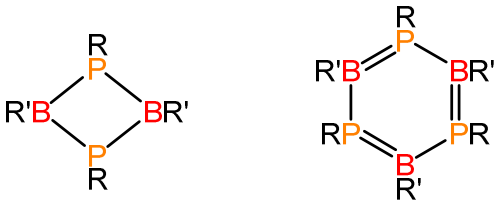

Figure 6.3. Four- and six membered boron–phosphorus rings

The use of a similar synthetic route to form four-membered rings involved the reaction of PhP(SiMe$_3$)$_2$ and RBX$_2$ (R = 2,2,6,6-tetramethylpiperidinoborane and X = Cl, Br) where [PhP=BR] was proposed as an intermediate.[6] Based on these results, the reactivity of similar substrates bearing R groups with less steric profile (R, R' = alkyl linear groups) will be undertaken. This could lead to the formation of [RP=BR'] monomers. These species could polymerise in a head-to-tail fashion to produce unsaturated PB polymers, in a similar manner to that previously reported for the thermolysis of Lewis-base stabilised phosphinoboranes (Scheme 6.3).[7] In the presence of *N*-heterocyclic carbenes (NHC) or Lewis bases (e.g. amines) the isolation of the intermediates [PhP–BR'L] (where L is a carbene or an amine) could be possible.

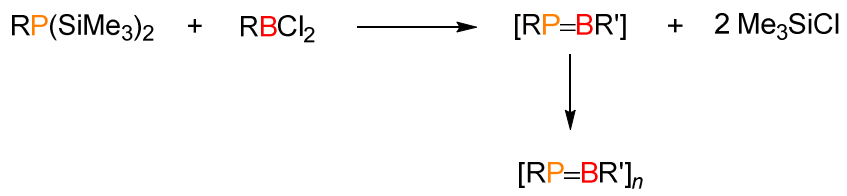

Scheme 6.3. Proposed Me_3SiCl elimination reaction for the formation of unsaturated polyaminoboranes

6.3 Polyamino and Polyphosphinoboranes as Precursors to Polymer-Derived Ceramics (PDC)

The use of the Polymer-Derived Ceramics (PDC) route to obtain non-oxide ceramics from polymeric precursors is well-established and has been successfully applied to organosilicon and organoboron polymer derivatives.[8,9] The PDC route has the advantage of controlling the composition and homogeneity at the atomic level. Moreover, the macromolecular precursors can be shaped by the different processing techniques developed in polymer science at mild temperatures. In this way, PDC circumvents the use of sintering additives which are required traditionally in powder technologies. The application of this concept to polyamino– and polyphosphinoboranes is necessary in order to maintain active this area of research. The ceramics derived from pyrolysis of polyamino– or polyphosphinoboranes could have similar inherent properties to boron nitride (BN) including chemical inertness, hardness, and high temperature stability. In addition, semiconducting properties have been attributed to boron phosphide (BP). This research will require the formation of an interdisciplinary group with knowledge in inorganic chemistry, polymer chemistry, and engineering.

In Chapter 4, the synthesis of polyaminoborane homopolymers and copolymers bearing aryl-substituted alkyl substituents at nitrogen was described. In particular, the synthesis of $[Ph(CH_2)_4NH–BH_2]_n–r–[NH_2–BH_2]_m$ [n: 1, m: 2] is interesting, as it is a soluble polyaminoborane that features high content of $[NH_2–BH_2]$ units. Further pyrolytic

studies of this polymer will be investigated. Initial cross-linking studies of polyaminoboranes were performed, and a slight improvement on the ceramic yield compared to the homopolymers was observed by TGA. Investigation on the formation of cross-linked BN polymeric materials using diamine–borane linkers, (BH_3·NH_2–R–NH_2·BH_3), with R groups consisting in long alkyl or ethylene glycol chains, will be explored.

In a similar manner, the pyrolysis of polyphosphinoboranes could be a potential route to obtain BP. In a previous report by *Manners* and coworkers, the synthesis of $[PhPH–BH_2]_n$ was achieved by the use of Rh-based precatalysts and the resulting polymer displayed high ceramic yields (75-80%) by TGA (1000 °C, 10 °C min^{-1}). Subsequent pyrolysis of this material (1000 °C, 10 °C min^{-1}, 24 h) under nitrogen gave a ceramic that, after analysis by powder X-ray diffraction, it was found to contain BP as the main crystalline component.[10] Detailed characterisation of the ceramic material was unpublished.

In Chapter 3, the thermal properties of a range of poly(alkylphosphinoboranes) were reported. The polymer $[MePH–BH_2]_n$ displayed the highest ceramic yield (75 %) by TGA (700 °C, 10 °C min^{-1}). We proposed that $[MePH–BH_2]_n$ could be a better precursor to boron phosphide (due to its low carbon content (20 % by mass)) than $[PhPH–BH_2]_n$ (59% by mass) as the former can potentially form more volatile carbon products that could lead to purer samples of BP. The synthesis of $[MePH–BH_2]_n$ on a larger scale and subsequent pyrolytic studies are under investigation. Also, detailed characterisation studies of the ceramic product will be performed.

6.4 Detailed studies of the solution behaviour of highly polar polyamino– and polyphosphinoboranes.

In Chapter 2 and Chapter 5, the formation of polyamino– and polyphosphinoboranes $[REH–BHR']_n$ (E= N or P) substituted by fluoro-containing groups (p-$CF_3C_6H_4$ or $m,m(CF_3)_2C_6H_3$) on the phenyl ring was described. In addition, we observed an inverse relationship between the polymer concentration and the apparent molar mass of the polymers, as observed by GPC. This is reminiscent of the behaviour of polyelectrolytes where the hydrodynamic radius (R_h) increases at low concentration due to the effect of osmotic pressure (Figure 6.4).[11] It is clear that further investigation is needed to uncover the nature of this unusual phenomenon in these polar inorganic polymers. These studies will include the use of static light scattering (SLS) as complementary technique to DLS. These studies will confirm the values given on the hydrodynamic radius obtained by DLS or the radius of gyration obtained by SLS, depend on the polymer concentration. If the radius of gyration does not depend on polymer concentration, then the phenomenon is exclusively related to a non-exclusion effect that occurs when the hydrophobic column in the GPC interacts with the polar polymers. In addition, we propose that the use of different concentrations of electrolytes in solution might counter the *polyelectrolyte effect* on polyaminoboranes and polyphosphinoboranes. Measurements by SLS, DLS and GPC will be performed. We also propose an investigation into non-ionic, polar organic polymers (e.g. fluorinated polystyrene $[RC_5H_4CH_2–CH_2]_n$ (R = CF_3), poly(2-vinylpyridine)s or poly(4-hydroxystyrene)) in polar solvents to confirm if similar *polyelectrolyte effects* occur. Recently, the use of ionic liquids, as the mobile phase in HPLC, have been used in the characterisation of polyelectrolytes. Also, the ionic liquid was found to counter the non-exclusion effects in some polyelectrolytes.[12] The use of a similar technique in our polymers could be possible to improve characterisation.

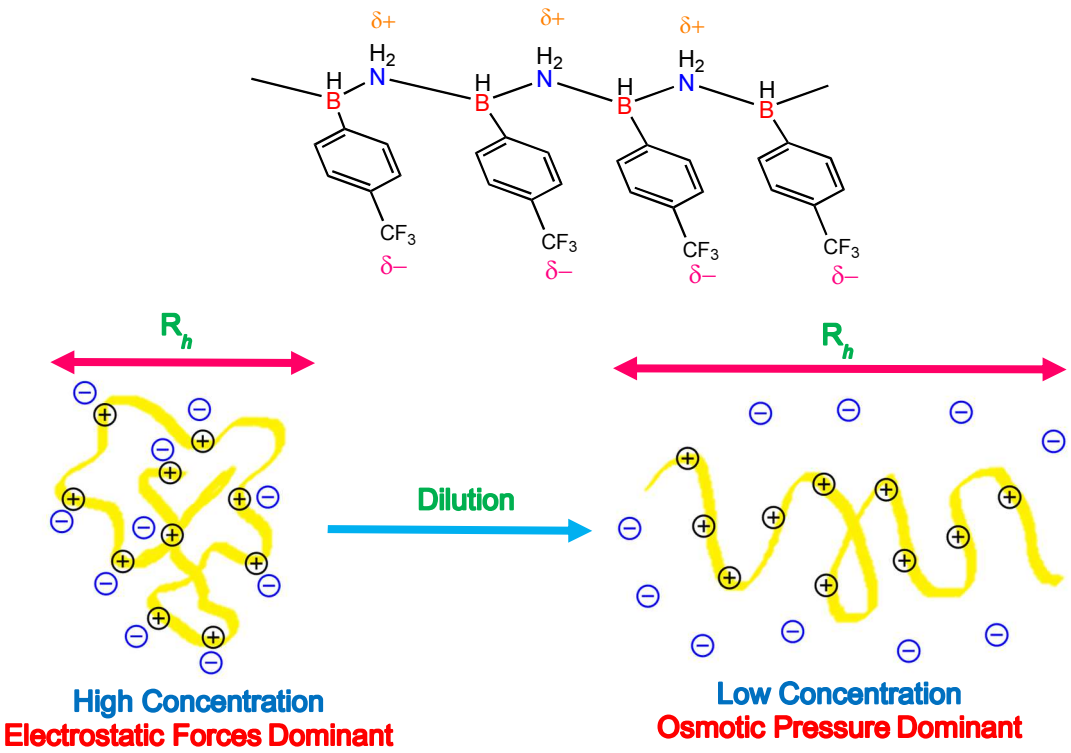

Figure 6.4. Representation of the *polyelectrolyte effect* on *B*-substituted polyaminoboranes.

6.5 Detailed mechanistic studies of the dehydropolymerisation of polyamino– and polyphosphinoboranes by [IrH$_2$(POCOP)] and [CpFe(CO)$_2$OTf] precatalysts.

The first example of well-defined homogeneous catalytic dehydropolymerisation was achieved using RNH$_2$·BH$_3$ (R = H, Me, ^{n}Bu) and an Ir(H)$_2$(POCOP) catalyst to form polyaminoboranes [RHNBH$_2$]$_n$.[13] In Chapter 4 and in Chapter 5, this dehydropolymerisation technique was extended to include other amine–boranes substrates. Although the [Ir] catalyst produced polyaminoboranes with high molar mass and reasonably low polydispersity, the key steps in the polymerisation are not completely understood, though some attempts have been made with other metal-based precatalysts.[14]

Understanding the difference in polymer molecular weights obtained via metal catalysed or catalyst-free processes will form part of our future work in this area. One of the challenges is the elucidation of the initial steps in the proposed chain growth mechanism

for the synthesis of polyaminoboranes, in which a slow initial dehydrogenation of $MeNH_2{\cdot}BH_3$ is followed by fast insertion of the resulting $MeNH{=}BH_2$.[13b]

It would be of interest to probe the proposed mechanism of dehydropolymerisation by experimental studies. To achieve this, we would use lower reaction temperatures and higher catalyst loading. The detection of intermediates by ESI-MS at early stages of the reaction, and their characterization by X-ray crystallography are key targets.

Mechanistic insight into the dehydropolymerisation process is needed to establish whether the dehydrogenation and coupling steps proceed *via* aminoborane or linear diborazane, as intermediates.[15] To probe this, we propose screening different primary amine–boranes $RNH_2{\cdot}BH_3$ (e. g. R = iPr) in order to find a suitable substrate to slow down the rate of catalysis, in order to gain better mechanistic insight. This may also be achieved by lowering reaction temperatures and performing the reactions in closed systems.

Based on previous studies of dehydrocoupling chemistry and model species,[16] a chain growth coordination-type mechanism was proposed for the dehydropolymerisation of primary phosphine–boranes *via* $[CpFe(CO)_2OTf]$.[17] In Chapter 2 and in Chapter 3, this synthetic methodology was applied to other phosphine–boranes containing either aryl or alkyl substituents. However, no mechanistic insight for these reactions was obtained. In order to find a general polymerisation mechanism further studies are needed. It has been established that the phosphidoborane $[CpFe(CO)_2(\eta^1\text{-}PRH{-}BH_3]$ complex, a likely intermediate, is also active as a catalyst in the dehydropolymerisation process. A study of the coordination chemistry of monomeric phosphine– and phosphinoboranes (and oligomeric species) with $[CpFe(CO)_2OTf]$ to model the different steps of the catalytic cycle will also be performed.

6.5 References

1. Gauthier, M. A.; Gibson, M. I.; Klok, H. A., *Angew. Chem. Int. Ed.* **2009,** *48*, 48-58.

2. Lee, V. Y., *Organosilicon Compounds: Experiment (Physico-Chemical Studies) and Applications*. Elsevier Science: 2017.

3. Shapland, P.; Vedejs, E., *J. Org. Chem.* **2004,** *69*, 4094-4100.

4. Paine, R. T.; Noth, H., *Chem. Rev.* **1995,** *95*, 343-379.

5. Dias, H. V. R.; Power, P. P., *J. Am. Chem. Soc.* **1989,** *111*, 144-148.

6. Escudie, J.; Couret, C.; Lazraq, M.; Garrigues, B., *Synth. React. Inorg. Met.-Org. Chem.* **1987,** *17*, 379-384.

7. Marquardt, C.; Jurca, T.; Schwan, K. C.; Stauber, A.; Virovets, A. V.; Whittell, G. R.; Manners, I.; Scheer, M., *Angew. Chem. Int. Ed.* **2015,** *54*, 13782-13786.

8. Colombo, P.; Mera, G.; Riedel, R.; Soraru, G. D., *J. Am. Ceram. Soc.* **2010,** *93*, 1805-1837.

9. https://starfiresystems

10. Dorn, H.; Rodezno, J. M.; Brunnhöfer, B.; Rivard, E.; Massey, J. A.; Manners, I., *Macromolecules* **2003,** *36*, 291-297.

11. Young, R. J.; Lovell, P. A., *Introduction to Polymers, Third Edition*. CRC Press: 2011.

12. Kuroda, K.; Ohno, H., *Chem. Commun.* **2015,** *51*, 10551-10553.

13. (a) Staubitz, A.; Soto, A. P.; Manners, I., *Angew. Chem. Int. Ed.* **2008,** *47*, 6212-6215; (b) Staubitz, A.; Sloan, M. E.; Robertson, A. P. M.; Friedrich, A.; Schneider, S.; Gates, P. J.; Günne, J. S. A. D.; Manners, I., *J. Am. Chem. Soc.* **2010,** *132*, 13332-13345.

14. (a) Johnson, H. C.; Hooper, T. N.; Weller, A. S., *Top. Organometal. Chem.* **2015,** *49*, 153-220; (b) Colebatch, A. L.; Gilder, B. W. H.; Whittell, G. R.; Oldroyd, N. L.; Manners, I.; Weller, A. S., *Chem. Eur. J.* **2018,** *24*, 5450-5455; (c) Adams, G. M.; Colebatch, A. L.; Skornia, J. T.; McKay, A. I.; Johnson, H. C.; Lloyd-Jones, G. C.; Macgregor, S. A.; Beattie, N. A.; Weller, A. S., *J. Am. Chem. Soc.* **2018,** *140*, 1481-1495; (d) Johnson, H. C.; Leitao, E. M.; Whitten, G. R.; Manners, I.; Lloyd-Jones, G. C.; Weller, A. S., *J. Am. Chem. Soc.* **2014,** *136*, 9078-9093; (e) Anke, F.; Han, D.; Klahn, M.; Spannenberg, A.; Beweries, T., *Dalton Trans.* **2017,** *46*, 6843-6847.

15. Robertson, A. P. M.; Leitao, E. M.; Jurca, T.; Haddow, M. F.; Helten, H.; Lloyd-Jones, G. C.; Manners, I., *J. Am. Chem. Soc.* **2013,** *135*, 12670-12683.

16. (a) Huertos, M. A.; Weller, A. S., *Chem. Commun.* **2012,** *48*, 7185-7187; (b) Huertos, M. A.; Weller, A. S., *Chem. Sci.* **2013,** *4*, 1881-1888; (c) Hooper, T. N.; Huertos, M. A.; Jurca, T.; Pike, S. D.; Weller, A. S.; Manners, I., *Inorg. Chem.* **2014,** *53*, 3716-3729; (d) Hooper, T. N.; Weller, A. S.; Beattie, N. A.; Macgregor, S. A., *Chem. Sci.* **2016,** *7*, 2414-2426; (e) Paul, U. S. D.; Braunschweig, H.; Radius, U., *Chem. Commun.* **2016,** *52*, 8573-8576.

17. Schäfer, A.; Jurca, T.; Turner, J.; Vance, J. R.; Lee, K.; Du, V. A.; Haddow, M. F.; Whittell, G. R.; Manners, I., *Angew. Chem. Int. Ed.* **2015,** *54*, 4836-4841.